

# HIGHLIGHTS OF POG 2019 - PLANT OXYGEN GROUP CONFERENCE

EDITED BY: Christian Lindermayr, Joerg Durner, Ann Cuypers,  
Jörg-Peter Schnitzler and Krystyna Oracz  
PUBLISHED IN: Frontiers in Plant Science







# frontiers

## Frontiers eBook Copyright Statement

The copyright in the text of individual articles in this eBook is the property of their respective authors or their respective institutions or funders. The copyright in graphics and images within each article may be subject to copyright of other parties. In both cases this is subject to a license granted to Frontiers.

The compilation of articles constituting this eBook is the property of Frontiers.

Each article within this eBook, and the eBook itself, are published under the most recent version of the Creative Commons CC-BY licence.

The version current at the date of publication of this eBook is CC-BY 4.0. If the CC-BY licence is updated, the licence granted by Frontiers is automatically updated to the new version.

When exercising any right under the CC-BY licence, Frontiers must be attributed as the original publisher of the article or eBook, as applicable.

Authors have the responsibility of ensuring that any graphics or other materials which are the property of others may be included in the CC-BY licence, but this should be checked before relying on the CC-BY licence to reproduce those materials. Any copyright notices relating to those materials must be complied with.

Copyright and source acknowledgement notices may not be removed and must be displayed in any copy, derivative work or partial copy which includes the elements in question.

All copyright, and all rights therein, are protected by national and international copyright laws. The above represents a summary only. For further information please read Frontiers' Conditions for Website Use and Copyright Statement, and the applicable CC-BY licence.

ISSN 1664-8714

ISBN 978-2-88966-576-1

DOI 10.3389/978-2-88966-576-1

## About Frontiers

Frontiers is more than just an open-access publisher of scholarly articles: it is a pioneering approach to the world of academia, radically improving the way scholarly research is managed. The grand vision of Frontiers is a world where all people have an equal opportunity to seek, share and generate knowledge. Frontiers provides immediate and permanent online open access to all its publications, but this alone is not enough to realize our grand goals.

## Frontiers Journal Series

The Frontiers Journal Series is a multi-tier and interdisciplinary set of open-access, online journals, promising a paradigm shift from the current review, selection and dissemination processes in academic publishing. All Frontiers journals are driven by researchers for researchers; therefore, they constitute a service to the scholarly community. At the same time, the Frontiers Journal Series operates on a revolutionary invention, the tiered publishing system, initially addressing specific communities of scholars, and gradually climbing up to broader public understanding, thus serving the interests of the lay society, too.

## Dedication to Quality

Each Frontiers article is a landmark of the highest quality, thanks to genuinely collaborative interactions between authors and review editors, who include some of the world's best academicians. Research must be certified by peers before entering a stream of knowledge that may eventually reach the public - and shape society; therefore, Frontiers only applies the most rigorous and unbiased reviews.

Frontiers revolutionizes research publishing by freely delivering the most outstanding research, evaluated with no bias from both the academic and social point of view. By applying the most advanced information technologies, Frontiers is catapulting scholarly publishing into a new generation.

## What are Frontiers Research Topics?

Frontiers Research Topics are very popular trademarks of the Frontiers Journals Series: they are collections of at least ten articles, all centered on a particular subject. With their unique mix of varied contributions from Original Research to Review Articles, Frontiers Research Topics unify the most influential researchers, the latest key findings and historical advances in a hot research area! Find out more on how to host your own Frontiers Research Topic or contribute to one as an author by contacting the Frontiers Editorial Office: [frontiersin.org/about/contact](https://frontiersin.org/about/contact)



# HIGHLIGHTS OF POG 2019 - PLANT OXYGEN GROUP CONFERENCE

Topic Editors:

**Christian Lindermayr**, Helmholtz-Gemeinschaft Deutscher Forschungszentren (HZ), Germany

**Joerg Durner**, Helmholtz-Gemeinschaft Deutscher Forschungszentren (HZ), Germany

**Ann Cuypers**, University of Hasselt, Belgium

**Jörg-Peter Schnitzler**, Helmholtz-Gemeinschaft Deutscher Forschungszentren (HZ), Germany

**Krystyna Oracz**, Warsaw University of Life Sciences, Poland

**Citation:** Lindermayr, C., Durner, J., Cuypers, A., Schnitzler, J.-P., Oracz, K., eds. (2021). Highlights of POG 2019 - Plant Oxygen Group Conference. Lausanne: Frontiers Media SA. doi: 10.3389/978-2-88966-576-1



# Table of Contents

- 05 Editorial: Highlights of POG 2019 - Plant Oxygen Group Conference**  
Christian Lindermayr, Krystyna Orazc, Ann Cuypers, Jörg-Peter Schnitzler and Jörg Durner
- 08 Fertilizer Rate-Associated Increase in Foliar Jasmonate Burst Observed in Wounded *Arabidopsis thaliana* Leaves is Attenuated at  $eCO_2$**   
Julian Martinez Henao, Louis Erik Demers, Katharina Grosser, Andreas Schedl, Nicole M. van Dam and Jacqueline C. Bede
- 25 Suppressor of Gamma Response 1 Modulates the DNA Damage Response and Oxidative Stress Response in Leaves of Cadmium-Exposed *Arabidopsis thaliana***  
Sophie Hendrix, Verena Iven, Thomas Eekhout, Michiel Huybrechts, Ingeborg Pecqueur, Nele Horemans, Els Keunen, Lieven De Veylder, Jaco Vangronsveld and Ann Cuypers
- 38 Superoxide Radical Metabolism in Sweet Pepper (*Capsicum annuum* L.) Fruits is Regulated by Ripening and by a NO-Enriched Environment**  
Salvador González-Gordo, Marta Rodríguez-Ruiz, José M. Palma and Francisco J. Corpas
- 52 Roles for Plant Mitochondrial Alternative Oxidase Under Normoxia, Hypoxia, and Reoxygenation Conditions**  
Jayamini Jayawardhane, Devin W. Cochrane, Poorva Vyas, Natalia V. Bykova, Greg C. Vanlerberghe and Abir U. Igamberdiev
- 66 Nitrated Nucleotides: New Players in Signaling Pathways of Reactive Nitrogen and Oxygen Species in Plants**  
Marek Petřivalský and Lenka Luhová
- 74 Effects of Antimony on Reactive Oxygen and Nitrogen Species (ROS and RNS) and Antioxidant Mechanisms in Tomato Plants**  
Francisco L. Espinosa-Vellarino, Inmaculada Garrido, Alfonso Ortega, Ilda Casimiro and Francisco Espinosa
- 91 Overexpression of ZePrx in *Nicotiana tabacum* Affects Lignin Biosynthesis Without Altering Redox Homeostasis**  
Alba García-Ulloa, Laura Sanjurjo, Sara Cimini, Antonio Encina, Romina Martínez-Rubio, Rebeca Bouza, Luis Barral, Graciela Estévez-Pérez, Esther Novo-Uzal, Laura De Gara and Federico Pomar
- 109 Identification of Sulfenylated Cysteines in *Arabidopsis thaliana* Proteins Using a Disulfide-Linked Peptide Reporter**  
Bo Wei, Patrick Willems, Jingjing Huang, Caiping Tian, Jing Yang, Joris Messens and Frank Van Breusegem
- 121 The Contribution of Plant Dioxxygenases to Hypoxia Signaling**  
Sergio Iacopino and Francesco Licausi



**129 *Novel Role of JAC1 in Influencing Photosynthesis, Stomatal Conductance, and Photooxidative Stress Signalling Pathway in Arabidopsis thaliana***

Weronika Czarnocka, Anna Rusaczek, Patrick Willems,  
Marzena Sujkowska-Rybikowska, Frank Van Breusegem and  
Stanisław Karpiński

**142 *Improving Air Quality by Nitric Oxide Consumption of Climate-Resilient Trees Suitable for Urban Greening***

Jiangli Zhang, Andrea Ghirardo, Antonella Gori, Andreas Albert, Franz Buegger,  
Rocco Pace, Elisabeth Georgii, Rüdiger Grote, Jörg-Peter Schnitzler,  
Jörg Durner and Christian Lindermayr





# Editorial: Highlights of POG 2019 - Plant Oxygen Group Conference

Christian Lindermayr<sup>1\*</sup>, Krystyna Oracz<sup>2</sup>, Ann Cuypers<sup>3</sup>, Jörg-Peter Schnitzler<sup>4</sup> and Jörg Durner<sup>1,5</sup>

<sup>1</sup> Institute of Biochemical Plant Pathology, Helmholtz Center Munich, Neuherberg, Germany, <sup>2</sup> Department of Plant Physiology, Institute of Biology, Warsaw University of Life Sciences, Warsaw, Poland, <sup>3</sup> Center for Environmental Sciences, Hasselt University, Diepenbeek, Belgium, <sup>4</sup> Research Unit Environmental Simulation, Institute of Biochemical Plant Pathology, Helmholtz Center Munich, Neuherberg, Germany, <sup>5</sup> Chair of Biochemical Plant Pathology, Technische Universität München, Freising, Germany

**Keywords:** reactive oxygen species, reactive nitrogen species, redox-signaling, S-sulfenylation, S-nitrosation, nitration

## Editorial on the Research Topic

### Highlights of POG 2019 - Plant Oxygen Group Conference

Redox reactions are evolutionarily conserved signaling principles, occurring in prokaryotes and eukaryotes. The most important redox molecules are reactive oxygen and nitrogen species (ROS and RNS). Due to their short half-life, high diffusion capability and ability to react with different components in the cell, ROS, and RNS are key signaling molecules participating in various signaling pathways involved in the regulation of transpiration, gas exchange, biotic/abiotic stress response, cell death, germination, and plant growth and development (Del Río, 2015; Mhamdi and Van Breusegem, 2018; Waszczak et al., 2018; Sánchez-Vicente et al., 2019; Smirnov and Arnaud, 2019; Sharma et al., 2020). In detail, they modify proteins and cellular metabolites and in this way alter their activity, function, stability, and/or intracellular localization (Mata-Pérez et al., 2017; Mittler, 2017; Czarnocka and Karpinski, 2018; Umbreen et al., 2018; Gupta et al., 2020). This Research Topic introduces active research in this rapidly moving field, including functional analysis of these redox-active molecules as well as technical developments in redox research.

## REDOX-SIGNALING MECHANISMS

Modification of biomolecules, such as proteins, lipids, or nucleic acids, by ROS and RNS represents one of the key mechanisms mediating the biological activity of these redox molecules. Petrivalský and Luhová discuss in their mini-review article the current knowledge on formation, metabolism and biological function of nitrated nucleotides focusing mainly on 8-nitroguanosine 3',5'-cyclic monophosphate (8-nitro-cGMP). 8-nitro-cGMP is formed by the reaction of peroxynitrite with free guanine nucleotide and possess the strongest redox-active and electrophilic properties among studied nitrated guanine derivatives. The signaling function of 8-nitro-cGMP is based on one side on its similarity to cGMP and on the other side on its electrophilic features and the chemical interaction with protein thiol groups resulting in the formation of a novel post-translational modification of cysteine residues termed S-guanylation. In plants, until now a physiological function of 8-nitro-cGMP has only been described in *Arabidopsis thaliana* stomatal guard cells, thus, it still requires intensive investigation to unravel mechanisms and biochemical and physiological functions of 8-nitro-cGMP and protein S-guanylation.

S-Sulfenylation is an oxidative modification of cysteine residues that can alter protein interaction, trafficking, conformation, and enzymatic activity. Wei et al. present an advanced non-invasive method for identifying sulfenylated cysteine residues. The method is based on

## OPEN ACCESS

### Edited by:

Michael James Considine,  
University of Western  
Australia, Australia

### Reviewed by:

Romy Schmidt,  
Bielefeld University, Germany  
Daniel James Gibbs,  
University of Birmingham,  
United Kingdom

### \*Correspondence:

Christian Lindermayr  
lindermayr@helmholtz-muenchen.de

### Specialty section:

This article was submitted to  
Plant Physiology,  
a section of the journal  
Frontiers in Plant Science

**Received:** 08 December 2020

**Accepted:** 11 January 2021

**Published:** 01 February 2021

### Citation:

Lindermayr C, Oracz K, Cuypers A,  
Schnitzler J-P and Durner J (2021)  
Editorial: Highlights of POG 2019 -  
Plant Oxygen Group Conference.  
Front. Plant Sci. 12:639262.  
doi: 10.3389/fpls.2021.639262



the redox-sensitive cysteine residue Cys598 of the yeast AP-1-like transcription factor, which specifically reacts with sulfenic acids resulting in the formation of a mixed disulfide bond. After tryptic digestion, the mixed disulfide-linked peptides can be enriched using an antibody against the Cys598-containing peptide. The presented novel labeling approach enables the identification of sulfenylated cysteines in any species that can be genetically modified and allows a deeper insight into the signaling function of S-sulfenylation.

## REDOX-REGULATION OF PLANT GROWTH AND DEVELOPMENT

Redox-dependent control of plant growth and development involves a network of interactions between redox-active molecules, antioxidants, and phytohormones. ROS are essential regulators of fruit ripening. Gonzalez-Gordo et al. focused on the superoxide metabolism during the non-climacteric sweet pepper ripening and revealed that superoxide generating NADPH oxidases accumulated during ripening. This superoxide generating system is modulated in a NO-enriched environment. Interestingly, the activity of different superoxide dismutase isoenzymes was unaffected during ripening suggesting that the basal superoxide dismutase activity is sufficient to keep the homeostasis of the necessary physiological superoxide production during sweet pepper ripening. Besides the importance for the ripening process, the superoxide production could also have additional benefits for the fruits as barrier preventing potential pathogen infections.

Class III plant peroxidases are involved in the oxidative polymerization of lignin. Comprehensive understanding of the lignification process has significant impact on industrial biofuel production, wood quality, and biodegradable plastic production. García-Ulloa et al. overexpressed *Zinnia elegans* basic peroxidase (ZePrx) in *Nicotiana tabacum* to further characterize its function in lignin biosynthesis and its interconnection with the antioxidative system *in planta*. According to the presented results, ZePrx functions in secondary cell wall biosynthesis by increasing sinapyl lignin in cell wall stems. Furthermore, increased ascorbate peroxidase activity and a reduced ascorbate redox state was observed confirming a role of ZePrx in maintaining the redox homeostasis.

## REDOX CONTROL OF PLANT STRESS RESPONSE

Plants are subjected to various abiotic and biotic stresses throughout their life cycle. Redox species play important functions in enabling stress tolerance. To optimize photosynthetic and acclimatory processes, regulation of light absorption under variable light conditions is essential. Czarnocka et al. identified new functions of the J domain-containing protein required for chloroplast accumulation response 1 (JAC1). So far, this protein was described in context of chloroplast movement. However, the presented results

demonstrate pleiotropic functions related to regulation of photosynthetic reactions, redox homeostasis, and cell death.

In plants, dioxygenases perform a variety of functions ranging from hormone biosynthesis to epigenetic rearrangements of chromatin. In their review, Iacopino and Licausi summarize the state of knowledge on the most important signaling functions of dioxygenases in plants. The focus of their article is on the importance of dioxygenases in adaptive processes under oxygen-deficient conditions, such as flooding. Due to their need for co-substrates and co-factors, such as oxygen, 2-oxoglutarate and iron ( $\text{Fe}^{2+}$ ), the authors propose a potential role of dioxygenases as metal sensors in plants.

Alternative oxidase (AOX) is a terminal oxidase in the plant's mitochondrial electron transport chain, which is not contributing to ATP synthesis. Jayawardhane et al. investigated the roles of AOX under different oxygen conditions using AOX overexpressing and knockdown *N. tabacum* plants. Interestingly, they observed the accumulation of NO under hypoxia and hypothesized that AOX is able to generate NO under hypoxia or that AOX activity reduces the amount of the NO scavenger superoxide. Overall, they demonstrated that AOX fulfills beneficial functions in low oxygen metabolism.

Cadmium (Cd) exposure causes an oxidative challenge and inhibits cell cycle progression. Such stress-induced effects on the cell cycle are often a consequence of activation of the DNA damage response (DDR). Hendrix et al. reported the involvement of Suppressor of Gamma Response 1 (SOG1) in the Cd-induced DDR in Arabidopsis leaves. Additionally, they described a new function for SOG1 in regulating the oxidative stress response in Cd-exposed plants. Hendrix et al. proposed that SOG1 might function as a general integrator of stress responses in plants.

Plants growing in mining areas can accumulate high levels of antimony (Sb) in their edible parts, causing potential health risks for herbivores and also for humans. In this respect, understanding the mechanisms involved in the uptake, toxicity, and detoxification of Sb is of great importance. Espinosa-Vellarino et al. analyzed the effects of Sb toxicity on plant growth, ROS/RNS, and the antioxidant systems in tomatoes. They show that Sb accumulation in roots impairs micro-elements uptake, plant growth, and photosynthetic performance. In response to Sb uptake, an increased production of reactive oxygen and nitrogen compounds occurs. Moreover, they demonstrate that this is accompanied by a strong expression of enzymes of the antioxidative system and causes tissue-specific changes in the levels and redox status of antioxidants. All this seems to be related to the ability of Sb to form complexes with thiol groups, which changes the redox homeostasis of plants.

## IMPACT OF REDOX-ACTIVE ATMOSPHERIC GASES ON PLANTS

Industrial processes, residential heating, and heavy traffic based on fossil fuels result in high levels of particles, nitrogen oxides ( $\text{NO}_x$ ), and other dangerous volatile organic compounds (VOCs) in urban and suburban areas. Since especially long-term exposure to such harmful particles/gases can negatively affect human

health, it is desirable to lower their concentration in cities. Zhang et al. determined the NO and NO<sub>2</sub> specific deposition velocities based on projected leaf area using a branch enclosure system and NO uptake in <sup>15</sup>NO fumigation experiments. They studied tree species that are regarded as suitable to be planted under predicted future urban climate conditions. Their results demonstrate that selection of appropriate tree species able to cope with increased heat and drought stress while keeping a high capacity to “clean” air may thus support urban planning strategies.

Plants are masters in adapting quickly and efficiently to changing environmental conditions. The expected increase in atmospheric CO<sub>2</sub> content will have a strong impact on plants, especially those that perform C3 photosynthesis. To develop sustainable management practices for agricultural crop protection, it is therefore crucial to understand how increased CO<sub>2</sub> levels affect plant-environment interactions, especially biotic stress caused by herbivores or microbial/fungal pathogens. In their work, Martinez Henao et al. applied a multifactorial design to analyze the effects of different N-fertilization (nitrate and ammonium) at ambient or elevated CO<sub>2</sub> concentrations on the response of *A. thaliana* plants to artificial injury, simulating an attack by herbivores or a necrotrophic pathogen. They show that artificial wounding leads to an increased oxidative status and to the accumulation of jasmonate phytohormones. The plant response to wounding, which depends on the type of fertilizer, is however, alleviated in plants grown under an increased CO<sub>2</sub> content. With this work the authors show that a deeper understanding of the mechanisms underlying plant defense is crucial for the development of strategies under future predicted climatic conditions.

## REFERENCES

- Czarnocka, W., and Karpinski, S. (2018). Friend or foe? Reactive oxygen species production, scavenging and signaling in plant response to environmental stresses. *Free Radic. Biol. Med.* 122, 4–20. doi: 10.1016/j.freeradbiomed.2018.01.011
- Del Río, L. A. (2015). ROS and RNS in plant physiology: an overview. *J. Exp. Bot.* 66, 2827–2837. doi: 10.1093/jxb/erv099
- Gupta, K. J., Kolbert, Z., Durner, J., Lindermayr, C., Corpas, F. J., Brouquisse, R., et al. (2020). Regulating the regulator: nitric oxide control of post-translational modifications. *New Phytol.* 227, 1319–1325. doi: 10.1111/nph.16622
- Mata-Pérez, C., Sánchez-Calvo, B., Padilla, M. N., Begara-Morales, J. C., Valderrama, R., Corpas, F. J., et al. (2017). Nitro-fatty acids in plant signaling: new key mediators of nitric oxide metabolism. *Redox Biol.* 11, 554–561. doi: 10.1016/j.redox.2017.01.002
- Mhamdi, A., and Van Breusegem, F. (2018). Reactive oxygen species in plant development. *Development* 145:dev164376. doi: 10.1242/dev.164376
- Mittler, R. (2017). ROS are good. *Trends Plant Sci.* 22, 11–19. doi: 10.1016/j.tplants.2016.08.002
- Sánchez-Vicente, I., Fernández-Espinosa, M. G., and Lorenzo, O. (2019). Nitric oxide molecular targets: reprogramming plant development upon stress. *J. Exp. Bot.* 70, 4441–4460. doi: 10.1093/jxb/erz339
- Sharma, A., Soares, C., Sousa, B., Martins, M., Kumar, V., Shahzad, B., et al. (2020). Nitric oxide-mediated regulation of oxidative stress in plants under metal stress: a review on molecular and biochemical aspects. *Physiol. Plant* 168, 318–344. doi: 10.1111/ppl.13004
- Smirnov, N., and Arnaud, D. (2019). Hydrogen peroxide metabolism and functions in plants. *New Phytol.* 221, 1197–1214. doi: 10.1111/nph.15488
- Umbreen, S., Lubega, J., Cui, B., Pan, Q., Jiang, J., and Loake, G. J. (2018). Specificity in nitric oxide signalling. *J. Exp. Bot.* 69, 3439–3448. doi: 10.1093/jxb/ery184
- Waszczak, C., Carmody, M., and Kangasjärvi, J. (2018). *Reactive oxygen species in plant signaling*. *Annu. Rev. Plant Biol.* 69, 209–236. doi: 10.1146/annurev-arplant-042817-040322

## CONCLUDING REMARKS

The collection of 11 research and review articles in this Research Topic reflects the broad spectrum of current research directions in the field of redox biology—from general plant cell metabolism, plant growth, and development, to abiotic and biotic stress effects and the identification of new antioxidant defense mechanisms. Plants produce ROS and RNS during growth/development and stress response. As the contributions to the RT “Highlights of POG 2019 - Plant Oxygen Group Conference” exemplarily shows, the redox-active molecules fulfill important signaling functions via various protein modifications, such as S-nitrosation, tyrosine nitration, or S-sulfonylation. Furthermore, nitrated nucleotides and functions of dioxygenases seem to be new players in ROS and RNS signaling. Depending on the stage of development or environmental stressors, different redox processes are induced in different cellular compartments, which proves the existence of a highly coordinated “redox network” in plants. Interestingly, atmospheric redox-active gases such as NO<sub>x</sub> can also disturb the cellular redox processes and influence plant growth/development and stress response. The work collected in this RT impressively demonstrates that research on reactive oxygen and nitrogen species remains central to a holistic understanding of the adaptation mechanisms of plants to their abiotic and living environment and their underlying regulatory networks.

## AUTHOR CONTRIBUTIONS

CL and J-PS wrote the initial draft of the Editorial. KO, AC, and JD made final comments. All authors contributed to the article and approved the submitted version.

**Conflict of Interest:** The authors declare that the research was conducted in the absence of any commercial or financial relationships that could be construed as a potential conflict of interest.

Copyright © 2021 Lindermayr, Oracz, Cuypers, Schnitzler and Durner. This is an open-access article distributed under the terms of the Creative Commons Attribution License (CC BY). The use, distribution or reproduction in other forums is permitted, provided the original author(s) and the copyright owner(s) are credited and that the original publication in this journal is cited, in accordance with accepted academic practice. No use, distribution or reproduction is permitted which does not comply with these terms.



# Fertilizer Rate-Associated Increase in Foliar Jasmonate Burst Observed in Wounded *Arabidopsis thaliana* Leaves is Attenuated at eCO<sub>2</sub>

Julian Martinez Henao<sup>1</sup>, Louis Erik Demers<sup>1</sup>, Katharina Grosser<sup>2</sup>, Andreas Schedl<sup>2</sup>, Nicole M. van Dam<sup>2</sup> and Jacqueline C. Bede<sup>1\*</sup>

<sup>1</sup> Department of Plant Science, McGill University, Ste-Anne-de-Bellevue, QC, Canada, <sup>2</sup> German Centre for Integrative Biodiversity Research (iDiv) Halle-Jena-Leipzig, Friedrich-Schiller-University Jena, Leipzig, Germany

## OPEN ACCESS

### Edited by:

Jörg-Peter Schnitzler,  
Helmholtz Center Munich, Germany

### Reviewed by:

Tong Zhang,  
Pacific Northwest National Laboratory  
(DOE), United States  
Amna Mhamdi,  
Ghent University, Belgium

### \*Correspondence:

Jacqueline C. Bede  
jacqueline.bede@mcgill.ca

### Specialty section:

This article was submitted to  
Plant Physiology,  
a section of the journal  
Frontiers in Plant Science

**Received:** 04 September 2019

**Accepted:** 20 November 2019

**Published:** 16 January 2020

### Citation:

Martinez Henao J, Demers LE,  
Grosser K, Schedl A, van Dam NM and  
Bede JC (2020) Fertilizer Rate-  
Associated Increase in Foliar  
Jasmonate Burst Observed in  
Wounded *Arabidopsis thaliana* Leaves  
is Attenuated at eCO<sub>2</sub>.  
Front. Plant Sci. 10:1636.  
doi: 10.3389/fpls.2019.01636

The predicted future increase in tropospheric carbon dioxide (CO<sub>2</sub>) levels will have major effects on C<sub>3</sub> plants and their interactions with other organisms in the biosphere. In response to attack by chewing arthropod herbivores or necrotrophic pathogens, many plants mount a rapid and intense increase in jasmonate-related phytohormones that results in a robust defense response; however, previous studies have shown that C<sub>3</sub> plants grown at elevated CO<sub>2</sub> may have lower induced jasmonate levels, particularly in well nitrate-fertilized plants. Given the relationship between atmospheric CO<sub>2</sub>, photorespiration, cellular reductant and redox status, nitrogen assimilation and phytohormones, we compared wound-induced responses of the C<sub>3</sub> plant *Arabidopsis thaliana*. These plants were fertilized at two different rates (1 or 10 mM) with nitrate or ammonium and grown at ambient or elevated CO<sub>2</sub>. In response to artificial wounding, an increase in cellular oxidative status leads to a strong increase in jasmonate phytohormones. At ambient CO<sub>2</sub>, increased oxidative state of nitrate-fertilized plants leads to a robust 7-iso-jasmonyl-L-isoleucine increase; however, the strong fertilizer rate-associated increase is alleviated in plants grown at elevated CO<sub>2</sub>. As well, the changes in ascorbate in response to wounding and wound-induced salicylic acid levels may also contribute to the suppression of the jasmonate burst. Understanding the mechanism underlying the attenuation of the jasmonate burst at elevated CO<sub>2</sub> has important implications for fertilization strategies under future predicted climatic conditions.

**Keywords:** ascorbate, carbon dioxide, glutathione, jasmonate, nitrogen fertilizer, oxidative stress, pyridine nucleotides, wounding

## INTRODUCTION

Climate change, in particular increasing tropospheric carbon dioxide (CO<sub>2</sub>) levels, will bring challenges to agriculture and forestry in terms of plant resistance to biotic stresses, such as pathogens and insect herbivores (Zavala et al., 2013; Zavala et al., 2017; Pincebourde et al., 2017; Kazan, 2018). To date, research on plant responses to biotic stresses under elevated CO<sub>2</sub> have been



somewhat contradictory which reflects our lack of understanding of these complex interactions and the integration of factors involved in the regulation of plant defenses. Yet, for global food production and security, it is imperative to understand how plant defense responses will change. This will allow us to make appropriate decisions in these rapidly changing environmental conditions.

In the last 50 years, atmospheric CO<sub>2</sub> levels have increased more than 20% from 322 to >410 ppm (<https://www.esrl.noaa.gov/gmd/ccgg/trends/>). These levels are predicted to reach between 600 to 1,000 ppm by the end of this century (Cox et al., 2000; Intergovernmental Panel on Climate Change, 2013; [www.ipcc-data.org/observ/ddc\\_co2.html](http://www.ipcc-data.org/observ/ddc_co2.html)). On the face of it, one might imagine an increase in plant productivity, particularly of C<sub>3</sub> plants. In C<sub>3</sub> plants, increased atmospheric CO<sub>2</sub> levels will result in more efficient photosynthesis by reducing flux through the C2 photorespiration pathway (Long et al., 2004; Ehlers et al., 2015). However, this has not always shown to be the case, emphasizing that plant productivity reflects complex interactions between carbon and nitrogen metabolism that also are linked to cellular redox status and stress signaling (Foyer et al., 2006; Long et al., 2006; Foyer et al., 2009; Foyer and Noctor, 2011; Foyer et al., 2011; Noctor et al., 2012; Noctor and Mhamdi, 2017).

Ribulose 1,5-bisphosphate carboxylase/oxygenase (Rubisco), one of the most abundant foliar enzymes, plays a key role in photosynthesis by fixing CO<sub>2</sub> to the 5C substrate, ribulose 1,5-bisphosphate in the Calvin-Benson-Bassham (CBB) cycle (**Figure 1**) (Carmo-Silva et al., 2015). However, if oxygen is fixed instead of CO<sub>2</sub>, then the resultant 2C phosphoglycolate must be salvaged through the C2 photorespiration pathway. Traditionally, the photorespiration pathway was viewed as wasteful as it requires ATP and NAD(P)H to regenerate a metabolically useful triose-phosphate and removes metabolic intermediates from the CBB cycle, thereby limiting the rate of this cycle and net photosynthesis by at least 25% (Ehlers et al., 2015). However, this view is rapidly changing as the importance of this pathway in integrating physiological process such as photosynthesis, nitrogen assimilation through redox balance and signaling is now recognized (Betti et al., 2016; Eisenhut et al., 2019).

As atmospheric CO<sub>2</sub> levels increase, Rubisco will be more efficient at fixing CO<sub>2</sub> over O<sub>2</sub> and flux through the

photorespiration pathway will be reduced. Therefore, in many C<sub>3</sub> plant species, exposure to elevated CO<sub>2</sub> (eCO<sub>2</sub>) levels results initially in an enhanced photosynthetic efficiency which often returns to basal levels over time, a process known as acclimation (Stitt and Krapp, 1999; Rogers and Humphries, 2000; Ainsworth and Rogers, 2007). A hallmark of photosynthetic acclimation is a decrease in plant nitrogen concentration, often resulting from a downregulation of Rubisco levels and activity, that act to lower the photosynthetic rate (Long et al., 2004). A number of factors contribute to this eCO<sub>2</sub>-associated adjustment of foliar nitrogen levels, including carbohydrate-mediated repression of genes that encode photosynthetic proteins as well as inhibition of nitrate assimilation (Leakey et al., 2009; Kant et al., 2012; Bloom, 2015a).

Nitrate assimilation is reported to be negatively impacted by eCO<sub>2</sub> in many plant species, particularly C<sub>3</sub> plants that assimilate nitrate in their leaves (Bloom, 2015a; Bloom, 2015b). The conversion of nitrate to organic nitrogen is energy intensive and begins with the NAD(P)H-dependent reduction of nitrate by nitrate reductase to produce the highly reactive, toxic nitrite that is rapidly transported into the plastid (Xu et al., 2012; Krapp, 2015; Huma et al., 2018). In photosynthetic tissue, nitrite reductase reduces nitrite to ammonium ion using reduced ferredoxin (Fd<sup>-</sup>), generated through the light-dependent reactions, as the electron donor. Therefore, when comparing the energy requirements of different fertilizer nitrogen sources, the use of nitrate fertilization costs an additional 8 e<sup>-</sup>/mole nitrogen compared to the direct use of ammonium fertilizer (Williams et al., 1987; Noctor and Foyer, 1998; Bloom, 2015b).

At eCO<sub>2</sub>, nitrate assimilation is impaired in the monocot wheat and the dicot *Arabidopsis thaliana* when plants were grown in growth chambers or wheat in the field under eCO<sub>2</sub> conditions (Bloom et al., 2010; Bloom et al., 2014). Under eCO<sub>2</sub> or elevated O<sub>2</sub>, both conditions that reduce photorespiration, a reduction in shoot nitrate assimilation was observed (Rachmilevitch et al., 2004; Bloom et al., 2010; Bloom 2015a), indicating a strong linkage between photorespiration and nitrate metabolism. Malate export from the chloroplast to the cytosol, that is linked to the photorespiration pathway, provides an important NADH source for nitrate reductase, therefore, under eCO<sub>2</sub> with the suppression of photorespiration, a decrease in cytosolic reducing power could negatively affect nitrate reduction (Scheibe, 2004; Scheibe et al., 2005; Bloom, 2015b). However, even in the night, eCO<sub>2</sub> inhibits nitrate, but not ammonium, assimilation (Rubio Asensio et al., 2015); therefore, other mechanisms, in addition to a link to photorespiration, must also be involved. At night, eCO<sub>2</sub> may negatively affect mitochondrial pathways to decrease energy supply. In both the day or night times, eCO<sub>2</sub> may also inhibit translocation of nitrite into the chloroplast (Bloom et al., 2002), though this seems unlikely given its toxicity. During the day, reduction of nitrite to ammonium in the chloroplast requires electrons from reduced Fd<sup>-</sup>. Therefore, there will be competition for reduced Fd between the Fd-dependent NADPH reductase (FNR), nitrite reductase and glutamine-oxoglutarate aminotransferase with FNR having the highest affinity for reduced Fd<sup>-</sup>. Therefore, at eCO<sub>2</sub>, as

**Abbreviations:** ABA, abscisic acid; aCO<sub>2</sub>, ambient carbon dioxide (450 ppm); ANOVA, analysis of variance; Asc, reduced form of ascorbate; C, carbon; CBB, Calvin-Benson-Bassham; CO<sub>2</sub>, carbon dioxide; DHA, dehydroascorbate, oxidized form of ascorbate; DW, dry weight; eCO<sub>2</sub>, elevated carbon dioxide (900 ppm); Fd, ferredoxin; FNR, ferredoxin-dependent NADPH reductase; FW, frozen weight; GSH, reduced glutathione; GSSG, oxidized glutathione; ICS1, isochorismate synthase1; NAD, oxidized form of nicotinamide adenine nucleotide; NADH, reduced form of nicotinamide adenine nucleotide; NADP, oxidized form of nicotinamide adenine nucleotide phosphate; NADPH, reduced form of nicotinamide adenine nucleotide phosphate; NH<sub>4</sub><sup>+</sup>, ammonium ion; NO<sub>3</sub><sup>-</sup>, nitrate; JA, jasmonic acid; JA-Ile, 7-jasmonyl-L-isoleucine; MANOVA, multivariate analysis of variance; N, nitrogen; NPR1, nonexpressor of pathogenesis-related protein1; OPDA, 12-oxo-phytyldienoic acid; ROS, reactive oxygen species; SA, salicylic acid.

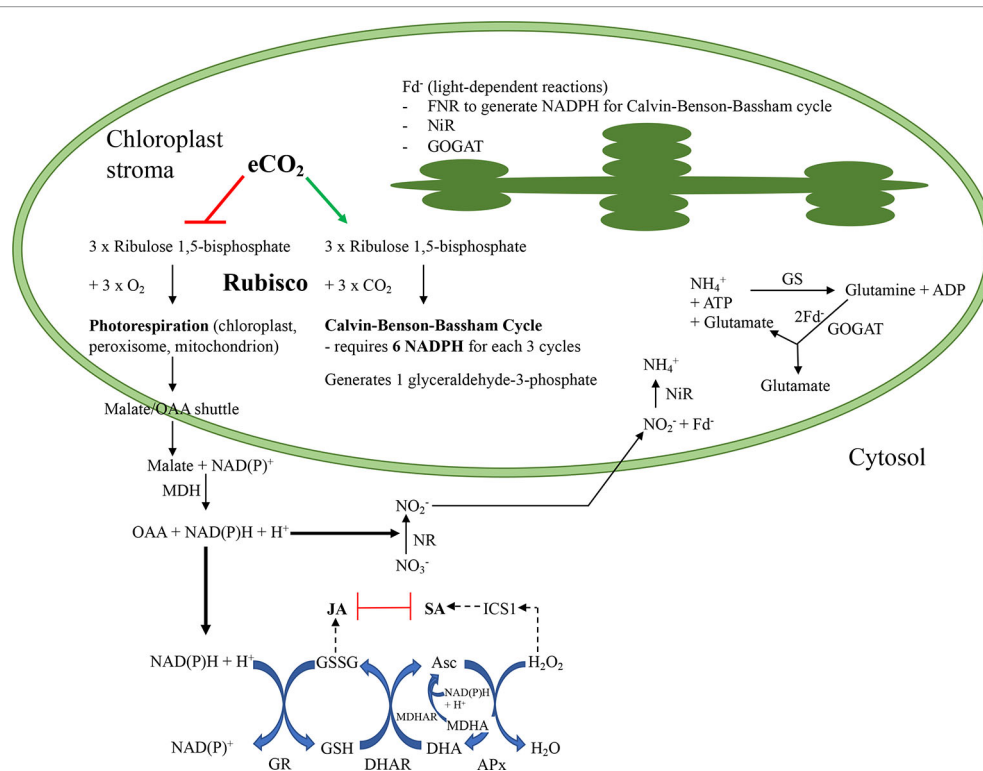


**FIGURE 1 |** Summary of putative interactions as atmospheric carbon dioxide levels increase in a C3 plant that assimilates nitrate in their leaves. At present atmospheric conditions, the enzyme ribulose 1,5-bisphosphate carboxylase/oxygenase (Rubisco) catalyzes both the carboxylation of ribulose 1,5-bisphosphate, utilizing ATP and NADPH + H<sup>+</sup> to generate triose-phosphates through the Calvin-Benson-Bassham (CBB) cycle that can be used in sucrose biosynthesis, or the oxygenation, to produce compounds that must be “salvaged” through photorespiration (PR). In the PR pathway, reductant equivalents are shuttled from the chloroplast through the malate/oxaloacetic acid (OAA) transporter to the cytosol and then peroxisome. A portion of these reductant equivalents remain in the cytosol where they are used for metabolic processes, such as to maintain redox homeostasis through the glutathione-ascorbate Foyer-Halliwel-Asada cycle or nitrate reduction. After nitrate is reduced, nitrite is transported into the chloroplast where it is reduced by nitrite reductase (NiR) and reduced ferredoxin (Fd<sup>-</sup>) to ammonium ion. Ammonium ion, either produced from nitrate assimilation or received via the phloem, is further converted to glutamine and then glutamate; this later conversion, catalyzed by glutamine-oxoglutarate aminotransferase (GOGAT) also requires Fd<sup>-</sup>. Thus, Fd<sup>-</sup> produced through the thylakoid-associated light-dependent reactions is necessary for nitrogen assimilation and also to generate NADPH required for the CBB cycle via the Fd<sup>-</sup>-dependent NADP<sup>+</sup> reductase (FNR). Under predicted future environmental conditions, elevated atmospheric carbon dioxide (eCO<sub>2</sub>) will favour the Rubisco carboxylation over oxygenation reaction, increasing the demand for NADPH, generated by FNR, in the CBB cycle. Cytosolic reductant levels may decrease as photorespiration decreases and this may affect cellular redox balance (Foyer-Halliwel-Asada cycle) that links to defence phytohormone levels as well as nitrate assimilation. The phytohormones jasmonic acid (JA) and salicylic acid (SA) have reciprocal negative effects on each other which allows the plant to fine tune its defense responses to the environment. Asc, reduced form of ascorbate; CBB, Calvin-Benson-Bassham cycle; DHA, dehydroascorbate, oxidized form of ascorbate; eCO<sub>2</sub>, elevated carbon dioxide; Fd<sup>-</sup>, reduced ferredoxin; FNR, ferredoxin-dependent NADPH reductase; GS, glutamine synthetase; GSH, reduced glutathione; GOGAT, glutamine-oxoglutarate aminotransferase; GR, glutathione reductase; GSSG, oxidized glutathione; H<sub>2</sub>O, water; H<sub>2</sub>O<sub>2</sub>, hydrogen peroxide; ICS1, isochlorismate synthase1; JA, jasmonic acid; MDH, malate dehydrogenase; MDHA, monodehydroascorbate; MDHAR, monodehydroascorbate reductase; NADP, oxidized form of nicotinamide adenine nucleotide phosphate; NADPH, reduced form of nicotinamide adenine nucleotide phosphate; NH<sub>4</sub><sup>+</sup>, ammonium ion; NiR, nitrite reductase; NO<sub>2</sub><sup>-</sup>, nitrite; NO<sub>3</sub><sup>-</sup>, nitrate; NR, nitrate reductase; OAA, oxaloacetic acid; PR, photorespiration; Rubisco, ribulose 1,5-bisphosphate carboxylase/oxygenase; SA, salicylic acid.

photosynthetic efficiency increases, stromal NADPH will be synthesized and used in the CBB cycle, at the expense of other pathways, such as nitrogen assimilation (Baysdorfer and Robinson, 1985; Huma et al., 2018). Though this is contentious and other studies have observed that atmospheric CO<sub>2</sub> levels did not affect nitrogen assimilation in *Phaseolus vulgaris* or wheat (Andrews et al., 2019). Photorespiration and nitrate assimilation also increase the rate of plant CO<sub>2</sub> uptake (Busch et al., 2018); CO<sub>2</sub> uptake declined when nitrate-fertilized plants were grown under conditions that limited photorespiration.

eCO<sub>2</sub> also affects the foliar pyridine nucleotide (NAD<sup>+</sup>/NADH, NADP<sup>+</sup>/NADPH) and redox (ascorbate, glutathione) pools that link important plant physiological pathways, such as seed germination, stomatal regulation, vegetative-to-reproductive transition and stress and defense responses (Figure 1) (Noctor et al., 2012; Considine and Foyer 2014; Noctor and Mhamdi, 2017; Igamberdiev and Bykova, 2018). Therefore, perturbation of the cellular pyridine nucleotide and redox status in plants grown at eCO<sub>2</sub> may affect the plant's ability to respond to biotic stresses, such as pathogens or insect

herbivores. The Foyer–Halliwell–Asada cycle is an interconnected series of reduction and oxidation (redox) reactions of glutathione and ascorbate that uses NAD(P)H as the final reductant (Foyer and Noctor, 2011; Noctor et al., 2012). This node integrates and translates plant metabolic status and environmental cues to changes in the cellular oxidative status to allow the plant to respond appropriately to the everchanging environment (Potters et al., 2010; Noctor et al., 2011). Dynamic changes cellular reductant (total and ratio oxidized/reduced pyridine nucleotides) and redox balance (total and oxidized/reduced ascorbate and glutathione pools) act to signal downstream molecular and biochemical responses. The photorespiration pathway provides input into the cellular redox balance by the generation of the reactive species hydrogen peroxide (H<sub>2</sub>O<sub>2</sub>) from the peroxisome and through the export of malate from chloroplasts into the cytosol to generate NADH (Scheibe, 2004; Scheibe and Dietz, 2012). The eCO<sub>2</sub>-associated reduction in photorespiration will lead to lower peroxisomal H<sub>2</sub>O<sub>2</sub> production that should translate into a more highly reduced cellular environment (Foyer et al., 2009; Bloom 2015a; Bloom, 2015b). However, in *Arabidopsis* grown at eCO<sub>2</sub>, there was activation of signaling pathways that reflected a more oxidative state (Mhamdi et al., 2013; Mhamdi and Noctor, 2016). This likely reflects a reduction in the malate shuttle and, hence, a decrease in cytosolic NAD(P)H as photorespiration decreases in plants grown at eCO<sub>2</sub> (Selinski and Scheibe, 2019). It also must be recognized that glutathione may also be linked to oxidative signaling independently of ascorbate (the Foyer–Halliwell–Asada cycle) through glutaredoxin–periredoxin or glutathione/thioredoxin peroxidase pathways (Noctor et al., 2012).

Developmental and environmental cues are integrated and reflected in the cellular redox balance that then signals the appropriate response through the actions of phytohormones (Noctor et al., 2011; Han et al., 2013a). Though phytohormones generally lead to specific types of downstream action, for example salicylic acid (SA) is involved in plant defense against biotrophic pathogens and 7-jasmonyl-isoleucine (JA-Ile) is involved in plant defense against chewing insect herbivores, these hormones often modify each other's actions through signaling nodes; a phenomenon referred to as “phytohormone cross-talk” (Koornneef and Pieterse, 2008; Caarls et al., 2015). Thus, SA and jasmonates often act antagonistically to modify the final response allowing the plant to integrate multiple developmental and environmental cues to respond appropriately (Caarls et al., 2015). Strong evidence is emerging for critical links between redox metabolites, in particular glutathione, and phytohormone signaling (Mhamdi et al., 2013; Han et al., 2013a; Han et al., 2013b).

Damage to leaves by mechanical wounding or chewing insect herbivores, such as caterpillars and beetles, activates signaling pathways that cause a rapid and vigorous increase in octadecanoid-derived phytohormones, collectively called jasmonates, that lead to induction of downstream defense responses (Arimura et al., 2011; Wasternack and Hause, 2013; Howe et al., 2018). The cellular state of oxidized glutathione (GSSG and GSSG/total glutathione) is highly correlated with

expression of jasmonate-dependent genes, such as *AtLOX3*, *AtMYB95*, *AtJAZ10*, and *AtVSP2* (Mhamdi et al., 2010; Gfeller et al., 2011; Han et al., 2013a); therefore, oxidative stress in response to damage may link to jasmonate levels and dependent gene expression. Glutathione regulates both the nonexpressor of pathogenesis-related protein1 (NPR1)-dependent and -independent SA signaling pathways (Han et al., 2013b; Kovacs et al., 2015). In recognition of biotrophic pathogens, a feedforward escalation between a SA and H<sub>2</sub>O<sub>2</sub> loop leads to changes in the cellular redox status to activate NPR1, which is regulated by through reduction of disulfide bridges regulated by H-type thioredoxins to lead to SA-dependent gene expression (Spoel et al., 2003; Koornneef et al., 2008; Tada et al., 2008). As well, an oxidative glutathione redox status is implicated in moderating the SA x jasmonate crosstalk but through an NPR1-independent, isochorismate synthase1 (ICS1)-dependent mechanism that is still not completely understood (Mhamdi et al., 2010; Han et al., 2013a; Han et al., 2013b).

In general, plants grown under eCO<sub>2</sub> have a higher cellular oxidative state resulting in increased foliar SA accumulation (Casteel et al., 2012a; Casteel et al., 2012b; Zavala et al., 2013; Mhamdi et al., 2013; Mhamdi and Noctor 2016; Gog et al., 2019). In *Arabidopsis*, eCO<sub>2</sub> did not affect redox ratios but total glutathione and NADPH pools were increased. This eCO<sub>2</sub>-associated increase in SA often translates into enhanced protection against biotrophic pathogens (Mhamdi and Noctor, 2016; Noctor and Mhamdi, 2017; Williams et al., 2018). However, this is not always the case, resistance to *Pseudomonas syringae* pv. *tomato* infection was compromised in *Arabidopsis* grown at eCO<sub>2</sub> (Zhou et al., 2019), pointing to the involvement of additional factors such as day length and nitrogen fertilization. In comparison, jasmonate levels are often suppressed in plants grown at eCO<sub>2</sub> leading to a higher susceptibility to chewing insect herbivores (Casteel et al., 2008; Zavala et al., 2013; Gog et al., 2019). Again, jasmonate levels at eCO<sub>2</sub> appear to be variable across different experiments, pointing to differences in plant species or involvement of other environmental factors, particularly light photoperiod and/or intensity (Matros et al., 2006; Casteel et al., 2012a; Casteel et al., 2012b; Zavala et al., 2013; Mhamdi and Noctor, 2016; Gog et al., 2019). Paudel et al. (2016) found that the foliar jasmonate burst that leads to induced resistance against chewing insect herbivores is attenuated in wounded plants grown at eCO<sub>2</sub> under high nitrate fertilization. Therefore, nitrogen may play a role in the plant's response to wounding stress at eCO<sub>2</sub>.

Given the relationship between eCO<sub>2</sub>, photorespiration, nitrate assimilation and cellular redox status and phytohormones that mediate plant defense responses, we conducted this study to compare responses to foliar wounding in *Arabidopsis* that were fertilized at two different rates (1 or 10 mM) of nitrate or ammonium in plants grown at aCO<sub>2</sub> or eCO<sub>2</sub>. *A. thaliana* is a C<sub>3</sub> plant that assimilates a significant proportion of nitrate in the leaves, compared to the roots (Kalcsits and Guy, 2013). In plants grown at eCO<sub>2</sub>, if the resultant lower photorespiration alters reductant availability necessary for nitrogen assimilation, then this should be reflected in pyridine nucleotide ratios and levels



(**Figure 1**). Lower pyridine nucleotide levels and/or changed oxidized-to-reduced ratios will affect cellular redox metabolites levels and ratios that may then be reflected in phytohormone levels. Therefore, through this research, we seek to further understand the mechanism underlying the suppression of the jasmonate burst in response to wounding of foliar tissues in well nitrate-fertilized *Arabidopsis* plants grown at eCO<sub>2</sub> (Paudel et al., 2016).

## MATERIALS AND METHODS

### Plants

*A. thaliana* Col-0 (TAIR CS3749) seeds, that were surface-sterilized in 3% (v/v) NaOCl for 10 min, followed by a rinse in 70% EtOH for 1 min and several washes in sterile ddH<sub>2</sub>O, were placed in Petri dishes containing Murashige and Skoog nutrient solution, 1% agar (Boyes et al., 2001). After cold treatment at 4°C for 72 h in the dark to break seed dormancy, plates were maintained at 20 ± 1°C, 60–70% relative humidity in continuous light (light intensity 250 μE m<sup>-2</sup> s<sup>-1</sup>, 23°C).

### Experimental Design

Plants with two true leaves were transferred into individual square pots (6.6 × 6.6 × 9 cm<sup>3</sup>) containing Farfard Agromix PV20 potting medium and randomly placed in the growth cabinet (12 h light at 22°C with light intensity ramped to 250 μE m<sup>-2</sup> s<sup>-1</sup> over 3 h; 12 h dark at 18°C ramped over 3 h) with controlled CO<sub>2</sub> concentrations, either 450 ± 50 or 900 ± 50 ppm. Plants were fertilized three times a week with half strength modified Hoagland's solution (macronutrients: 0.5 mM KH<sub>2</sub>PO<sub>4</sub>, 0.5 mM CaCl<sub>2</sub>, 0.25 mM MgSO<sub>4</sub>, 0.05 mM Na<sub>2</sub>EDTA<sup>III</sup>; micronutrients: 46 μM H<sub>3</sub>BO<sub>3</sub>, 9 μM MnSO<sub>4</sub>, 0.32 μM CuSO<sub>4</sub>·5H<sub>2</sub>O, 0.76 μM Zn SO<sub>4</sub>·H<sub>2</sub>O, 0.16 μM Na<sub>2</sub>MoO<sub>4</sub>·2H<sub>2</sub>O, 0.002 μM CoCl<sub>2</sub>·6H<sub>2</sub>O) with either KNO<sub>3</sub> (1 or 10 mM) or (NH<sub>4</sub>)<sub>2</sub>SO<sub>4</sub> (1 or 10 mM) as the nitrogen source. Nitrogen treatment was randomized. Ammonium is toxic to many plant species when present in excess (Li et al., 2014). *Arabidopsis* is negatively affected by 5-mM ammonium when grown hydroponically (Podgórska et al., 2015). At the time of our experiment, we did not visually observe a difference between plants fertilized with nitrate or ammonium that likely reflects that our plants were grown in potting media.

When plants were 4 weeks old (stage 3.9; Boyes et al., 2001), a subset of plants were frozen in liquid nitrogen (N<sub>2</sub>) to measure foliar carbon (C) and nitrogen (N) levels. Half of the remaining plants were wounded on the largest six rosette leaves with a hole punch, carefully ensuring that the midvein was not damaged, at 5 pm (1.5 h before end of the day). A plexiglass panel was used to separate wounded and unwounded plants to minimize any volatile signaling between plants (Lan et al., 2014). For the measurement of pyridine nucleotides and redox metabolites, whole rosettes were immediately frozen in N<sub>2</sub> over a time course (15, 30, and 45 min). Rosettes for phytohormone analyses were taken 24 h after mechanical damage and immediately flash-frozen in N<sub>2</sub> and stored at -80°C until

analysis. The experiment was temporally repeated at least four times with one biological replicate being sampled at each independent replication (total n = 4).

### Nutrient Controls

Plants were fertilized with different nitrogen sources, either nitrate (NO<sub>3</sub><sup>-</sup>) or ammonium (NH<sub>4</sub><sup>+</sup>), that represent an anion or cation. Therefore, controls must be conducted to ensure that the differences in the counterion (K<sup>+</sup> for nitrate and SO<sub>4</sub><sup>-</sup> for ammonium ion) do not influence experimental results (Vatter et al., 2015). Therefore, controls of the addition of 9.2 or 9 mM K<sub>2</sub>SO<sub>4</sub> to either 1 mM of nitrate or ammonium fertilizer were used. Osmolality and osmotic pressure were calculated according to Trejo-Téllez and Gómez-Merino (2012) (**Supplemental Table 1**).

### Carbon and Nitrogen Quantification

*Arabidopsis* foliar carbon and nitrogen levels were measured by a CN elemental analyzer (Vario EL cube analyzer, Elementar Analysensysteme). Lyophilized samples were ground using a sonicator (Qiagen TissueLyser II). Then after transport to Germany, re-dried in an oven at 70°C for 2 h. Samples were weighed into tin boats (4 × 4 × 11 mm<sup>3</sup>, Elementar Analysensysteme) using an analytical microbalance (Cubis MSA, Sartorius AG). The tin boats were closed tightly over the samples and sealed to minimize air infiltration. The final pellet was reweighed and stored in a dessicator until measurement. Elemental carbon and nitrogen were quantified following manufacturer's protocol.

### Pyridine Nucleotide Quantification

Pyridine nucleotide (NAD<sup>+</sup>, NADH, NADP<sup>+</sup>, NADPH) levels were measured based on an enzymatic cycling method, with alcohol dehydrogenase to determine the NAD<sup>+</sup> pool and glucose 6-phosphate dehydrogenase (G6PDH) to determine the NADH<sup>+</sup> pool, which is visualized through the reduction of dichlorophenolindophenol by phenazine methosulfate (Quevel and Noctor, 2007; Noctor et al., 2016). Carefully weighed frozen leaf material (approximately 100 mg) was finely ground in liquid nitrogen. An acid extraction (cold 0.2 M HCl) was used to prepare samples for NAD<sup>+</sup> or NADP<sup>+</sup> analysis whereas tissue was extracted in cold 0.2 M NaOH for NADH or NADPH analysis. To remove cellular debris, samples were centrifuged at 16,000 g for 10 min, 4°C and the supernatant transferred to a sterile tube. Samples (0.2 ml) were boiled for 1 min and then placed immediately on ice. Phosphate buffer (0.2 M, pH 5.6, 35 μl) was added and the samples were neutralized by carefully and the samples were neutralized by carefully adding small volumes of 0.2 N NaOH to the acidic extracts (NAD<sup>+</sup> or NADP<sup>+</sup>) extracts with vortexing until pH 6–7 was reached whereas for the basic extracts (NADH or NADPH), small volumes of 0.2 N HCl were carefully added with vortexing until a neutral pH was reached. The added volume was noted and taken into account in the final calculations. To determine NAD<sup>+</sup> and NADH levels, 20 μl of the neutralized acidic (NAD<sup>+</sup>) or neutralized basic (NADH) extract was added to a reaction mixture with a final concentration of 50 mM HEPES buffer containing 1 mM EDTA, pH 7.5, 12 μM

2,6-dichlorophenolindophenol, 1 mM phenazine methosulfate and 125 U alcohol dehydrogenase in triplicate in a 96-well plate. After addition of ethanol (final concentration 7.4%), the change in absorbance at 600 nm was measured at 30-s intervals for 5 min using a Tecan Infinite M200 spectrophotometer. For NADP<sup>+</sup> and NADPH<sup>+</sup>, the same general reaction mixture was used except that the substrate is 0.5 mM glucose-6-phosphate, instead of ethanol, and the enzyme is 0.01 U G6PDH, instead of alcohol dehydrogenase. The linear reaction rate is used to calculate the concentration by comparison to a standard curve of the respective pyridine nucleotide (ranging from 0 to 0.2 μM) performed in triplicate.

## Redox Metabolite Quantification

Redox metabolite (Asc, DHA, GSH, GSSG) levels were measured based on an enzymatic cycling method (Quevel and Noctor, 2007; Noctor et al., 2016). Carefully weighed frozen leaf material (approximately 100 mg) was finely ground in liquid nitrogen and extracted in cold 0.2 M HCl. To remove cellular debris, samples were centrifuged at 16,000 g for 10 min, 4°C. Phosphate buffer (0.2 M, pH 5.6, 0.5 ml) was added and the extracts brought to pH 4–5 by carefully adding small volumes of 0.2 N NaOH with vortexing. The added volume was noted and taken into account in the final calculations.

To determine the total glutathione pool, in triplicate in a 96-well plate, 10 μl of the neutralized extract was added to a reaction mixture where the final concentration was 0.1 M phosphate buffer containing 5 mM EDTA, pH 7.5, 0.5 mM NADPH and 0.6 mM 5,5 dithiobis 2-nitro-benzoic acid, pH 7.5. After shaking, the reaction was initiated by the addition of glutathione reductase (final concentration 0.01 U). The reaction was monitored at 412 nm for 2 min at 5 s intervals and the slope of the line from the first 90 s was used to determine total glutathione concentration, using a standard curve of free GSH (ranging from 0 to 250 pmol). To measure GSSG, the neutralized plant extracts as well as a concentration range of GSSG standards (0–100 pmol) were incubated with 2-vinylpyridine, which forms an insoluble precipitate with GSH. After centrifugation at 16,000 g for 10 min, room temperature, GSSG concentration was determined by the assay as described above. Reduced GSH was calculated by subtracting 2 × GSSG from the total GSH.

To determine reduced ascorbate (Asc) levels, in triplicate in a 96-well plate, 40 μl of the neutralized extract was added to a reaction mixture of 0.1 M phosphate buffer, pH 5.6 (final concentration). After shaking, the absorbance was read at 265 nm. The reaction initiated by the addition of 0.2 U of ascorbate oxidase, prepared in 0.2 M phosphate buffer, and incubated with gentle shaking for 8 min at room temperature. Again, the absorbance was read at 265 nm and the difference used to calculate Asc levels based on an Asc standard curve (ranging from 40 to 240 μM) that was included on each plate. In parallel, 100 μl of extract was added to a reaction mixture with a final concentration of 0.1 M phosphate buffer, pH 5.6 and 1.25 mM dithiothreitol, that reduces dehydroascorbate to Asc. After incubation for 30 min at room temperature, total ascorbate levels were measured.

## Phytohormone Quantification

Phytohormone analysis of *Arabidopsis* rosette tissues was conducted by ultrahigh performance liquid chromatography-triple quadrupole mass spectrometry (UHPLC-EVOQ-TQ-MS, Bruker). Homogenized, lyophilized foliar samples (approximately 20 mg) were extracted in ethyl acetate (MS-grade, VWR) containing a mixture of isotopically-labeled standards of the acidic phytohormones (D6-JA and D6-JA-Ile (HPC Standards) and D4-SA and D6-ABA (OlChemIm. s.r.o.)). After vortexing for 10 min, cellular debris was removed by centrifugation at 18,994 g for 10 min, 4°C. The supernatant was transferred to a new tube and the solvent evaporated using a vacuum concentrator at room temperature. The pellet was resuspended in 70% methanol (v/v) and sonicated to fully solubilize the pellet and again centrifuged for 5 min at 18,994 g, 4°C.

Samples were separated by reverse phase UHPLC on a Zorbax Extend-C<sub>18</sub> column (4.6 × 50 mm, 1.8 μm, Agilent). For the first 30 s, the mobile phase was stationary at 5% ACN, 0.05% formic acid, then this was increased to 50% ACN, 0.05% formic acid over 2 min. The mobile phase was kept at 100% ACN, 0.05% formic acid for 1 min and then return to the initial conditions over the next minute. All solvents used were liquid chromatography–mass spectrometry grade. The column temperature was 42°C.

After separation, compounds were nebulized by electron spray ionization in the negative mode using the following conditions: capillary voltage 4,500, cone 35 arbitrary units (a.u.)/350°C, probe 60 a.u./475°C, nebulizer gas (N<sub>2</sub>) 60 a.u. Phytohormones were identified based on retention time and monitoring the transition m/z (**Supplemental Table 2**). Phytohormone level was calculated based on the peak area of the corresponding internal standard and initial weight.

## Statistics

Foliar carbon, nitrogen and their ratio were analyzed by three-factor analysis-of-variance (ANOVA) (factors: CO<sub>2</sub>, nitrogen source, nitrogen level) using the statistical software SPSS (ver. 16). Reducing power and redox metabolite levels were compared at 15, 30, and 45 min after mechanical wounding by four-factor ANOVA (factors: CO<sub>2</sub>, nitrogen source, nitrogen level, treatment). Changes in response to mechanical damage often reflected the time after wounding. Effects of CO<sub>2</sub>, nitrogen source and nitrogen level were only considered significant if consistent across the time points. OPDA and JA are intermediates to biologically active form of JA-Ile (Wasternack and Hause, 2013; Howe et al., 2018). Given this relationship, the effect of CO<sub>2</sub>, nitrogen source, nitrogen level, and wounding on phytohormone levels was analyzed by four factor-multiple ANOVA (MANOVA). SA and ABA levels were analyzed by four-factor ANOVA. In all analyses, outliers were identified by the maximal normed residual test (Grubb's test) (Stefanski, 1971).

In all analyses, normalization was performed if data did not follow a normal distribution and violated Levene's test of homogeneity. The square root of OPDA and JA phytohormone data were used. The log<sub>10</sub> of ratios, JA-Ile and ABA data were analyzed. Statistical differences ( $p \leq 0.05$ ) were determined by Tukey HST *post-hoc* tests.

## RESULTS

### Counterion and Sodicity Controls

To ensure that observed effects were due to the nitrogen source and not the counterion complement of the nitrogen [*i.e.* KNO<sub>3</sub> vs (NH<sub>4</sub>)<sub>2</sub>SO<sub>4</sub>] or changes in sodicity, controls to account for the potassium or sulfate imbalances were included. At either aCO<sub>2</sub> or eCO<sub>2</sub>, a difference in foliar carbon (C), nitrogen (N), C:N, phytohormone, reducing agents (NAD, NADP, NADH, NADPH, and their log ratios) or redox metabolites (oxidized and reduced glutathione and ascorbate and their log ratios) was not observed (**Supplemental Table 3**).

### Foliar Carbon and Nitrogen Levels

Foliar carbon levels were significantly affected by the nitrogen source but not by nitrogen levels [Source  $F_{(1,24)} = 13.612$ ;  $p = 0.002$ ; Levels  $F_{(1,24)} < 0.001$ ;  $p = 0.986$ ]; carbon levels were elevated by 6% in ammonium-fertilized plants (**Figure 2A**). As expected, nitrogen fertilization level, but not type, affected foliar nitrogen, with an increase of leaf nitrogen in well-fertilized plants [Source  $F_{(1,24)} = 0.936$ ;  $p = 0.347$ ; Levels  $F_{(1,24)} =$ ;  $p = 0.004$ ] (**Figure 2B**). This is reflected in the foliar log C:N ratio, where well fertilized plants had a lower C:N ratio [Levels  $F_{(1,24)} = 10.099$ ;  $p = 0.006$ ] (**Figure 2C**).

Experiments were conducted in controlled climate chambers. Under these conditions, the soil may be exposed to microbes that could influence the fertilization form; for example, *Nitrosomas* and *Nitrobacter* bacteria involved in ammonia conversion to nitrate (Burger and Jackson, 2003). Even though, this is a possibility, nitrate- and ammonium ion-specific responses suggest that microbial conversion of the added fertilizer was minimal.

### Foliar Reducing Power and Redox Metabolites Reflect Nitrogen Source

Foliar NADH levels varied with the nitrogen fertilizer used; NADH levels in ammonium-fertilized plants were over 20% higher than in nitrate-fertilized plants (**Figure 3A**). NAD(P)H supplies the reductant for the Foyer-Halliwell-Asada cycle (Foyer and Noctor, 2011). As foliar levels of reductant, such as NADH, increases, one would predict this to be reflected in GSH and Asc levels. Similar to NADH, GSH levels are higher in ammonium-fertilized plants compared to nitrate-fertilized plants (**Figure 3B**). GSSG and total glutathione levels are also higher in ammonium-fertilized plants (**Figures 3C, D**); thus, the ratio of GSH/GSSG was not affected by nitrogen treatment (**Figure 3E**). In comparison, total ascorbate levels are higher in nitrate-fertilized plants compared to those fertilized with ammonium (**Figure 3F**).

### Foliar Reducing Power and Redox Metabolite Dynamics in Wounded Leaves

Wounding resulted in a rapid decrease in *Arabidopsis* foliar levels of reduced Asc and concomitant increase in oxidized DHA, that both return to basal levels 30 min after damage (15 min, **Figures 4A, B**); this translates into a wound-associated increase in the DHA/Asc ratio (**Figure 4C**). The foliar NADP/

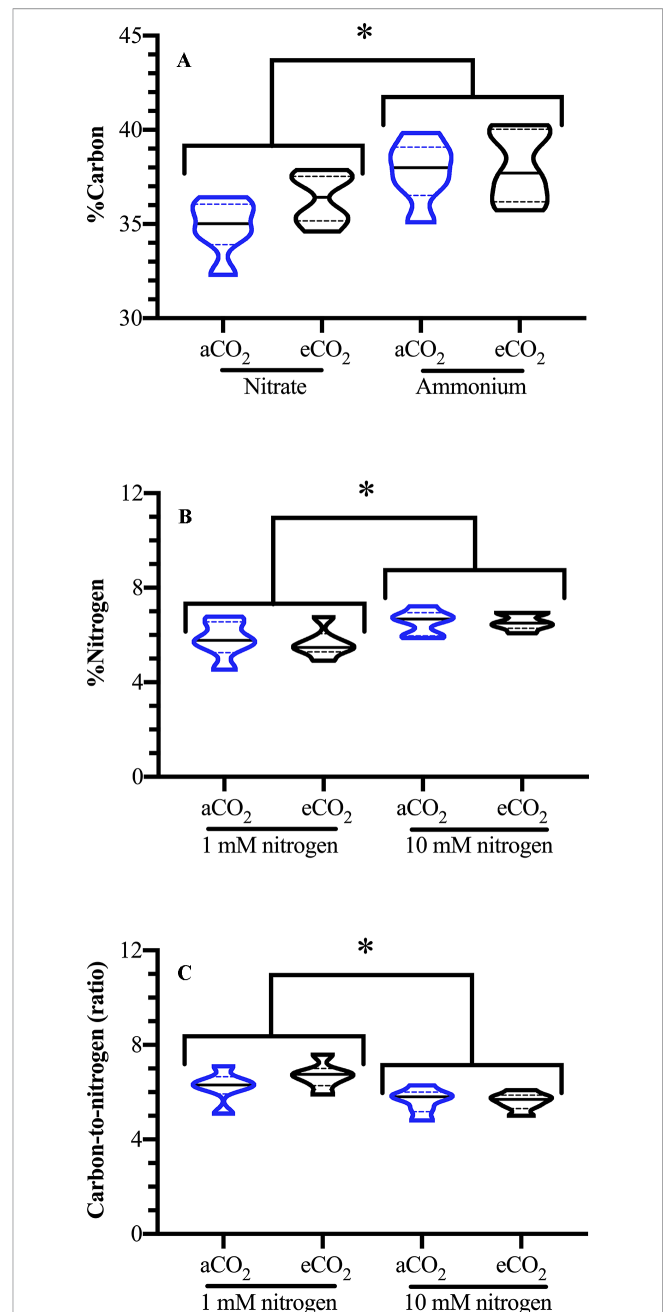


**FIGURE 2 |** Effect of atmospheric carbon dioxide and nitrogen fertilization on *Arabidopsis* foliar carbon and nitrogen levels. *Arabidopsis thaliana* plants were grown either at ambient (aCO<sub>2</sub>, 450 ppm) or elevated (eCO<sub>2</sub>, 900 ppm) carbon dioxide and fertilized with either nitrate or ammonium ion (1 or 10 mM). Foliar **(A)** carbon (%C), **(B)** nitrogen (%N), and **(C)** ratio carbon to nitrogen (C:N); blue denotes plants grown at aCO<sub>2</sub> and black denotes plants grown at eCO<sub>2</sub>. The experiment was repeated four times and outliers removed by the maximal normed residual test ( $n = 3-4$ ). C:N ratio data was normalized by log<sub>10</sub> transformation. Statistical differences were determined by three-factor ANOVA (treatments: nitrogen source, nitrogen level, CO<sub>2</sub>;  $p \leq 0.05$ ) followed by Tukey honestly significant difference *post hoc* test. Only significant effects are graphically represented. Data is represented by violin plots with the median indicated by a solid line and the interquartile by dashed lines. Significant differences are indicated by asterisks; \* represents  $p \leq 0.02$ .



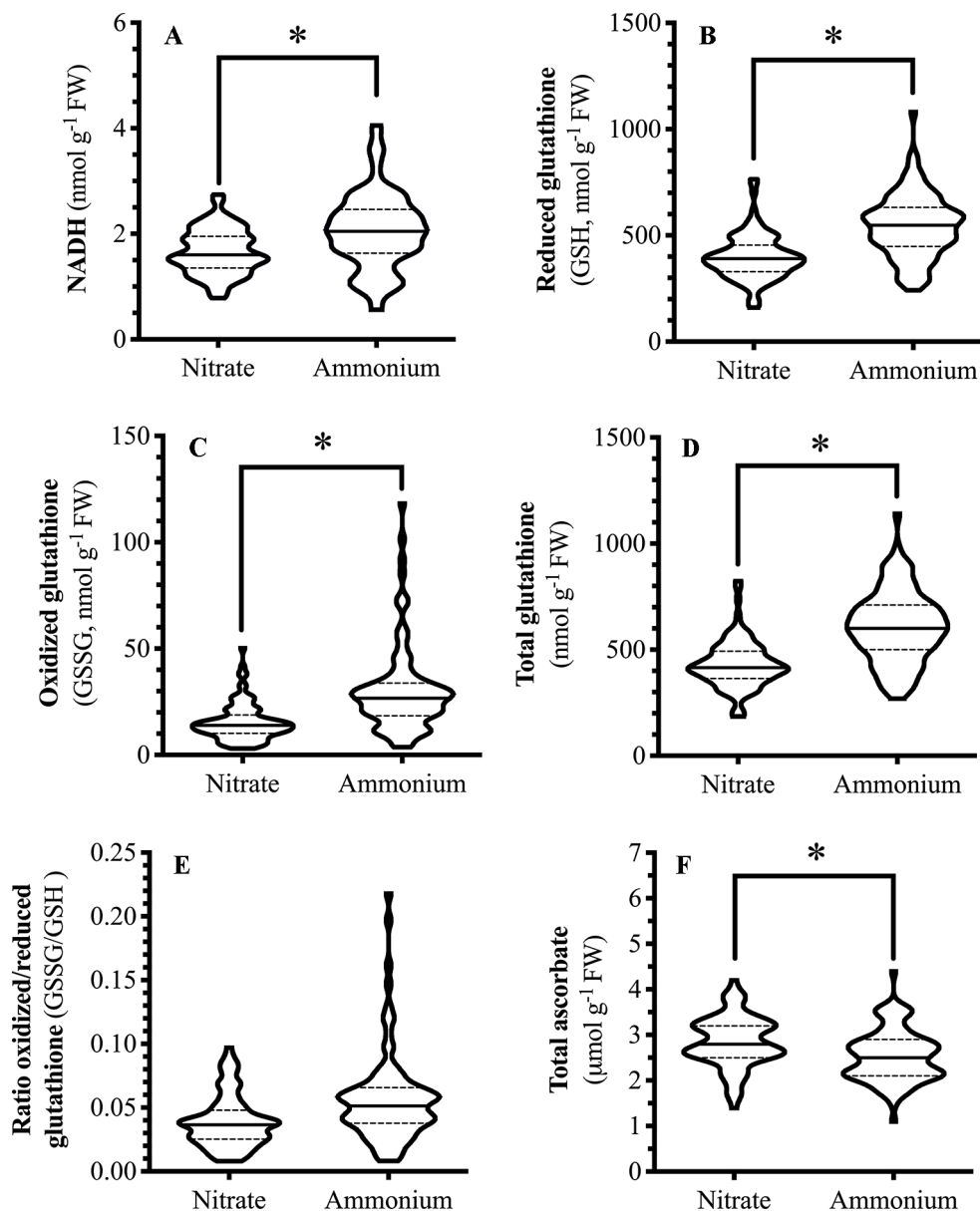


**FIGURE 3 |** Effect of nitrogen source on *Arabidopsis* foliar pyridine nucleotides and redox metabolite levels. *Arabidopsis thaliana* plants were grown either at ambient (aCO<sub>2</sub>, 450 ppm) or elevated (eCO<sub>2</sub>, 900 ppm) carbon dioxide and fertilized with either nitrate or ammonium ion (1 or 10 mM). Rosette tissue of a subset of plants was mechanically damaged. Metabolite (A) NADH (B) GSH (C) GSSG (D) total glutathione (E) ratio GSSG/GSH (F) total ascorbate levels. The experiment was repeated four times and outliers removed by the maximal normed residual test ( $n = 3-4$ ). GSSG/GSH ratio data was normalized by log<sub>10</sub> transformation. Statistical differences were determined by four-factor ANOVA (treatments: nitrogen source, nitrogen level, CO<sub>2</sub>, mechanical damage;  $p \leq 0.05$ ) followed by Tukey honestly significant difference *post hoc* test. Only significant effects are graphically represented and effects were only considered significant if consistent across the time points (15, 30, 45 min.). Data is represented by violin plots with the median indicated by a solid line and the interquartile by dashed lines. Significant differences are indicated by asterisks; \*represents  $p \leq 0.05$ . FW, frozen weight; GSH, reduced glutathione; GSSG, oxidized glutathione; NADH, reduced form of nicotinamide adenine nucleotide.

NADPH ratio rapidly decreased within 30 min after being damaged (Figure 4D). As well, the GSSG/GSH ratio increased in plants 30 min after wounding (Figure 4E). At 45 min after damage, the GSSG/GSH ratio returned to basal levels but foliar GSSG levels remained high (Figure 4F). Together, these metabolic changes reflect a cellular oxidative environment in response to wounding stress.

A wound-dependent connection between pyridine nucleotide and redox status and atmospheric CO<sub>2</sub> was observed. The decrease in foliar NADP levels 30 min after wounding was observed in plants grown at aCO<sub>2</sub>, but not in plants grown at eCO<sub>2</sub> (Figure 5A). As well, 45 min after wounding, foliar NAD levels increased in ammonium-fertilized plants that were grown at eCO<sub>2</sub> (Figure 5B). In plants grown at eCO<sub>2</sub>, total ascorbate

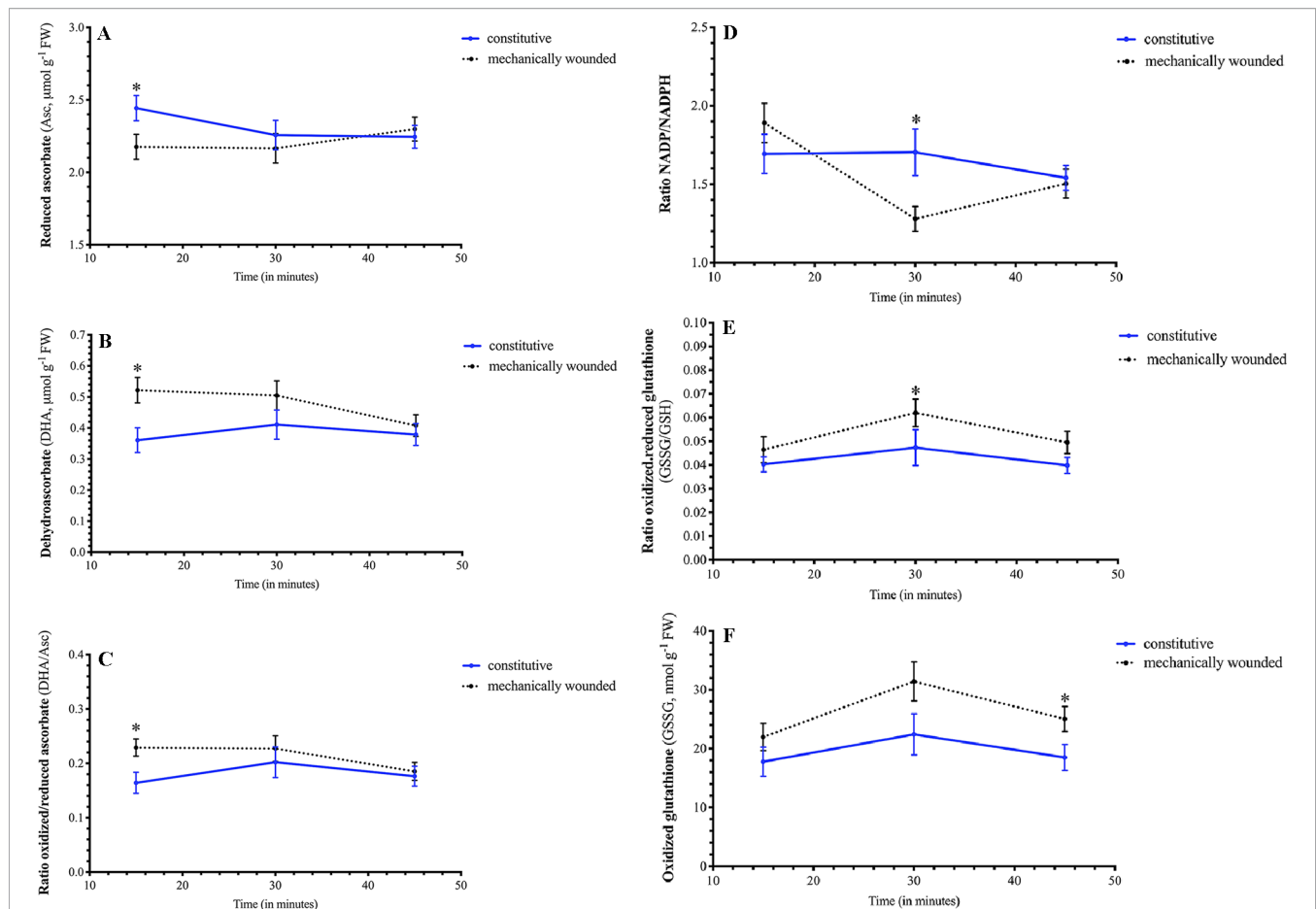


**FIGURE 4 |** Effect of wounding on *Arabidopsis* foliar pyridine nucleotide and redox metabolite levels. *Arabidopsis thaliana* plants were grown either at ambient (aCO<sub>2</sub>, 450 ppm) or elevated (eCO<sub>2</sub>, 900 ppm) carbon dioxide and fertilized with either nitrate or ammonium ion (1 or 10 mM). Rosette tissue of a subset of plants was mechanically damaged. Wounding effected foliar levels of **(A)** reduced Asc, **(B)** oxidized DHA, **(C)** DHA/Asc ratio, **(D)** NADP/NADPH ratio, **(E)** GSSG/GSH ratio, and **(F)** GSSG. Blue solid lines represent constitutive levels and black dashed lines represent levels in wounded plants. The experiment was repeated four times and outliers removed by the maximal normed residual test ( $n = 3-4$ ). DHA/Asc, NADP/NADPH and GSSG/GSH ratio data was normalized by log<sub>10</sub> transformation. Statistical differences were determined by 4-factor ANOVA (treatments: nitrogen source, nitrogen level, CO<sub>2</sub>, mechanical damage;  $p \leq 0.05$ ) at each time point followed by Tukey honestly significant difference *post hoc* test. Only significant effects are graphically represented and significant differences are indicated by an asterisk; \*represents  $p \leq 0.05$ . DHA, dehydroascorbate (oxidized form of ascorbate); FW, frozen weight; GSH, reduced glutathione; GSSG, oxidized glutathione; NADP, oxidized form of nicotinamide adenine nucleotide phosphate; NADPH, reduced form of nicotinamide adenine nucleotide phosphate.

leaf levels rapidly changed in plants within 45 min after wounding (**Figure 5C**). This primarily reflects changes in reduced Asc levels that increase in wounded plants grown at eCO<sub>2</sub> but remain stable in plants grown at aCO<sub>2</sub> (**Figure 5D**).

## Foliar Phytohormone Levels

### Jasmonates

Given that OPDA, JA and JA-Ile are biosynthetically related, a MANOVA was used to compare treatments on metabolite levels. In response to wounding, a robust increase in all three jasmonates is observed [square root OPDA  $F_{(1,58)} = 102.21$   $p < 0.001$ ; square root JA  $F_{(1,58)} = 52.52$   $p < 0.001$ ; log<sub>10</sub> JA-Ile  $F_{(1,58)} = 295.25$   $p < 0.001$ ] (**Figure 6A**).

Lower foliar JA levels are observed in plants grown at eCO<sub>2</sub> [square root JA  $F_{(1,58)} = 5.510$   $p = 0.023$ ]; this reflects a 25% reduction in JA levels compared to plants grown at aCO<sub>2</sub> (**Figure 6B**).

Wound-induced JA-Ile levels vary with nitrogen source; the JA-Ile burst is higher in nitrate-fertilized than ammonium-fertilized plants [ $\log_{10}$  JA-Ile  $F_{(1,58)} = 5.71$   $p = 0.021$ ]. Higher levels are observed in well-fertilized plants [ $\log_{10}$  JA-Ile  $F_{(1,58)} = 4.91$   $p = 0.032$ ]; however, this increase in JA-Ile levels seen in response to nitrogen fertilization in plants grown at aCO<sub>2</sub> is attenuated at eCO<sub>2</sub> [CO<sub>2</sub> × N level;  $\log_{10}$  JA-Ile  $F_{(1,58)} = 4.51$   $p = 0.040$ ]. At ambient CO<sub>2</sub>, JA-Ile levels were approximately double in well fertilized plants; this enhancement was not observed in plants grown at eCO<sub>2</sub>.

Together, these data suggest that at aCO<sub>2</sub>, higher nitrogen fertilization rates result in a stronger jasmonate burst in response to wounding of foliar tissue. Fertilizer effects the magnitude of the 7-jasmonyl-isoleucine burst, which is higher in nitrate-fertilized plants. This strong increase, regardless of the fertilizer source, ammonium or nitrate, is suppressed at eCO<sub>2</sub> (**Figures 6B, C**).

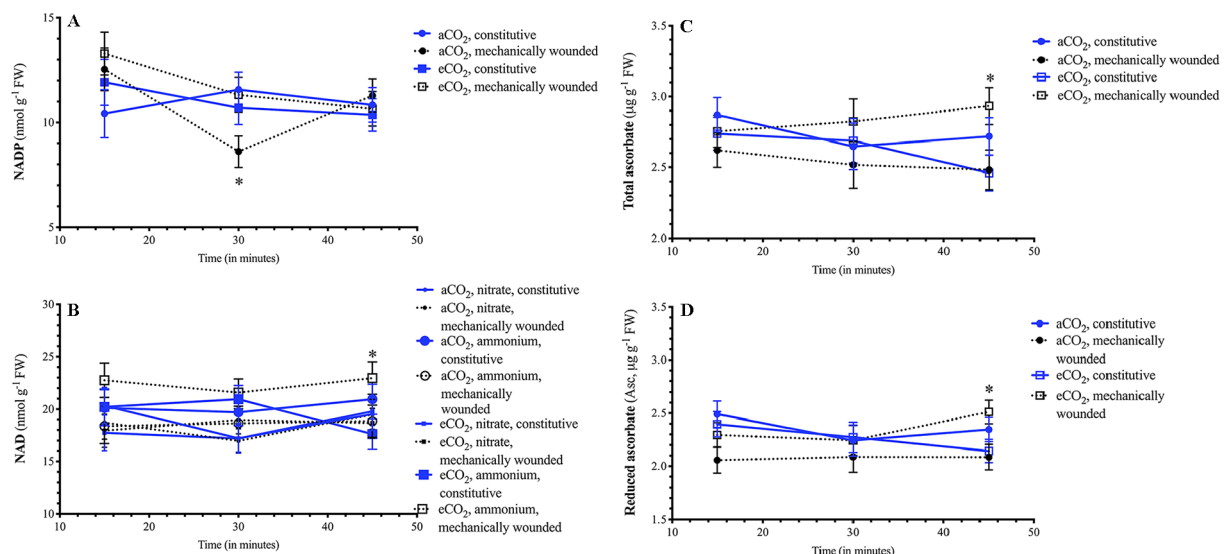


**FIGURE 5 |** Effect of wounding on *Arabidopsis* foliar pyridine nucleotide and redox metabolite levels in plants grown at different carbon dioxide levels. *Arabidopsis thaliana* plants were grown either at ambient (aCO<sub>2</sub>, 450 ppm) or elevated (eCO<sub>2</sub>, 900 ppm) carbon dioxide and fertilized with either nitrate or ammonium ion (1 or 10 mM). Rosette tissue of a subset of plants was mechanically damaged. Depending on the atmospheric CO<sub>2</sub> plants were grown in a differential effect of wounding was observed on (A) NADP, (B) NAD, (C) total ascorbate and (D) reduced Asc levels. Blue solid lines represent constitutive levels and black dashed lines represent levels in wounded plants. Circles (o) indicate plants that were grown at aCO<sub>2</sub> and squares (□) indicate plants that were grown at eCO<sub>2</sub>. For NAD, the size of the symbol indicates the nitrogen source (small = nitrate, large = ammonium). The experiment was repeated four times and outliers removed by the maximal normed residual test ( $n = 3-4$ ). Statistical differences were determined by 4-factor ANOVA (treatments: nitrogen source, nitrogen level, CO<sub>2</sub>, mechanical damage;  $p \leq 0.05$ ) at each time point followed by Tukey honestly significant difference *post hoc* test. Only significant effects are graphically represented and significant differences are indicated by an asterisk; \*represents  $p \leq 0.05$ . FW, frozen weight; NAD, oxidized form of nicotinamide adenine nucleotide; NADP, oxidized form of nicotinamide adenine nucleotide phosphate.

## Salicylic Acid

SA levels are 20% lower in plants grown under eCO<sub>2</sub> [ $F_{(1,63)} = 46.97$   $p < 0.001$ ] (Figure 6D). As seen previously (Ogawa et al., 2010), SA levels are induced in response to wounding [ $F_{(1,63)} = 10.73$   $p = 0.002$ ]. A CO<sub>2</sub> × nitrogen source interaction is observed ( $F_{(1,63)} = 17.425$   $p < 0.001$ ); the increased foliar SA levels in response to ammonium ion fertilization seen in *Arabidopsis* grown at aCO<sub>2</sub> is not observed at eCO<sub>2</sub>.

## Absciscic Acid

Foliar ABA levels are affected by nitrogen source and level and atmospheric CO<sub>2</sub> [ $\log_{10}$  nitrogen source  $F_{(1,63)} = 16.77$   $p < 0.001$ ; nitrogen level  $F_{(1,63)} = 6.26$   $p = 0.016$ ; CO<sub>2</sub>  $F_{(1,63)} = 5.52$   $p = 0.023$ ] (Figure 6E). A nitrogen source × nitrogen level interaction is observed where higher ABA levels are observed in response to ammonium fertilization and also enhanced fertilization rate [ $\log_{10}$   $F_{(1,63)} = 10.01$   $p = 0.003$ ]; this effect is not seen in response to nitrate fertilization. This observation is also particularly striking at aCO<sub>2</sub>; the increase in ABA that reflects nitrogen fertilization is seen at aCO<sub>2</sub> but not eCO<sub>2</sub> [ $\log_{10}$  CO<sub>2</sub> × N source  $F_{(1,63)} = 4.81$   $p = 0.033$ ].

## DISCUSSION

The increase in atmospheric CO<sub>2</sub> predicted to be reached by the end of the century will have dramatic effects on plant physiology and productivity, particularly of C3 plants. Increase carboxylase activity of Rubisco and decreased photorespiration should

enhance plant productivity. However, studies have also found that induced levels of defensive jasmonate phytohormones are suppressed in C3 plants grown at eCO<sub>2</sub> (Guo et al., 2012; Sun et al., 2013; Vaughan et al., 2014; Li et al., 2016; Paudel et al., 2016; Lu et al., 2018). Our study has found links between the source of nitrogen, nitrate or ammonium, and cellular reductant levels and redox metabolites. The more oxidized cellular environment of nitrate-fertilized plants translates into a wound-associated increase in the defense-related phytohormone 7-*iso*-jasmonyl-L-isoleucine. However, the fertilizer rate-associate enhancement of the jasmonate burst is damped in plants grown at eCO<sub>2</sub>. Under this condition, ascorbate and salicylic acid levels in wounded leaves possibly contribute to the suppression of the jasmonate burst.

## Arabidopsis Foliar Nitrogen Level and Carbon: Nitrogen Ratio Reflect Fertilization Rate

Foliar nitrogen content reflected the fertilizer rate but not the source; higher leaf nitrogen content (%N) and lower C:N ratio is observed in well fertilized plants (10 mM) (Figures 2B, C). Even though there are reports of decreased total N levels in plants grown at eCO<sub>2</sub> (Cotrufo et al., 2002; Sun et al., 2002; Yin, 2002; Teng et al., 2006; Bloom et al., 2010), we did not find this; instead fertilizer nitrogen concentration was the major driver effecting foliar percent nitrogen. However, this may reflect a difference in the nitrate concentration that was used in the experiments. In Bloom et al. (2010), nitrate assimilation was inhibited at eCO<sub>2</sub>



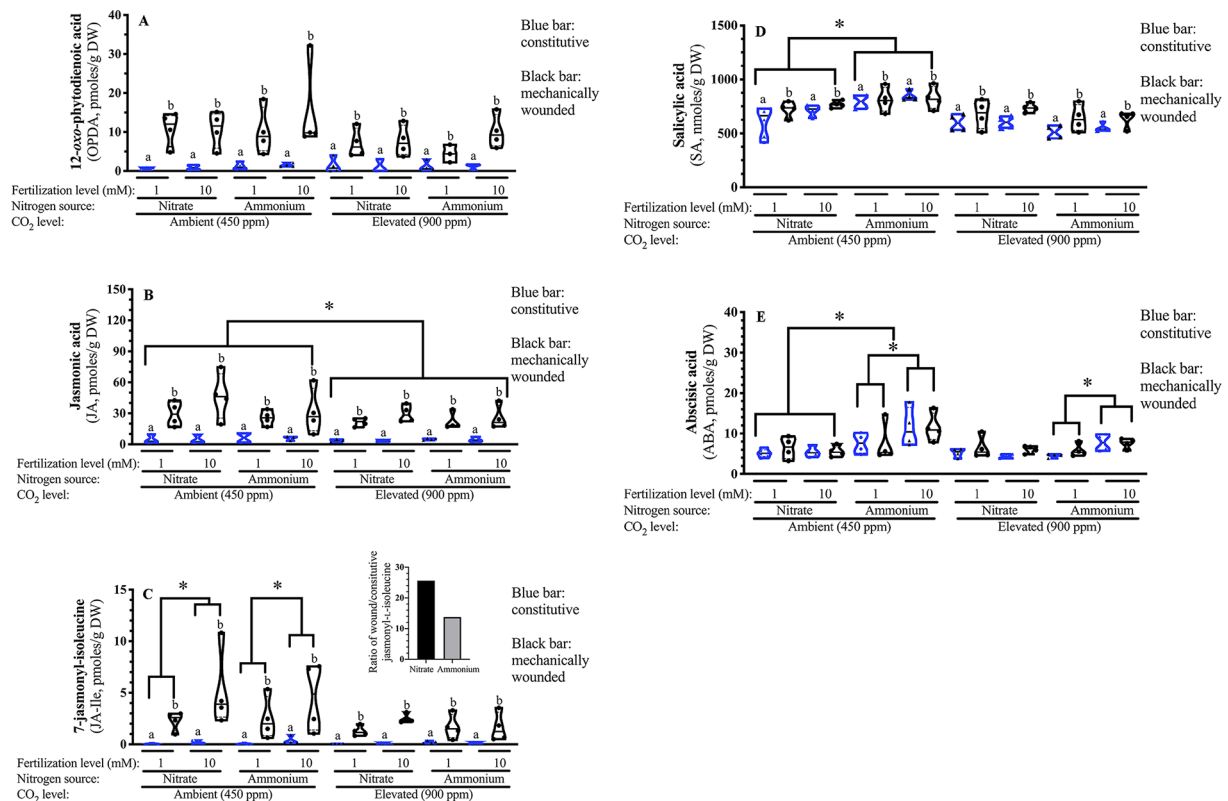


**FIGURE 6 |** Effect of atmospheric carbon dioxide, nitrogen fertilization and wounding on *Arabidopsis* foliar phytohormone levels. *Arabidopsis thaliana* were grown either at ambient (aCO<sub>2</sub>, 450 ppm) or elevated (eCO<sub>2</sub>, 900 ppm) carbon dioxide and fertilized with either nitrate or ammonium ion (1 or 10 mM). Rosette tissue of a subset of plants was mechanically damaged. Foliar (A) 12-oxo-phytodienoic acid (OPDA) (B) Jasmonic acid (JA) (C) 7-Jasmonyl-isoleucine (JA-Ile) (D) Salicylic acid (SA) (E) Abscisic acid (ABA). Constitutive phytohormone levels are indicated by clear blue boxes. Wound-induced phytohormone levels are indicated by black boxes. The experiment was repeated 4 times and outliers removed by the maximal normed residual test ( $n = 3-4$ ). Data was transformed as follows: OPDA and JA data were squared and the  $\log_{10}$  of JA-Ile and ABA data was used. Statistical differences in foliar OPDA, JA and JA-Ile levels were determined by four-factor MANOVA (treatments: nitrogen source, nitrogen level, CO<sub>2</sub>, mechanical damage;  $p \leq 0.05$ ) followed by Tukey honestly significant difference *post-hoc* test. Statistical differences in foliar SA and ABA levels were determined by four-factor ANOVA (treatments: nitrogen source, nitrogen level, CO<sub>2</sub>, mechanical damage;  $p \leq 0.05$ ) followed by Tukey honestly significant difference *post-hoc* test. Data is represented by violin plots with the median indicated by a solid line and the interquartile by dashed lines. Significant wound-related differences are indicated by alphabetical letters. Other significant differences are indicated by asterisks (\*). DW, dry weight.

when *Arabidopsis* plants were fertilized with relatively low nitrate rates (0.2–1 mM) compared to this study (1–10 mM). Other studies have also found that atmospheric CO<sub>2</sub> levels have a minimal effect on nitrogen assimilation (Andrews et al., 2019).

## Nitrogen Source Affects *Arabidopsis* Carbon and Nitrogen, Reductant and Redox Metabolite Levels

The leaves of nitrate-fertilized plants have lower NADH levels that may reflect the additional requirements of reductant for nitrate reduction and assimilation as compared to ammonium (Figure 3A); these results are in agreement with Podgórska et al. (2015), who observed a decrease in the NAD(P)<sup>+</sup>/NAD(P)H ratio in ammonium-fertilized *Arabidopsis* plants in comparison to nitrate. Compared to ammonium fertilize, the use of nitrate fertilizer by the plant is energetically expensive and requires an additional 8 e<sup>-</sup>/mole nitrogen for nitrate assimilation (Williams et al., 1987; Noctor and Foyer, 1998; Bloom, 2015b). In general,

nitrate-fertilized plants have lower CO<sub>2</sub> assimilation rates, that would translate into lower percent carbon, because of the competition with the CBB cycle for reductant (Scheibe, 2004; Scheibe et al., 2005; Bloom, 2015b). Thus, plants fertilized with nitrate had a lower foliar percent carbon compared to ammonium-fertilized plants (Figure 3A).

A number of studies have observed increased mitochondrial respiration and cellular oxidative state in ammonium-fertilized plants, which reflects higher levels of mitochondria-associated reactive oxygen species (Guo et al., 2005; Patterson et al., 2010; Podgórska et al., 2013; Podgórska et al., 2015; Hachiya and Sakakibara, 2017). In ammonium-fertilized plants, excess reducing equivalents must be oxidized by the mitochondria resulting in increased ROS produced by the electron transport chain; It should also be noted that even though under today's conditions, mitochondrial-generated ROS is significantly less than the ROS produced through photorespiration and photorespiration will be suppressed in C<sub>3</sub> plants grown under

eCO<sub>2</sub> (Foyer et al., 2011). We found that foliar GSSG, GSH and total glutathione levels are higher in plants fertilized with ammonium than nitrate, but there was no difference in the GSSG/GSH ratio (Figures 3B–E). Also, total ascorbate levels are lower in ammonium-fertilized plants (Figure 3F). Similar to our study, a number of other investigations have also found an increase in total glutathione levels in ammonium-fertilized *Arabidopsis* compared to nitrate-treated plants (Medici et al., 2004; Podgórska et al., 2015); though the ratio of GSSG/GSH was also higher in Medici et al. (2004) study which we did not observe but this study was focused on root tissues. Often, a negative correlation between glutathione and ascorbate exists and, though there is some variability in the literature, lower foliar ascorbate levels in ammonium-fertilized plants have also been reported by others (Kerchev et al., 2011; Podgórska et al., 2015). In fact, decreasing nitrate fertilization is used as a strategy to increase fruit and vegetable vitamin C (ascorbate) content (Stefanelli et al., 2010). Together, these data support the observation that the cellular redox state is more oxidized in nitrate-fertilized plants compared to ammonium (Figures 3A–F).

### Nitrogen Source Affects *Arabidopsis* Phytohormones in Plants Grown at aCO<sub>2</sub> (450 ppm)

SA, a key hormone involved in signaling defense pathway against biotrophic pathogens (Boatwright and Pajerowska-Mukhtar, 2013), is also recognized to play an antagonistic role against jasmonate signaling allowing the plant to respond appropriately to environmental stresses (Caarls et al., 2015). SA levels moderate jasmonate levels through phytohormone cross-talk patterns; often a reciprocal, negative correlation between these two hormones is observed (Caarls et al., 2015). Foliar NADH and SA levels were higher in ammonium-fertilized *Arabidopsis* (Figures 3A and 6D). A number of studies have found that increased foliar NADH levels are correlated with higher SA pools and enhance resistance to avirulent biotrophic pathogens as well as a recent study using chemically-induced expression of the ADP-ribose/NADH pyrophosphohydrolase AtNUDX7 that also found a positive relationship between foliar NADH and SA levels (Noctor et al., 2011; Pétriacq et al., 2012; Ogawa et al., 2016). Therefore, there may be a relationship between the higher NADH levels in the ammonium-fertilized plants that lead to higher constitutive SA levels observed here (Figure 3A); however, it is unclear why this fertilizer-associated effect is attenuated in plants grown at eCO<sub>2</sub>. One possibility is that at eCO<sub>2</sub>, reduced photorespiration may affect the localization of reductant that is linked to SA biosynthesis.

Though best recognized for the key regulatory roles in abiotic stresses, such as cold, drought and salinity (Sah et al., 2016), ABA is also involved in plant responses to mechanical and insect damage (Erb et al., 2012). ABA acts antagonistically to the Erf/ORF59 branch of the jasmonate-dependent signaling pathway that leads to defenses such as defensin (PDF1.2) (Kazan 2018). ABA also attenuates SA-mediated defense responses by stimulating the 26S-proteasome-mediated degradation of NPR1 (Ding et al., 2016). In plants grown at aCO<sub>2</sub>, higher ABA levels are also observed in

ammonium-fertilized plants and this is more pronounced under a high fertilizer rate (Figure 6E); this may reflect the relationship with ascorbate which is lower in ammonium-fertilized plants as a negative correlation is often observed between ascorbate and ABA levels (Figure 3F) (Pastori et al., 2003; Kerchev et al., 2011). It is unclear why this pattern is only observed in plants grown at aCO<sub>2</sub>, however, other studies have also found lower ABA levels in plants grown at eCO<sub>2</sub> (Teng et al., 2006).

### Wounding of *Arabidopsis* Leaves Results in an Increased Oxidative State and Elevated Phytohormone Levels

Dynamic changes in redox metabolites and pyrrolidine nucleotide levels occurred in wounded *Arabidopsis* leaves. Initially, an increase in DHA/Asc occurred within 15 min of wounding that reflected an increase in oxidized ascorbate (DHA) and decrease in reduced ascorbate (Asc) (Figures 4A–C). In a similar manner, Suza et al. (2010) observed that crushing of *Arabidopsis* leaves with a haemostat increased total ascorbate levels over the initial 6 h period after treatment. In our time course, this is followed by a decrease in NADP<sup>+</sup>/NADPH ratio and an increase in GSSG/GSH and, at 45 min after wounding, an increase in foliar GSSG levels continues (Figures 4D–F). Together our data indicates an increase in cellular oxidative state in damaged leaves. GSSG accumulation is often linked with increases in SA levels (Mhamdi et al., 2010; Mhamdi et al., 2013); we observed a consistent, slight increase in wound-induced SA levels that may reflect GSSG levels (Figure 6D).

Han et al. (2013a) have proposed that glutathione is key for the upregulation of the SA and jasmonate phytohormone pathways and the cross-talk between them. Mechanical damage of *Arabidopsis* leaves results in a vigorous increase in jasmonate-related phytohormones (Glauser et al., 2008; Wasternack and Hause, 2013); known as the jasmonate burst. Key representatives of these hormones, that are involved in regulation of plant responses to wounding, are 12-*oxo*-phytodienoic acid (OPDA), jasmonic acid and 7-jasmonyl-isoleucine (JA-Ile). We observed a robust increase in these phytohormones in wounded plants (Figures 6A–C).

### The Wound-Induced Jasmonate Burst is Attenuated in *Arabidopsis* Grown at eCO<sub>2</sub> (900 ppm)

Atmospheric CO<sub>2</sub> affects how *Arabidopsis* responds to mechanical damage. In the hour after damage, foliar NADP levels decline in wounded plants grown at aCO<sub>2</sub> (Figure 5A). As well there is a concomitant increase in NAD levels in wounded *Arabidopsis* grown at eCO<sub>2</sub> and fertilized with ammonium (Figure 5B); therefore, in plants grown at eCO<sub>2</sub>, that will reduce photorespiration, NAD levels in nitrate-fertilized plants is lower than in ammonium-fertilized plants which reflects the increased need for reductant in nitrate assimilation. Reduced and total ascorbate levels increase in the damaged leaves of these plants grown at eCO<sub>2</sub> (Figures 5C, D).

The jasmonate burst is the hallmark of the plant defense signaling pathway leading to resistance against chewing herbivores and necrotrophic pathogens (Wasternack and Hause,

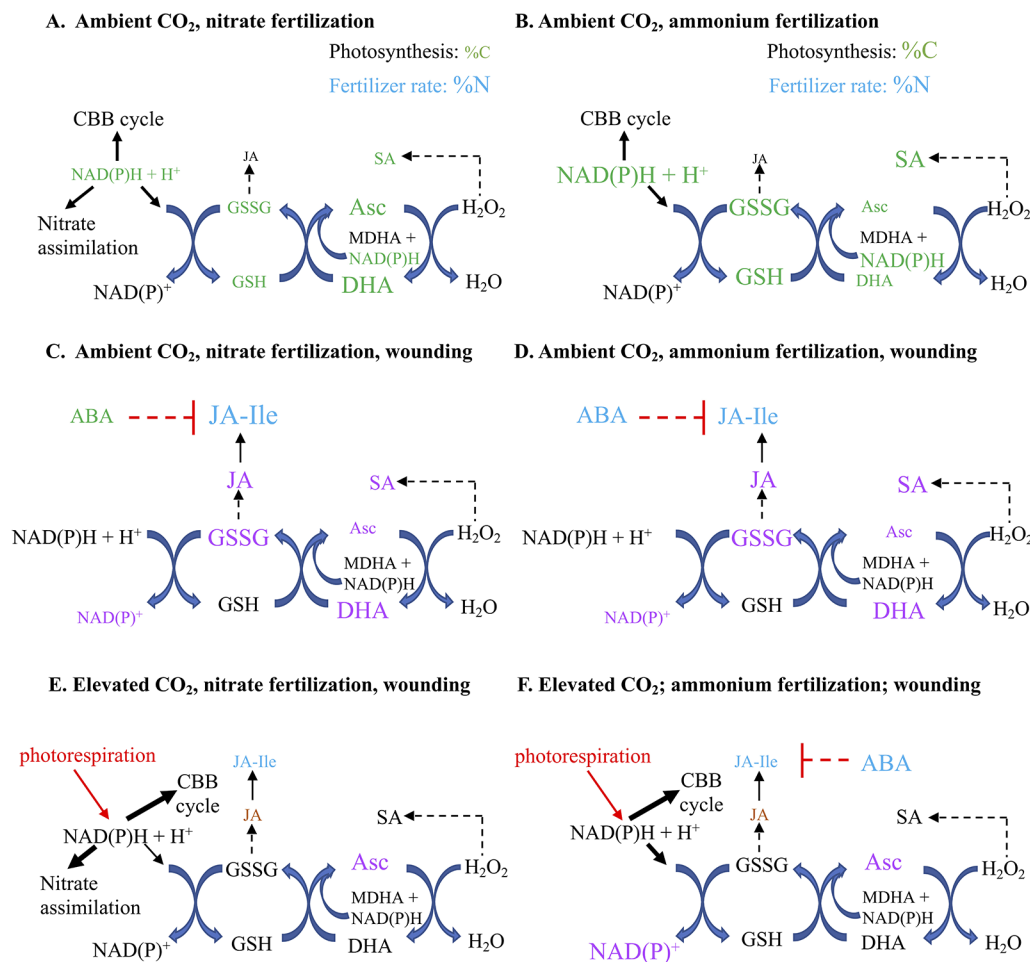


**FIGURE 7 |** Proposed model of the effect of nitrogen fertilizer on wound-induced foliar defense responses of *Arabidopsis thaliana*, a C3 plant that assimilates nitrate in its leaves, grown under predicted future carbon dioxide levels. Foliar percent carbon (%C) and nitrogen (%N), redox metabolite and pyridine nucleotide levels are represented in *Arabidopsis* fertilized by (A) nitrate or (B) ammonium. Overall, this reflected a slightly higher oxidative cellular state in plants fertilized by nitrate, which may explain the higher wound-induced JA-Ile levels in (C) nitrate compared to (D) ammonium fertilized plants (Figure 6C inset). At elevated carbon dioxide (eCO<sub>2</sub>) levels, there is a less strong oxidative state in (E) nitrate- or (F) ammonium-fertilized plants compared to ambient CO<sub>2</sub> that may, at least partially, account for the suppressed JA-Ile burst in response to wounding. Differences in metabolite levels are indicated by the relative size of their font. The colours represent the treatment effect; green indicates fertilizer type (nitrate or ammonium), blue represents fertilizer rate (1 or 10 mM), purple indicates mechanical damage, red indicates negative interactions and dashed lines indicate putative relationships. ABA, abscisic acid; aCO<sub>2</sub>, ambient carbon dioxide (450 ppm); Asc, reduced form of ascorbate; C, carbon; CBB, Calvin-Benson-Bassham; DHA, dehydroascorbate, oxidized form of ascorbate; eCO<sub>2</sub>, elevated carbon dioxide (900 ppm); GSH, reduced glutathione; GSSG, oxidized glutathione; NAD(P), oxidized form of nicotinamide adenine nucleotide (phosphate); NAD(P)H, reduced form of nicotinamide adenine nucleotide (phosphate); JA, jasmonic acid; JA-Ile: 7-jasmonyl-L-isoleucine; N, nitrogen; OPDA, 12-oxo-phytyldienoic acid; SA: salicylic acid.

2013; Howe et al., 2018). However, this burst is strongly attenuated in wounded plants grown at eCO<sub>2</sub> (Figures 6B, C). Early steps in the pathway, i.e. OPDA levels, are not affected by fertilizer or CO<sub>2</sub> levels, suggesting that regulation of this pathway occur after OPDA biosynthesis (Figure 6A). In contrast, lower JA levels are observed at eCO<sub>2</sub>, which has also been noted in other studies (Guo et al., 2012; Sun et al., 2013; Vaughan et al., 2014; Li et al., 2016; Lu et al., 2018). As well, the wound-associated increase in the bioactive JA-Ile levels that positively reflects nitrogen fertilizer and rate is not observed in *Arabidopsis* grown at eCO<sub>2</sub> (Figure 6C). It is of interest that the wound-induced increase in JA-Ile is higher in nitrate- than ammonium-fertilized plants which likely reflects the more oxidative state in these plants (Figure 6C, inset). Plants grown

at aCO<sub>2</sub> show a more robust JA-Ile increase in well-fertilized plants that is attenuated at eCO<sub>2</sub>, an observation similar to that reported by Paudel et al. (2016) who also noted that the jasmonate burst was attenuated at eCO<sub>2</sub> and more markedly in well-fertilized plants.

High constitutive SA levels observed in *Arabidopsis* grown at eCO<sub>2</sub> is proposed to be responsible for the decreased jasmonate levels also observed at eCO<sub>2</sub> (Casteel et al., 2012a; Zavala et al., 2013; Mhamdi and Noctor, 2016; Gog et al., 2019). Numerous plants species grown at elevated CO<sub>2</sub> have increased SA levels (Casteel et al., 2012a; Huang et al., 2012; Sun et al., 2013; Mhamdi et al., 2013; Zhang et al., 2015; Li et al., 2019; Gog et al., 2019); though this appears to be plant species- or cultivar-specific and influenced by other environmental factors (Matros et al., 2006;

Casteel et al., 2012b; Mhamdi and Noctor, 2016; Noctor and Mhamdi, 2017; Zhou et al., 2019). In fact, in our study, a decrease in SA levels are observed at eCO<sub>2</sub> which may reflect the photoperiod used in these experiments (12:12 L:D, **Figure 6D**), compared to others conducted under long day conditions (16:8) (Matros et al., 2006; Sun et al., 2013; Zhang et al., 2015; Mhamdi and Noctor, 2016; Gog et al., 2019). *Arabidopsis* plants that have higher SA levels also have increased resistance to hemibiotrophic and necrotrophic pathogens, such as *Pseudomonas syringae* DC3000 and *Botrytis cinerea* (Mhamdi and Noctor, 2016); however, a recent study found that resistance of *Arabidopsis* to *P. syringae* pv tomato was reduced in plants grown at eCO<sub>2</sub> (Zhou et al., 2019), which also points to the involvement of other factors, such as light or nitrogen, in this network. A wound-induced increase in SA levels was observed as has been seen in previous studies; a transient increase in SA levels 24 h after carborundum-induced mechanical damage of *Arabidopsis* leaves has been previously reported (Ogawa et al., 2010). Given the well-established cross-talk between the SA x jasmonate pathways (Caarls et al., 2015), this may, in part, explain the suppression of the jasmonate burst observed in plants grown at eCO<sub>2</sub> (**Figure 6C**).

## CONCLUSION

At aCO<sub>2</sub>, overall, a more cellular oxidative state was observed in nitrate-fertilized plants that translates into a higher jasmonate burst in wounded plants (**Figure 7**). In undamaged plants, ammonium fertilization results in higher reductant levels (NADH, **Figure 3A**) and redox buffering capacity (GSSG, GSH, total glutathione; **Figures 3B–D**) that likely reflects the requirement for additional reductant in nitrate assimilation. Therefore, in ammonium-fertilized plants, the additional reductant could be used in the CBB cycle that translates into higher carbon fixation (**Figure 2A**). In contrast, total ascorbate levels are higher in nitrate-fertilized plants (**Figure 2F**). Within 15 min after mechanical wounding, an increase in oxidized DHA and concomitant decrease in reduced Asc is observed (**Figures 4A, B**). This is followed by an increase in GSSG and decrease in NADP<sup>+</sup>/NADPH levels (**Figures 4E, D**). This variance in cellular oxidative state may translate into the noted differences in wound-associated levels of jasmonate and SA phytohormones (**Figures 6A–D**). Nitrate-fertilized plants have a more oxidative cellular environment, albeit moderate, compared to ammonium-fertilized plants and this potentially is reflected in the increase in wound-associated JA-Ile levels compared to ammonium-fertilized plants (**Figure 6C**, inset). In addition, the JA-Ile burst is strongest in well-fertilized plants (**Figure 6C**).

At eCO<sub>2</sub>, the decrease in photorespiration is expected to decrease cellular reductant levels which has the potential to effect oxidative signaling in response to wound stress. In response to mechanical damage, the wound-associated decrease in NADP<sup>+</sup> is only observed in plants grown at aCO<sub>2</sub> but not eCO<sub>2</sub> (**Figure 5A**); this may reflect lower NADPH levels due to a decreased photorespiration-associated malate shuttle. In contrast NAD<sup>+</sup> levels increase in wounded ammonium-fertilized plants grown at

eCO<sub>2</sub>, but not aCO<sub>2</sub> (**Figure 5B**). Ammonium fertilization results in higher foliar NADH levels (**Figure 3A**); the wound-associated increase in NAD<sup>+</sup> may be more pronounced at eCO<sub>2</sub> reflecting changes in mitochondrial respiration. As well, there is a wound-associated increase in reduced and total ascorbate levels only observed in plants grown at eCO<sub>2</sub> (**Figures 5C, D**). Therefore, at eCO<sub>2</sub>, in response to wounding, there is less strong oxidative state compared to plants grown at aCO<sub>2</sub>. This translates into a muted JA-Ile burst in response to wounding, particularly in well-fertilized plants grown at eCO<sub>2</sub>, in agreement with previous studies (Paudel et al., 2016) (**Figure 6C**). However, at the fertilization rates used, a difference in wound-induced jasmonates between ammonium- or nitrate-fertilized plants is not observed; therefore, this suppression may be linked to competition for nitrogen assimilation at eCO<sub>2</sub>, but downstream of nitrate reduction and/or foliar ascorbate and SA levels. Wound-induced total ascorbate, which strongly reflects foliar reduced Asc levels, is higher in plants grown at eCO<sub>2</sub> and a negative correlation between ascorbate and jasmonate signaling pathways has been previously observed (Kerchev et al., 2011). As well, the increase in SA levels induced by wounding may also act to suppress induced jasmonate levels (**Figure 6D**) (Koornneef and Pieterse, 2008; Caarls et al., 2015).

Therefore, in response to damage, dynamic fluctuations in redox metabolites, particular glutathione-related metabolites, indicate an increase in cellular oxidative status in wounded *Arabidopsis* leaves leading to a robust jasmonate burst (**Figures 4A–C** and **6A–C**). Well-fertilized *Arabidopsis* plants grown at aCO<sub>2</sub> exhibit stronger JA-Ile increases in damaged leaves, which is heightened in nitrate-fertilized plants, that possibly reflects the cellular oxidative state (**Figures 3A–D**, **3F**, **5B**, and **6C**). In *Arabidopsis* grown at eCO<sub>2</sub>, the oxidative state and jasmonate burst is muted in wounded plants (**Figure 6C**). The increase in ascorbate and SA in response to wounding may contribute to the suppression of the JA burst (**Figures 5C** and **6D**).

Plants are sophisticated in their approaches to integrate and respond to everchanging environmental conditions. In the next 50 years, dramatic increases in atmospheric CO<sub>2</sub> levels are predicted to occur and this will greatly impact plants, particularly those who conduct C<sub>3</sub> photosynthesis. Understanding how eCO<sub>2</sub> will impact future plant-interactions, particularly those in response to negative biotic stresses, such as chewing insects or necrotrophic pathogens, is critical to develop sustainable management practices for agricultural crop protection.

## DATA AVAILABILITY STATEMENT

The datasets generated for this study are available on request to the corresponding author.

## AUTHOR CONTRIBUTIONS

Conceived and designed the experiments: JM and JB. Performed the experiments: JH, LD, KG, and AS. Analyzed the data: JM and JB. Wrote the manuscript: JM, KG, AS, ND, and JB.



## ACKNOWLEDGMENTS

We are grateful to Zhihong Zhang, Ruoxi Liu, and Maike Huszarik for assisting with experiments. We are grateful to Sonia Dorion and Jean Rivoal for training JHM in pyridine nucleotide and redox metabolite assays. We thank the two reviewers of this article for their insightful comments. This research was funded through a Fonds de recherche du Québec—Nature et technologies (FRQNT)-funded network grant awarded to the Centre de recherche en sciences du végétal (SEVE) (2018-RS-203283) and a grant from

the Natural Sciences and Engineering Research Council (NSERC) (RGPIN-2013-04516) to JCB.

## SUPPLEMENTARY MATERIAL

The Supplementary Material for this article can be found online at: <https://www.frontiersin.org/articles/10.3389/fpls.2019.01636/full#supplementary-material>

## REFERENCES

- Ainsworth, E. A., and Rogers, A. (2007). The response of photosynthesis and stomatal conductance to rising [CO<sub>2</sub>]: mechanisms and environmental interactions. *Plant Cell Environ.* 30, 258–270. doi: 10.1111/j.1365-3040.2007.01641.x
- Andrews, M., Condrón, L. M., Kemp, P. D., Topping, J. F., Lindsey, K., Hodge, S., et al. (2019). Elevated CO<sub>2</sub> effects on nitrogen assimilation and growth of C<sub>3</sub> vascular plants are similar regardless of N-form assimilated. *J. Exp. Bot.* 70, 683–390. doi: 10.1093/jxb/ery371
- Arimura, G.-I., Ozawa, R., and Maffei, M. E. (2011). Recent advances in plant early signaling in response to herbivory. *Int. J. Mol. Sci.* 12, 3723–3739. doi: 10.3390/ijms12063723
- Baysdorfer, C., and Robinson, J. M. (1985). Metabolic interactions between spinach leaf nitrite reductase and ferredoxin-NADP reductase. Competition for reduced ferredoxin. *Plant Physiol.* 77, 318–320. doi: 10.1104/pp.77.2.318
- Betti, M., Bauwe, H., Busch, F. A., Fernie, A. R., Keech, O., Levey, M., et al. (2016). Manipulating photorespiration to increase plant productivity: recent advances and perspectives for crop improvement. *J. Exp. Bot.* 67, 2977–2988. doi: 10.1093/jxb/erw076
- Bloom, A. J., Smart, D. R., Nguyen, D. T., and Searles, P. S. (2002). Nitrogen assimilation and growth of wheat under elevated carbon dioxide. *Proc. Natl. Acad. Sci.* 99, 1730–1735. doi: 10.1073/pnas.022627299
- Bloom, A. J., Burger, M., Rubio Asensio, J. S., and Cousins, A. B. (2010). Carbon dioxide enrichment inhibits nitrate assimilation in wheat. *Science* 328, 899–903. doi: 10.1126/science.1186440
- Bloom, A. J., Burger, M., Kimball, B. A., and Pinter, P. J. Jr. (2014). Nitrate assimilation is inhibited by elevated CO<sub>2</sub> in field-grown wheat. *Nat. Clim. Change* 4, 477–480. doi: 10.1038/NClimate2183
- Bloom, A. J. (2015a). Photorespiration and nitrate assimilation: a major intersection between plant carbon and nitrogen. *Photosynth. Res.* 123, 117–128. doi: 10.1007/s11120-014-0056-y
- Bloom, A. J. (2015b). The increasing importance of distinguishing among plant nitrogen sources. *Curr. Opin. Plant Biol.* 25, 10–16. doi: 10.1016/j.pbi.2015.03.002
- Boatwright, J. L., and Pajeroska-Mukhtar, K. (2013). Salicylic acid: an old hormone up to new tricks. *Mol. Plant Pathol.* 14, 623–634. doi: 10.1111/mp.12035
- Boyes, D. C., Zayed, A. M., Ascenzi, R., McCaskill, A. J., Hoffman, N. E., Davis, K. R., et al. (2001). Growth stage-based phenotypic analysis of Arabidopsis: a model for high throughput functional genomics in plants. *Plant Cell* 13, 1499–1510. doi: 10.1105/tpc.010011
- Burger, M., and Jackson, L. E. (2003). Microbial immobilization of ammonium and nitrate in relation to ammonification and nitrification rates in organic and conventional cropping systems. *Soil Biol. Biochem.* 35, 29–36. doi: 10.1016/S0038-0717(01)00233-X
- Busch, F. A., Sage, R. F., and Farquhar, G. D. (2018). Plants increase CO<sub>2</sub> uptake by assimilating nitrogen via the photorespiratory pathway. *Nat. Plants* 4, 46–54. doi: 10.1038/s41477-017-0065-x
- Caarls, L., Pieterse, C. M. J., and Van Wees, S. C. M. (2015). How salicylic acid takes over transcriptional control over jasmonic acid signaling. *Front. Plant Sci.* 6, 170. doi: 10.3389/fpls.2015.00170
- Carmo-Silva, E., Scales, J. C., Madgwick, P. J., and Parry, M. A. J. (2015). Optimizing Rubisco and its regulation for greater resource use efficiency. *Plant Cell Environ.* 38, 1817–1832. doi: 10.1111/pce.12425
- Casteel, C. L., O'Neill, B. F., Zavala, J. A., Bilgin, D. D., and Berenbaum, M. R. (2008). Transcriptional profiling reveals elevated CO<sub>2</sub> and elevated O<sub>3</sub> alter resistance of soybean (*Glycine max*) to Japanese beetles (*Popillia japonica*). *Plant Cell Environ.* 31, 419–434. doi: 10.1111/j.1365-3040.2008.01782.x
- Casteel, C. L., Niziolek, O. K., Leakey, A. D. B., Berenbaum, M. R., and DeLucia, E. H. (2012a). Effects of elevated CO<sub>2</sub> and soil water content on phytohormone transcript induction in *Glycine max* after *Popillia japonica* feeding. *Arthropod-Plant Interact.* 6, 439–447. doi: 10.1007/s11829-012-9195-2
- Casteel, C. L., Segal, L. M., Niziolek, O. K., Berenbaum, M. R., and DeLucia, E. H. (2012b). Elevated carbon dioxide increases salicylic acid in *Glycine max*. *Environ. Entomol.* 41, 1435–1442. doi: 10.1603/En12196
- Considine, M. J., and Foyer, C. H. (2014). Redox regulation of plant development. *Antioxid. Redox Signaling* 21, 1305–1326. doi: 10.1089/ars.20135665
- Cotrufo, M. F., Ineson, P., and Scott, A. (2002). Elevated CO<sub>2</sub> reduces the nitrogen concentration of plant tissues. *Global Change Biol.* 4, 43–54. doi: 10.1046/j.1365-2486.1998.00101.x
- Cox, P. M., Betts, R. A., Jones, C. D., Spall, S. A., and Totterdell, I. J. (2000). Acceleration of global warming due to carbon-cycle feedbacks in a coupled climate model. *Nature* 408, 184–187. doi: 10.1038/35041539
- Ding, Z., Dommel, M., and Mou, Z. (2016). Abscissic acid promotes proteasome-mediated degradation of the transcription coactivator NPR1 in *Arabidopsis thaliana*. *Plant J.* 86, 20–34. doi: 10.1111/tpj.13141
- Ehlers, I., Augusti, A., Betson, T. R., Nilsson, M. G., Marshall, J. D., and Schleucher, J. (2015). Detecting long-term metabolic shifts using isotopomers: CO<sub>2</sub>-driven suppression of photorespiration in C<sub>3</sub> plants over the 20<sup>th</sup> century. *Proc. Natl. Acad. Sci.* 112, 15585–15590. doi: 10.1073/pnas.1504493112
- Eisenhut, M., Roell, M.-S., and Weber, A. P. M. (2019). Mechanistic understanding of photorespiration paves the way to a new green revolution. *New Phytol.* 223, 1762–1769. doi: 10.1111/nph.15872
- Erb, M., Meldau, S., and Howe, G. A. (2012). Role of phytohormones in insect-specific plant reactions. *Trends Plant Sci.* 17, 250–259. doi: 10.1016/j.tplants.2012.01.003
- Foyer, C. H., and Noctor, G. (2011). Ascorbate and glutathione: The heart of the redox hub. *Plant Physiol.* 155, 2–18. doi: 10.1104/pp.110.167569
- Foyer, C. H., Noctor, G., and Verrier, P. (2006). “Chapter 12. Photosynthetic carbon-nitrogen interactions: modelling inter-pathway control and signalling,” in *Annual Plant Reviews Vol. 22: Control of Primary Metabolism in Plants*. Eds. W. C. Plaxton and M. T. McManus (Oxford, UK: Blackwell Publishing Ltd.), 325–347. doi: 10.1002/9780470988640.ch12
- Foyer, C. H., Bloom, A. J., Queval, G., and Noctor, G. (2009). Photorespiratory metabolism: genes, mutants, energetics, and redox signaling. *Ann. Rev. Plant Biol.* 60, 455–484. doi: 10.1146/annurev.arplant.043008.091948
- Foyer, C. H., Noctor, G., and Hodges, M. (2011). Respiration and nitrogen assimilation: targeting mitochondria-associated metabolism as a means to enhance nitrogen use efficiency. *J. Exp. Bot.* 62, 1467–1482. doi: 10.1093/jxb/erq453
- Gfeller, A., Baerenfaller, K., Loscos, J., Chetelat, A., Baginsky, S., and Farmer, E. E. (2011). Jasmonate controls polypeptide patterning in undamaged tissue in wounded arabidopsis leaves. *Plant Physiol.* 156, 1797–1807. doi: 10.1104/pp.111.181008
- Glauser, G., Grata, E., Dubugnon, L., Rudaz, S., Farmer, E. E., and Wolfender, J.-L. (2008). Spatial and temporal dynamics of jasmonate synthesis and accumulation in *Arabidopsis* in response to wounding. *J. Biol. Chem.* 283, 16400–16407. doi: 10.1074/jbc.M801760200
- Gog, L., Berenbaum, M. R., and DeLucia, E. H. (2019). Mediation of impacts of elevated CO<sub>2</sub> and light environment on *Arabidopsis thaliana* (L.) chemical defense against insect herbivory via photosynthesis. *J. Chem. Ecol.* 45, 61–73. doi: 10.1007/s10886-018-1035-0

- Guo, S., Schinner, K., Sattelmacher, B., and Hansen, U.-P. (2005). Different apparent CO<sub>2</sub> compensation points in nitrate- and ammonium-grown *Phaseolus vulgaris* and their relationship to non-photorespiratory CO<sub>2</sub> evolution. *Physiol. Plant.* 123, 288–301. doi: 10.1111/j.1399-3054.2005.00467.x
- Guo, H., Sun, Y., Ren, Q., Zhu-Salzman, K., Kang, L., Wang, C., et al. (2012). Elevated CO<sub>2</sub> reduces the resistance and tolerance of tomato plants to *Helicoverpa armigera* by suppressing the JA signaling pathway. *PLoS One* 7, e41426. doi: 10.1371/journal.pone.0041426
- Hachiya, T., and Sakakibara, H. (2017). Interactions between nitrate and ammonium in their uptake, allocation, assimilation, and signaling in plants. *J. Exp. Bot.* 68, 2501–2512. doi: 10.1093/jxb/erw449
- Han, Y., Hhamdi, A., Chaouch, S., and Noctor, G. (2013a). Regulation of basal and oxidative stress-triggered jasmonic acid-related gene expression by glutathione. *Plant Cell Environ.* 36, 1135–1146. doi: 10.1111/pce.12048
- Han, Y., Chaouch, S., Mhamdi, A., Queval, G., Zechmann, B., and Noctor, G. (2013b). Functional analysis of *Arabidopsis* mutants points to novel roles of glutathione in coupling H<sub>2</sub>O<sub>2</sub> to activation of salicylic acid accumulation and signaling. *Antioxid. Redox Signaling* 18, 2106–2121. doi: 10.1089/ars.20125052
- Howe, G. A., Major, I. T., and Koo, A. J. (2018). Modularity in jasmonate signaling for multistress resilience. *Ann. Rev. Plant Biol.* 69, 20.1–20.29. doi: 10.1146/annurev-arplant-042817-040047
- Huang, L., Ren, Q., Sun, Y., Ye, L., Cao, H., and Ge, F. (2012). Lower incidence and severity of tomato virus in elevated CO<sub>2</sub> is accompanied by modulated plant induced defense in tomato. *Plant Biol.* 14, 905–913. doi: 10.1111/j.1438-8677.2012.00582.x
- Huma, B., Kundu, S., Poolman, M. G., Kruger, N. J., and Fell, D. A. (2018). Stoichiometric analysis of the energetics and metabolic impact of photorespiration in C3 plants. *Plant J.* 96, 1228–1241. doi: 10.1111/tjp.14105
- Igamberdiev, A. U., and Bykova, N. V. (2018). Role of organic acids in the integration of cellular redox metabolism and mediation of redox signaling in photosynthetic tissues of higher plants. *Free Radical Biol. Med.* 122, 74–85. doi: 10.1016/j.freeradbiomed.2018.01.016
- Intergovernmental Panel on Climate Change (2013) (Cambridge, UK).
- Kalcsits, L. A., and Guy, R. D. (2013). Whole-plant and organ-level nitrogen isotope discrimination indicates modification of partitioning of assimilation, fluxes and allocation of nitrogen in knockout lines of *Arabidopsis thaliana*. *Physiol. Plant.* 149, 249–259. doi: 10.1111/ppl.12038
- Kant, S., Seneweera, S., Rodin, J., Materne, M., Burch, D., Rothstein, S. J., et al. (2012). Improving yield potential in crops under elevated CO<sub>2</sub>: integrating the photosynthetic and nitrogen utilization efficiencies. *Front. Plant Sci.* 3, 162. doi: 10.3389/fpls.2012.00162
- Kazan, K. (2018). Plant-biotic interactions under elevated CO<sub>2</sub>: a molecular perspective. *Environ. Exp. Bot.* 153, 249–261. doi: 10.1016/j.envexpbot.2018.06.005
- Kerchev, P. I., Peliny, T. K., Diaz Vivancos, P., Kiddle, G., Hedden, P., Driscoll, S., et al. (2011). The transcription factor ABI4 is required for the ascorbic acid-dependent regulation of growth and regulation of jasmonate-dependent defense signaling pathways in *Arabidopsis*. *Plant Cell* 23, 3319–3334. doi: 10.1105/tpc.111.090100
- Koornneef, A., and Pieterse, C. M. J. (2008). Cross talk in defense signaling. *Plant Physiol.* 146, 839–844. doi: 10.1104/pp.107.112029
- Koornneef, A., Leon-Reyes, A., Ritsema, T., Verhage, A., Den Otter, F. C., Van Loon, L. C., et al. (2008). Kinetics of salicylate-mediated suppression of jasmonate signaling reveal a role for redox modulation. *Plant Physiol.* 147, 1358–1368. doi: 10.1104/pp.108.121392
- Kovacs, I., Durner, J., and Lindermayr, C. (2015). Crosstalk between nitric oxide and glutathione is required for nonexpressor of pathogenesis-related genes 1 (NPR1)-dependent defense signaling in *Arabidopsis thaliana*. *New Phytol.* 208, 860–872. doi: 10.1111/nph.13502
- Krapp, A. (2015). Plant nitrogen assimilation and its regulation: a complex puzzle with missing pieces. *Curr. Opin. Plant Biol.* 25, 115–122. doi: 10.1016/j.pbi.2015.05.010
- Lan, Z., Krosse, S., Achard, P., van Dam, N. M., and Bede, J. C. (2014). DELLA proteins modulate *Arabidopsis* defenses induced in response to caterpillar herbivory. *J. Exp. Bot.* 65, 571–583. doi: 10.1093/jxb/ert420
- Leakey, A. D. B., Ainsworth, E. A., Bernacchi, C. J., Rogers, A., Long, S. P., and Ort, D. R. (2009). Elevated CO<sub>2</sub> effects on plant carbon, nitrogen, and water relations: six important lessons from FACE. *J. Exp. Bot.* 60, 2859–2876. doi: 10.1093/jxb/erp096
- Li, B., Li, G., Kronzucker, H. J., Baluška, F., and Shi, W. (2014). Ammonium stress in *Arabidopsis*: signaling, genetic loci, and physiological targets. *Trends Plant Sci.* 19, 107–114. doi: 10.1016/j.tplants.2013.09.004
- Li, X., Jalal, G., Li, Z., Tang, M., Yan, P., and Han, W. (2016). Decreased biosynthesis of jasmonic acid via lipoxygenase pathway compromised flavonoid biosynthesis in tea plant *Camellia sinensis* L. *Environ. Exp. Bot.* 161, 367–374. doi: 10.1016/j.envexpbot.2018.11.012
- Long, S. P., Ainsworth, E. A., Rogers, A., and Ort, D. R. (2004). Rising atmospheric carbon dioxide: plants FACE the future. *Ann. Rev. Plant Biol.* 55, 591–628. doi: 10.1146/annurev-arplant.55.031903.141610
- Long, S. P., Ainsworth, E. A., Leakey, A. D. B., Nösberger, J., and Ort, D. R. (2006). Food for thought: lower-than-expected crop yield stimulation with rising CO<sub>2</sub> concentrations. *Science* 312, 1918–1921. doi: 10.1126/science.1114722
- Lu, C., Qi, J., Hattenhausen, C., Lei, Y., Zhang, J., Zhang, M., et al. (2018). Elevated CO<sub>2</sub> differentially affects tobacco and rice defense against lepidopteran larvae via the jasmonic acid signaling pathway. *J. Integr. Plant Biol.* 60, 412–431. doi: 10.1111/jipb.12633
- Matros, A., Amme, S., Ketting, B., Buck-Sorlin, G. H., Sonnwald, U., and Mock, H. P. (2006). Growth at elevated CO<sub>2</sub> concentrations lead to modified profiles of secondary metabolites in tobacco cv. SamsunNN and to increased resistance against infection with potato virus Y. *Plant Cell Environ.* 29, 126–137. doi: 10.1111/j.1365-3040.2005.01406.x
- Medici, L. O., Azevedo, R. A., Smith, R. J., and Lea, P. J. (2004). The influence of nitrogen supply on antioxidant enzymes in plant roots. *Funct. Plant Biol.* 31, 1–9. doi: 10.1071/FP03130
- Mhamdi, A., and Noctor, G. (2016). High CO<sub>2</sub> primers plant biotic stress defences through redox-linked pathways. *Plant Physiol.* 172, 929–942. doi: 10.1104/pp.16.01129
- Mhamdi, A., Hager, J., Chaouch, S., Queval, G., Han, Y., Taconnat, L., et al. (2010). *Arabidopsis* glutathione reductase1 plays a crucial role in leaf responses to intracellular hydrogen peroxide and in ensuing appropriate gene expression through both salicylic acid and jasmonic acid signaling pathways. *Plant Physiol.* 153, 1144–1160. doi: 10.1104/pp.110.153767
- Mhamdi, A., Han, Y., and Noctor, G. (2013). Glutathione-dependent phytohormone responses. Teasing apart signaling and antioxidant functions. *Plant Signaling Behav.* 8, 5. doi: 10.4161/psb.24181
- Noctor, G., and Foyer, C. H. (1998). A re-evaluation of the ATP : NADPH budget during C<sub>3</sub> photosynthesis: a contribution from nitrate assimilation and its associated respiratory activity? *J. Exp. Bot.* 49, 1895–1908. doi: 10.1093/jxb/49.3291895
- Noctor, G., and Mhamdi, A. (2017). Climate change, CO<sub>2</sub>, and defense: The metabolic, redox, and signaling perspectives. *Trends Plant Sci.* 22, 857–870. doi: 10.1016/j.tplants.2017.07.007
- Noctor, G., Hager, J., and Li, S. (2011). Biosynthesis of NAD and its manipulation in plants. *Adv. Bot. Res.* 58, 153–201. doi: 10.1016/B978-0-12-386479-6.00002-0
- Noctor, G., Mhamdi, A., Chaouch, S., Han, Y., Neukermans, J., Marquez-Garcia, B., et al. (2012). Glutathione in plants: an integrated overview. *Plant Cell Environ.* 35, 454–484. doi: 10.1111/j.1365-3040.2011.02400.x
- Noctor, G., Mhamdi, A., and Foyer, C. H. (2016). Oxidative stress and antioxidative systems: recipes for successful data collection and interpretation. *Plant Cell Environ.* 39, 1140–1160. doi: 10.1111/pce.12726
- Ogawa, T., Muramoto, K., Takada, R., Nakagawa, S., Shigeoka, S., and Yoshimura, K. (2016). Modulation of NADH levels by *Arabidopsis* Nudix hydrolases, AtNUDX6 and 7, and the respective proteins themselves play distinct roles in the regulation of various cellular responses involved in biotic/abiotic stresses. *Plant Cell Physiol.* 57, 1295–1308. doi: 10.1093/pcp/pcw078
- Ogawa, T., Ara, T., Aoki, K., Suzuki, H., and Shibata, D. (2010). Transient increase in salicylic acid and its glucose conjugates after wounding in *Arabidopsis* leaves. *Plant Biotechnol.* 27, 205–209. doi: 10.5511/plantbiotechnology.27.205

- Pastori, G. M., Kiddle, G., Antoniq, J., Bernard, S., Veljovic-Jovanovic, S., Verrier, P. J., et al. (2003). Leaf vitamin C contents modulate plant defense transcripts and regulate genes that control development through hormone signaling. *Plant Cell* 15, 939–951. doi: 10.1105/tpc.010538
- Patterson, K., Cakmak, T., Cooper, A., Lager, I., Rasmusson, A. G., and Escobar, M. A. (2010). Distinct signalling pathways and transcriptome response signatures differentiate ammonium- and nitrate-supplied plants. *Plant Cell Environ.* 33, 1486–1501. doi: 10.1111/j-1365-3040.2010.02158.x
- Paudel, J. R., Amirizian, A., Krosse, S., Giddings, J., Ismail, S. A. A., Xia, J., et al. (2016). Effect of atmospheric carbon dioxide levels and nitrate fertilization on glucosinolate biosynthesis in mechanically damaged *Arabidopsis* plants. *BMC Plant Biol.* 16, 68. doi: 10.1186/s12870-016-0752-1
- Pétriacy, P., de Bont, L., Hager, J., Didierlaurent, L., Mauve, C., Guérard, F., et al. (2012). Inducible NAD overproduction in *Arabidopsis* alters metabolic pools and gene expression correlated with increase salicylate content and resistance to *Pst-AvrRpm1*. *Plant J.* 70, 650–665. doi: 10.1111/j.1365-3113x.2012.04920.x
- Pincebourde, S., van Baaren, J., Rasmann, S., Rasmont, P., Rodet, G., Martinet, B., et al. (2017). Plant-insect interactions in a changing world. *Adv. Bot. Res.* 81, 289–332. doi: 10.1016/bs.abr.2016.09.009
- Podgórska, A., Gieczewska, K., Łukawska-Kuźma, K., Gardeström, P., Rasmusson, A. G., and Szal, B. (2013). Long-term ammonium nutrition of *Arabidopsis* increases the extrachloroplastic NAD(P)H/NAD(P)<sup>+</sup> ratio and mitochondrial reactive oxygen species level in leaves but does not impair photosynthetic capacity. *Plant Cell Environ.* 36, 2034–2045. doi: 10.1111/pce.12113
- Podgórska, A., Ostaszewska, M., Gardeström, P., Rasmusson, A. G., and Szal, B. (2015). In comparison with nitrate nutrition, ammonium nutrition increase growth of the *frostbite1* *Arabidopsis* mutant. *Plant Cell Environ.* 38, 224–237. doi: 10.1111/pce.12404
- Potters, G., Horemans, N., and Jansen, M. A. K. (2010). The cellular redox state in plant stress biology – a charging concept. *Plant Physiol. Biochem.* 48, 292–300.
- Quevel, G., and Noctor, G. (2007). A plant reader method for the measurement of NAD, NADP, glutathione and ascorbate in tissue extracts: Application to redox profiling during *Arabidopsis* rosette development. *Anal. Biochem.* 363, 58–69. doi: 10.1016/j.ab.2007.01.005
- Rachmilevitch, S., Cousins, A. B., and Bloom, A. J. (2004). Nitrate assimilation in plant shoots depends on photorespiration. *Proc. Natl. Acad. Sci.* 101, 11506–11510. doi: 10.1073/pnas.0404388101
- Rogers, A., and Humphries, S. W. (2000). A mechanistic evaluation of photosynthetic acclimation at elevated CO<sub>2</sub>. *Global Change Biol.* 6, 1005–1011. doi: 10.1046/j.1365-2486.2000.00375.x
- Rubio Asensio, J. S., Rachmilevitch, S., and Bloom, A. J. (2015). Responses of *Arabidopsis* and wheat to rising CO<sub>2</sub> depend on nitrogen source and nighttime CO<sub>2</sub> levels. *Plant Physiol.* 168, 156–163. doi: 10.1104/pp.15.00110
- Sah, S. K., Reddy, K. R., and Li, J. (2016). Abscisic acid and abiotic stress tolerance in crop plants. *Front. Plant Sci.* 7, e571. doi: 10.3389/fpls.2016.00571
- Scheibe, R., and Dietz, K.-J. (2012). Reduction-oxidation network for flexible adjustment of cellular metabolism in photoautotrophic cells. *Plant Cell Environ.* 35, 202–216. doi: 10.1111/j.1365-2040.2011.02319.x
- Scheibe, R., Backhausen, J. E., Emmerlich, V., and Holtgreffe, S. (2005). Strategies to maintain redox homeostasis during photosynthesis under changing conditions. *J. Exp. Bot.* 56, 1481–1489. doi: 10.1093/jxb/eri181
- Scheibe, R. (2004). Malate valves to balance cellular energy supply. *Physiol. Plant.* 120, 21–26. doi: 10.1111/j.0031-9317.2004.0222.x
- Selinski, J., and Scheibe, R. (2019). Malate valves: old shuttles with new perspectives. *Plant Biol.* 21, 21–30. doi: 10.1111/plb.12869
- Spoel, S. H., Koornneef, A., Claessens, S. M. C., Korzelius, J. P., Van Pelt, J. A., Mueller, M. J., et al. (2003). NPR1 modulates cross-talk between salicylate- and jasmonate-dependent defense pathways through a novel function in the cytosol. *Plant Cell* 15, 760–770. doi: 10.1105/tpc.009159
- Stefanelli, D., Goodwin, I., and Jones, R. (2010). Minimal nitrogen and water use in horticulture: effects on quality and content of selected nutrients. *Food Res. Int.* 43, 1833–1843. doi: 10.1016/j.foodres.2010.04.022
- Stefanski, W. (1971). Rejecting outliers by maximum normed residual. *Ann. Math. Stat.* 42, 35–45.
- Stitt, M., and Krapp, A. (1999). The interaction between elevated carbon dioxide and nitrogen nutrition: the physiological and molecular background. *Plant Cell Environ.* 22, 583–621.
- Sun, J., Gibson, K. M., Kiirats, O., Okita, T. W., and Edwards, G. E. (2002). Interactions of nitrate and CO<sub>2</sub> enrichment on growth, carbohydrates, and Rubisco in *Arabidopsis* starch mutants. Significance of starch and hexose. *Plant Physiol.* 130, 1573–1583. doi: 10.1104/pp.010058
- Sun, Y., Guo, H., Zhu-Salzman, K., and Ge, F. (2013). Elevated CO<sub>2</sub> increase the abundance of the peach aphid on *Arabidopsis* by reducing jasmonic acid defenses. *Plant Sci.* 210, 128–140. doi: 10.1016/j.plantsci.2013.05.014
- Suza, W. P., Avila, C. A., Carruthers, K., Kulkarni, S., Goggin, F. L., and Lorence, A. (2010). Exploring the impact of wounding and jasmonates on ascorbate metabolism. *Plant Physiol. Biochem.* 48, 337–350. doi: 10.1016/j.plaphy.2010.02.004
- Tada, Y., Spoel, S. H., Pajeroska-Mukhtar, K., Mou, Z., Song, J., Wang, C., et al. (2008). Plant immunity requires conformational changes of NPR1 via S-nitrosylation and thioredoxins. *Science* 321, 952–956. doi: 10.1126/science.1156970
- Teng, N., Wang, J., Chen, T., Wu, X., Wang, Y., and Lin, J. (2006). Elevated CO<sub>2</sub> induces physiological, biochemical and structural changes in leaves of *Arabidopsis thaliana*. *New Phytol.* 172, 92–103. doi: 10.1111/j.1469-8137.2006.01818.x
- Trejo-Téllez, L. L., and Gómez-Merino, F. C. (2012). “Nutrient solutions for hydroponic systems,” in *Hydroponics – A Standard Methodology of Plant Biological Researches*. Ed. T. Asao (London: IntechOpen), 1–22. doi: 10.5772/37578
- Vatter, T., Neuhauser, B., Stetter, M., and Ludewig, U. (2015). Regulation of length and density of *Arabidopsis* root hairs by ammonium and nitrate. *J. Plant Res.* 128, 839–848.
- Vaughan, M. M., Huffaker, A., Schmeltz, E. A., Dafoe, N. J., Christensen, S., Sims, J., et al. (2014). Effects of elevated [CO<sub>2</sub>] on maize defence against mycotoxigenic *Fusarium verticillioides*. *Plant Cell Environ.* 37, 2691–2706.
- Wasternack, C., and Hause, B. (2013). Jasmonates: biosynthesis, perception, signal transduction and action in plant stress response, growth and development. An update to the 2007 review in *Annals of Botany*. *Ann. Bot.* 111, 1021–1058. doi: 10.1093/aob/mct067
- Williams, K., Percival, F., Merino, J., and Mooney, H. A. (1987). Estimation of tissue construction cost from heat of combustion and organic nitrogen content. *Plant Cell Environ.* 10, 725–734. doi: 10.1111/1356-3040.ep11604754
- Williams, A., Pétriacy, P., Schwarzenbacher, R. E., Beerling, D. J., and Ton, J. (2018). Mechanisms of glacial-to-future atmospheric CO<sub>2</sub> effects on plant immunity. *New Phytol.* 218, 752–761. doi: 10.1111/nph.15018
- Xu, G., Fan, X., and Miller, A. J. (2012). Plant nitrogen assimilation and use efficiency. *Ann. Rev. Plant Biol.* 63, 153–182. doi: 10.1146/annurev-arplant-042811-105532
- Yin, X. (2002). Responses of leaf nitrogen concentration and specific leaf area to atmospheric CO<sub>2</sub> enrichment: a retrospective synthesis across 62 species. *Global Change Biol.* 8, 631–642. doi: 10.1046/j.1365-2486.2002.00497.x
- Zavala, J. A., Nabity, P. D., and DeLucia, E. H. (2013). An emerging understanding of mechanisms governing insect herbivory under elevated CO<sub>2</sub>. *Ann. Rev. Entomol.* 58, 79–97.
- Zavala, J. A., Gog, L., and Giacometti, R. (2017). Anthropogenic increases in carbon dioxide modifies plant-insect interactions. *Ann. Appl. Biol.* 170, 68–77. doi: 10.1111/aab.12319.3
- Zhang, S., Li, X., Sun, Z., Shao, S., Hu, L., Ye, M., et al. (2015). Antagonism between phytohormone signalling underlies the variation in disease susceptibility of tomato plants under elevated CO<sub>2</sub>. *J. Exp. Bot.* 66, 1951–1963.
- Zhou, Y., Van Leeuwen, S. K., Pieterse, C. M. J., Bakker, P. A. H. M., and Van Wees, S. C. M. (2019). Effect of atmospheric CO<sub>2</sub> on plant defense against leaf and root pathogens of *Arabidopsis*. *Eur. J. Plant Physiol.* 154, 31–42. doi: 10.1007/s10658-019-01716-1

**Conflict of Interest:** The authors declare that the research was conducted in the absence of any commercial or financial relationships that could be construed as a potential conflict of interest.

Copyright © 2020 Martínez Henao, Demers, Grosser, Schedl, van Dam and Bede. This is an open-access article distributed under the terms of the Creative Commons Attribution License (CC BY). The use, distribution or reproduction in other forums is permitted, provided the original author(s) and the copyright owner(s) are credited and that the original publication in this journal is cited, in accordance with accepted academic practice. No use, distribution or reproduction is permitted which does not comply with these terms.





# Suppressor of Gamma Response 1 Modulates the DNA Damage Response and Oxidative Stress Response in Leaves of Cadmium-Exposed *Arabidopsis thaliana*

Sophie Hendrix<sup>1\*</sup>, Verena Iven<sup>1</sup>, Thomas Eekhout<sup>2,3</sup>, Michiel Huybrechts<sup>1</sup>, Ingeborg Pecqueur<sup>1</sup>, Nele Horemans<sup>1,4</sup>, Els Keunen<sup>1</sup>, Lieven De Veylder<sup>2,3</sup>, Jaco Vangronsveld<sup>1</sup> and Ann Cuypers<sup>1</sup>

<sup>1</sup> Environmental Biology, Centre for Environmental Sciences, Hasselt University, Diepenbeek, Belgium, <sup>2</sup> Department of Plant Biotechnology and Bioinformatics, Ghent University, Ghent, Belgium, <sup>3</sup> Center for Plant Systems Biology, VIB, Ghent, Belgium, <sup>4</sup> Biosphere Impact Studies, Belgian Nuclear Research Centre (SCKCEN), Mol, Belgium

## OPEN ACCESS

### Edited by:

Han Asard,  
University of Antwerp, Belgium

### Reviewed by:

Dawei Xue,  
Hangzhou Normal University, China  
Naoko Ohkama-Ohtsu,  
Tokyo University of Agriculture  
and Technology, Japan

### \*Correspondence:

Sophie Hendrix  
sophie.hendrix@uhasselt.be

### Specialty section:

This article was submitted to  
Plant Abiotic Stress,  
a section of the journal  
Frontiers in Plant Science

**Received:** 30 October 2019

**Accepted:** 13 March 2020

**Published:** 03 April 2020

### Citation:

Hendrix S, Iven V, Eekhout T,  
Huybrechts M, Pecqueur I,  
Horemans N, Keunen E, De Veylder L,  
Vangronsveld J and Cuypers A (2020)  
Suppressor of Gamma Response 1  
Modulates the DNA Damage  
Response and Oxidative Stress  
Response in Leaves  
of Cadmium-Exposed *Arabidopsis*  
*thaliana*. *Front. Plant Sci.* 11:366.  
doi: 10.3389/fpls.2020.00366

Cadmium (Cd) exposure causes an oxidative challenge and inhibits cell cycle progression, ultimately impacting plant growth. Stress-induced effects on the cell cycle are often a consequence of activation of the DNA damage response (DDR). The main aim of this study was to investigate the role of the transcription factor SUPPRESSOR OF GAMMA RESPONSE 1 (SOG1) and three downstream cyclin-dependent kinase inhibitors of the SIAMESE-RELATED (SMR) family in the Cd-induced DDR and oxidative challenge in leaves of *Arabidopsis thaliana*. Effects of Cd on plant growth, cell cycle regulation and the expression of DDR genes were highly similar between the wildtype and *smr4/5/7* mutant. In contrast, *sog1-7* mutant leaves displayed a much lower Cd sensitivity within the experimental time-frame and significantly less pronounced upregulations of DDR-related genes, indicating the involvement of SOG1 in the Cd-induced DDR. Cadmium-induced responses related to the oxidative challenge were disturbed in the *sog1-7* mutant, as indicated by delayed Cd-induced increases of hydrogen peroxide and glutathione concentrations and lower upregulations of oxidative stress-related genes. In conclusion, our results attribute a novel role to SOG1 in regulating the oxidative stress response and connect oxidative stress to the DDR in Cd-exposed plants.

**Keywords:** *Arabidopsis thaliana*, cadmium, DNA damage response, oxidative stress response, SIAMESE-related, suppressor of gamma response 1

## INTRODUCTION

Cadmium (Cd) is known to indirectly increase reactive oxygen species (ROS) production in plants, thereby causing oxidative stress (Rodríguez-Serrano et al., 2006; Cuypers et al., 2011). Although ROS fulfil important roles as signaling molecules, they can damage macromolecules such as proteins, lipids and DNA in cells when present in high concentrations (Gallego et al., 2012; Cuypers et al., 2016). In order to protect themselves against oxidative stress, plants possess an extensive



antioxidative defense system, consisting of both enzymatic and non-enzymatic antioxidants. An important non-enzymatic antioxidant in plants is glutathione (GSH), which functions in reducing hydrogen peroxide ( $H_2O_2$ ) and is also involved in Cd chelation (Jozefczak et al., 2012).

As a consequence of increased ROS production, Cd exposure was reported to cause DNA damage in a variety of plant species, including *Arabidopsis thaliana* (Wang et al., 2016; Cao et al., 2018), *Triticum vulgare* (Mutlu and Mutlu, 2015), *Oryza sativa* (Zhang et al., 2015), *Allium cepa* and *Lactuca sativa* (Silveira et al., 2017). When cells perceive DNA damage, the activity of cyclin-dependent kinases (CDKs) can be affected, thereby inhibiting cell cycle progression (Hu et al., 2016). During the classical cell cycle, CDK activity reaches two threshold levels: one for DNA replication and one for mitosis. In addition to the classical cell cycle, plant cells can also undergo endoreplication (also termed “endoreduplication”), a process that is involved in plant growth and development but is also often induced during stress conditions (De Veylder et al., 2011). During this alternative cell cycle mode, CDK activity only reaches the threshold for DNA replication but not that for mitosis. As a result, nuclear DNA is replicated without subsequent cell division, resulting in endopolyploidy. The reduced mitotic CDK activity can be accomplished in three ways: (1) transcriptional downregulation of mitotic cyclins and CDKs, (2) proteasome-mediated degradation of mitotic cyclins, and (3) inhibition of CDK activity by CDK inhibitors (De Veylder et al., 2011).

Plant CDK inhibitors are classified into two families: the KIP-RELATED PROTEINS (KRPs) and SIAMESE-RELATED (SMR) proteins. Whereas SMRs appear to be plant-specific, KRPs display limited sequence identity with CDK inhibitors from other organisms. To date, 7 KRPs and 17 SMR proteins have been identified in *A. thaliana*. Some SMR proteins have been suggested to play a role in the DNA damage response (DDR) (Yi et al., 2014; Kumar and Larkin, 2017). Yi et al. (2014) demonstrated that exposure to hydroxyurea induced DNA double strand breaks (DSBs), likely through induction of ROS, and increased *SMR5* and *SMR7* transcript levels in *A. thaliana* roots. This transcriptional induction of *SMR5* and *SMR7* depends on SUPPRESSOR OF GAMMA RESPONSE 1 (SOG1), a NAC [no apical meristem (NAM), *A. thaliana* transcription activation factor (ATAF1/2) and cup-shaped cotyledon (CUC2)] transcription factor, which is phosphorylated and thereby activated by the cell cycle checkpoint kinase ATAXIA-TELANGIECTASIA MUTATED (ATM) in response to the detection of DSBs (Yoshiyama et al., 2013). This plant-specific transcription factor plays a key role in the plant DDR and its function strongly resembles that of the human p53, as it regulates various processes including cell cycle progression, DNA repair and programmed cell death (Yoshiyama, 2015; Ogita et al., 2018). Furthermore, SOG1 can also be phosphorylated by ATM AND RAD3-RELATED (ATR), activated in response to single strand breaks (SSBs) and stalled replication forks (Sjogren et al., 2015). In addition to *SMR5* and *SMR7*, *OXIDATIVE SIGNAL INDUCIBLE 1 (OXI1)* was shown to be a direct target gene of

SOG1 (Ogita et al., 2018). Interestingly, *OXI1* plays a key role in the oxidative signaling pathway induced in *A. thaliana* upon Cd exposure (Smeets et al., 2013; Schellingen et al., 2015b). Through activation of MAP kinases (MPKs), *OXI1* enhances the expression and activity of ethylene biosynthesis enzymes, thereby contributing to the fast increase in ethylene release observed in plants acutely exposed to Cd (Schellingen et al., 2014; Schellingen et al., 2015b).

As results of our previous study have shown that Cd exposure significantly inhibited both cell division and endoreplication and increased expression levels of several direct SOG1 target genes, including *SMR4*, *SMR5* and *SMR7* in *A. thaliana* leaves (Hendrix et al., 2018), the main hypothesis of this study is that SOG1 mediates the Cd-induced inhibition of cell cycle progression in leaves. Furthermore, we also aim to determine the involvement of *SMR4*, *SMR5* and *SMR7* in this response. To this end, Cd-induced responses are compared between leaves of wild-type (WT), *smr4/5/7* and *sog1-7* knockout *A. thaliana* plants. Cadmium-induced effects on cell cycle progression, DNA repair and programmed cell death – all known to be regulated by SOG1 – are determined and compared between leaves of all genotypes. In addition, the involvement of SOG1 in the Cd-induced oxidative stress response is analyzed.

## MATERIALS AND METHODS

### Generation of the *smr4/5/7* Mutant

A construct targeting two distinct sites in the *SMR4* gene (*AT5G02220*) was designed using the pEn-Chimera and pDe-Cas9 vectors as described by Fauser et al. (2014). The resulting construct was transformed into *Arabidopsis smr5/7* mutant plants (Yi et al., 2014) using the floral dip method (Clough and Bent, 1998). Primary transformants were selected on agar plates containing kanamycin and propagated in the greenhouse, after which kanamycin-sensitive T2 plants were selected and genotyped at the *SMR4* locus using Sanger sequencing. Oligos to generate the construct and primers for sequencing are listed in **Supplementary Table S1**.

### Growth Conditions and Cadmium Exposure

Wild-type, *smr4/5/7* and *sog1-7* (Sjogren et al., 2015) mutant *A. thaliana* seeds (ecotype Col-0) were surface-sterilized and cultivated in a hydroponic system using a modified Hoagland solution (Smeets et al., 2008). Growth conditions were set as previously described (Keunen et al., 2011). At day 14 or day 19 after sowing, plants were either exposed to 5  $\mu$ M  $CdSO_4$  via the roots or further grown under control conditions. Individual leaves or complete leaf rosettes were harvested after 24 h, 72 h or 8 days of exposure. Unless otherwise stated, samples were snap-frozen in liquid nitrogen and stored at  $-80^\circ C$  until further analysis. **Supplementary Figure S1** provides a visual representation of the different Cd exposure set-ups employed in this study. The mutant genotype of *smr4/5/7* and *sog1-7* plants was verified as described in **Supplementary Table S2**.

## Flow Cytometric Analysis of Endoreplication

To determine the extent of endoreplication, nuclear ploidy levels were determined in individual leaves using the CyStain® PI Absolute P kit (Sysmex Partec, Görlitz, Germany). Before harvest, leaves were scanned using a conventional flatbed scanner to enable determination of leaf surface area in ImageJ (Schneider et al., 2012). Sample preparation and flow cytometric analysis were performed as described by Hendrix et al. (2018). Data were analyzed using FCS Express 4 software (De Novo Software, Pasadena, CA, USA). The endoreplication index indicating the average number of endocycles per cell was calculated as follows:  $[(0 \times \% 2C) + (1 \times \% 4C) + (2 \times \% 8C) + (3 \times \% 16C) + (4 \times \% 32C)] / 100$  (Cookson et al., 2006; Boudolf et al., 2009).

## Determination of Element Concentrations

In order to determine leaf Cd concentrations, complete leaf rosettes were harvested and rinsed using distilled water. Subsequently, samples were oven-dried at 80°C and digested in HNO<sub>3</sub> (70–71%) in a heat block. Cadmium concentrations in the leaf extracts were determined using inductively coupled plasma-optical emission spectrometry (ICP-OES 710, Agilent Technologies, Santa Clara, CA, USA).

## Gene Expression Analysis

To determine gene expression levels in complete rosettes, frozen samples were first ground using two stainless steel beads in the Retsch Mixer Mill MM 400 (Retsch, Haan, Germany). RNA extraction and cDNA synthesis were performed as previously described (Hendrix et al., 2018). Quantitative real-time PCR (qPCR) was performed using the 7500 Fast Real-Time PCR System (Applied Biosystems, Thermo Fisher Scientific, Waltham, MA, USA) and the Quantinova™ SYBR® Green PCR Kit (Qiagen, Hilden, Germany). Reactions contained 2 µL diluted cDNA sample, 5 µL Quantinova™ SYBR® Green dye, 0.05 µL ROX reference dye, 2.35 µL RNase-free H<sub>2</sub>O and forward and reverse primers (300 nM each, unless stated otherwise in **Supplementary Table S3**) in a total reaction volume of 10 µL. Amplification occurred at the following cycling conditions: 2 min at 95°C, 40 cycles of 5 s at 95°C and 25 s at 60°C. A dissociation curve was generated to confirm product specificity. Relative gene expression levels were determined via the  $2^{-\Delta C_q}$  method and normalized against the expression of at least three stably expressed reference genes, selected using the GrayNorm algorithm (Remans et al., 2014). Forward and reverse primer sequences are shown in **Supplementary Table S3**. **Supplementary Table S4** shows the qPCR parameters according to the Minimum Information for publication of qPCR Experiments (MIQE) guidelines (Bustin et al., 2009).

## Determination of Glutathione Levels and Redox State

Concentrations of total GSH and glutathione disulfide (GSSG) were determined in complete leaf rosettes using a plate reader method for measuring redox couples adapted from Queval and Noctor (2007), as described by dos Reis et al. (2018).

## Determination of Hydrogen Peroxide Levels

Relative H<sub>2</sub>O<sub>2</sub> levels were determined in complete leaf rosettes using the Amplex™ Red Hydrogen Peroxide/Peroxidase Assay Kit (Invitrogen, Thermo Fisher Scientific), as previously described by Hendrix et al. (2018).

## Determination of Lipid Peroxidation Levels

To determine the extent of lipid peroxidation, the concentration of thiobarbituric acid-reactive metabolites (TBArm) was determined in complete leaf rosettes. Samples were homogenized in 1 mL 0.1% trichloroacetic acid (TCA) using mortar and pestle. After centrifugation (20 000 g; 10 min; 4°C), 400 µL supernatant was added to 1 mL 0.5% TBA and samples were incubated at 95°C for 30 min, quickly cooled down and again centrifuged. The absorbance of the supernatant at 532 nm was determined and corrected for non-specific absorbance at 600 nm. All samples were analyzed *in duplo*.

## Statistical Analysis

All statistical analyses were performed in R version 3.3.1 (R Core Team, 2019). Normal distribution and homoscedasticity of the data were verified using the Shapiro-Wilk and Bartlett's test, respectively. When these assumptions were not met, data were transformed (square root, inverse, exponent, logarithm). Gene expression data were standardly log-transformed. Depending on the number of variables, data were statistically analyzed using either a one-way or two-way ANOVA within each time point, followed by a *post hoc* Tukey-Kramer test to correct for multiple comparisons. If the (transformed) data did not meet the normality assumption, a non-parametric Kruskal-Wallis test was used, followed by the Wilcoxon rank sum test. Outliers were determined using the Extreme Studentized Deviate method (GraphPad Software, San Diego, CA, USA) at significance level 0.05.

## RESULTS

Cadmium is well known to disturb plant growth and development and was shown to significantly inhibit cell division as well as endoreplication in *A. thaliana* leaves in a time-dependent manner (Hendrix et al., 2018). Furthermore, previous research demonstrated that the expression of *SMR4*, *SMR5* and *SMR7* was strongly induced in *A. thaliana* leaves upon Cd exposure (Hendrix et al., 2018). Via ChIP sequencing, these genes were shown to be direct target genes of the transcription factor SOG1 (Bourbousse et al., 2018; Ogita et al., 2018). Therefore, this study aimed to investigate the involvement of these plant-specific CDK inhibitors and their upstream regulator SOG1 in Cd-induced plant responses. To this end, responses were compared between leaves of WT, *smr4/5/7* triple knockouts and *sog1-7* mutant *A. thaliana* plants grown in hydroponics and exposed to 5 µM Cd in a short-term (24 and 72 h) and long-term (8 days) set-up (**Supplementary Figure S1**).

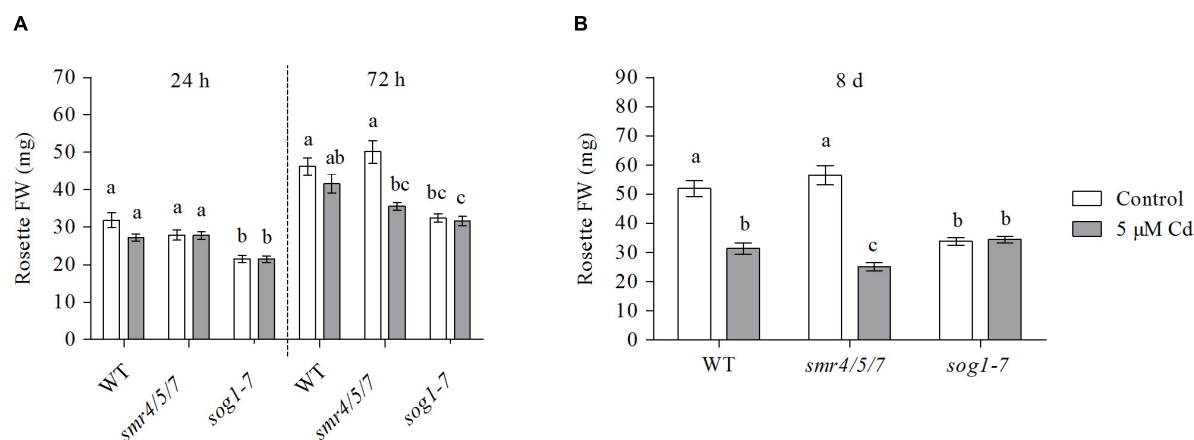


**FIGURE 1 |** Rosette fresh weight (mg) of hydroponically grown wild-type (WT), *smr4/5/7* and *sog1-7* mutant *A. thaliana* plants exposed to 0 (white bars) or 5  $\mu$ M CdSO<sub>4</sub> (gray bars) for **(A)** 24 h or 72 h from day 19 after sowing or **(B)** 8 days from day 14 after sowing. Values represent the average  $\pm$  S.E. of at least 9 biological replicates. Different letters indicate significant differences between conditions (2-way ANOVA per exposure duration;  $P < 0.05$ ).

## Leaf Growth of the *sog1-7* Mutant Is Not Affected by Cadmium Exposure

Leaf fresh weight (FW) of the *smr4/5/7* mutant did not differ from that of WT plants grown under control conditions (**Figure 1**). In contrast, leaf FW of *sog1-7* mutant plants was significantly lower (approximately 1.5-fold) as compared to that of WT plants. The FW of both WT and *smr4/5/7* leaves was negatively affected by exposure to 5  $\mu$ M Cd, a response which was most pronounced after 8 days. However, rosette weight of *sog1-7* mutants was not affected by Cd exposure at any of the time points studied (**Figure 1** and **Supplementary Table S5**), suggesting that this genotype is less sensitive to Cd than WT plants within the experimental time frame.

Rosette diameter and the surface area of leaves 1 (the oldest rosette leaf) and 3 were compared between plants of all genotypes grown under control conditions or exposed to 5  $\mu$ M Cd for 8 days. Whereas leaf 1 was already present at the start of Cd exposure, leaf 3 had only just emerged when exposure was

initiated. Results show a pattern highly similar to that observed for leaf FW. Indeed, rosette diameter and the surface area of the leaves analyzed of *sog1-7* mutants were significantly smaller as compared to those of WT plants grown under control conditions, whereas they were highly similar between *smr4/5/7* mutants and WT plants (**Table 1**). Furthermore, Cd exposure negatively affected rosette diameter and leaf surface area of WT and *smr4/5/7* plants, whereas this response was generally absent in *sog1-7* mutants (**Table 1**), again pointing toward a lower Cd sensitivity of this genotype.


## Cadmium-Induced Effects on Endoreplication Are Less Pronounced in Leaves of the *sog1-7* Mutant

The extent of endoreplication in leaves 1 and 3 was compared between WT, *smr4/5/7* and *sog1-7* mutant plants grown under control conditions or exposed to 5  $\mu$ M Cd for 8 days. Representative histograms displaying the ploidy distribution


**TABLE 1 |** Rosette diameter (mm), surface area (mm<sup>2</sup>) of leaves 1 and 3 and representative pictures of hydroponically grown wild-type (WT), *smr4/5/7* and *sog1-7* mutant *A. thaliana* plants exposed to 0 or 5  $\mu$ M CdSO<sub>4</sub> for 8 days from day 14 after sowing.

	WT		<i>smr4/5/7</i>		<i>sog1-7</i>	
	Control	5 $\mu$ M Cd	Control	5 $\mu$ M Cd	Control	5 $\mu$ M Cd
Rosette diameter (mm)	33.67 $\pm$ 1.17 <sup>a</sup>	22.02 $\pm$ 0.37 <sup>b</sup>	35.67 $\pm$ 1.80 <sup>a</sup>	20.99 $\pm$ 0.29 <sup>b</sup>	25.81 $\pm$ 0.43 <sup>c</sup>	23.19 $\pm$ 0.48 <sup>bc</sup>
Surface area leaf 1 (mm <sup>2</sup> )	36.44 $\pm$ 2.27 <sup>a</sup>	23.59 $\pm$ 0.80 <sup>b</sup>	37.18 $\pm$ 3.26 <sup>ac</sup>	23.19 $\pm$ 1.44 <sup>b</sup>	32.39 $\pm$ 0.74 <sup>c</sup>	31.16 $\pm$ 1.06 <sup>c</sup>
Surface area leaf 3 (mm <sup>2</sup> )	57.34 $\pm$ 2.72 <sup>a</sup>	30.58 $\pm$ 2.13 <sup>bd</sup>	63.29 $\pm$ 4.31 <sup>a</sup>	28.57 $\pm$ 1.30 <sup>b</sup>	45.07 $\pm$ 1.13 <sup>c</sup>	35.67 $\pm$ 0.53 <sup>d</sup>


  




WT  
Control




5  $\mu$ M Cd




*smr4/5/7*  
Control



5  $\mu$ M Cd



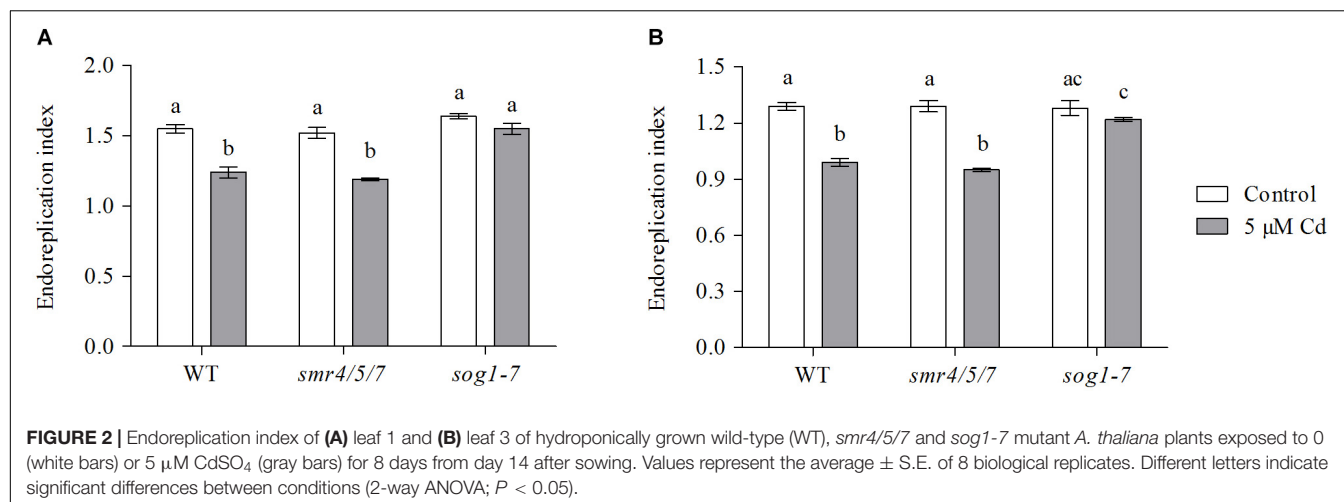
*sog1-7*  
Control



5  $\mu$ M Cd

1 cm scale bar is shown next to the WT Control plant.

Values represent the average  $\pm$  S.E. of 8 biological replicates. Different letters indicate significant differences between conditions (2-way ANOVA;  $P < 0.05$ ).



within each experimental condition are shown in **Supplementary Figure S2**). The obtained results show that the endoreplication index – representing the average number of endocycles per cell – of these leaves was significantly lower in Cd-exposed WT and *smr4/5/7* mutant plants as compared to their control counterparts. This effect was not observed in the *sog1-7* mutant (**Figure 2**). These data support the lower Cd sensitivity of the *sog1-7* mutant.

### Leaf Cadmium Concentrations Are Similar Between WT, *smr4/5/7* and *sog1-7* Plants

To investigate whether the observed difference in Cd sensitivity was related to the extent of Cd uptake in all genotypes, leaf Cd concentrations were compared between WT, *smr4/5/7* and *sog1-7* mutant plants exposed to 5  $\mu\text{M}$  Cd for 24 h, 72 h or 8 days. Results demonstrate that Cd concentrations in leaf rosettes did not differ between mutant and WT plants at any of the time points investigated (**Table 2**; **Supplementary Table S5**).

### Cadmium-Induced Effects on the Expression of Genes Involved in the DNA Damage Response Are Less Pronounced in Leaves of the *sog1-7* Mutant

As negative effects of stress factors on cell cycle progression are an intrinsic part of the DDR, this response was further investigated at the transcriptional level in leaves of the *sog1-7* mutant to gain more insight into the mechanisms underlying its lowered Cd sensitivity. In addition to regulating cell cycle progression, the DDR also coordinates DNA repair and cell death. Therefore, expression levels of selected genes related to each of these three mechanisms (cell cycle regulation, DNA repair and cell death) were compared between leaves of WT and *sog1-7* mutant plants grown under control conditions or exposed to 5  $\mu\text{M}$  Cd for 24 and 72 h (short-term). Expression levels of many of the genes analyzed were considerably increased by

Cd in leaves of WT plants after both exposure durations. For most genes, this response was significantly less pronounced in the *sog1-7* mutant after 24 h of exposure and even completely absent after 72 h of exposure (**Table 3**). Whereas cell death-related genes responded most strongly after 24 h of Cd exposure, the upregulation of genes involved in cell cycle regulation and DNA repair was mainly pronounced after 72 h of exposure (**Table 3**).

To determine (1) whether the difference in response between leaves of WT plants and *sog1-7* mutants could also be observed after long-term exposure and (2) whether the absence of a differential response between WT plants and *smr4/5/7* mutants at the cell cycle level coincided with a lack of differential gene expression, a subset of these genes was measured in leaves of *sog1-7* mutant plants after 8 days of exposure and *smr4/5/7* mutants upon 24 and 72 h of exposure. As shown in **Table 4**, transcript levels of the majority of the genes studied were also significantly upregulated in leaves of the WT after long-term Cd exposure. Again, this response was completely absent in leaves of the *sog1-7* mutant (**Table 4**). Furthermore, highly similar responses were observed in leaves of the *smr4/5/7* mutant upon short-term exposure (**Table 5**), which agrees with the fact that Cd sensitivity is unaltered in this genotype.

**TABLE 2 |** Cadmium concentrations ( $\text{mg kg}^{-1}$  DW) in leaf rosettes of hydroponically grown wild-type (WT), *smr4/5/7* and *sog1-7* mutant *A. thaliana* plants exposed to 5  $\mu\text{M}$   $\text{CdSO}_4$  for 24 h or 72 h from day 19 after sowing or for 8 days from day 14 after sowing.

	WT	<i>smr4/5/7</i>	<i>sog1-7</i>
24 h	748.19 $\pm$ 29.82 <sup>ab</sup>	831.03 $\pm$ 33.15 <sup>a</sup>	616.07 $\pm$ 47.89 <sup>b</sup>
72 h	1124.67 $\pm$ 106.78 <sup>a</sup>	1414.87 $\pm$ 48.57 <sup>a</sup>	1161.43 $\pm$ 69.87 <sup>a</sup>
8 d	1479.58 $\pm$ 479.91 <sup>a</sup>	1209.00 $\pm$ 259.97 <sup>a</sup>	1320.96 $\pm$ 49.37 <sup>a</sup>

Values represent the average  $\pm$  S.E. of 3 biological replicates. Different letters indicate significant differences between conditions (1-way ANOVA per exposure duration;  $P < 0.05$ ). Cadmium concentrations in non-exposed plants were below the detection limit.



**TABLE 3 |** Normalized expression levels of genes involved in the DNA damage response in leaf rosettes of hydroponically grown wild-type (WT) and *sog1-7* mutant *A. thaliana* plants exposed to 5  $\mu$ M CdSO<sub>4</sub> for 24 h or 72 h from day 19 after sowing.

24 h			72 h	
WT	<i>sog1-7</i>	Gene	WT	<i>sog1-7</i>
<b>Cell cycle regulation</b>				
1.75 $\pm$ 0.10	1.86 $\pm$ 0.11	<i>SOG1</i>	1.66 $\pm$ 0.07	1.22 $\pm$ 0.04
1.35 $\pm$ 0.16	2.22 $\pm$ 0.22	<i>SMR4</i>	3.03 $\pm$ 0.31	1.08 $\pm$ 0.06*
2.85 $\pm$ 0.20	1.33 $\pm$ 0.07*	<i>SMR5</i>	9.99 $\pm$ 1.77	2.42 $\pm$ 0.36*
1.72 $\pm$ 0.44	0.92 $\pm$ 0.05	<i>SMR7</i>	54.94 $\pm$ 10.46	2.46 $\pm$ 0.63*
0.65 $\pm$ 0.07	1.30 $\pm$ 0.01*	<i>WEE1</i>	1.59 $\pm$ 0.09	1.28 $\pm$ 0.05*
0.35 $\pm$ 0.04	1.16 $\pm$ 0.14*	<i>CYC1;1</i>	2.28 $\pm$ 0.27	1.38 $\pm$ 0.07*
<b>DNA repair</b>				
0.61 $\pm$ 0.03	1.14 $\pm$ 0.08*	<i>PARP1</i>	1.91 $\pm$ 0.18	1.20 $\pm$ 0.00*
2.01 $\pm$ 0.03	1.84 $\pm$ 0.15	<i>PARP2</i>	13.13 $\pm$ 1.90	2.39 $\pm$ 0.17*
0.75 $\pm$ 0.10	1.29 $\pm$ 0.08	<i>BRCA1</i>	5.40 $\pm$ 0.52	1.66 $\pm$ 0.12*
3.12 $\pm$ 0.20	1.43 $\pm$ 0.18*	<i>XRCC1</i>	1.71 $\pm$ 0.03	0.95 $\pm$ 0.02*
2.50 $\pm$ 0.14	1.63 $\pm$ 0.25*	<i>LIG4</i>	1.75 $\pm$ 0.01	1.13 $\pm$ 0.08*
0.61 $\pm$ 0.06	1.42 $\pm$ 0.15*	<i>RAD51</i>	4.24 $\pm$ 0.50	1.51 $\pm$ 0.05*
<b>Cell death</b>				
22.02 $\pm$ 1.97	3.32 $\pm$ 1.02*	<i>SAG14</i>	4.26 $\pm$ 0.69	0.58 $\pm$ 0.07*
2.53 $\pm$ 0.23	1.19 $\pm$ 0.18*	<i>SAG18</i>	1.91 $\pm$ 0.11	1.39 $\pm$ 0.07*
1.97 $\pm$ 0.17	1.65 $\pm$ 0.05	<i>SAG20</i>	2.41 $\pm$ 0.23	1.45 $\pm$ 0.11*
14.86 $\pm$ 1.20	7.02 $\pm$ 2.14	<i>SAG21</i>	3.15 $\pm$ 0.55	0.73 $\pm$ 0.12*
4.74 $\pm$ 0.51	1.21 $\pm$ 0.28*	<i>ATG8H</i>	2.19 $\pm$ 0.14	1.13 $\pm$ 0.13*
5.25 $\pm$ 0.79	1.68 $\pm$ 0.40*	<i>BI1</i>	1.72 $\pm$ 0.06	0.62 $\pm$ 0.05*
5.63 $\pm$ 0.84	3.88 $\pm$ 0.77	<i>MC8</i>	2.07 $\pm$ 0.03	1.10 $\pm$ 0.01

Values represent the average  $\pm$  S.E. of 5 biological replicates and are expressed relative to the average of the same genotype under control conditions at the same time point (set at 1.00). Significant Cd-induced upregulations and downregulations for both normalized and non-normalized data are highlighted in green and red, respectively. Asterisks (\*) indicate a significantly different Cd-induced response between both genotypes for both normalized and non-normalized data (2-way ANOVA per exposure duration;  $P < 0.05$ ). Direct SOG1 target genes according to Ogita et al. (2018) are underlined. ATG8H, autophagy 8H; BI1, Bax inhibitor 1; BRCA1, breast cancer susceptibility 1; CYC, cyclin; MC8, metacaspase 8; PARP, poly(ADP-ribose) polymerase; SOG1, suppressor of gamma response 1; RAD51, DNA repair protein RAD51 homolog 1; SAG, senescence-associated gene; SMR, SIAMESE-related; WEE1, WEE1 kinase homolog; XRCC1, homolog of X-ray repair cross complementing 1.

## Cadmium-Induced Effects on Expression Levels of Oxidative Stress-Related Genes Are Less Pronounced in Leaves of the *sog1-7* Mutant

Taken together, the data obtained in the first part of this study indicate that the *sog1-7* mutant is less sensitive to acute Cd exposure. As oxidative stress is an important process well known to be involved in Cd-induced stress responses (Cuypers et al., 2011; Gallego et al., 2012), the involvement of SOG1 in oxidative stress and signaling pathways was investigated in the second part of this study. To this end, transcript levels of oxidative stress-related genes were determined in leaves of WT and *sog1-7* mutant plants grown under control conditions or exposed to 5  $\mu$ M Cd for 24 and 72 h. As shown in Table 6, Cd exposure significantly increased the expression of five oxidative stress hallmark genes in WT leaves. These increases were significantly less pronounced or even completely absent in leaves of the *sog1-7* mutant. Similar

**TABLE 4 |** Normalized expression levels of genes involved in the DNA damage response in leaf rosettes of hydroponically grown wild-type (WT) and *sog1-7* mutant *A. thaliana* plants exposed to 5  $\mu$ M CdSO<sub>4</sub> for 8 d from day 14 after sowing.

Gene	WT	<i>sog1-7</i>
<b>Cell cycle regulation</b>		
<i>SMR4</i>	1.59 $\pm$ 0.18	0.87 $\pm$ 0.11
<i>SMR5</i>	2.71 $\pm$ 0.47	1.19 $\pm$ 0.07*
<i>SMR7</i>	3.84 $\pm$ 1.18	0.91 $\pm$ 0.08*
<i>WEE1</i>	1.43 $\pm$ 0.07	1.02 $\pm$ 0.05
<i>CYC1;1</i>	1.17 $\pm$ 0.12	1.11 $\pm$ 0.09
<b>DNA repair</b>		
<i>PARP2</i>	3.87 $\pm$ 0.88	1.42 $\pm$ 0.15*
<i>BRCA1</i>	1.53 $\pm$ 0.12	1.09 $\pm$ 0.03
<i>XRCC1</i>	1.40 $\pm$ 0.05	0.96 $\pm$ 0.10
<b>Cell death</b>		
<i>SAG14</i>	9.09 $\pm$ 4.28	0.34 $\pm$ 0.09*
<i>SAG18</i>	1.89 $\pm$ 0.13	1.04 $\pm$ 0.04
<i>ATG8H</i>	2.51 $\pm$ 0.58	1.00 $\pm$ 0.06
<i>BI1</i>	2.21 $\pm$ 0.18	0.82 $\pm$ 0.12*
<i>MC8</i>	5.27 $\pm$ 0.78	0.79 $\pm$ 0.20*

Values represent the average  $\pm$  S.E. of 5 biological replicates and are expressed relative to the average of the same genotype under control conditions (set at 1.00). Significant Cd-induced upregulations for both normalized and non-normalized data are highlighted in green. Asterisks (\*) indicate a significantly different Cd-induced response between both genotypes for both normalized and non-normalized data (2-way ANOVA;  $P < 0.05$ ). Direct SOG1 target genes according to Ogita et al. (2018) are underlined. ATG8H, autophagy 8H; BI1, Bax inhibitor 1; BRCA1, breast cancer susceptibility 1; CYC, cyclin; MC8, metacaspase 8; PARP, poly(ADP-ribose) polymerase; SAG, senescence-associated gene; SMR, SIAMESE-related; WEE1, WEE1 kinase homolog; XRCC1, homolog of X-ray repair cross complementing 1.

responses were observed for *RBOHC* and *RBOHF*, encoding NADPH oxidases involved in superoxide (O<sub>2</sub><sup>•−</sup>) production. Furthermore, Cd-induced effects on transcript levels of several antioxidative genes were significantly less pronounced in leaves of the mutant (Table 6).

As *OXII* was recently described as a SOG1 target gene (Ogita et al., 2018) and is a key player in the Cd-induced oxidative signaling response (Opdenakker et al., 2012; Schellingen et al., 2015b), the expression of genes involved in the OXI1-MPK signaling pathway was also compared between leaves of both genotypes upon short-term Cd exposure. All genes analyzed were significantly upregulated upon Cd exposure in WT plants, whereas they were significantly less affected in the *sog1-7* mutant (Table 6), pointing toward the involvement of SOG1 in oxidative signaling processes. The expression of the ethylene biosynthesis genes *ACS2* and *ACS6* and the ethylene marker gene *ERF1* showed the same pattern (Table 6). Similarly, transcript levels of GSH biosynthesis genes *GSH1* and *GSH2* were increased by Cd exposure in leaves of WT plants but not in *sog1-7* mutants (Table 6).

The expression of most genes involved in the DNA damage response and the oxidative stress response did not differ between leaves of WT plants and *sog1-7* mutants grown under control conditions (Supplementary Table S6), suggesting that SOG1 is mostly involved in transcriptional regulation in stress-exposed plants.

**TABLE 5 |** Normalized expression levels of genes involved in the DNA damage response in leaf rosettes of hydroponically grown wild-type (WT) and *smr4/5/7* mutant *A. thaliana* plants exposed to 5  $\mu$ M CdSO<sub>4</sub> for 24 h or 72 h from day 19 after sowing.

24 h		Gene	72 h	
WT	<i>smr4/5/7</i>		WT	<i>smr4/5/7</i>
Cell cycle regulation				
2.00 ± 0.22	2.07 ± 0.12	<i>SOG1</i>	1.99 ± 0.16	1.80 ± 0.08
0.82 ± 0.11	0.73 ± 0.06	<i>WEE1</i>	1.97 ± 0.12	1.80 ± 0.10
0.58 ± 0.10	0.47 ± 0.08	<i>CYCB1;1</i>	1.71 ± 0.14	1.68 ± 0.23
DNA repair				
1.56 ± 0.14	2.20 ± 0.12	<i>PARP2</i>	4.08 ± 1.30	3.46 ± 0.19
1.08 ± 0.13	0.81 ± 0.11	<i>BRCA1</i>	2.16 ± 0.16	2.29 ± 0.16
2.84 ± 0.31	3.59 ± 0.16	<i>XRCC1</i>	1.74 ± 0.12	1.60 ± 0.10
Cell death				
27.40 ± 3.82	34.65 ± 3.83	<i>SAG14</i>	5.87 ± 1.55	3.39 ± 0.75
2.44 ± 0.06	2.83 ± 0.04	<i>SAG18</i>	1.75 ± 0.18	1.67 ± 0.19
6.68 ± 0.98	8.38 ± 0.97	<i>ATG8H</i>	2.20 ± 0.45	1.54 ± 0.18
5.27 ± 0.77	7.15 ± 0.61	<i>BI1</i>	2.03 ± 0.15	1.68 ± 0.05
10.45 ± 1.12	8.99 ± 0.82	<i>MC8</i>	7.00 ± 0.69	4.75 ± 0.49

Values represent the average ± S.E. of 5 biological replicates and are expressed relative to the average of the same genotype under control conditions at the same time point (set at 1.00). Significant Cd-induced upregulations and downregulations for both normalized and non-normalized data are highlighted in green and red, respectively (2-way ANOVA per exposure duration;  $P < 0.05$ ). Direct SOG1 target genes according to Ogita et al. (2018) are underlined. *ATG8H*, autophagy 8H; *BI1*, Bax inhibitor 1; *BRCA1*, breast cancer susceptibility 1; *CYC*, cyclin; *MC8*, metacaspase 8; *PARP*, poly(ADP-ribose) polymerase; *SOG1*, suppressor of gamma response 1; *SAG*, senescence-associated gene; *WEE1*, WEE1 kinase homolog; *XRCC1*, homolog of X-ray repair cross complementing 1.

## Cadmium-Induced Glutathione Biosynthesis Is Delayed in Leaves of the *sog1-7* Mutant

To investigate whether the lack of induction of both GSH biosynthesis genes upon Cd exposure in the *sog1-7* mutant was reflected at the metabolite level, GSH concentrations and redox state were determined in leaves of WT plants and *sog1-7* mutants exposed to Cd for 24 h, 72 h and 8 days.

After 24 h of exposure, reduced GSH levels did not change in either genotype (Figure 3A). In contrast, GSSG concentrations significantly decreased (Figure 3B), resulting in an elevated GSH/GSSG ratio (Figure 3C). This response was highly similar between both genotypes. After 72 h of exposure, reduced GSH levels were significantly increased in leaves of WT plants, whereas this effect was not observed in the *sog1-7* mutant (Figure 3A). The negative effect of Cd exposure on GSSG levels persisted after 72 h in both genotypes (Figure 3B). After 8 days of exposure, reduced GSH levels were also significantly increased in leaves of the *sog1-7* mutant, although to a smaller extent than in WT leaves (Figure 3A). In contrast, GSSG concentrations were no longer affected by Cd exposure after this prolonged exposure duration (Figure 3B). It is interesting to notice that reduced GSH concentrations were generally slightly higher in mutant as compared to WT leaves under control conditions (Figure 3A).

**TABLE 6 |** Normalized expression levels of genes involved in the oxidative stress response in leaf rosettes of hydroponically grown wild-type (WT) and *sog1-7* mutant *A. thaliana* plants exposed to 5  $\mu$ M CdSO<sub>4</sub> for 24 h or 72 h from day 19 after sowing.

24 h			72 h	
WT	<i>sog1-7</i>	Gene	WT	<i>sog1-7</i>
Oxidative stress markers				
9.81 ± 1.81	2.70 ± 0.21*	<i>UPOX</i>	5.14 ± 1.32	2.72 ± 0.36
14.92 ± 2.15	2.12 ± 0.35*	<i>TI1</i>	5.12 ± 0.28	2.59 ± 0.23*
20.44 ± 3.07	5.79 ± 1.29*	<i>AT1G19020</i>	2.87 ± 0.24	0.98 ± 0.08
17.90 ± 3.33	1.49 ± 0.59*	<i>AT1G05340</i>	8.10 ± 1.44	2.00 ± 0.84*
16.22 ± 2.53	2.01 ± 0.46*	<i>TIR-class</i>	2.11 ± 0.23	0.22 ± 0.01*
Pro-oxidants				
48.25 ± 9.99	10.28 ± 1.90*	<i>RBOHC</i>	6.46 ± 2.37	1.03 ± 0.30*
2.25 ± 0.33	2.16 ± 0.26	<i>RBOHD</i>	2.16 ± 0.12	1.57 ± 0.01
3.61 ± 0.12	1.84 ± 0.33	<i>RBOHF</i>	3.46 ± 0.33	1.89 ± 0.09*
Antioxidants				
2.09 ± 0.28	0.62 ± 0.11*	<i>CSD1</i>	0.66 ± 0.05	0.20 ± 0.02*
0.45 ± 0.08	0.42 ± 0.14	<i>CSD2</i>	0.22 ± 0.02	0.18 ± 0.01
0.74 ± 0.25	3.35 ± 0.44	<i>FSD1</i>	0.63 ± 0.23	1.93 ± 0.49
1.75 ± 0.20	1.07 ± 0.07*	<i>APX1</i>	0.83 ± 0.14	0.50 ± 0.10
6.50 ± 1.19	3.34 ± 0.38	<i>APX2</i>	3.36 ± 0.45	1.38 ± 0.25*
2.78 ± 0.26	1.36 ± 0.19*	<i>CAT1</i>	1.23 ± 0.12	0.56 ± 0.06*
0.50 ± 0.06	0.81 ± 0.03	<i>CAT2</i>	0.73 ± 0.04	0.85 ± 0.05
1.88 ± 0.05	1.22 ± 0.11*	<i>CAT3</i>	1.73 ± 0.39	1.04 ± 0.18
Oxidative signalling				
31.50 ± 3.77	8.21 ± 0.58*	<i>OXI1</i>	9.72 ± 2.93	2.09 ± 0.36*
3.80 ± 0.18	2.36 ± 0.30	<i>MPK3</i>	2.42 ± 0.18	1.07 ± 0.05*
2.15 ± 0.12	1.39 ± 0.11*	<i>MPK6</i>	1.18 ± 0.06	0.96 ± 0.01
28.54 ± 4.28	5.33 ± 2.06*	<i>ACS2</i>	8.16 ± 1.00	1.46 ± 0.43*
8.69 ± 0.66	5.62 ± 0.72	<i>ACS6</i>	3.03 ± 0.43	1.16 ± 0.05*
47.71 ± 4.79	29.73 ± 3.85	<i>ERF1</i>	5.61 ± 1.59	1.19 ± 0.13
Glutathione biosynthesis				
1.42 ± 0.03	1.10 ± 0.06	<i>GSH1</i>	1.11 ± 0.05	1.08 ± 0.04
2.69 ± 0.07	1.29 ± 0.06*	<i>GSH2</i>	1.43 ± 0.03	1.16 ± 0.02*

Values represent the average ± S.E. of 5 biological replicates and are expressed relative to the average of the same genotype under control conditions at the same time point (set at 1.00). Significant Cd-induced upregulations and downregulations for both normalized and non-normalized data are highlighted in green and red, respectively. Asterisks (\*) indicate a significantly different Cd-induced response between both genotypes for both normalized and non-normalized data (2-way ANOVA per exposure duration;  $P < 0.05$ ). Direct SOG1 target genes according to Ogita et al. (2018) are underlined. *ACS*, 1-amino-cyclopropane-1-carboxylate synthase; *APX*, ascorbate peroxidase; *CAT*, catalase; *CSD*, Cu/Zn superoxide dismutase; *ERF1*, ethylene response factor 1; *FSD*, Fe superoxide dismutase; *GSH1*, glutamate-cysteine ligase; *GSH2*, glutathione synthetase; *MPK*, mitogen-activated protein kinase; *OXI1*, oxidative signal-inducible 1; *RBOH*, respiratory burst oxidase homolog; *TI1*, trypsin inhibitor 1; *TIR1*, toll/interleukin receptor 1; *UPOX*, upregulated by oxidative stress.

## Cadmium-Induced Hydrogen Peroxide Production Is Delayed in Leaves of the *sog1-7* Mutant

To obtain insight into the evolution of ROS levels in both genotypes over time, relative H<sub>2</sub>O<sub>2</sub> concentrations were determined in leaves of WT and *sog1-7* mutant plants exposed to 5  $\mu$ M Cd for 24 h, 72 h and 8 days. As shown in Figure 4A,

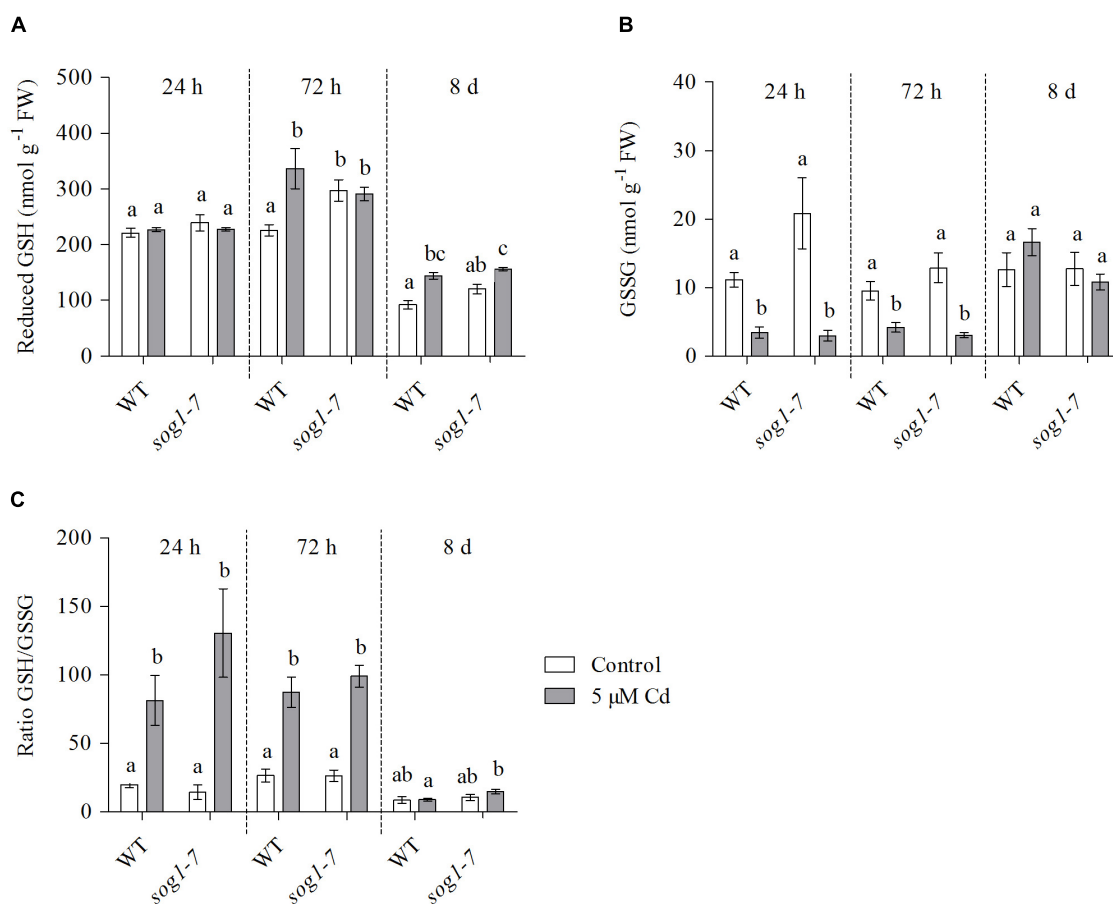


**FIGURE 3 | (A)** Reduced glutathione (GSH) (nmol g<sup>-1</sup> FW) concentrations, **(B)** glutathione disulfide (GSSG) (nmol g<sup>-1</sup> FW) concentrations and **(C)** reduced-to-oxidized GSH ratio in leaf rosettes of hydroponically grown wild-type (WT) and *sog1-7* mutant *A. thaliana* plants exposed to 0 (white bars) or 5 μM CdSO<sub>4</sub> (gray bars) for 24 h, 72 h or 8 days from day 19 after sowing. Values represent the average ± S.E. of at least 4 biological replicates. Different letters indicate significant differences between conditions (2-way ANOVA per exposure duration;  $P < 0.05$ ).

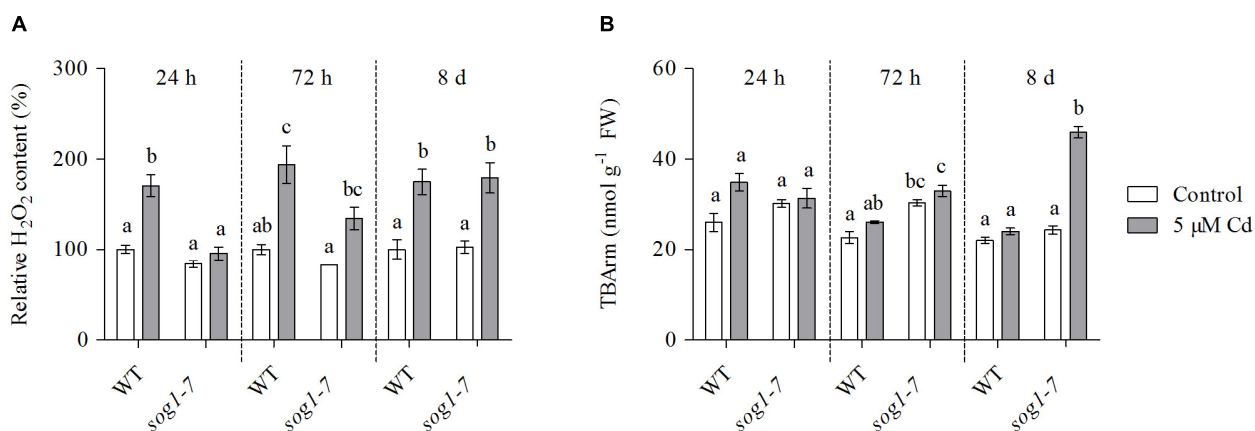


**FIGURE 4 | (A)** Hydrogen peroxide (H<sub>2</sub>O<sub>2</sub>) content (%) relative to wild-type (WT) control and **(B)** TBA-reactive metabolites (TBArm) concentrations (nmol g<sup>-1</sup> FW) in leaf rosettes of hydroponically grown WT and *sog1-7* mutant *A. thaliana* plants exposed to 0 (white bars) or 5 μM CdSO<sub>4</sub> (gray bars) for 24 h, 72 h and 8 days from day 19 after sowing. Values represent the average ± S.E. of at least 3 biological replicates. Different letters indicate significant differences between conditions (2-way ANOVA per exposure duration;  $P < 0.05$ ).

H<sub>2</sub>O<sub>2</sub> levels were significantly increased after 24 h of Cd exposure in leaves of WT plants, whereas they were unaffected in the *sog1-7* mutant. After 72 h of exposure, H<sub>2</sub>O<sub>2</sub> concentrations were significantly higher in leaves of Cd-exposed as compared to control plants of both genotypes, although this was less obvious in the mutant (**Figure 4A**). After a prolonged exposure duration of 8 days, H<sub>2</sub>O<sub>2</sub> levels were increased to the same extent in both genotypes (**Figure 4A**). Taken together, these data suggest that the Cd-induced increase of ROS levels is delayed in the *sog1-7* mutant.

### The Extent of Lipid Peroxidation Is Increased in Leaves of the *sog1-7* Mutant After Long-Term Cadmium Exposure

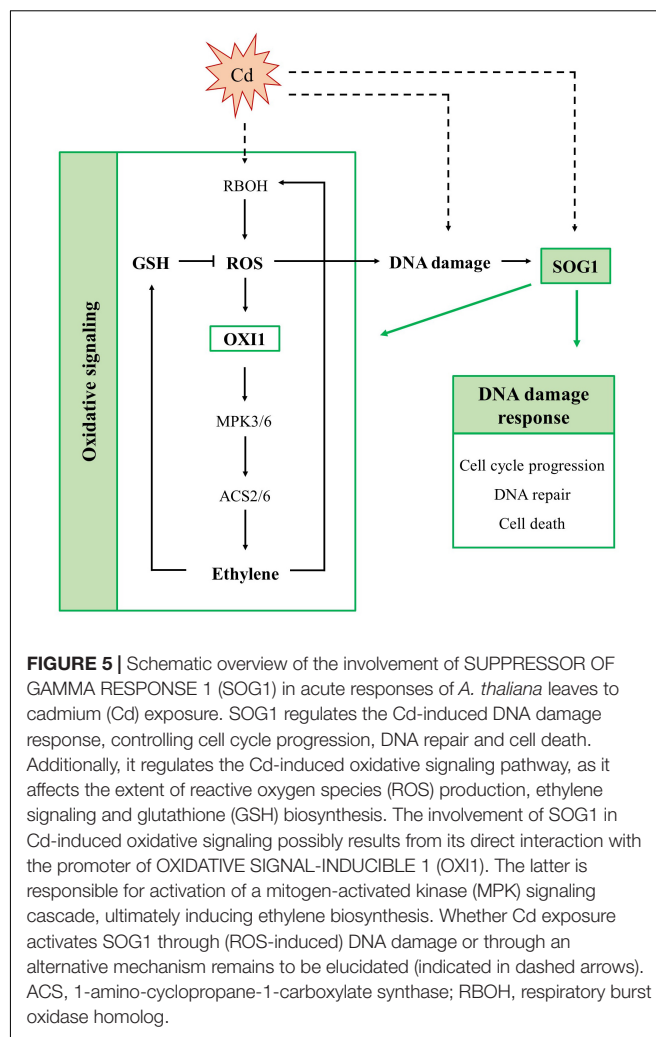
In a final part of this study, the extent of lipid peroxidation was studied in both genotypes, as a measure of the extent of ROS-induced damage to cellular components. To this end, TBArm concentrations – a marker for lipid peroxidation – were measured in leaves of WT and *sog1-7* mutant plants exposed to 5  $\mu$ M Cd for 24 h, 72 h and 8 days. Whereas the extent of lipid peroxidation was not affected by Cd exposure after 24 and 72 h of exposure (**Figure 4B**), it was significantly higher in leaves of the *sog1-7* mutant after long-term exposure for 8 days. However, this response was not observed in WT plants (**Figure 4B**).

## DISCUSSION

Cadmium exposure inhibits cell division and endoreplication and increases the expression of SOG1-regulated genes, including *SMR4*, *SMR5* and *SMR7* in leaves of *A. thaliana* (Hendrix et al., 2018). Therefore, the main aim of this study was to further explore the involvement of these CDK inhibitors and their upstream regulator SOG1 in Cd-induced stress responses in *A. thaliana*. To this end, Cd-induced effects were compared between leaves of WT, *smr4/5/7* and *sog1-7* plants exposed to 5  $\mu$ M Cd in a short-term (24 and 72 h) or long-term (8 days) exposure set-up (**Supplementary Figure S1**). A schematic overview of the proposed role of SOG1 in the Cd-induced DDR and oxidative signaling is provided in **Figure 5**.

### The Cadmium-Induced DNA Damage Response in *A. thaliana* Leaves Is Modulated by SOG1

The *sog1-7* mutant was substantially less sensitive to acute Cd exposure in comparison to WT plants, as indicated by the lack of a significant Cd-induced reduction in rosette FW (**Figure 1** and **Supplementary Table S5**), rosette diameter and leaf surface area (**Table 1**). This mutant was also reported to exhibit a lower aluminum (Al) sensitivity, as shown by a smaller Al-induced reduction of root length (Sjogren et al., 2015). It should be noticed that the *sog1-7* mutant is characterized by significantly smaller leaf rosettes as compared to WT plants under our control conditions (**Table 1**). The underlying reason for this altered phenotype is currently unclear and requires further investigation.



In contrast to the *sog1-7* mutant, Cd sensitivity of the *smr4/5/7* mutant was highly similar to that of the WT (**Figure 1** and **Table 1**). At the cellular level, Cd exposure inhibited endoreplication in WT leaves (**Figure 2**), corresponding with results of our previous study (Hendrix et al., 2018). In general, this response was absent in leaves of the *sog1-7* mutant, whereas *smr4/5/7* knockout plants behaved similar to WT plants (**Figure 2**). The lack of Cd-induced effects on endoreduplication in leaves of *sog1-7* mutants supports a role for SOG1 in cell cycle regulation. Furthermore, it likely contributes to the reduced Cd sensitivity of this genotype. The involvement of SOG1 in the regulation of endoreplication is supported by the fact that cell expansion – often coinciding with endoreplication – induced by the DSB-inducing agent zeocin is suppressed in sepal epidermal cells of the *sog1-1* mutant (Adachi et al., 2011). Furthermore, Chen and Umeda (2015) reported that the zeocin-induced reduction of root length observed in WT plants was absent in *sog1-1* mutants. Root meristem size was decreased in WT roots exposed to zeocin, whereas this effect was not observed in *sog1-1* mutant roots, indicating that SOG1 is required for the zeocin-induced early onset of endoreplication (Chen and Umeda, 2015).



A similar result was described by Johnson et al. (2018), showing that the inhibition of DNA replication and cell division observed in the mitotic zone of WT roots shortly after exposure to ionizing radiation was absent in *sog1-1* mutants. Our data indicate that the Cd-induced inhibition of endoreplication in WT plants is also absent in the *sog1-7* mutants (Figure 2), suggesting that under these stress conditions, SOG1 is responsible for the inhibition rather than activation of endoreplication. The fact that Cd-induced effects on endoreplication in the *smr4/5/7* mutant were highly similar to those observed in the WT (Figure 2) suggests that these CDK inhibitors are not responsible for the inhibition of endoreplication observed in leaves of Cd-exposed plants. It cannot be excluded, however, that a (SOG1-regulated) bypass mechanism is activated in the *smr4/5/7* mutant compensating for the lack of functional SMR4, SMR5 and SMR7. This mechanism might involve other proteins of the SMR or KRP families, also involved in regulating cell cycle progression. Furthermore, the highly similar extent of endoreplication between *smr4/5/7* and WT leaves upon Cd exposure might be explained by redundancy between these SMR proteins and WEE1, as the latter is a known SOG1 target (Ogita et al., 2018). Nevertheless, the inhibition of endoreplication in Cd-exposed plants might occur independently of SMR4, SMR5 and SMR7 through SOG1-mediated regulation of other cell cycle-related genes such as *CYCB1;1*. This mitotic cyclin was previously shown to be a direct SOG1 target gene (Ogita et al., 2018). After 24 h of Cd exposure, its expression significantly decreased, whereas it showed an increasing trend upon 72 h of exposure in leaves of WT plants as well as *smr4/5/7* mutants (Table 5). However, in *sog1-7* mutants, no alterations in *CYCB1;1* transcript levels were observed after Cd exposure (Table 3). Whether or not SOG1-dependent regulation of *CYCB1;1* transcription contributes to the observed inhibition of endoreplication in leaves of Cd-exposed plants requires further investigation.

To gain more insight into the involvement of SOG1 in early responses to Cd exposure, transcript levels of genes involved in the DDR were determined in control and Cd-exposed WT and *sog1-7* mutant plants. As previous results indicated that Cd-induced effects on gene expression levels are similar between different leaves (Hendrix et al., 2018), gene expression analyses were performed in entire leaf rosettes. In contrast to Sjogren et al. (2015) who did not observe any effect on SOG1 gene expression in roots of Al-exposed *Arabidopsis*, we found a significant SOG1 upregulation in leaves of Cd-exposed seedlings (Table 3). An induction of SOG1 by Cd exposure was also observed in roots of *A. thaliana* (Cao et al., 2018). Taken together with the fact that SOG1 is known to be regulated at the post-translational level through phosphorylation (Yoshiyama, 2015), this would imply that under certain stress conditions SOG1 could also be regulated at the transcriptional in addition to the post-translational level. Many genes related to the DDR (i.e., related to cell cycle progression, DNA repair and cell death) were induced upon Cd exposure after 24 h and/or 72 h in leaves of WT plants, suggesting the occurrence of Cd-induced DNA damage. Cadmium was previously reported to cause DNA damage in a large range of plant species, as recently reviewed

by Huybrechts et al. (2019). The observed Cd-induced DDR was significantly less pronounced or even completely absent in the *sog1-7* mutant (Table 3). These results were confirmed in plants exposed to Cd for 8 days in a long-term exposure set-up (Table 4). In contrast, Cd-induced effects on the transcription of these genes did not differ between leaves of *smr4/5/7* and WT plants (Table 5). The key role of SOG1 in the DDR was also demonstrated by the lack of induction of cell cycle-related and DNA repair genes in *sog1-1* mutants exposed to gamma irradiation (Yoshiyama et al., 2013, 2017) and mitomycin C (Horvath et al., 2017) and *sog1-7* mutants exposed to Al (Sjogren et al., 2015). Furthermore, Ogita et al. (2018) recently reported that several of the genes shown in Table 3 were either directly or indirectly regulated by SOG1 in *A. thaliana* seedlings treated with 15  $\mu$ M zeocin and contained the consensus SOG1 binding motif. These SOG1 target genes were confirmed by Bourbousse et al. (2018) in seedlings exposed to gamma irradiation.

Our data demonstrate that additional genes could be under the control of SOG1 in leaves of Cd-exposed seedlings, as suggested by their induction in WT plants but not in *sog1-7* mutants. These include *XRCC1* and *LIG4* (involved in DNA repair), several senescence-associated genes (SAGs) and genes involved in autophagy and cell death regulation. Whether these genes are direct SOG1 targets or are indirectly regulated by other transcription factors downstream of SOG1 remains to be investigated. Previous studies have shown that functional SOG1 is required for the induction of cell death in the stem cell region of *A. thaliana* roots exposed to UV-B, gamma irradiation and zeocin (Furukawa et al., 2010; Yoshiyama et al., 2013, 2017). This SOG1-mediated cell death causes the removal of a subset of stem cells and induces a regeneration response in the surrounding root apical meristem. As a consequence, a functional stem cell niche is regained, enabling continued root growth (Johnson et al., 2018). A similar mechanism might be induced by SOG1 upon Cd exposure, as Cd was also shown to induce cell death in the root meristem of *Pisum sativum* (Lehotai et al., 2011) and *A. cepa* (Behboodi and Samadi, 2004).

Taken together, our data indicate that SOG1 is a key player in the Cd-induced DDR in *Arabidopsis* leaves, regulating the expression of a large array of genes involved in cell cycle regulation, DNA repair and cell death-related processes (Figure 5). As transcript levels of some of these genes were slightly increased upon Cd exposure in leaves of *sog1-7* mutant plants – although to a significantly lower extent than in WT plants – it is likely that they are regulated by additional, SOG1-independent pathways. Despite the smaller phenotype of *sog1-7* mutants, the expression of most genes analyzed did not differ between leaves of the WT and the *sog1-7* mutant under control conditions (Supplementary Table S6), indicating that SOG1 is mainly involved in transcriptional regulation under stress conditions. It should be noted, however, that the expression of *SMR4*, *UPOX* and *APX2* was significantly higher in leaves of *sog1-7* mutants as compared to WT plants under control conditions. Although *SMR4* is a known direct SOG1 target gene (Bourbousse et al., 2018; Ogita et al., 2018), these data suggest that additional, SOG1-independent mechanisms are responsible

for *SMR4* transcriptional regulation. Furthermore, the elevated transcript levels of the oxidative stress hallmark gene *UPOX* and the stress-responsive gene *APX2* might indicate an increased basal stress level in the *sog1-7* mutant.

## The Cadmium-Induced Oxidative Stress Response in *A. thaliana* Leaves Is Regulated by SOG1

As oxidative stress is an important process involved in plant responses to Cd exposure (Benavides et al., 2005; Cuypers et al., 2010; Gallego et al., 2012), Cd-induced effects on several oxidative stress-related parameters were compared between leaves of WT and *sog1-7* mutant plants to gain additional insight into the role of SOG1 in early Cd-induced stress responses. Cadmium exposure significantly increased the expression of five oxidative stress hallmark genes (Gadjev et al., 2006) in leaves of WT plants exposed for 24 h and/or 72 h (Table 6). These transcriptional inductions were either significantly less pronounced or even completely absent in the *sog1-7* mutant, suggesting a disturbed oxidative stress response in this genotype. Interestingly, *UPOX*, encoding a mitochondrial oxidative stress hallmark gene, was recently reported to be regulated by SOG1 in response to zeocin treatment (Ogita et al., 2018). It is plausible that the oxidative stress hallmark genes are indirectly regulated by SOG1, as the list of SOG1 target genes contains a large number of transcription factors (Bourbousse et al., 2018; Ogita et al., 2018) that could be responsible for their upregulation.

Furthermore, the extent of Cd-induced *RBOHC* and *RBOHF* upregulation was significantly lower in *sog1-7* leaves as compared to WT leaves (Table 6). These genes encode NADPH oxidases located in the plasma membrane and are involved in  $O_2^{\cdot-}$  production in Cd-exposed *A. thaliana* leaves (Remans et al., 2010). In general, the expression of antioxidative genes involved in  $O_2^{\cdot-}$  and  $H_2O_2$  detoxification was also less increased or even decreased in *sog1-7* mutants (Table 6). These data suggest a lower degree of Cd-induced ROS production and antioxidative defense in *sog1-7* mutant leaves, possibly leading to a disturbance in oxidative signaling processes.

A key player in the Cd-induced oxidative signaling pathway is OXI1. As proposed by Schellingen et al. (2015b), Cd exposure increases ROS production through the activation of NADPH oxidases. Increased ROS levels are then perceived by OXI1, which subsequently activates MPK3 and MPK6 through phosphorylation. Interestingly, OXI1 was recently shown to contain a SOG1 binding motif (Ogita et al., 2018) and could hence function as a link between SOG1 and Cd-induced oxidative signaling (Figure 5). Our results showed that Cd exposure significantly increased transcript levels of *OXI1*, *MPK3* and *MPK6* after 24 and 72 h of exposure in WT plants. This effect was significantly less pronounced or even completely abolished in the *sog1-7* mutant (Table 6). As MPK3 and MPK6 are known to affect the transcription and activity of ACS2 and ACS6, involved in ethylene biosynthesis, transcript levels of both genes were also determined and *ERF1* gene expression was measured as a marker for ethylene signaling. Results showed a pattern highly

similar to that of *OXI1*, *MPK3* and *MPK6*, with significantly less pronounced Cd-induced upregulations in the *sog1-7* mutant (Table 6). In addition, the expression of GSH biosynthesis genes *GSH1* and *GSH2* was determined, as GSH is a key player in plant responses to Cd stress through its antioxidative and Cd-chelating functions (Jozefczak et al., 2012). As shown in Table 6, *GSH1* and *GSH2* transcript levels were significantly upregulated upon Cd exposure in WT leaves but not in *sog1-7* mutant leaves.

To determine whether differences in Cd-induced effects on the expression of GSH biosynthesis genes were also reflected at the metabolite level, reduced and oxidized GSH concentrations were determined in leaves of WT and *sog1-7* mutant *A. thaliana* plants exposed to Cd for 24 h, 72 h and 8 days. Concentrations of GSSG showed an immediate decrease upon Cd exposure in leaves of both genotypes (Figure 3B). This response is often observed in leaves of Cd-exposed *A. thaliana* and generally coincides with elevated transcript levels of glutathione reductase (GR), suggesting an increased reduction of GSSG to GSH (Jozefczak et al., 2014; Keunen et al., 2015; Schellingen et al., 2015a). In addition, Cd-induced increases in reduced GSH levels were observed from 72 h of exposure in WT plants, but were delayed in *sog1-7* mutants (Figure 3A). These data agree with the lack of a Cd-induced upregulation of *GSH1* and *GSH2* in the mutant after short-term exposure (Table 6). A lack of transcriptional induction of the GSH biosynthesis genes and the absence of increases in GSH concentrations after exposure to 5  $\mu$ M Cd was also observed in leaves of the ethylene insensitive *etr1-1* and *ein2-1* mutants (Schellingen et al., 2015b). Interestingly, these mutants showed a decreased Cd sensitivity as compared to the WT (Schellingen et al., 2015b). Our data indicate that a similar connection between ethylene and GSH metabolism might exist in the leaves of *sog1-7* mutant plants, as both the expression of ethylene-related genes and reduced GSH concentrations were less affected by Cd exposure in this genotype. Taken together, these data point toward a key role for SOG1 in acute Cd-induced oxidative signaling (Figure 5). The reduced Cd-induced effects on oxidative signaling in leaves of the *sog1-7* mutant could either be explained by a lower degree of ROS production in the mutant or by a reduced ability of the mutant to induce oxidative signaling pathways.

Therefore, Cd-induced effects on leaf  $H_2O_2$  concentrations were compared between WT and *sog1-7* plants exposed to 5  $\mu$ M Cd for 24 h, 72 h and 8 days. Cadmium-induced increases in  $H_2O_2$  levels were delayed in the mutant (Figure 4A). Chen and Umeda (2015) reported that root  $H_2O_2$  levels were increased by 24 h of zeocin exposure in WT *A. thaliana* plants, but not in a *sog1-1* mutant. This response corresponded with the absence of a zeocin-induced upregulation of *FLAVIN-DEPENDENT MONOOXYGENASE 1* (*FMO1*), involved in ROS production in roots (Chen and Umeda, 2015). The fact that  $H_2O_2$  production did not increase in leaves of the mutant after 24 h of Cd exposure (Figure 4A) possibly underlies the absence of a transcriptional induction of the oxidative signaling pathway (Table 6). As a result, an induction of a clear defense response is absent in *sog1-7* mutants after 72 h of Cd exposure. Therefore, increased levels of oxidative damage might be expected in the

mutant after prolonged Cd exposure, since increased H<sub>2</sub>O<sub>2</sub> concentrations were observed at this time point. This was confirmed by a significant increase in TBArm in leaves of mutant but not WT plants after 8 days of exposure (Figure 4B). Taken together, our work shows that Cd-induced ROS production is delayed in leaves of the *sog1-7* mutant. As a consequence, oxidative signaling and a clear defense response are insufficiently induced, resulting in an increased extent of oxidative damage after prolonged exposure.

In conclusion, our data strongly support the involvement of SOG1 in the Cd-induced DDR in leaves of *A. thaliana*. Interestingly, the obtained results also imply an additional role for SOG1 in regulating the oxidative stress response in Cd-exposed plants. The involvement of SOG1 in this process has never been described before and suggests that this protein functions in additional pathways besides the DNA damage response. Therefore, we propose that SOG1 might function as a general integrator of stress responses in plants exposed to Cd and possibly additional stress factors as well. A Cd-induced transcriptional upregulation of *SOG1* was also reported in *A. thaliana* roots (Cao et al., 2018). Hence, future research should aim to identify whether a similar SOG1-mediated response is activated by Cd exposure in roots.

## DATA AVAILABILITY STATEMENT

The datasets generated for this study are available on request to the corresponding author.

## REFERENCES

- Adachi, S., Minamisawa, K., Okushima, Y., Inagaki, S., Yoshiyama, K., Kondou, Y., et al. (2011). Programmed induction of endoreduplication by DNA double-strand breaks in *Arabidopsis*. *Proc. Natl. Acad. Sci. U.S.A.* 108, 10004–10009. doi: 10.1073/pnas.1103584108
- Behboodi, B. S., and Samadi, L. (2004). Detection of apoptotic bodies and oligonucleosomal DNA fragments in cadmium-treated root apical cells of *Allium cepa* Linnaeus. *Plant Sci.* 167, 411–416. doi: 10.1016/j.plantsci.2004.04.024
- Benavides, M. P., Gallego, S. M., and Tomaro, M. L. (2005). Cadmium toxicity in plants. *Braz. J. Plant Physiol.* 17, 21–34. doi: 10.1590/S1677-04202005000100003
- Boudolf, V., Lammens, T., Boruc, J., Van Leene, J., Van Den Daele, H., Maes, S., et al. (2009). CDKB1;1 forms a functional complex with CYCA2;3 to suppress endocycle onset. *Plant Physiol.* 150, 1482–1493. doi: 10.1104/pp.109.140269
- Bourbousse, C., Vegesna, N., and Law, J. A. (2018). SOG1 activator and MYB3R repressors regulate a complex DNA damage network in *Arabidopsis*. *Proc. Natl. Acad. Sci. U.S.A.* 115, E12453–E12462. doi: 10.1073/pnas.1810582115
- Bustin, S. A., Benes, V., Garson, J. A., Hellems, J., Kubista, M., Mueller, R., et al. (2009). The MIQE guidelines: minimum information for publication of quantitative real-time PCR experiments. *Clin. Chem.* 55, 611–622. doi: 10.1373/clinchem.2008.112797
- Cao, X., Wang, H. T., Zhuang, D. F., Zhu, H., Du, Y., Cheng, Z., et al. (2018). Roles of MSH2 and MSH6 in cadmium-induced G2/M checkpoint arrest in *Arabidopsis* roots. *Chemosphere* 201, 586–594. doi: 10.1016/j.chemosphere.2018.03.017
- Chen, P. Y., and Umeda, M. (2015). DNA double-strand breaks induce the expression of flavin-containing monooxygenase and reduce root meristem size in *Arabidopsis thaliana*. *Genes Cells* 20, 636–646. doi: 10.1111/gtc.12255
- Clough, S. J., and Bent, A. F. (1998). Floral dip: a simplified method for *Agrobacterium*-mediated transformation of *Arabidopsis thaliana*. *Plant J.* 16, 735–743. doi: 10.1046/j.1365-3113x.1998.00343.x

## AUTHOR CONTRIBUTIONS

SH, EK, and AC envisioned the project and designed the experiments. SH, VI, and IP carried out the experiments. TE generated the *smr4/5/7* mutant. SH analyzed the data and together with AC, wrote the manuscript. MH, LD, NH, and JV revised the article critically for important intellectual content. All authors have read and approved the manuscript.

## FUNDING

This work was supported by Hasselt University through Ph.D. grants to SH (grant number BOF14DOC04) and VI (grant number BOF18DOC02). Additional funding came from FWO projects to AC (grant numbers G0B6716N and G0C7518N).

## ACKNOWLEDGMENTS

We thank Ann Wijgaerts and Carine Put for their skillful technical assistance.

## SUPPLEMENTARY MATERIAL

The Supplementary Material for this article can be found online at: <https://www.frontiersin.org/articles/10.3389/fpls.2020.00366/full#supplementary-material>

- Cookson, S. J., Radziejewski, A., and Granier, C. (2006). Cell and leaf size plasticity in *Arabidopsis*: what is the role of endoreduplication? *Plant Cell Environ.* 29, 1273–1283. doi: 10.1111/j.1365-3040.2006.01506.x
- Cuyppers, A., Hendrix, S., dos Reis, R., De Smet, S., Deckers, J., Gielen, H., et al. (2016). Hydrogen peroxide, signaling in disguise during metal phytotoxicity. *Front. Plant Sci.* 7:470. doi: 10.3389/fpls.2016.00470
- Cuyppers, A., Plusquin, M., Remans, T., Jozefczak, M., Keunen, E., Gielen, H., et al. (2010). Cadmium stress: an oxidative challenge. *Biometals* 23, 927–940. doi: 10.1007/s10534-010-9329-x
- Cuyppers, A., Smeets, K., Ruytinx, J., Opdenakker, K., Keunen, E., Remans, T., et al. (2011). The cellular redox state as a modulator in cadmium and copper responses in *Arabidopsis thaliana* seedlings. *J. Plant Physiol.* 168, 309–316. doi: 10.1016/j.jplph.2010.07.010
- De Veylder, L., Larkin, J. C., and Schnittger, A. (2011). Molecular control and function of endoreplication in development and physiology. *Trends Plant Sci.* 16, 624–634. doi: 10.1016/j.tplants.2011.07.001
- dos Reis, R., Keunen, E., Mourato, M. P., Martins, L. L., Vangronsveld, J., and Cuyppers, A. (2018). Accession-specific life strategies affect responses in leaves of *Arabidopsis thaliana* plants exposed to excess Cu and Cd. *J. Plant Physiol.* 223, 37–46. doi: 10.1016/j.jplph.2018.01.008
- Fausser, F., Schiml, S., and Puchta, H. (2014). Both CRISPR/Cas-based nucleases and nickases can be used efficiently for genome engineering in *Arabidopsis thaliana*. *Plant J.* 79, 348–359. doi: 10.1111/tpj.12554
- Furukawa, T., Curtis, M. J., Tominey, C. M., Duong, Y. H., Wilcox, B. W. L., Aggoune, D., et al. (2010). A shared DNA-damage-response pathway for induction of stem-cell death by UVB and by gamma irradiation. *DNA Repair.* 9, 940–948. doi: 10.1016/j.dnarep.2010.06.006
- Gadjev, I., Vanderauwera, S., Gechev, T. S., Laloi, C., Minkov, I. N., Shulaev, V., et al. (2006). Transcriptomic footprints disclose specificity of reactive oxygen species signaling in *Arabidopsis*. *Plant Physiol.* 141, 436–445. doi: 10.1104/pp.106.078717
- Gallego, S. M., Pena, L. B., Barcia, R. A., Azpilicueta, C. E., Lannone, M. F., Rosales, E. P., et al. (2012). Unravelling cadmium toxicity and tolerance in



- plants: insight into regulatory mechanisms. *Environ. Exp. Bot.* 83, 33–46. doi: 10.1016/j.envexpbot.2012.04.006
- Hendrix, S., Keunen, E., Mertens, A. I. G., Beemster, G. T. S., Vangronsveld, J., and Cuypers, A. (2018). Cell cycle regulation in different leaves of *Arabidopsis thaliana* plants grown under control and cadmium-exposed conditions. *Environ. Exp. Bot.* 155, 441–452. doi: 10.1016/j.envexpbot.2018.06.026
- Horvath, B. M., Kourova, H., Nagy, S., Nemeth, E., Magyar, Z., Papdi, C., et al. (2017). *Arabidopsis* Retinoblastoma related directly regulates DNA damage responses through functions beyond cell cycle control. *EMBO J.* 36, 1261–1278. doi: 10.15252/embj.201694561
- Hu, Z. B., Cools, T., and De Veylder, L. (2016). Mechanisms used by plants to cope with DNA damage. *Annu. Rev. Plant Biol.* 67, 439–462. doi: 10.1146/annurev-arplant-043015-111902
- Huybrechts, M., Cuypers, A., Deckers, J., Iven, V., Vandionant, S., Jozefczak, M., et al. (2019). Cadmium and plant development: an agony from seed to seed. *Int. J. Mol. Sci.* 20:3971. doi: 10.3390/ijms20163971
- Johnson, R. A., Conklin, P. A., Tjahjadi, M., Missirian, V., Toal, T., Brady, S. M., et al. (2018). Suppressor of Gamma response1 links DNA damage response to organ regeneration. *Plant Physiol.* 176, 1665–1675. doi: 10.1104/pp.17.01274
- Jozefczak, M., Keunen, E., Schat, H., Blik, M., Hernández, L. E., Carleer, R., et al. (2014). Differential response of *Arabidopsis* leaves and roots to cadmium: glutathione-related chelating capacity vs antioxidant capacity. *Plant Physiol. Biochem.* 83, 1–9. doi: 10.1016/j.plaphy.2014.07.001
- Jozefczak, M., Remans, T., Vangronsveld, J., and Cuypers, A. (2012). Glutathione is a key player in metal-induced oxidative stress defenses. *Int. J. Mol. Sci.* 13, 3145–3175. doi: 10.3390/ijms13033145
- Keunen, E., Schellingen, K., Van Der Straeten, D., Remans, T., Colpaert, J., Vangronsveld, J., et al. (2015). Alternative Oxidase1a modulates the oxidative challenge during moderate Cd exposure in *Arabidopsis thaliana* leaves. *J. Exp. Bot.* 66, 2967–2977. doi: 10.1093/jxb/erv035
- Keunen, E., Truyens, S., Bruckers, L., Remans, T., Vangronsveld, J., and Cuypers, A. (2011). Survival of Cd-exposed *Arabidopsis thaliana*: are these plants reproductively challenged? *Plant Physiol. Biochem.* 49, 1084–1091. doi: 10.1016/j.plaphy.2011.07.013
- Kumar, N., and Larkin, J. C. (2017). Why do plants need so many cyclin-dependent kinase inhibitors? *Plant Signal. Behav.* 12:e1282021. doi: 10.1080/15592324.2017.1282021
- Lehotai, N., Peto, A., Bajkán, S., Erdei, L., Tari, I., and Kolbert, S. (2011). In vivo and in situ visualization of early physiological events induced by heavy metals in pea root meristem. *Acta Physiol. Plant.* 33, 2199–2207. doi: 10.1007/s11738-011-0759-z
- Mutlu, F., and Mutlu, B. (2015). Genotoxic effects of cadmium on tolerant and sensitive wheat cultivars. *J. Environ. Biol.* 36, 689–694.
- Ogita, N., Okushima, Y., Tokizawa, M., Yamamoto, Y. Y., Tanaka, M., Seki, M., et al. (2018). Identifying the target genes of SUPPRESSOR OF GAMMA RESPONSE 1, a master transcription factor controlling DNA damage response in *Arabidopsis*. *Plant J.* 94, 439–453. doi: 10.1111/tpj.13866
- Opdenakker, K., Remans, T., Keunen, E., Vangronsveld, J., and Cuypers, A. (2012). Exposure of *Arabidopsis thaliana* to Cd or Cu excess leads to oxidative stress mediated alterations in MAPKinase transcript levels. *Environ. Exp. Bot.* 83, 53–61. doi: 10.1016/j.envexpbot.2012.04.003
- Queval, G., and Noctor, G. (2007). A plate reader method for the measurement of NAD, NADP, glutathione, and ascorbate in tissue extracts: application to redox profiling during *Arabidopsis rosette* development. *Anal. Biochem.* 363, 58–69. doi: 10.1016/j.ab.2007.01.005
- R Core Team (2019). *R: A Language and Environment for Statistical Computing*. Vienna: R Foundation for Statistical Computing.
- Remans, T., Keunen, E., Bex, G. J., Smeets, K., Vangronsveld, J., and Cuypers, A. (2014). Reliable gene expression analysis by reverse transcription-quantitative PCR: reporting and minimizing the uncertainty in data accuracy. *Plant Cell* 26, 3829–3837. doi: 10.1105/tpc.114.130641
- Remans, T., Opdenakker, K., Smeets, K., Mathijsen, D., Vangronsveld, J., and Cuypers, A. (2010). Metal-specific and NADPH oxidase dependent changes in lipoxygenase and NADPH oxidase gene expression in *Arabidopsis thaliana* exposed to cadmium or excess copper. *Funct. Plant Biol.* 37, 532–544. doi: 10.1071/FP09194
- Rodríguez-Serrano, M., Romero-Puertas, M. C., Zabalza, A., Corpas, F. J., Gómez, M., Del Río, L. A., et al. (2006). Cadmium effect on oxidative metabolism of pea (*Pisum sativum* L.) roots. Imaging of reactive oxygen species and nitric oxide accumulation in vivo. *Plant Cell Environ.* 29, 1532–1544. doi: 10.1111/j.1365-3040.2006.01531.x
- Schellingen, K., Van Der Straeten, D., Remans, T., Loix, C., Vangronsveld, J., and Cuypers, A. (2015a). Ethylene biosynthesis is involved in the early oxidative challenge induced by moderate Cd exposure in *Arabidopsis thaliana*. *Environ. Exp. Bot.* 117, 1–11. doi: 10.1016/j.envexpbot.2015.04.005
- Schellingen, K., Van Der Straeten, D., Remans, T., Vangronsveld, J., Keunen, E., and Cuypers, A. (2015b). Ethylene signalling is mediating the early cadmium-induced oxidative challenge in *Arabidopsis thaliana*. *Plant Sci.* 239, 137–146. doi: 10.1016/j.plantsci.2015.07.015
- Schellingen, K., Van Der Straeten, D., Vandenbussche, F., Prinsen, E., Remans, T., Vangronsveld, J., et al. (2014). Cadmium-induced ethylene production and responses in *Arabidopsis thaliana* rely on ACS2 and ACS6 gene expression. *BMC Plant Biol.* 14:214. doi: 10.1186/s12870-014-0214-6
- Schneider, C. A., Rasband, W. S., and Eliceiri, K. W. (2012). NIH Image to ImageJ: 25 years of image analysis. *Nat. Methods* 9, 671–675. doi: 10.1038/nmeth.2089
- Silveira, G. L., Lima, M. G., Reis, G. B., Palmieri, M. J., and Andrade-Vieria, L. F. (2017). Toxic effects of environmental pollutants: comparative investigation using *Allium cepa* L. and *Lactuca sativa* L. *Chemosphere* 178, 359–367. doi: 10.1016/j.chemosphere.2017.03.048
- Sjogren, C. A., Bolaris, S. C., and Larsen, P. B. (2015). Aluminum-dependent terminal differentiation of the *Arabidopsis* root tip is mediated through an ATR-, ALT2-, and SOG1-regulated transcriptional response. *Plant Cell* 27, 2501–2515. doi: 10.1105/tpc.15.00172
- Smeets, K., Opdenakker, K., Remans, T., Forzani, C., Hirt, H., Vangronsveld, J., et al. (2013). The role of the kinase OXI1 in cadmium- and copper-induced molecular responses in *Arabidopsis thaliana*. *Plant Cell Environ.* 36, 1228–1238. doi: 10.1111/pce.12056
- Smeets, K., Ruytinx, J., Van Belleghem, F., Semane, B., Lin, D., Vangronsveld, J., et al. (2008). Critical evaluation and statistical validation of a hydroponic culture system for *Arabidopsis thaliana*. *Plant Physiol. Biochem.* 46, 212–218. doi: 10.1016/j.plaphy.2007.09.014
- Wang, H. T., He, L., Song, J., Cui, W., Zhang, Y., Jia, C., et al. (2016). Cadmium-induced genomic instability in *Arabidopsis*: molecular toxicological biomarkers for early diagnosis of cadmium stress. *Chemosphere* 150, 258–265. doi: 10.1016/j.chemosphere.2016.02.042
- Yi, D., Avim Kamei, C. L., Cools, T., Vanderauwera, S., Takahashi, N., Okushima, Y., et al. (2014). The *Arabidopsis* SIAMESE-RELATED cyclin-dependent kinase inhibitors SMR5 and SMR7 regulate the DNA damage checkpoint in response to reactive oxygen species. *Plant Cell* 26, 296–309. doi: 10.1105/tpc.113.118943
- Yoshiyama, K. O. (2015). SOG1: a master regulator of the DNA damage response in plants. *Genes Genet. Syst.* 90, 209–216. doi: 10.1266/ggs.15-00011
- Yoshiyama, K. O., Kaminoyama, K., Sakamoto, T., and Kimura, S. (2017). Increased phosphorylation of Ser-Gln sites on SUPPRESSOR OF GAMMA RESPONSE1 strengthens the DNA damage response in *Arabidopsis thaliana*. *Plant Cell* 29, 3255–3268. doi: 10.1105/tpc.17.00267
- Yoshiyama, K. O., Kobayashi, J., Ogita, N., Ueda, M., Kimura, S., Maki, H., et al. (2013). ATM-mediated phosphorylation of SOG1 is essential for the DNA damage response in *Arabidopsis*. *EMBO Rep.* 14, 817–822. doi: 10.1038/embor.2013.112
- Zhang, X. Q., Chen, H. N., Jiang, H., Lu, W. Y., Pan, J. J., Qian, Q., et al. (2015). Measuring the damage of heavy metal cadmium in rice seedlings by SRAP analysis combined with physiological and biochemical parameters. *J. Sci. Food Agric.* 95, 2292–2298. doi: 10.1002/jsfa.6949

**Conflict of Interest:** The authors declare that the research was conducted in the absence of any commercial or financial relationships that could be construed as a potential conflict of interest.

Copyright © 2020 Hendrix, Iven, Eekhout, Huybrechts, Pecqueur, Horemans, Keunen, De Veylder, Vangronsveld and Cuypers. This is an open-access article distributed under the terms of the Creative Commons Attribution License (CC BY). The use, distribution or reproduction in other forums is permitted, provided the original author(s) and the copyright owner(s) are credited and that the original publication in this journal is cited, in accordance with accepted academic practice. No use, distribution or reproduction is permitted which does not comply with these terms.





# Superoxide Radical Metabolism in Sweet Pepper (*Capsicum annuum* L.) Fruits Is Regulated by Ripening and by a NO-Enriched Environment

Salvador González-Gordo, Marta Rodríguez-Ruiz, José M. Palma and Francisco J. Corpas\*

Group of Antioxidants, Free Radicals and Nitric Oxide in Biotechnology, Food and Agriculture, Department of Biochemistry, Cell and Molecular Biology of Plants, Estación Experimental del Zaidín, Spanish National Research Council (CSIC), Granada, Spain

## OPEN ACCESS

### Edited by:

Christian Lindermayr,  
Helmholtz Zentrum München,  
Germany

### Reviewed by:

Shi-Lin Tian,  
Huanghuai University, China  
Francisca Sevilla,  
Center for Edaphology and Applied  
Biology of Segura, Spanish National  
Research Council, Spain

### \*Correspondence:

Francisco J. Corpas  
javier.corpas@eez.csic.es

### Specialty section:

This article was submitted to  
Plant Physiology,  
a section of the journal  
Frontiers in Plant Science

**Received:** 17 January 2020

**Accepted:** 31 March 2020

**Published:** 14 May 2020

### Citation:

González-Gordo S,  
Rodríguez-Ruiz M, Palma JM and  
Corpas FJ (2020) Superoxide Radical  
Metabolism in Sweet Pepper  
(*Capsicum annuum* L.) Fruits Is  
Regulated by Ripening and by  
a NO-Enriched Environment.  
Front. Plant Sci. 11:485.  
doi: 10.3389/fpls.2020.00485

Superoxide radical ( $O_2^{\bullet-}$ ) is involved in numerous physiological and stress processes in higher plants. Fruit ripening encompasses degradative and biosynthetic pathways including reactive oxygen and nitrogen species. With the use of sweet pepper (*Capsicum annuum* L.) fruits at different ripening stages and under a nitric oxide (NO)-enriched environment, the metabolism of  $O_2^{\bullet-}$  was evaluated at biochemical and molecular levels considering the  $O_2^{\bullet-}$  generation by a NADPH oxidase system and its dismutation by superoxide dismutase (SOD). At the biochemical level, seven  $O_2^{\bullet-}$ -generating NADPH-dependent oxidase isozymes [also called respiratory burst oxidase homologs (RBOHs) I–VII], with different electrophoretic mobility and abundance, were detected considering all ripening stages from green to red fruits and NO environment. Globally, this system was gradually increased from green to red stage with a maximum of approximately 2.4-fold increase in red fruit compared with green fruit. Significantly, breaking-point (BP) fruits with and without NO treatment both showed intermediate values between those observed in green and red peppers, although the value in NO-treated fruits was lower than in BP untreated fruits. The  $O_2^{\bullet-}$ -generating NADPH oxidase isozymes I and VI were the most affected. On the other hand, four SOD isozymes were identified by non-denaturing electrophoresis: one Mn-SOD, one Fe-SOD, and two CuZn-SODs. However, none of these SOD isozymes showed any significant change during the ripening from green to red fruits or under NO treatment. In contrast, at the molecular level, both RNA-sequencing and real-time quantitative PCR analyses revealed different patterns with downregulation of four genes *RBOH A, C, D*, and *E* during pepper fruit ripening. On the contrary, it was found out the upregulation of a *Mn-SOD* gene in the ripening transition from immature green to red ripe stages, whereas a *Fe-SOD* gene was downregulated. In summary, the data reveal a contradictory behavior between activity and gene expression of the enzymes involved in the metabolism of

$O_2^{\bullet-}$  during the ripening of pepper fruit. However, it could be concluded that the prevalence and regulation of the  $O_2^{\bullet-}$  generation system (NADPH oxidase-like) seem to be essential for an appropriate control of the pepper fruit ripening, which, additionally, is modulated in the presence of a NO-enriched environment.

**Keywords:** NADPH oxidase, nitric oxide, nitration, pepper fruit, respiratory burst oxidase homolog, S-nitrosation, superoxide dismutase, ripening

## INTRODUCTION

Fruit ripening is a genetically coordinated developmental process that involves important physiological and biochemical changes affecting their organoleptic properties such as color, flavor, aroma, texture, and nutritional quality (Giovannoni, 2001; Osorio et al., 2013; Karlova et al., 2014). The ripening process occurs naturally when the fruits are in the plant, but it can also take place during the period of postharvest and storage especially in those types of fruits whose ripening depends on ethylene (climacteric fruits), such as tomato (*Solanum lycopersicum* L.), custard apple (*Annona squamosa* L.), banana (*Musa* spp.), or mango (*Mangifera indica* L.).

Pepper (*Capsicum* spp.) fruit, a non-climacteric one, belongs to the Solanaceae family, which includes other members such as tomatoes, potatoes, or eggplant. Fresh or processed pepper fruits are widely consumed around the world, so they have a great economic importance. Pepper fruit including many types and varieties differ in size, shape, color, and degree of pungency (hotness), being this last feature due to the presence of capsaicin (8-methyl-*N*-vanillyl-trans-6-nonenamide), and an alkaloid produced as a secondary metabolite. Furthermore, pepper fruits contain a high level of vitamin C and other vitamins such as A, E, B1, and B2 (Rodríguez-Ruiz et al., 2017). Pepper fruit ripening has an associated drastic change in color because the initial green color due to chlorophylls is progressively decomposed and is substituted by a different range of carotenoids including  $\beta$ -carotene, lutein, violaxanthin, capsanthin, violaxanthin, and zeaxanthin among others, which contribute to provide a variety of color (red, yellow, orange, purple/violet, etc.) in the ripe stage (Pascual et al., 2010; Gómez-García and Ochoa-Alejo, 2013; Ou et al., 2013; Liu et al., 2020). In fact, this variety of color and shape is even being used for ornamental purposes. In general, the main function of these carotenoids is the protection against oxidative damage because they can interact with singlet oxygen ( $^1O_2$ ) as well as scavenger of peroxy radicals (LOO $\cdot$ ), but also they are precursors of phytohormones such as abscisic acid (ABA) or strigolactones (Fanciullino et al., 2014).

Reactive oxygen and nitrogen species (ROS/RNS) are two families of molecules that are part of the physiological metabolism in all types of cells. Some of these molecules such as hydrogen peroxide ( $H_2O_2$ ) or nitric oxide (NO) have regulatory functions in many physiological processes including seed germination, plant growth and development, and senescence, but also these reactive species could be also overproduced under adverse environmental conditions being involved in nitro-oxidative processes (Corpas and Barroso, 2013). Recently,

biochemical evidences support that both ROS and RNS interact and seem to be involved in fruit ripening (Tanou et al., 2015; Palma et al., 2015, 2019; Corpas et al., 2018; Corpas and Palma, 2018; Léchaudel et al., 2018; Rodríguez-Ruiz et al., 2019).

NADPH oxidase (NOX), also called respiratory burst oxidase homolog (RBOH), is one of the main enzymatic sources of superoxide radicals ( $O_2^{\bullet-}$ ) in plants (Sagi and Fluhr, 2006; Suzuki et al., 2011; Marino et al., 2012). RBOHs participate in a wide range of function including cellular signal transduction, cell growth and development, pollen germination and tube growth, stomatal movements, plant interaction with beneficial organism, plant defense against pathogens (Müller et al., 2009; Jiménez-Quesada et al., 2016, 2019; Qu et al., 2017; Wang et al., 2018; Fonseca-García et al., 2019; Kaya et al., 2019). The number of RBOH genes reported thus far differs among the different plant species. Thus, 10 RBOH genes have been identified in the model plant *Arabidopsis*, nine in rice (*Oryza sativa*) (Wang et al., 2013; Kaur and Pati, 2018) and common bean (*Phaseolus vulgaris*) (Montiel et al., 2012), eight in tomato (*Solanum lycopersicum*) (Li et al., 2015) and seven in strawberry (*Fragaria*  $\times$  *ananassa* cv. Toyonaka) (Zhang et al., 2018), grape (*Vitis vinifera*) (Cheng et al., 2013), and pepper (*Capsicum annuum* L.). This diversity of RBOH genes suggests that the corresponding proteins could have specific function according to their organ location (root, stem, leaf, flower, or fruit), physiological stage (seedling or flowering plants), or environmental conditions.

Superoxide dismutases (SODs) are metalloenzymes that catalyze the disproportionation of  $O_2^{\bullet-}$  into  $O_2$  and  $H_2O_2$  and are associated with stress, development, and senescence conditions in plants (Houmani et al., 2016; del Río et al., 2018). Moreover, the type and number of SOD isozymes can differ between different plant species and their corresponding organs (Asada et al., 1973; Bridges and Salin, 1981; Almansa et al., 1989; Corpas et al., 1991, 2006; Pinilla et al., 2019). In preliminary studies, the presence of four SOD and seven  $O_2^{\bullet-}$ -generating NOX isozymes, which seemed to be differentially regulated during ripening in different sweet pepper cultivars, was reported (Mateos et al., 2013; Chu-Puga et al., 2019). Moreover, additional research has identified and characterized other enzymatic and non-enzymatic antioxidant systems in pepper fruit (Jiménez et al., 2003; Mateos et al., 2009; Martí et al., 2009, 2011; Camejo et al., 2015; Chiaiese et al., 2019; Rodríguez-Ruiz et al., 2019; Ribes-Moya et al., 2020). With the goal to get a deeper knowledge of the physiological function and the regulation of the  $O_2^{\bullet-}$  metabolism in the ripening of sweet pepper fruit, biochemical and molecular approach-based in-gel activity assays and RNA-Seq/real-time quantitative PCR (RT-qPCR) analyses were accomplished in fruits at different ripening stages and in

the presence of a NO-enriched environment. The data provide differential profile between biochemical and molecular results; however, it can be concluded that during ripening of sweet pepper from green to red stage, there is a prevalence of  $O_2^{\bullet-}$  generation, which seems to be negatively modulated in the presence of a NO-enriched environment.

## MATERIALS AND METHODS

### Plant Material and Nitric Oxide Gas Treatment

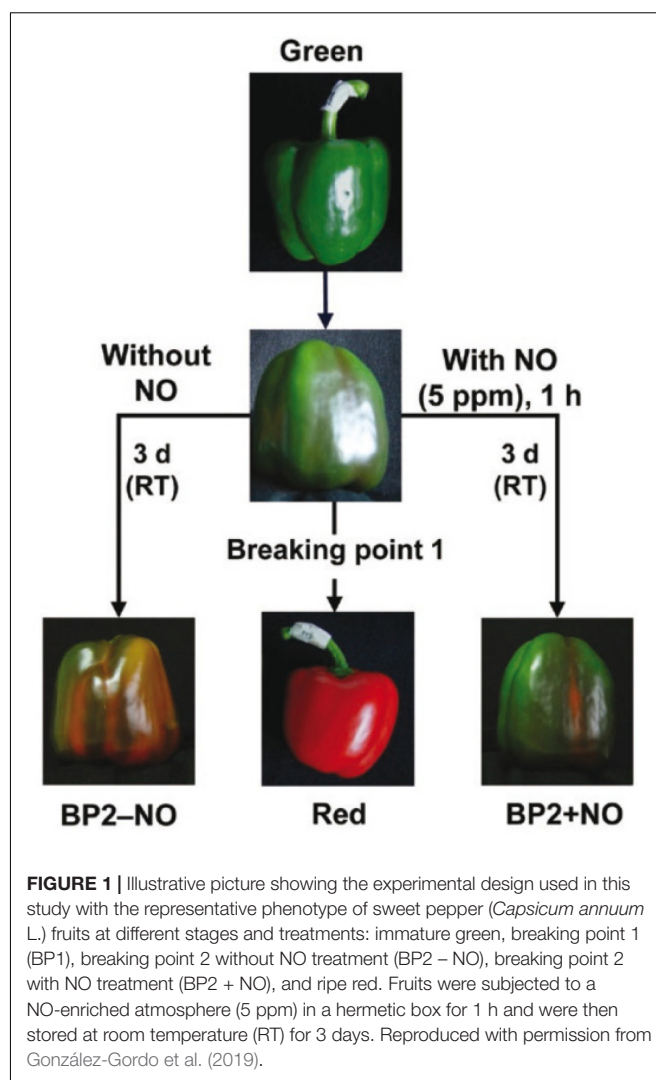
California-type sweet pepper (*Capsicum annuum* L., cv. Melchor) fruits were collected at three different developmental stages – green immature (G), breaking point (BP1), and red ripe (R) – from plants grown in plastic-covered experimental greenhouses (Zeraim Iberica S.A./Syngenta Seeds, Ltd., El Ejido, Almería, Spain). **Supplementary Figure S1** shows a typical distribution of fruits at the three stages mentioned above (G, BP, and R) in pepper plants. In addition, to study the exogenous NO gas effect on the fruit ripening, we set two additional groups: treated fruits with 5 ppm NO for 1 h (BP2 + NO) and another parallel group that was not treated with NO (BP2 – NO) (Palma et al., 2018; González-Gordo et al., 2019). After 3 days, all fruits from the five groups were chopped into small cubes (5 mm/edge), frozen under liquid nitrogen, and then stored at  $-80^\circ\text{C}$  until use. **Figure 1** provides a comprehensive picture of the experimental design used in this study, which is based on a previous report (González-Gordo et al., 2019).

### Preparation of Pepper Samples for Biochemical Analyses

The pericarp of pepper fruits stored at  $-80^\circ\text{C}$  of the different groups were ground under liquid nitrogen in an IKA A11 Basic mill and then dissolved in a ratio 1:1 (w/v) with 50 mM of Tris-HCl buffer, pH 7.5, 0.1 mM of EDTA, 0.1% (v/v) Triton X-100, 10% (v/v) glycerol, and 5 mM of dithiothreitol (DTT). In all cases, pericarp samples were prepared from, at least, five fruits (biological replicates) at each stage and treatments. Homogenates were filtered through two layers of Miracloth and centrifuged at  $27,000 \times g$  at  $4^\circ\text{C}$  for 30 min. The supernatants were used for the enzymatic assays.

### In-Gel Isozyme Profile of NADPH Oxidase and Superoxide Dismutase Activity Assays

Protein samples were separated using non-denaturing polyacrylamide gel electrophoresis (PAGE) on 6% acrylamide gels, and  $O_2^{\bullet-}$ -generating NOX isozymes were visualized by a photochemical nitro blue tetrazolium (NBT) reduction method described previously (Airaki et al., 2012; Chu-Puga et al., 2019). Briefly, after the electrophoresis, the gels were incubated in the dark for 20 min in a reaction mixture solution containing 50 mM of Tris-HCl buffer (pH 7.4), 0.2 mM of NBT, 0.1 mM of  $MgCl_2$ , and 1 mM of  $CaCl_2$ . Subsequently, 0.2 mM of NADPH was added, and the appearance of the blue formazan bands



was monitored. The reaction was stopped by immersing the gels in distilled water. As controls, gels were preincubated 30 min with 50  $\mu\text{M}$  of diphenyleneiodonium (DPI), a specific inhibitor of NADPH-dependent  $O_2^{\bullet-}$  generation activity (Leterrier et al., 2012).

Superoxide dismutase (SOD) isozymes were separated by non-denaturing PAGE on 10% acrylamide gels, and activity was localized in gels by the NBT reduction method with  $O_2^{\bullet-}$  radicals generated photochemically (Beauchamp and Fridovich, 1971). To identify the type of SOD isozymes, the gels were preincubated separately at  $25^\circ\text{C}$  for 30–45 min in 50 mM of K-phosphate, pH 7.8, in the presence or absence of either 5 mM of KCN or 5 mM of  $H_2O_2$ . CuZn-SOD is inhibited by KCN and  $H_2O_2$ ; Fe-SOD is inhibited by  $H_2O_2$  but not by KCN, and Mn-SOD is not inhibited by either KCN or  $H_2O_2$  (Corpas et al., 1998).

For the *in vitro* assay of the effect of some RNS and oxidizing/reducing agents on the isozyme SOD activity, pepper samples were preincubated with different chemicals including 4 mM of 3-morpholinosydnonimine (SIN-1), a peroxynitrite ( $ONOO^-$ ) donor, 4 mM of S-nitrosoglutathione (GSNO) and



4 mM of diethylamine NONOate (DEA NONOate) as NO donors, 10 mM of H<sub>2</sub>O<sub>2</sub> as an oxidant; 4 mM of reduced glutathione (GSH), and 10 mM of DTT as reductants. All preincubations were done at 25°C for 2 h in the dark. Then, electrophoresis gels were stained for SOD activity as it has been previously described. In certain assays as those described in **Figure 7**, gels were preincubated for 30 min under dark conditions with either 5 mM of H<sub>2</sub>O<sub>2</sub> or 5 mM of GSH before staining for SOD activity.

Protein concentration was determined using the Bio-Rad protein assay (Hercules, CA, United States), with bovine serum albumin as standard. Band intensity of RBOH isozymes was quantified using ImageJ 1.45 software<sup>1</sup>.

## RNA Extraction, Sequencing, and Real-Time Quantitative PCR

Total RNA was isolated from pepper fruits using a two-step method based on TRIzol® Reagent (Gibco BRL) and the RNeasy Plant Mini Kit (Qiagen), following the manufacturer's instructions. Libraries were prepared using an optimized Illumina protocol and were sequenced on an Illumina NextSeq550 comprising four independent replicates belonging to the green stage and five to each of the other stages (González-Gordo et al., 2019). RNA (1 µg) was used for cDNA synthesis. It was added to a mixture containing 0.67 mM of dNTPs and 5 µM of oligo d(T)23VN in a volume of 15 µl. This mix was incubated 5 min at 65°C. Afterward, reaction buffer [75 mM of Tris-HCl, pH 9.0, 2 mM of MgCl<sub>2</sub>, 50 mM of KCl, and 20 mM of (NH<sub>4</sub>)<sub>2</sub>SO<sub>4</sub>], 1 U/µl of RnaseOUT™ (Invitrogen), and 10 U/µl of SuperScript™ II Reverse Transcriptase (Invitrogen) were added in a final reaction volume of 20 µl. Finally, cDNA synthesis was performed at 42°C for 50 min, followed by an inactivation step of 15 min at 70°C.

In order to get our reference transcriptome and differentially expressed (DE) genes among the ripening stages and the NO treatment, we analyzed 24 biological replicates (4 × G, 5 × BP1, 5 × BP2 + NO, 5 × BP2 – NO, and 5 × R) and followed an optimized workflow to process all the data. Data processing involved several bioinformatic tools (TransFlow, Seoane et al., 2018 and DEgenes Hunter, González-Gayte et al., 2017), which apply different algorithms with their own statistical tests, to validate the whole experiment. The trends found in the expression patterns in the RNA-Seq experiments were confirmed by performing the real-time quantitative PCR (RT-qPCR) experiments.

Real-time quantitative PCR experiments were performed on a QuantStudio 3 Real-Time PCR System (Applied Biosystems, Foster City, CA, United States) with QUANTIMIX HotSplit Easy kit (Biotools, B&M Labs, Madrid, Spain) following manufacturer's instructions and using specific primers (see **Supplementary Table S1**). *Actin* and *glyceraldehyde-3-phosphate dehydrogenase* (*GAPDH*) were used as housekeeping genes (Wan et al., 2011; Bin et al., 2012). Reactions were performed with an initial step at 95°C for 30 s and then cycled at 95°C for 1 min, 67°C for 1 min, and 72°C

for 15 s for 40 cycles. Each PCR was performed at least three times (technical replicates), with three independent samples (biological replicates). Relative gene expression was calculated using the 2<sup>–ΔΔCt</sup> method (Schmittgen and Livak, 2008). A time-course expression analysis of *RBOH* and *SOD* genes constitutes a trustworthy visual representation of the expression values obtained by RNA-Seq.

## Phylogenetic Analysis and Conserved Respiratory Burst Oxidase Homolog Protein Sequences

Alignment of plant RBOH proteins was performed using the ClustalW tool with default parameters. Then, a phylogenetic tree was generated using MEGA 7.0 and edited with Figtree software. Sequence logos of conserved motifs were created by WebLogo 3.

## Statistical Analysis

A one-way analysis of variance (ANOVA) was used to test the statistical significance between relative expression values obtained using RT-qPCR. *Post hoc* comparisons of means were made by using a Tukey honestly significant difference (HSD) test. Statistical significance was considered at the conventional 5% level ( $P \leq 0.05$ ). All calculations were performed using R Studio.

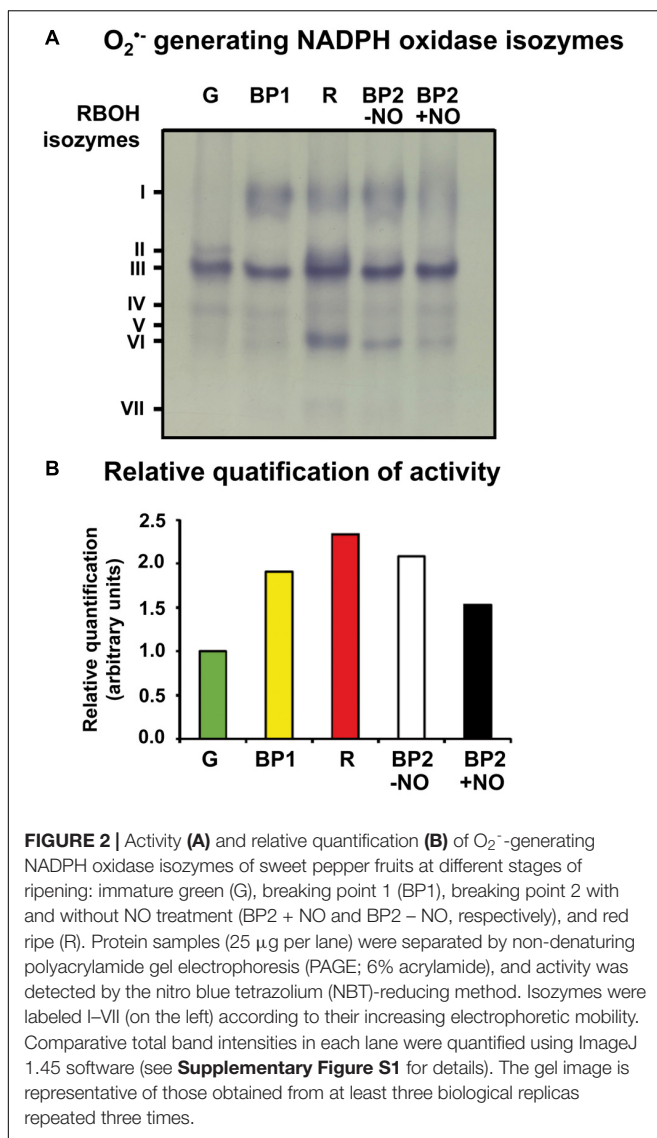
## RESULTS

The main goal of this study is to understand how O<sub>2</sub>•<sup>–</sup> metabolism is modulated during pepper fruit ripening with special focus in the activity of two groups of isozymes, O<sub>2</sub>•<sup>–</sup>-generating NOXs and the antioxidant SODs. Additionally, it was evaluated how these two enzymatic systems could be affected in the presence of a NO-enriched environment during the ripening of sweet pepper fruits.

With the use of these group of samples, **Figure 2A** shows the O<sub>2</sub>•<sup>–</sup>-generating NOX isozymes profile of sweet pepper fruits at different stages of ripening: immature green, BP1, BP2 with and without NO (BP2 + NO and BP2 – NO, respectively), and red. Thus, a total of seven O<sub>2</sub>•<sup>–</sup>-generating NOX isozymes, with different electrophoretic mobility and abundance, were globally detected during the ripening from green to red fruits considering all the different stages and the NO treatment. They were designated as I to VII according to their increasing electrophoretic mobility. **Supplementary Figure S2** illustrates the relative quantification of each O<sub>2</sub>•<sup>–</sup>-generating NOX isozyme in the analyzed ripening stages, with isozyme III being the most prominent in all ripening stages. **Figure 2B** shows the total relative quantification considering all the O<sub>2</sub>•<sup>–</sup>-generating NOX isozymes present in each ripening stages. Thus, a gradual increased activity was observed throughout ripening with a maximum of about 2.4-fold increase in red fruit compared with green fruit. Significantly, pepper fruits both with and without NO treatment (BP2 + NO and BP2 – NO) showed intermediate values to those observed for green and red peppers (**Figure 2B**), with the value in NO-treated fruits being lower than in untreated fruits. In this case, isozymes I and VI seemed to be the most affected.

<sup>1</sup><https://imagej.nih.gov/ij/>





To get deeper knowledge about this  $O_2^{\bullet-}$ -generating NOX isoymes during ripening, the identification of *RBOH* genes in the transcriptome of sweet pepper previously reported (González-Gordo et al., 2019) and their corresponding protein sequences were accomplished. With this information, one could make a comparative analysis of the percentage of identities among the protein sequences of the 10 *Arabidopsis* *RBOH* isoymes (A to J) with the seven identified sweet pepper *RBOH* isoymes because *Arabidopsis thaliana* provides the most complete information on this subject (Figure 3A). Considering the highest degree of protein identities with respect to the *Arabidopsis* *RBOH*s, the seven sweet pepper *RBOH* isoymes identified here were designated with letters A, B, C, D, E, H, and J.

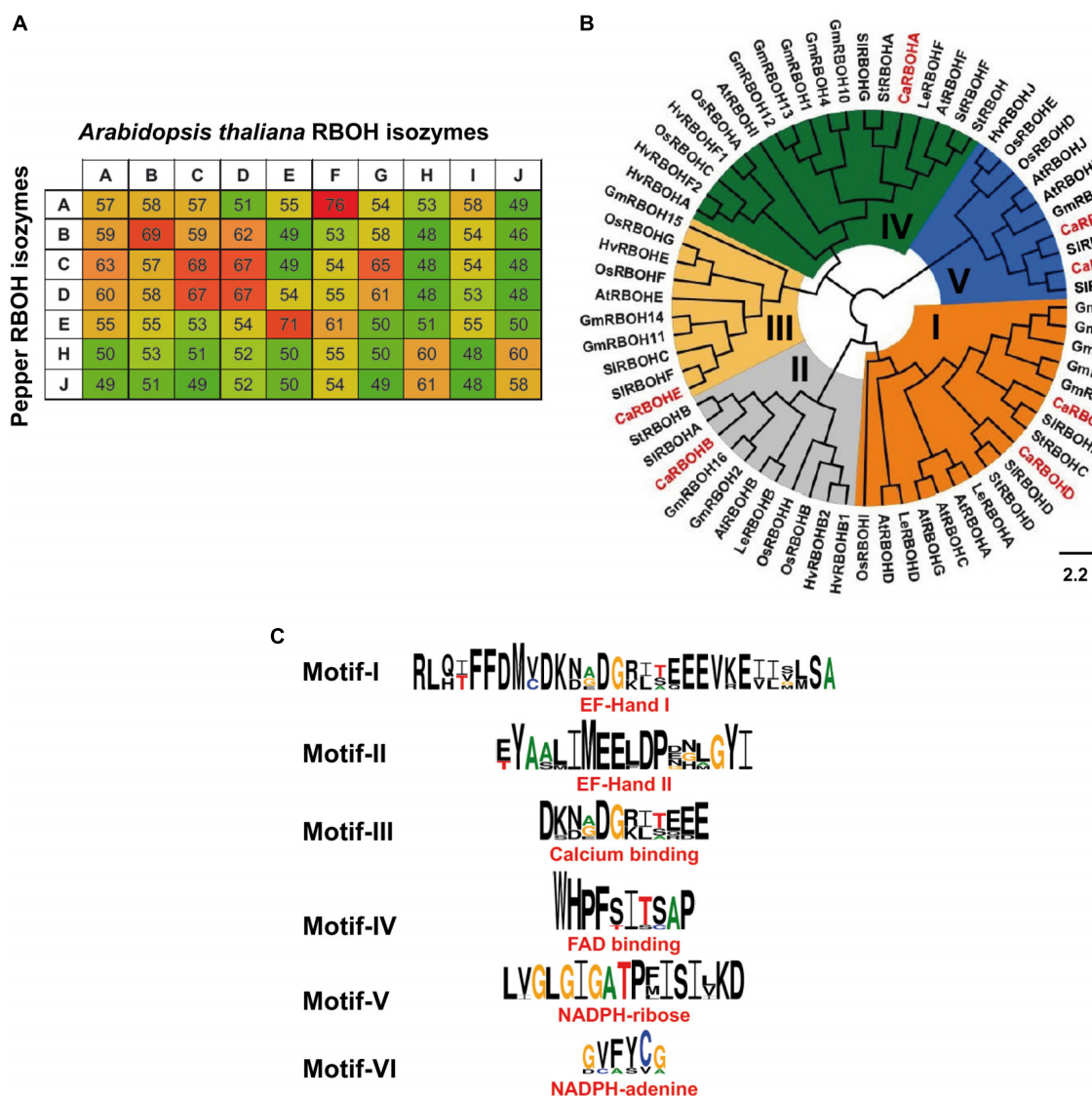
Figure 3B illustrates the phylogenetic comparative analysis among *RBOH* proteins from eight plant species including sweet pepper (*Capsicum annuum*), *Arabidopsis thaliana*, garden cress (*Lepidium sativum*), soybean (*Glycine max*), barley (*Hordeum vulgare*), rice (*Oryza sativa*), and two species of the *Solanum*

genus: tomato (*Solanum lycopersicum*) and potato (*Solanum tuberosum*). This allowed to identify five main *RBOH* groups designated as I to V, which are depicted with different colors in the diagram. CaRBOH A, reported in this work, was included in group IV, CaRBOH B was present in group II, CaRBOH C and D are in group I, CaRBOH E is in group III, and CaRBOH H and J are in group V. Figure 3C shows the identification of six conserved motifs of plant *RBOH*s present in sweet pepper *RBOH* protein sequences, which correspond to EF-Hand I and II, calcium and FAD binding, NADPH-ribose, and NADPH-adenine motifs, respectively.

With the seven identified *RBOH* genes in the sweet pepper transcriptome (RNA-Seq) (González-Gordo et al., 2019), a time-course analysis was done, and among these seven genes, only the designated *RBOH* A, C, D, and E were found to show expression changes in our experimental design. Figure 4A shows the time-course expression analysis of these four *RBOH* genes by RNA-Seq of sweet pepper fruits at different stages of ripening mentioned before including the NO treatment. In all four cases, the *RBOH* gene expression was downregulated from green (G) to red (R) stage. In general, the gene expression in fruits with and without NO treatment (BP2 + NO and BP2 – NO, respectively) both showed intermediate values between those observed for green and red peppers, but in all cases, the NO treatment increased the expression of the four *RBOH* genes. To corroborate these data, RT-qPCR analyses of the genes were done using the same fruit sample set to perform the RNA-Seq approach (Figure 4B). Thus, the expression of the four *RBOH* genes was also downregulated throughout ripening. Additionally, the NO effect (BP2 + NO) in the gene expression did not show significant difference regarding the BP – NO group, with the exception of *RBOH* C expression, which was downregulated.

As part of the  $O_2^{\bullet-}$  metabolism analysis, the SOD system activity and its gene expression during pepper fruit ripening were also studied. Figure 5A depicts the SOD isozyme profile in non-denaturing polyacrylamide gel of sweet pepper fruits at the different ripening stages used in this work: immature green (G), BP1, BP2 with and without NO treatment (BP2 + NO and BP2 – NO, respectively), and ripe red (R). According to the mobility in gels and the response to inhibitors, a total of four SOD isoymes were identified: one Mn-SOD, one Fe-SOD, and two CuZn-SODs. It is remarkable to point out that after the quantification of the SOD in-gel activity, none of the isoymes showed any significant change either during the ripening from green to red fruits or considering the different stages after the NO treatment (Figure 5B).

The search of SOD genes in the sweet pepper transcript database previously obtained by RNA-Seq (González-Gordo et al., 2019) allowed finding a total of eight SOD genes including two *Mn*-SODs, three *Fe*-SODs, and three *CuZn*-SODs. Figure 6A shows the time-course expression analysis of these eight SOD genes (RNA-Seq) of sweet pepper fruits at the different ripening stages reported above. Among these eight SOD genes, only two, *Mn*-SOD I and *Fe*-SOD I, were modulated during ripening and under the NO treatments. Whereas the *Mn*-SOD I expression increased during ripening, the *Fe*-SOD I showed an opposite behavior. Additionally, under NO treatment, the expression of

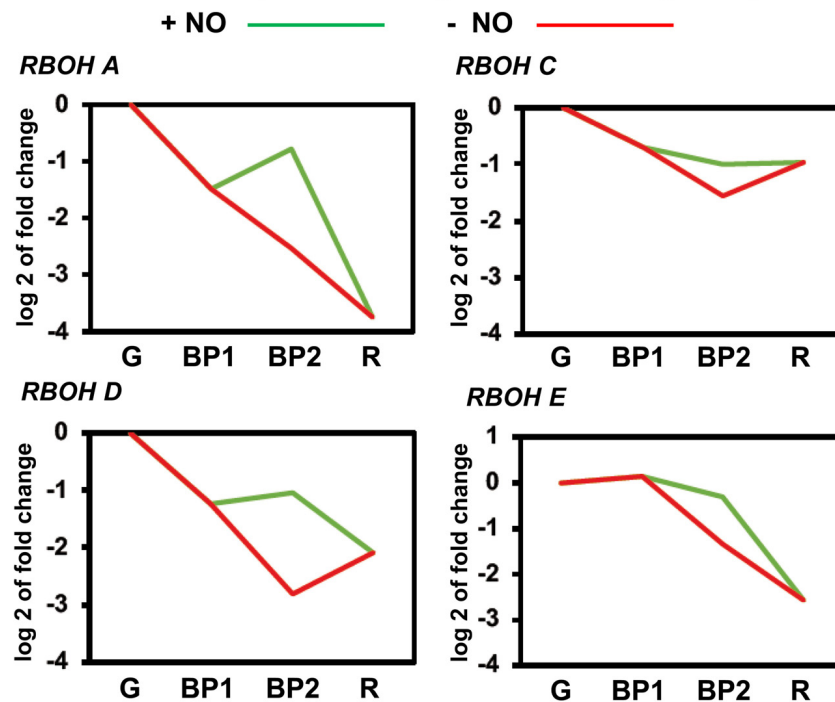
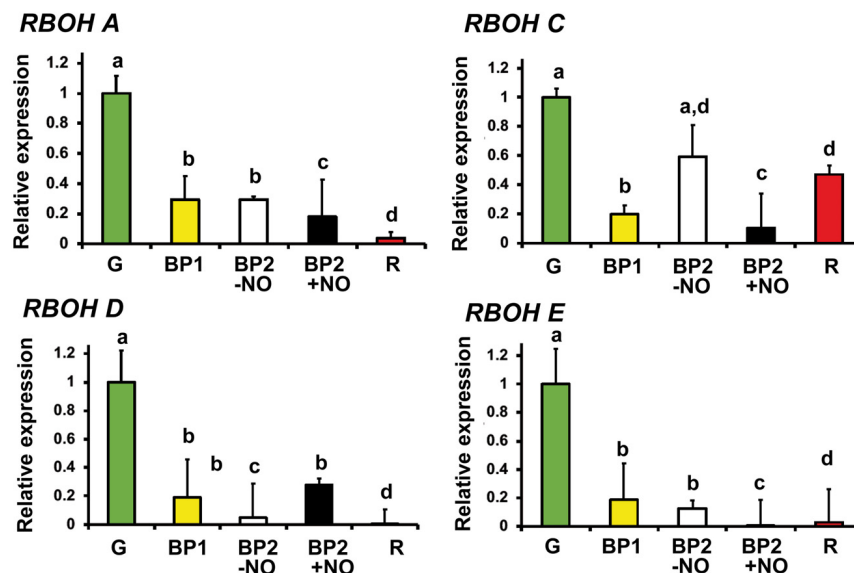


**FIGURE 3 |** Analyses of sweet pepper respiratory burst oxidase homolog (RBOH) isozyms based on their protein sequences. **(A)** Percentage of protein sequence identity among the 10 *Arabidopsis* RBOH isozyms with the seven sweet pepper RBOH isozyms. High, intermediate, and low identities are shown as green, yellow, and red color, respectively. **(B)** Phylogenetic analysis and conserved regions of sweet pepper RBOH proteins. Maximum-likelihood tree of 67 plant RBOH protein sequences. Identified CaRBOH proteins are highlighted in red color. The scale bar represents the phylogenetic branch length. Different subgroups of RBOHs are depicted in different colors (I–VI). Species abbreviations: At (*Arabidopsis thaliana*), Ca (*Capsicum annuum*), Gm (*Glycine max*), Hv (*Hordeum vulgare*), Ls (*Lepidium sativum*), Os (*Oryza sativa*), SI (*Solanum lycopersicum*), and St (*Solanum tuberosum*). **(C)** Conservation of sequence motifs (I–VI) of sweet pepper RBOH protein sequences.

these two genes was also different because *Mn-SOD I* was downregulated after NO treatment whereas *Fe-SOD I* expression increased. The data of the two genes obtained by RNA-Seq were corroborated by RT-qPCR (Figure 6B).

In a previous study, we showed that in sweet pepper, the  $O_2^{\bullet-}$  generation by a NOX system was inhibited in the presence of NO donors, ONOO<sup>-</sup>, and GSH, suggesting that the responsible enzymes could be regulated by S-nitrosation, Tyr-nitration, or glutathionylation, respectively (Chu-Puga et al., 2019). However, to our knowledge, there is no such similar analysis of SOD isozyms from pepper fruits. Consequently, we performed a

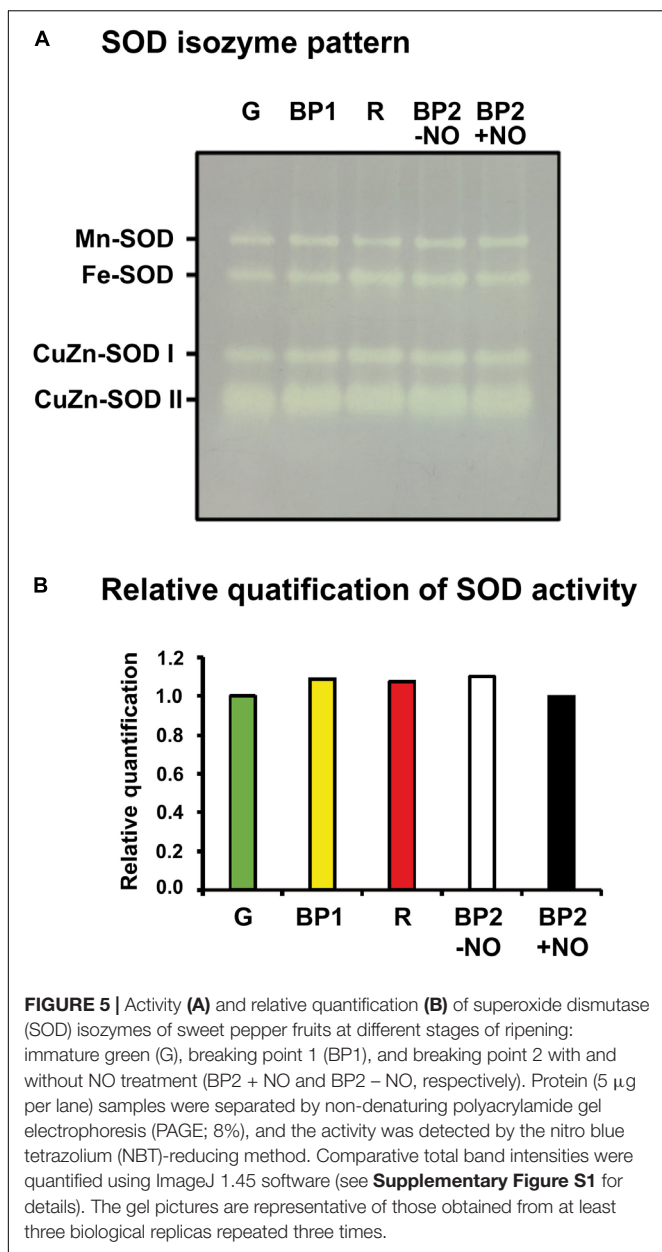
series of biochemical *in vitro* assays of the SOD activity in the presence of different chemicals including 4 mM of SIN-1 as ONOO<sup>-</sup> donor, 4 mM of GSNO and 4 mM of DEA NONOate as NO donor, 4 mM of GSH and 10 mM of DTT as reductants, and 10 mM of H<sub>2</sub>O<sub>2</sub> as oxidant. Figure 7A shows that, except for the slight changes in the electrophoretic mobility of CuZn-SOD II, none of the SOD isozyms present in the red fruits were affected for any of the treatments. To discard potential masking effect, considering that both CuZn-SOD and Fe-SOD activities are well known to be inhibited by H<sub>2</sub>O<sub>2</sub>, it was decided to repeat the experiments, but in this case, the gel was incubated in the

**A Time-course expression analysis of *CaRBOH* genes (RNA-Seq)****B Validation of RNA-Seq using real-time PCR (qRT-PCR)**

**FIGURE 4 | (A)** Time-course expression analysis of four *CaRBOH* genes (RNA-Seq). **(B)** Validation of RNA-Seq data using real-time quantitative PCR (RT-qPCR). Samples of sweet pepper fruits at different stages of ripening correspond to immature green (G), breaking point 1 (BP1), and breaking point 2 with and without NO treatment (BP2 + NO and BP2 - NO, respectively). Each PCR was performed at least three times, with three independent samples. Different letters indicate significant differences ( $P < 0.05$ ).

presence of 5 mM of  $H_2O_2$  once the samples were incubated with the chemicals and the electrophoresis was completed. As observed in **Figure 7B**, and as expected, both CuZn-SODs and Fe-SOD were indeed inhibited whereas the Mn-SOD was unaffected in all cases. With the goal to get deeper knowledge

about SOD isozyme activities and their potential regulation by RNS and distinct redox conditions, a similar analysis was done, but in this case, the gel was incubated with 5 mM of GSH (**Figure 7C**). In this situation, it was observed that none of the SOD isozymes underwent significant changes in its activity.



However, we detected a new CuZn-SOD band close to and faster than the CuZn-SOD I in the samples treated with DEA NONOate and  $H_2O_2$ .

## DISCUSSION

Reactive oxygen species generation is part of the cellular metabolism, and depending on the levels of production and the ROS type, they could have either toxic effects or signal properties. There are evidences that ROS metabolism is involved in a diverse range of plant processes, and the available data indicate that fruit development and ripening have an active ROS metabolism in different species such as grapevine berry

(Pilati et al., 2014), mango (Rosalie et al., 2015), peach (Huan et al., 2016), tomato (Kumar et al., 2016; Zhu et al., 2017), grape berry (Xi et al., 2017), or guava (Mondal et al., 2009; Batista-Silva et al., 2018). In previous reports on sweet pepper ripening, we focused on the  $H_2O_2$  metabolism, and it was found that catalase activity and their gene expression were diminished during ripening. Moreover, catalase was downregulated by NO-mediated posttranslational modifications including Tyr-nitration and S-nitrosation (Chaki et al., 2015; Rodríguez-Ruiz et al., 2019). To get deeper knowledge on the ROS metabolism during sweet pepper ripening, the present study has been focused on another main ROS, specifically in  $O_2^{\bullet-}$ , to analyze some of the biochemical players involved in their generation and decomposition. With the goal to get a deeper understanding of the ROS metabolism during sweet pepper fruit ripening, especially on the metabolism of  $O_2^{\bullet-}$  and its potential modulation under a NO-enrichment environment, we have based on a previous study where we reported the first transcriptome of sweet pepper at different ripening stages, being also compared with the transcriptome under a NO-enrichment environment (González-Gordo et al., 2019). In such study, it was observed that during fruit ripening the ROS metabolism was altered with an increase of lipid oxidation and that NO reduced this parameter with a concomitant increase in the content of GSH and ascorbate peroxidase (APX) activity.

## $O_2^{\bullet-}$ Generation by a NADPH-Dependent Oxidase System Increases During Ripening but Is Negatively Modulated by NO

It should be mentioned that to our knowledge there are only few reports focused on the function of a specific RBOH activity during fruit ripening. In an early study, we found up to seven NADPH-oxidase isozymes that were differently regulated during the ripening of sweet pepper fruits (Chu-Puga et al., 2019). It should be remarked that the identification of the seven isozymes in non-denaturing gel activity assays involved the optimization of the amount of loaded protein samples for each stage being determined in green fruit by almost two-fold the amount found in red fruits. Thus, these seven NADPH-oxidase isozymes with different electrophoretic mobility and abundance were detected considering both green and red fruits. The present data corroborate those previous data, but the analysis of the intermediate ripening stages in the presence of NO (BP2 + NO) showed a fine regulation of this system because isozymes I and III displayed lower activities when they were compared with the BP2 without NO treatment (BP2 – NO); however, one cannot discard the existence of additional isozymes whose activity may be too low for their detection in our experimental conditions. To our knowledge, the only identified NOX that has been reported to be negatively regulated by NO corresponds to the *Arabidopsis* RBOH isozyme D activity (AtRBOHD) that was inhibited by S-nitrosation at Cys825, thus disturbing the mechanism of the immune response (Yun et al., 2011). Very recently, it has been reported that this AtRBOHD is also susceptible to undergo



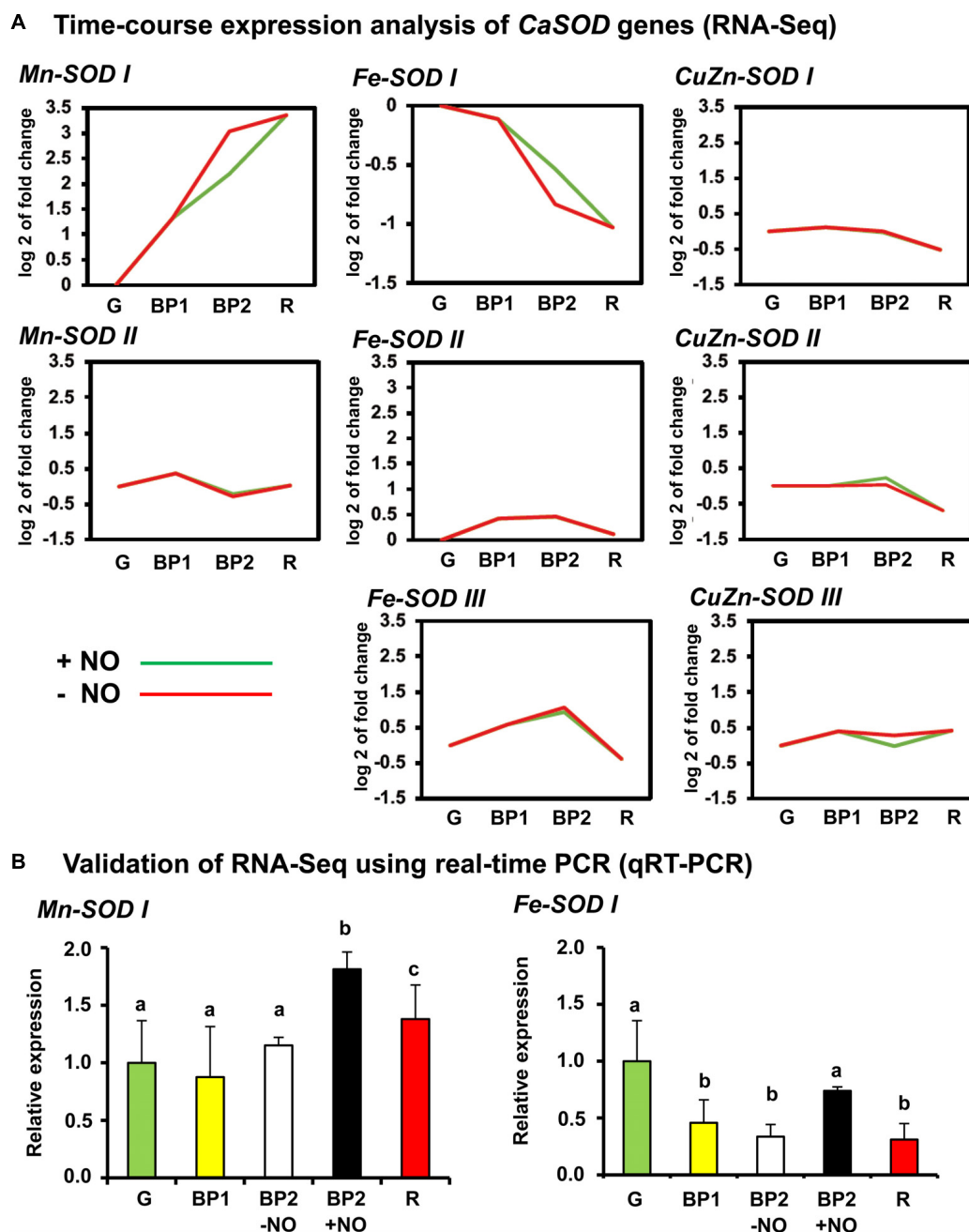
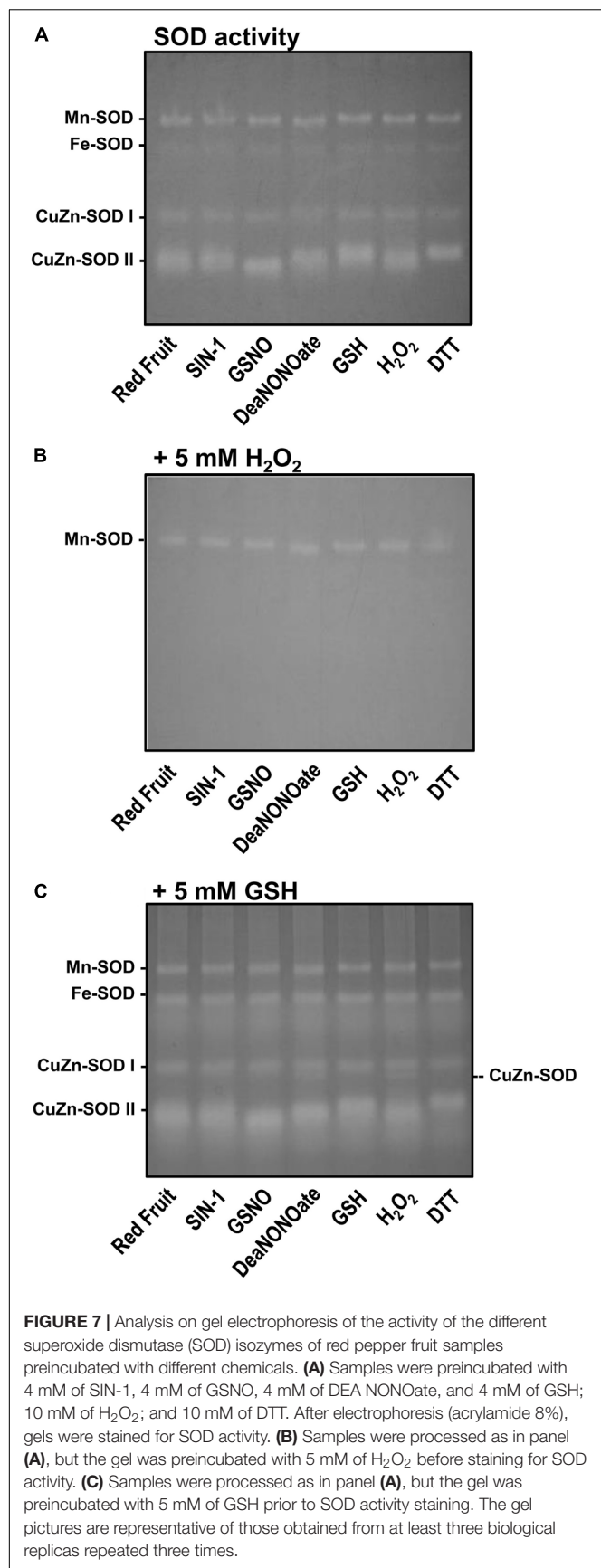


**FIGURE 6 | (A)** Time-course expression analysis of *CaSOD* genes (RNA-Seq). **(B)** Validation of RNA-Seq for *Mn-SOD I* and *Fe-SOD I* genes using real-time quantitative PCR (RT-qPCR). Each PCR was performed at least three times, with three independent samples. Different letters indicate significant differences ( $P < 0.05$ ).

persulfidation, a posttranslational modification mediated by hydrogen sulfide ( $H_2S$ ) (Corpas et al., 2019), at Cys825 and Cys890, provoking an increase in the  $O_2^{\bullet-}$  production, which was relevant in the ABA signaling to induce stomatal closure (Shen et al., 2020). In pepper fruit, we have previously described that the content of endogenous  $H_2S$  increases at ripening (Muñoz-Vargas et al., 2018) and that it could be hypothesized that this  $H_2S$  might be involved in the observed increase of

NOX activity. However, future analyses should be carried out to corroborate this and to identify what isozyme(s) could be the target of persulfidation in our plant model.

On the other hand, these data indicate that this increase in NOX activity might be necessary in the physiological ripening process, and this is concomitant with the enhanced NADPH-generating systems described during sweet pepper ripening, specifically NADP-malic enzyme and 6-phosphogluconate



dehydrogenase activities (Muñoz-Vargas et al., 2020). However, the  $O_2^{\bullet-}$  generation could have other beneficial effects in pepper fruit as a mechanism to prevent potential pathogen infections (Tian et al., 2013). In this sense, the latest results in apricot fruit treated exogenously with polyamines showed that the activities and gene expression levels of NOX systems were triggered, allowing the resistance to the fungus *Alternaria alternata* (Li et al., 2019). Recently, it has been described by *in silico* analyses the identification of the *RBOH* family genes in Chinese white pear (*Pyrus bretschneideri*), which contains 10 *RBOH*s. Among these genes, it was found that *PbRBOHA* and *PbRBOHD* were specially accumulated in pear stone cells, suggesting the involvement of ROS metabolism in the lignification of these cells (Cheng et al., 2019).

### Sweet Pepper Fruit Transcriptome Contains Seven Respiratory Burst Oxidase Homolog Isozymes

Based on the comparative analysis between the *Arabidopsis* *RBOH* genes with the sweet pepper fruit transcriptome (González-Gordo et al., 2019) and their corresponding protein sequences, the seven pepper *RBOH* proteins were designated with the letters A, B, C, D, E, H, and J. All these *RBOH* proteins showed the six characteristic conserved motifs of plant *RBOH*s, which correspond to EF-Hand I and II, calcium and FAD binding sites, NADPH-ribose, and NADPH-adenine (Torres and Dangel, 2005; Kaur et al., 2018). However, the correspondence between the seven NOX isozymes identified with the seven *RBOH* genes reported here need to be confirmed by future experiments where each pepper *RBOH* protein encoded by its respective gene needs to be purified, and their mobility needs be evaluated under non-denaturing gel electrophoresis.

### There Is No Correlation Between NADPH Oxidase and Superoxide Dismutase Isoenzymatic Activities and the Corresponding Genes

In our experimental model of sweet pepper, it should be pointed out that the analyses of activity and gene expression of both NOX and SOD isozymes have different behaviors. Thus, it was found that whereas  $O_2^{\bullet-}$  generation by NOX isoenzymes increased during ripening, the identified *RBOH* genes were downregulated. Comparative observation could be made with the activity of SOD isozymes, which did not show any significant variations, whereas the gene expression of *Mn-SOD* increased, *Fe-SOD* decreased, and *CuZn-SOD* did not change. This apparent contradiction between enzyme activity and gene expression is not unusual, and there are numerous examples where the inexistent correlation between gene expression and their corresponding protein activity has been described. Recently, the analysis of protein and transcript abundance during tomato fruit development and ripening showed a poor correlation owing to, among other factors, the rate of protein translation and degradation; in fact, the levels of transcripts were more reduced than the protein levels (Belouah et al., 2019). Among other factors that could support

these discrepancies, the protein posttranslational modifications including those mediated by ROS or RNS could be considered.

## The Superoxide Dismutase Isoenzymatic Pattern Was Unaffected Either During Ripening or by a NO-Enriched Environment

In a previous study, we showed by *in vitro* analyses that the  $O_2^{\bullet-}$  generation by the NADPH-oxidase system was inhibited in the presence of NO donors, ONOO<sup>-</sup>, and GSH, suggesting that the responsible enzymes can undergo S-nitrosation, Tyronitration, and glutathionylation, respectively (Chu-Puga et al., 2019). Although we did not observe any apparent change in the SOD isoenzymatic activity during ripening or in the NO-enriched atmosphere, we decided to prepare *in vitro* analyses to study the pepper SOD isoenzymatic activity because in the *in vitro* analysis of the seven *Arabidopsis* SOD isozymes, it was reported that, using GSNO as NO donor, none of the *Arabidopsis* SODs were affected. Conversely, peroxyntirite (a nitrating agent) triggered the inhibition of the mitochondrial Mn-SOD, peroxisomal CuZn-SOD (CSD3), and chloroplastic iron SOD3 (FSD3), whereas the other SODs were unaffected (Holzmeister et al., 2015). In our experimental conditions of sweet pepper, neither GSNO nor peroxyntirite seems to affect any of the SOD isozymes. Nevertheless, it was found that the pretreatment of pepper sample with NO and H<sub>2</sub>O<sub>2</sub> previous to the gel analysis of the SOD isozymes allowed to identify a new CuZn-SOD with mobility higher than that of the CuZn-SOD I but slower than that of CuZn-SOD II. A reasonable explanation of the appearance of a new isoenzyme could be due to the presence of two different oxidation states of the CuZn-SOD I corresponding to a mixed Cu(I)/Cu(II) redox pair after these mentioned treatments, such as it has been described in bovine and human CuZn-SOD after isoelectrofocusing analyses (Chevreux et al., 2009). A similar behavior of the potential oxidation of a CuZn-SOD that affected the electrophoretic mobility of the enzyme was also reported for the cytosolic CuZn-SOD from watermelon cotyledons (Palma et al., 1997).

## CONCLUSION

Reactive oxygen species metabolism is of great importance for fruit ripening because it is involved in the process of development and quality (Decros et al., 2019). The present study has focused on the  $O_2^{\bullet-}$  metabolism in the non-climacteric sweet pepper ripening, and the data support that  $O_2^{\bullet-}$ -generating NOX production increases during ripening being regulated by NO. On the other hand, the SOD activity of the different isoenzymes was unaffected during ripening, and it should be pointed out that none of the SOD isozymes were significantly affected by any of the assayed *in vitro* nitro-oxidative conditions. This suggests that the basal SOD activity is sufficient to keep the homeostasis of the necessary physiological  $O_2^{\bullet-}$  production during sweet pepper ripening. This prevalence of  $O_2^{\bullet-}$  production could have additional benefits because they could be a barrier to prevent

potential pathogen infections. Moreover, these new data of the prevalence of  $O_2^{\bullet-}$ -generating NOX during sweet pepper fruit ripening should be also integrated with the NADPH-generating system constituted by a group of NADP-dehydrogenases, which are regulated by signal molecules such as NO and H<sub>2</sub>S (Muñoz-Vargas et al., 2018, 2020). Additionally, future analyses should be developed to understand the integration of the redox homeostasis with the phytohormones including ABA, indole-3-acetic acid, gibberellins, cytokinins, or jasmonic acid involved in the ripening of sweet pepper considering that it is a non-climacteric fruit (Symons et al., 2012; Fuentes et al., 2019; Sun et al., 2019). This will allow to extend our knowledge of the complex network of involved signal molecules in this physiological process.

## DATA AVAILABILITY STATEMENT

The datasets generated for this study are available on request to the corresponding author.

## AUTHOR CONTRIBUTIONS

FC and JP conceived and designed the experiments. SG-G and MR-R performed the experiments. SG-G, JP, and FC analyzed the data. All authors contributed to drafting the work, revised the final manuscript, and approved submission.

## FUNDING

The research work of FC and JP is supported by a European Regional Development Fund-cofinanced grant from the Ministry of Economy and Competitiveness (AGL2015-65104-P and PID2019-103924GB-I00), the Plan Andaluz de Investigación, Desarrollo e Innovación (PAIDI 2020) (P18-FR-1359), and Junta de Andalucía (group BIO192), Spain.

## ACKNOWLEDGEMENTS

SG-G acknowledges a “Formación de Personal Investigador” contract (BES-2016-078368) from the Ministry of Economy and Competitiveness, Spain. The provision of pepper fruits by Zeraim Iberica/Syngenta Seeds Ltd. (El Ejido, Almería, Spain) is acknowledged, especially Víctor J. Domínguez, Lidia Martín, and Manuel Solís. The valuable technical assistance of Mrs. María J. Campos, Mr. Carmelo Ruiz-Torres, and Dr. Pancraccio is deeply acknowledged.

## SUPPLEMENTARY MATERIAL

The Supplementary Material for this article can be found online at: <https://www.frontiersin.org/articles/10.3389/fpls.2020.00485/full#supplementary-material>

## REFERENCES

- Airaki, M., Letierrier, M., Mateos, R. M., Valderrama, R., Chaki, M., Barroso, J. B., et al. (2012). Metabolism of reactive oxygen species and reactive nitrogen species in pepper (*Capsicum annuum* L.) plants under low temperature stress. *Plant Cell Environ.* 35, 281–295. doi: 10.1111/j.1365-3040.2011.02310.x
- Almansa, M. S., del Río, L. A., Alcaraz, C. F., and Sevilla, F. (1989). Isoenzyme pattern of superoxide dismutase in different varieties of *Citrus* plants. *Physiol. Plant* 76, 563–568.
- Asada, K., Urano, M., and Takahashi, M. (1973). Subcellular location of superoxide dismutase in spinach leaves and preparation and properties of crystalline spinach superoxide dismutase. *Eur. J. Biochem.* 36, 257–266. doi: 10.1111/j.1432-1033.1973.tb02908.x
- Batista-Silva, W., Cosme Silva, G. M., Santana, D. B., Salvador, A. R., Medeiros, D. B., Belghith, I., et al. (2018). Chitosan delays ripening and ROS production in guava (*Psidium guajava* L.) fruit. *Food Chem.* 242, 232–238. doi: 10.1016/j.foodchem.2017.09.052
- Beauchamp, C., and Fridovich, I. (1971). Superoxide dismutase: improved assays and an assay applicable to acrylamide gels. *Anal. Biochem.* 44, 276–287. doi: 10.1016/0003-2697(71)90370-8
- Belouah, I., Nazaret, C., Pétiacq, P., Prigent, S., Bénard, C., Mengin, V., et al. (2019). Modeling protein destiny in developing fruit. *Plant Physiol.* 180, 1709–1724. doi: 10.1104/pp.19.00086
- Bin, W. S., Wei, L. K., Ping, D. W., Li, Z., Wei, G., Bing, L. J., et al. (2012). Evaluation of appropriate reference genes for gene expression studies in pepper by quantitative real-time PCR. *Mol. Breed.* 30, 1393–1400.
- Bridges, S. M., and Salin, M. L. (1981). Distribution of iron-containing superoxide dismutase in vascular plants. *Plant Physiol.* 68, 275–278. doi: 10.1104/pp.68.2.275
- Camejo, D., Jiménez, A., Palma, J. M., and Sevilla, F. (2015). Proteomic identification of mitochondrial carbonylated proteins in two maturation stages of pepper fruits. *Proteomics* 15, 2634–2642. doi: 10.1002/pmic.201400370
- Chaki, M., Álvarez de Morales, P., Ruiz, C., Begara-Morales, J. C., Barroso, J. B., Corpas, F. J., et al. (2015). Ripening of pepper (*Capsicum annuum*) fruit is characterized by an enhancement of protein tyrosine nitration. *Ann. Bot.* 116, 637–647. doi: 10.1093/aob/mcv016
- Cheng, C., Xu, X., Gao, M., Li, J., Guo, C., Song, J., et al. (2013). Genome-wide analysis of respiratory burst oxidase homologs in grape (*Vitis vinifera* L.). *Int. J. Mol. Sci.* 14, 24169–24186. doi: 10.3390/ijms141224169
- Cheng, X., Li, G., Manzoor, M. A., Wang, H., Abdullah, M., Su, X., et al. (2019). In silico genome-wide analysis of respiratory burst oxidase homolog (RBOH) family genes in five fruit-producing trees, and potential functional analysis on lignification of stone cells in chinese white pear. *Cells* 8:E520. doi: 10.3390/cells8060520
- Chevieux, S., Roudeau, S., Frayssé, A., Carmona, A., Devès, G., Solari, P. L., et al. (2009). Multimodal analysis of metals in copper-zinc superoxide dismutase isoforms separated on electrophoresis gels. *Biochimie* 91, 1324–1327. doi: 10.1016/j.biochi.2009.05.016
- Chiaiese, P., Corrado, G., Minutolo, M., Barone, A., and Errico, A. (2019). Transcriptional regulation of ascorbic acid during fruit ripening in pepper (*Capsicum annuum*) varieties with low and high antioxidants content. *Plants (Basel)* 8:206. doi: 10.3390/plants8070206
- Chu-Puga, Á., González-Gordo, S., Rodríguez-Ruiz, M., Palma, J. M., and Corpas, F. J. (2019). NADPH oxidase (Rboh) activity is up regulated during sweet pepper (*Capsicum annuum* L.) fruit ripening. *Antioxidants (Basel)* 8:E9. doi: 10.3390/antiox8010009
- Corpas, F. J., Fernández-Ocaña, A., Carreras, A., Valderrama, R., Luque, F., and Esteban, F. J. (2006). The expression of different superoxide dismutase forms is cell-type dependent in olive (*Olea europaea* L.) leaves. *Plant Cell Physiol.* 47, 984–994. doi: 10.1093/pcp/pcj071
- Corpas, F. J., Freschi, L., Rodríguez-Ruiz, M., Miotto, P. T., González-Gordo, S., and Palma, J. M. (2018). Nitro-oxidative metabolism during fruit ripening. *J. Exp. Bot.* 69, 3449–3463. doi: 10.1093/jxb/erx453
- Corpas, F. J., González-Gordo, S., Cañas, A., and Palma, J. M. (2019). Nitric oxide and hydrogen sulfide in plants: which comes first? *J. Exp. Bot.* 70, 4391–4404. doi: 10.1093/jxb/erz031
- Corpas, F. J., and Palma, J. M. (2018). Nitric oxide on/off in fruit ripening. *Plant Biol.* 20, 805–807. doi: 10.1111/plb.12852
- Corpas, F. J., Sandalio, L. M., del Río, L. A., and Trelease, R. N. (1998). Copper-zinc superoxide dismutase is a constituent enzyme of the matrix of peroxisomes in the cotyledons of oilseed plants. *New Phytol.* 138, 307–314.
- Corpas, F. J., Sandalio, L. M., Palma, J. M., Leidi, E. O., Hernández, J. A., Sevilla, F., et al. (1991). Subcellular distribution of superoxide dismutase in leaves of ureide-producing leguminous plant. *Physiol. Plant.* 82, 285–291.
- Decros, G., Baldet, P., Beauvoit, B., Stevens, R., Flandin, A., Colombié, S., et al. (2019). Get the balance right: ROS homeostasis and redox signalling in fruit. *Front. Plant Sci.* 10:1091. doi: 10.3389/fpls.2019.01091
- del Río, L. A., Corpas, F. J., López-Huertas, E., and Palma, J. M. (2018). “Plant superoxide dismutases: function under abiotic stress conditions,” in *Antioxidants and Antioxidant Enzymes in Higher Plants*, eds D. K. Gupta, J. M. Palma, and F. J. Corpas, (Cham: Springer International Publishing), 1–26.
- Fanciullino, A. L., Bidel, L. P., and Urban, L. (2014). Carotenoid responses to environmental stimuli: integrating redox and carbon controls into a fruit model. *Plant Cell Environ.* 37, 273–289. doi: 10.1111/pce.12153
- Fonseca-García, C., Zayas, A. E., Montiel, J., Nava, N., Sánchez, F., and Quinto, C. (2019). Transcriptome analysis of the differential effect of the NADPH oxidase gene RbohB in *Phaseolus vulgaris* roots following *Rhizobium tropici* and *Rhizophagus irregularis* inoculation. *BMC Genomics*. 20:800. doi: 10.1186/s12864-019-6162-7
- Fuentes, L., Carlos, R., Figuero, C. R., and Valdenegro, M. (2019). Recent advances in hormonal regulation and cross-talk during non-climacteric fruit development and ripening. *Horticulturae* 5:45.
- Giovannoni, J. (2001). Molecular biology of fruit maturation and ripening. *Annu. Rev. Plant Physiol. Plant Mol. Biol.* 52, 725–749. doi: 10.1146/annurev.arplant.52.1.725
- Gómez-García, M. R., and Ochoa-Alejo, N. (2013). Biochemistry and molecular biology of carotenoid biosynthesis in chili peppers (*Capsicum* spp.). *Int. J. Mol. Sci.* 14, 19025–19053. doi: 10.3390/ijms140919025
- González-Gayte, I., Moreno, R. B., Zonjic, P. S., and Claros, M. G. (2017). DEgenes Hunter – a flexible R pipeline for automated RNA-seq studies in organisms without reference genome. *Genomics Comput. Biol.* 3:31.
- González-Gordo, S., Bautista, R., Claros, M. G., Cañas, A., Palma, J. M., and Corpas, F. J. (2019). Nitric oxide-dependent regulation of sweet pepper fruit ripening. *J. Exp. Bot.* 70, 4557–4570. doi: 10.1093/jxb/erz136
- Holzmeister, C., Gaupels, F., Geerlof, A., Sarioglu, H., Sattler, M., Durner, J., et al. (2015). Differential inhibition of *Arabidopsis* superoxide dismutases by peroxynitrite-mediated tyrosine nitration. *J. Exp. Bot.* 66, 989–999. doi: 10.1093/jxb/eru458
- Houmani, H., Rodríguez-Ruiz, M., Palma, J. M., Abdelly, C., and Corpas, F. J. (2016). Modulation of superoxide dismutase (SOD) isozymes by organ development and high long-term salinity in the halophyte *Cakile maritima*. *Protoplasma* 253, 885–894. doi: 10.1007/s00709-015-0850-1
- Huan, C., Jiang, L., An, X., Yu, M., Xu, Y., Ma, R., et al. (2016). Potential role of reactive oxygen species and antioxidant genes in the regulation of peach fruit development and ripening. *Plant Physiol. Biochem.* 104, 294–303. doi: 10.1016/j.plaphy.2016.05.013
- Jiménez, A., Romojaro, F., Gómez, J. M., Llanos, M. R., and Sevilla, F. (2003). Antioxidant systems and their relationship with the response of pepper fruits to storage at 20 degrees C. *J. Agric. Food Chem.* 51, 6293–6299. doi: 10.1021/jf030052i
- Jiménez-Quesada, M. J., Traverso, J. Á., and Alché, J. D. (2016). NADPH oxidase-dependent superoxide production in plant reproductive tissues. *Front. Plant Sci.* 7:359. doi: 10.3389/fpls.2016.00359
- Jiménez-Quesada, M. J., Traverso, J. A., Potocký, M., Žárský, V., and Alché, J. D. (2019). Generation of superoxide by OeRbohH, a NADPH oxidase activity during olive (*Olea europaea* L.) pollen development and germination. *Front. Plant Sci.* 10:1149. doi: 10.3389/fpls.2019.01149
- Karlova, R., Chapman, N., David, K., Angenent, G. C., Seymour, G. B., and de Maagd, R. A. (2014). Transcriptional control of fleshy fruit development and ripening. *J. Exp. Bot.* 65, 4527–4541. doi: 10.1093/jxb/eru316
- Kaur, G., and Pati, P. K. (2018). In silico insights on diverse interacting partners and phosphorylation sites of respiratory burst oxidase homolog (Rbohs) gene families from *Arabidopsis* and rice. *BMC Plant Biol.* 18:161. doi: 10.1186/s12870-018-1378-2



- Kaur, G., Guruprasad, K., Temple, B. R. S., Shirvanyants, D. G., Dokholyan, N. V., and Pati, P. K. (2018). Structural complexity and functional diversity of plant NADPH oxidases. *Amino Acids* 50, 79–94. doi: 10.1007/s00726-017-2491-5
- Kaya, H., Takeda, S., Kobayashi, M. J., Kimura, S., Iizuka, A., Imai, A., et al. (2019). Comparative analysis of the reactive oxygen species-producing enzymatic activity of Arabidopsis NADPH oxidases. *Plant J.* 98, 291–300. doi: 10.1111/tj.14212
- Kumar, V., Irfan, M., Ghosh, S., Chakraborty, N., Chakraborty, S., and Datta, A. (2016). Fruit ripening mutants reveal cell metabolism and redox state during ripening. *Protoplasma* 253, 581–594. doi: 10.1007/s00709-015-0836-z
- Léchaudel, M., Darnaudery, M., Joët, T., Fournier, P., and Joas, J. (2018). Genotypic and environmental effects on the level of ascorbic acid, phenolic compounds and related gene expression during pineapple fruit development and ripening. *Plant Physiol. Biochem.* 130, 127–138. doi: 10.1016/j.plaphy.2018.06.041
- Leterrier, M., Airaki, M., Palma, J. M., Chaki, M., Barroso, J. B., and Corpas, F. J. (2012). Arsenic triggers the nitric oxide (NO) and S-nitrosoglutathione (GSNO) metabolism in *Arabidopsis*. *Environ. Pollut.* 166, 136–143. doi: 10.1016/j.envpol.2012.03.012
- Li, Y., Ma, Y., Zhang, T., Bi, Y., Wang, Y., and Prusky, D. (2019). Exogenous polyamines enhance resistance to *Alternaria alternata* by modulating redox homeostasis in apricot fruit. *Food Chem.* 301:125303. doi: 10.1016/j.foodchem.2019.125303
- Liu, Y., Lv, J., Liu, Z., Wang, J., Yang, B., Chen, W., et al. (2020). Integrative analysis of metabolome and transcriptome reveals the mechanism of color formation in pepper fruit (*Capsicum annuum* L.). *Food Chem.* 306:125629. doi: 10.1016/j.foodchem.2019.125629
- Li, X., Zhang, H., Tian, L., Huang, L., Liu, S., Li, D., et al. (2015). Tomato SlRbohB, a member of the NADPH oxidase family, is required for disease resistance against Botrytis cinerea and tolerance to drought stress. *Front. Plant Sci.* 6:463. doi: 10.3389/fpls.2015.00463
- Marino, D., Dunand, C., Puppo, A., and Pauly, N. (2012). A burst of plant NADPH oxidases. *Trends Plant Sci.* 17, 9–15. doi: 10.1016/j.tplants.2011.10.001
- Martí, M. C., Camejo, D., Olmos, E., Sandalio, L. M., Fernández-García, N., Jiménez, A., et al. (2009). Characterisation and changes in the antioxidant system of chloroplasts and chromoplasts isolated from green and mature pepper fruits. *Plant Biol. (Stuttg)* 11, 613–624. doi: 10.1111/j.1438-8677.2008.00149.x
- Martí, M. C., Camejo, D., Vallejo, F., Romojaro, F., Bacarizo, S., Palma, J. M., et al. (2011). Influence of fruit ripening stage and harvest period on the antioxidant content of sweet pepper cultivars. *Plant Foods Hum. Nutr.* 66, 416–423. doi: 10.1007/s11130-011-0249-x
- Mateos, R. M., Bonilla-Valverde, D., del Río, L. A., Palma, J. M., and Corpas, F. J. (2009). NADP-dehydrogenases from pepper fruits: effect of maturation. *Physiol. Plant* 135, 130–139. doi: 10.1111/j.1399-3054.2008.01179.x
- Mateos, R. M., Jiménez, A., Román, P., Romojaro, F., Bacarizo, S., Leterrier, M., et al. (2013). Antioxidant systems from pepper (*Capsicum annuum* L.): involvement in the response to temperature changes in ripe fruits. *Int. J. Mol. Sci.* 14, 9556–9580. doi: 10.3390/ijms14059556
- Mondal, K., Malhotra, S. P., Jain, V., and Singh, R. (2009). Oxidative stress and antioxidant systems in guava (*Psidium guajava* L.) fruits during ripening. *Physiol. Mol. Biol. Plants* 15, 327–334. doi: 10.1007/s12298-009-0037-3
- Montiel, J., Nava, N., Cárdenas, L., Sánchez-López, R., Arthikala, M. K., Santana, O., et al. (2012). A *Phaseolus vulgaris* NADPH oxidase gene is required for root infection by Rhizobia. *Plant Cell Physiol.* 53, 1751–1767. doi: 10.1093/pcp/pcs120
- Müller, K., Carstens, A. C., Linkies, A., Torres, M. A., and Leubner-Metzger, G. (2009). The NADPH-oxidase AtrbohB plays a role in *Arabidopsis* seed after-ripening. *New Phytol.* 184, 885–897. doi: 10.1111/j.1469-8137.2009.03005.x
- Muñoz-Vargas, M. A., González-Gordo, S., Cañas, A., López-Jaramillo, J., Palma, J. M., and Corpas, F. J. (2018). Endogenous hydrogen sulfide (H<sub>2</sub>S) is up-regulated during sweet pepper (*Capsicum annuum* L.) fruit ripening. In vitro analysis shows that NADP-dependent isocitrate dehydrogenase (ICDH) activity is inhibited by H<sub>2</sub>S and NO. *Nitric Oxide* 81, 36–45. doi: 10.1016/j.niox.2018.10.002
- Muñoz-Vargas, M. A., González-Gordo, S., Palma, J. M., and Corpas, F. J. (2020). Inhibition of NADP-malic enzyme activity by H<sub>2</sub>S and NO in sweet pepper (*Capsicum annuum* L.) fruits. *Physiol. Plant* 168, 278–288. doi: 10.1111/ppl.13000
- Osorio, S., Scossa, F., and Fernie, A. R. (2013). Molecular regulation of fruit ripening. *Front. Plant Sci.* 4:198. doi: 10.3389/fpls.2013.00198
- Ou, L. J., Zhang, Z. Q., Dai, X. Z., and Zou, X. X. (2013). Photooxidation tolerance characters of a new purple pepper. *PLoS One* 8:e63593. doi: 10.1371/journal.pone.0063593
- Palma, J. M., de Morales, P. Á., del Río, L. A., and Corpas, F. J. (2018). The proteome of fruit peroxisomes: sweet pepper (*Capsicum annuum* L.) as a model. *Subcell Biochem.* 89, 323–341. doi: 10.1007/978-981-13-2233-4\_14
- Palma, J. M., Freschi, L., Rodríguez-Ruiz, M., González-Gordo, S., and Corpas, F. J. (2019). Nitric oxide in the physiology and quality of fleshy fruits. *J. Exp. Bot.* 70, 4405–4417. doi: 10.1093/jxb/erz350
- Palma, J. M., Pastori, G. M., Bueno, P., Distefano, S., and del Río, L. A. (1997). Purification and properties of cytosolic copper, zinc superoxide dismutase from watermelon (*Citrullus vulgaris* Schrad.) cotyledons. *Free Radic. Res.* 26, 83–91. doi: 10.3109/10715769709097787
- Palma, J. M., Sevilla, F., Jiménez, A., del Río, L. A., Corpas, F. J., Álvarez de Morales, P., et al. (2015). Physiology of pepper fruit and the metabolism of antioxidants: chloroplasts, mitochondria and peroxisomes. *Ann. Bot.* 116, 627–636. doi: 10.1093/aob/mcv121
- Palma, J. M., Ruiz, C., and Corpas, F. J. (2018). A simple and useful method to apply exogenous no gas to plant systems: bell pepper fruits as a model. *Methods Mol. Biol.* 1747, 3–11. doi: 10.1007/978-1-4939-7695-9\_1
- Pascual, I., Azcona, I., Aguirreola, J., Morales, F., Corpas, F. J., Palma, J. M., et al. (2010). Growth, yield, and fruit quality of pepper plants amended with two sanitized sewage sludges. *J. Agric. Food Chem.* 58, 6951–6959. doi: 10.1021/jf100282f
- Pinilla, M., Iglesias-Moya, J., Campos, M. J., Corpas, F. J., and Palma, J. M. (2019). Pomegranate (*Punica granatum* L.) fruits: characterization of the main enzymatic antioxidants (peroxisomal catalase and SOD isozymes) and the NADPH-regenerating system. *Agronomy* 9:338.
- Pilati, S., Brazzale, D., Guella, G., Milli, A., Ruberti, C., Biasioli, F., et al. (2014). The onset of grapevine berry ripening is characterized by ROS accumulation and lipoxygenase-mediated membrane peroxidation in the skin. *BMC Plant Biol.* 14:87. doi: 10.1186/1471-2229-14-87
- Qu, Y., Yan, M., and Zhang, Q. (2017). Functional regulation of plant NADPH oxidase and its role in signaling. *Plant Signal. Behav.* 12:e1356970. doi: 10.1080/15592324.2017.1356970
- Ribes-Moya, A. M., Adalid, A. M., Raigón, M. D., Hellín, P., Fita, A., and Rodríguez-Burruezo, A. (2020). Variation in flavonoids in a collection of peppers (*Capsicum* sp.) under organic and conventional cultivation: effect of the genotype, ripening stage, and growing system. *J. Sci. Food Agric.* 100, 2208–2223. doi: 10.1002/jsfa.10245
- Rodríguez-Ruiz, M., Mateos, R. M., Codesido, V., Corpas, F. J., and Palma, J. M. (2017). Characterization of the galactono-1,4-lactone dehydrogenase from pepper fruits and its modulation in the ascorbate biosynthesis. Role of nitric oxide. *Redox Biol.* 12, 171–181. doi: 10.1016/j.redox.2017.02.009
- Rodríguez-Ruiz, M., Mito, P., Palma, J. M., and Corpas, F. J. (2017). S-nitrosoglutathione reductase (GSNOR) activity is down-regulated during pepper (*Capsicum annuum* L.) fruit ripening. *Nitric Oxide* 68, 51–55. doi: 10.1016/j.niox.2016.12.011
- Rodríguez-Ruiz, M., González-Gordo, S., Cañas, A., Campos, M. J., Paradela, A., Corpas, F. J., et al. (2019). Sweet pepper (*Capsicum annuum* L.) fruits contain an atypical peroxisomal catalase that is modulated by reactive oxygen and nitrogen species. *Antioxidants (Basel)* 8:E374. doi: 10.3390/antiox8090374
- Rosalie, R., Joas, J., Deytieu-Belleau, C., Vulcain, E., Payet, B., Dufossé, L., et al. (2015). Antioxidant and enzymatic responses to oxidative stress induced by pre-harvest water supply reduction and ripening on mango (*Mangifera indica* L. cv. 'Cogshall') in relation to carotenoid content. *J. Plant Physiol.* 184, 68–78. doi: 10.1016/j.jplph.2015.05.019
- Sagi, M., and Fluhr, R. (2006). Production of reactive oxygen species by plant NADPH oxidases. *Plant Physiol.* 141, 336–340. doi: 10.1104/pp.106.078089
- Schmittgen, T. D., and Livak, K. J. (2008). Analyzing real-time PCR data by the comparative C T method. *Nat. Protoc.* 3, 1101–1108. doi: 10.1038/nprot.2008.73
- Seoane, P., Espigares, M., Carmona, R., Polonio, Á., Quintana, J., Cretazzo, E., et al. (2018). TransFlow: a modular framework for assembling and assessing accurate de novo transcriptomes in non-model organisms. *BMC Bioinform.* 19:416. doi: 10.1186/s12859-018-2384-y

- Shen, J., Zhang, J., Zhou, M., Zhou, H., Cui, B., Gotor, C., et al. (2020). Persulfidation-based modification of cysteine desulphydrase and the NADPH oxidase RBOHD controls guard cell abscisic acid signaling. *Plant Cell* 32, 1000–1017. doi: 10.1105/tpc.19.00826
- Sun, L. R., Zhao, Z. J., and Hao, F. S. (2019). NADPH oxidases, essential players of hormone signalings in plant development and response to stresses. *Plant Signal. Behav.* 14:1657343. doi: 10.1080/15592324.2019.1657343
- Suzuki, N., Miller, G., Morales, J., Shulaev, V., Torres, M. A., and Mittler, R. (2011). Respiratory burst oxidases: the engines of ROS signaling. *Curr. Opin. Plant Biol.* 14, 691–699. doi: 10.1016/j.pbi.2011.07.014
- Symons, G. M., Chua, Y. J., Ross, J. J., Quittenden, L. J., Davies, N. W., and Reid, J. B. (2012). Hormonal changes during non-climacteric ripening in strawberry. *J. Exp. Bot.* 63, 4741–4750. doi: 10.1093/jxb/ers147
- Tanou, G., Minas, I. S., Karagiannis, E., Tsikou, D., Audebert, S., Papadopoulou, K. K., et al. (2015). The impact of sodium nitroprusside and ozone in kiwifruit ripening physiology: a combined gene and protein expression profiling approach. *Ann. Bot.* 116, 649–662. doi: 10.1093/aob/mcv107
- Tian, S., Qin, G., and Li, B. (2013). Reactive oxygen species involved in regulating fruit senescence and fungal pathogenicity. *Plant Mol. Biol.* 82, 593–602. doi: 10.1007/s11103-013-0035-2
- Torres, M. A., and Dangel, J. L. (2005). Functions of the respiratory burst oxidase in biotic interactions, abiotic stress and development. *Curr. Opin. Plant Biol.* 8, 397–403. doi: 10.1016/j.pbi.2005.05.014
- Wan, H., Yuan, W., Ruan, M., Ye, Q., Wang, R., Li, Z., et al. (2011). Identification of reference genes for reverse transcription quantitative real-time PCR normalization in pepper (*Capsicum annuum* L.). *BBRC* 416, 24–30. doi: 10.1016/j.bbrc.2011.10.105
- Wang, G. F., Li, W. Q., Li, W. Y., Wu, G. L., Zhou, C. Y., and Chen, K. M. (2013). Characterization of rice NADPH oxidase genes and their expression under various environmental conditions. *Int. J. Mol. Sci.* 14, 9440–9458. doi: 10.3390/ijms14059440
- Wang, W., Chen, D., Zhang, X., Liu, D., Cheng, Y., and Shen, F. (2018). Role of plant respiratory burst oxidase homologs in stress responses. *Free Radic. Res.* 52, 826–839. doi: 10.1080/10715762.2018.1473572
- Xi, F. F., Guo, L. L., Yu, Y. H., Wang, Y., Li, Q., Zhao, H. L., et al. (2017). Comparison of reactive oxygen species metabolism during grape berry development between ‘Kyoho’ and its early ripening bud mutant ‘Fengzao’. *Plant Physiol. Biochem.* 118, 634–642. doi: 10.1016/j.plaphy.2017.08.007
- Yun, B. W., Feechan, A., Yin, M., Saidi, N. B., Le Bihan, T., Yu, M., et al. (2011). S-nitrosylation of NADPH oxidase regulates cell death in plant immunity. *Nature* 478, 264–268. doi: 10.1038/nature10427
- Zhang, Y., Li, Y., He, Y., Hu, W., Zhang, Y., Wang, X., et al. (2018). Identification of NADPH oxidase family members associated with cold stress in strawberry. *FEBS Open Bio* 8, 593–605. doi: 10.1002/2211-5463.12393
- Zhu, Z., Chen, Y., Shi, G., and Zhang, X. (2017). Selenium delays tomato fruit ripening by inhibiting ethylene biosynthesis and enhancing the antioxidant defense system. *Food Chem.* 219, 179–184. doi: 10.1016/j.foodchem.2016.09.138

**Conflict of Interest:** The authors declare that the research was conducted in the absence of any commercial or financial relationships that could be construed as a potential conflict of interest.

Copyright © 2020 González-Gordo, Rodríguez-Ruiz, Palma and Corpas. This is an open-access article distributed under the terms of the Creative Commons Attribution License (CC BY). The use, distribution or reproduction in other forums is permitted, provided the original author(s) and the copyright owner(s) are credited and that the original publication in this journal is cited, in accordance with accepted academic practice. No use, distribution or reproduction is permitted which does not comply with these terms.



# Roles for Plant Mitochondrial Alternative Oxidase Under Normoxia, Hypoxia, and Reoxygenation Conditions

Jayamini Jayawardhane<sup>1</sup>, Devin W. Cochrane<sup>1</sup>, Poorva Vyas<sup>1</sup>, Natalia V. Bykova<sup>2</sup>, Greg C. Vanlerberghe<sup>3,4</sup> and Abir U. Igamberdiev<sup>1\*</sup>

<sup>1</sup> Department of Biology, Memorial University of Newfoundland, St. John's, NL, Canada, <sup>2</sup> Morden Research and Development Centre, Agriculture and Agri-Food Canada, Morden, MB, Canada, <sup>3</sup> Department of Biological Sciences, University of Toronto Scarborough, Toronto, ON, Canada, <sup>4</sup> Department of Cell and Systems Biology, University of Toronto Scarborough, Toronto, ON, Canada

## OPEN ACCESS

### Edited by:

Christian Lindermayr,  
Helmholtz Zentrum München,  
Germany

### Reviewed by:

David M. Rhoads,  
California State University,  
San Bernardino, United States  
Bożena Szal,  
University of Warsaw, Poland

### \*Correspondence:

Abir U. Igamberdiev  
igamberdiev@mun.ca

### Specialty section:

This article was submitted to  
Plant Abiotic Stress,  
a section of the journal  
Frontiers in Plant Science

**Received:** 20 February 2020

**Accepted:** 16 April 2020

**Published:** 15 May 2020

### Citation:

Jayawardhane J, Cochrane DW, Vyas P, Bykova NV, Vanlerberghe GC and Igamberdiev AU (2020) Roles for Plant Mitochondrial Alternative Oxidase Under Normoxia, Hypoxia, and Reoxygenation Conditions. *Front. Plant Sci.* 11:566. doi: 10.3389/fpls.2020.00566

Alternative oxidase (AOX) is a non-energy conserving terminal oxidase in the plant mitochondrial electron transport chain (ETC) that has a lower affinity for oxygen than does cytochrome (cyt) oxidase. To investigate the role(s) of AOX under different oxygen conditions, wild-type (WT) *Nicotiana tabacum* plants were compared with AOX knockdown and overexpression plants under normoxia, hypoxia (near-anoxia), and during a reoxygenation period following hypoxia. Paradoxically, under all the conditions tested, the AOX amount across plant lines correlated positively with leaf energy status (ATP/ADP ratio). Under normoxia, AOX was important to maintain respiratory carbon flow, to prevent the mitochondrial generation of superoxide and nitric oxide (NO), to control lipid peroxidation and protein S-nitrosylation, and possibly to reduce the inhibition of cyt oxidase by NO. Under hypoxia, AOX was again important in preventing superoxide generation and lipid peroxidation, but now contributed positively to NO amount. This may indicate an ability of AOX to generate NO under hypoxia, similar to the nitrite reductase activity of cyt oxidase under hypoxia. Alternatively, it may indicate that AOX activity simply reduces the amount of superoxide scavenging of NO, by reducing the availability of superoxide. The amount of inactivation of mitochondrial aconitase during hypoxia was also dependent upon AOX amount, perhaps through its effects on NO amount, and this influenced carbon flow under hypoxia. Finally, AOX was particularly important in preventing nitro-oxidative stress during the reoxygenation period, thereby contributing positively to the recovery of energy status following hypoxia. Overall, the results suggest that AOX plays a beneficial role in low oxygen metabolism, despite its lower affinity for oxygen than cytochrome oxidase.

**Keywords:** alternative oxidase, hypoxia, mitochondria, nitric oxide, reactive oxygen species, reoxygenation

## INTRODUCTION

The plant mitochondrial electron transport chain (ETC) is branched so that electrons in the ubiquinone pool can pass to oxygen via the usual cytochrome (cyt) pathway [involving Complex III, cyt c and cyt oxidase (EC 1.9.3.1)] or via alternative oxidase (AOX; EC 1.10.3.11) (Vanlerberghe, 2013; Del-Saz et al., 2018; Selinski et al., 2018). Electron flow from ubiquinol to oxygen via the cyt

pathway is coupled to proton translocation and hence contributes to the synthesis of ATP. However, electron flow from ubiquinol to oxygen via AOX is not coupled to proton translocation, hence not contributing to ATP synthesis. Having two pathways with different energy yields provides a means to maintain carbon, redox, and/or energy balance in response to the changing demands on metabolism imposed by internal (e.g., developmental) and external (e.g., environmental stress) factors (Millar et al., 1998; Ribas-Carbo et al., 2005; Sieger et al., 2005; Giraud et al., 2008; Smith et al., 2009; Chai et al., 2010; Cvetkovska and Vanlerberghe, 2012b; Dahal and Vanlerberghe, 2017, 2018a).

One consequence of AOX respiration is that it can influence the generation of reactive oxygen species (ROS) and reactive nitrogen species by the mitochondrial ETC. For example, studies have shown that chemical inhibition or genetic knockdown/knockout of AOX can increase mitochondrial amounts of such species, including superoxide ( $O_2^-$ ) and nitric oxide (NO) (Purvis, 1997; Maxwell et al., 1999; Parsons et al., 1999; Giraud et al., 2008; Smith et al., 2009; Cvetkovska and Vanlerberghe, 2012a; Alber et al., 2017).

Studies using different plant species and tissues have shown that AOX amount can change in response to hypoxia, anoxia, or reoxygenation after a low oxygen treatment (Amor et al., 2000; Tsuji et al., 2000; Klok et al., 2002; Szal et al., 2003; Millar et al., 2004; Liu et al., 2005; Kreuzwieser et al., 2009; Skutnik and Rychter, 2009; Narsai et al., 2011; Gupta et al., 2012; Vergara et al., 2012; Rivera-Contreras et al., 2016; Vishwakarma et al., 2018; Guan et al., 2019; Panozzo et al., 2019; Wany et al., 2019). The majority, but not all, of these studies indicate an increase of AOX transcript, protein and/or maximum activity (capacity) under such conditions. These findings hint at an increased role for AOX during conditions of low or fluctuating oxygen concentrations. On the other hand, AOX has a lower affinity for oxygen than cyt oxidase, suggesting that it may be a less prominent component of respiration at low oxygen concentration (Millar et al., 1994; Ribas-Carbo et al., 1994; Affourtit et al., 2001). The discrepancy between these two views may be due to another complicating factor, which is the potential for NO production in the mitochondrion at low oxygen (Gupta et al., 2018). For example, at low oxygen, cyt oxidase displays a nitrite reductase activity, generating NO from nitrite (Castello et al., 2006; Poyton et al., 2009). Further, this NO can then inhibit the oxidase activity of the enzyme (Poyton et al., 2009). On the other hand, AOX is NO-resistant, continuing to function effectively as an oxidase in the presence of NO (Millar and Day, 1997). Hence, at low oxygen, there could be a shift in the consumption of oxygen away from cyt oxidase and toward AOX, despite the lower affinity for oxygen of AOX compared to cyt oxidase.

In the current study, we compared wild-type (WT) tobacco plants to both AOX knockdown and overexpression plants under different oxygen conditions, including normoxia, hypoxia (near-anoxia), and reoxygenation following hypoxia. Our results show that AOX amount influences leaf carbon and energy metabolism under all these conditions. This indicates that AOX has role(s) in low oxygen metabolism, despite its lower affinity for oxygen than cyt oxidase.

## MATERIALS AND METHODS

### Plant Material and Growth Conditions

Tobacco (*Nicotiana tabacum* L. cv. Petit Havana SR1) WT, AOX knockdown (RI9, RI29) and AOX overexpression (B7, B8) plants were grown for 1 month in controlled environment growth chambers (Model PGR-15, Conviron, Winnipeg, MB, Canada) with a 14 h photoperiod, temperature of 26°C/20°C (light/dark), relative humidity of 50%, and photosynthetic photon flux density of 150  $\mu\text{mol m}^{-2} \text{s}^{-1}$ . Plants were irrigated every other day and fertilized every 2 weeks with a 20-20-20 fertilizer containing 5.9% of nitrate nitrogen. The transgenic lines used in this study have been characterized earlier (Amirsadeghi et al., 2006; Wang et al., 2011; Wang and Vanlerberghe, 2013; Dahal and Vanlerberghe, 2018a). Amongst these, RI29 is the most effective knockdown (no detectable leaf AOX protein), while faint amounts of leaf AOX protein can still sometimes be detected in RI9. B8 and B7 are both effective AOX overexpressors, with B8 showing slightly higher amounts of AOX protein than B7. Previous studies have shown that under optimal (well-watered, ambient  $\text{CO}_2$ ) growth conditions, all these plant lines (WT, RI9, RI29, B7, and B8) display similar growth, respiratory rates, photosynthetic properties, and maximal cyt oxidase activities and protein amounts (Dahal and Vanlerberghe, 2017, 2018a,b; Dahal et al., 2017).

### Normoxia, Hypoxia, and Reoxygenation Treatments

To test the plants under oxygen deficiency, they were placed in a custom-built, sealed, 2 L, dark chamber for 4 h. A steady inflow of nitrogen gas was maintained at 120  $\text{mL min}^{-1}$  (Alphagaz 1 grade having  $\sim 0.001\%$  oxygen) at one opening and unidirectional air valves facing outward in the openings to maintain ambient pressure within the chamber while preventing ambient air from entering (Cochrane et al., 2017). In a few experiments, the nitrogen gas contained either 0.1% or 3% oxygen. The chamber was opaque to obscure any light and contained two small openings on either side. The control plants (normoxia treatment) were flushed with air at the same flow rate in the same chamber for 4 h. Fully developed fourth or fifth leaves of the plants were harvested immediately after the treatment, frozen in liquid nitrogen and stored at  $-80^\circ\text{C}$  for subsequent analyses. For the post-hypoxia or reoxygenation treatment, the plants were flushed with normal air for 15 and 120 min after the hypoxia treatment.

### Reactive Oxygen Species

Fresh leaf biomass (100 mg) was crushed using a mortar and pestle over ice in 1 mL of 8 M KOH and then centrifuged (15,000 g, 10 min,  $4^\circ\text{C}$ ). The amount of superoxide anion ( $O_2^-$ ) in the supernatant was then measured at 550 nm by reduction of cyt c using a method modified from Sun and Trumpower (2003), as described in Ma et al. (2016).

For  $\text{H}_2\text{O}_2$  measurements, fresh leaf biomass (100 mg) was crushed using a mortar and pestle over ice, homogenized for 30 min in 6% trichloroacetic acid (TCA) and then centrifuged (15,000 g, 10 min,  $4^\circ\text{C}$ ).  $\text{H}_2\text{O}_2$  content in the supernatant



was determined using a Pierce Quantitative Peroxide Assay kit (Thermo Fisher Scientific).

## Lipid and Protein Modifications

Lipid peroxidation was measured as malondialdehyde (MDA) content, using the thiobarbituric acid (TBA) method described earlier (Heath and Parker, 1968), with minor modifications. Fresh leaf biomass (250 mg) was homogenized in 5 mL of 0.1% TCA and centrifuged (10,000 g, 5 min, 4°C). A 1 mL aliquot of supernatant was combined with 4 mL of 20% TCA containing 0.5% TBA. This mixture was incubated (95°C, 30 min), quickly cooled in crushed ice, and centrifuged (10,000 g, 10 min, 4°C). The absorbance of the sample was measured spectrophotometrically at 532 and 600 nm. The non-specific absorbance at 600 nm was subtracted from the absorbance at 532 nm and the concentration of MDA was calculated using an extinction coefficient of  $155 \text{ mM}^{-1} \text{ cm}^{-1}$ .

The measurement of protein S-nitrosylation was performed by reducing R-SNO to R-SH in the presence of ascorbate and then assaying free thiol groups using 5,5'-dithiol-bis (2-nitrobenzoic acid) (DTNB) (Ma et al., 2016). Leaf biomass (100 mg) was homogenized in 1.8 mL of 50 mM HEPES (pH 8.0) containing 1 mM EDTA, 0.1 mM neocuproine, 0.2% (w/v) SDS and 0.5% (w/v) CHAPS. The homogenate was centrifuged (15,000 g, 10 min, 4°C) and proteins in the supernatant were precipitated by two volumes of ice cold acetone (-20°C) overnight. The protein precipitate was collected by centrifugation (15,000 g, 10 min, 4°C) and washed four times with chilled 70% acetone before resuspension in the same volume of extraction buffer. The protein solution was separated into two 0.9 mL samples. One sample (experimental) was combined with 50  $\mu\text{L}$  of 100 mM ascorbate and the other sample (control) was combined with 50  $\mu\text{L}$  of water. After incubating for 1 h at 25°C, 50  $\mu\text{L}$  of 10 mM DTNB in 75 mM phosphate buffer (pH 7.0) was added to each sample, and each were then measured spectrophotometrically at 412 nm. Samples without protein were used as blanks, and the difference between experimental and control samples was used to calculate the quantity of R-SNO. The total concentration of protein was measured using Bradford reagent (Sigma-Aldrich, United States).

## Adenylates

The extraction of ATP and ADP was modified from Dordas et al. (2003) as described earlier (Cochrane et al., 2017). Fresh leaf biomass (100 mg) was rapidly frozen in liquid nitrogen and homogenized in 1 mL of 2.4 M HCl using a mortar and pestle. The homogenate was then transferred to a microcentrifuge tube, neutralized using 5 M KOH and centrifuged (20,000 g, 10 min, 4°C). ATP and ADP in the supernatant were then measured using a luciferase-based bioluminescent assay (EnzyLight™ ADP/ATP ratio Assay Kit ELDT-100 by BioAssay Systems, CA, United States) and FB 12 Single Tube Luminometer by Titertek-Berthold (Berthold Detection Systems, GmbH, Germany).

## NO Measurements Under Hypoxia

Leaves were detached, weighed and immediately placed in 20 mM Hepes buffer (pH 7.0) containing 50 mM sodium nitrate. When inhibitors were used, this buffer also contained either 2 mM potassium cyanide (KCN), 5 mM salicylhydroxamic acid

(SHAM) or 300  $\mu\text{M}$  sodium tungstate ( $\text{Na}_2\text{WO}_4$ ). The leaves in buffer were then placed in an air tight chamber as described earlier with a constant inflow of nitrogen gas at  $120 \text{ mL min}^{-1}$  (0.001%  $\text{O}_2$ ). NO was measured by chemiluminescence detection (Planchet et al., 2005). In brief, a constant flow of measuring gas (purified air or nitrogen) at  $120 \text{ mL min}^{-1}$  was pulled through the chamber and subsequently through the chemiluminescence detector (CLD 770 AL ppt; Eco-Physics, Dürnten, Switzerland; detection limit 20 ppt; 20 s time resolution) by a vacuum pump connected to an ozone destroyer. The ozone generator of the chemiluminescence detector was supplied with dry oxygen (99%). The inflowing gas (air or nitrogen) was made NO free by passing it through a NO scrubber (Eco Physics Ltd, Switzerland). Calibration was routinely carried out with NO free air (0 ppt NO) and with various concentrations of NO (1–35 ppb) adjusted by mixing the calibration gas (500 ppb NO in nitrogen; Messer Griesheim, Darmstadt, Germany) with NO-free air. Flow controllers (Fisher Scientific) were used to adjust all gas flows.

## Aconitase (EC 4.2.1.3) Activity

Fresh leaf biomass (100 mg) was homogenized in 1 mL of cold extraction buffer (50 mM Tris-HCl [pH 7.4], 1 mM dithiothreitol, 5 mM  $\text{MgCl}_2$ , 2 mM trisodium citrate and 0.4 M mannitol). The extract was centrifuged (3,000 g, 5 min, 4°C) and the supernatant was then centrifuged again (10,000 g, 20 min, 4°C). The pellet (containing mitochondria) was then resuspended in a buffer containing 50 mM Tris-HCl (pH 7.4), 2 mM trisodium citrate, 5 mM dithiothreitol and 100 mM  $\text{MgCl}_2$  and used to measure mitochondrial aconitase activity. The supernatant was also collected and used to measure cytosolic aconitase activity. Cross-contamination between the mitochondrial and cytosolic fractions was determined using marker enzymes (succinate dehydrogenase for mitochondria, lactate dehydrogenase for cytosol), as described earlier (Eprintsev et al., 2017). Cross-contamination did not exceed 10%. To measure aconitase activity, 0.1 mL of extract was added to 0.9 mL of assay buffer (50 mM Tris-HCl [pH 7.4] and 40 mM citrate). Enzyme activity was measured spectrophotometrically (240 nm) for 10 min using an Ultraspec 4300 (Biochrom). An extinction coefficient of  $3.6 \text{ mM}^{-1} \text{ cm}^{-1}$  was used for cis-aconitate (Baumgart and Bott, 2011).

## Metabolomics

Metabolomics was performed using NMR analysis (Psychogios et al., 2011). Leaf tissue was flash frozen in liquid nitrogen and powdered using ceramic beads and a tabletop centrifuge. The resulting powder was homogenized in 2 M perchloric acid and incubated at room temperature for 1 h. Homogenates were neutralized on ice to pH 7 using 3 M KOH and the subsequent potassium perchlorate precipitate was removed by centrifugation (15 000 g, 10 min, 4 °C). Samples were then freeze-dried for 48 h before being homogenized in heavy water ( $\text{D}_2\text{O}$ ) using a ceramic mortar. After incubation for 24 h at room temperature, the solutions were centrifuged and an aliquot of the supernatant (aqueous extract) with a volume of  $\sim 0.6 \text{ mL}$  was placed in a vial for NMR analysis. Subsequently, 140  $\mu\text{L}$  of a standard buffer solution (54%  $\text{D}_2\text{O}$ : 46% 150 mM  $\text{KH}_2\text{PO}_4$  pH 7.0

v/v containing 5.0 mM DSS-d6 (2,2-dimethyl-2-silcepentane-5-sulphonate), 5.84 mM 2-chloropyrimidine-5 carboxylate, and 0.1% NaN<sub>3</sub> in H<sub>2</sub>O) was added to the sample. The plant sample (350  $\mu$ L) was then transferred to a 3 mm SampleJet NMR tube for subsequent spectral analysis (Canam et al., 2013). All <sup>1</sup>H-NMR spectra were collected on a 700 MHz Avance III (Bruker) spectrometer equipped with a 5 mm HCN Z-gradient pulsed-field gradient (PFG) cryoprobe. <sup>1</sup>H-NMR spectra were acquired at 25°C using the first transient of the NOESY pre-saturation pulse sequence (noesy1dpr), chosen for its high degree of quantitative accuracy. All FID's (free induction decays) were zero-filled to 250 K data points. The singlet produced by the DSS methyl groups was used as an internal standard for chemical shift referencing (set to 0 ppm) and for quantification. All <sup>1</sup>H-NMR spectra were processed and analyzed using the Chenomx NMR Suite Professional software package version 8.1 (Chenomx Inc., Edmonton, AB, United States). The Chenomx NMR Suite software allows for qualitative and quantitative analysis of an NMR spectrum by manually fitting spectral signatures from an internal database to the spectrum. Typically, 90% of visible peaks were assigned to a compound and more than 90% of the spectral area could be routinely fit using the Chenomx spectral analysis software. Most of the visible peaks are annotated with a compound name.

## Total Phenolics and Flavonoids

Soluble phenolics and flavonoids were extracted from leaves by homogenizing in 80% (v/v) acetone with 0.2% (m/v) formic acid in a ratio of 1:10. The homogenate was then shaken (8 h, 4°C) and then centrifuged (20,000 g, 20 min, 4°C). The residue was extracted twice again under the same conditions and the supernatants were combined.

Total soluble phenolic content was determined using Folin-Ciocalteu reagent as described by Chandrasekara and Shahidi (2011) with modifications (Vyas et al., 2013). The Folin-Ciocalteu reagent (0.5 mL) was combined with 0.5 mL of leaf extract and mixed well. Saturated sodium carbonate solution (1 mL) was then added to neutralize the reaction. The final volume was adjusted to 10 mL by adding water and vortexing for 1 min. The samples were then kept in the dark (35 min, room temperature), and then centrifuged (4,000 g, 10 min). The absorbance was measured at 725 nm. Total soluble phenolic content of each sample was determined using a gallic acid standard curve and expressed as gallic acid equivalents (GAE) per leaf fresh weight.

Total flavonoid content was measured by aluminum chloride colorimetric assay (Zhishen et al., 1999). The above soluble extract (1 mL) or a standard solution of catechin (0.5 mL) was mixed with 4 mL of water followed by addition of 0.3 mL of 5% (m/v) NaNO<sub>2</sub>, 0.3 mL of 10% (m/v) AlCl<sub>3</sub> (after 5 min) and 2 mL of 1 M NaOH (1 min later). The volume was adjusted with water to 10 mL. The absorbance was measured spectrophotometrically at a wavelength of 510 nm. Total flavonoid content was expressed as catechin equivalent (CE) per leaf fresh weight.

## Statistical Analyses

All experiments were repeated at least three times. Statistical analyses were performed using Prism 5.0 (GraphPad Software).

Two-way ANOVA analyses were followed by a Bonferroni post-test to compare plant lines within a treatment.

## RESULTS

### Normoxia, Hypoxia, and Reoxygenation Experiment

Wild-type, AOX knockdown (RI9, RI29) and AOX overexpression (B7, B8) tobacco plants were compared in an experiment in which potted plants were subjected to either a 4 h normoxia (normal air) treatment, a 4 h hypoxia (0.001% oxygen, i.e., near anoxia) treatment, or a 4 h hypoxia treatment followed by a reoxygenation (normal air) treatment for 15 min or 120 min. Following treatment, leaf tissue was collected for a number of analyses, the results of which are described below.

Under normoxia, leaf O<sub>2</sub><sup>-</sup> amount was similar between WT and overexpression plants, but significantly higher in the knockdowns (**Figure 1A**). In response to the hypoxia treatment, O<sub>2</sub><sup>-</sup> amount increased only slightly in the overexpressors, but more dramatically in the WT and knockdowns. Hence, following hypoxia, O<sub>2</sub><sup>-</sup> amount was significantly lower in the overexpressors and significantly higher in the knockdowns, compared to WT. These differences across plant lines were also evident during the reoxygenation period (**Figure 1A**).

The hypoxia treatment increased H<sub>2</sub>O<sub>2</sub> amount in all plant lines, compared to the normoxia treatment (**Figure 1B**). Following reoxygenation, H<sub>2</sub>O<sub>2</sub> amount declined in all plant lines, particularly by the 120 min time point, when amounts had returned to at or below that measured following the normoxia treatment. However, unlike the results with O<sub>2</sub><sup>-</sup>, the relationship between H<sub>2</sub>O<sub>2</sub> amount and AOX amount across the plant lines was complex, regardless of the treatment conditions. Under all conditions, the knockdowns had significantly higher H<sub>2</sub>O<sub>2</sub> amount than WT. This was particularly evident following hypoxia and at the early stage (15 min) of reoxygenation. However, the AOX overexpressors also had higher H<sub>2</sub>O<sub>2</sub> amounts than WT following hypoxia and after 15 min of reoxygenation (**Figure 1B**).

Under normoxia, the amount of protein S-nitrosylation (R-SNO) was significantly lower in the AOX overexpressors, compared to the WT and knockdowns (**Figure 2A**). R-SNO amount was significantly higher in one knockdown line (RI9) compared to WT, but WT and RI29 showed similar R-SNO amount. In response to hypoxia, R-SNO amount decreased in the WT and knockdown plants, while increasing slightly in the overexpressors. Under these conditions, R-SNO amount was only slightly lower in the overexpressors and slightly higher in the knockdowns, compared to WT. Compared to the hypoxia treatment, there was little change in the R-SNO amount in WT and overexpression plants following reoxygenation. However, the R-SNO amount in knockdown plants increased during reoxygenation. Hence, at both the 15 and 120 min time points, R-SNO amounts were significantly higher in the knockdowns than other plant lines (**Figure 2A**).

The amount of lipid peroxidation (MDA equivalents) was lowest in the normoxia-treated plants. Under this condition, WT

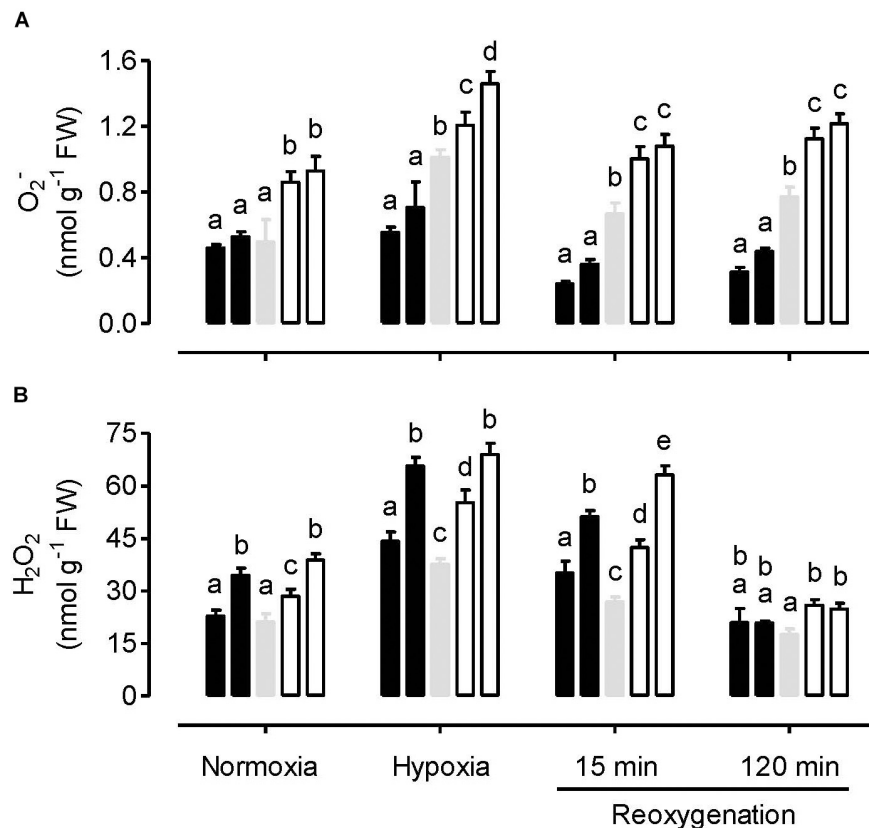


**FIGURE 1 |** Leaf  $O_2^-$  amount (A) and  $H_2O_2$  amount (B) in tobacco plants treated under either normoxia conditions, hypoxia conditions (for 4 h), or reoxygenation conditions (for 15 or 120 min) following a 4 h hypoxia treatment. Data are presented for WT (gray bar), alternative oxidase overexpressors (B8, left closed bar; B7, right closed bar) and alternative oxidase knockdowns (RI9, left open bar; RI29, right open bar). Each experiment included single individuals for each plant line and treatment. Data are the mean  $\pm$  SD of three independent experiments ( $n = 3$ ). Within a treatment, plant lines not sharing a common letter are significantly different from one another ( $P < 0.05$ ).

and overexpression plants displayed similar amounts, while the knockdowns displayed significantly higher amounts (Figure 2B). The hypoxia treatment increased MDA amount in all plant lines, compared to normoxia. Now, MDA amounts were significantly lower in the overexpressors, compared to WT. MDA amounts were higher in the knockdowns than WT, although this result was only significant in the case of RI29. Re-oxygenation increased MDA amounts further across all plant lines. At both time points following reoxygenation, MDA amounts were significantly lower in the overexpressors and significantly higher in the knockdowns, compared to WT (Figure 2B).

Under normoxia, the ATP/ADP ratio was similar between the WT and AOX knockdown plants, but slightly higher in the overexpressors (Figure 3). In response to hypoxia, the ATP/ADP ratio decreased in all plant lines. The ratio remained significantly higher in the overexpressors compared to WT. Further, the knockdowns now displayed lower ATP/ADP ratios than the WT, although this difference was only significant in the case of RI29. Re-oxygenation increased the ATP/ADP ratio of all plant lines, but also magnified the differences in ATP/ADP ratio between the plant lines. Particularly by the 120 min time point of reoxygenation, the ATP/ADP ratio was much higher in the

overexpressors and much lower in the knockdowns, compared to WT (Figure 3). Interestingly, while the ATP/ADP ratio of the knockdowns recovered to values similar to that seen in the normoxia treatment, the WT, and overexpression plants now displayed ATP/ADP ratios that were much higher than measured during the normoxia treatment.

Interestingly, following the hypoxia treatment, the overexpression plants were more visibly upright, healthy and robust than the WT and knockdown plants, an observation that may relate to some of the above factors (such as energy status) but which requires further investigation (Figure 4).

## Nitric Oxide Emission From Hypoxia Treated Leaves

Nitric oxide emission rates were measured from leaves incubated in nitrate solution and in an atmosphere containing 0.001% oxygen. Under these hypoxic conditions, NO emission rate was significantly higher in AOX overexpressors and significantly lower in AOX knockdowns, compared to WT (Figure 5). Further, tungstate treatment could dramatically lower NO production in all plant lines, while KCN treatment ceased NO production in all plant lines (data not shown).

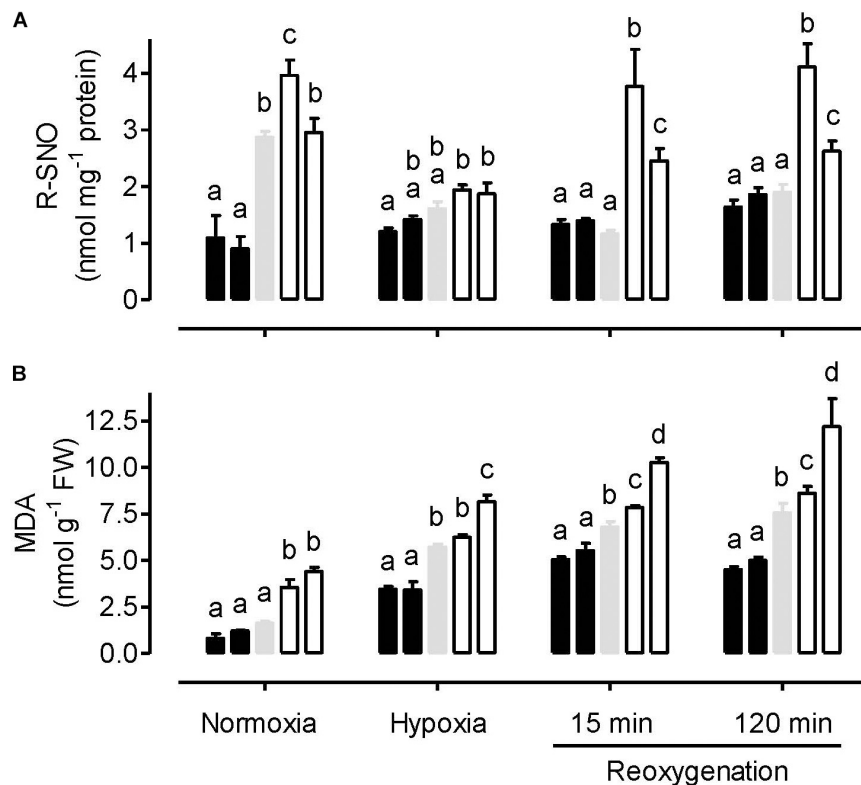


**FIGURE 2 |** Leaf R-SNO amount (A) and MDA amount (B) in tobacco plants treated under either normoxia conditions, hypoxia conditions (for 4 h), or reoxygenation conditions (for 15 or 120 min) following a 4 h hypoxia treatment. Data are presented for WT (gray bar), alternative oxidase overexpressors (B8, left closed bar; B7, right closed bar) and alternative oxidase knockdowns (RI9, left open bar; RI29, right open bar). Each experiment included single individuals for each plant line and treatment. Data are the mean  $\pm$  SD of three independent experiments ( $n = 3$ ). Within a treatment, plant lines not sharing a common letter are significantly different from one another ( $P < 0.05$ ).

When leaves were pre-treated with the AOX inhibitor SHAM, the rates of NO emission decreased in all plant lines (Figure 5). However, the absolute decrease in NO emission rate was greatest in the overexpressors (particularly B8), and least in the knockdowns (particularly RI29), with WT plants showing an intermediate response.

For three of the plant lines, NO emission was also measured at 0.1% O<sub>2</sub>. The absolute rates (in units of ppb NO g<sup>-1</sup> FW h<sup>-1</sup>) were: B7, 5.69; WT, 5.65; and RI9, 3.87. Overall, these rates are much lower than measured at 0.001% O<sub>2</sub> (compare to Figure 5). Also, while the WT and overexpressor display similar rates under these conditions, the rate in the knockdown remains significantly lower than in the other plant lines. In 3% oxygen or in ambient air, no NO emission could be detected by the chemiluminescence method.

### Aconitase Activity in Normoxia and Hypoxia Treated Plants

Both leaf cytosolic aconitase and leaf mitochondrial aconitase activities were measured in plants following a normoxia or hypoxia (3 h, 0.001% O<sub>2</sub>) treatment. Under normoxia, the mitochondrial (Figure 6A) and cytosolic (Figure 6B) activities were comparable to one another, and each activity was

similar between the WT, AOX knockdown (RI9) and AOX overexpression (B7) plants. The hypoxia treatment had a relatively small impact on cytosolic aconitase activity, decreasing by 13% in RI9, 8% in WT and just 2% in B7 (Figure 6B). However, the hypoxia treatment led to substantial losses of mitochondrial aconitase activity (Figure 6A). Further, this loss was most severe in the overexpressor (95% decrease in activity compared to normoxia) and least severe in the knockdown (39% decrease in activity), with the WT showing an intermediate response (80% decrease in activity).

### Metabolite Amounts in Normoxia and Hypoxia Treated Plants

A range of primary metabolites (including two sugars, six organic acids, and eight amino acids) were identified and quantified using a <sup>1</sup>H-NMR metabolomics technique. Under normoxia conditions, the amount of sugars (glucose and galactose) and organic acids (lactate, acetate, pyruvate, citrate, succinate and malate) in leaves were similar between the WT and AOX overexpressor (B7) (Figures 7A–H). In most cases, however, these metabolites were significantly higher in the AOX knockdown (RI9) than other plant lines. In WT plants, hypoxia had either little impact on the amount of these metabolites (in



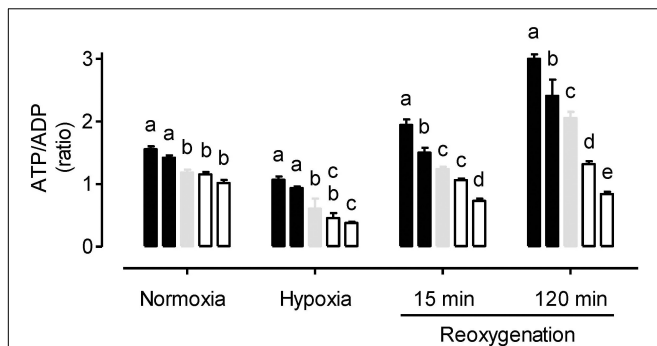


**FIGURE 3 |** Leaf ATP/ADP ratio in tobacco plants treated under either normoxia conditions, hypoxia conditions (for 4 h), or reoxygenation conditions (for 15 or 120 min) following a 4 h hypoxia treatment. Data are presented for WT (gray bar), alternative oxidase overexpressors (B8, left closed bar; B7, right closed bar) and alternative oxidase knockdowns (RI9, left open bar; RI29, right open bar). Each experiment included single individuals for each plant line and treatment. Data are the mean  $\pm$  SD of three independent experiments ( $n = 3$ ). Within a treatment, plant lines not sharing a common letter are significantly different from one another ( $P < 0.05$ ).

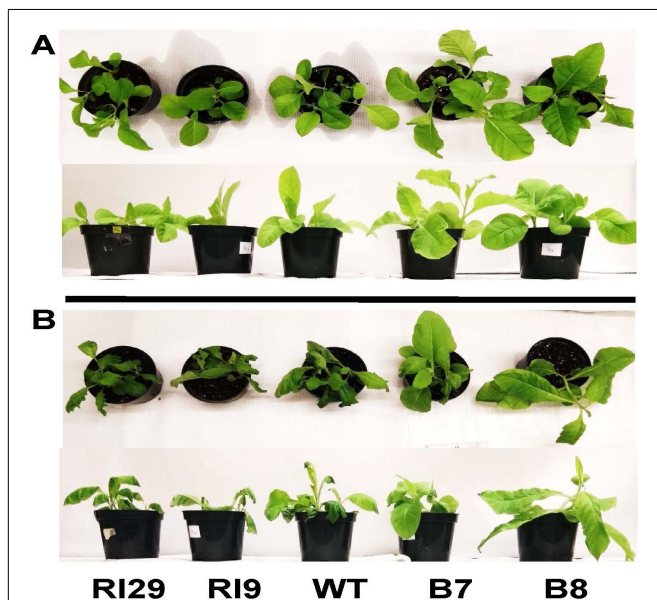


**FIGURE 4 |** Typical appearance of wild-type (WT), AOX knockdown (RI9, RI29), and AOX overexpression (B7, B8) plants following either the normoxia (A) or 4 h hypoxia (B) treatment.

the case of glucose, galactose, lactate and acetate) or reduced their amounts by half or more (in the case of pyruvate, citrate, succinate and malate). In the knockdown, hypoxia reduced the amounts of glucose and galactose, while organic acid amounts were unaffected. Hence, the knockdown maintained higher organic acid amounts in leaves than WT under both the normoxia and hypoxia conditions (Figures 7C–H). The AOX overexpressor showed a different pattern following hypoxia. Sugar amounts were unchanged by hypoxia and were similar to WT amounts under hypoxia. Succinate, malate, lactate and

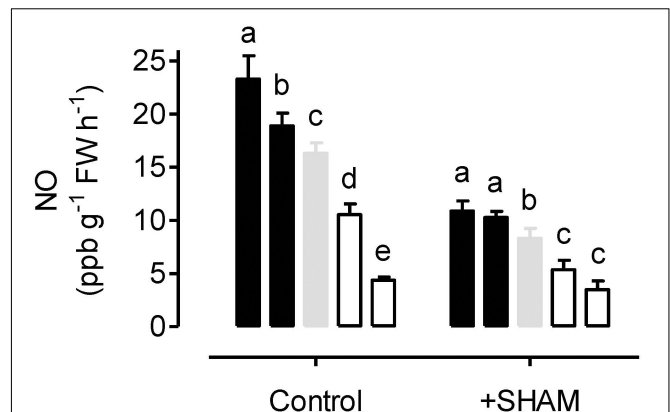


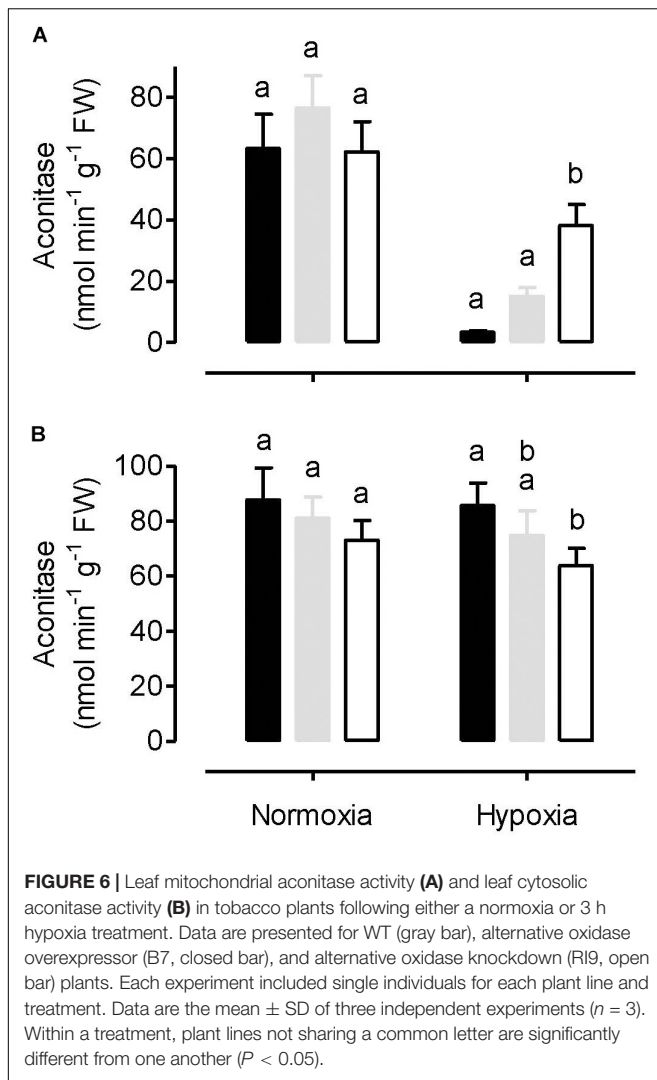
**FIGURE 5 |** Nitric oxide (NO) emission rates from tobacco leaves in the presence of 50 mM sodium nitrate (control) or 50 mM sodium nitrate plus 5 mM SHAM. NO emission was measured in an atmosphere containing approximately 0.001% oxygen. Data are presented for WT (gray bar), alternative oxidase overexpressors (B8, left closed bar; B7, right closed bar) and alternative oxidase knockdowns (RI9, left open bar; RI29, right open bar). Each experiment included single individuals for each plant line and treatment. Data are the mean  $\pm$  SD of three independent experiments ( $n = 3$ ). Within a treatment, plant lines not sharing a common letter are significantly different from one another ( $P < 0.05$ ).

acetate increased in the overexpressor under hypoxia and were now higher than in the WT under hypoxia. Finally, pyruvate and citrate showed a small decline in leaves following hypoxia, similar to that seen in the WT response to hypoxia (Figures 7A–H).

Under normoxia, the amount of most amino acids measured was similar between the WT and AOX knockdown, but serine and glycine amounts were significantly higher in the knockdown (Figures 7I–P). The amount of several amino acids was also similar between the WT and overexpressor under normoxia, but leucine and isoleucine were significantly lower in the overexpressor than WT (Figures 7I–P). Following hypoxia, serine and glycine amounts decreased in the knockdown and were now similar to the other plant lines (Figures 7K,L). While alanine tended to increase in all plant lines in response to hypoxia, the increase was particularly pronounced in the overexpressor, such that its alanine amount was now significantly higher than the other plant lines. In response to hypoxia, asparagine increased in the WT, but this response was not seen in either the overexpressor or knockdown plants (Figure 7M). The amount of GABA increased in all plant lines in response to hypoxia and was significantly higher in the overexpressor than WT (Figure 7P).

## Antioxidant Amounts in Normoxia and Hypoxia Treated Plants

The amount of total leaf phenolics and total leaf flavonoids were measured in plants following a normoxia or hypoxia (3 h, 0.001%  $O_2$ ) treatment. Under normoxia, phenolics (Figure 8A) and flavonoids (Figure 8B) were slightly lower in WT plants, compared to either the AOX knockdown or overexpression plants. However, these differences were only significant in the case of the phenolics amount in the knockdown. Following the hypoxia treatment, the amount of phenolics and flavonoids



increased in both the WT and overexpression plants, but not in the knockdown. Hence, following hypoxia, the content of phenolics and flavonoids was significantly greater in the WT and overexpressor, compared to the knockdown (**Figure 8**).

## DISCUSSION

We investigated the significance of mitochondrial AOX under different oxygen conditions by comparing WT tobacco plants to AOX knockdown and AOX overexpression plants following either: (1) a normoxia (normal air) treatment; (2) a short-term (3–4 h) hypoxia (near-anoxia) treatment; (3) a reoxygenation period (of 15 or 120 min) following a hypoxia treatment. The discussion below deals with each of these treatments in sequence.

### Normoxia

Under normoxia conditions, knockdown of AOX increased the leaf amount of  $O_2^-$  (**Figure 1A**). This is evidence that AOX respiration is important in controlling ROS generation

by the mitochondrial ETC. The results confirm previous fluorescent imaging studies in tobacco leaf using the MitoSOX mitochondrial  $O_2^-$  indicator (Cvetkovska and Vanlerberghe, 2012a). In that study, knockdown of AOX increased the amount of mitochondria-localized  $O_2^-$  relative to WT, while overexpression of AOX had little effect, similar to the results seen here. Interestingly, the pattern of  $O_2^-$  amount across plant lines was mirrored by the pattern of MDA amount across plant lines, which was also elevated in the knockdowns, but unaffected in the overexpressors, relative to WT (**Figure 2B**). These results suggest that increased ROS generation by the mitochondrial ETC can increase the amount of oxidative damage (lipid peroxidation) in leaf tissues. Overall, these results are consistent with a large body of evidence indicating that AOX respiration reduces mitochondrial ETC-generated ROS under normal oxygen conditions (Purvis, 1997; Maxwell et al., 1999; Parsons et al., 1999; Giraud et al., 2008; Smith et al., 2009; Cvetkovska and Vanlerberghe, 2012a).

Similar to  $O_2^-$ , knockdown of AOX also increased the leaf amount of  $H_2O_2$  under normoxia (**Figure 1B**). However, the relationship between AOX amount and  $H_2O_2$  amount appears more complex since overexpression of AOX also increased leaf  $H_2O_2$  amount, at least in one of the two overexpressors (B7). One possibility is that the aberrant amount of ROS generation by the mitochondrial ETC can signal changes in the capacity of ROS-scavenging systems within the cell, leading to unexpected changes in  $H_2O_2$  amount. This was reported before in tobacco plants with altered AOX amount. In one study, overexpression of AOX dampened the induction of scavenging systems, resulting paradoxically in an increase in  $H_2O_2$  amount (Pasqualini et al., 2007) while in another study, knockdown of AOX was shown to magnify the induction of scavenging systems (Wang et al., 2011). Overall, such results suggest that, in evaluating the influence of AOX respiration on ROS generation by the mitochondrial ETC, the likely most unambiguous approach is to measure the primary product of that process ( $O_2^-$ ) rather than  $H_2O_2$ , the amount of which will depend upon the secondary processes associated with its formation and scavenging. Interestingly, the overall pattern of  $H_2O_2$  amount across plant lines mirrored the pattern of antioxidants (phenolics, flavonoids), which also tended to be higher in both RI9 and B7, relative to WT (**Figure 8**). These results suggest that the production of these secondary metabolites in tobacco leaf is responsive to the  $H_2O_2$ -load on the cell.

Previously, it was shown that AOX knockdown tobacco plants under normoxia have higher amounts of leaf mitochondria-localized NO, compared to WT plants (Cvetkovska and Vanlerberghe, 2012a). Alber et al. (2017) provided evidence that the increase in NO was due to an increased leak of mitochondrial ETC electrons to nitrite, possibly at Complex III, as postulated earlier (Igamberdiev et al., 2010). One important consequence of NO is that it can result in the S-nitrosylation of target proteins (Baudouin, 2011; Zaffagnini et al., 2016). Indeed, the amount of protein S-nitrosylation (R-SNO) did differ across the plant lines under normoxia (**Figure 2A**). Amounts were lowest in the overexpressors and highest in the knockdowns, consistent with the idea that AOX respiration can act to reduce the mitochondrial ETC generation of NO under normoxia.

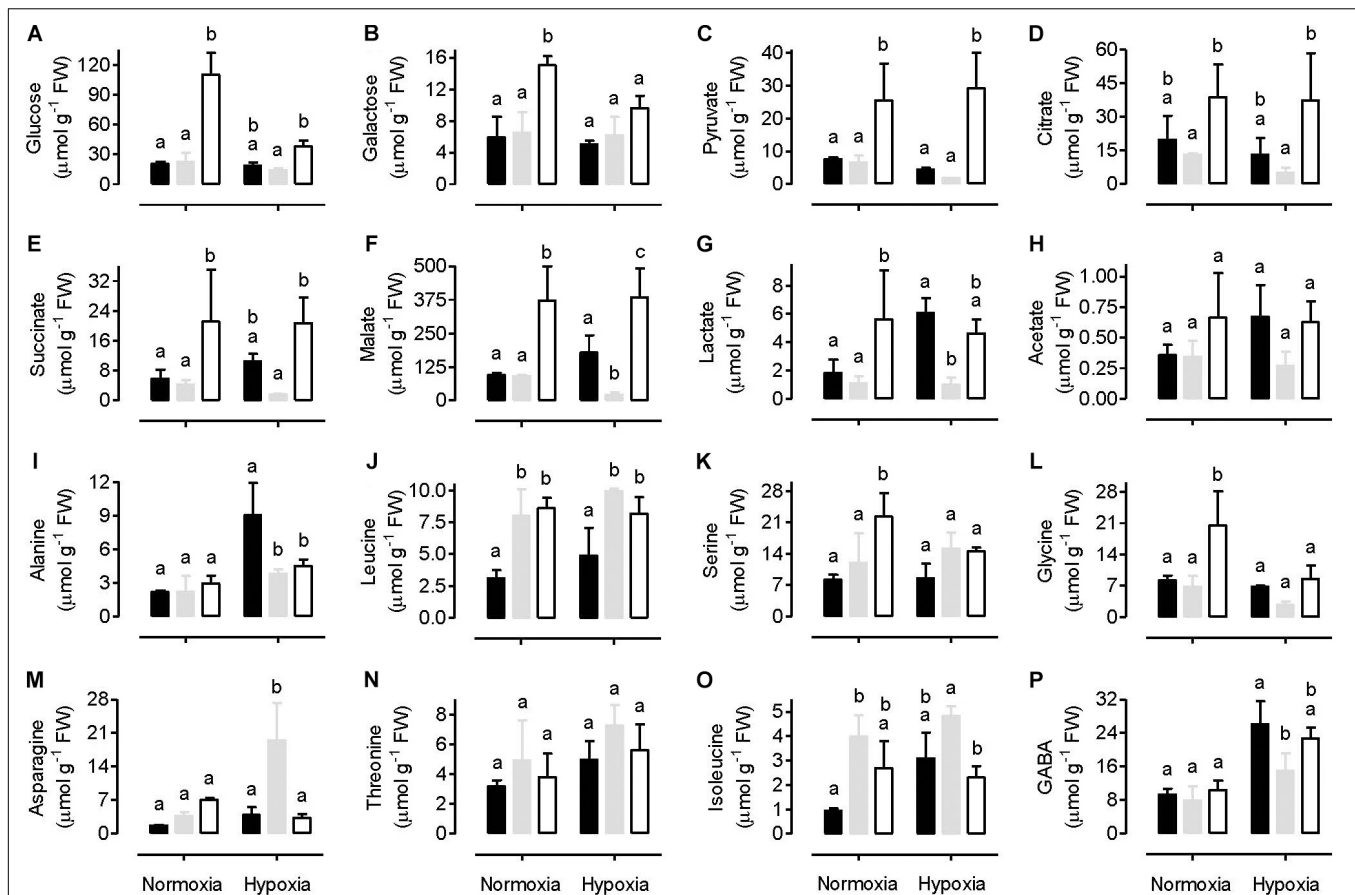
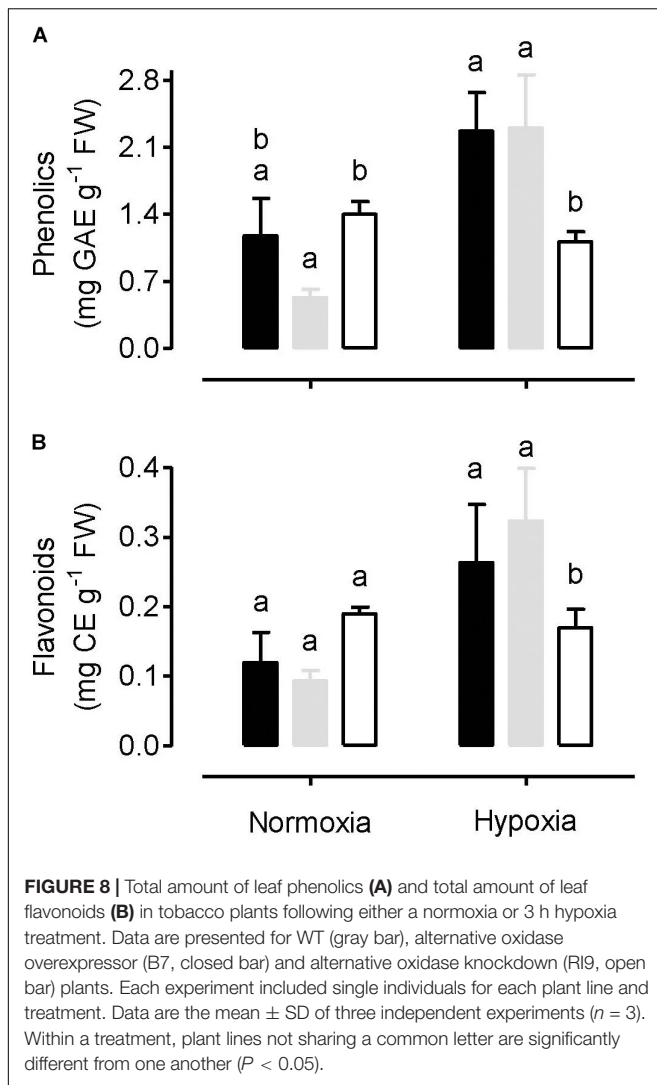


**FIGURE 7 |** Leaf metabolite amounts in tobacco plants following either a normoxia or 3 h hypoxia treatment. Data are presented for WT (gray bar), alternative oxidase overexpressor (B7, closed bar) and alternative oxidase knockdown (RI9, open bar) plants. The metabolites include various sugars (A,B), organic acids (C-H), and amino acids (I-P). Each experiment included single individuals for each plant line and treatment. Data are the mean  $\pm$  SD of three independent experiments ( $n = 3$ ). Within a treatment, plant lines not sharing a common letter are significantly different from one another ( $P < 0.05$ ).

Electron flow from ubiquinol to oxygen through AOX is not coupled to proton translocation from matrix to inter-membrane space. Hence, knockdown of AOX could enhance overall proton translocation and oxidative phosphorylation by diverting additional electrons toward Complex's III and IV. Similarly, overexpression of AOX might decrease overall proton translocation and oxidative phosphorylation by diverting electrons away from Complex's III and IV and toward AOX. To examine these possibilities, we measured the energy status (ATP/ADP ratio) of the different plant lines. Paradoxically, the ATP/ADP ratio was significantly higher in the AOX overexpressors than WT (Figure 5). It was also slightly lower in the knockdowns than WT, although this result was not significant. These results suggest that increased AOX respiration can improve leaf energy status despite its non-energy conserving nature. More investigation is required to uncover the mechanistic basis of this observation. One possibility is that aberrant amounts of NO in the transgenic lines, as discussed above, is partly responsible. NO is a potent inhibitor of cyt oxidase, so higher amounts of NO in the mitochondrion (knockdown lines) could be acting to restrict cyt oxidase activity (hence

lowering the ATP/ADP ratio), while lower amounts of NO in the mitochondrion (overexpression lines) could result in increased cyt oxidase activity (hence increasing the ATP/ADP ratio). Interestingly, it was previously shown that lower NO in barley roots following overexpression of a non-symbiotic phytohemoglobin did increase respiration rates under normoxia (Gupta et al., 2014).

Of the two sugars and six organic acids analyzed, all but one of these were significantly higher in amount in AOX knockdown than WT plants under normoxia (Figures 7A-H). The exception was acetate, which, while still approximately twofold higher in the knockdown than the WT, was not significantly different in amount. Two (of eight) amino acids analyzed (serine and glycine) were also significantly higher in the knockdown than WT, while the others were similar to WT (Figures 7I-P). One interpretation of these results is that lack of AOX respiration can significantly impede upstream respiratory carbon metabolism, resulting in the accumulation of carbon intermediates. Likely, the lack of AOX primarily restricts ETC activity (as suggested by the higher amounts of  $\text{O}_2^-$ , Figure 1A) and this restriction then secondarily backs up carbon metabolism, particularly organic



acid metabolism by the tricarboxylic acid (TCA) cycle. Of particular interest is the accumulation of pyruvate and lactate (Figures 7C,G). Pyruvate is an important biochemical activator of AOX (Selinski et al., 2018). Hence, pyruvate accumulation is thought to activate AOX in order to stimulate TCA cycle carbon flow, and hence draw down the pyruvate amount (Vanlerberghe et al., 1995). Consistent with this model, our results show that, in the absence of AOX, pyruvate does accumulate. A consequence of this accumulation is the overflow of pyruvate into fermentation pathways, such as seen here by the accumulation of lactate. On the other hand, the large majority of metabolites tested did not differ significantly between the WT and overexpressor under normoxia, except for two amino acids (leucine and isoleucine) that were less abundant in the overexpressor. These plants also displayed similar  $O_2^-$  amount to the WT (Figure 1A).

In summary, AOX does significantly influence respiratory metabolism in tobacco leaf under normoxia. A lack of AOX disrupted mitochondrial ETC activity, increasing  $O_2^-$  generation, and restricting respiratory carbon flow.

Overexpression of AOX had less pervasive effects, likely due in part to the fact that the protein is subject to tight post-translational biochemical controls over its activity (Guy and Vanlerberghe, 2005). However, overexpression did lower R-SNO amounts relative to WT, suggestive of less NO generation by the mitochondrial ETC, and it did increase the ATP/ADP ratio relative to WT, suggestive of higher cytochrome oxidase activity. These two observations may be linked (Gupta et al., 2014).

## Hypoxia

Alternative oxidase has a much lower affinity for oxygen than does cytochrome oxidase. The  $K_m$  for oxygen is estimated at 10  $\mu$ M for AOX, compared to 0.08–0.16  $\mu$ M for cytochrome oxidase (Hoshi et al., 1993; Millar et al., 1994; Affourtit et al., 2001). While this difference might be expected to limit AOX activity at low oxygen concentrations, others factors may actually favor AOX activity under these conditions. First, AOX is subject to biochemical controls (Millar et al., 1993; Umbach and Siedow, 1993; Vanlerberghe et al., 1995; Selinski et al., 2018) that may favor AOX activity under hypoxia. The more reducing conditions [higher NAD(P)H/NAD(P)<sup>+</sup> ratios] typical of hypoxia will favor reduction of an AOX regulatory disulfide bond to its component sulfhydryls. These sulfhydryls can then interact with 2-oxoacids, most notably pyruvate, resulting in a strong activation of AOX activity. Under hypoxia, a stimulation of glycolysis combined with a slowing of the TCA cycle might increase pyruvate amount, as reported in some studies (Rocha et al., 2010; António et al., 2016). Second, under hypoxia, cytochrome oxidase displays a nitrite reductase activity that generates NO from nitrite (Poyton et al., 2009). This NO can then inhibit the oxidase activity of the enzyme (Poyton et al., 2009). On the other hand, AOX is NO-resistant (Millar and Day, 1997). The inhibition of cytochrome oxidase by NO slows oxygen consumption such that, even in an atmosphere of almost pure nitrogen (0.001% oxygen), the oxygen concentration in the cell can remain in the micromolar range (Benamar et al., 2008; Gupta et al., 2009, 2018). Hence, under hypoxia, there could be a shift in the consumption of oxygen away from cytochrome oxidase and toward AOX, despite the lower affinity for oxygen of AOX compared to cytochrome oxidase. Another potentially confounding factor is the possibility of nitrite reduction to NO by AOX itself under hypoxia. Initially, this hypothesis was based on pharmacological evidence, where the AOX inhibitor SHAM was shown to decrease NO emission rates from tobacco leaf under hypoxia (Planchet et al., 2005). More recently, additional support for this hypothesis has come from a study showing that *Arabidopsis* plants overexpressing AOX display increased NO emission rates under hypoxia (Vishwakarma et al., 2018).

As might be expected, the severe hypoxia treatment reduced the ATP/ADP ratio of all the plant lines, relative to normoxia (Figure 3). However, the relatively small differences in energy status between the plant lines seen under normoxia were magnified by the hypoxia treatment. These results establish an important role for AOX activity in the maintenance of energy status under hypoxia. One possibility is that AOX becomes a key electron sink to maintain electron flow to any available oxygen, under conditions when NO is inhibiting cytochrome oxidase (see more below). Even with AOX activity alone (i.e., complete inhibition of



cyt oxidase), proton translocation could still proceed at Complex I and allow for some oxidative phosphorylation. Another indication that AOX is acting as a key electron sink under these conditions are the results regarding  $O_2^-$  amount. Following hypoxia,  $O_2^-$  amounts are much lower in the overexpressors and much higher in the knockdowns, relative to WT, an indication that AOX is providing a means to prevent over-reduction of the ETC under these conditions (**Figure 1A**). Consistent with this, while oxidative damage (MDA amount) increased in all plant lines following hypoxia, this damage was least abundant in the overexpressors and most abundant in the knockdowns, with WT showing an intermediate response (**Figure 2B**).

Under hypoxia, NO emission rates were highest in the overexpressors, and lowest in the knockdowns, with WT showing an intermediate response (**Figure 5**). The large difference across plant lines may provide some explanation why R-SNO amounts following hypoxia increased slightly in the overexpressors (relative to normoxia) but decreased strongly in the WT and knockdowns (**Figure 2A**). The positive relationship between NO emission rates and AOX amount across plant lines is consistent with the hypothesis that AOX is able to produce NO from nitrite under hypoxia (Planchet et al., 2005; Vishwakarma et al., 2018). If this is the case, AOX could be contributing to the maintenance of energy status (ATP/ADP ratio) not so much by maintaining electron flow to oxygen (as discussed above), but rather by contributing to the phytohemoglobin-NO cycle. In this cycle, nitrite (rather than oxygen) acts as a terminal electron acceptor in the mitochondrial ETC, allowing for the maintenance of some proton translocation and oxidative phosphorylation. The NO then leaks from the mitochondrion and the nitrogen is cycled back to nitrate using non-symbiotic class 1 phytohemoglobins with extremely high affinity for oxygen (Igamberdiev and Hill, 2004; Stoimenova et al., 2007; Gupta et al., 2011). The cycle depends upon cyt oxidase (to act as a nitrite reductase) and nitrate reductase (to convert nitrate back to nitrite). In the current study, either the cyt oxidase inhibitor KCN or the nitrate reductase inhibitor tungstate dramatically reduced NO emission rates under hypoxia, indicating that this cycle is active. However, the AOX inhibitor SHAM could also reduce NO emission rates significantly and this inhibition was most pronounced in the overexpressors and least pronounced in the knockdowns (**Figure 5**). This is again consistent with the hypothesis that AOX can produce NO. However, results with SHAM should be considered with caution since its specificity is quite low, allowing it to inhibit peroxidases and other redox proteins as well (Rich et al., 1978).

While aberrant amounts of NO emission in the knockdown and overexpression plants (**Figure 5**) is consistent with AOX being capable of nitrite reduction to NO under hypoxia, an alternative explanation should also be considered. NO can be scavenged by its very fast reaction with  $O_2^-$  to produce peroxynitrite, which in turn can be detoxified by mitochondrial peroxidases (de Oliveira et al., 2008; Wulff et al., 2009; Quijano et al., 2016). Since AOX influences the generation of mitochondrial  $O_2^-$ , it could affect the rate of mitochondrial NO scavenging by this reaction, thereby influencing the rate of leaf NO emission. If AOX knockdowns produce more  $O_2^-$  than WT

plants under hypoxia (**Figure 1A**), then their lower NO emission rates (**Figure 5**) could be due to more effective NO scavenging in the mitochondrion. Similarly, lower  $O_2^-$  production in overexpressors would decrease NO scavenging, hence increasing NO emissions. Further, the lower NO emission rates in SHAM-treated plants (particularly the WT and overexpression plants) could be explained in this manner. Inhibition of AOX in these plants by SHAM would increase  $O_2^-$  generation and hence NO scavenging.

As discussed earlier, under normoxia, knockdown of AOX altered the abundance of the majority of the metabolites measured in this study (9 out of 16 metabolites differed significantly from WT), while overexpression of AOX had relatively little effect (2 out of 16 metabolites differed significantly from WT) (**Figure 7**). However, following hypoxia, the number of metabolites with significantly altered abundance relative to WT was similar between the knockdown (7 out of 16 metabolites) and overexpression (6 out of 16 metabolites) plants. These results suggest that AOX overexpression was more disruptive to carbon metabolism under hypoxia than under normoxia. For example, while lactate and alanine were similar between the WT and overexpression plants under normoxia, they were higher in the overexpressor than WT following hypoxia (**Figures 7G,I**).

One site of disruption of carbon metabolism in the overexpressor following hypoxia was at mitochondrial aconitase. The overexpressor retained only 5% of this activity following hypoxia (relative to normoxia), while the WT and knockdown retained 20 and 61%, respectively (**Figure 6A**). Aconitase is susceptible to oxidative stress (Sweetlove et al., 2002; Armstrong et al., 2004; Quijano et al., 2016), but if this were responsible for the losses of activity seen here, then one would predict the greatest losses to have occurred in the knockdown, which in fact saw the least loss of activity. However, aconitase may also be susceptible to inactivation by NO (Navarre et al., 2000; Gupta et al., 2012). Indeed, the exaggerated loss of activity in the overexpressor relative to WT corresponds with its higher rate of NO emission under hypoxia (**Figure 5**). Similarly, the greater retention of activity in the knockdown relative to WT corresponds with its lower rate of NO emission. These results provide compelling (yet circumstantial) evidence that, under hypoxia, mitochondrial aconitase may be susceptible to inactivation by NO. On the other hand, cytosolic aconitase activity decreased only slightly in response to hypoxia, and this decline was similar across plant lines (**Figure 6B**).

In summary, AOX clearly remains relevant at very low oxygen concentrations, despite its much lower affinity for oxygen than cyt oxidase. AOX activity under these conditions supports energy generation, at a time when mitochondria-generated NO is inhibiting cyt oxidase. AOX prevents excessive nitro-oxidative stress under these conditions.

## Reoxygenation

Within 15 min of reoxygenation, leaf energy status (i.e., ATP/ADP ratio) of all plant lines improved relative to hypoxia, suggestive of a rapid recovery of ETC activity (**Figure 3**). Nonetheless, the differences in ATP/ADP ratio across plant lines

persisted, suggesting that AOX was contributing positively to this recovery of energy status during reoxygenation. In fact, by 120 min, those plants containing AOX (WT and overexpression plants) had ATP/ADP ratios that now far exceeded those measured in the normoxia treatment, while this was not the case in the knockdowns. Nonetheless,  $O_2^-$  amounts remained low in the WT and overexpressors (particularly the overexpressors), while the knockdown plants showed high amounts of  $O_2^-$ . In fact, the differences in  $O_2^-$  amount across plant lines during the reoxygenation period were as great as, or greater, than seen under hypoxia. As a result, the differences in oxidative damage (MDA amount) across plant lines was greater following 120 min of reoxygenation than with any other treatment (**Figure 2B**). Overall, these results confirm that reoxygenation can elicit oxidative stress (Blokhina et al., 2003; Chang et al., 2012; Shingaki-Wells et al., 2014). Further, AOX provides a means to dampen this stress and improve the recovery of energy status.

Reoxygenation resulted in a spike in protein S-nitrosylation that was specific to the AOX knockdowns (**Figure 2A**). These results are consistent with previous studies indicating that, under normoxia, AOX respiration reduces NO generation by the ETC, by preventing over-reduction of Complex III (Cvetkovska and Vanlerberghe, 2012a,b; Alber et al., 2017).

In summary, reoxygenation represents a condition in which AOX appears particularly important in preventing excessive nitro-oxidative stress. In doing so, AOX improved the ability of leaf tissue to rapidly recover its energy status.

## Conclusion

The results show that AOX amount influences leaf carbon and energy metabolism under normoxia, hypoxia, and during a reoxygenation period following hypoxia. Under all these conditions, an optimal AOX amount was necessary to support metabolism and to prevent excessive nitro-oxidative stress.

## REFERENCES

- Affourtit, C., Krab, K., and Moore, A. L. (2001). Control of plant mitochondrial respiration. *Biochim. Biophys. Acta* 1504, 58–69. doi: 10.1016/s0005-2728(00)00239-5
- Alber, N. A., Sivanesan, H., and Vanlerberghe, G. C. (2017). The occurrence and control of nitric oxide generation by the plant mitochondrial electron transport chain. *Plant Cell Environ.* 40, 1074–1085. doi: 10.1111/pce.12884
- Amirsadeghi, S., Robson, C. A., McDonald, A. E., and Vanlerberghe, G. C. (2006). Changes in plant mitochondrial electron transport alter cellular levels of reactive oxygen species and susceptibility to cell death signaling molecules. *Plant Cell Physiol.* 47, 1509–1519. doi: 10.1093/pcp/pcl016
- Amor, Y., Chevion, M., and Levine, A. (2000). Anoxia pretreatment protects soybean cells against  $H_2O_2$ -induced cell death: possible involvement of peroxidases and of alternative oxidase. *FEBS Lett.* 477, 175–180. doi: 10.1016/s0014-5793(00)01797-x
- Antônio, C., Pöpke, C., Rocha, M., Diab, H., Limami, A. M., Obata, T., et al. (2016). Regulation of primary metabolism in response to low oxygen availability as revealed by carbon and nitrogen isotope redistribution. *Plant Physiol.* 170, 43–56. doi: 10.1104/pp.15.00266
- Armstrong, J. S., Whiteman, M., Yang, H., and Jones, D. P. (2004). The redox regulation of intermediary metabolism by a superoxide-aconitase rheostat. *BioEssays* 26, 894–900. doi: 10.1002/bies.20071

## DATA AVAILABILITY STATEMENT

The datasets generated for this study are available on request to the corresponding author.

## AUTHOR CONTRIBUTIONS

JJ performed the experiments on normoxia, hypoxia, and reoxygenation including NO measurements, participated in discussion of results, and contributed to writing the manuscript. DC determined the aconitase activity, prepared the samples for metabolomics analysis, analyzed the results, and contributed to writing the manuscript. PV determined the phenolic and flavonoid content, and prepared the samples for metabolomics analysis. NB planned and supervised the experiments, analyzed the results, and contributed to writing the manuscript. GV developed the transgenic lines, analyzed the results, and contributed to writing the manuscript and shaping its final version. AI supervised the design, execution, and interpretation of the experiments, and prepared the manuscript for submission.

## FUNDING

This work was supported by grants from the Natural Sciences and Engineering Research Council of Canada (RGPIN-2013-55753 to AI and RGPIN-2019-04362 to GV).

## ACKNOWLEDGMENTS

The authors gratefully acknowledge the NMR analysis performed by Dr. Rupasri Mandal and coworkers at the Metabolomics Innovation Centre (TMIC) (Edmonton, AB, Canada).

- Baudouin, E. (2011). The language of nitric oxide signaling. *Plant Biol.* 13, 233–242. doi: 10.1111/j.1438-8677.2010.00403.x
- Baumgart, M., and Bott, M. (2011). Biochemical characterisation of aconitase from *Corynebacterium glutamicum*. *J. Biotechnol.* 154, 163–170. doi: 10.1016/j.jbiotec.2010.07.002
- Benamar, A., Rolletschek, H., Borisjuk, L., Avelange-Macherel, M. H., Curien, G., Mostefai, H. A., et al. (2008). Nitrite-nitric oxide control of mitochondrial respiration at the frontier of anoxia. *Biochim. Biophys. Acta* 1777, 1268–1275. doi: 10.1016/j.bbabi.2008.06.002
- Blokhina, O., Virolainen, E., and Fagerstedt, K. V. (2003). Antioxidants, oxidative damage and oxygen deprivation stress: a review. *Ann. Bot.* 91, 179–194. doi: 10.1093/aob/mcf118
- Canam, T., Li, X., Holowachuk, J., Yu, M., Xia, J., Mandal, R., et al. (2013). Differential metabolite profiles and salinity tolerance between two genetically related brown-seeded and yellow-seeded *Brassica carinata* lines. *Plant Sci.* 198, 17–26. doi: 10.1016/j.plantsci.2012.09.011
- Castello, P. R., David, P. S., McClure, T., Crook, Z., and Poyton, R. O. (2006). Mitochondrial cytochrome oxidase produces nitric oxide under hypoxic conditions: implications for oxygen sensing and hypoxic signaling in eukaryotes. *Cell Metab.* 3, 277–287. doi: 10.1016/j.cmet.2006.02.011
- Chai, T.-T., Simmonds, D., Day, D. A., Colmer, T. D., and Finnegan, P. M. (2010). Photosynthetic performance and fertility are repressed in GmAOX2b antisense soybean. *Plant Physiol.* 152, 1638–1649. doi: 10.1104/pp.109.149294

- Chandrasekara, N., and Shahidi, F. (2011). Effect of roasting on phenolic content and antioxidant activities of whole cashew nuts, kernels, and testa. *J. Agric. Food Chem.* 59, 5006–5014. doi: 10.1021/jf2000772
- Chang, R., Jang, C. J. H., Branco-Price, C., Nghiem, P., and Bailey-Serres, J. (2012). Transient MPK6 activation in response to oxygen deprivation and reoxygenation is mediated by mitochondria and aids seedling survival in *Arabidopsis*. *Plant Mol. Biol.* 78, 109–122. doi: 10.1007/s11103-011-9850-5
- Cochrane, D. W., Shah, J. K., Hebelstrup, K. H., and Igamberdiev, A. U. (2017). Expression of phytohemoglobin affects nitric oxide metabolism and energy state of barley plants exposed to anoxia. *Plant Sci.* 265, 124–130. doi: 10.1016/j.plantsci.2017.10.001
- Cvetkovska, M., and Vanlerberghe, G. C. (2012a). Alternative oxidase modulates leaf mitochondrial concentrations of superoxide and nitric oxide. *New Phytol.* 195, 32–39. doi: 10.1111/j.1469-8137.2012.04166.x
- Cvetkovska, M., and Vanlerberghe, G. C. (2012b). Coordination of a mitochondrial superoxide burst during the hypersensitive response to bacterial pathogen in *Nicotiana tabacum*. *Plant Cell Environ.* 35, 1121–1136. doi: 10.1111/j.1365-3040.2011.02477.x
- Dahal, K., Martyn, G. D., Alber, N. A., and Vanlerberghe, G. C. (2017). Coordinated regulation of photosynthetic and respiratory components is necessary to maintain chloroplast energy balance in varied growth conditions. *J. Exp. Bot.* 68, 657–671. doi: 10.1093/jxb/erw469
- Dahal, K., and Vanlerberghe, G. C. (2017). Alternative oxidase respiration maintains both mitochondrial and chloroplast function during drought. *New Phytol.* 213, 560–571. doi: 10.1111/nph.14169
- Dahal, K., and Vanlerberghe, G. C. (2018a). Growth at elevated CO<sub>2</sub> requires acclimation of the respiratory chain to support photosynthesis. *Plant Physiol.* 178, 82–100. doi: 10.1104/pp.18.00712
- Dahal, K., and Vanlerberghe, G. C. (2018b). Improved chloroplast energy balance during water deficit enhances plant growth: more crop per drop. *J. Exp. Bot.* 69, 1183–1197. doi: 10.1093/jxb/erx474
- de Oliveira, H. C., Wulff, A., Saviani, E. E., and Salgado, I. (2008). Nitric oxide degradation by potato tuber mitochondria: evidence for the involvement of external NAD(P)H dehydrogenases. *Biochim. Biophys. Acta* 1777, 470–476. doi: 10.1016/j.bbapbio.2008.02.006
- Del-Saz, N. F., Ribas-Carbo, M., McDonald, A. E., Lambers, H., Fernie, A. R., and Florez-Sarasa, I. (2018). An in vivo perspective of the role(s) of the alternative oxidase pathway. *Trends Plant Sci.* 23, 206–219. doi: 10.1016/j.tplants.2017.1.1.006
- Dordas, C., Hasinoff, B. B., Igamberdiev, A. U., Manac'h, N., Rivoal, J., and Hill, R. D. (2003). Expression of a stress-induced haemoglobin affects NO levels produced by alfalfa root cultures under hypoxic stress. *Plant J.* 35, 763–770. doi: 10.1046/j.1365-3113x.2003.01846.x
- Eprintsev, A. T., Fedorin, D. N., Dobychna, M. A., and Igamberdiev, A. U. (2017). Expression and promoter methylation of succinate dehydrogenase and fumarate genes in maize under anoxic conditions. *J. Plant Physiol.* 216, 197–201. doi: 10.1016/j.jplph.2017.06.011
- Giraud, E., Ho, L. H. M., Clifton, R., Carroll, A., Estavillo, G., Tan, Y.-F., et al. (2008). The absence of ALTERNATIVE OXIDASE1a in *Arabidopsis* results in acute sensitivity to combined light and drought stress. *Plant Physiol.* 147, 595–610. doi: 10.1104/pp.107.115121
- Guan, B., Lin, Z., Liu, D., Li, C., Zhou, Z., Mei, F., et al. (2019). Effect of waterlogging-induced autophagy on programmed cell death in *Arabidopsis* roots. *Front. Plant Sci.* 10:468. doi: 10.3389/fpls.2019.00468
- Gupta, K. J., Hebelstrup, K. H., Kruger, N. J., and Ratcliffe, R. G. (2014). Nitric oxide is required for homeostasis of oxygen and reactive oxygen species in barley roots under aerobic conditions. *Mol. Plant.* 7, 747–750. doi: 10.1093/mp/sst167
- Gupta, K. J., Hebelstrup, K. H., Mur, L. A. J., and Igamberdiev, A. U. (2011). Plant hemoglobins: important players at the crossroads between oxygen and nitric oxide. *FEBS Lett.* 585, 3843–3849. doi: 10.1016/j.febslet.2011.10.036
- Gupta, K. J., Kumari, A., Florez-Sarasa, I., Fernie, A. R., and Igamberdiev, A. U. (2018). Interaction of nitric oxide with the components of the plant mitochondrial electron transport chain. *J. Exp. Bot.* 69, 3413–3424. doi: 10.1093/jxb/ery119
- Gupta, K. J., Shah, J. K., Brotman, Y., Jahnke, K., Willmitzer, L., and Kaiser, W. M. (2012). Inhibition of aconitase by nitric oxide leads to induction of the alternative oxidase and to a shift of metabolism towards biosynthesis of amino acids. *J. Exp. Bot.* 63, 1773–1784. doi: 10.1093/jxb/ers053
- Gupta, K. J., Zabalza, A., and van Dongen, J. T. (2009). Regulation of respiration when the oxygen availability changes. *Physiol. Plant.* 137, 383–391. doi: 10.1111/j.1399-3054.2009.01253.x
- Guy, R. D., and Vanlerberghe, G. C. (2005). Partitioning of respiratory electrons in the dark in leaves of transgenic tobacco with modified levels of alternative oxidase. *Physiol. Plant.* 125, 171–180. doi: 10.1111/j.1399-3054.2005.00557.x
- Heath, R. L., and Parker, L. (1968). Photoperoxidation in isolated chloroplasts. I. Kinetics and stoichiometry of fatty acid peroxidation. *Arch. Biochem. Biophys.* 125, 189–198. doi: 10.1016/0003-9861(68)90654-1
- Hoshi, Y., Hazeki, O., and Tamura, M. (1993). Oxygen dependence of redox state of copper in cytochrome oxidase in vitro. *J. Appl. Physiol.* 74, 1622–1627. doi: 10.1152/jappl.1993.74.4.1622
- Igamberdiev, A. U., Bykova, N. V., Shah, J. K., and Hill, R. D. (2010). Anoxic nitric oxide cycling in plants: participating reactions and possible mechanisms. *Physiol. Plant.* 138, 393–404. doi: 10.1111/j.1399-3054.2009.01314.x
- Igamberdiev, A. U., and Hill, R. D. (2004). Nitrate. NO and haemoglobin in plant adaptation to hypoxia: an alternative to classic fermentation pathways. *J. Exp. Bot.* 55, 2473–2482. doi: 10.1093/jxb/erh272
- Klok, E. J., Wilson, I. W., Wilson, D., Chapman, S. C., Ewing, R. M., and Somerville, S. C. (2002). Expression profile analysis of the low-oxygen response in *Arabidopsis* root cultures. *Plant Cell* 14, 2481–2494. doi: 10.1105/tpc.004747
- Kreuzwieser, J., Hauberg, J., Howell, K. A., Carroll, A., Rennenberg, H., Millar, A. H., et al. (2009). Differential response of gray poplar leaves and roots underpins stress adaptation during hypoxia. *Plant Physiol.* 149, 461–473. doi: 10.1104/pp.108.125989
- Liu, F., VanToai, T., Moy, L. P., Bock, G., Linford, L. D., and Quackenbush, J. (2005). Global transcription profiling reveals comprehensive insights into hypoxic response in *Arabidopsis*. *Plant Physiol.* 137, 1115–1129. doi: 10.1104/pp.104.055475
- Ma, Z., Marsolais, F., Bykova, N. V., and Igamberdiev, A. U. (2016). Nitric oxide and reactive oxygen species mediate metabolic changes in barley seed embryo during germination. *Front. Plant Sci.* 7:138. doi: 10.3389/fpls.2016.00138
- Maxwell, D. P., Wang, Y., and McIntosh, L. (1999). The alternative oxidase lowers mitochondrial reactive oxygen production in plant cells. *Proc. Natl. Acad. Sci. U.S.A.* 96, 8271–8276. doi: 10.1073/pnas.96.14.8271
- Millar, A. H., Atkin, O. K., Menz, R. I., Henry, B., Farquhar, G., and Day, D. A. (1998). Analysis of respiratory chain regulation in roots of soybean seedlings. *Plant Physiol.* 117, 1083–1093. doi: 10.1104/pp.117.3.1083
- Millar, A. H., Bergensen, F. J., and Day, D. A. (1994). Oxygen affinity of terminal oxidases in soybean mitochondria. *Plant Physiol. Biochem.* 32, 847–852.
- Millar, A. H., and Day, D. A. (1997). Alternative solutions to radical problems. *Trends Plant Sci.* 2, 289–290. doi: 10.1016/S1360-1385(97)89948-7
- Millar, A. H., Trend, A. E., and Heazlewood, J. L. (2004). Changes in the mitochondrial proteome during the anoxia to air transition in rice focus around cytochrome-containing respiratory complexes. *J. Biol. Chem.* 279, 39471–39478. doi: 10.1074/jbc.M406015200
- Millar, A. H., Wiskich, J. T., Whelan, J., and Day, D. A. (1993). Organic acid activation of the alternative oxidase of plant mitochondria. *FEBS Lett.* 329, 259–262. doi: 10.1016/0014-5793(93)80233-k
- Narsai, R., Rocha, M., Geigenberger, P., Whelan, J., and van Dongen, J. T. (2011). Comparative analysis between plant species of transcriptional and metabolic responses to hypoxia. *New Phytol.* 190, 472–487. doi: 10.1111/j.1469-8137.2010.03589.x
- Navarre, D. A., Wendehenne, D., Durner, J., Noad, R., and Klessig, D. F. (2000). Nitric oxide modulates the activity of tobacco aconitase. *Plant Physiol.* 122, 573–582. doi: 10.1104/pp.122.2.573
- Panozzo, A., Dal Cortivo, C., Ferrari, M., Vicelli, B., Varotto, S., and Vamerali, T. (2019). Morphological changes and expressions of AOX1A, CYP81D8, and putative PFP genes in a large set of commercial maize hybrids under extreme waterlogging. *Front. Plant Sci.* 10:62. doi: 10.3389/fpls.2019.00062
- Parsons, H. L., Yip, J. Y. H., and Vanlerberghe, G. C. (1999). Increased respiratory restriction during phosphate-limited growth in transgenic tobacco cells lacking alternative oxidase. *Plant Physiol.* 121, 1309–1320. doi: 10.1104/pp.121.4.1309
- Pasqualini, S., Paolocci, F., Borgogni, A., Moretti, R., and Ederli, L. (2007). The overexpression of an alternative oxidase gene triggers ozone sensitivity in tobacco plants. *Plant Cell Environ.* 30, 1545–1556. doi: 10.1111/j.1365-3040.2007.01730.x



- Planchet, E., Gupta, K. J., Sonoda, M., and Kaiser, W. M. (2005). Nitric oxide emission from tobacco leaves and cell suspensions: rate limiting factors and evidence for the involvement of mitochondrial electron transport. *Plant J.* 41, 732–743. doi: 10.1111/j.1365-313X.2005.02335.x
- Poyton, R. O., Ball, K. A., and Castello, P. R. (2009). Mitochondrial generation of free radicals and hypoxic signaling. *Trends Endocrinol. Metab.* 20, 332–340. doi: 10.1016/j.tem.2009.04.001
- Psychogios, N., Hau, D. D., Peng, J., Guo, A. C., Mandal, R., Bouatra, S., et al. (2011). The human serum metabolome. *PLoS One* 6:e16957. doi: 10.1371/journal.pone.0016957
- Purvis, A. C. (1997). Role of the alternative oxidase in limiting superoxide production by plant mitochondria. *Physiol. Plant.* 100, 165–170. doi: 10.1111/j.1399-3054.1997.tb03468.x
- Quijano, C., Trujillo, M., Castro, L., and Trostchansky, A. (2016). Interplay between oxidant species and energy metabolism. *Redox Biol.* 8, 28–42. doi: 10.1016/j.redox.2015.11.010
- Ribas-Carbo, M., Berry, J. A., Azcon-Bieto, J., and Siedow, J. N. (1994). The reaction of the plant mitochondrial cyanide-resistant alternative oxidase with oxygen. *Biochim. Biophys. Acta* 118, 205–212. doi: 10.1016/0005-2728(94)90037-X
- Ribas-Carbo, M., Taylor, N. L., Giles, L., Busquets, S., Finnegan, P. M., Day, D. A., et al. (2005). Effects of water stress on respiration in soybean leaves. *Plant Physiol.* 139, 466–473. doi: 10.1104/pp.105.065565
- Rich, P. R., Wiegand, N. K., Blum, H., Moore, A. L., and Bonner, W. D. Jr. (1978). Studies on the mechanism of inhibition of redox enzymes by substituted hydroxamic acids. *Biochim. Biophys. Acta* 525, 325–337. doi: 10.1016/0005-2744(78)90227-9
- Rivera-Contreras, I. K., Zamora-Hernández, T., Huerta-Heredia, A. A., Capataz-Tafur, J., Barrera-Figueroa, B. E., and Juntawong, P. (2016). Transcriptomic analysis of submergence-tolerant and sensitive *Brachypodium distachyon* ecotypes reveals oxidative stress as a major tolerance factor. *Sci. Rep.* 6:27686. doi: 10.1038/srep27686
- Rocha, M., Licausi, F., Araújo, W. L., Nunes-Nesi, A., Sodek, L., and Fernie, A. R. (2010). Glycolysis and the tricarboxylic acid cycle are linked by alanine aminotransferase during hypoxia induced by waterlogging of *Lotus japonicus*. *Plant Physiol.* 152, 1501–1513. doi: 10.1104/pp.109.150045
- Selinski, J., Scheibe, R., Day, D. A., and Whelan, J. (2018). Alternative oxidase is positive for plant performance. *Trends Plant Sci.* 23, 588–597. doi: 10.1016/j.tplants.2018.03.012
- Shingaki-Wells, R., Millar, A. H., Whelan, J., and Narsai, R. (2014). What happens to plant mitochondria under low oxygen? An omics review of the responses to low oxygen and reoxygenation. *Plant Cell Environ.* 37, 2260–2277. doi: 10.1111/pce.12312
- Sieger, S. M., Kristensen, B. K., Robson, C. A., Amirsadeghi, S., Eng, E. W. Y., Abdel-Mesih, A., et al. (2005). The role of alternative oxidase in modulating carbon use efficiency and growth during macronutrient stress in tobacco cells. *J. Exp. Bot.* 56, 1499–1515. doi: 10.1093/jxb/eri146
- Skutnik, M., and Rychter, A. M. (2009). Differential response of antioxidant systems in leaves and roots of barley subjected to anoxia and post-anoxia. *J. Plant Physiol.* 166, 926–937. doi: 10.1016/j.jplph.2008.11.010
- Smith, C. A., Melino, V. J., Sweetman, C., and Soole, K. L. (2009). Manipulation of alternative oxidase can influence salt tolerance in *Arabidopsis thaliana*. *Physiol. Plant.* 137, 459–472. doi: 10.1111/j.1399-3054.2009.01305.x
- Stoimenova, M., Igamberdiev, A. U., Gupta, K. J., and Hill, R. D. (2007). Nitrite-driven anaerobic ATP synthesis in barley and rice root mitochondria. *Planta* 226, 465–474. doi: 10.1007/s00425-007-0496-0
- Sun, J., and Trumpower, B. L. (2003). Superoxide anion generation by the cytochrome bc<sub>1</sub> complex. *Arch. Biochem. Biophys.* 419, 198–206. doi: 10.1016/j.abb.2003.08.028
- Sweetlove, L. J., Heazlewood, J. L., Herrald, V., Holtzapffel, R., Day, D. A., Leaver, C. J., et al. (2002). The impact of oxidative stress on Arabidopsis mitochondria. *Plant J.* 32, 891–904. doi: 10.1046/j.1365-313x.2002.01474.x
- Szal, B., Jolivet, Y., Hasenfratz-Sauder, M.-P., Dizengremel, P., and Rychter, A. M. (2003). Oxygen concentration regulates alternative oxidase expression in barley roots during hypoxia and post-hypoxia. *Physiol. Plant.* 119, 494–502. doi: 10.1046/j.1399-3054.2003.00161.x
- Tsuji, H., Nakazono, M., Saisho, D., Tsutsumi, N., and Hirai, A. (2000). Transcript levels of the nuclear-encoded respiratory genes in rice decrease by oxygen deprivation: evidence for involvement of calcium in expression of the alternative oxidase 1a gene. *FEBS Lett.* 471, 201–204. doi: 10.1016/S0014-5793(00)01411-3
- Umbach, A. L., and Siedow, J. N. (1993). Covalent and noncovalent dimers of the cyanide-resistant alternative oxidase protein in higher plant mitochondria and their relationship to enzyme activity. *Plant Physiol.* 103, 845–854. doi: 10.1104/pp.103.3.845
- Vanlerberghe, G. C. (2013). Alternative oxidase: a mitochondrial respiratory pathway to maintain metabolic and signaling homeostasis during abiotic and biotic stress in plants. *Int. J. Mol. Sci.* 14, 6805–6847. doi: 10.3390/ijms14046805
- Vanlerberghe, G. C., Day, D. A., Wiskich, J. T., Vanlerberghe, A. E., and McIntosh, L. (1995). Alternative oxidase activity in tobacco leaf mitochondria: dependence on tricarboxylic acid cycle-mediated redox regulation and pyruvate activation. *Plant Physiol.* 109, 353–361. doi: 10.1104/pp.109.2.353
- Vergara, R., Parada, F., Rubio, S., and Pérez, J. (2012). Hypoxia induces H<sub>2</sub>O<sub>2</sub> production and activates antioxidant defence system in grapevine buds through mediation of H<sub>2</sub>O<sub>2</sub> and ethylene. *J. Exp. Bot.* 63, 4123–4131. doi: 10.1093/jxb/ers094
- Vishwakarma, A., Kumari, A., Mur, L. A. J., and Gupta, K. J. (2018). A discrete role for alternative oxidase under hypoxia to increase nitric oxide and drive energy production. *Free Radic. Biol. Med.* 122, 40–51. doi: 10.1016/j.freeradbiomed.2018.03.045
- Vyas, P., Debnath, S. C., and Igamberdiev, A. U. (2013). Metabolism of glutathione and ascorbate in lingonberry cultivars during in vitro and ex vitro propagation. *Biol. Plant.* 57, 603–612. doi: 10.1007/s10535-013-0339-8
- Wang, J., Rajakulendran, N., Amirsadeghi, S., and Vanlerberghe, G. C. (2011). Impact of mitochondrial alternative oxidase expression on the response of *Nicotiana tabacum* to cold temperature. *Physiol. Plant.* 142, 339–351. doi: 10.1111/j.1399-3054.2011.01471.x
- Wang, J., and Vanlerberghe, G. C. (2013). A lack of mitochondrial alternative oxidase compromises capacity to recover from severe drought stress. *Physiol. Plant.* 149, 461–473. doi: 10.1111/ppl.12059
- Wany, A., Gupta, A. K., Kumari, A., Mishra, S., Singh, N., Pandey, S., et al. (2019). Nitrate nutrition influences multiple factors in order to increase energy efficiency under hypoxia in Arabidopsis. *Ann. Bot.* 123, 691–705. doi: 10.1093/aob/mcy202
- Wulff, A., Oliveira, H. C., Saviani, E. E., and Salgado, I. (2009). Nitrite reduction and superoxide-dependent nitric oxide degradation by Arabidopsis mitochondria: influence of external NAD(P)H dehydrogenases and alternative oxidase in the control of nitric oxide levels. *Nitric Oxide* 21, 132–139. doi: 10.1016/j.niox.2009.06.003
- Zaffagnini, M., De Mía, M., Morisse, S., Di Giacinto, N., Marchand, C. H., Maes, A., et al. (2016). Protein S-nitrosylation in photosynthetic organisms: a comprehensive overview with future perspectives. *Biochim. Biophys. Acta* 1864, 952–966. doi: 10.1016/j.bbapap.2016.02.006
- Zhishen, J., Mengcheng, T., and Jianming, W. (1999). The determination of flavonoid contents in mulberry and their scavenging effect on superoxide radicals. *Food Chem.* 64, 555–559. doi: 10.1016/S0308-8146(98)00102-2

**Conflict of Interest:** The authors declare that the research was conducted in the absence of any commercial or financial relationships that could be construed as a potential conflict of interest.

Copyright © 2020 Jayawardhane, Cochrane, Vyas, Bykova, Vanlerberghe and Igamberdiev. This is an open-access article distributed under the terms of the Creative Commons Attribution License (CC BY). The use, distribution or reproduction in other forums is permitted, provided the original author(s) and the copyright owner(s) are credited and that the original publication in this journal is cited, in accordance with accepted academic practice. No use, distribution or reproduction is permitted which does not comply with these terms.





# Nitrated Nucleotides: New Players in Signaling Pathways of Reactive Nitrogen and Oxygen Species in Plants

Marek Petřivalský\* and Lenka Luhová

Department of Biochemistry, Faculty of Science, Palacký University, Olomouc, Czechia

## OPEN ACCESS

### Edited by:

Christian Lindermayr,  
Helmholtz Zentrum München,  
Germany

### Reviewed by:

Takaaki Akaike,  
Tohoku University, Japan  
Chris Gehring,  
University of Perugia, Italy  
Agepati S. Raghavendra,  
University of Hyderabad, India

### \*Correspondence:

Marek Petřivalský  
marek.petrivalsky@upol.cz

### Specialty section:

This article was submitted to  
Plant Physiology,  
a section of the journal  
Frontiers in Plant Science

**Received:** 21 January 2020

**Accepted:** 20 April 2020

**Published:** 19 May 2020

### Citation:

Petrivalský M and Luhová L (2020)  
Nitrated Nucleotides: New Players  
in Signaling Pathways of Reactive  
Nitrogen and Oxygen Species  
in Plants. *Front. Plant Sci.* 11:598.  
doi: 10.3389/fpls.2020.00598

Nitration of diverse biomolecules, including proteins, lipids and nucleic acid, by reactive nitrogen species represents one of the key mechanisms mediating nitric oxide (NO) biological activity across all types of organisms. 8-nitroguanosine 3'5'-cyclic monophosphate (8-nitro-cGMP) has been described as a unique electrophilic intermediate involved in intracellular redox signaling. In animal cells, 8-nitro-cGMP is formed from guanosine-5'-triphosphate by a combined action of reactive nitrogen (RNS) and oxygen species (ROS) and guanylate cyclase. As demonstrated originally in animal models, 8-nitro-cGMP shows certain biological activities closely resembling its analog cGMP; however, its regulatory functions are mediated mainly by its electrophilic properties and chemical interactions with protein thiols resulting in a novel protein post-translational modification termed S-guanylation. In *Arabidopsis thaliana*, 8-nitro-cGMP was reported to mediate NO-dependent signaling pathways controlling abscisic acid (ABA)-induced stomatal closure, however, its derivative 8-mercapto-cGMP (8-SH-cGMP) was later shown as the active component of hydrogen sulfide (H<sub>2</sub>S)-mediated guard cell signaling. Here we present a survey of current knowledge on biosynthesis, metabolism and biological activities of nitrated nucleotides with special attention to described and proposed functions of 8-nitro-cGMP and its metabolites in plant physiology and stress responses.

**Keywords:** nitration, nitric oxide, plant, persulfidation, reactive nitrogen species, reactive oxygen species, signaling, S-guanylation

## INTRODUCTION

Nitric oxide (NO) is a crucial gaseous signaling molecule which plays vital roles in a broad spectrum of physiological and developmental processes throughout the plant life, including germination, development of leaves, roots and reproductive organs, stomata movement and plant senescence (Yu et al., 2014; Astier et al., 2018). NO also participates in signaling pathways of plant reactions to biotic and abiotic stresses (Corpas and Barroso, 2015; Farnese et al., 2016). Signaling functions of NO in plants are mediated namely through three key NO-dependent post-translational modifications (PTM): metal nitrosylation in metalloproteins, S-nitrosation of cysteine

thiols, and tyrosine nitration (Begara-Morales et al., 2016; Umbreen et al., 2018). Nitration of proteins, lipids, nucleic acid and free nucleotides occurs in plants as a part of NO-dependent signaling pathways within redox regulations and during plant responses to diverse environmental stress stimuli (reviewed in Arasimowicz-Jelonek and Floryszak-Wieczorek, 2019). Here we present a concise overview of current knowledge on formation, metabolism and biological activities of nitrated nucleotides with special attention to described and proposed functions of 8-nitro-cGMP and its metabolites in plants.

## FORMATION OF NITRATED NUCLEOTIDES

The possibility of covalent modification of nucleotides and related compounds has been studied since the early years of NO research in animals. 8-Nitroguanine was reported to originate in a dose-dependent manner from a rapid reaction of peroxynitrite with free guanine nucleotide (Yermilov et al., 1995a) as well with guanine in calf thymus and epidermal keratinocytes DNA *in vitro* (Yermilov et al., 1995b; Spencer et al., 1996). *In vivo* formation of 8-nitroguanine and related nitrated derivatives was reported in livers of hamsters after infection with *Opisthorchis viverrini* (Pinlaor et al., 2003) and in human gastric mucosa upon *H. pylori* infection (Ma et al., 2004). Guanosine can be also readily nitrated by reactive nitrogen species *in vitro* (Niles et al., 2001; Sodum and Fiala, 2001). 8-Nitroguanosine formation occurred in RNA of peroxynitrite-treated human lung carcinoma cells (Masuda et al., 2002), whereas its production in mice cells during viral pneumonia was found to proceed via inducible NO synthase (iNOS)-dependent NO overproduction (Akaike et al., 2003). *In vitro*, 8-nitropurine can be converted by a nucleophilic action of peroxynitrite to 8-oxopurine and this compound can be further oxidized by peroxynitrite to uric acid and its oxidation products (Lee et al., 2002).

As an important breakthrough, the formation of 8-nitro-cGMP, a nitrated cyclic nucleotide, was discovered in mouse macrophages with an active expression of iNOS. Importantly, 8-nitro-cGMP was found to possess the strongest redox-active and electrophilic properties among studied nitrated guanine derivatives (Sawa et al., 2007). Furthermore, 8-nitro-cGMP shows unique dual signaling functions, derived from its structural similarity to cGMP (i.e., activation of cGMP-dependent protein kinases) and its electrophilic properties due to the reactive nitro group (i.e., reactivity toward reduced thiols). *In vivo*, the formation of 8-nitro-cGMP does not proceed by the nitration of cGMP. 8-Nitro-cGMP is synthesized via the nitration of abundant GTP and subsequent action of guanylate cyclase on 8-nitroGTP to produce 8-nitro-cGMP (Fujii et al., 2010; Kunieda et al., 2015). Moreover, higher levels of 8-nitro-cGMP ( $\geq 40 \mu\text{M}$ ) compared to cGMP levels ( $4.6 \mu\text{M}$ ) were detected, uncovering 8-nitro-cGMP as the major intracellular cyclic nucleotide. After myocardial infarction, the 8-nitro-cGMP formation did not occur in mouse hearts deficient in iNOS, confirming the essential role of iNOS-derived NO for 8-nitro-cGMP formation (Nishida et al., 2012). Superoxide produced in mitochondria

was identified as a determinant of 8-nitro-cGMP synthesis, whereas peroxynitrite as the molecular species involved in the reaction mechanism of guanine nitration; however, nitrite with  $\text{H}_2\text{O}_2$  and myeloperoxidase can also nitrate guanine nucleotides in particular cellular environments (Ahmed et al., 2012). In LPS-treated rat glioma cells, the direct conversion of cGMP to 8-nitro-cGMP appeared unlikely, as the intracellular cGMP concentrations were one order of magnitude lower than 8-nitro-cGMP and inhibitors of soluble guanylate cyclase suppressed intracellular 8-nitro-cGMP generation.

## METABOLISM OF NITRATED NUCLEOTIDES

In contrast to cGMP, 8-nitro-cGMP is not degraded by the hydrolytic activity of phosphodiesterases (Sawa et al., 2013). The relative stability in the cellular environment presents a well-documented chemical feature of 8-nitro-cGMP, which enables to maintain its signaling functions. 8-nitro-cGMP shows electrophilicity much lower than other cellular electrophiles like unsaturated aldehydes and fatty acids, or nitroalkenes originating from lipid nitration. Consequently, the reaction rate of 8-nitro-cGMP and GSH thiol group is 20–10,000 times slower compared to these electrophiles (Sawa et al., 2010). Due to its relative chemical stability, 8-nitro-cGMP is expected to occur at noticeable concentrations even under high levels of reduced GSH. Moreover, several tested isoforms of glutathione transferases did not show any catalytical action to accelerate 8-nitro-cGMP degradation via its conjugation with GSH (Akaike et al., 2013). Nevertheless, it should be noted that 8-nitro-cGMP was unstable in degassed neutral phosphate buffer upon irradiation with the blue light ( $400 \pm 16 \text{ nm}$ ) and decomposed to 8-nitrosoguanine and an open form of ribonolactone, with a half-life of  $67.4 \pm 1.8 \text{ min}$  (Samanta et al., 2014). However, the biological relevance of light-driven 8-nitro-cGMP decomposition has not been so far addressed *in vivo*.

Metabolic fate of 8-nitro-cGMP in cell culture was assayed using stable  $^{18}\text{O}$ -labeled compound and LC-MS analysis. A novel nucleotide derivative, 8-amino-cGMP, was identified together with the S-guanylation products of 8-nitro-cGMP reaction with glutathione or cysteine (Saito et al., 2012). Immunochemical study based on prepared 8-amino-cGMP antibodies corroborated that the catabolism of 8-nitro-cGMP in LPS-triggered mouse macrophages proceeds to the formation of 8-amino-cGMP. Surprisingly, isotope-labeled 8-amino-cGMP was further converted to unmodified cGMP, suggesting oxidative modifications like guanine nitration and reducing pathways such as cGMP production would operate simultaneously during oxidative stress.

Hydrogen sulfide ( $\text{H}_2\text{S}$ ) belongs to reactive sulfur species with recognized signaling role across a wide range of organisms. In animals,  $\text{H}_2\text{S}$  biosynthesis is controlled by two crucial enzymes: cystathionine  $\beta$ -synthase (CBS) and cystathionine  $\gamma$ -lyase (CSE). Knockdown of CBS and CSE resulted in elevated 8-nitro-cGMP concentrations, indicating that its activity might be regulated

by sulfur species (Nishida et al., 2012). 8-mercapto-cGMP (8-SH-cGMP) was discovered by LC-MS analysis as a plausible product of S-guanylation reaction of 8-nitro-cGMP with  $H_2S$  in mammalian cells. Treatment of 8-SH-cGMP *in vitro* with  $H_2O_2$  or RNS provided intact cGMP. Thus inside cells, both 8-SH-cGMP and 8-amino-cGMP can be transformed into cGMP. However, the role of  $H_2S$  in the formation of 8-SH-cGMP was later put to the question because of the *in vitro* reaction of 8-nitro-cGMP with the sulfide anion generates mainly 8-amino-cGMP (Terzič et al., 2014). Thus, endogenous  $H_2S$  might act as a reductant in the transformation of 8-nitro-cGMP to 8-amino-cGMP; however, key roles of reactive hydropersulfides and related polysulfides in redox signaling and modifications of protein cysteines have been currently recognized (Akaike et al., 2017; Fukuto et al., 2018). In mice, hydropersulfides mitigated chronic heart failure after myocardial infarction, and this cardioprotective effect was mediated by repression of H-Ras pathway triggered by electrophilic action of 8-nitro-cGMP as a redox messenger for NO and ROS signaling. Hydropersulfide was shown to effectively thiolate cellular electrophiles, represented by 8-nitro-cGMP, indicating that electrophile thiolation can be considered a singular mechanism within ROS signaling and regulation of intracellular redox environment (Akaike et al., 2013). Later investigations revealed that CBS and CSE produce persulfide species showing higher nucleophilicity compared to  $H_2S$ . Persulfides of cysteine and glutathione are namely produced and react with 8-nitro-cGMP to substitution products, which are then converted to 8-SH-cGMP by a thiol-disulfide exchange (Ida et al., 2014). The biological relevance of 8-SH-cGMP is indicated by the fact that it was recognized as the most abundant cGMP derivative in several mouse organs (Ida et al., 2014). Certainly, elucidation of redox signaling mechanisms of reactive persulfides counting low-molecular thiols and proteins together with protein S-guanylation opens a new era of redox biology, physiology, and pathophysiology (Kasamatsu et al., 2016), which awaits its investigation and recognition in plant sciences.

## BIOLOGICAL ACTIVITIES OF NITRATED NUCLEOTIDES

In early studies, nitrated derivatives of guanine or guanosine were considered rather as markers of nitrosative damage occurring in cells under stress conditions. Important redox-active features of 8-nitroguanosine, including generation of superoxide catalyzed by NADPH-cytochrome P450 reductase and NOS isoenzymes, were reported (Sawa et al., 2003). Soon after, 8-nitroguanosine was demonstrated to induce mutagenesis in animal cell culture (Yoshitake et al., 2004). Increased production of ROS and RNS was implicated in the development of lung cancer mediated by nitrosative and oxidative DNA modifications. Nitrosative stress associated with 8-nitroguanine generation results in lung epithelial injury in idiopathic pulmonary fibrosis (Terasaki et al., 2006). Oxidized and nitrated guanine derivatives were detected in cell cultures, tissues and organs from humans with degenerative diseases, cancer, viral pneumonia and other inflammatory conditions (Ohshima et al., 2006).

Later experiments evidenced biological activities and signaling functions of 8-nitro-cGMP were in major extent mediated by a PTM of protein thiols termed S-guanylation (Ihara et al., 2011; Nishida et al., 2016). Mechanisms of regulation of S-guanylation as protein PTM are actually not fully understood. It needs clarification if intracellular levels and distribution of NO and ROS may explain the observed site- and time-specific modulations of S-guanylation. S-guanylation, proceeding by a nucleophilic attack of the nitro group on protein cysteines, is considered an irreversible thiol modification. It is noteworthy that a similar replacement of the nitro group with thiol had not been reported previously. The reactivity of each cysteine residue varies considerably depending on its surrounding chemical and steric environment. The values of cysteines pKa in the target protein are affected by neighboring amino acid residues. Cysteine residues with lower pKa dissociate to sulfur anions that show higher reactivity with 8-nitro-cGMP. Basal levels of protein S-guanylation occurring in physiological conditions are elevated by inflammatory conditions. Due to the presence of numerous reactive cysteine residues, guanylation of protein Keap1 (Kelch-like ECH-associated1) was observed to occur even under a high excess of reduced glutathione (Sawa et al., 2007).

The discovery of new S-guanylated proteins provided further hints to biological roles of 8-nitro-cGMP. Protocols for S-guanylation proteomics have been developed and used to analyse the regulatory roles of protein S-guanylation in mitochondrial ROS export in animal cells stimulated with LPS or cytokines (Rahaman et al., 2014). S-guanylation of two key cysteine residues, Cys160 and Cys257, in heat-shock protein 60 controls the opening of mitochondrial permeability transition pore and export of mitochondrial ROS into the cytosol. In mice, increased levels of 8-nitro-cGMP following myocardial infarction suggested its role in the pathogenesis of heart failure (Nishida et al., 2012). In this experimental model, 8-nitro-cGMP acts as a physiological ligand activating H-Ras protein, when S-guanylation at Cys184 drives H-Ras translocation to non-raft membrane domains and activation of its downstream signaling pathways.

Hepatocyte growth factor ameliorated high glucose-induced oxidative stress in rat mesangial cells by elevated NO-dependent 8-nitro-cGMP production (Guoguo et al., 2012). 1-nitro-2-phenylethane restricted taurocholate-induced cell death in pancreatic cells by increasing 8-nitro-cGMP production mediated by the sGC (Cosker et al., 2014). 8-nitro-cGMP also showed significant cytoprotective capacity in dopaminergic neurons by S-guanylation leading to induction of hem oxygenase 1 (HO-1) (Kurauchi et al., 2013; Kasamatsu et al., 2014). Similarly, HO-1 activated by NO-dependent 8-nitro-cGMP production participates in macrophage defense to *Salmonella* infection (Zaki et al., 2009). In studies of the Alzheimer disease, 8-nitro-cGMP guanylated cysteine residues in two tau proteins, which eliminated their capacity to form tau aggregates (Yoshitake et al., 2016). Cell exposure to the exogenous electrophile methylmercury, which triggers NO and ROS signaling, elevated intracellular 8-nitro-cGMP, depleted reactive persulfides and 8-SH-cGMP, increased S-guanylation and activation of H-Ras leading to damaged cerebellar neurons (Ihara et al., 2017).

8-nitro-cGMP was found to S-guanylate thiol groups of cGMP-dependent protein kinases (PKG), the primary sensor proteins of intracellular cGMP known to control an array of cellular reactions (Ahmed et al., 2017). S-guanylation of PKG occurs specifically at two susceptible residues Cys42 and Cys195 among 11 cysteine residues of PKG. Notably, S-guanylation of Cys195, positioned in the cGMP binding domain, results in an enduring activation of the enzyme activity. In mice, S-guanylation of PKG was observed without any treatment and was strongly increased by LPS treatment (Akashi et al., 2016). It was suggested that degradation of S-guanylated proteins might proceed by autophagy (Taguchi et al., 2012). Interestingly, induction of autophagy was revealed as another important function of 8-nitro-cGMP in animals (Ito et al., 2013; Rawet-Slobodkin and Elazar, 2013; Abada and Elazar, 2014). Autophagy can efficiently function as an innate defense to pathogen infection (Nakagawa et al., 2004; Mizushima and Komatsu, 2011). 8-nitro-cGMP supported autophagic elimination of infecting group A *Streptococci* in mice macrophages, where autophagosome-encapsulated pathogens showed higher S-guanylation compared to pathogens in the cytosol, indicating S-guanylation might be exploited to tag bacteria or disease-related fragments and cellular debris for autophagic removal (Ito et al., 2013; Takahashi et al., 2019). Inversely, bacteria are capable to interfere with autophagy-mediated pathogen clearance via production and release of reactive persulfides which inhibit autophagy signaling by the degradation of 8-nitro-cGMP in host cells (Khan et al., 2018).

## BIOLOGICAL FUNCTIONS IN PLANTS

The currently accumulated evidence has unraveled roles of cyclic nucleotides including cGMP in multiple plant physiological processes, including plant growth and development from germination to flowering (Lemtiri-Chlieh et al., 2011; Gehring and Turek, 2017). Compared to animals, the reaction pathways and signaling function of cGMP are not completely described and no homologs of animal cGMP-producing enzymes have been identified in higher plants; however, NO-dependent cGMP pathway participates in multiple signaling mechanisms in plants, namely in the regulation of stomata opening and defense response to pathogenic challenge (Gross and Durner, 2016). However, the molecular mechanisms of cGMP signal transduction to cellular effectors, including cGMP-dependent kinases G, are still poorly characterized (Świeżawska et al., 2018). Recent reports described the identification of cGMP-dependent protein kinase with a role in mediating gibberellin responses in rice (Shen et al., 2019) and a plant cGMP-activated phosphodiesterase involved in the UVA-induced cGMP degradation in *Arabidopsis* stomata (Isner et al., 2019). Signaling pathways involved in the regulation of stomatal movements by external stimuli and phytohormones comprise, beside cGMP, diverse components like NO, ROS, cytosolic pH, calcium ions and phospholipids (Daszkowska-Golec and Szarejko, 2013; Gayatri et al., 2013; Agurla et al., 2014; Agurla and Raghavendra, 2016). Moreover, protein PTMs by phosphorylation and redox modifications have key functions in the regulation of

stomatal movement. These modifications control molecular components of signal perception, second messenger production and downstream events within guard cell signaling (Balmant et al., 2016). NO fulfills crucial functions in modulation of stomatal movement, namely in abscisic acid-induced stomatal closure. NO is involved in stomatal closure induced by H<sub>2</sub>S, polyamines and methyl jasmonate (Sun et al., 2019) as well as microbe-associate molecular patterns (Ye and Murata, 2016). Interactions and cross-talk of the signaling pathway of NO and H<sub>2</sub>S are quite complex and both gasotransmitters regulate stomatal movement independently or in united action, in ABA-dependent signaling cascades or ABA-independent mechanisms (Scuffi et al., 2016).

Intriguing observations that cGMP was needed but not sufficient for stomatal closure induced by ABA were in agreement with experiments using *Arabidopsis* mutants in cGMP-dependent calcium channels which were not impaired in ABA-triggered stomatal closure (Dubovskaya et al., 2011; Wang et al., 2013). Later, the occurrence and functional implications of 8-nitro-cGMP in *Arabidopsis* stomatal guard cells were discovered (Joudoi et al., 2013). cGMP and 8-nitro-cGMP appear to show contrasting impact on stomata function: 8-nitro-cGMP induced stomatal closure in the light, whereas 8-Br-cGMP, an extensively utilized cGMP analog, did not. On the contrary, 8-Br-cGMP but not cGMP induced stomata opening in the dark. 8-nitro-cGMP signaling is mediated by modulation of Ca<sup>2+</sup>, cyclic adenosine-5'-diphosphate ribose, and the SLAC1 (*SLOW ANION CHANNEL1*) channels. Increased levels of RNS, produced by ROS and NO reactions, resulted in 8-nitro-cGMP production triggering increased levels of cytosolic Ca<sup>2+</sup> which activated the SLAC1 anion channels to promote stomata closure. In the following study, the 8-nitro-cGMP metabolite 8-SH-cGMP was also observed to induce closure of stomata pores (Honda et al., 2015). Nevertheless, the participation of protein S-guanylation in 8-SH-cGMP signaling was not evidenced (Figure 1).

It can be expected that similar to animal models (Sawa et al., 2007), 8-nitro-cGMP retains the capacity to activate plant cGMP-dependent protein kinases. In animal cells, intracellular 8-nitro-cGMP levels are supposed to be comparable or higher than cGMP levels during infection or inflammatory conditions (Fujii et al., 2010; Kunieda et al., 2015). Therefore, the role of 8-nitro-cGMP and its metabolites 8-amino-cGMP and 8-SH-cGMP as PKs activators in plant physiology and stress responses requires further investigation.

In plants, autophagy mediates selective destruction of viruses as well limits infection by bacterial and filamentous pathogens. Emerging evidence indicates that autophagy is a key regulator of plant innate immunity and contributes with both pro-death and pro-survival functions to antimicrobial defenses, depending on the pathogenic lifestyle (Hofius et al., 2017; Leary et al., 2019). The role of H<sub>2</sub>S in regulating plant autophagy has been recently demonstrated (Gotor et al., 2013; Laureano-Marín et al., 2016). Sulfide, but no other molecules such as sulfur-containing molecules or ammonium, was able to inhibit autophagy machinery induced in *A. thaliana* roots under nitrogen deprivation via a redox-independent mechanism. H<sub>2</sub>S-mediated signaling in autophagy has been suggested to be



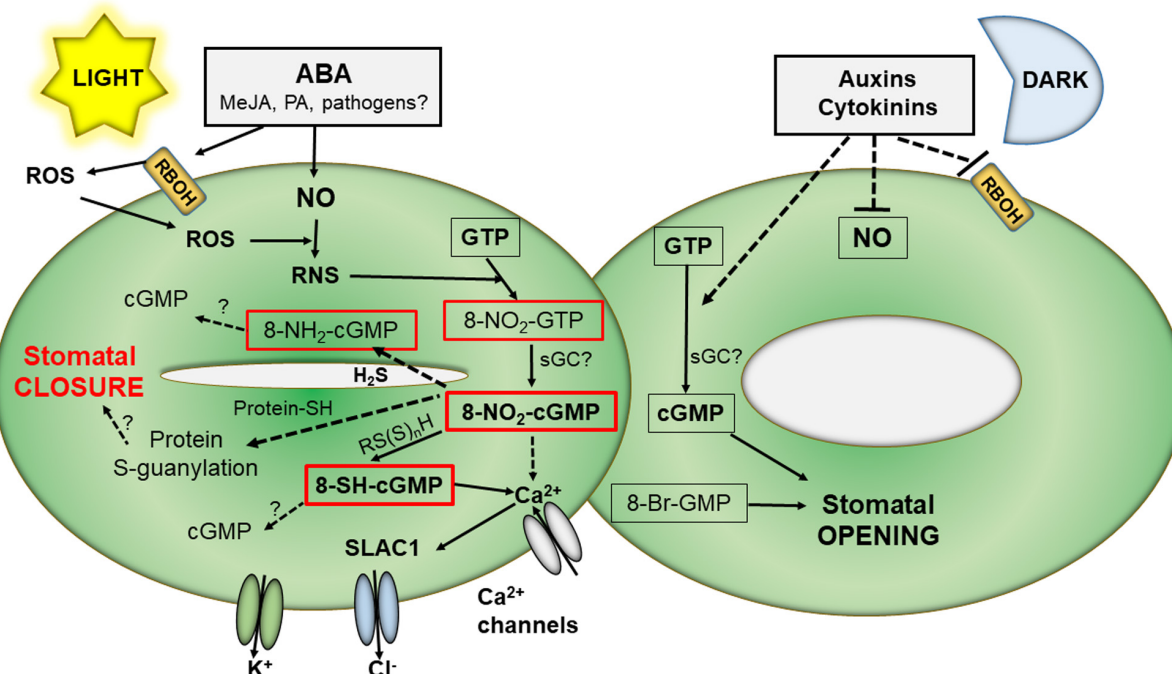


**FIGURE 1 |** Overview of 8-Nitro-cGMP reaction pathways in stomata signaling. In the light, external stimuli like ABA induce in stomata guard cells increased NO synthesis as well as activation of ROS production by membrane NADPH oxidase. ROS react with NO to form RNS which can nitrate GTP to 8-nitro-GTP which is then converted to 8-nitro-cGMP, possibly by action of sGC. 8-Nitro-cGMP, and/or 8-SH-cGMP formed by its reaction with reactive persulfides, trigger elevated cytoplasmic  $\text{Ca}^{2+}$  levels and subsequently activation of slow anion channels leading to stomatal closure. In the dark, other plant hormones, including cytokinins and auxin, decreases both NO and ROS levels resulting in increased cGMP and stomatal opening. ABA, abscisic acid; cGMP, 3',5'-cyclic guanosine monophosphate; GTP, guanosine triphosphate; MeJA, methyl jasmonate; PA, polyamines; RBOH, NADPH oxidase; RNS, reactive nitrogen species; ROS, reactive oxygen species;  $\text{RS(S)}_n\text{H}$ , persulfides; sGC, soluble guanylate cyclase; SLAC, slow anion channels.

mediated by post-translational modifications of the enzymes involved in the ubiquitinylation process or of other proteins involved in the initiation and completion of the autophagosome. The action of  $\text{H}_2\text{S}$  may include protein S-persulfidation at the reactive cysteine residue(s) of the target proteins. Polyamine spermine was reported to induce autophagy in plants, mediated by increased generation of ROS and NO required for effective triggering of autophagy (Dmitrieva et al., 2018). Combined effects of NO and ROS is required for autophagy and necrotic HR cell death induced by *Alternaria alternata* toxin in tobacco BY-2 cells (Sadhu et al., 2019). In Arabidopsis, glycolate oxidase activity is induced by avirulent Pst DC3000 AvrRpm1 and this response is suppressed by a synergic action of NO and cGMP. The enzyme activity *in vitro* was inhibited by combined treatment with cGMP and NO donor, but it is not known if this effect was mediated by 8-nitro-cGMP (Donaldson et al., 2016). Given the widely demonstrated role of 8-nitro-cGMP in autophagy processes in animals, this deserves further investigations on plant cells and components both *in vitro* and *in vivo*.

## FUTURE PERSPECTIVES

To date, only two scientific reports investigated the functions of 8-nitro-cGMP and 8-SH-GMP in plant cell signaling and

regulation. Further progress in this field may be hampered by several experimental obstacles: the pure chemical standards of described compounds are not commercially available, their synthesis requires dubious purification and analytical techniques requires mass-spectrometry instrumentation. A reporter system has been developed for specific and sensitive detection of cyclic nucleotides including cGMP in bacteria and plants; however, if this system shows response also to cGMP derivatives has not been tested (Wheeler et al., 2013). It should be also considered that available commercial antibodies might lack required specificity, i.e., to show affinity to 8-nitroguanine and 8-nitroguanosine but also 8-nitroxanthine (Sawa et al., 2006). Furthermore, very limited information exists on how and in what extent S-guanylation might function as protein PTM in plant cells. As discussed above, it requires further investigations to clarify if cysteine pKa may control the required specificity of S-guanylation targets in cellular signaling and autophagy; thus, the nature of putative enzymes that might catalyze S-guanylation continues an essential point for the advances in this research area both in plants and animals. Moreover, a combined application of available transcriptomic, proteomic and metabolomics tools to plant cells treated with 8-nitro-cGMP and its metabolites can provide new insights in their role in NO- and ROS-dependent plant signaling.

## AUTHOR CONTRIBUTIONS

MP and LL designed the manuscript. MP wrote the initial version of the manuscript. LL read and corrected the final version.

## REFERENCES

- Abada, A., and Elazar, Z. (2014). Getting ready for building: signaling and autophagosome biogenesis. *EMBO Rep.* 15, 839–852. doi: 10.15252/embr.201439076
- Agurla, S., Gayatri, G., and Raghavendra, A. S. (2014). Nitric oxide as a secondary messenger during stomatal closure as a part of plant immunity response against pathogens. *Nitric Oxide* 43, 89–96. doi: 10.1016/j.niox.2014.07.004
- Agurla, S., and Raghavendra, A. S. (2016). Convergence and divergence of signaling events in guard cells during stomatal closure by plant hormones or microbial elicitors. *Front. Plant Sci.* 7:1332. doi: 10.3389/fpls.2016.01332
- Ahmed, K. A., Sawa, T., Ihara, H., Kasamatsu, S., Yoshitake, J., Rahaman, M. M., et al. (2012). Regulation by mitochondrial superoxide and NADPH oxidase of cellular formation of nitrated cyclic GMP: potential implications for ROS signalling. *Biochem. J.* 441, 719–730. doi: 10.1042/BJ20111130
- Ahmed, K. A., Zhang, T., Ono, K., Tsutsuki, H., Ida, T., Akashi, S., et al. (2017). Synthesis and characterization of 8-nitroguanosine 3',5'-cyclic monophosphorothioate Rp-Isomer as a potent inhibitor of protein kinase G1α. *Biol. Pharm. Bull.* 40, 365–374. doi: 10.1248/bpb.b16-00880
- Akaike, T., Ida, T., Wei, F. Y., Nishida, M., Kumagai, Y., Alam, M. M., et al. (2017). CysteinyI-tRNA synthetase governs cysteine polysulfidation and mitochondrial bioenergetics. *Nat. Comm.* 8:1177. doi: 10.1038/s41467-017-01311-y
- Akaike, T., Nishida, M., and Fujii, S. (2013). Regulation of redox signalling by an electrophilic cyclic nucleotide. *J. Biochem.* 153, 131–138. doi: 10.1093/jb/mvs145
- Akaike, T., Okamoto, S., Sawa, T., Yoshitake, J., Tamura, F., Ichimori, K., et al. (2003). 8-Nitroguanosine formation in viral pneumonia and its implication for pathogenesis. *Proc. Natl. Acad. Sci. U. S. A.* 100, 685–690. doi: 10.1073/pnas.0235623100
- Akashi, S., Ahmed, K. A., Sawa, T., Ono, K., Tsutsuki, H., Burgoyne, J. R., et al. (2016). Persistent activation of cGMP-Dependent protein kinase by a nitrated cyclic nucleotide via site specific protein S-Guanylation. *Biochemistry* 55, 751–761. doi: 10.1021/acs.biochem.5b00774
- Arasimowicz-Jelonek, M., and Floryszak-Wieczorek, J. (2019). A physiological perspective on targets of nitration in NO-based signaling networks in plants. *J. Exp. Bot.* 70, 4379–4389. doi: 10.1093/jxb/erz300
- Astier, J., Gross, I., and Durner, J. (2018). Nitric oxide production in plants: an update. *J. Exp. Bot.* 69, 3401–3411. doi: 10.1093/jxb/erx420
- Balmant, K. M., Zhang, T., and Chen, S. (2016). Protein phosphorylation and redox modification in stomatal guard cells. *Front. Physiol.* 7:26. doi: 10.3389/fphys.2016.00026
- Begara-Morales, J. C., Sánchez-Calvo, B., Chaki, M., Valderrama, R., Mata-Pérez, C., Padilla, M. N., et al. (2016). Antioxidant systems are regulated by nitric oxide-mediated post-translational modifications (NO-PTMs). *Front. Plant Sci.* 7:152. doi: 10.3389/fpls.2016.00152
- Corpas, F. J., and Barroso, J. B. (2015). Nitric oxide from a “green” perspective. *Nitric Oxide* 45, 15–19. doi: 10.1016/j.niox.2015.01.007
- Cosker, F., Lima, F. J., Lahlou, S., and Magalhaes, P. J. (2014). Cytoprotective effect of 1-nitro-2-phenylethane in mice pancreatic acinar cells subjected to taurocholate: putative role of guanylyl cyclase-derived 8-nitro-cyclic-GMP. *Biochem. Pharmacol.* 15, 191–201. doi: 10.1016/j.bcp.2014.07.030
- Daszkowska-Golec, A., and Szarejko, I. (2013). Open or close the gate - stomata action under the control of phytohormones in drought stress conditions. *Front. Plant Sci.* 4:138. doi: 10.3389/fpls.2013.00138
- Dmitrieva, S. A., Ponomareva, A. A., Gurjanov, O. P., Mazina, A. B., Andrianov, V. V., Iyudin, V. S., et al. (2018). Spermine induces autophagy in plants: possible role of no and reactive oxygen species. *Dokl. Biochem. Biophys.* 483, 341–343. doi: 10.1134/S1607672918060121
- Donaldson, L., Meier, S., and Gehring, C. (2016). The *Arabidopsis* cyclic nucleotide interactome. *Cell Commun. Signal.* 14:10. doi: 10.1186/s12964-016-0133-2
- Dubovskaya, L. V., Bakakina, Y. S., Kolesneva, E. V., Sodel, D. L., Mcainsh, M. R., Hetherington, A. M., et al. (2011). cGMP-dependent ABA-induced stomatal closure in the ABA-insensitive *Arabidopsis* mutant abi1-1. *New Phytol.* 191, 57–69. doi: 10.1111/j.1469-8137.2011.03661.x
- Farnese, F. S., Menezes-Silva, P. E., Gusman, G. S., and Oliveira, J. A. (2016). When bad guys become good ones: the key role of reactive oxygen species and nitric oxide in the plant responses to abiotic stress. *Front. Plant Sci.* 7:471. doi: 10.3389/fpls.2016.00471
- Fujii, S., Sawa, T., Ihara, H., Tong, K. I., Ida, T., Okamoto, T., et al. (2010). The critical role of nitric oxide signaling, via protein S-guanylation and nitrated cyclic GMP, in the antioxidant adaptive response. *J. Biol. Chem.* 285, 23970–23984. doi: 10.1074/jbc.M110.145441
- Fukuto, J. M., Ignarro, L. J., Nagy, P., Wink, D. A., Kevil, C. G., Feelisch, M., et al. (2018). Biological hydropersulfides and related polysulfides - a new concept and perspective in redox biology. *FEBS Lett.* 592, 2140–2152. doi: 10.1002/1873-3468.13090
- Gayatri, G., Agurla, S., and Raghavendra, A. S. (2013). Nitric oxide in guard cells as an important secondary messenger during stomatal closure. *Front. Plant Sci.* 4:425. doi: 10.3389/fpls.2013.00425
- Gehring, C., and Turek, I. S. (2017). Cyclic nucleotide monophosphates and their cyclases in plant signaling. *Front. Plant Sci.* 8:1704. doi: 10.3389/fpls.2017.01704
- Gotor, C., García, I., Crespo, J. L., and Romero, L. C. (2013). Sulfide as a signaling molecule in autophagy. *Autophagy* 9, 609–611. doi: 10.4161/auto.23460
- Gross, I., and Durner, J. (2016). In search of enzymes with a role in 3', 5'-cyclic guanosine monophosphate metabolism in plants. *Front. Plant Sci.* 7:576. doi: 10.3389/fpls.2016.00576
- Guoguo, S., Akaike, T., Tao, J., Qi, C., Nong, Z., and Hui, L. (2012). HGF-mediated inhibition of oxidative stress by 8-nitro-cGMP in high glucose-treated rat mesangial cells. *Free Radic. Res.* 46, 1238–1248. doi: 10.3109/10715762.2012.701292
- Hofius, D., Li, L., Hafrén, A., and Coll, N. S. (2017). Autophagy as an emerging arena for plant-pathogen interactions. *Curr. Opin. Plant Biol.* 38, 117–123. doi: 10.1016/j.pbi.2017.04.017
- Honda, K., Yamada, N., Yoshida, R., Ihara, H., Sawa, T., Akaike, T., et al. (2015). 8-Mercapto-cyclic GMP mediates hydrogen sulfide-induced stomatal closure in *Arabidopsis*. *Plant Cell Physiol.* 56, 1481–1489. doi: 10.1093/pcp/pcv069
- Ida, T., Sawa, T., Ihara, H., Tsuchiya, Y., Watanabe, Y., Kumagai, Y., et al. (2014). Reactive cysteine persulfides and S-polythiolation regulate oxidative stress and redox signaling. *Proc. Natl. Acad. Sci. U.S.A.* 111, 7606–7611. doi: 10.1073/pnas.1321232111
- Ihara, H., Kasamatsu, S., Kitamura, A., Nishimura, A., Tsutsuki, H., Ida, T., et al. (2017). Exposure to electrophiles impairs reactive persulfide-dependent redox signaling in neuronal cells. *Chem. Res. Toxicol.* 30, 1673–1684. doi: 10.1021/acs.chemrestox.7b00120
- Ihara, H., Sawa, T., Nakabeppu, Y., and Akaike, T. (2011). Nucleotides function as endogenous chemical sensors for oxidative stress signaling. *J. Clin. Biochem. Nutr.* 48, 33–39. doi: 10.3164/jcbn.11-003FR
- Isner, J.-C., Olteanu, V.-A., Hetherington, A. J., Coupel-Ledru, A., Sun, P., Pridgeon, A. J., et al. (2019). Short- and long-term effects of UVA on *Arabidopsis* are mediated by a novel cGMP phosphodiesterase. *Curr. Biol.* 29, 2580–2585. doi: 10.1016/j.cub.2019.06.071
- Ito, C., Saito, Y., Nozawa, T., Fujii, S., Sawa, T., Inoue, H., et al. (2013). Endogenous nitrated nucleotide is a key mediator of autophagy and innate defense against bacteria. *Mol. Cell* 52, 794–804. doi: 10.1016/j.molcel.2013.10.024
- Joudoi, T., Shichiri, Y., Kamizono, N., Akaike, T., Sawa, T., Yoshitake, J., et al. (2013). Nitrated cyclic GMP modulates guard cell signaling in *Arabidopsis*. *Plant Cell* 25, 558–571. doi: 10.1105/tpc.112.105049
- Kasamatsu, S., Nishimura, A., Morita, M., Matsunaga, T., Abdul Hamid, H., and Akaike, T. (2016). Redox signaling regulated by cysteine persulfide and protein polysulfidation. *Molecules* 121:E1721. doi: 10.3390/molecules21121721

## FUNDING

This research project was funded by the Internal Grant Scheme of Palacký University in Olomouc (IGA\_PrF\_2020\_013).

- Kasamatsu, S., Watanabe, Y., Sawa, T., Akaike, T., and Ihara, H. (2014). Redox signal regulation via nNOS phosphorylation at Ser847 in PC12 cells and rat cerebellar granule neurons. *Biochem. J.* 459, 251–263. doi: 10.1042/BJ20131262
- Khan, S., Fujii, S., Matsunaga, T., Nishimura, A., Ono, K., Ida, T., et al. (2018). Reactive persulfides from *Salmonella typhimurium* downregulate autophagy-mediated innate immunity in macrophages by inhibiting electrophilic signaling. *Cell Chem. Biol.* 25, 1403.e4–1413.e4. doi: 10.1016/j.chembiol.2018.08.007
- Kunieda, K., Tsutsuki, H., Ida, T., Kishimoto, Y., Kasamatsu, S., Sawa, T., et al. (2015). 8-Nitro-cGMP enhances SNARE complex formation through S-guanylation of Cys90 in SNAP25. *ACS Chem. Neurosci.* 6, 1715–1725. doi: 10.1021/acschemneuro.5b00196
- Kurauchi, Y., Hisatsune, A., Isohama, Y., Sawa, T., Akaike, T., and Katsuki, H. (2013). Nitric oxide/soluble guanylyl cyclase signaling mediates depolarization-induced protection of rat mesencephalic dopaminergic neurons from MPP+ cytotoxicity. *Neurosci.* 231, 206–215. doi: 10.1016/j.neuroscience.2012.11.044
- Laureano-Marín, A. M., Moreno, I., Romero, L. C., and Gotor, C. (2016). Negative regulation of autophagy by sulfide is independent of reactive oxygen species. *Plant Physiol.* 171, 1378–1391. doi: 10.1104/pp.16.00110
- Leary, A. Y., Savage, Z., Tumas, Y., and Bozkurt, T. O. (2019). Contrasting and emerging roles of autophagy in plant immunity. *Curr. Opin. Plant Biol.* 52, 46–53. doi: 10.1016/j.pbi.2019.07.002
- Lee, J. M., Niles, J. C., Wishnok, J. S., and Tannenbaum, S. R. (2002). Peroxynitrite reacts with 8-nitropurines to yield 8-oxopurines. *Chem. Res. Toxicol.* 15, 7–14. doi: 10.1021/tx010093d
- Lemtiri-Chlieh, F., Thomas, L., Marondedze, C., Irving, H., and Gehring, C. (2011). “Cyclic nucleotides and nucleotide cyclases in plant stress responses, abiotic stress Response,” in *Plants - Physiological, Biochemical and Genetic Perspectives*, ed. A. Shanker (Venkateswarlu: IntechOpen).
- Ma, N., Adachi, Y., Hiraku, Y., Horiki, N., Horiike, S., Imoto, I., et al. (2004). Accumulation of 8-nitroguanine in human gastric epithelium induced by *Helicobacter pylori* infection. *Biochem. Biophys. Res. Commun.* 319, 506–510. doi: 10.1016/j.bbrc.2004.04.193
- Masuda, M., Nishino, H., and Ohshima, H. (2002). Formation of 8-nitroguanine in cellular RNA as a biomarker of exposure to reactive nitrogen species. *Chem. Biol. Interact.* 139, 187–197. doi: 10.1016/s0009-2797(01)00299-x
- Mizushima, N., and Komatsu, M. (2011). Autophagy: renovation of cells and tissues. *Cell* 147, 728–741. doi: 10.1016/j.cell.2011.10.026
- Nakagawa, I., Amato, A., Mizushima, N., Yamamoto, A., Yamaguchi, H., Kamimoto, T., et al. (2004). Autophagy defends cells against invading group A *Streptococcus*. *Science* 306, 1037–1040. doi: 10.1126/science.1103966
- Niles, J. C., Wishnok, J. S., and Tannenbaum, S. R. (2001). A novel nitroimidazole compound formed during the reaction of peroxynitrite with 2,3,5-tri-O-acetyl-guanosine. *J. Am. Chem. Soc.* 123, 12147–12151. doi: 10.1021/ja004296k
- Nishida, M., Kumagai, Y., Ihara, H., Fujii, S., Motohashi, H., and Akaike, T. (2016). Redox signaling regulated by electrophiles and reactive sulfur species. *J. Clin. Biochem. Nutr.* 58, 91–98. doi: 10.3164/jcbn.15-111
- Nishida, M., Sawa, T., Kitajima, N., Ono, K., Inoue, H., Ihara, H., et al. (2012). Hydrogen sulfide anion regulates redox signaling via electrophile sulphydration. *Nat. Chem. Biol.* 8, 714–724. doi: 10.1038/nchembio.1018
- Ohshima, H., Sawa, T., and Akaike, T. (2006). 8-nitroguanine, a product of nitrative DNA damage caused by reactive nitrogen species: formation, occurrence, and implications in inflammation and carcinogenesis. *Antioxid. Redox Signal.* 8, 1033–1045. doi: 10.1089/ars.2006.8.1033
- Pinlaor, S., Yongvanit, P., Hiraku, Y., Ma, N., Semba, R., Oikawa, S., et al. (2003). 8-Nitroguanine formation in the liver of hamsters infected with *Opisthorchis viverrini*. *Biochem. Biophys. Res. Commun.* 309, 567–571. doi: 10.1016/j.bbrc.2003.08.039
- Rahaman, M. M., Sawa, T., Ahtesham, A. K., Khan, S., Inoue, H., Irie, A., et al. (2014). S-guanylation proteomics for redox-based mitochondrial signaling. *Antioxid. Redox. Signal.* 20, 295–307. doi: 10.1089/ars.2012.4606
- Rawet-Slobodkin, M., and Elazar, Z. (2013). 8-nitro-cGMP a new player in antibacterial autophagy. *Mol. Cell* 52, 767–768. doi: 10.1016/j.molcel.2013.1.2006
- Sadhu, A., Moriyasu, Y., Acharya, K., and Bandyopadhyay, M. (2019). Nitric oxide and ROS mediate autophagy and regulate *Alternaria alternata* toxin-induced cell death in tobacco BY-2 cells. *Sci. Rep.* 9:8973. doi: 10.1038/s41598-019-45470-y
- Saito, Y., Sawa, T., Yoshitake, J., Ito, C., Fujii, S., Akaike, T., et al. (2012). Nitric oxide promotes recycling of 8-nitro-cGMP, a cytoprotective mediator, into intact cGMP in cells. *Mol. Biosyst.* 8, 2909–2915. doi: 10.1039/c2mb25189b
- Samanta, A., Thunemann, M., Feil, R., and Stafforst, T. (2014). Upon the photostability of 8-nitro-cGMP and its caging as a 7-dimethylaminocoumarinyl ester. *Chem. Commun.* 50, 7120–7123. doi: 10.1039/c4cc02828g
- Sawa, T., Akaike, T., Ichimori, K., Akuta, T., Kaneko, K., Nakayama, H., et al. (2003). Superoxide generation mediated by 8-nitroguanosine, a highly redox-active nucleic acid derivative. *Biochem. Biophys. Res. Commun.* 311, 300–306. doi: 10.1016/j.bbrc.2003.10.003
- Sawa, T., Arimoto, H., and Akaike, T. (2010). Regulation of redox signaling involving chemical conjugation of protein thiols by nitric oxide and electrophiles. *Bioconjug. Chem.* 21, 1121–1129. doi: 10.1021/bc900396u
- Sawa, T., Ihara, H., Ida, T., Fujii, S., Nishida, M., and Akaike, T. (2013). Formation, signaling functions, and metabolisms of nitrated cyclic nucleotide. *Nitric Oxide* 34, 10–18. doi: 10.1016/j.niox.2013.04.004
- Sawa, T., Tatemichi, T., Akaike, T., Barbina, A., and Ohshima, H. (2006). Analysis of urinary 8-nitroguanine, a marker of nitrative nucleic acid damage, by high-performance liquid chromatography-electrochemical detection coupled with immunoaffinity purification: association with cigarette smoking. *Free Radic. Biol. Med.* 40, 711–720. doi: 10.1016/j.freeradbiomed.2005.09.035
- Sawa, T., Zaki, M. H., Okamoto, T., Akuta, T., Tokutomi, Y., Kim-Mitsuyama, S., et al. (2007). Protein S-guanylation by the biological signal 8-nitroguanosine 3',5'-cyclic monophosphate. *Nat. Chem. Biol.* 3, 727–735. doi: 10.1038/nchembio.2007.33
- Scuffi, D., Lamattina, L., and García-Mata, C. (2016). Gasotransmitters and stomatal closure: is there redundancy. *Concerted Action, or Both? Front. Plant Sci.* 7, 277. doi: 10.3389/fpls.2016.00277
- Shen, Q., Zhan, X., Yang, P., Li, J., Chen, J., and Tang, B. (2019). Dual activities of plant cGMP-dependent protein kinase and its roles in gibberellin signaling and salt stress. *Plant Cell* 31, 3073–3091. doi: 10.1105/tpc.19.00510
- Sodum, R. S., and Fiala, E. S. (2001). Analysis of peroxynitrite reactions with guanine, xanthine, and adenine nucleosides by high-pressure liquid chromatography with electrochemical detection: c8-nitration and -oxidation. *Chem. Res. Toxicol.* 14, 438–450. doi: 10.1021/tx000189s
- Spencer, J. P., Wong, J., Jenner, A., Aruoma, O. I., Cross, C. E., and Halliwell, B. (1996). Base modification and strand breakage in isolated calf thymus DNA and in DNA from human skin epidermal keratinocytes exposed to peroxynitrite or 3-morpholinopyridine. *Chem. Res. Toxicol.* 9, 1152–1158. doi: 10.1021/tx960084i
- Sun, L. R., Yue, C. M., and Hao, F. S. (2019). Update on roles of nitric oxide in regulating stomatal closure. *Plant Signal. Behav.* 14:e1649569. doi: 10.1080/15592324.2019.1649569
- Świeżawska, B., Duszyn, M., Jaworski, K., and Szmidt-Jaworska, A. (2018). Downstream targets of cyclic nucleotides in plants. *Front. Plant Sci.* 9:1428. doi: 10.3389/fpls.2018.01428
- Taguchi, K., Fujikawa, N., Komatsu, M., Ishii, T., Unno, M., Akaike, T., et al. (2012). Keap1 degradation by autophagy for the maintenance of redox homeostasis. *Proc. Natl. Acad. Sci. U.S.A.* 109, 13561–13566. doi: 10.1073/pnas.1121572109
- Takahashi, D., Moriyama, J., Nakamura, T., Miki, E., Takahashi, E., Sato, A., et al. (2019). AUTACS: cargo-specific degraders using selective autophagy. *Mol. Cell* 76, 797.e10–810.e10. doi: 10.1016/j.molcel.2019.09.009
- Terasaki, Y., Akuta, T., Terasaki, M., Sawa, T., Mori, T., Okamoto, T., et al. (2006). Guanine nitration in idiopathic pulmonary fibrosis and its implications for carcinogenesis. *Am. J. Respir. Crit. Care Med.* 174, 665–673. doi: 10.1164/rccm.200510-1580OC
- Terzić, V., Padovani, D., Balland, V., Artaud, I., and Galardon, E. (2014). Electrophilic sulphydration of 8-nitro-cGMP involves sulfane sulfur. *Org. Biomol. Chem.* 12, 5360–5364. doi: 10.1039/c4ob00868e
- Umbreen, S., Lubega, J., Cui, B., Pan, Q., Jiang, J., and Loake, G. J. (2018). Specificity in nitric oxide signalling. *J. Exp. Bot.* 69, 3439–3448. doi: 10.1093/jxb/ery184
- Wang, Y. F., Munemasa, S., Nishimura, N., Ren, H. M., Robert, N., Han, M., et al. (2013). Identification of Cyclic GMP-activated nonselective Ca<sup>2+</sup>-permeable cation channels and associated CNGC5 and CNGC6 genes in *Arabidopsis* guard cells. *Plant Physiol.* 163, 578–590. doi: 10.1104/pp.113.225045

- Wheeler, J. I., Freihat, L., and Irving, H. R. (2013). A cyclic nucleotide sensitive promoter reporter system suitable for bacteria and plant cells. *BMC Biotechnol.* 13:97. doi: 10.1186/1472-6750-13-97
- Ye, W., and Murata, Y. (2016). Microbe associated molecular pattern signaling in guard cells. *Front. Plant Sci.* 7:583. doi: 10.3389/fpls.2016.00583
- Yermilov, V., Rubio, J., Becchi, M., Friesen, M. D., Pignatelli, B., and Ohshima, H. (1995a). Formation of 8-nitroguanine by the reaction of guanine with peroxynitrite in vitro. *Carcinogenesis* 16, 2045–2050. doi: 10.1093/carcin/16.9.2045
- Yermilov, V., Rubio, J., and Ohshima, H. (1995b). Formation of 8-nitroguanine in DNA treated with peroxynitrite in vitro and its rapid removal from DNA by depurination. *FEBS Lett.* 376, 207–210. doi: 10.1016/0014-5793(95)01281-6
- Yoshitake, J., Akaike T., Akuta, T., Tamura, F., Ogura, T., Esumi, H., et al. (2004). Nitric oxide as an endogenous mutagen for sendai virus without antiviral activity. *J. Virol.* 78, 8709–8719. doi: 10.1128/JVI.78.16.8709-8719.2004
- Yoshitake, J., Soeda, Y., Ida, T., Sumioka, A., Yoshikawa, M., Matsushita, K., et al. (2016). Modification of Tau by 8-Nitroguanosine 3',5'-Cyclic Monophosphate (8-Nitro-cGMP): effects of nitric oxide-linked chemical modification on tau aggregation. *J. Biol. Chem.* 291, 22714–22720. doi: 10.1074/jbc.M116.734350
- Yu, M., Lamattina, L., Spoel, S. H., and Loake, G. J. (2014). Nitric oxide function in plant biology: a redox cue in deconvolution. *New Phytol.* 202, 1142–1156. doi: 10.1111/nph.12739
- Zaki, M. H., Fujii, S., Okamoto, T., Islam, S., Khan, S., Ahmed, K. A., et al. (2009). Cytoprotective function of heme oxygenase 1 Induced by a nitrated cyclic nucleotide formed during murine salmonellosis. *J. Immunol.* 182, 3746–3756. doi: 10.4049/jimmunol.0803363

**Conflict of Interest:** The authors declare that the research was conducted in the absence of any commercial or financial relationships that could be construed as a potential conflict of interest.

Copyright © 2020 Petrivalský and Luhová. This is an open-access article distributed under the terms of the Creative Commons Attribution License (CC BY). The use, distribution or reproduction in other forums is permitted, provided the original author(s) and the copyright owner(s) are credited and that the original publication in this journal is cited, in accordance with accepted academic practice. No use, distribution or reproduction is permitted which does not comply with these terms.





# Effects of Antimony on Reactive Oxygen and Nitrogen Species (ROS and RNS) and Antioxidant Mechanisms in Tomato Plants

Francisco L. Espinosa-Vellarino, Inmaculada Garrido, Alfonso Ortega, Ilda Casimiro and Francisco Espinosa\*

Research Group of Physiology, Cellular and Molecular Biology of Plants, University of Extremadura, Badajoz, Spain

## OPEN ACCESS

### Edited by:

Jörg-Peter Schnitzler,  
Helmholtz Zentrum München,  
Germany

### Reviewed by:

Francisco J. Corpas,  
Estación Experimental del Zaidín  
(EEZ), Spain  
Vijay Pratap Singh,  
Allahabad University, India

### \*Correspondence:

Francisco Espinosa  
espinosa@unex.es

### Specialty section:

This article was submitted to  
Plant Physiology,  
a section of the journal  
Frontiers in Plant Science

**Received:** 14 February 2020

**Accepted:** 29 April 2020

**Published:** 27 May 2020

### Citation:

Espinosa-Vellarino FL, Garrido I,  
Ortega A, Casimiro I and Espinosa F  
(2020) Effects of Antimony on  
Reactive Oxygen and Nitrogen  
Species (ROS and RNS)  
and Antioxidant Mechanisms  
in Tomato Plants.  
Front. Plant Sci. 11:674.  
doi: 10.3389/fpls.2020.00674

This research studies the effects that Sb toxicity (0.0, 0.5, and 1.0 mM) has on the growth, reactive oxygen and nitrogen species, and antioxidant systems in tomato plants. Sb is accumulated preferentially in the roots, with little capacity for its translocation to the leaves where the concentration is much lower. The growth of the seedlings is reduced, with alteration in the content in other nutrients. There is a decrease in the content of Fe, Mg, and Mn, while Cu and Zn increase. The contents in chlorophyll a and b decrease, as does the photosynthetic efficiency. On the contrary the carotenoids increase, indicating a possible action as antioxidants and protectors against Sb. The phenolic compounds do not change, and seem not to be involved in the defense response of the tomato against the stress by Sb. The water content of the leaves decreases while that of proline increases in response to the Sb toxicity. Fluorescence microscopy images and spectrofluorometric detection showed increases in the production of  $O_2^{\cdot-}$ ,  $H_2O_2$ , NO, and  $ONOO^-$ , but not of nitrosothiols. The Sb toxicity induces changes in the SOD, POX, APX, and GR antioxidant activities, which show a clear activation in the roots. In leaves, only the SOD and APX increase. The DHAR activity is inhibited in roots but undergoes no changes in the leaves, as is also the case for the POX and GR activities. Ascorbate increases while GSH decreases in the roots. The total AsA + DHA content increases in the roots, but the total GSH + GSSG content decreases, while neither is altered in the leaves. Under Sb toxicity increases the expression of the SOD, APX, and GR genes, while the expression of GST decreases dramatically in roots but increases in leaves. In addition, an alteration is observed in the pattern of the growth of the cells in the elongation zone, with smaller and disorganized cells. All these effects appear to be related to the ability of the Sb to form complexes with thiol groups, including GSH, altering both redox homeostasis and the levels of auxin in the roots and the quiescent center.

**Keywords:** antimony, antioxidants, ascorbate, glutathione, reactive oxygen species, reactive nitrogen species, tomato

## INTRODUCTION

The metalloid antimony (Sb) is found in soils at concentrations typically ranging between 0.3 and 8.4 mg kg<sup>-1</sup> (Tschan et al., 2009). Antimony has an atomic weight of 121.76 (atomic number 51), and is a trace element that is not essential for plants, but which can be absorbed by them. Depending on the redox state of the soil, Sb can be found as either antimonite (Sb[III]), or antimonate (Sb[V]), with Sb[III] being more toxic than Sb[V] (Filella et al., 2002; Rajabpoor et al., 2019). It is one of the most toxic metalloids for both plants and animals including humans (Feng et al., 2013; Li et al., 2018; Zhang et al., 2018). Its toxic effects on human health cause respiratory, cardiovascular, and cancerous conditions (Filella et al., 2009). Its presence in soils and waters has increased considerably in recent decades. This increase is anthropogenic, coming from mining and industrial processes as a consequence of the considerable growth in the use of Sb products in flame retardant additives, pigments, alloys, batteries, and semiconductors (Okkenhaug et al., 2011; García-Lorenzo et al., 2015; Li et al., 2017; Liu and Qiu, 2018; Wen et al., 2018). Rising Sb levels in soils, especially the degraded soils in mining areas, contribute significantly to the alteration of ecosystems (Fawcett et al., 2015; Zhou et al., 2017). The amounts of Sb detected in such soils can reach very high values, e.g., 19–4400 mg kg<sup>-1</sup> in Italy (Cidu et al., 2014), 10–5633 mg kg<sup>-1</sup> in China (He et al., 2012; Ning et al., 2015), 125–15,100 mg kg<sup>-1</sup> in Spain (Murciego et al., 2007), 22,000 mg kg<sup>-1</sup> in Australia (Warnken et al., 2017), and 80,200 mg kg<sup>-1</sup> in New Zealand (Wilson et al., 2004).

Despite Sb not being an essential element for plants, they absorb it in its soluble forms (Baroni et al., 2000). Its transport system is unknown, although it could involve a nodulin 26 linked to intrinsic membrane proteins that has been identified in *Arabidopsis* (Kamiya and Fujiwara, 2009). It is also possible that Sb enters through aquaporins (Bienert et al., 2008). The absorption capacity is strongly dependent on the plant species and on Sb's bioavailability in the soil (Shtangeeva et al., 2012; Natasha et al., 2019). This latter itself depends on such characteristics of the soil as pH, redox potential, and the presence of other mineral elements such as P and Ca that can alter cation exchange (Spuller et al., 2007; Okkenhaug et al., 2011).

Plant cells produce reactive oxygen species (ROS) that are involved in both physiological and stress response processes (Apel and Hirt, 2004). They include superoxide anion (O<sub>2</sub><sup>•-</sup>), hydrogen peroxide (H<sub>2</sub>O<sub>2</sub>), and hydroxyl ion (OH<sup>-</sup>) which are produced in different cell compartments (Apel and Hirt, 2004; Waszczak et al., 2018). Stress conditions not only alter plants' ROS levels, resulting in clear imbalances of redox homeostasis (Das and Roychoudhury, 2014), but also lead to the production of reactive nitrogen species (RNS) including nitric oxide (NO), peroxyxynitrite (ONOO<sup>-</sup>), and S-nitrosoglutathione (GSNO) (Wang et al., 2013). Their accumulation in the cells develops what is called nitrosative stress (Corpas et al., 2011; Corpas and Barroso, 2013), and the interaction between ROS and RNS induces nitro-oxidative stress (Corpas et al., 2011; Sahay and Gupta, 2017; Kohli et al., 2019; Kolbert et al., 2019).

Heavy metal and metalloid toxicity causes a strong increase in ROS and RNS production (Feng et al., 2009; Tschan et al., 2009; Pan et al., 2011; Corpas and Barroso, 2014, 2017; Feigl et al., 2015; Chai et al., 2016; Karacan et al., 2016; Ortega et al., 2017). Consequently, growth and biomass production, the content of photosynthetic pigments and levels of photosynthesis, and the absorption and distribution of other nutrients are all altered (Natasha et al., 2019). As a protection against the damage caused by this ROS and RNS imbalance, plants have developed both enzymatic and non-enzymatic antioxidant systems capable of eliminating these reactive species more efficiently (Mittler, 2002; Verma and Dubey, 2003; Zhang et al., 2007; Ahsan et al., 2009; Gill and Tuteja, 2010). The imbalance in the redox state induced by Sb toxicity alters the activities of superoxide dismutase (SOD), peroxidase (POX), ascorbate peroxidase (APX), dehydroascorbate reductase (DHAR), glutathione reductase (GR), and nitrosoglutathione reductase (GSNOR) (Xu et al., 2013; Vaculiková et al., 2014; Feng et al., 2016; Chai et al., 2017; Ortega et al., 2017). The many non-enzymatic antioxidant compounds also involved in the control of this stress include phenolics, flavonoids, phenylpropanoid glycosides (PPGs), carotenoids, and the components of the ascorbate-glutathione (AsA/GSH) cycle (Sharma et al., 2012; Anjum et al., 2014; Xue et al., 2015; Ji et al., 2017; Ortega et al., 2017). The AsA and GSH together with their oxidized forms and the related enzymes, control the cellular redox equilibrium. The AsA/GSH cycle intervenes in the scavenging and control of the ROS produced under stress conditions. The GSH carries out a key role in the plants' defense against the oxidative stress induced by heavy metals. The GSH/GSSG, besides contributing to the redox homeostasis and to the antioxidant defense, is fundamental in detoxification processes. The GSH contributes to the detoxification both forming phytochelatinas as well as through the direct bond between its thiol groups with the metals. The GSH/GSSG alteration is also key in cellular signaling (Noctor et al., 2012; Anjum et al., 2014). The increased production of ROS and RNS and their interactions may act on the antioxidant systems involved in the response to heavy metals, both inducing the activity of these systems and modifying the expression of the genes involved in them (Sahay and Gupta, 2017; Kohli et al., 2019).

While there has been extensive study of the physiological, biochemical, and molecular effects on plants of many heavy metals and metalloids (Yadav, 2010; Hossain et al., 2012), in the case of Sb, there have only been a relatively few studies (Feng et al., 2013; Vaculiková et al., 2014; Peško et al., 2016; Ortega et al., 2017). More seldomly studied is the intervention of RNS and its connection with ROS. In sunflower subject to stress by Sb, an increase in the nitrosothiols production has been observed (Ortega et al., 2017). Tomato is a widely used model plant due to the high consumption of its fruits as food around the world. The objective of the present work was to investigate the physiological and molecular response of this important crop plant to Sb toxicity. In particular, we considered the potential alterations in growth, ROS and RNS production, enzymatic and non-enzymatic antioxidant systems, and gene expression.

## MATERIALS AND METHODS

### Plant Material, Growth Conditions, and Treatments

Seeds of tomato (*Solanum lycopersicum*, L., cv. Muchamiel) seeds were surface sterilized for 15 min in a 10% sodium hypochlorite solution (40 g L<sup>-1</sup>), rinsed several times with distilled water, and, before germination, were imbibed in distilled water, aerated, and agitated for 2 h at room temperature. After imbibition, the seeds were germinated in a plastic container (30 cm × 20 cm × 10 cm) filled with a sterilized perlite mixture substrate wetted with Hoagland solution, at 27°C, in darkness for 72 h. After germination, the seedlings were cultivated for 5 days at 27°C with 85% relative humidity and under constant illumination at a photosynthetic photon flux density of 350 μmol m<sup>-2</sup> s<sup>-1</sup>.

After 7 days, the plants were grown in hydroponic culture for 7 days in lightweight polypropylene trays (30 cm × 20 cm × 10 cm; 4 plants per container) and the same environmental conditions as before except for relative humidity of 50%. The plants were treated with a basal nutrient solution consisting of 4 mM KNO<sub>3</sub>, 3 mM Ca(NO<sub>3</sub>)<sub>2</sub> · 4H<sub>2</sub>O, 2 mM MgSO<sub>4</sub> · 7H<sub>2</sub>O, 6 mM KH<sub>2</sub>PO<sub>4</sub>, 1 mM NaH<sub>2</sub>PO<sub>4</sub> · 2H<sub>2</sub>O, 10 μM ZnSO<sub>4</sub> · 7H<sub>2</sub>O, 2 μM MnCl<sub>2</sub> · 4H<sub>2</sub>O, 0.25 μM CuSO<sub>4</sub> · 5H<sub>2</sub>O, 0.1 μM Na<sub>2</sub>MoO<sub>4</sub> · 2H<sub>2</sub>O, 10 μM H<sub>3</sub>BO<sub>3</sub>, and 20 μM NaFeIII-EDTA. For the Sb treatment, the basal solution was supplemented with KSb(OH)<sub>6</sub> to final concentrations of 0.00 (control), 0.50 mM, and 1.00 mM Sb. Each culture solution was adjusted to pH 5.8, continuously aerated, and changed every 4 days. The plants were exposed to the Sb for 14 days (their total age at the end of the experiment was 28 days). Plants from each treatment were divided into roots and stems which were rinsed with distilled water, dried on filter paper, and weighed to obtain the fresh weight (FW). Half of the roots and leaves from each treatment were dried in a forced-air oven at 70°C for 24 h to obtain the dry weight (DW), followed by the subsequent determination of the Sb concentration. The other halves of the roots and leaves were used for biochemical analysis.

### Determination of Relative Water Content (%RWC)

The RWC of the stems was determined at the time of harvest from fresh material in accordance with the method described by Smart and Bingham (1974). Leaf disks were collected from the different treatments, and their FWs determined. They were then immersed in distilled water for 1 h, dried externally with filter paper, and weighed again to obtain the turgid weight (TW). Finally, they were oven-dried at 70°C for 24 h, and weighed to obtain the DW. The RWC was calculated as  $RWC\% = (FW - DW)/(TW - DW) \times 100$ .

### Determination of Sb and Mineral Contents

To determine the concentrations of Sb in the soil and roots and leaves, the samples were maintained at 70°C for 72 h, and then crushed in a ceramic mortar. The assays were performed

by inductively coupled plasma mass spectrometry (ICP-MS) (Lehotai et al., 2012).

### Determination of Photosynthetic Pigment Contents and Photosynthetic Efficiency

Disks were taken from fresh adult leaves and incubated in methanol for 24 h in darkness at room temperature. The chlorophyll a, chlorophyll b, and carotenoid contents were determined spectrophotometrically by measuring A<sub>666</sub>, A<sub>653</sub>, and A<sub>470</sub>. The total chlorophyll and carotenoid contents were calculated in accordance with Wellburn (1994).

The maximum photosynthetic efficiency (F<sub>V</sub>/F<sub>M</sub>) was determined on fresh leaves of intact plants, before being collected, using a “ChlorophyllFluorometer OS-30p” device (Opti-Sciences). Prior to the excitation, the leaves being sampled were kept in darkness for 10 min, then illuminated so as to measure the fluorescence emitted and calculate the F<sub>V</sub>/F<sub>M</sub> ratio (Oxborough and Baker, 1997).

### Determination of Phenolic Content

Phenols, flavonoids, and PPGs were extracted from roots and leaves by homogenization in methanol, chloroform, and 1% NaCl (1:1:0.5), filtering, and centrifuging at 3200 g for 10 min. Total phenols were determined spectrophotometrically at A<sub>765</sub> with Folin–Ciocalteu reagent (Singleton et al., 1985), expressing the result as μg caffeic acid g<sup>-1</sup> FW. Total flavonoid content was measured at A<sub>415</sub> (Kim et al., 2003), expressing the result as μg of rutin g<sup>-1</sup> FW. The PPGs were determined at A<sub>525</sub> (Gálvez et al., 2008), expressing the result as μg verbascoside g<sup>-1</sup> FW.

### Determination of Proline Content

The proline content was determined in accordance with the method of Bates et al. (1973). Briefly, 0.5 g/1.0 g of roots and leaves were homogenized in 2.5 ml of 3% sulfosalicylic acid, filtered, centrifuged at 10,000 g for 10 min, and 500 μL of the supernatant was added to a mixture of the same volumes of glacial acetic acid and ninhydrin. The resulting mixture was incubated at 100°C for 1 h, then placed into ice to stop the reaction. To each reaction tube, 1.5 mL of toluene blue was added, followed by vortexing for 20 s. After 5 min left at rest, the absorbance at 520 nm was measured, expressing the result as μg proline g<sup>-1</sup> FW.

### Determination of Lipid Peroxidation

The peroxidation of membrane lipids was determined spectrophotometrically from the formation of MDA (malondialdehyde) from TBA (2-thiobarbituric acid). To this end, roots and leaves were homogenized in 0.25% TBA and 10% TCA (trichloroacetic acid), incubated at 95°C for 30 min, filtered, and centrifuged at 8800 g for 10 min. The amount of MDA was determined from A<sub>532</sub> – A<sub>600</sub> with extinction coefficient ε = 155 mM<sup>-1</sup> cm<sup>-1</sup>, expressing the result as μmol MDA g<sup>-1</sup> FW (Fu and Huang, 2001).

## Determination of Enzymatic Oxidant and Antioxidant Activities

Roots and leaves were homogenized at 4°C in 50 mM pH 6.0 phosphate buffer, 1 mM EDTA (ethylene diamine tetra-acetic acid), 0.5 mM PMSF (phenylmethylsulfonyl fluoride), 1 mM  $\beta$ -mercaptoethanol, 1 g L<sup>-1</sup> PVPP (polyvinylpyrrolidone). The homogenate was filtered and centrifuged at 39,000 g for 30 min at 4°C, and the supernatant was used for the enzyme determinations.

The protein content was determined using the Bradford method (Bradford, 1976). The production of O<sub>2</sub>·<sup>-</sup> was measured from the formation of adrenochrome at A<sub>480</sub> ( $\epsilon$  = 4.020 mM<sup>-1</sup> cm<sup>-1</sup>) (Misra and Fridovich, 1972; Garrido et al., 2012). Polyphenoloxidase (PPO, EC 1.14.18.1) activity was determined by measuring A<sub>390</sub> at 30°C in a medium containing the enzyme extract, 100 mM phosphate buffer, Triton X-100, and 30  $\mu$ M caffeic acid (Thipyapong et al., 1995). Superoxide dismutase (SOD, EC 1.15.1.1) activity was determined at A<sub>560</sub> in a medium containing 50 mM phosphate buffer pH 7.8, 0.1 mM EDTA, 1.3  $\mu$ M riboflavin, 13 mM methionine, and 63  $\mu$ M 4-nitro blue tetrazolium (NBT) (Beauchamp and Fridovich, 1971). The peroxidase (POX, EC 1.11.1.7) activity was determined at A<sub>590</sub> ( $\epsilon$  = 47.6 mM<sup>-1</sup> cm<sup>-1</sup>) (Ngo and Lenhoff, 1980) in 3.3 mM DMAB, 66.6  $\mu$ M MBTH, and 50 mM phosphate buffer pH 6.0. The glutathione reductase (GR EC 1.6.4.2) activity was determined at A<sub>340</sub> from the oxidation of NADPH ( $\epsilon$  = 6.22 mM<sup>-1</sup> cm<sup>-1</sup>) (De Gara et al., 2003) in a medium (1.5 mL) containing 0.1 M phosphate buffer (pH 7.5), 0.5 mM EDTA, 0.5 mM GSSG, 0.2 mM NADPH, and enzyme extract. The dehydroascorbate reductase (DHAR EC 1.6.4.2) activity was determined from the oxidation of DHA at A<sub>265</sub> ( $\epsilon$  = 14 mM<sup>-1</sup> cm<sup>-1</sup>) (De Gara et al., 2003) in a medium containing 0.1 M phosphate buffer (pH 6.5), 0.5 mM EDTA, 2.5 mM GSH, 0.5 mM DHA, and enzyme extract.

## Determination of the Components of the AsA/GSH Cycle

To determine the AsA, DHA, GSH, and GSSG contents, roots and leaves (1 g mL<sup>-1</sup>) were homogenized at 4°C in 5% metaphosphoric acid in a porcelain mortar. The homogenate was filtered and centrifuged at 16,000 g for 20 min at 4°C. The total ascorbate and glutathione assays were done in accordance with De Pinto et al. (1999). The total ascorbate pool was determined in a reaction medium containing the extract, 150 mM phosphate buffer (pH 7.4), and 5 mM EDTA, which was incubated for 15 min in darkness. The result was then complemented with 0.5% NEM (*N*-ethylmaleimide), 10% TCA, 44% orthophosphoric acid, 4% dipyridyl, and 110 mM FeCl<sub>3</sub>, followed by incubation at 40°C for 40 min in darkness. The reaction was halted with ice, and the A<sub>525</sub> was measured. To determine the amount of AsA, 10 mM DTT (DL-dithiothreitol) was added to the reaction medium before incubation in darkness, while 100  $\mu$ L of water was added to determine the ascorbate pool. The concentration of DHA was estimated from the difference between the total ascorbate pool (AsA + DHA) and AsA.

The total glutathione pool was determined by adding 0.4  $\mu$ L of extract to 0.6  $\mu$ L of 0.5 mM phosphate buffer (pH 7.5). The reaction medium containing the extract, 0.3 mM NADPH, 150 mM phosphate buffer (pH 7.4), 5 mM EDTA, and 0.6 mM DTNB [5,5'-dithiobis-(2-nitrobenzoic acid)] was stirred for 4 min, then 2 U mL<sup>-1</sup> GR was added and the A<sub>412</sub> was measured. To determine the GSSG content, the mixture was incubated for 1 h in darkness with 2-vinylpyridine (20  $\mu$ L) to eliminate GSH, and, to determine the glutathione pool, 20  $\mu$ L of water was added. The amount of GSH was obtained by the difference between the total pool (GSH + GSSG) and the amount of GSSG.

## Visualization and Spectrofluorometric Detection of ROS and RNS

The primary roots (20 mm) of the control and Sb-treated plants were incubated for 30 min at 37°C in darkness with 25  $\mu$ M DCF-DA (for H<sub>2</sub>O<sub>2</sub> detection) or 10  $\mu$ M DHE (for O<sub>2</sub>·<sup>-</sup> detection) in 10 mM Tris-HCl, pH 7.4. They were then rinsed thrice (for 15 min each) with the same buffer (Valderrama et al., 2007). For the determination of NO and ONOO<sup>-</sup>, the roots were incubated for 60 min at 25°C in darkness with 10  $\mu$ M DAF-2DA (for NO detection) or 10  $\mu$ M APF (for ONOO<sup>-</sup> detection) in 10 mM Tris HCl, pH 7.4. They were then rinsed thrice (for 15 min each) with the same buffer (Valderrama et al., 2007). For the detection of RSNOs, intact root samples were incubated for 60 min at 25°C in darkness with 10 mM NEM, and rinsed thrice (for 15 min each) with 10 mM Tris-HCl, pH 7.4. The roots were then incubated for 60 min at 25°C in darkness with 10  $\mu$ M Alexa-Fluor 488 Hg-link phenylmercury (Corpas et al., 2008) followed by rinsing thrice (for 15 min each) with the same buffer. Finally, the whole roots (not fixed) were sectioned into the apical (AZ), elongation (EZ), and mature (MZ) zones by placing them on a slide and examining them under fluorescence microscopy (Axioplan-Zeiss microscope). As negative controls, before treatment with the respective probes, primary roots were pre-incubated for 120 min at 37°C in darkness in 1 mM ascorbate (H<sub>2</sub>O<sub>2</sub> scavenger), 1 mM TMP (O<sub>2</sub>·<sup>-</sup> scavenger), 400  $\mu$ M cPTIO (NO scavenger), or 20  $\mu$ M Ebselen (ONOO<sup>-</sup> scavenger). In the case of the negative control for RSNOs, no pre-incubation in 10 mM NEM was done.

Images were processed and analyzed using the ImageJ program, and fluorescence intensity was expressed in arbitrary units. At least five roots were tested under each experimental condition, and five independent repetitions were analyzed.

The amounts of ROS and RNS were also determined spectrofluorometrically. Briefly, 1-g aliquots of primary roots of each treatment were crushed in liquid nitrogen, and homogenized in darkness in 5 mL 1 mM EDTA, 2 mM DTT, 1 mM PMSF, 0.2% Triton X-100, and 50 mM Tris-HCl pH 7.4, and centrifuged at 17,000 g for 30 min at 4°C. The precipitate was discarded. For each sample, the reaction medium comprised 100  $\mu$ L of crude extract and 900  $\mu$ L of 10 mM Tris-HCl, pH 7.2 alone (blank) or containing the respective fluorescent probe (25  $\mu$ M DCF-DA, 10  $\mu$ M DHE, 10  $\mu$ M DAF-2DA, 10  $\mu$ M APF, or 10  $\mu$ M Alexa-Fluor 488 Hg-link phenylmercury, final concentrations



**TABLE 1** | Oligonucleotides used for real-time quantitative RT-PCR analysis of the actin 41, SOD, APX, GR, and GST genes.

Gene	ID Gene	Forward primer	Reverse primer	Size (bp)
Actin-41	NP_001317048	GAATGGAAGCTGCAGGAATC	AGCAATACCTGGGAACATGG	128
APX	Solyc06g005150	TCTGGTTTGTAGGGACCTTG	GCTTTGTCTGATGGCAACTG	113
GR	Solyc09g065900	TAGCAAAGTTCTGGGCTTG	AACCTGCTTTGACTGCAAC	84
GST	Solyc01g099590	TGGGCTCGTTTGTGTATG	CCCTCTGCTTTTGTCTCC	80
SOD	Solyc02g021140	GGATTGGCTTGCTTGAGC	CGATCAGGGGGATATCATTC	99

respectively). The respective probe scavengers were used for negative controls. The reaction mixture was incubated at 37°C for 1 h, and the fluorescence was measured in a spectrofluorometer. In each case,  $\lambda_{exc}$  and  $\lambda_{em}$  were adjusted to the respective probe (Valderrama et al., 2007; Corpas et al., 2008; Gaupels et al., 2011; Airaki et al., 2012; Signorelli et al., 2016). The fluorescence was expressed in arbitrary units (AU) per  $\mu\text{g}$  protein.

### Real-Time Quantitative PCR

Roots and leaves (3rd leaf) were used from plants grown under the different experimental conditions (control, 0.5 mM Sb, and 1.0 mM Sb) described above. The RNA was isolated using a “Spectrum Plant Total RNA Kit” (Sigma-Aldrich®) together with the “RNase-Free DNase Set” (Cat No. 79254; QIAGEN®). The concentration (in  $\text{ng } \mu\text{L}^{-1}$ ) and quality of the extract were evaluated with a biophotometer (Eppendorf), calculating the  $A_{260}/A_{280}$  ratio. Samples of RNA with a value of 2.0 for this ratio were considered to be of quality, and integrity was determined by running part of the samples on 1.5% agarose gel. Samples of 1–2  $\mu\text{g}$  of purified RNA were reverse transcribed with the High Capacity cDNA Reverse Transcription Kit (Applied Biosystems®) with RNase inhibitor (Applied Biosystems®). Once the reverse transcription mix had been made, an Eppendorf® thermal cycler was programmed with a first 10-min 25°C phase to anneal the primers, followed by a 120-min 37°C phase for the reverse transcriptase to act, and finally inactivation of the procedure by warming to 85°C for 5 min.

For each qPCR, first an RT-PCR was performed with the different cDNAs using the *Thermus* spp. recombinant DNA polymerase (error rate of  $1-10 \times 10^{-6}$ ) from the Biotools kit, using the primers (Table 1) designed to perform the qPCR to ensure that there were no non-specific amplifications. The tomato housekeeping gene actin was selected as the reference gene (Mascia et al., 2010). All reactions were repeated three times. Together, three independent biological assays (three seedlings each assay) were performed. The relative expression levels of each gene were calculated using the  $2^{-\Delta\Delta\text{CT}}$  method. The RT-PCRs were done using an Eppendorf thermal cycler (Eppendorf®, Hauppauge, NY, United States). Aliquots of 25  $\mu\text{L}$  of sample from each of the PCR products were mixed with 2  $\mu\text{L}$  Thermo-Fisher® loading buffer. As indicator of the size of the fragments, 1 kb plus Ladder (Thermo-Fisher®) was used. The samples and Ladder were loaded onto 1% agarose gels with TAE (Tris-acetate-EDTA) buffer from Fisher Reagent® 1× and ethidium bromide as intercalating agent (0.075%). After

**FIGURE 1** | Representative photographs of 28-day-old untreated (control) and Sb toxicity (14-day under Sb treatment) tomato plants.

electrophoresis, the gels were visualized with UV light using a GeneFlash transilluminator (Syngene) which has an 8-bit  $768 \times 582$  pixel camera to take black and white photographs of the gels. The photographs were printed using the Sony® Video Graphic Printer.

Real-time amplification was performed with SYBR green (Thermo Fisher Scientific®) in a QuantStudio 1 amplification and detection instrument (Applied Biosystems, Thermo Fisher Scientific®).

### Statistical Analyses

The data presented are the means  $\pm$  SD of at least 10 replicates obtained from three independent experiments. Statistical analyses were performed using the Mann–Whitney *U*-test. Statistical differences in molecular data were estimated by Student's *t*-test and differences are presented (\* $p < 10^{-3}$ ; \*\* $p < 10^{-6}$ ; \*\*\* $p < 10^{-15}$ ).

## RESULTS

### Effect of Sb on Growth, RWC, Proline Content and Lipid Peroxidation of Tomato Plants

In tomato plants grown for 14 days in the presence of 0.5 mM and 1.0 mM Sb, we observed a significant reduction in root length compared to the control (**Figure 1** and **Table 2**), with a decrease of 12% for both Sb concentrations. The length of the stems was hardly affected at all. With respect to the fresh weight, there was a 25% decrease in the roots for both Sb concentrations, and this effect was greater in the stems (27% for the 0.5 mM concentration, and 35% for the 1.0 mM Sb concentration). The root-to-stem fresh weight ratios were higher than the control for both concentrations. This result indicates that the stems were more strongly affected by the Sb toxicity. With respect to the dry weight, there was a decrease of 20% in the roots for both concentrations, and of 25% in the stems, with no differences between the two concentrations. There were no alterations in the root-to-stem dry weight ratios. The phenotype of the tomato plants grown under Sb stress showed chlorosis and necrotic lesions, especially in the case of 1.0 mM Sb (**Figure 1**).

The amounts of MDA detected in the roots showed the development of oxidative damage induced by the Sb. In particular, relative to the control values, there were increases of 8 and 29% in the MDA levels for the 0.5 and 1.0 mM Sb concentrations, respectively. In the stems, however, the effect was less marked, with no alteration for 0.5 mM Sb and only a 9% increase for 1 mM Sb (**Table 3**). The response of the osmolyte proline was the opposite. There was no significant alteration in the roots, but in the leaves there were increases that reached 50% (for 0.5 mM Sb) relative to the control value. The RWC was reduced by the growth in Sb, falling from 93 to 84% for 0.5 mM Sb (a decrease of 10% relative to the control) and to 75% for 1.0 mM Sb (a decrease of 20% relative to the control).

### Effect of Sb in the Culture Medium on the Accumulation of Sb and Other Mineral Elements

Increase in the amount of Sb in the culture medium led to significant and strong increases in the absorption and accumulation of this element in both the roots and leaves (**Table 4**). The greater the amount of Sb present in the medium, the greater was the absorption and transport to the leaves. For both Sb concentrations, the roots showed a greater accumulation

capacity than the leaves. The values of the bioaccumulation factor (BF) clearly showed the tomato roots' great capacity to absorb and accumulate Sb, especially for the 0.5 mM Sb concentration. The highest levels of BF in the leaves were also observed with this concentration. There was thus an apparent tendency toward saturation. With respect to the values of the translocation factor (TF), these clearly depended on the concentration affecting the roots, being 0.030 for 0.5 mM, and 0.42 for 1.0 mM Sb.

The presence of Sb in the medium and its absorption by the tissues also altered the absorption and accumulation of other essential mineral elements. **Table 5** lists the concentrations of Fe, Mg, Mn, Cu, and Zn in roots and leaves. With 1.0 mM Sb, the roots' Fe, Mn, and Mg contents decreased markedly (by 80, 35, and 37%, respectively), but their Cu and Zn contents increased significantly (by 82 and 26%, respectively). In the leaves, Fe and Mg decreased, Mn and Zn remained unaltered, and Cu increased ( $\times 2$ ).

### Effect of Sb on Photosynthetic Pigment Content and Photosynthetic Efficiency

The chlorophyll a and chlorophyll b contents decreased in the leaves of plants grown with Sb, the more so the greater the Sb concentration in the medium (**Table 6**). The total chlorophyll content fell 32% with 0.5 mM Sb and 40% with 1.0 mM Sb. These changes in chlorophyll levels translated into an increase in the chl a/chl b ratio, which passed from 1.98 to 2.27 for 0.5 mM Sb and 2.35 for 1.0 mM Sb. The carotenoid levels were unaltered for 0.5 mM Sb, and increased by 20% for 1.0 mM Sb. The carotenoid/chlorophyll ratio also increased. The photosynthetic efficiency was reduced by approximately 24% with Sb in the growth medium.

### Effect of Sb on the Oxidant and Antioxidant Activities

In the roots, the Sb toxicity strongly enhanced the  $O_2^{\cdot-}$  production activity (**Figure 2A**), reaching a 72.9% increase for 0.5 mM Sb in the growth medium with respect to the controls. In the leaves however, the levels of  $O_2^{\cdot-}$  were similar to those of the controls.

The SOD activity increased in both roots and leaves due to the Sb treatment (**Figure 2B**). Relative to the controls, these increases were 29.9 and 40% in the roots, and 74.8 and 58.2% in the leaves for 0.5 mM and 1.0 mM Sb, both respectively. The POX activity (**Figure 2C**) was influenced only by treatment with 0.5 mM Sb in the roots, with an increase of 65.5%, while

**TABLE 2 |** Effect of Sb on the length (L), fresh weight (FW), and dry weight (DW) of the roots and stems of tomato plants.

Treatments	Length (cm)		FW (mg)		DW (mg)	
	Roots	Stems	Roots	Stems	Roots	Stems
Control	29.05 $\pm$ 2.25 <sup>a</sup>	17.33 $\pm$ 1.61 <sup>a</sup>	1840 $\pm$ 450 <sup>a</sup>	9371 $\pm$ 678 <sup>a</sup>	85.87 $\pm$ 7.14 <sup>a</sup>	589.89 $\pm$ 43.78 <sup>a</sup>
0.5 mM Sb	25.77 $\pm$ 1.74 <sup>b</sup>	16.45 $\pm$ 1.49 <sup>a</sup>	1390 $\pm$ 200 <sup>b</sup>	6882 $\pm$ 798 <sup>b</sup>	64.50 $\pm$ 7.55 <sup>b</sup>	436.15 $\pm$ 50.22 <sup>b</sup>
1.0 mM Sb	24.49 $\pm$ 1.91 <sup>b</sup>	16.73 $\pm$ 1.97 <sup>a</sup>	1691 $\pm$ 130 <sup>ab</sup>	6145 $\pm$ 839 <sup>b</sup>	69.88 $\pm$ 6.33 <sup>b</sup>	466.74 $\pm$ 49.67 <sup>b</sup>

The data are from 10 independent experiments, each carried out in triplicate (different letters indicate significant differences at  $p < 0.05$ , Mann-Whitney U-test).

**TABLE 3 |** Effect of Sb on the membrane lipid peroxidation, proline content, and relative water content (RWC) in tomato plants.

Treatments	Lipid peroxidation ( $\mu\text{mol MDA g}^{-1}\text{ FW}$ )		Proline content ( $\mu\text{g g}^{-1}\text{ FW}$ )		RWC (%)
	Roots	Leaves	Roots	Leaves	
Control	$3.95 \pm 0.68^b$	$29.74 \pm 2.23^a$	$9.46 \pm 0.42^a$	$18.37 \pm 1.53^b$	$93.40 \pm 2.50^a$
0.5 mM Sb	$4.27 \pm 0.66^{ab}$	$29.45 \pm 3.36^a$	$8.09 \pm 1.56^a$	$27.58 \pm 3.21^a$	$84.51 \pm 2.07^b$
1.0 mM Sb	$5.10 \pm 0.99^a$	$32.41 \pm 2.69^a$	$8.66 \pm 1.30^a$	$21.59 \pm 3.02^b$	$74.83 \pm 1.78^c$

The data are from 10 independent experiments, each carried out in triplicate (different letters indicate significant differences at  $p < 0.05$ , Mann–Whitney U-test).

there was no alteration observed in the leaves. With regard to the APX activity (**Figure 2D**), in roots this only increased (by 27%) in the plants grown in 1.0 mM Sb, but in leaves there were increases for both Sb concentrations (0.5 mM Sb, 12.6%; 1.0 mM Sb, 49.7%). The DHAR activity (**Figure 2E**) decreased in the roots treated with Sb (by 22% and 34.3% for 0.5 mM and 1.0 mM Sb, respectively), but was unaffected in the leaves. With respect to GR (**Figure 2F**), there was a slight increase (12%) in its activity only in the roots treated with 0.5 mM Sb, but no change in the leaves.

**TABLE 4 |** The Sb content of roots and leaves and the corresponding bioaccumulation factor (BF) and translocation factor (TF) values in tomato plants.

Treatments	Sb ( $\mu\text{g Sb g}^{-1}\text{ FW}$ )		BF		TF
	Roots	Leaves	Roots	Leaves	
Control	$4.1 \pm 1.1^c$	nd	Nd	nd	nd
0.5 mM Sb	$11332.0 \pm 450.4^b$	$327.4 \pm 28.2^b$	$182.3^a$	$5.46^a$	$0.030^b$
1.0 mM Sb	$13183.1 \pm 375.3^a$	$554.9 \pm 48.3^a$	$109.6^b$	$4.74^a$	$0.042^a$

The data are from 10 independent experiments, each carried out in triplicate (different letters indicate significant differences at  $p < 0.05$ , Mann–Whitney U-test). BF, the ratio between the concentration of element in the roots or leaves and that present in the soil. TF, the ratio between the concentration of element in the leaves and in the roots.

The contents of total phenols, flavonoids, and PPGs were all unaltered by the Sb treatment in the roots or the leaves (**Figures 3A–C**) except for a decrease in total flavonoids in leaves subjected to 0.5 mM Sb. With respect to the PPO activity (**Figure 3D**), this remained unchanged in the roots, but showed an Sb-concentration dependent increase in the leaves.

Treatment with 0.5 mM Sb caused a decrease in AsA content in the roots, but not with 1.0 mM Sb for which there was no change in this content (**Table 6**). Both concentrations, however, produced increases in AsA content in the leaves. The DHA content presented the opposite behavior, with increases in the roots at 1.0 mM Sb but no alteration at 0.5 mM Sb, and decreases in the leaves for both concentrations. These alterations caused the total AsA + DHA content to decrease in both roots and leaves for 0.5 mM Sb and increase for 1.0 mM Sb. As for the AsA/DHA ratio, this decreased in roots and increased in leaves, both cases being dependent on the Sb concentration.

The total level of GSH (**Table 7**) decreased in the roots (by 33 and 27% for 0.5 mM and 1.0 mM Sb, respectively), but in the leaves it increased by 24% only for 1.0 mM Sb, with no modification for 0.5 mM Sb. The GSSG content in the roots presented a similar response to the Sb treatment, decreasing to a greater extent with 0.5 mM Sb (44%) than with 1.0 mM Sb (30%). In the leaves, there was no significant

**TABLE 5 |** Effect of Sb on the Fe, Mn, Cu, Mg, and Zn content in roots and leaves of tomato plants.

Treatments	Fe ( $\mu\text{g g}^{-1}\text{ DW}$ )		Mn ( $\mu\text{g g}^{-1}\text{ DW}$ )		Cu ( $\mu\text{g g}^{-1}\text{ DW}$ )		Mg ( $\text{mg g}^{-1}\text{ DW}$ )		Zn ( $\mu\text{g g}^{-1}\text{ DW}$ )	
	Roots	Leaves	Roots	Leaves	Roots	Leaves	Roots	Leaves	Roots	Leaves
Control	$633.5 \pm 70.3^a$	$84.9 \pm 6.1^a$	$368.3 \pm 40.1^a$	$43.8 \pm 3.9^b$	$15.7 \pm 2.1^b$	$4.8 \pm 1.1^c$	$8.2 \pm 0.5^a$	$9.5 \pm 0.7^a$	$45.0 \pm 0.8^b$	$37.5 \pm 0.4^a$
0.5 mM Sb	$234.7 \pm 22.6^b$	$89.9 \pm 9.1^a$	$307.0 \pm 33.5^a$	$50.6 \pm 6.2^a$	$15.3 \pm 1.3^b$	$6.4 \pm 1.3^b$	$6.8 \pm 0.7^b$	$8.0 \pm 0.9^b$	$46.7 \pm 1.0^b$	$33.4 \pm 0.4^c$
1.0 mM Sb	$112.6 \pm 12.8^c$	$69.4 \pm 8.5^b$	$239.6 \pm 21.8^b$	$45.1 \pm 2.7^{ab}$	$28.6 \pm 2.9^a$	$10.2 \pm 1.9^a$	$5.2 \pm 0.6^c$	$4.9 \pm 0.4^c$	$56.6 \pm 1.2^a$	$35.0 \pm 0.5^b$

The data are from 10 independent experiments, each carried out in triplicate (different letters indicate significant differences at  $p < 0.05$ , Mann–Whitney U-test).

**TABLE 6 |** Effect of Sb on the chlorophyll a and b and total chlorophyll contents, chlorophyll a/b ratio, total carotenoids (Car), carotenoid/chlorophyll ratio, and photosynthetic efficiency ( $F_V/F_M$ ) in tomato leaves.

Treatments	Chl a ( $\mu\text{g g}^{-1}\text{ FW}$ )	Chl b ( $\mu\text{g g}^{-1}\text{ FW}$ )	Chl a + b ( $\mu\text{g g}^{-1}\text{ FW}$ )	Chl a/chl b	Carotenoids ( $\mu\text{g g}^{-1}\text{ FW}$ )	Carotenoids/total chl	$F_V/F_M$
Control	$1947.0 \pm 77.7^a$	$979.8 \pm 109.4^a$	$2947.8^a$	$1.98^b$	$185.4 \pm 12.9^b$	$0.070^c$	$0.771 \pm 0.045^a$
0.5 mM Sb	$1375.6 \pm 76.2^b$	$607.47 \pm 38.7^b$	$1968.3^b$	$2.27^a$	$178.2 \pm 38.7^b$	$0.095^b$	$0.605 \pm 0.058^b$
1.0 mM Sb	$1221.4 \pm 65.2^c$	$523.2 \pm 38.4^c$	$1796.5^c$	$2.35^a$	$225.3 \pm 23.2^a$	$0.132^a$	$0.586 \pm 0.036^c$

The data are from 10 independent experiments, each carried out in triplicate (different letters indicate significant differences at  $p < 0.05$ , Mann–Whitney U-test).

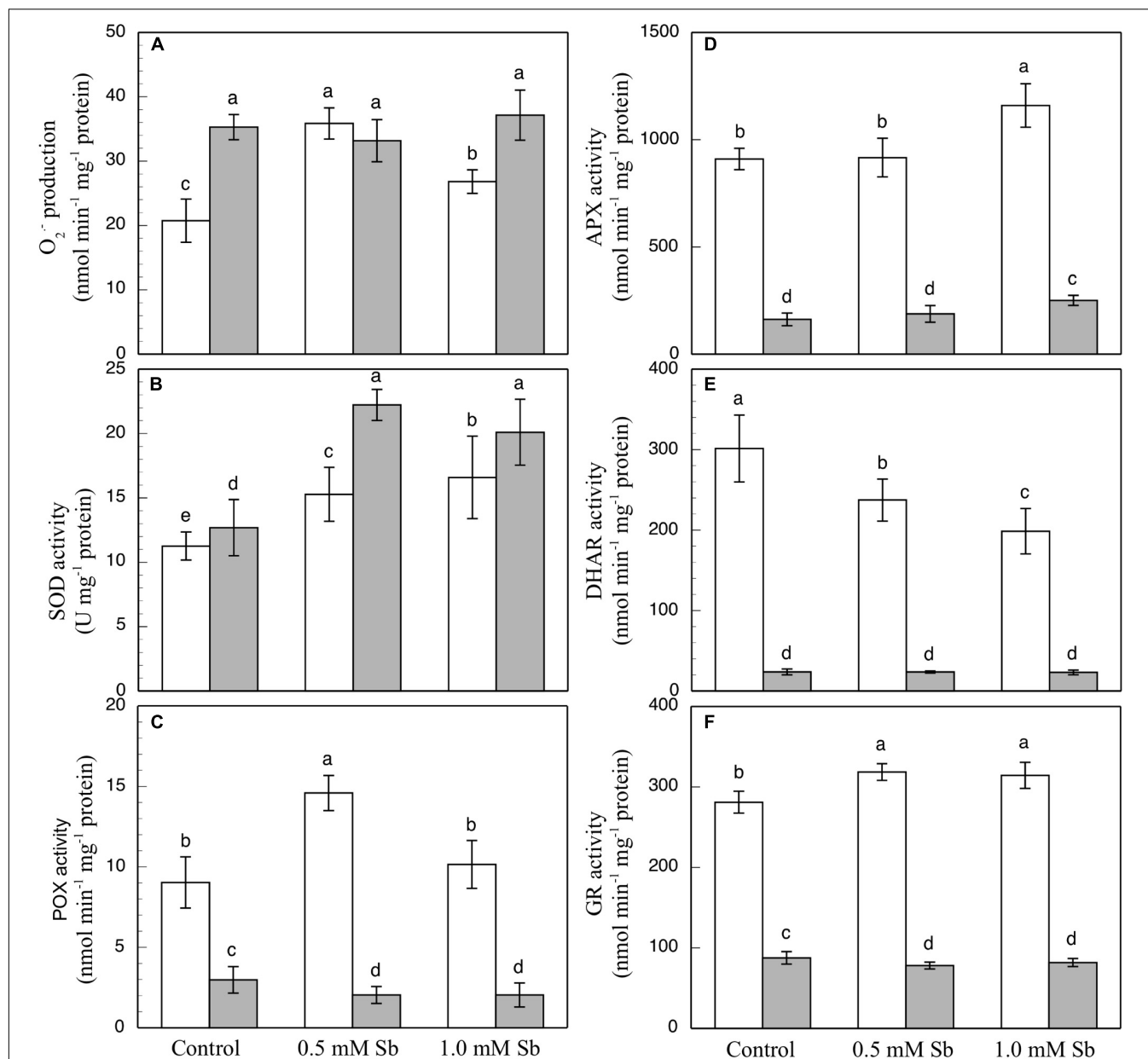


**FIGURE 2 |** Effect of Sb on O<sub>2</sub><sup>•-</sup> production (A) and on the SOD (B), POX (C), APX (D), DHAR (E), and GR (F) activities, in roots (white) and leaves (gray) of tomato plants. The data are from 10 independent experiments, each carried out in triplicate (different letters indicate significant differences at  $p < 0.05$ , Mann-Whitney  $U$ -test).

alteration in this content. These alterations in GSH and GSSG meant that the total content of the two declined in the roots, but remained unchanged in the leaves. The GSH/GSSG ratio in the roots increased from 0.316 to 0.385 with 0.5 mM Sb, but was unchanged with the higher Sb concentration. In the leaves, this ratio declined for the lower Sb concentration, but increased significantly for the higher one of 1.0 mM Sb.

Roots grown for 14 days under conditions of 0.5 and 1.0 mM Sb toxicity presented increases in the amounts of O<sub>2</sub><sup>•-</sup>, H<sub>2</sub>O<sub>2</sub>, NO, ONOO<sup>-</sup> and RSNOs as visualized in the

intact roots, and also as quantified by the pixel intensity of the images (Figures 4A–J). For O<sub>2</sub><sup>•-</sup>, NO and ONOO<sup>-</sup> accumulation (Figures 4A,B,E–H), this increase was only significant with 1.0 mM Sb, but not with 0.5 mM Sb. For H<sub>2</sub>O<sub>2</sub> (Figures 4C,D) however, there were strong increases with both Sb concentrations. For the RSNOs (Figures 4I,J) increase slightly under toxicity of Sb. Figure 5 shows the ROS and RNS values obtained by spectrofluorometry, using the same probes as in the microscopy images for their detection. One observes that Sb causes a significant increase in both ROS and RNS, coinciding with the estimates made from the fluorescence images. Thus,



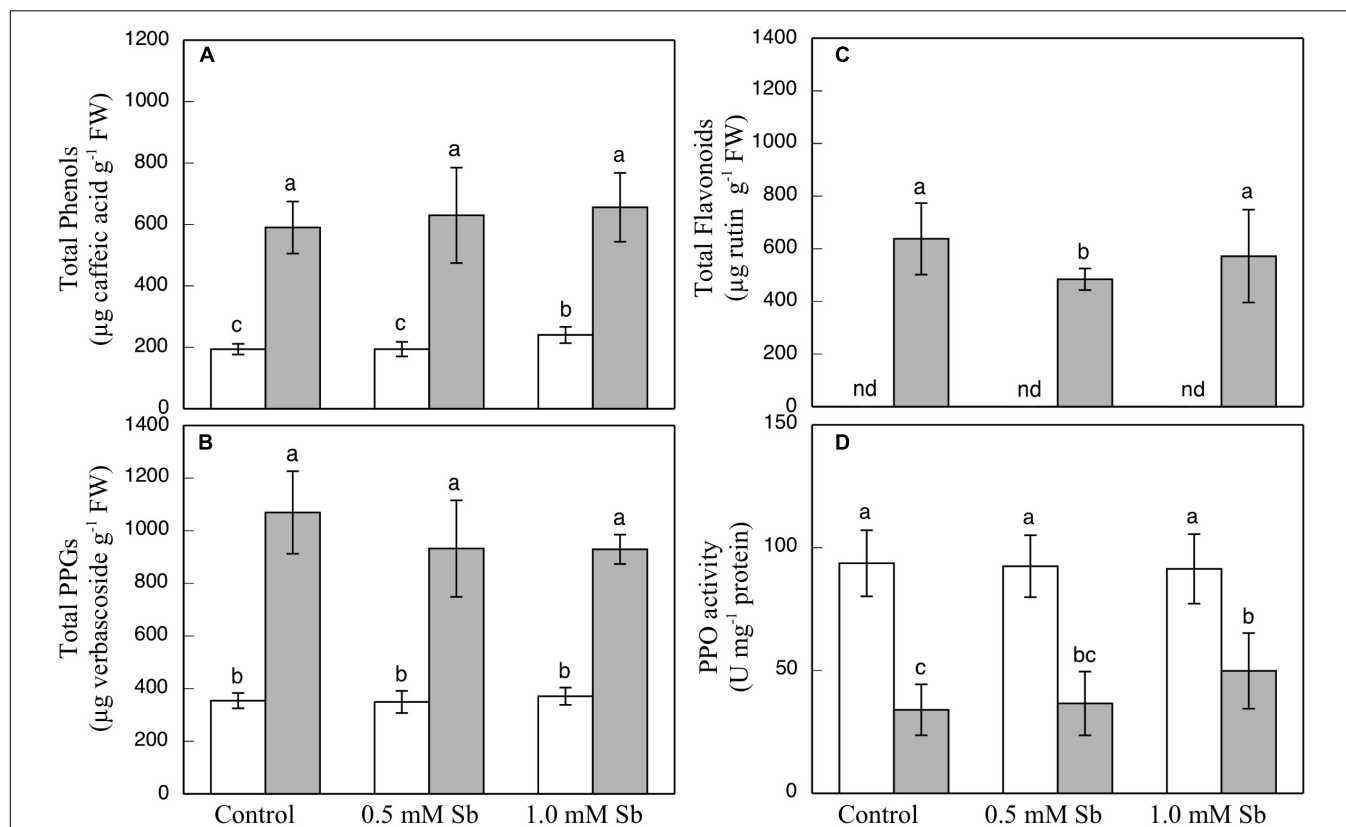


**FIGURE 3 |** Effect of Sb on the total phenol (A), flavonoid (B), and PPG (C) contents, and the PPO activity (D) in roots (white) and leaves (gray) of tomato plants. The data are from 10 independent experiments, each carried out in triplicate (different letters indicate significant differences at  $p < 0.05$ , Mann-Whitney  $U$ -test).

$\text{O}_2^{\cdot-}$  increases ( $\times 1.5$ ) under 1.0 mM Sb toxicity, while  $\text{H}_2\text{O}_2$  increases for both 0.5 mM and 1.0 mM Sb (Figures 5A,B). Both NO and ONOO $^-$  increase considerably with respect to the control (Figures 5C,D), with ONOO $^-$  presenting very high values for both Sb concentrations. On the contrary, the RSNOs (Figure 5E) do not undergo any change, with the values being very similar to the controls. This behavior of the RSNOs reflects

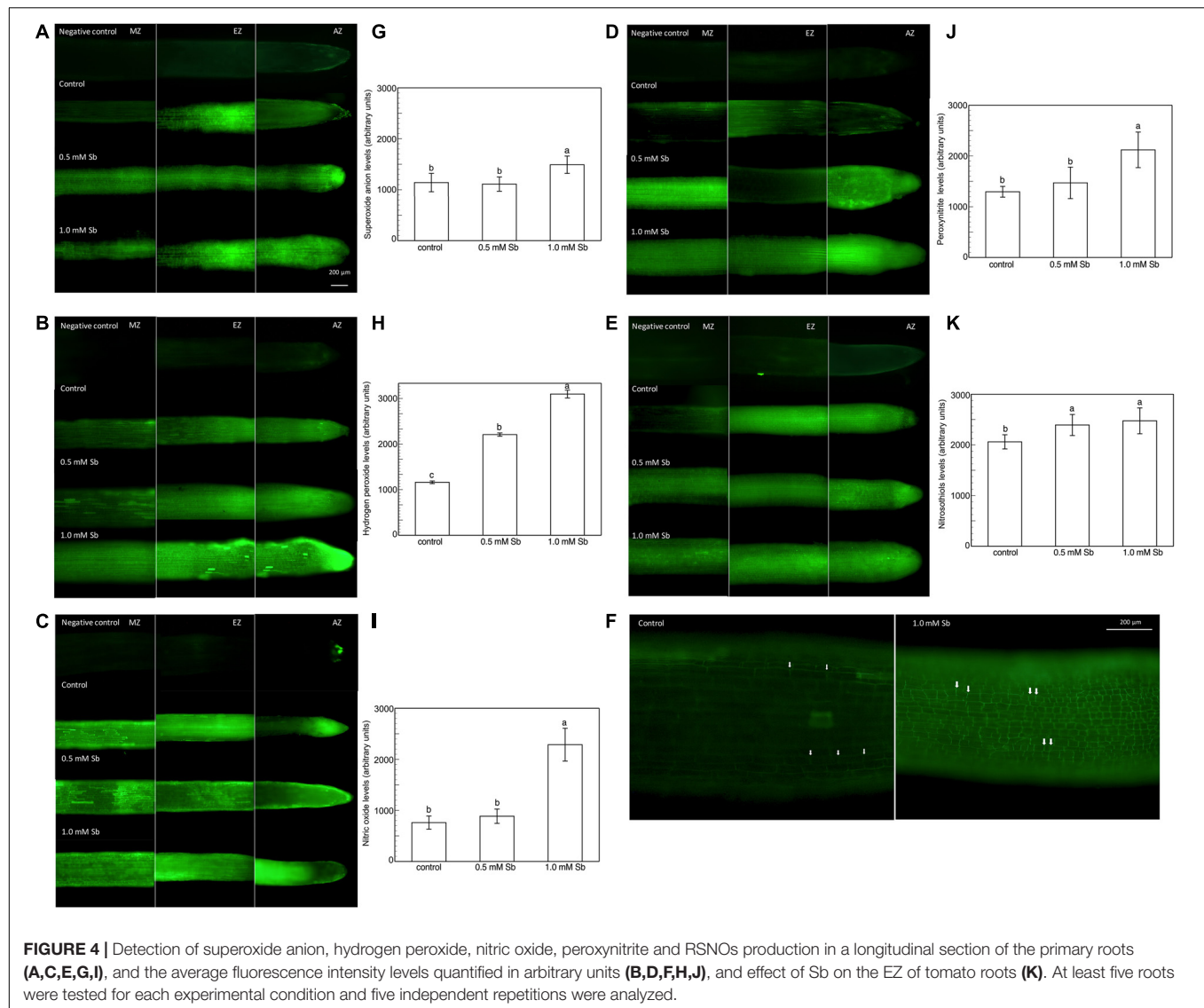
Sb's capacity to interact with thiol groups, preventing the binding of NO, which could explain the marked increase in the amount of NO detected under Sb toxicity ( $\times 3$  with respect to the control values).

The elongation zone (EZ), especially in the roots subjected to 1.0 mM Sb, showed a clear alteration in the size and arrangement of the cells (Figure 4K). This alteration consisted

**TABLE 7 |** Effect of Sb on the AsA, DHA, and ascorbate pool (AsA + DHA) contents, the AsA/DHA ratio, the GSH, GSSG, and glutathione pool (GSH + GSSG) contents, and the GSH/GSSG ratio, in roots and leaves of tomato plants.

Treatments	AsA (nmol g $^{-1}$ FW)		DHA (nmol g $^{-1}$ FW)		AsA + DHA (nmol g $^{-1}$ FW)		AsA/DHA	
	Roots	Leaves	Roots	Leaves	Roots	Leaves	Roots	Leaves
Control	95.23 $\pm$ 9.73 <sup>a</sup>	223.38 $\pm$ 35.36 <sup>b</sup>	388.10 $\pm$ 28.17 <sup>b</sup>	2195.65 $\pm$ 143.33 <sup>a</sup>	483.33 $\pm$ 51.5 <sup>b</sup>	2419.03 $\pm$ 133.36 <sup>a</sup>	0.249 $\pm$ 0.011 <sup>a</sup>	0.102 $\pm$ 0.089 <sup>b</sup>
0.5 mM Sb	68.07 $\pm$ 5.51 <sup>b</sup>	234.17 $\pm$ 38.63 <sup>b</sup>	324.22 $\pm$ 34.83 <sup>b</sup>	2127.77 $\pm$ 161.99 <sup>a</sup>	361.14 $\pm$ 29.8 <sup>c</sup>	2361.53 $\pm$ 208.86 <sup>a</sup>	0.237 $\pm$ 0.021 <sup>a</sup>	0.109 $\pm$ 0.008 <sup>b</sup>
1.0 mM Sb	103.63 $\pm$ 6.64 <sup>a</sup>	361.95 $\pm$ 45.60 <sup>a</sup>	580.94 $\pm$ 69.43 <sup>a</sup>	2053.25 $\pm$ 270.45 <sup>a</sup>	684.56 $\pm$ 55.7 <sup>a</sup>	2430.20 $\pm$ 224.06 <sup>a</sup>	0.179 $\pm$ 0.009 <sup>b</sup>	0.180 $\pm$ 0.021 <sup>a</sup>
Treatments	GSH (nmol g $^{-1}$ FW)		GSSG (nmol g $^{-1}$ FW)		GSH + GSSG (nmol g $^{-1}$ FW)		GSH/GSSG	
	Roots	Leaves	Roots	Leaves	Roots	Leaves	Roots	Leaves
Control	13.15 $\pm$ 2.0 <sup>a</sup>	18.71 $\pm$ 3.1 <sup>b</sup>	43.1 $\pm$ 3.9 <sup>a</sup>	79.95 $\pm$ 8.2 <sup>a</sup>	56.25 $\pm$ 5.8 <sup>a</sup>	98.66 $\pm$ 11.4 <sup>a</sup>	0.316 $\pm$ 0.029 <sup>a</sup>	0.247 $\pm$ 0.013 <sup>b</sup>
0.5 mM Sb	8.83 $\pm$ 1.4 <sup>b</sup>	17.62 $\pm$ 2.6 <sup>b</sup>	24.24 $\pm$ 3.5 <sup>c</sup>	85.84 $\pm$ 9.1 <sup>a</sup>	33.06 $\pm$ 4.1 <sup>c</sup>	103.46 $\pm$ 8.5 <sup>a</sup>	0.385 $\pm$ 0.030 <sup>a</sup>	0.205 $\pm$ 0.091 <sup>b</sup>
1.0 mM Sb	9.7 $\pm$ 1.6 <sup>b</sup>	23.24 $\pm$ 3.0 <sup>a</sup>	30.32 $\pm$ 2.2 <sup>b</sup>	72.82 $\pm$ 6.5 <sup>a</sup>	40.02 $\pm$ 3.6 <sup>b</sup>	96.06 $\pm$ 10.5 <sup>a</sup>	0.316 $\pm$ 0.025 <sup>a</sup>	0.333 $\pm$ 0.021 <sup>a</sup>

The data are from 10 independent experiments, each carried out in triplicate (different letters indicate significant differences at  $p < 0.05$ , Mann-Whitney  $U$ -test).



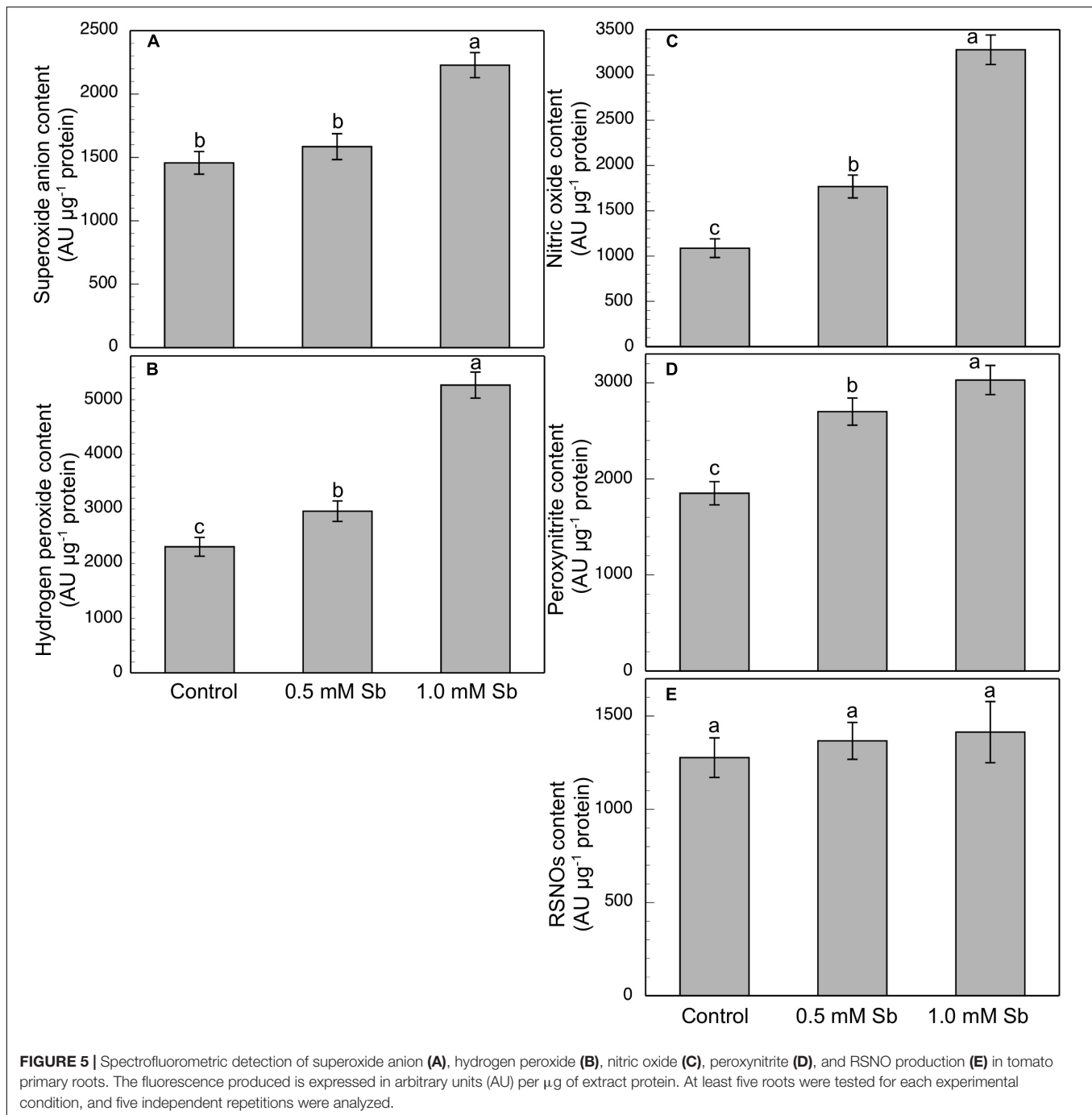
of a disorganization of this area, leading to less cell elongation (the cells being much shorter than those of the control roots in this same area) and disorganization of the cell columns, causing abnormal EZ thickening.

## Effect of Sb on Antioxidant Enzyme Gene Expression

In general, there were increases in the expression of genes related to antioxidant systems induced by Sb toxicity. Thus, there was a strong increase in the expression of APX genes both roots and leaves (Figure 6). There was a significant increase in SOD expression only for the 1.0 mM Sb concentration. With regard to GR expression, this increased in the roots, but in the leaves there was a decrease with 0.5 mM Sb and an increase with 1.0 mM Sb. Finally, the GST expression is strongly inhibited in roots but on the contrary, showed an increase when considering the leaves.

## DISCUSSION

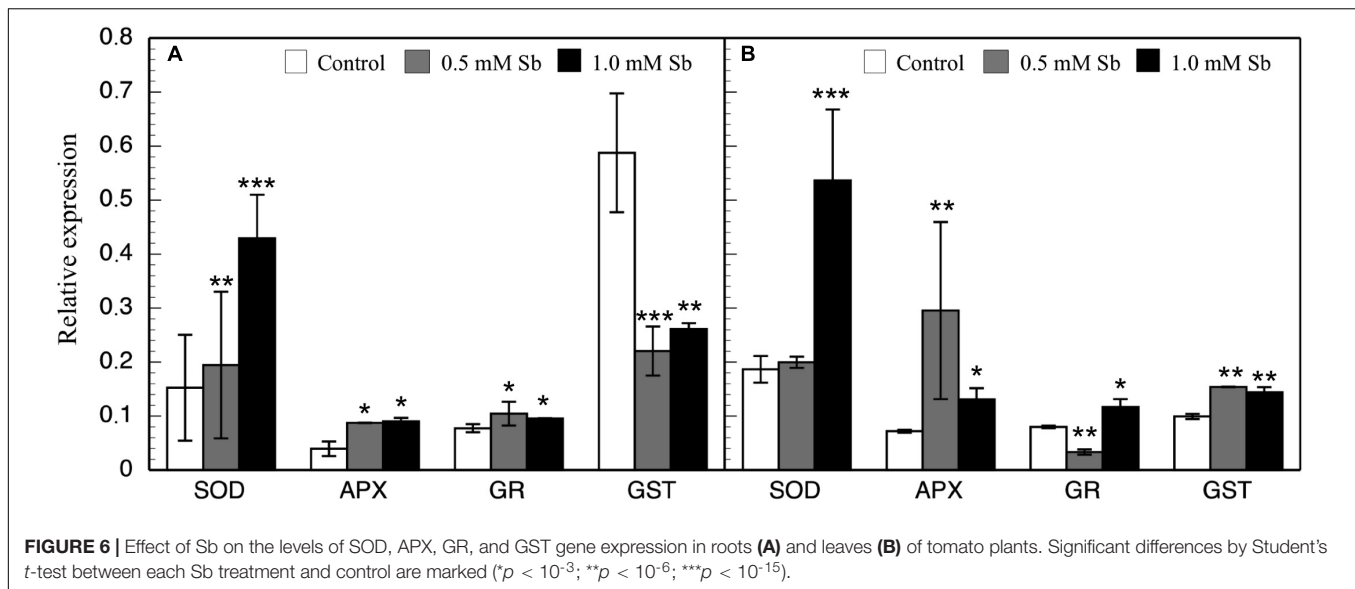
The growth of the tomato plants shows the effects of the Sb-induced toxicity. The fresh and dry weight, of both roots and stems, is reduced under Sb toxicity to very similar levels for the two concentrations used. Root growth is also affected, but to a lesser extent than that of the stems. Roots show greater accumulation of this element, with values much greater than those of the leaves. The effect of Sb on the growth has also been observed in other plants (Pan et al., 2011; Shtangeeva et al., 2011; Bech et al., 2012; Cai et al., 2016; Chai et al., 2017; Ortega et al., 2017; Zhou et al., 2018). For tomatoes, Peško et al. (2016) report a different behavior – the lower concentrations produce an increase in dry weight and the higher ones a reduction in both the stems and roots. In other cases, growth alterations have been reported as either mild (Feng et al., 2011) or absent as described by Tschan et al. (2008) in maize and sunflowers, although the concentrations they used were lower (Feng et al., 2011) or much



lower (Tschan et al., 2008) than those of the present study. For the EZ, we observed alterations in cell size and organization that could be due to Sb's toxic effect through its interaction with GSH. The participation of GSH in the regulation of auxin levels in the root apices and in the alteration of the quiescent center has been clearly demonstrated (Koprivova et al., 2010). Thus, any alteration in the GSH content translates into an alteration in the development of these root meristems. Vernoux et al. (2000) demonstrated that *Arabidopsis* mutants with a very reduced content of GSH showed a drastic decline in root meristem

development. Sb's capacity to bind to -SH groups (Sun et al., 2000; Ortega et al., 2017) to form Sb phytochelatin (GS-Sb) similar to the GS-Cd observed for Cd (Mendoza-Cózat et al., 2008) as a system of Sb detoxification can act to sharply reduce the amount of GSH, and alter root development.

In these plants the BF values obtained show a clear accumulation of Sb in the roots (182.3 and 109.6 for 0.5 and 1.0 mM Sb, respectively), much higher than the levels detected in the leaves (5.46 and 4.74 for 0.5 and 1.0 mM Sb, respectively). The TF values are also low (0.029 and 0.042 for 0.5 and



1.0 mM Sb, respectively), which indicates a very low translocation capacity of Sb within the tomato plant. These TFs are much lower than those described in other plants subjected to stress by Sb (Zhou et al., 2018). It is clear that there is a strong dependence of Sb TFs on the plant species and also on the Sb concentration (Pan et al., 2011). The observed TFs are greater in plants capable of supporting high Sb concentrations, e.g., *Dittrichia viscosa* (Pérez-Sirvent et al., 2012) and *Acorus calamus* (Zhou et al., 2018).

The Sb toxicity also alters the absorption and transport of other mineral elements. Thus, as the amount of Sb in the medium increases, Fe and Mg decrease in both roots and leaves, while Mn only does so in roots. The content of Cu, however, increases under 1.0 mM Sb, and Zn is the least affected element studied since it only shows an increase in roots. These changes reflect the interaction between these elements and Sb at the transport level. They partially agree with those observed by other workers. Thus, under Sb toxicity, Feng et al. (2013) describe a decrease in the content of Mg, Fe, Mn, Cu, and Zn. In an earlier study with sunflower plants (Ortega et al., 2017), we observed an increase in the content of Mg and Cu, while Fe and Zn decreased. With Zn toxicity, Feigl et al. (2015) report an increase in Cu content and decreases in Fe and Mn.

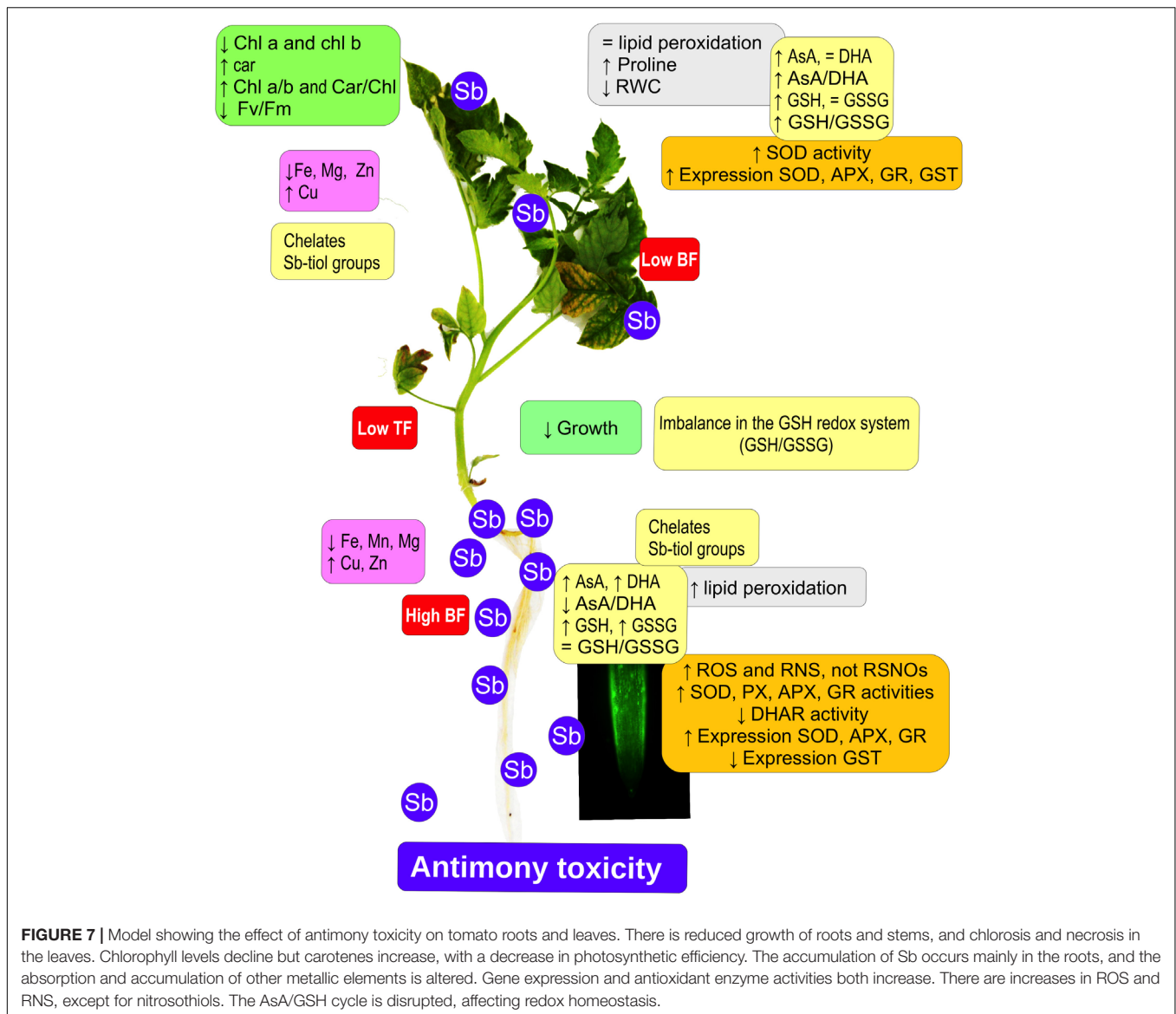
The total chlorophyll content decreases, due to the falls in both chlorophyll a and chlorophyll b content, although the latter is the more affected. This decrease may be related, like the other alterations already described, to the interaction between Sb and the -SH groups, which affects the functionality of the enzyme systems involved in the biosynthesis of these compounds and the stability of the chloroplasts themselves (Zhou et al., 2018). These results coincide with those observed by Pan et al. (2011) in *Zea mays* and by Xue et al. (2015) in *Miscanthus sinensis*, who attribute this decrease to an effect of Sb on the biosynthesis of these pigments. Also the alteration in the content of cations such as Mg, which is reduced by almost half in leaves, can affect the total chlorophyll content. The increase in the chl a/chl b ratio

is interesting since it reflects changes in the functionality of the thylakoids, modifying their appressed state (Anderson and Aro, 1994), and is known to reduce electron transfer (Chow, 1999) and can lead to photoinhibition in the leaves (Zhou et al., 2018). As a consequence of these Sb-induced alterations, photosynthetic efficiency decreases sharply (by 24%), possibly due to the effect of Sb on PSII in altering the appression and fluidity of the thylakoids (Pan et al., 2011; Zhou et al., 2018). On the contrary, both the carotenoid content and the carotenoid/chlorophyll ratio increase. This coincides with the observations of Chai et al. (2017), and reflects the action of carotenoids as antioxidants and photoprotectors, but it is not concordant with those of Zhou et al. (2018) who describe decreases in the carotenoid content and carotenoid/chlorophyll ratio in response to Sb toxicity in *Acorus calamus*.

The total content of these compounds is unaltered in both roots and leaves of tomato plants, unlike the case of sunflowers subjected to Sb toxicity (Ortega et al., 2017) in which the content of phenolic compounds, especially flavonoids, increases. Rajabpoor et al. (2019) also observed in *Salvia spinosa* large increases in the total content of phenols and flavonoids, increases which could have been involved in the constitutive defense of tolerance to Sb. Only the PPO activity in leaves under 1 mM Sb toxicity seems to increase, as it also did for this same concentration of Sb in *Helianthus annuus* (Ortega et al., 2017). This result would indicate the non-intervention of these antioxidant compounds in the antioxidant defense machinery against Sb-induced stress.

There is no alteration in the levels of lipid peroxidation in leaves, and only a slight increase in roots. This suggests that the participation of the antioxidant system seems to prevent damage at the level of peroxidation of the membranes in the leaves, but is not enough to prevent such damage in the roots. Our results coincide with those described by other workers (Feng et al., 2011; Corrales et al., 2014) regarding the low incidence of Sb on lipid peroxidation. Other studies on different





species show a clear increase in lipid peroxidation induced by Sb (Paoli et al., 2013; Xue et al., 2015; Chai et al., 2016, 2017; Ortega et al., 2017). Sb toxicity induces an increase in the proline content of leaves, similar to that described by other workers (Xue et al., 2015; Rajabpoor et al., 2019). The increase produced by this osmolyte in leaves may be related to the need to counteract the decrease in solute potential due to the Sb-induced alteration of the RWC. Water stress caused by the reduction in RWC can lead to increased synthesis of osmoprotective proline, preventing dehydration and protein inactivation (Verbruggen and Hermans, 2008). This increase in the leaves' proline content could also act by directly scavenging OH (Signorelli et al., 2014) and maintaining the stability of the membranes (Hayat et al., 2012), or by the induction of antioxidant enzymes but not scavenging  $O_2^{\cdot-}$ , NO, or ONOO<sup>-</sup> (Signorelli et al., 2016). In *Zea mays* subjected to stress by Sb, there is a marked increase in the proline content of

the roots (Vaculiková et al., 2014), which is not the case in the present study.

Sb induces an increase in  $O_2^{\cdot-}$  production in tomato roots, but not in the leaves. This effect is similar to that observed in sunflowers by Ortega et al. (2017), although in sunflowers the increase in  $O_2^{\cdot-}$  occurs in both roots and leaves. Other workers also describe increases in the production of  $O_2^{\cdot-}$  under heavy metal toxicity. Feigl et al. (2015) observe a similar increase in  $O_2^{\cdot-}$  in response to Zn toxicity in *B. napus*, but not in *B. juncea*. A similar increase is described by Srivastava et al. (2014) in roots and leaves of rice under Cd toxicity. The increases in the content of NO and ONOO<sup>-</sup> that we obtained in the roots are very similar to those described for Zn toxicity (Feigl et al., 2015). The increase in the ONOO<sup>-</sup> content may explain the moderate increase in the content of NO and  $O_2^{\cdot-}$  (Feigl et al., 2015). However, the RSNO content is unaltered, although in conditions of biotic stress it is known

to increase (Chaki et al., 2009). Also, the spectrofluorometric determination of ROS and RNS showed them both to increase under Sb toxicity, which could be indicative of a nitro-oxidative stress having been produced (Corpas and Barroso, 2013). The increases in the NO and ONOO<sup>-</sup> content that we observed under Sb toxicity contrast with the results of Rodríguez-Ruíz et al. (2019) for pea plants subjected to As toxicity who observed strong decreases in both reactive species in roots, but an increase (NO) or no change (ONOO<sup>-</sup>) in leaves. The rise in O<sub>2</sub><sup>-</sup> is in line with the strong observed increases in SOD gene expression and SOD activity, especially under 1.0 mM Sb toxicity, reflecting the induction of the antioxidant system. A similar effect on increase of SOD activity was observed by Feng et al. (2019) in rice plants under stress caused by different forms of Sb. These increases in both SOD expression and activity may explain the observed low incidence of Sb toxicity on membrane lipid peroxidation. The peroxidase behavior shows differences. Thus, POX has increased activity in roots but not in leaves, while APX has increased expression and activity in both organs. The increases in SOD, POX, and APX activity reflect the involvement of the antioxidant machinery in the response to toxicity from Sb (Feng et al., 2009, 2019; Benhamdi et al., 2014; Vaculiková et al., 2014; Ortega et al., 2017) and from other heavy metals (Srivastava et al., 2014; Feigl et al., 2015; Rodríguez-Ruíz et al., 2019). Other activities such as DHAR and GR are not significantly altered under Sb toxicity in leaves, but in roots, the DHAR activity is inhibited while that of GR is slightly increased. The expression of GR increases in roots and leaves, although only for 1.0 mM Sb in the latter, which explains the observed increase in GR activity. These results coincide with the response to As described by Singh et al. (2015) and Rodríguez-Ruíz et al. (2019) who report an increase in GR activity with inhibition of DHAR activity. In contrast, Feng et al. (2009) describe inhibition of GR activity as an effect of Sb.

The ascorbate/glutathione cycle component content is modified in response to Sb toxicity. In tomato roots, the content of AsA and DHA increases, although the latter does so in a greater proportion which causes a decrease in the AsA/DHA ratio. In leaves, the ratio increases since the DHA content decreases. In roots, GSH and GSSG decline, while in leaves, GSH increases and GSSG is unaltered. The GSH/GSSG ratio is only modified in leaves, in which it increases. The effect of Sb on AsA and GSH coincides in part with the results obtained in response to Cd (Srivastava et al., 2014) and As (Singh et al., 2015) toxicity. The roots are the organ more affected by Sb toxicity. The results show an imbalance between the components of the ascorbate/glutathione cycle. While the total content of AsA and DHA increases in roots, the content in GSH and GSSG decreases, with a clear imbalance in the cycle and with alteration of the enzymatic activities related to it. These results coincide with those described by Rodríguez-Ruíz et al. (2019) for the effect of As toxicity on hydroponically grown pea plants. The As toxicity caused an increase in APX and GR activities in both roots and leaves, the DHAR and MDAR activities decreased in roots but were unaffected in leaves, and, in both organs, the GSH and GSSG content decreased, the AsA content was

unaltered, and there was a marked increase in phytochelatin. In our case, in tomato plants we found that Sb toxicity induces increases in both antioxidant activities and in the GSH and GSSG content in roots, with a behavior similar to that described for As. In addition, in roots, there is a sharp decrease in the expression of GST, while in leaves it increases. In roots with high amounts of accumulated Sb, the inhibition of GST expression, the increase in GR activity, and the decrease in DHAR activity favor the availability of GSH for the formation of chelates with Sb (Noctor et al., 2012). This is a protective mechanism against Sb toxicity and against that of other heavy metals (Yadav, 2010; Hossain et al., 2012; Natasha et al., 2019). The ability of Sb to form complexes with -SH groups (Sun et al., 2000; Foyer and Noctor, 2005) could be the cause of the imbalance observed in the antioxidant components, as well as the effects on growth in tomato plants.

## CONCLUSION

Tomato plants subjected to Sb toxicity (**Figure 7**) show a great capacity to accumulate Sb, especially in their roots, resulting in growth disturbance, changes in the capacity to absorb other mineral elements such as Fe and Mg, and decreased chlorophyll content and photosynthetic efficiency. There are increases in ROS and RNS production, and in SOD, POX, APX, and GR activities but not DHAR in the roots, limiting transport to the aerial parts, with induction of SOD, APX, and GR expression and activities, inhibition of GST expression, and alteration of redox homeostasis. Our results suggest that the effects induced by Sb toxicity may be due to the element's capacity to interact with -SH groups, including GSH thiol groups. The GSH content also intervenes in the maintenance of levels of auxins in the roots and quiescent center, so that root development is disturbed.

## DATA AVAILABILITY STATEMENT

The raw data supporting the conclusions of this article will be made available by the authors, without undue reservation, to any qualified researcher.

## AUTHOR CONTRIBUTIONS

AO, FE, FE-V, IC, and IG contributed conception, design and realization on the study. AO performed the molecular analysis. FE, FE-V, and IG performed the biochemical analysis. FE-V and IC performed the microcopy analysis. FE wrote the manuscript. All authors contributed to manuscript revision, read and approved the submitted version.

## FUNDING

This study was made possible thanks to the Junta de Extremadura/FEDER for the Research Project IB16078 and the support given to the Research Group FBCMP (GR18168).

## REFERENCES

- Ahsan, N., Renaut, J., and Komatsu, S. (2009). Recent developments in the application of proteomics to the analysis of plant responses to heavy metals. *Proteomics* 9, 2602–2621. doi: 10.1002/pmic.200800935
- Airaki, M., Leterrier, M., Mateos, R. M., Valderrama, R., Chaki, M., Barroso, J. B., et al. (2012). Metabolism of reactive oxygen species and reactive nitrogen species in pepper (*Capsicum annuum* L.) plants under low temperature stress. *Plant Cell Environ.* 35, 281–295. doi: 10.1111/j.1365-3040.2011.02310.x
- Anderson, J. M., Aro, E. M. (1994). Grana stacking and protection of photosystem II in thylakoid membranes of higher plant leaves under sustained high irradiance: an hypothesis. *Photosynth. Res.* 41, 315–326. doi: 10.1007/BF00019409
- Anjum, N. A., Gill, S. S., Gill, R., Hasanuzzaman, M., Duarte, A. C., Pereira, E., et al. (2014). Metal/metalloid stress tolerance in plants: role of ascorbate, its redox couple, and associated enzymes. *Protoplasma* 251, 1265–1283. doi: 10.1007/s00709-014-0636-x
- Apel, K., and Hirt, H. (2004). Reactive oxygen species: metabolism, oxidative stress, and signal transduction. *Annu. Rev. Plant Biol.* 55, 373–399. doi: 10.1146/annurev.arplant.55.031903.141701
- Baroni, F., Boscagli, A., Protano, G., and Riccobono, F. (2000). Antimony accumulation in *Achillea ageratum*, *Plantago lanceolata* and *Silene vulgaris* growing in an old Sb-mining area. *Environ. Pollut.* 109, 347–352. doi: 10.1016/S0269-7491(99)00240-7
- Bates, L. S., Waldren, R. P., Teare, I. D. (1973). Rapid determination of free proline for water-stress studies. *Plant Soil* 39, 205–207. doi: 10.1007/BF00018060
- Beauchamp, C., and Fridovich, I. (1971). Superoxide dismutase: improved assays and an assay applicable to acrylamide gels. *Anal. Biochem.* 44, 276–287. doi: 10.1016/0003-2697(71)90370-8
- Bech, J., Corrales, I., Tume, P., Barceló, J., Duran, P., Roca, N., et al. (2012). Accumulation of antimony and other potentially toxic elements in plants around a former antimony mine located in the Ribes Valley (Eastern Pyrenees). *J. Geochem. Explor.* 113, 100–105. doi: 10.1016/j.gexplo.2011.06.006
- Benhamdi, A., Bentellis, A., Rached, O., Du Laing, G., and Mechakra, A. (2014). Effects of antimony and arsenic on antioxidant enzyme activities two steppic plant species in an old antimony mining area. *Biol. Trace Elem. Res.* 158, 96–104. doi: 10.1007/s12011-014-9917-7
- Bienert, G. P., Thorsen, M., Schuüssler, M. D., Nilsson, H. R., Wagner, A., Tamás, M. J., et al. (2008). A subgroup of plant aquaporins facilitate the bi-directional diffusion of As (OH)<sub>3</sub> and Sb(OH)<sub>3</sub> across membranes. *BMC Biol.* 6, 26. doi: 10.1186/1741-7007-6-26
- Bradford, M. M. (1976). A rapid and sensitive method for the quantitation of microgram quantities of protein utilizing the principle of protein-dye binding. *Anal. Biochem.* 72, 248–254. doi: 10.1016/0003-2697(76)90527-3
- Cai, F., Ren, J., Tan, S., and Wang, S. (2016). Uptake, translocation and transformation of antimony in rice (*Oryza sativa* L.) seedling. *Environ. Pollut.* 209, 169–176. doi: 10.1016/j.envpol.2015.11.033
- Chai, L. Y., Mubarak, H., Yang, Z. H., Yong, W., Tang, C. J., and Mirza, N. (2016). Growth, photosynthesis and defense mechanism of antimony (Sb)-contaminated *Boehmeria nivea* (L.). *Environ. Sci. Pollut. Res.* 23, 7470–7481. doi: 10.1007/s11356-015-5987-0
- Chai, L. Y., Wang, Y., Yang, Z. H., Mubarak, H., and Mirza, N. (2017). Physiological characteristics of *Ficus tikoua* under antimony stress. *Transact. Nonferr. Metal. Soc.* 27, 939–945. doi: 10.1016/S1003-6326(17)60106-7
- Chaki, M., Valderrama, R., Fernández-Ocaña, A., Carreras, A., Gómez-Rodríguez, M. V., Pedrajas, J. R., et al. (2009). Involvement of reactive nitrogen and oxygen species (RNS and ROS) in sunflower mildew interaction. *Plant Cell Physiol.* 50, 265–279. doi: 10.1093/pcp/pcn196
- Chow, W. S. (1999). Grana formation: entropy-assisted local order in chloroplasts? *Aust. J. Plant Physiol.* 26, 641–647.
- Cidu, R., Biddau, R., Dore, E., Vacca, A., and Marini, L. (2014). Antimony in the soil–water–plant system at the Su Suergiu abandoned mine (Sardinia, Italy): strategies to mitigate contamination. *Sci. Total Environ.* 497–498, 319–331. doi: 10.1016/j.scitotenv.2014.09.024
- Corpas, F. J., and Barroso, J. B. (2013). Nitro-oxidative stress vs oxidative or nitrosative stress in higher plants. *New Phytol.* 199, 633–635. doi: 10.1111/nph.12380
- Corpas, F. J., and Barroso, J. B. (2014). Peroxynitrite (ONOO<sup>−</sup>) is endogenously produced in Arabidopsis peroxisomes and is overproduced under cadmium stress. *Ann. Bot.* 113, 87–96. doi: 10.1093/aob/mct260
- Corpas, F. J., and Barroso, J. B. (2017). Lead-induced stress, which triggers the production of nitric oxide (NO) and superoxide anion (O<sub>2</sub><sup>−</sup>) in Arabidopsis peroxisomes, affects catalase activity. *Nitric Oxide* 68, 103–110. doi: 10.1016/j.niox.2016.12.010
- Corpas, F. J., Carreras, A., Esteban, F., Chaki, M., Valderrama, R., and del Río, L. A. (2008). Localization of S-nitrosothiols and assay of nitric oxide synthase and S-nitrosoglutathione reductase activity in plants. *Methods Enzymol.* 437, 559–572. doi: 10.1016/S0076-6879(07)37028-6
- Corpas, F. J., Leterrier, M., Valderrama, R., Airaki, M., Chaki, M., Palma, J. M., et al. (2011). Nitric oxide imbalance provokes a nitrosative response in plants under abiotic stress. *Plant Sci.* 181, 604–611. doi: 10.1016/j.plantsci.2011.04.005
- Corrales, I., Barceló, J., Bech, J., and Poschenrieder, C. (2014). Antimony accumulation and toxicity tolerance mechanisms in Trifolium species. *J. Geochem. Explor.* 147, 167–172. doi: 10.1016/j.gexplo.2014.07.002
- Das, K., and Roychoudhury, A. (2014). Reactive oxygen species (ROS) and response of antioxidants as ROS-scavengers during environmental stress in plants. *Front. Environ. Sci.* 2:53. doi: 10.3389/fenvs.2014.00053
- De Gara, L., De Pinto, M. C., Moliterni, V. M. C., and D'Égidio, M. G. (2003). Redox regulation and storage processes during maturation in kernels of *Triticum durum*. *J. Exp. Bot.* 54, 249–258. doi: 10.1093/jxb/erg021
- De Pinto, M. C., Francis, D., and De Gara, L. (1999). The redox state of ascorbate-dehydroascorbate pair as a specific sensor of cell division in tobacco TBV-2 cells. *Protoplasma* 209, 90–97. doi: 10.1007/BF01415704
- Fawcett, S. E., Jamieson, H. E., Nordstrom, D. K., and McCleskey, R. B. (2015). Arsenic and antimony geochemistry of mine wastes, associated waters and sediments at the Giant Mine, Yellowknife, Northwest Territories, Canada. *Appl. Geochem.* 62, 3–17. doi: 10.1016/j.apgeochem.2014.12.012
- Feigl, G., Lehotai, N., Molnár, A., Ördög, A., Rodríguez-Ruiz, M., Palma, J. M., et al. (2015). Zinc induces distinct changes in the metabolism of reactive oxygen and nitrogen species (ROS and RNS) in the roots of two *Brassica* species with different sensitivity to zinc stress. *Ann. Bot.* 116, 613–625. doi: 10.1093/aob/mcu246
- Feng, R., Lei, L., Su, J., Zhang, R., Zhu, Y., Chen, W., et al. (2019). Toxicity of different forms of antimony to rice plant: effects on root exudates, cell wall components, endogenous hormones and antioxidant system. *Sci. Total Environ.* 711:134589. doi: 10.1016/j.scitotenv.2019.134589
- Feng, R., Liao, G., Guo, J., Wang, R., Xu, Y., Ding, Y., et al. (2016). Responses of root growth and antioxidative systems of paddy rice exposed to antimony and selenium. *Environ. Exp. Bot.* 122, 29–38. doi: 10.1016/j.envexpbot.2015.08.007
- Feng, R., Wei, C., Tu, S., Ding, Y., Wang, R., and Guo, J. (2013). The uptake and detoxification of antimony by plants: a review. *Environ. Exp. Bot.* 96, 28–34. doi: 10.1016/j.envexpbot.2013.08.006
- Feng, R., Wei, C., Tu, S., Tang, S., and Wu, F. (2011). Simultaneous hyperaccumulation of arsenic and antimony in Cretan brake fern: evidence of plant uptake and subcellular distributions. *Microchem. J.* 97, 38–43. doi: 10.1016/j.microc.2010.05.010
- Feng, R., Wei, C., Tu, S., Wu, F., and Yang, L. (2009). Antimony accumulation and antioxidative responses in four fern plants. *Plant Soil* 317, 93–101. doi: 10.1007/s11104-008-9790-2
- Filella, M., Belzile, N., and Chen, Y. W. (2002). Antimony in the environment: a review focused on natural waters I. Occurrence. *Earth Sci. Rev.* 57, 125–176. doi: 10.1016/S0012-8252(01)00070-8
- Filella, M., Williams, P. A., and Belzile, N. (2009). Antimony in the environment: knowns and unknowns. *Environ. Chem.* 6, 95–105. doi: 10.1071/EN09007
- Foyer, C. H., and Noctor, G. (2005). Oxidant and antioxidant signalling in plants: a re-evaluation of the concept of oxidative stress in a physiological context. *Plant Cell Environ.* 28, 1056–1071. doi: 10.1111/j.1365-3040.2005.01327.x
- Fu, J., and Huang, B. (2001). Involvement of antioxidants and lipid peroxidation in the adaptation of two cool-season grasses to localized drought stress. *Environ. Exp. Bot.* 45, 105–114. doi: 10.1016/S0098-8472(00)00084-8
- Gálvez, M., Martín-Cordero, C., Houghton, P. J., and Ayuso, M. J. (2008). Antioxidant activity of methanol extracts obtained from *Plantago* species. *J. Agric. Food Chem.* 53, 1927–1933. doi: 10.1021/jf048076s



- García-Lorenzo, M. L., Martínez-Sánchez, M. J., Pérez-Sirvent, C., López-Sánchez, J., Molina-Ruiz, J., and Tudela, M. L. (2015). Geogenic distribution of arsenic (As) and antimony (Sb) in soils of the murcia region in Spain. *Environ. Forensics* 16, 88–95. doi: 10.1080/15275922.2014.991435
- Garrido, I., García-Sánchez, M., Casimiro, I., Casero, J., García-Romera, I., Ocampo, J. A., et al. (2012). Oxidative stress induced in sunflower seedling roots by aqueous dry olive-mill residues. *PLoS One* 7:e46137. doi: 10.1371/journal.pone.0046137
- Gaupels, F., Spiazzi-Vandelle, E., Yang, D., and Delledonne, M. (2011). Detection of peroxynitrite accumulation in *Arabidopsis thaliana* during the hypersensitive defense response. *Nitric Oxide* 25, 222–228. doi: 10.1016/j.niox.2011.01.009
- Gill, S. S., and Tuteja, N. (2010). Reactive oxygen species and antioxidant machinery in abiotic stress tolerance in crop plants. *Plant Physiol. Biochem.* 40, 909–930. doi: 10.1016/j.plaphy.2010.08.016
- Hayat, S., Hayat, Q., Alyemeni, M. N., Wani, A. S., Pichtel, J., and Ahmad, A. (2012). Role of proline under changing environments: a review. *Plant Signal. Behav.* 7, 1456–1466. doi: 10.4161/psb.21949
- He, M., Wang, X., Wu, F., and Fu, Z. (2012). Antimony pollution in China. *Sci. Total Environ.* 421–422, 41–50. doi: 10.1016/j.scitotenv.2011.06.009
- Hossain, M. A., Piyatida, P., Teixeira da Silva, J. A., and Fujita, M. (2012). Molecular mechanism of heavy metal toxicity and tolerance in plants: central role of glutathione in detoxification of reactive oxygen species and methylglyoxal and in heavy metal chelation. *J. Bot.* 2012:872875. doi: 10.1155/2012/872875
- Ji, Y., Sarret, G., Schulin, R., and Tandy, S. (2017). Fate and chemical speciation of antimony (Sb) during uptake, translocation and storage by rye grass using XANES spectroscopy. *Environ. Pollut.* 231, 1322–1329. doi: 10.1016/j.envpol.2017.08.105
- Kamiya, T., and Fujiwara, T. (2009). *Arabidopsis* NIP1;1 transports antimonite and determines antimonite sensitivity. *Plant Cell Physiol.* 50, 1977–1981. doi: 10.1093/pcp/pcp130
- Karacan, M. S., Rodionova, M. V., Tunç, T., Venedik, K. B., Mamaş, S., Shitov, A. V., et al. (2016). Characterization of nineteen antimony(III) complexes as potent inhibitors of photosystem II, carbonic anhydrase, and glutathione reductase. *Photosynth. Res.* 130, 1–16. doi: 10.1007/s11120-016-0236-z
- Kim, D., Jeong, S. W., and Leo, C. Y. (2003). Antioxidant capacity of phenolic phytochemicals from various cultivars of plums. *Food Chem.* 81, 321–326. doi: 10.1016/S0308-8146(02)00423-5
- Kohli, S. K., Khanna, K., Bhardwaj, R., Abd\_Allah, E. F., Ahmad, P., and Corpas, F. J. (2019). Assessment of subcellular ROS and NO metabolism in higher plants: multifunctional signaling molecules. *Antioxidants* 8:641. doi: 10.3390/antiox8120641
- Kolbert, Z., Barroso, J. B., Brouquisse, R., Corpas, F. J., Gupta, K. J., Lindermayr, C., et al. (2019). A forty year journey: the generation and roles of NO in plants. *Nitric Oxide* 93, 53–70. doi: 10.1016/j.niox.2019.09.006
- Koprivova, A., Mugford, S. T., and Kopriva, S. (2010). *Arabidopsis* root growth dependence on glutathione is linked to auxin transport. *Plant Cell Rep.* 29, 1157–1167. doi: 10.1007/s00299-010-0902-0
- Lehotai, N., Kolbert, Z., Petó, A., Feigl, G., Ördög, O., Kumar, D., et al. (2012). Selenite-induced hormonal and signalling mechanisms during root growth of *Arabidopsis thaliana* L. *J. Exp. Bot.* 65, 5677–5687. doi: 10.1093/jxb/ers222
- Li, J., Zheng, B., He, Y., Zhou, Y., Chen, X., Ruan, S., et al. (2018). Antimony contamination, consequences and removal techniques: a review. *Ecotoxicol. Environ. Saf.* 156, 125–134. doi: 10.1016/j.ecoenv.2018.03.024
- Li, X., Yang, H., Zhang, C., Zeng, G., Liu, Y., Xu, W., et al. (2017). Spatial distribution and transport characteristics of heavy metals around an antimony mine area in central China. *Chemosphere* 170, 17–24. doi: 10.1016/j.chemosphere.2016.12.011
- Liu, T., and Qiu, K. (2018). Removing antimony from waste lead storage batteries alloy by vacuum displacement reaction technology. *J. Hazard. Mater.* 347, 334–340. doi: 10.1016/j.jhazmat.2018.01.017
- Mascia, T., Santovito, E., Gallitelli, D., Cillo, F. (2010). Evaluation of reference genes for quantitative reverse-transcription polymerase chain reaction normalization in infected tomato plants. *Mol. Plant Pathol.* 11, 805–816. doi: 10.3390/cells8080822
- Mendoza-Cózatl, D. G., Butko, E., Springer, F., Torpey, J. W., Komives, E. A., Kehr, J., et al. (2008). Identification of high levels of phytochelators, glutathione and cadmium in the phloem sap of *Brassica napus*. A role for thiol-peptides in the long-distance transport of cadmium and the effect of cadmium on iron translocation. *Plant J.* 54, 249–259. doi: 10.1111/j.1365-3113X.2008.03410.x
- Misra, H. P., and Fridovich, I. (1972). The role of superoxide anion in the autoxidation of epinephrine and a simple assay for superoxide dismutase. *J. Biol. Chem.* 247, 3170–3175.
- Mittler, R. (2002). Oxidative stress, antioxidants and stress tolerance. *Trends Plant Sci.* 7, 405–410. doi: 10.1016/s1360-1385(02)02312-9
- Murciego, A., García-Sánchez, A., Rodríguez-González, M. A., Pinilla, E., Toro, C., Cabezas, J., et al. (2007). Antimony distribution and mobility in topsoils and plants (*Cytisus striatus*, *Cistus ladanifer* and *Dirichia viscosa*) from polluted Sb-mining areas in Extremadura (Spain). *Environ. Pollut.* 145, 15–21. doi: 10.1016/j.envpol.2006.04.004
- Natasha, Shahid, M., Khalid, S., Dumat, C., Pierart, A., and Niazi, N. K. (2019). Biogeochemistry of antimony in soil-plant system: ecotoxicology and human health. *Appl. Geochem.* 106, 45–59. doi: 10.1016/j.apgeochem.2019.04.006
- Ngo, T. T., and Lenhoff, H. M. (1980). A sensitive and versatile chromogenic assay for peroxidase and peroxidase-coupled reactions. *Anal. Biochem.* 195, 389–397. doi: 10.1016/0003-2697(80)90475-3
- Ning, Z., Xiao, T., and Xiao, E. (2015). Antimony in the soil-plant system in an Sb mining/smeltering area of Southwest China. *Int. J. Phytoremediat.* 17, 1081–1089. doi: 10.1080/15226514.2015.1021955
- Noctor, G., Mhamdi, A., Chaouch, S., Han, Y., Neukemans, J., Marquez-García, B., et al. (2012). Glutathione in plants: an integrated overview. *Plant Cell Environ.* 35, 454–484. doi: 10.1111/j.1365-3040.2011.02400.x
- Okkenhaug, G., Zhu, Y. -G., Luo, L., Lei, M., Li, X., and Mulder, J. (2011). Distribution, speciation and availability of antimony (Sb) in soils and terrestrial plants from an active Sb mining area. *Environ. Pollut.* 159, 2427–2434. doi: 10.1016/j.envpol.2011.06.028
- Ortega, A., Garrido, I., Casimiro, I., and Espinosa, F. (2017). Effects of antimony on redox activities and antioxidant defence systems in sunflower (*Helianthus annuus* L.) plants. *PLoS One* 12:e0183991. doi: 10.1093/treephys/28.1.45
- Oxborough, K., and Baker, N. R. (1997). Resolving chlorophyll a fluorescence images of photosynthetic efficiency into photochemical and non-photochemical components – calculation of qP and Fv-/ Fm-, without measuring Fo-. *Photosynth. Res.* 54, 135–142. doi: 10.1023/A:1005936823310
- Pan, X., Zhang, D., Chen, X., Bao, A., and Li, L. (2011). Antimony accumulation, growth performance, antioxidant defense system and photosynthesis of *Zea mays*, in response to antimony pollution in soil. *Water Air Soil Pollut.* 215, 517–523. doi: 10.1007/s11270-010-0496-8
- Paoli, L., Fiorini, E., Munzi, S., Sorbo, S., Basile, A., and Loppi, S. (2013). Antimony toxicity in the lichen *Xanthoria parietina* (L.). *Th. Fr. Chemosphere* 93, 2269–2275. doi: 10.1016/j.chemosphere.2013.07.082
- Pérez-Sirvent, C., Martínez-Sánchez, M. J., Martínez-López, S., Bech, J., Bolan, N. (2012). Distribution and bioaccumulation of arsenic and antimony in *Dirichia viscosa* growing in mining-affected semiarid soils in southeast Spain. *J. Geochem. Explor.* 123, 128–135. doi: 10.1016/j.gexplo.2012.08.002
- Peško, M., Molnárová, M., and Fargašová, A. (2016). Response of tomato plants (*Solanum lycopersicum*) to stress induced by Sb (III). *Acta Environ. Univ. Comenianae* 24, 42–47. doi: 10.1515/aeuc-2016-0006
- Rajabpoor, S., Ghaderian, S. M., and Schat, H. (2019). Effects of antimony on enzymatic and non-enzymatic antioxidants in a metalcolous and a non-metalcolous population of *Salvia spinosa* L. *Plant Physiol. Biochem.* 144, 386–394. doi: 10.1016/j.plaphy.2019.10.011
- Rodríguez-Ruiz, M., Aparicio-Chacón, M. V., José, M. Palma, J. M., Corpas, F. J. (2019). Arsenate disrupts ion balance, sulfur and nitric oxide metabolisms in roots and leaves of pea (*Pisum sativum* L.) plants. *Environ. Exp. Bot.* 161, 143–156. doi: 10.1016/j.envexpbot.2018.06.028
- Sahay, S., and Gupta, M. (2017). An update on nitric oxide and its benign role in plant responses under metal stress. *Nitric Oxide* 67, 39–52. doi: 10.1016/j.niox.2017.04.011
- Shtangeeva, I., Bali, R., and Harris, A. (2011). Bioavailability and toxicity of antimony. *J. Geochem. Explorat.* 110, 40–45. doi: 10.1016/j.gexplo.2010.07.003
- Shtangeeva, I., Steinnes, E., and Lierhagen, S. (2012). Uptake of different forms of antimony by wheat and rye seedlings. *Environ. Sci. Pollut. Res. Int.* 19, 502–509. doi: 10.1007/s11356-011-0589-y
- Sharma, P., Jha, A. B., Dubey, R. S., and Pessarakli, M. (2012). Reactive oxygen species, oxidative damage, and antioxidative defense mechanism in plants under stressful conditions. *J. Bot.* 2012, 217037. doi: 10.1155/2012/217037



- Signorelli, S., Coitiño, E. L., Borsani, O., and Monza, J. (2014). Molecular mechanisms for the reaction between OH radicals and proline: insights on the role as Reactive Oxygen Species scavenger in plant stress. *J. Phys. Chem. B* 118, 37–47. doi: 10.1021/jp407773u
- Signorelli, S., Imparatta, C., Rodríguez-Ruiz, M., Borsani, O., Corpas, F. J., Monza, J. (2016). *In vivo* and *in vitro* approaches demonstrate proline is not directly involved in the protection against superoxide, nitric oxide, nitrogen dioxide and peroxyxynitrite. *Funct. Plant Biol.* 43, 870–879. doi: 10.1071/FP16060
- Singh, V. P., Singh, S., Kumar, J., and Prasad, S. M. (2015). Investigating the roles of ascorbate-glutathione cycle and thiol metabolism in arsenate tolerance in ridged *Luffa* seedlings. *Protoplasma* 252, 1217–1229. doi: 10.1007/s00709-014-0753-6
- Singleton, V. L., Salgues, M., Zaya, J., and Troudsale, E. (1985). Caftaric acid disappearance and conversion to products of enzymatic oxidation in grape must and wine. *Am. J. Enol. Viticul.* 36, 50–56.
- Smart, R. E., and Bingham, G. E. (1974). Rapid estimates of relative water content. *Plant Physiol.* 53, 258–260. doi: 10.1104/pp.53.2.258
- Spuller, C., Weigand, H., and Marb, C. (2007). Trace metal stabilization in a shooting range soil: mobility and phytotoxicity. *J. Hazard. Mater.* 141, 378–387. doi: 10.1016/j.jhazmat.2006.05.082
- Srivastava, R. K., Pandey, P., Rajpoot, R., Rani, A., and Dubey, R. S. (2014). Cadmium and lead interactive effects on oxidative stress and antioxidative responses in rice seedlings. *Protoplasma* 251, 1047–1065. doi: 10.1007/s00709-014-06143
- Sun, H., Yan, S. C., and Cheng, W. S. (2000). Interaction of antimony tartrate with the tripeptide glutathione. *Implication for its mode of action. Eur. J. Biochem.* 207, 5450–5457. doi: 10.1046/j.1432-1327.2000.01605.x
- Thipyapong, P., Hunt, M. D., and Steffens, J. C. (1995). Systemic wound induction of potato (*Solanum tuberosum*) polyphenol oxidase. *Phytochemistry* 40, 673–676. doi: 10.1016/0031-9422(95)00359-F
- Tschan, M., Robinson, B. H., and Schulin, R. (2008). Antimony uptake by *Zea mays* (L.) and *Helianthus annuus* (L.) from nutrient solution. *Environ. Geochem. Health* 30, 187–191. doi: 10.1007/s10653-008-9142-4
- Tschan, M., Robinson, B. H., and Schulin, R. (2009). Antimony in the soil–plant system—a review. *Environ. Chem.* 6, 106–115. doi: 10.1071/EN08111
- Vaculiková, M., Vaculik, M., Šimková, L., Fialov, I., Kochanová, Z., Sedláková, B., et al. (2014). Influence of silicon on maize roots exposed to antimony—Growth and antioxidative response. *Plant Physiol. Biochem.* 83, 279–284. doi: 10.1016/B978-0-12-799963-0.00007-1
- Valderrama, R., Corpas, F. J., Carreras, A., Fernández-Ocaña, A., Chaki, M., and Luque, F. et al. (2007). Nitrosative stress in plants. *FEBS Lett.* 581, 453–461. doi: 10.1016/j.febslet.2007.01.006
- Verbruggen, N., and Hermans, C. (2008). Proline accumulation in plants: a review. *Amino Acids* 35, 753–759. doi: 10.1007/s00726-008-0061-6
- Verma, S., and Dubey, R. S. (2003). Lead toxicity induces lipid peroxidation and alters the activities of antioxidant enzymes in growing rice plants. *Plant Sci.* 164, 645–655. doi: 10.1016/S0168-9452(03)00022-0
- Vernoux, T., Wilson, R. C., Seeley, K. A., Reichheld, J. P., Muroy, S., Brown, S., et al. (2000). The *ROOT MERISTEMLESS1/CADMIUM SENSITIVE2* gene defines a glutathione-dependent pathway involved in initiation and maintenance of cell division during postembryonic root development. *Plant Cell* 12, 97–110. doi: 10.1105/tpc.12.1.97
- Wang, Y., Loake, G. J., and Chu, C. (2013). Cross-talk of nitric oxide and reactive oxygen species in plant programmed cell death. *Front. Plant Sci.* 4:314. doi: 10.3389/fpls.2013.00314
- Warnken, J., Ohlsson, R., Welsh, D. T., Teasdale, P. R., Chelsky, A., and Bennett, W. W. (2017). Antimony and arsenic exhibit contrasting spatial distributions in the sediment and vegetation of a contaminated wetland. *Chemosphere* 180, 388–395. doi: 10.1016/j.chemosphere.2017.03.142
- Waszczak, C., Carmody, M., and Kangasjärvi, J. (2018). Reactive oxygen species in plant signaling. *Ann. Rev. Plant Biol.* 69, 209–236.
- Wellburn, A. R. (1994). The spectral determination of chlorophyll a and chlorophyll b, as well as total carotenoids, using various solvents with spectrophotometers of different resolution. *J. Plant Physiol.* 144, 307–313. doi: 10.1016/S0176-1617(11)81192-2
- Wen, B., Zhou, J., Zhou, A., Liu, C., and Li, L. (2018). A review of antimony (Sb) isotopes analytical methods and application in environmental systems. *Int. Biodeter. Biodegr.* 128, 109–116. doi: 10.1016/j.ibiod.2017.01.008
- Wilson, N. J., Craw, D., and Hunter, K. (2004). Antimony distribution and environmental mobility at an historic antimony smelter site, New Zealand. *Environ. Pollut.* 129, 257–266. doi: 10.1016/j.envpol.2003.10.014
- Xue, L., Ren, H., Li, S., Gao, M., Shi, S., Chang, E., et al. (2015). Comparative proteomic analysis in *Miscanthus sinensis* exposed to antimony stress. *Environ. Pollut.* 201, 150–160. doi: 10.1016/j.envpol.2015.03.004
- Xue, L., Ren, H., Li, S., Gao, M., Shi, S., Chang, E., et al. (2015). Comparative proteomic analysis in *Miscanthus sinensis* exposed to antimony stress. *Environ. Pollut.* 201, 150–160. doi: 10.1016/j.envpol.2015.03.004
- Xu, S., Guerra, D., Lee, U., and Vierling, E. (2013). S-nitrosogluthathione reductases are low-copy number, cysteine-rich proteins in plants that control multiple developmental and defense responses in Arabidopsis. *Front. Plant Sci.* 4:430. doi: 10.3389/fpls.2013.00430
- Yadav, S. K. (2010). Heavy metals toxicity in plants: an overview on the role of glutathione and phytochelatin in heavy metals stress tolerance of plants. *S. Afr. J. Bot.* 76, 167–179. doi: 10.1016/j.sajb.2009.10.007
- Zhang, C., Lu, C., Wang, Z., Feng, G., Du, E., Liu, Y., et al. (2018). Antimony enhances c-Myc stability in prostate cancer via activating CtBP2-ROCK1 signaling pathway. *Ecotoxicol. Environ. Saf.* 164, 61–68. doi: 10.1016/j.ecoenv.2018.07.070
- Zhang, F. Q., Wang, Y.-S., Lou, Z. P., and Dong, J. D. (2007). Effect of heavy metal stress on antioxidative enzymes and lipid peroxidation in leaves and roots of two mangrove plant seedlings (*Kandelia candel* and *Bruguiera gymnorrhiza*). *Chemosphere* 67, 44–50. doi: 10.1016/j.chemosphere.2006.10.007
- Zhou, J., Nyirenda, M. T., Xie, L., Li, Y., Zhou, B., Zhu, Y., et al. (2017). Mine waste acidic potential and distribution of antimony and arsenic in waters of the Xikuangshan mine, China. *Appl. Geochem.* 77, 52–61. doi: 10.1016/j.apgeochem.2016.04.010
- Zhou, X., Sun, C., Zhu, P., and Liu, F. (2018). Effects of antimony stress on photosynthesis and growth of *Acorus calamus*. *Front. Plant Sci.* 9:579. doi: 10.3389/fpls.2018.00579

**Conflict of Interest:** The authors declare that the research was conducted in the absence of any commercial or financial relationships that could be construed as a potential conflict of interest.

Copyright © 2020 Espinosa-Vellarino, Garrido, Ortega, Casimiro and Espinosa. This is an open-access article distributed under the terms of the Creative Commons Attribution License (CC BY). The use, distribution or reproduction in other forums is permitted, provided the original author(s) and the copyright owner(s) are credited and that the original publication in this journal is cited, in accordance with accepted academic practice. No use, distribution or reproduction is permitted which does not comply with these terms.



# Overexpression of *ZePrx* in *Nicotiana tabacum* Affects Lignin Biosynthesis Without Altering Redox Homeostasis

Alba García-Ulloa<sup>1</sup>, Laura Sanjurjo<sup>1</sup>, Sara Cimini<sup>2\*</sup>, Antonio Encina<sup>3</sup>,  
Romina Martínez-Rubio<sup>3</sup>, Rebeca Bouza<sup>4</sup>, Luis Barral<sup>4</sup>, Graciela Estévez-Pérez<sup>5</sup>,  
Esther Novo-Uzal<sup>6</sup>, Laura De Gara<sup>2</sup> and Federico Pomar<sup>1</sup>

<sup>1</sup> Departamento de Biología, Centro de Investigaciones Científicas Avanzadas, Universidade da Coruña, A Coruña, Spain,

<sup>2</sup> Unit of Food Science and Human Nutrition, Department of Science and Technology for Humans and the Environment, Campus Bio-Medico University, Rome, Italy, <sup>3</sup> Área de Fisiología Vegetal, Departamento de Ingeniería y Ciencias Agrarias, Universidad de León, León, Spain, <sup>4</sup> Grupo de Polímeros, Departamento de Física y Ciencias de la Tierra Escuela Universitaria Politécnica, Universidade da Coruña, Serantes, Ferrol, Spain, <sup>5</sup> Department of Mathematics, Universidade da Coruña, A Coruña, Spain, <sup>6</sup> Instituto Gulbenkian de Ciência, Oeiras, Portugal

## OPEN ACCESS

### Edited by:

Christian Lindermayr,  
Helmholtz Zentrum München,  
Germany

### Reviewed by:

Akiyoshi Kawaoka,  
Akita Jujo Chemicals Co., Ltd., Japan  
Yuree Lee,  
Seoul National University,  
South Korea

### \*Correspondence:

Sara Cimini  
s.cimini@unicampus.it

### Specialty section:

This article was submitted to  
Plant Physiology,  
a section of the journal  
Frontiers in Plant Science

**Received:** 20 March 2020

**Accepted:** 02 June 2020

**Published:** 26 June 2020

### Citation:

García-Ulloa A, Sanjurjo L,  
Cimini S, Encina A, Martínez-Rubio R,  
Bouza R, Barral L, Estévez-Pérez G,  
Novo-Uzal E, De Gara L and Pomar F  
(2020) Overexpression of *ZePrx*  
in *Nicotiana tabacum* Affects Lignin  
Biosynthesis Without Altering Redox  
Homeostasis.  
Front. Plant Sci. 11:900.  
doi: 10.3389/fpls.2020.00900

Class III plant peroxidases (Prxs) are involved in the oxidative polymerization of lignins. *Zinnia elegans* Jacq. Basic peroxidase (*ZePrx*) has been previously characterized as capable of catalyzing this reaction *in vitro* and the role in lignin biosynthesis of several of its *Arabidopsis thaliana* homologous has been previously confirmed. In the present work, *ZePrx* was overexpressed in *Nicotiana tabacum* to further characterize its function *in planta* with particular attention to its involvement in lignin biosynthesis. Since Prxs are known to alter ROS levels by using them as electron acceptor or producing them in their catalytic activity, the impact of this overexpression in redox homeostasis was studied by analyzing the metabolites and enzymes of the ascorbate-glutathione cycle. In relation to the modification induced by *ZePrx* overexpression in lignin composition and cellular metabolism, the carbohydrate composition of the cell wall as well as overall gene expression through RNA-Seq were analyzed. The obtained results indicate that the overexpression of *ZePrx* caused an increase in syringyl lignin in cell wall stems, suggesting that *ZePrx* is relevant for the oxidation of sinapyl alcohol during lignin biosynthesis, coherently with its S-peroxidase nature. The increase in the glucose content of the cell wall and the reduction of the expression of several genes involved in secondary cell wall biosynthesis suggests the occurrence of a possible compensatory response to maintain cell wall properties. The perturbation of cellular redox homeostasis occurring as a consequence of *ZePrx* overexpression was kept under control by an increase in APX activity and a reduction in ascorbate redox state. In conclusion, our results confirm the role of *ZePrx* in lignin biosynthesis and highlight that its activity alters cellular pathways putatively aimed at maintaining redox homeostasis.

**Keywords:** class III peroxidases, lignins, syringyl, secondary cell wall, redox homeostasis, RNA-Seq

## INTRODUCTION

Peroxidases (EC 1.11.1) are enzymes capable of oxidize many substrates using hydrogen peroxide ( $H_2O_2$ ) as co-substrate (De Gara, 2004; Oliva et al., 2009). Higher plants contain at least four types of peroxidases that exist as multigene families: glutathione peroxidase (EC 1.11.1.9), catalase (EC 1.11.1.7), ascorbate peroxidase (APX, class I peroxidase, EC 1.11.1.11), and class III peroxidases (Prxs, EC 1.11.1.17). Ascorbate peroxidase controls  $H_2O_2$  levels by oxidizing ascorbate in the first reaction of the ascorbate (ASC)–glutathione (GSH) cycle, a system that keeps  $H_2O_2$  levels under control (De Gara, 2004; Foyer and Noctor, 2011). Prxs are apoplastic and vacuolar plant peroxidases presenting a double catalytic-cycle, which allow them to both consume and produce reactive oxygen species (ROS; Chen and Schopfer, 1999; Zámocky and Obinger, 2010). Several reverse genetic studies, focused on the catalytic properties of these enzymes as well as on their specialized function, demonstrate that Prxs can be involved in a diverse range of functions (reviewed in Shigeto and Tsutsumi, 2016). The diverse functions of Prxs are accomplished through the oxidation of specific molecules such as lignin precursors during lignin polymerization (Sasaki et al., 2004; Gabaldón et al., 2006) and/or through the regulation of specific ROS levels (Kawaoka et al., 2003; Liszkay et al., 2003; Kim et al., 2008; Sundaravelpandian et al., 2013; Peters et al., 2017). The study of Prxs function is challenged by the numerous roles that one isoform can play in plants. Nevertheless, one of the aspects drawing more attention is Prx involvement in lignification (reviewed in Marjamaa et al., 2009).

Lignins, alongside with cellulose and xylan, are the main components of the secondary cell wall (Zhong and Ye, 2015). The biosynthesis of these three macromolecules is finely modulated during plant development and in response to environmental signals in order to accomplish a correct assembly of the secondary cell wall. Several transcription factors (TFs), mainly belonging to NAC and MYB families, are responsible for the regulation of secondary cell wall deposition (Zhong and Ye, 2014; Taylor-Teeples et al., 2015). Thanks to this joint control, changes in the biosynthesis of one of these components can be made up with changes in the biosynthesis of another one, keeping stable the properties of the cell wall (Mélida et al., 2015). Lignins are responsible of making the cell wall hydrophobic and resistant. They are complex and amorphous phenolic polymers, synthesized by oxidative polymerization of three precursors (*p*-coumaryl, coniferyl, and sinapyl alcohols) through a cross-linking reaction initiated by Prxs and laccases in the apoplast (Vanholme et al., 2010). This process increases the strength and rigidity of the cell walls thus with a positive impact on the plant responses to several environmental constraint conditions (Vanholme et al., 2010; Hamann, 2012). Studies performed on *Arabidopsis thaliana* L. mutants for Prx4, Prx52, and Prx72 demonstrated the participation of these enzymes in lignin biosynthesis, especially in the incorporation of syringyl groups to lignins in the interfascicular fibers of the stem (Herrero et al., 2013a; Fernández-Pérez et al., 2014, 2015). These three peroxidases shared features with the *Zinnia elegans* Jacq. basic

peroxidase (ZePrx; Herrero et al., 2013b), which has been previously proposed to catalyze the oxidation of monolignols in cells undergoing active lignification such as those of the xylem. It is also able to *in vitro* catalyze lignin precursor oxidative polymerization into molecules enriched in  $\beta$ -O-4 links (Ros Barceló et al., 2002; Gabaldón et al., 2005, 2006).

Due to the lack of ZePrx mutants or protocols for the stable transformation of *Z. elegans* plants, no further studies had been conducted until now to deepen into the function of ZePrx. The increase of our knowledge on lignification process, cell wall stiffening and cellular redox homeostasis has impact on several applicative aspects such as agronomy yield, biofuel production and plant resilience during environmental constraint conditions. In the present work, *Nicotiana tabacum* L. transgenic plants overexpressing ZePrx were obtained and characterized, in order to study the involvement of this enzyme in lignification *in planta* and the redox homeostasis in these overexpressing transgenic plants.

## MATERIALS AND METHODS

### Plant Material

All plants were kept under controlled conditions on a day/night cycle of 16/8 h at 25/18°C temperature in a growth chamber with white light ( $150 \mu\text{mol m}^{-2} \text{s}^{-1}$ ). *Z. elegans* cv. Envy were grown over sterile paper and collected six days after germination. *N. tabacum* plants were grown in sterilized TOPF (Plantaflor) substrate.

### RNA Extraction and cDNA Synthesis

Total RNA from *Z. elegans* hypocotyls and from *N. tabacum* leaves and stems was extracted using Aurum<sup>TM</sup> Total RNA Mini Kit (Bio-Rad) following the manufacturer's instructions. For cDNA synthesis with iScript<sup>TM</sup> cDNA Synthesis Kit (Bio-Rad), 200 ng of RNA were used following the manufacturer's instructions.

### ZePrx Cloning and Expression Vector Construction

ZePrx coding region (AJ880395.1) was amplified by PCR using the ZePrxCLO primers (Table 1) and *Pfu* DNA polymerase (Thermo Fisher Scientific). After purification, the PCR product was cloned into the *Hind*III – *Eco*RI site of the MCS of pJIT62 vector using a T4 ligase (Thermo Fisher Scientific). This vector was cloned into chemically competent *Escherichia coli* DH5 $\alpha$ . Positive colonies selected after screening on LB medium with 0.01% carbenicillin were confirmed by PCR with ZePrxCLO primers (Table 1). The *Kpn*I–*Xho*I fragment of this vector was purified and introduced into a pGreen II 0179 vector (Hellens et al., 2000a,b), that was cloned into chemically competent *E. coli* XL1 blue cells. Colonies were selected in LB medium supplemented with 0.005% kanamycin, 0.02% X-Gal and 1 mM IPTG and confirmed by PCR with B5 and B3 primers (Table 1). The final vector was sequenced using the primers in Table 1 in a genetic analyzer 3130xl (Applied Biosystems).

**TABLE 1** | Sequences of the different primers used for transgenic lines production.

Primer	Sequence	RE	Purpose
ZePrxCLOF	GAGAAAGCTTATGAGTTATCATAAGTCAAGTGGA	<i>Hind</i> III	Cloning of <i>ZePrx</i> , colony screening and sequencing
ZePrxCLOR	GAGAGAATTCTTAAGTGGGATTACCGCAAAGAG	<i>Eco</i> RI	
ZePrxSEC5	TGTGGTATCGTAAAGGTGG	–	Sequencing
ZePrxSEC3	ATGTCAACAATCCTGCAACG	–	
B5	GGTAACGCCAGGGTTTTCCAGT	–	Colony screening and sequencing
B3	CCCGGGCTGCAGGAATTCGAT	–	
ZePrxF	TCTTCCAAGAGGGAACATGG	–	Semiquantitative PCR
ZePrxR	CCGAGTGTGTGAGATCCTGA	–	
NtBTub1F	GAAGGAATGGACGAGATGGA	–	
NtBTub1R	TTCACCTTCGTCATCAGCAG	–	

Underlined sequences correspond with the restriction enzymes recognition sequences used for *ZePrx* cloning into *pJIT60*.

Chemically competent *Agrobacterium tumefaciens* AGL1 (Wise et al., 2006) were transformed simultaneously with pGreen II 0179 and pSoup plasmids (Hellens et al., 2000b). Two types of transformed *A. tumefaciens* were obtained: empty vector lines (EV), transformed with the pGreen II 0179 EV to obtain control plants and plant lines transformed with the pGreen II 0179 vector containing *ZePrx* gene under the control of CaMV 35S promoter to obtain overexpressing (OE) lines. Two independent OE lines were obtained: OE1 and OE2.

## N. tabacum Transformation

Surface sterilized seeds of *N. tabacum* cv. Petit Havana (SR1) were sowed on solid half strength MS medium supplemented with 1% sucrose. Leaf fragments of the *N. tabacum* plants were transformed as described in Clemente (2006). Transgenic seeds from self-pollinated plants were harvested and stored at 4°C. Resistance analysis was performed to identify T1 lines with only one insertion and T2 homozygous plants through a segregation analysis sowing seeds in a half strength MS medium with hygromycin. Briefly, in order to select transgenic lines with one insertion, we used only T1 lines that showed a 3:1 ratio (resistant:sensible) in the segregation analysis (Bent, 2006; Cosio et al., 2017). Transgenic seeds were harvested and stored at 4°C. Sterilized seeds were sowed in half strength MS solid medium supplemented with 0.1% sucrose and 0.005% hygromycin B. The number of resistant and sensitive plants was determined three weeks after sowing.

## ZePrx Expression Levels

Leaves from three weeks-old and stems from six weeks-old EV and OE plants were collected, frozen in liquid nitrogen and stored at –80°C until used. The expression of *ZePrx* (target gene: AJ880395.1) and *NtBTub1* housekeeping gene (reference gene: U91564.2) (Schmidt and Delaney, 2010) were analyzed by using NZYTaq DNA Polymerase (NZYTech) and *ZePrx* and *NtBTub1* primer pairs (Table 1).

## Growth and Development

The stem of *N. tabacum* transgenic plants was measured every three days from the emergence of the first true leave until the opening of the first flower. Its reproductive development was

also registered classifying the plants in five categories: vegetative, pre-bloom, budding, flowering and open flower.

## Cell Wall Protein Extraction and Peroxidase Activity

Stems from six and eight weeks-old plants were collected and used fresh for protein extraction. Stems were cut in 0.5 cm long fragments, vacuum infiltrated with 50 mM Tris-acetate 1 M KCl pH 5.0 buffer and centrifuged to collect the intercellular wash fluid (IWF). The IWF was recovered according to Ros Barceló et al. (2002, 2007). This protocol allows the extraction of cell wall components with an irrelevant cytoplasmic contamination (Ros Barceló et al., 2002, 2007; De Pinto and De Gara, 2004). In brief, leaf tissue was homogenized in 50 mM Tris-HCl 1 M KCl 1 mM EDTA pH 7.5 buffer at 4°C. After centrifugation, the supernatant was recovered. All protein samples were dialyzed overnight against their extraction buffer without KCl or EDTA using cellulose membranes with a 14 kDa pore size (Sigma). The protein samples were stored at –20°C until analyzed.

Peroxidase activity was assayed spectrophotometrically at 25°C in a reaction buffer containing 50 mM Tris acetate buffer pH 5.0 for the IWF samples and 50 mM Tris-HCl buffer pH 7.5 for the symplastic ones. The substrates assayed were 1 mM 4-methoxy- $\alpha$ -naftol (4MN) ( $\epsilon_{593} = 21 \mu\text{M}^{-1} \text{cm}^{-1}$ ), 50  $\mu\text{M}$  syringaldazine ( $\epsilon_{530} = 27 \mu\text{M}^{-1} \text{cm}^{-1}$ ), 100  $\mu\text{M}$  coniferyl alcohol ( $\epsilon_{291} = 9.75 \mu\text{M}^{-1} \text{cm}^{-1}$ ) and 100  $\mu\text{M}$  sinapyl alcohol ( $\epsilon_{271} = 4.14 \mu\text{M}^{-1} \text{cm}^{-1}$ ). In all the assays 500  $\mu\text{M}$  H<sub>2</sub>O<sub>2</sub> was used as co-substrate. Total proteins were quantified using Quick Start Bradford (Bio-Rad).

SDS-PAGE gels were prepared according to Laemmli (1970) and proteins were stained with the PlusOne Silver Staining Kit (Pharmacia). Isoelectrofocusing gels were prepared according to Wrigley (1971), migration was performed as described by López-Serrano et al. (2004) and peroxidases were revealed with 4-methoxy- $\alpha$ -naphthol (Ferrer et al., 1990).

## Histochemical Analyses

Cross sections were manually obtained at 1 cm from the base of stem from *N. tabacum* plants. Wiesner staining was performed according to Pomar et al. (2002). For Mäule



staining (Strivastava, 1966) the stem cross sections were vacuum infiltrated 5 min in  $\text{KMnO}_4$  1%, rinsed 2 min in HCl 37%, stained with 0.5 M  $\text{NH}_3$ , washed with distilled water and photographed. A preliminary analysis allowed us to define 5–6 weeks after sowing the starting of lignification of the secondary xylem (data not shown).

## Cell Wall Isolation and Characterization

The stem fragments from IWF extraction were homogenized with 50 mM Tris-HCl, 1 M KCl, 1 mM EDTA, pH 7.5 buffer at 4°C. After centrifugation, the pellet was dried at 60°C and, then, milled in a Mini BeadBeater (Biospec Products). The material was washed with 1% Triton X-100 (five times), distilled water (twice), 70% ethanol (once), and 96% ethanol (four times). The pellet was rinsed twice in diethyl ether and dried at 37°C for 48 h (Espiñeira et al., 2011).

Lignin content of the cell walls was determined using the acetyl bromide method. Briefly, 3 mg of cell walls were mixed with 500  $\mu\text{L}$  of acetyl bromide 2.33 M in acetic acid and kept at 70°C for 30 min. NaOH was added to a final concentration of 0.2 N and the final volume was adjusted to 10 mL with acetic acid. Finally, the absorbance at 290 nm was determined and a 20.09  $\text{g}^{-1} \text{cm}^{-1}$  factor was used for lignin quantification (Iiyama and Wallis, 1988).

Lignin composition was studied by thioacidolysis (Novo-Uzal et al., 2009), adding 0.5 mg of tetracosane to each sample as an internal standard. We used a Thermo Finnigan Trace GC gas chromatograph with a DB-XLB, J&W column (60 m length  $\times$  0.25 mm internal diameter) and a Thermo Finnigan Polaris Q mass spectrometer. Mass spectra were recorded at 70 eV. Quantification was performed as described in Yue et al. (2011).

The carbohydrate composition of the cell walls, cellulose, uronic acid sugars and neutral sugars, was determined as described in Mérida et al. (2015). Cell walls were fractioned with KOH extractions (0.1 and 4 N) and total sugar content in these fractions and digestion samples was determined by the phenol-sulfuric method as described in Rebaque et al. (2017). Xyloglucan content was determined on the KOH fractions by iodine sodium sulfate assay (Kooiman, 1960).

Fourier transform infrared spectra (FTIR) of the cell walls were recorded with a Bruker Vector 22 (Bruker Optics).

## Mechanical Tests

The stems of eight weeks-old plants were divided in four segments. Each was subjected to tensile tests performed using a 5566 series Instron universal testing machine (maximum load = 500 N, speed = 0.005–500  $\text{mm min}^{-1}$ ,  $l = 1135$  mm, accuracy =  $\pm 0.01\%$ ). All the assays were performed with a displacement speed of  $\text{mm min}^{-1}$ . Tension ( $\sigma$ ) and deformation ( $\epsilon$ ) were used to obtain  $\sigma = \sigma(\epsilon)$  curves for each segment.

## Analysis of Hydrogen Peroxide and Redox Systems

Hydrogen peroxide was measured in EV and OE plants according to potassium iodide (KI) method (Junglee et al., 2014).

Briefly, 0.1 g of leaves were collected and quickly grounded in liquid nitrogen and homogenized with 0.5 ml of 0.1% cold trichloroacetic acid. After centrifugation at maximum speed for 15 min, 0.25 ml of the supernatant were mixed with 0.25 ml of 10 mM potassium phosphate buffer (pH 7.0) and 0.5 ml of KI 1M. The samples were incubated for 15 min at room temperature and then the absorbance at 350 nm was measured.  $\text{H}_2\text{O}_2$  levels of extracts were determined based on a  $\text{H}_2\text{O}_2$  standard curve.

Ascorbate and GSH were extracted as reported in Ferrer et al. (2018). Approximately 0.3 g of leaves were collected from three weeks-old *N. tabacum* plantlets and grinded in liquid nitrogen. The pulverized tissue was homogenized with six volumes of 5% metaphosphoric acid at 4°C. The homogenate was centrifuged at 20,000 g for 15 min at 4°C and the supernatant used for the determination of levels and redox states as described in De Pinto et al. (1999). Ascorbate and GSH levels were expressed as  $\text{nmol mg}^{-1}$  protein.

For the enzymatic activities, leaves from EV and ZePrx OE lines were ground in liquid nitrogen and homogenized at 4°C in six volumes of 50 mM Tris-HCl (pH 7.5), added with 0.05% (W/v) cysteine, 0.1% (W/v) BSA and 1 mM ASC. The homogenate was centrifuged at 20,000 g for 15 min at 4°C and the supernatant was collected and analyzed by spectrophotometry. The activities of ASC peroxidase (APX) (L-ASC:  $\text{H}_2\text{O}_2$  oxidoreductase, EC 1.11.1.11), DHAR (GSH: dehydroascorbate oxidoreductase, EC 1.8.5.1) and GR (NADPH:GSH disulfide oxidoreductase, EC 1.6.4.2) were determined as previously described (Ferrer et al., 2018).

Non-denaturing-PAGE (protein extraction, gel preparation and staining) was carried out as described in Locato et al. (2008).

## RNA-Seq Analysis

Total RNA from 6 weeks-old stems was extracted using Aurum<sup>TM</sup> Total RNA Mini Kit (Bio-Rad) following the manufacturer's instructions. RNA concentration and quality were checked using a Bioanalyzer 2100 (Agilent Technologies). Only samples with a RIN over seven were used.

The RNA-Seq analyses were performed by Macrogen Inc. (Korea Republic). A library was constructed for each biological sample (a total of six) using the TruSeq RNA Sample Prep v2 (Illumina) according to the manufacturer's instructions. The paired-end sequencing was conducted in an Illumina HiSeq 2500 sequencer with the TruSeq SBS v4 (Illumina) kit.

Data quality was assessed with the software FastQC v0.11.5. The sequences were trimmed using the SLIDINGWINDOW option of Trimmomatic 0.32 (Bolger et al., 2014). Trimmed sequences were aligned to the reference genome (Edwards et al., 2017) with the software HISAT2 v2.0.5 (Kim et al., 2015) and the transcripts were assembled with StringTie v1.3.3b (Pertea et al., 2015). The abundance of each transcript was determined with the  $-e$  option of StringTie (Pertea et al., 2016).

## rt-qPCR

One microgram of RNA was used for cDNA synthesis with iScript<sup>TM</sup> cDNA Synthesis Kit (Bio-Rad), following the manufacturer's instructions. The amplification was performed with a FastStart SYBR Green Master mix (Roche). Specific

primers at 0.3  $\mu$ M concentration and 125 ng of cDNA were used for rt-qPCR reaction under the following conditions: 10 min at 95°C, 40 cycles of 30 s at 95°C, 30 s at 55°C, 1 min at 72°C and a final extension of 5 min at 72°C. The analyzed genes and the primers used are depicted in **Table 2**.

## Statistical Analysis

At least three biological replicates for each analysis have been considered. Statistical analysis was performed using SPSS v17.0. Levene test was used to check the homogeneity of variances. ANOVA test was performed to check differences among OE and EV lines. Kruskal–Wallis test was the chosen alternative when ANOVA data requirements were not met. Finally, Tukey or Dunnett *post hoc* tests were used to check for homogenous subsets. In peroxidase activity assays we used the moment of sowing as a random factor, since the effect of this variable was found to be significant.

For FTIR analysis, 10 biological replicates were analyzed. The spectra were baselined corrected and normalized with the OPUS 5.5 (Bruker) software. SPSS v17.0 was used for principal component analysis and the R v3.5.1 package to perform a FANOVA with the FANOVA and *fda.usc* functions.

The RNA-Seq analysis of differentially expressed genes (DEG) was performed using R Bioconductor after transforming and normalizing the abundance values with the *preprocessCore* R library. Only genes with an absolute value of fold change over two and a *p*-value under 0.05 were considered as DEGs. These genes were grouped according to their expression profile using a hierarchical cluster (Euclidean distance and whole linkage). We performed a Gene Ontology (GO) Enrichment Analysis on all the genes with a *p*-value under 0.05 using the PANTHER enrichment analysis tool (Mi et al., 2019). A Fisher test was performed using a Benjamini–Hochberg False Discovery Rate correction with a 0.05 cut-off value. We used the REVIGO tool in order to eliminate redundant categories (Supek et al., 2011). We analyzed separately upregulated and downregulated genes.

## RESULTS

### Characterization of Overexpressing ZePrx Transgenic Lines

#### Overexpressing ZePrx Transformed Lines Accumulated High Level of an Active Protein

*N. tabacum* plants were transformed with the ZePrx coding sequence under the control of the strong and constitutive CaMV35S promoter and eleven stable independent transformed lines were obtained. The expression of ZePrx was confirmed both in stems and leaves. Semi-quantitative rt-PCR analysis performed on stem and leaves revealed that ZePrx gene expression was higher in most of the OE compared to EV lines where the ZePrx gene expression was undetectable (**Supplementary Figures S1A,B**). Two OE lines (named 2.15 and 7.2) and two EV lines (10.3 and 15.14) were selected and further characterized. In the following results we present the mean value for EV lines, as they showed a similar behavior.

Since ZePrx has been reported to catalyze the last step of lignin biosynthesis (Gabaldón et al., 2005), the impact of its overexpression was firstly investigated in the stem, an organ in which the lignification is pivotal, especially during its secondary growth. At this purpose, two developmental stages have been considered for subsequent analysis based on direct observation of the plants growing in our experimental conditions: six weeks-old plants, when stems are starting their secondary growth, and eight weeks-old plants, when secondary growth has already occurred and stems are widely lignified.

ZePrx protein presence in stems collected from EV and OE lines at six weeks-old developmental stage was confirmed by SDS-PAGE and isoelectrofocusing. Protein separation by SDS-PAGE showed the presence of an additional band, of approximately 30 kDa, in the apoplastic fluid of OE lines (**Figure 1A**). Eight weeks-old plants showed the same protein and isoenzyme pattern (data not shown). The presence of active ZePrx protein in OE lines was confirmed by isoelectrofocusing stained for Prx activity (**Figure 1B**).

**TABLE 2** | Genes analyzed through qPCR.

Gene	ID	Primer	Sequence	Efficiency (%)
PAL	Nitab4.5_0000582g0180	NtPALF NtPALR	GGGCATGGTCCACTAACACT CTTGCTCACAGCGGTTGATA	93
MYB15	Nitab4.5_0006658g0010	NtMYB15F NtMYB15R	GCTGGTGCCCATAGTACCTC TGCGAGTTCTCTTGCTGATG	92
CesA4	Nitab4.5_0002389g0020	NtCesA4F NtCesA4R	CTCATCCCAACCAACTCTCT AAGAGAGGACCCCATGAACC	90
GT43	Nitab4.5_0000669g0220	NtGT43F NtGT43R	AATTGAGGGATTGGGACAT ATGCCACCCATAACTTCAG	93
$\beta$ -Tub1	U91564.2	NtBTub1F NtBTub1R	GAAGGAATGGACGAGATGGA TTCACCTTCGTATCAGCAG	100
Actin	AB158612	NtActF NtActR	GGCATTGCAGATCGTATGAG CCTTGATCTTCATGCTGCTG	97

ID, identification code in the annotation of *N. tabacum* genome (Edwards et al., 2017) or accession in the NCBI database.  $\beta$ -Tub1 (Schmidt and Delaney, 2010) and actin (Duwadi et al., 2015) were used as reference genes.

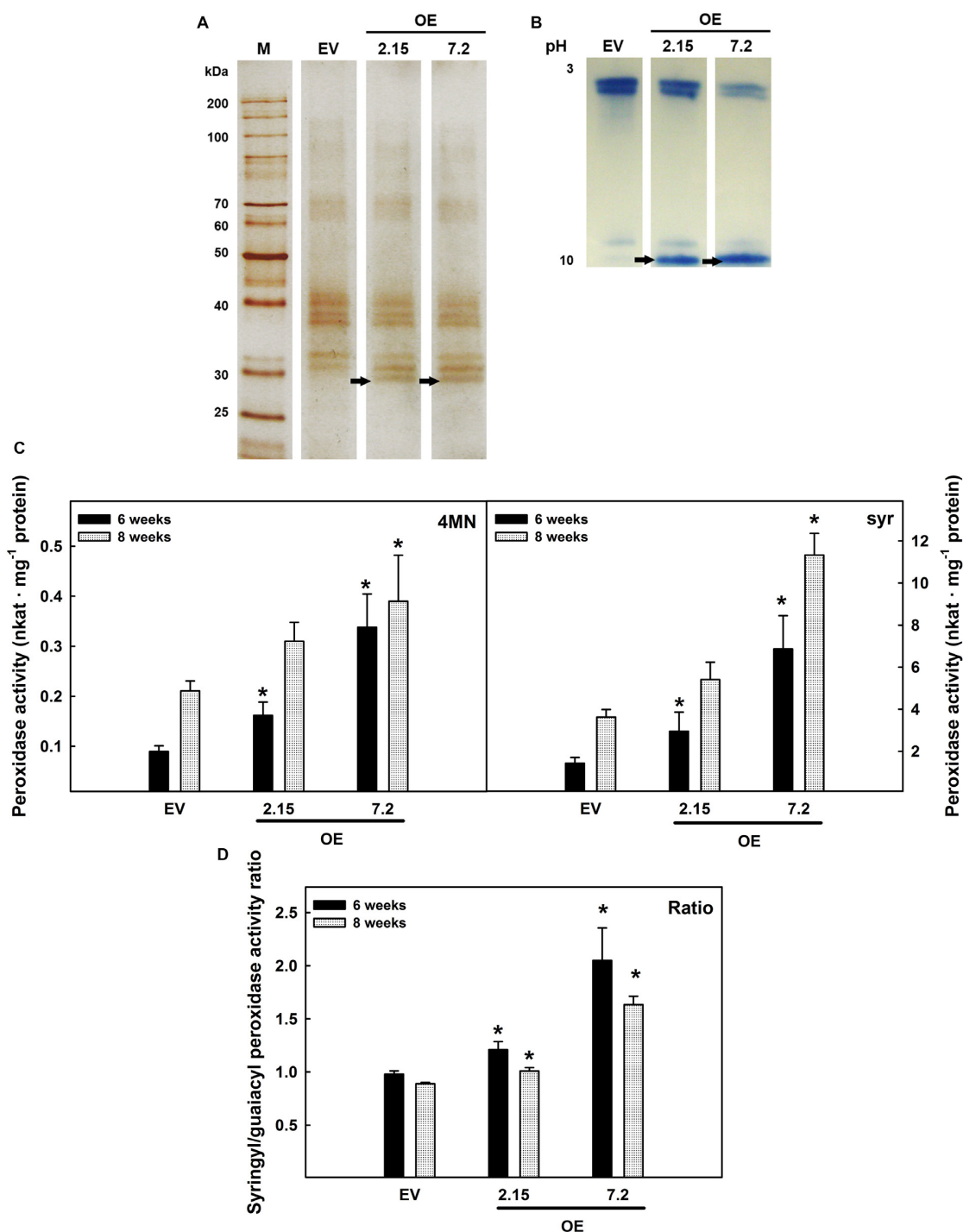


**FIGURE 1 |** ZePrx detection and peroxidase activity in the intercellular wash fluid from stems. **(A)** SDS-PAGE gels and **(B)** Isoelectrofocusing gels of proteins from the apoplast of the stems of 6 weeks-old *N. tabacum* transgenic plants. EV, empty vector; OE, *ZePrx* overexpressing lines. Arrows signal the extra band corresponding to the presence of ZePrx. **(C)** Peroxidase activity on the apoplastic fluid of six and eight weeks-old stems of *N. tabacum* transgenic plants. Total peroxidase activity was determined using 4-methoxy- $\alpha$ -naphthol (4MN) and syringyl-peroxidase activity, with syringaldazine (syr). **(D)** Ratio S/G, between the peroxidase activity measured with sinapyl alcohol (syringyl) and coniferyl alcohol (guaiacyl). The figure shows the mean and standard error for each of the lines. EV, empty vector; OE, *ZePrx* overexpressing lines; Con Alc, coniferyl alcohol; Con Ald, coniferaldehyde; Sin Alc, sinapyl alcohol; Sin Ald, sinapaldehyde. Asterisks (\*) indicate which OE lines were found to be significant different from the control in a Dunnett *post hoc* test at 0.05 level of significance. *n* = 3 for each line. EV is the mean of four EV lines (*n* = 12).

An isoelectric point close to 10 that corresponds to basic peroxidases characterized this additional band. The size and the isoelectric point of this additional protein detected in the OE lines were coherent to those previously determined for ZePrx (Gabaldón et al., 2005).

### ZePrx Overexpression Caused an Increase in Stem Peroxidase Activity but Did Not Have any Effects on Development

The peroxidase activity in the IWF obtained from stem of six and eight weeks-old plants was measured using four different substrates: 4MN and syringaldazine, synthetic substrates, as well as coniferyl and sinapyl alcohol, two lignin building blocks. The peroxidase activity measured using 4MN substrate (which measures the total peroxidase activity) and syringaldazine (which measures the so-called S-peroxidase activity) was significantly increased in the IWF of both OE lines at six-weeks-old and at eight weeks-old stems in OE 7.2 line (Figures 1C,D). In both cases, the peroxidase activity measured in OE 7.2 line was higher than that measured in 2.15 OE line (Figure 1C). This behavior agrees with the ZePrx overexpression level detected in the two transgenic lines. The ratio between the peroxidase activity measured using sinapyl alcohol (syringyl activity) and coniferyl alcohol (guaiacyl activity) was also analyzed in order to verify if the overexpression of a ZePrx affected it. This ratio, referred as sinapyl/guaiacyl (S/G ratio) gives information about the type of lignin precursors that the peroxidases are able to oxidize, since not all the Prxs are capable of oxidizing sinapyl alcohol (Sasaki et al., 2004). Both OE lines showed a higher S/G activity ratio when compared to EV lines (Figure 1D).

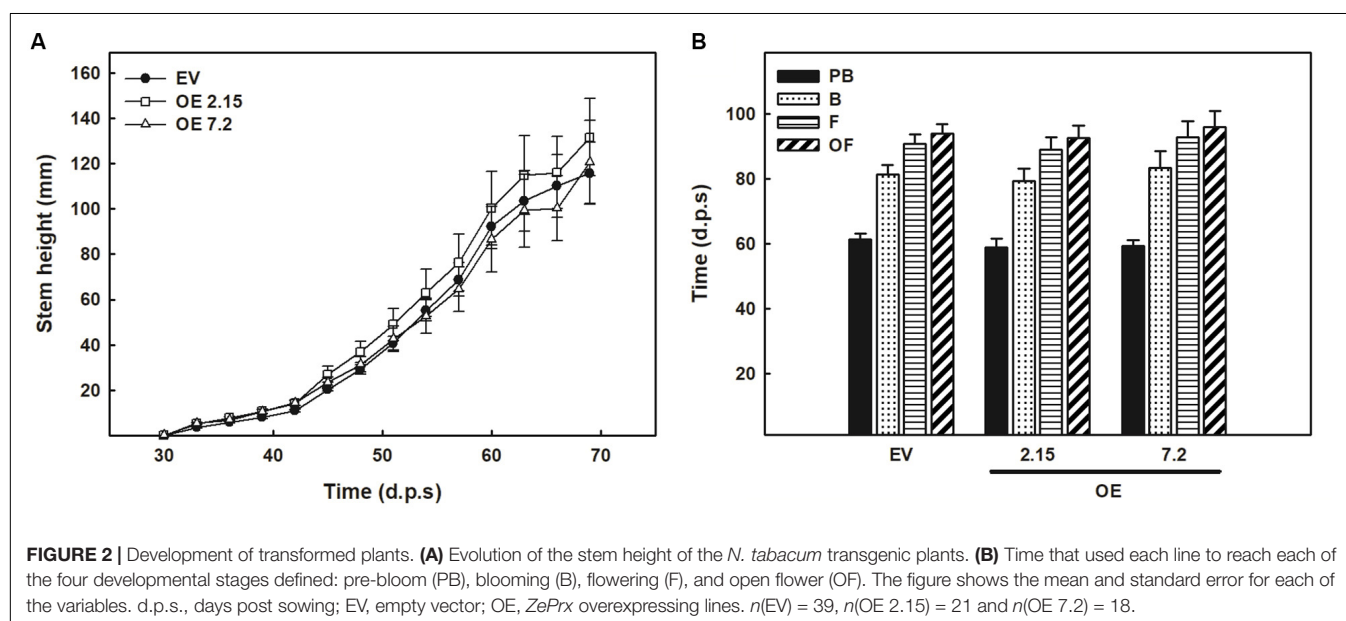
OE and EV lines did not show any differences in stem height during its vegetative growth (Figure 2A). Moreover, no differences in the time needed to reach different stages of floral development were evident between OE and EV lines (Figure 2B).

### Redox Homeostasis in OE Lines Required the Involvement of APX

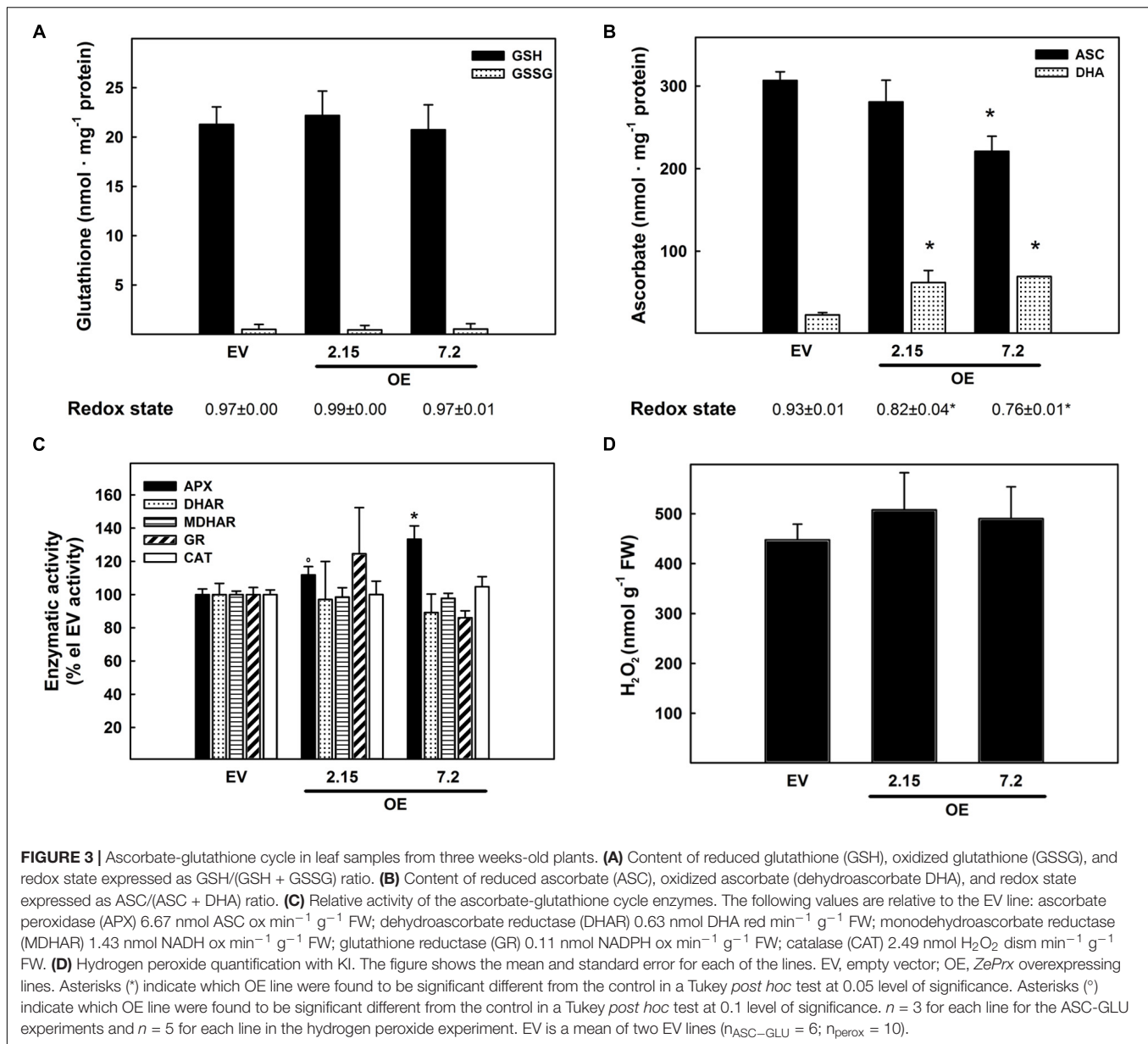
Since it is well known that the diverse peroxidase activities can facilitate opposite reactions in plants, such as generation and scavenging of ROS thus affecting plant homeostatic capacity, the effects of ZePrx overexpression on antioxidative systems and  $H_2O_2$  content were investigated.

The effects of ZePrx overexpression on the ASC-GSH cycle was analyzed by measuring the content of these two antioxidants, their relative redox state and the activities of the enzymes involved in this cycle. The activity of catalase (CAT) was also measured. All these parameters were monitored in the leaves (see Materials and Methods), which also overexpressed ZePrx (Supplementary Figure S1C) and where ASC-GSH cycle plays a pivotal role for maintaining cellular homeostasis (De Gara et al., 2010). Leaves did not show any statistically significant difference in the content of the reduced (GSH) and oxidized forms (GSSG) of glutathione between the analyzed lines (Figure 3A). The content of total ascorbate pool was also not changed between EV and OE lines but an increase in the content of the oxidized form, dehydroascorbate (DHA), and a decrease in the content of the reduced form, ASC, was observed in the two OE lines compared to EV lines. Therefore, a decrease in the ascorbate redox state occurred in OE plants (Figure 3B). Consistently, the activity of APX, the first enzyme of the ASC-GSH cycle controlling  $H_2O_2$  levels by using ascorbate as reducing agent, was significantly higher in the two OE lines than in the EV lines (Figure 3C). None of the other ASC-GSH cycle enzymes as well as CAT were significantly altered in the transformed lines (Figure 3C).

To check whether the overexpressed ZePrx was, itself, responsible for the increased ASC oxidation in the OE lines, the pattern of the peroxidases able to use ASC as electron donor was analyzed by non-denaturing PAGE. The absence of an extra band in the APX isoenzyme profile of OE lines compared with EV ones (Supplementary Figure S2), confirmed that the rise in ASC







oxidation and APX activity was not directly due to *ZePrx* activity. To get deeper insights into redox impairment putatively due to *ZePrx* overexpression, the H<sub>2</sub>O<sub>2</sub> content was also measured in the leaves. The increased observed in H<sub>2</sub>O<sub>2</sub> content in OE lines was not statistically significant (Figure 3D).

### ***ZePrx* Overexpression Caused Few Changes in Cell Wall Composition**

As a first approach to study the changes induced in cell wall composition by *ZePrx* overexpression, FTIR analysis was used. This technique offers global information of cell wall composition by an infrared-spectrum (see section “Materials and Methods”). The obtained data did not show relevant differences in OE and EV spectra when statistically analyzed (Figures 4A–C). However,

since small changes in specific cell wall components are hard to be detected by FTIR analysis, lignin deposition and carbohydrates composition of cell wall were analyzed in EV and OE lines. The total lignin content was measured by acetyl bromide method. EV and OE lines showed no statistically significant differences in lignin content in six weeks-old stems, where the lignin content was about 70 μg mg<sup>-1</sup> cell wall, and in eight weeks-old stems, with lignin values around 87 μg mg<sup>-1</sup> cell wall (Table 3). The absence of overall changes in lignin deposition was also confirmed through histochemical analysis that did not show differences between EV and OE lines on the amount and/or distribution of cinnamaldehydes (Wiesner staining) and syringyl lignins (Mäule staining). These latest tests also showed that vascular structure was not affected by the overexpression of *ZePrx* (Supplementary Figure S3).

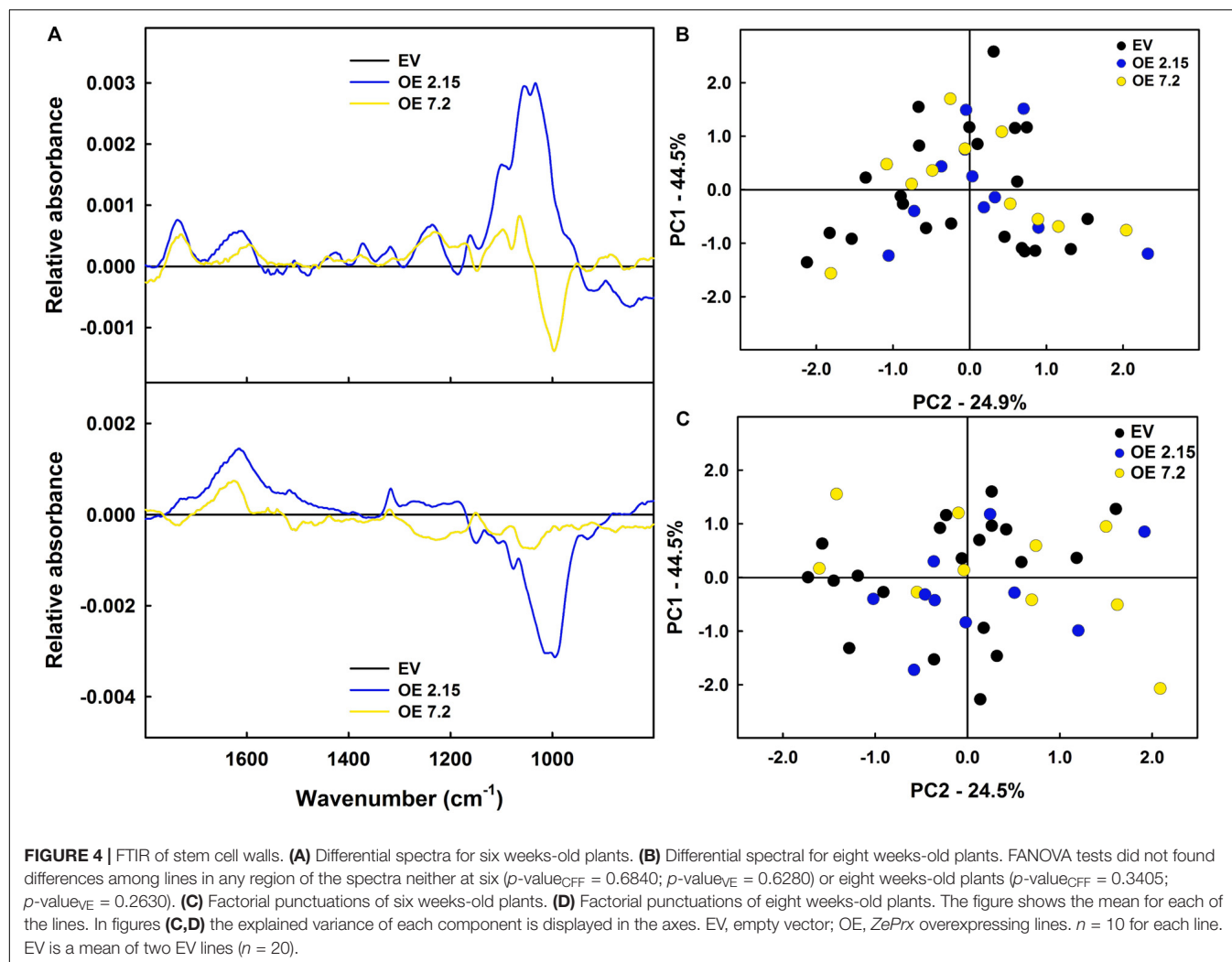


**TABLE 3 |** Lignin quantification and composition of the stems of *N. tabacum* transgenic plants.

Line	Lignin ( $\mu\text{g mg}^{-1}$ cell wall)	Monomeric composition (%)				S/G ratio
		Con Alc	Con Ald	Sin Alc	Sin Ald	
6 weeks-old stems						
EV	71.51 $\pm$ 6.49	45.57 $\pm$ 1.29*	2.09 $\pm$ 0.20	49.17 $\pm$ 1.43*	2.93 $\pm$ 0.24	1.11 $\pm$ 0.06*
OE 2.15	71.17 $\pm$ 4.85	45.74 $\pm$ 1.87*	2.20 $\pm$ 0.31	48.73 $\pm$ 2.71*	3.33 $\pm$ 0.79	1.09 $\pm$ 0.09*
OE 7.2	69.93 $\pm$ 1.40	43.94 $\pm$ 0.98*	2.08 $\pm$ 0.25	50.91 $\pm$ 1.43*	3.08 $\pm$ 0.20	1.18 $\pm$ 0.06*
8 weeks-old stems						
EV	87.40 $\pm$ 4.53	42.38 $\pm$ 0.28*	1.53 $\pm$ 0.06	53.66 $\pm$ 0.34*	2.43 $\pm$ 0.44	1.28 $\pm$ 0.01*
OE 2.15	86.43 $\pm$ 5.63	42.09 $\pm$ 0.39*	1.55 $\pm$ 0.07	53.89 $\pm$ 0.41*	2.47 $\pm$ 0.16	1.29 $\pm$ 0.02*
OE 7.2	87.98 $\pm$ 12.16	39.78 $\pm$ 1.00*	1.47 $\pm$ 0.07	56.49 $\pm$ 0.79*	2.26 $\pm$ 0.26	1.43 $\pm$ 0.06*

Lignin quantification through acetyl bromide method and monomeric composition determined by thioacidolysis. The mean and standard error values are provided. EV, empty vector; OE, ZePrx overexpressing lines; Con Alc, coniferyl alcohol; Con Ald, coniferaldehyde; Sin Alc, sinapyl alcohol; Sin Ald, sinapaldehyde. Asterisks (\*) indicate which OE lines were found to be significantly different from the control in a Dunnet post hoc test at 0.05 level of significance.  $n = 3$  for each line. EV is a mean of 2 EV lines ( $n = 6$ ).

Lignin composition was more in depth studied by thioacidolysis in order to determine the percentage of lignin derived from coniferyl alcohol, coniferaldehyde, sinapyl alcohol and sinapaldehyde in six and eight weeks-old stems.

In addition, the S/G ratio was calculated to check for differences in the proportion of syringyl to coniferyl units in the lignins characterizing OE and EV lines (Table 3). While there were no changes in lignin composition in six weeks-old plants, an

increase in lignin derived from sinapyl alcohol was found at 8 weeks-old in the OE 7.2 line and, consequently, an increase in S/G ratio (Table 3).

The analysis of the cell wall was extended to carbohydrate composition in OE and EV lines stems of eight weeks-old plants, a developmental stage in which there were significant changes in lignin composition in OE 7.2 line. Most of the monosaccharides present in cell walls showed no differences among lines. However, there was a significant increase in the glucose content in the OE 7.2 line (Figure 5A). In cell wall, glucose is present in two main polysaccharides: cellulose and hemicelluloses. Therefore, the content of these two polysaccharides was analyzed. Neither cellulose content (Figure 5B) nor hemicellulose content and distribution (Figure 5C) revealed significant differences among EV and OE lines. Since xyloglucan is the hemicellulose with the highest glucose content, xyloglucan content in the hemicellulose fractions was also measured but no differences were observed (Figure 5D).

### Cell Wall Properties Were Not Affected by ZePrx Overexpression

Changes in cell wall composition can alter cell wall mechanical properties. For this reason, a tensile test measuring elasticity (E-modulus), tensile strength and deformation, was performed in eight weeks-old stems of the EV and OE 7.2 lines (Figures 6A–C). For these experiments the OE 7.2 line was selected since it has a higher peroxidase activity compared with OE 2.5 line and also a significant modification of the cell wall composition. No differences were observed in the E-modulus, the tension nor the deformation that the stems can bear between EV and OE 7.2 lines (Figures 6A–C).

### ZePrx Overexpression Caused Changes in the Secondary Cell Wall Biosynthesis Network

An RNA-Seq analysis was performed on six weeks-old stems in order to further deepen in the impact of ZePrx overexpression on the overall plant metabolism. The OE 7.2 line was again selected for this analysis along with the EV 15.14 line. 781 genes showed a significant change in *fc* ( $p$ -value < 0.05 and a  $fc \geq |1|$ ). 354 of these genes were downregulated and 427 upregulated (Supplementary Table S1). An enrichment analysis has been performed in order to identify the GO categories overrepresented in both groups (Figure 7). These results showed that OE 7.2 line had an upregulation of genes related to RNA modification and different metabolic processes (Figure 7A) and a downregulation of genes related to cell wall biosynthesis, both carbohydrates and lignin (Figure 7B).

We enlarge the analysis by including DEGs with a bigger change in their expression ( $fc > |2|$ ). From this analysis have emerged 22 DEGs (18 downregulated and 4 upregulated) (Figure 8A and Supplementary Table S2). Through a hierarchical clustering, it was possible to divide the 22 DEGs into three groups (Figure 8A). The first group includes genes that code for proteins involved in secondary cell wall biosynthesis. All these genes were repressed in the OE line.

A phenylalanine ammonio lyase (PAL) and a laccase, both involved in lignins biosynthesis; two cellulose synthase isoforms (CesA4 and CesA7) and a COBRA-like protein (COBL4), responsible for secondary cell wall cellulose biosynthesis; two glycosyltransferases (GT43 and GT8) and three proteins with a DUF579 domain (two isoforms of a IRX15L protein and a GUX protein), contributing to xylan biosynthesis; an arabinogalactan protein fasciclin-like that keeps cell wall structure; and four proteins related to cell death (a germin-like protein, a CaM-binding protein, a nepenthesin-like protein and a peptidoglycan binding protein with a LysM domain). The other two groups contained genes involved in signaling. Group 2 contained four genes that were induced in the OE 7.2 line: a MYB TF (*MYB15*), a Kunitz-like protease inhibitor, a tyrosine phosphatase and a protein of unknown function. Meanwhile group 3 contained three genes that were repressed in the OE 7.2 line: a methyl jasmonate esterase, a sulfate adiniltransferase ATP-sulfurilase and Zinc-finger protein GRF-like. These groups, especially the first one, showed a correspondence with the GO enrichment analysis for the genes with a significant  $fc \geq |1|$ , since genes involved in cell wall biosynthesis were especially represented.

In order to confirm the information derived from RNA-Seq analysis, the expression of four genes was analyzed by qPCR: *PAL* (lignin), *CesA4* (cellulose), *GT43* (xylan), and *MYB15* (Figure 8B). The first three genes were selected in order to corroborate the changes in expression of genes directly involved in the biosynthesis of the main components of secondary cell wall and *MYB15*, since it is a TF belonging to one of the main families that regulate secondary cell wall biosynthesis. Consistently with the RNA-Seq analysis, the expression of the first three genes, involved in secondary cell wall biosynthesis, was strongly reduced in OE lines compared to EV lines. On the other hand, the expression of *MYB15* was induced in OE lines in comparison with EV lines in accordance with the RNA-Seq analysis (Figure 8B).

## DISCUSSION

Prxs are classical secretory peroxidases involved in numerous biological processes in plants being one isoform possibly involved in more than one function (Cosio and Dunand, 2009; Shigeto and Tsutsumi, 2016). This is the case of AtPrx33 and AtPrx34, involved in plant defense and root elongation (Shigeto and Tsutsumi, 2016). Other example is *swpa4*, a sweet potato peroxidase that, when overexpressed in tobacco, is capable of increasing lignin biosynthesis and tolerance to biotic and abiotic stimuli (Kim et al., 2008). The use of expression studies, biochemical characterization and mutants or transgenic plants has been very useful to assign a precise function to a specific Prx (Cosio and Dunand, 2009). Plant transformation has provided numerous evidences of the *in planta* function of various isoenzymes (El Mansouri et al., 1999; Kawaoka et al., 2003; Kim et al., 2008; Herrero et al., 2013a; Fernández-Pérez et al., 2014, 2015; Cosio et al., 2017; Wu et al., 2017).

ZePrx belongs to class III peroxidase and it is considered responsible of lignin polymerization in *Z. elegans* since its

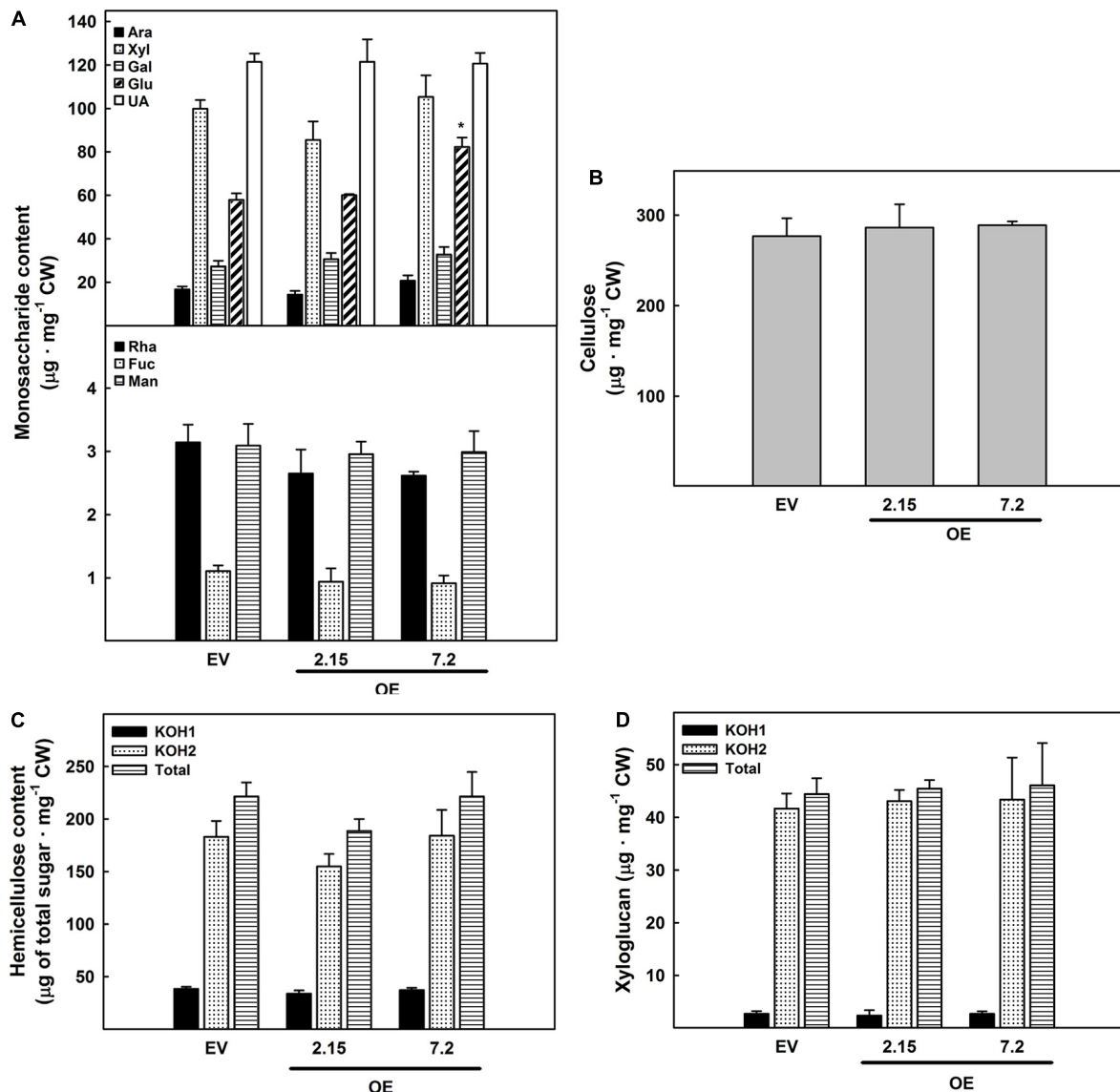
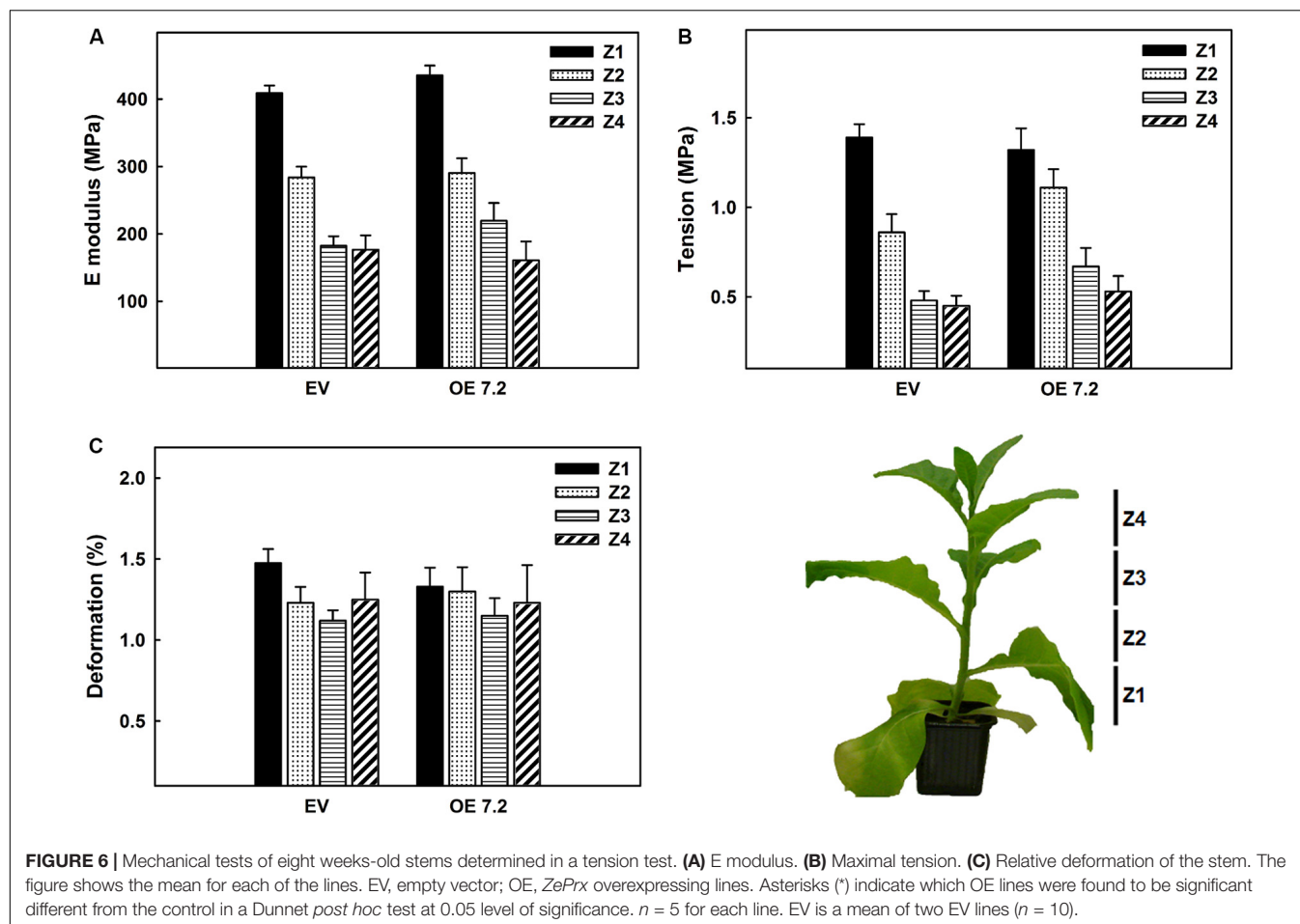


**FIGURE 5 |** Carbohydrate composition of eight weeks-old stems cell walls. **(A)** Monosaccharide composition (Ara, arabinose; Xyl, xylose; Gal, galactose; Glu, glucose; UA, uronic acid; Rha, rhamnose; Fuc, fucose; and Man, mannose). **(B)** Cellulose content. **(C)** Total sugar content of the two different hemicellulose fractions of the cell wall (KOH1: fraction extracted with KOH 0.1N and KOH2: fraction extracted with KOH 4N). **(D)** Xyloglucan content of the different hemicellulose fractions of the cell wall. The figure shows the mean and standard error for each of the lines. EV, empty vector; OE, *ZePrx* overexpressing lines. Asterisks (\*) indicate which OE lines were found to be significant different from the control in a Dunnet *post hoc* test at 0.05 level of significance.  $n = 3$  for each line and  $n = 6$  for total sugar content in the hemicellulose fractions. EV is a mean of two EV lines ( $n = 6$ ).

expression in the stem is temporally correlated with its lignification (Ros Barceló et al., 2002). Moreover, this enzyme is capable of oxidizing *in vitro* the three main lignin precursors (*p*-coumaryl, coniferyl, and sinapyl alcohols) to polymers similar to lignins (Gabaldón et al., 2006). The promoter of this enzyme has multiple motifs that respond to signals usually involved in the regulation of vascular development and lignification (Gutiérrez et al., 2009; López Núñez-Flores et al., 2010), backing its role in lignin biosynthesis. In the present work, heterologous overexpression of *ZePrx* in *N. tabacum* plants has been used to further characterize the function of this enzyme.

Transgenic OE plants showed a higher expression of *ZePrx* compared to EV lines. The presence of an active *ZePrx* in *N. tabacum* OE lines is confirmed by the identification of an extra band of 30 kDa with an isoelectric point of 10, consistently with the characteristics previously determined for *ZePrx* (Gabaldón et al., 2005) and an increase in the peroxidase catalytic activity. The shift toward a higher capability of oxidizing sinapyl alcohol, given by the increase in S/G activity ratio, is coherent with the overexpression of a S-peroxidase (Gabaldón et al., 2005). Indeed, *ZePrx* has five characteristic motifs in its sequence, which determine a wider catalytic site compared





to the so-called guaiacyl or G-peroxidases. As a result, they can accommodate larger substrates such as sinapyl alcohol or syringaldazine (Ros Barceló et al., 2007). Under optimal growing conditions, OE transgenic plants are not phenotypically altered, in terms of plant growth and development. These results agree with those of Fernández-Pérez et al. (2014) and Cosío et al. (2017). In the first case, *A. thaliana* knock-out mutants for *AtPrx52*, which codifies a *ZePrx* orthologous involved in lignin polymerization, did not show any growth or development changes (Fernández-Pérez et al., 2014). In the second one, the authors observed that *AtPrx17*, codifying for another peroxidase involved in lignification, caused notable changes in development when suppressed, but mild ones or none when overexpressed (Cosío et al., 2017).

Prxs are able to produce  $H_2O_2$ , besides using it as substrate in lignin polymerization (Kim et al., 2008). Indeed, these enzymes undergoes a peroxidative cycle, which consumes  $H_2O_2$  by oxidizing different compounds, as well as a hydroxylic and an oxidative cycle through which they produce different types of ROS (Chen and Schopfer, 1999).  $H_2O_2$  is considered the main ROS acting in cells, due to its relatively long half-life and its capability to cross biological membranes through aquaporins (Wang et al., 2020). Recently, mechanisms for extracellular  $H_2O_2$  perception and integration with internal

cues have been suggested to be pivotal for sensing the outside stress conditions (Wu et al., 2020).  $H_2O_2$  modulation is crucial, since it is a signaling or damaging molecule, depending on concentration, timing and localization of its production as well as the presence or other signals specifically generated by stressing conditions (De Gara et al., 2010; Noctor et al., 2018). In our case non-significant increase in  $H_2O_2$  was observed in OE lines. However, this could be the consequence of the increase in APX activity and ASC oxidation observed in both OE lines. The maintenance of an overall redox homeostasis is also confirmed by RNA-Seq analysis, since no genes included in the redox category have been identified as differentially expressed between OE and EV lines. The interaction between  $H_2O_2$ -producing peroxidases and APX has been already reported in literature as determinant in various physiological processes, first among all in stress defense responses. Peters et al., found that *Sporisorium scitamineum* (smut pathogen) induces an early modulation of the production and scavenging of ROS during defense responses in resistant sugarcane. In particular, in the resistant genotype infected by *S. scitamineum*, the expression of a protein belonging to class III peroxidases seems to be positively related to an increase in APX activity aimed at reducing intracellular  $H_2O_2$  increase (Peters et al., 2017).

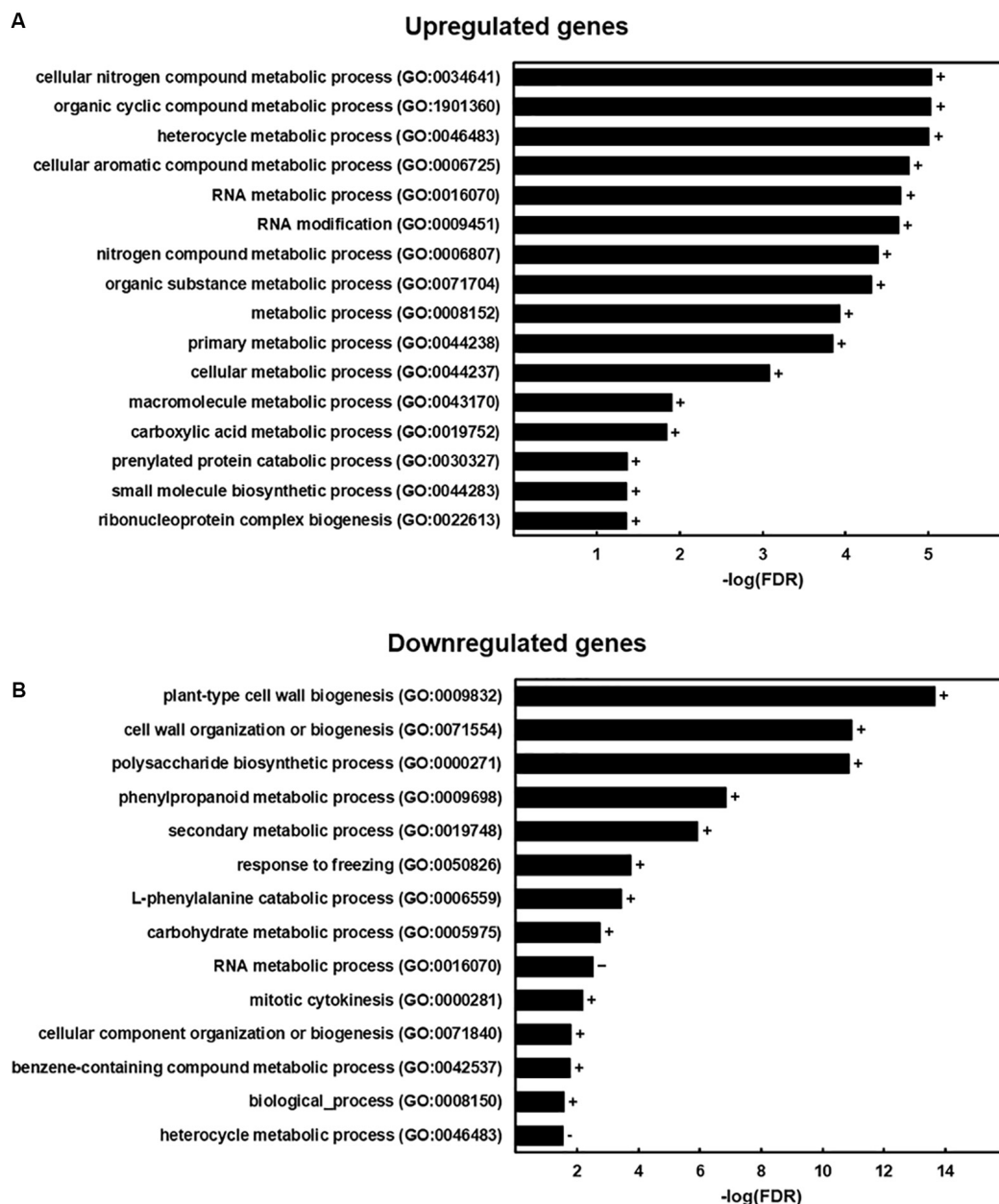
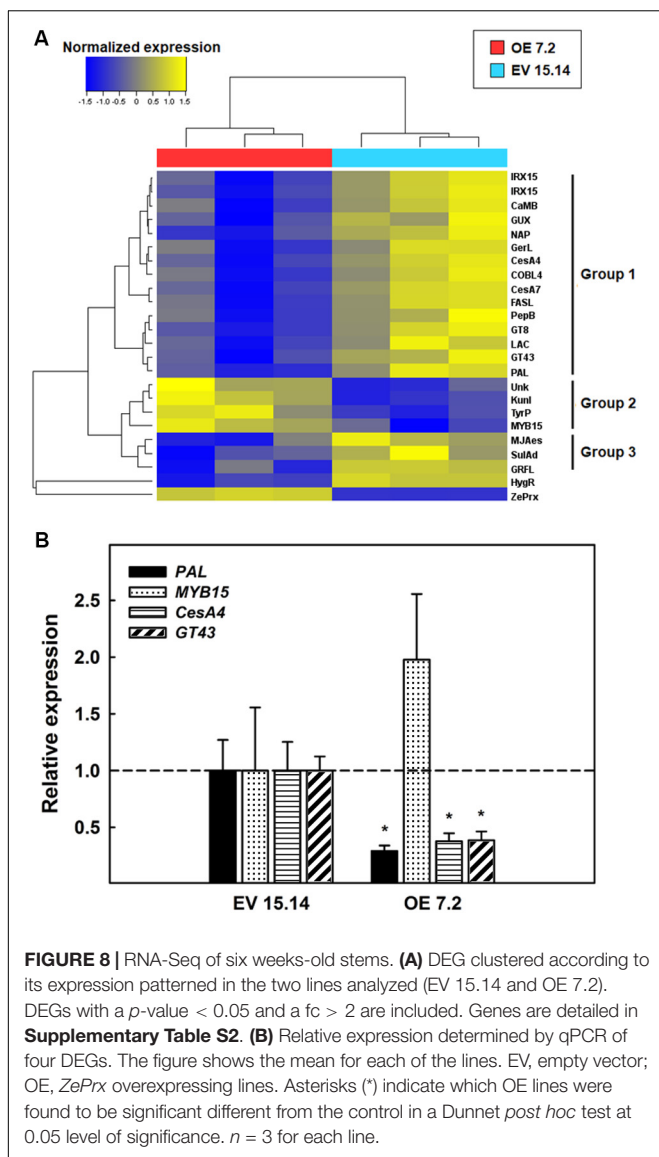


**FIGURE 7 |** GO enrichment analysis. GO terms that were more represented in the genes with a significant change in expression of the RNA-Seq analysis ( $p$ -value < 0.05) that in *N. tabacum* genome. **(A)** Results for the group of upregulated genes (427 total genes, but 297 were assigned with a GO category and included in the analysis). **(B)** Results for the group of downregulated genes (354 total genes, but 274 were assigned with a GO category and included in the analysis). The figure shows the  $-\log(\text{FDR})$  for each category obtained with a Benjamini-Hochberg FDR correction. Signs next to the bars indicate if a category was overrepresented (+) or underrepresented (−) in the sample.

Several studies focused on the Prxs involved in lignin biosynthesis showed that its overexpression causes an increase in lignin content (El Mansouri et al., 1999; Kim et al., 2008; Cosio et al., 2017; Wu et al., 2017). However, the overexpression of *ZePrx* in *N. tabacum* plants does not seem to cause a lignin accumulation at higher levels than EV plants, when analyzed by histochemical staining or the acetyl bromide method. These results contrast with previous studies

in which mutants of *A. thaliana* lacking the *ZePrx* orthologous *AtPrx4*, *AtPrx52*, and *AtPrx72*, presented a reduction in lignin deposition (Herrero et al., 2013a; Fernández-Pérez et al., 2014, 2015). Nevertheless, it should be considered that lignin biosynthesis is a major carbon sink for the plant and has a high energy cost (Amthor, 2003). Plants have evolved a complex control system over lignin biosynthesis in order to avoid unnecessary deposition of lignin thus limiting the

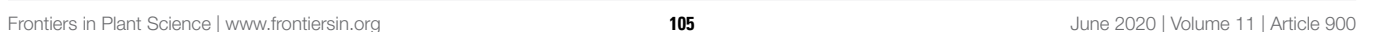


carbon flux into the lignin biosynthetic pathway through the control of the expression of different key enzymes (Anterola et al., 2002; Richet et al., 2011). Furthermore, some studies have pointed out that lignin precursors are not stored in large quantities in the cell, but transported to the apoplast to become part of lignins as soon as they are synthesized (Anterola et al., 1999; Smith et al., 2013). Since peroxidases are involved in the last step of lignin biosynthesis (Vanholme et al., 2010), lignins precursor availability is a limiting factor influencing the quantity of lignin that plants generate. In this context, an increase in the activity of enzymes involved in the oxidative polymerization, such as *ZePrx*, will not result in a higher amount of lignins biosynthesis when precursors are scarce. Instead, in the case of mutants with a reduced expression of peroxidases involved in lignin polymerization, the peroxidase activity becomes insufficient for lignin biosynthesis, causing a reduction of total lignins (Herrero et al., 2013a;

Fernández-Pérez et al., 2014, 2015; Cosio et al., 2017). RNA-Seq results also showed that the OE line 7.2 had a reduced expression of two genes involved in lignin biosynthesis a PAL and a laccase (Vanholme et al., 2010). Therefore, the plant seems to respond to the expression of an additional peroxidase by limiting the production of monolignols (decrease in PAL) and its incorporation to the lignin polymer (decrease in laccase), thus avoiding an unnecessary increase in lignin deposition due to *ZePrx* overexpression. This does not occur in OE line 2.15 in which only a smaller increase in *ZePrx* activity was observed in comparison with OE line 7.2. The increase in peroxidase activity occurring in OE 2.15 line seems not to be sufficient to induce a change in lignin composition. Therefore, the two analyzed transgenic lines, 2.15 and 7.2 OE lines, differ from the EV line with respect to a higher peroxidase activity, a higher Syringyl/Guaiacyl peroxidase activity ratio and a higher ASC content and ascorbate peroxidase activity. However, the OE 7.2 line presents a more marked increase in peroxidase activity and a stronger increase of Syringyl/Guaiacyl peroxidase activity ratio compared to the 2.15 line. The change in the peroxidase activity observed at six weeks developmental stage in the 7.2 OE line could be considered not sufficient to cause variation in lignin composition. On the contrary, at eight weeks, developmental stage in which the increase in peroxidase activity was stronger, an interesting variation in lignin composition was observed, further supporting a dose dependent effect of the peroxidase activity on lignification process.

It is worth noting that mutants of *A. thaliana*, lacking the *ZePrx* orthologous showed a reduced S/G ratio (Herrero et al., 2013a; Fernández-Pérez et al., 2014, 2015). Consistently, in our *N. tabacum* plants overexpressing *ZePrx* the increase in S-peroxidase activity promotes a higher incorporation of syringyl units within lignins thus causing an increase in S/G ratio. This effect seems to be dose dependent, since it increased in the OE lines during time, following the increase of *Prx* activity. Therefore, the overexpression of *ZePrx* determine a change in lignin composition, without increasing its content. This dose dependent effect, has been also previously observed in similar studies in which mutant lines with a higher peroxidase activity showed a higher modification of lignins content (Elfstrand et al., 2001, 2002; Kim et al., 2008). Elfstrand and coworkers, demonstrate that the overexpression of a peroxidase in *Norway spruce* resulted in an enrichment in coniferaldehyde groups, without affecting to the total lignin quantity. Additionally, in this case the change in lignin composition has effects on lignin structure, since syringyl units are only involved in  $\beta$ -O-4 links and this links generate a linear lignin polymer (Sasaki et al., 2004). Lignins with such a structure contribute to cell walls being less elastic (higher E-modulus) than the ones with guaiacyl-type lignins (Koehler et al., 2006). In our case, despite the increase in S/G ratio, the increase in E-modulus was not statistically significant. This might be due to other compensatory alteration on the cell wall. The analysis of cell wall polysaccharides composition only showed an increase in glucose content in OE 7.2 line compared to EV lines. Nevertheless, this increase could not be explained by changes in cellulose, hemicellulose or xylan contents, which are the main storage of glucose in the cell wall.

Therefore, *ZePrx* overexpression seems to trigger a compensatory response in the cell wall biosynthesis. **Figure 9** shows a possible explanation of gene expression reorganization induced by *ZePrx* overexpression, based on RNA-Seq analysis. Besides genes involved in secondary cell wall biosynthesis and





programed cell death which share the same expression pattern, the expression of *ZePrx* also affected the expression of genes involved in signaling. The alteration of TFs of MYB family is of particular interest since this family has a major role in controlling secondary cell wall formation. Specifically, this MYB15 TF is homologous to *AtMYB15*, which has been related to lignin biosynthesis in constraint situations like exposure to cold (Agarwal et al., 2006). In addition, this gene has been reported to be induced by methyl jasmonate (Almagro et al., 2014), which could be accumulate in the OE 7.2 plants as a result of the reduced expression of a methyl jasmonate esterase observed in these plants. This is also the case for some protease inhibitors (Wu et al., 2008), that share with *MYB15* the same gene expression pattern (Figures 8A, 9). Therefore, the alteration of the expression of these genes could contribute to reduce changes in the mechanical properties of the stem putatively induced by the increase in syringyl lignins caused by *ZePrx* overexpression. Nevertheless, further research is needed to fully understand the role of its genes in cell wall homeostasis.

In conclusion, our data suggests that *ZePrx* participates in lignification *in planta* by altering cell wall composition, in particular the S/G ratio. In the absence of other external stimuli, such as biotic or abiotic stress, the OE lines seem to be able to overcome changes in cell wall mechanical properties by altering the metabolic pathways controlling cell wall structure as well. They were also able to avoid changes in redox homeostasis by modulating APX activity and ASC oxidation. Further research is needed to fully understand the whole function of *ZePrx in planta*, and in particular, its interconnections with redox systems and its possible involvement in stress defense responses.

## DATA AVAILABILITY STATEMENT

The datasets presented in this study can be found in online repositories. The names of the repository/repositories and accession number(s) can be found below: <https://www.ncbi.nlm.nih.gov/sra/PRJNA607100>.

## REFERENCES

- Agarwal, M., Hao, Y., Kappor, A., Dong, C. H., Fujii, H., Zheng, X., et al. (2006). A R2R3 type MYB transcription factor is involved in the cold regulation of CBF genes and in acquired freezing tolerance. *J. Biol. Chem.* 281, 37636–37645. doi: 10.1074/jbc.M605895200
- Almagro, L., Carbonell-Bejerano, P., Belchí-Navarro, S., Bru, R., Martínez-Zapater, J. M., Lijavetzky, D., et al. (2014). Dissecting the transcriptional response to elicitors in *Vitis vinifera* cells. *PLoS One* 9:e109777. doi: 10.1371/journal.pone.0109777
- Amthor, J. S. (2003). Efficiency of lignin biosynthesis: a quantitative analysis. *Ann. Bot.* 91, 673–695. doi: 10.1093/aob/mcg073
- Anterola, A. M., Jeon, J. H., Davin, L. B., and Lewis, N. G. (2002). Transcriptional control of monolignol biosynthesis in *Pinus taeda*. Factors affecting monolignol ratios and carbon allocation in phenylpropanoid metabolism. *J. Biol. Chem.* 277, 18272–18280. doi: 10.1074/jbc.M112051200
- Anterola, A. M., van Rensburg, H., van Heerden, P. S., Davin, L. B., and Lewis, N. G. (1999). Multi-site modulation of flux during monolignol formation in loblolly pine (*Pinus taeda*). *Biochem. Biophys. Res.* 261, 652–657. doi: 10.1006/bbrc.1999.1097

## AUTHOR CONTRIBUTIONS

AG-U carried out the experiments, participated in the study, contributed to design and drafted the manuscript. LS designed and participated in the transformation experiments. SC contributed to design the study, to analyze the data and to write the manuscript. AE and RM-R coordinated and performed the carbohydrates experiments. RB and LB designed and performed the tensile tests. GE-P statistically analyzed the FTIR data. LD coordinated the redox experiments and reviewed the manuscript. EN-U contributed to designed the study, coordinated the experiments on lignin composition and helped to draft the manuscript. FP designed the study, coordinated the experiments concerning lignin composition and reviewed the manuscript. All authors contributed to the article and approved the submitted version.

## FUNDING

AG-U held an FPU grant from MECO (Spain) (FPU13/04835). This research was possible thanks to the funding of Xunta de Galicia (Spain) (ED431C 2018/57).

## ACKNOWLEDGMENTS

We are grateful to the Molecular Biology section and Dr. Gerardo Fernández from Chromatography Section of Servicio de Apoyo a la Investigación (SAI) from Universidade da Coruña.

## SUPPLEMENTARY MATERIAL

The Supplementary Material for this article can be found online at: <https://www.frontiersin.org/articles/10.3389/fpls.2020.00900/full#supplementary-material>

- Bent, A. (2006). “*Arabidopsis thaliana* floral dip transformation method,” in *Agrobacterium Protocols. Methods in Molecular Biology*, 343, ed. K. Wang (Totowa, NJ: Humana Press), 87–103.
- Bolger, A. M., Lohse, M., and Usadel, B. (2014). Trimmomatic: a flexible trimmer for Illumina sequence data. *Bioinformatics* 30, 2114–2120. doi: 10.1093/bioinformatics/btu170
- Chen, S. X., and Schopfer, P. (1999). Hydroxyl-radical production of physiological reactions. A novel function of peroxidase. *FEBS J.* 260, 726–735. doi: 10.1046/j.1432-1327.1999.00199.x
- Clemente, T. (2006). “*Nicotiana glauca* (Nicotiana glauca, Nicotiana glauca),” in *Agrobacterium Protocols. Methods in Molecular Biology*, Vol. 343, ed. K. Wang (Totowa, NJ: Humana Press), 132–154.
- Cosio, C., and Dunand, C. (2009). Specific functions of individual class III peroxidase genes. *J. Exp. Bot.* 60, 391–408. doi: 10.1093/jxb/ern318
- Cosio, C., Ranocha, P., Francoz, E., Burlat, V., Zheng, Y., Perry, S. E., et al. (2017). The class III peroxidase PRX17 is a direct target of the MADS-box transcription factor AGAMOUS-LIKE15 (AGL15) and participates in lignified tissue formation. *New Phytol.* 213, 250–263. doi: 10.1111/nph.14127
- De Gara, L. (2004). Class III peroxidases and ascorbate metabolism in plants. *Phytochem. Rev.* 3, 195–205. doi: 10.1023/B:PHYT.0000047795.82713.99

- De Gara, L., Locato, V., Dipierro, S., and de Pinto, M. C. (2010). Redox homeostasis in plants. The challenge of living with endogenous oxygen production. *Resp. Physiol. Neurobi.* 173S, S13–S19. doi: 10.1016/j.resp.2010.02.007
- De Pinto, M. C., and De Gara, L. (2004). Changes in the ascorbate metabolism of both apoplastic and symplastic spaces are involved in cell differentiation. *J. Exp. Bot.* 55, 2559–2569. doi: 10.1093/jxb/erh253
- De Pinto, M. C., Francis, D., and De Gara, L. (1999). The redox state of the ascorbate-dehydroascorbate pair as a specific sensor of cell division in tobacco BY-2 cells. *Protoplasma* 209, 90–97. doi: 10.1007/BF01415704
- Duwadi, K., Chen, L., Menassa, R., and Dhaubhadel, S. (2015). Identification, characterization and down-regulation of *cysteine protease* genes in tobacco for use in recombinant protein production. *PLoS One* 10:e0130556. doi: 10.1371/journal.pone.0130556
- Edwards, K. D., Fernández-Pozo, N., Drake-Stowe, K., Humphry, M., Evans, A. D., Bombarely, A., et al. (2017). A reference genome for *Nicotiana tabacum* enables map-based cloning of homeologous loci implicated in nitrogen utilization efficiency. *BMC Genom.* 18:448–461. doi: 10.1186/s12864-017-3791-6
- El Mansouri, I., Mercado, J. A., Santiago-Dómenech, N., Pliego-Alfaro, F., Valpuesta, V., and Quesada, M. A. (1999). Biochemical and phenotypical characterization of transgenic tomato plants overexpressing a basic peroxidase. *Physiol. Plant.* 106, 355–362. doi: 10.1034/j.1399-3054.1999.106401.x
- Elfstrand, M., Fosdall, C., Sitbon, F., Olsson, O., Lönnberg, A., and von Arnold, S. (2001). Overexpression of the endogenous peroxidase-like gene *spi 2* in transgenic Norway spruce plants results in increased total peroxidase activity and reduced growth. *Plant Cell Rep.* 20, 596–603. doi: 10.1007/s002990100360
- Elfstrand, M., Sitbon, F., Lapiere, C., Bottin, A., and von Arnold, S. (2002). Altered lignin structure and resistance to pathogens in *spi 2*-expressing tobacco plants. *Planta* 214, 708–716. doi: 10.1007/s00425-001-0681-5
- Espíñeira, J. M., Novo Uzal, E., Gómez Ros, L. V., Carrión, J. S., Merino, F., Ros Barceló, A., et al. (2011). Distribution of lignin monomers and the evolution of lignification among lower plants. *Plant Biol.* 13, 59–68. doi: 10.1111/j.1438-8677.2010.00345.x
- Fernández-Pérez, F., Pomar, F., Pedreño, M. A., and Novo-Uzal, E. (2014). The suppression of *AtPrx52* affects fibers but not xylem lignification in *Arabidopsis* by altering the proportion of syringyl units. *Physiol. Plant.* 154, 395–406. doi: 10.1111/ppl.12310
- Fernández-Pérez, F., Vivar, T., Pomar, F., Pedreño, M. A., and Novo-Uzal, E. (2015). Peroxidase 4 is involved in syringyl lignin formation in *Arabidopsis thaliana*. *J. Plant Physiol.* 175, 86–94. doi: 10.1016/j.jplph.2014.11.006
- Ferrer, M. A., Calderón, A. A., Muñoz, R., and Ros Barceló, A. (1990). 4-methoxy- $\alpha$ -naphthol as a specific substrate for kinetic, zymographic and cytochemical studies on plant peroxidase activities. *Phytochem. Anal.* 1, 63–69. doi: 10.1002/pca.2800010203
- Ferrer, M. A., Cimini, S., López-Orenes, A., Calderón, A. A., and De Gara, L. (2018). Differential Pb tolerance in metallicolous and non-metallicolous *Zygophyllum fabago* populations involves the strengthening of the antioxidative pathways. *Environ. Exper. Bot.* 150, 141–151. doi: 10.1016/j.envexpbot.2018.03.010
- Foster, C. E., Martin, T. M., and Pauly, M. (2010). Comprehensive compositional analysis of plant cell walls (lignocellulosic biomass) part II: Carbohydrates II. *J. Vis. Exp.* 37:e1837. doi: 10.3791/1837
- Foyer, C. H., and Noctor, G. (2011). Ascorbate and glutathione: the heart of the redox hub. *Plant Physiol.* 155, 2–18. doi: 10.1104/pp.110.167569
- Gabaldón, C., López-Serrano, M., Pedreño, M. A., and Ros Barceló, A. (2005). Cloning and molecular characterization of the basic peroxidase isoenzyme from *Zinnia elegans*, an enzyme involved in lignin biosynthesis. *Plant Physiol.* 139, 1138–1154. doi: 10.1104/pp.105.069674
- Gabaldón, C., López-Serrano, M., Pomar, F., Merino, F., Cuello, J., Pedreño, M. A., et al. (2006). Characterization of the last step of lignin biosynthesis in *Zinnia elegans* suspension cell cultures. *FEBS Lett.* 580, 4311–4316. doi: 10.1016/j.febslet.2006.06.088
- Gibson, L. J. (2012). The hierarchical structure and mechanics of plant materials. *J. R. Soc. Interface* 9, 2749–2766. doi: 10.1098/rsif.2012.0341
- Gutiérrez, J., López Núñez-Flores, M. J., Gómez-Ros, L. V., Novo-Uzal, E., Carrasco, A. E., Díaz, J., et al. (2009). Hormonal regulation of the basic peroxidase isoenzyme from *Zinnia elegans*. *Planta* 230, 767–778. doi: 10.1007/s00425-009-0982-7
- Hamann, T. (2012). Plant cell wall integrity maintenance as an essential component of biotic stress response mechanisms. *Front. Plant Sci.* 3:77. doi: 10.3389/fpls.2012.00077
- Hellens, R., Mullineaux, P., and Klee, H. (2000a). A guide to *Agrobacterium* binary Ti vectors. *Trends Plant Sci.* 5, 446–451. doi: 10.1016/S1360-1385(00)01740-4
- Hellens, R. P., Edwards, E. A., Leyland, N. R., Bean, S., and Mullineaux, P. (2000b). pGreen: a versatile and flexible binary Ti vector for *Agrobacterium*-mediated plant transformation. *Plant Mol. Biol.* 42, 819–832. doi: 10.1023/A:1006496308160
- Herrero, J., Fernández-Pérez, F., Yebra, T., Novo-Uzal, E., Pomar, F., Pedreño, M. A., et al. (2013a). Bioinformatic and functional characterization of the basic peroxidase 72 from *Arabidopsis thaliana* involved in lignin biosynthesis. *Planta* 237, 1599–1612. doi: 10.1007/s00425-013-1865-5
- Herrero, J., Esteban-Carrasco, A., and Zapata, J. M. (2013b). Looking for *Arabidopsis thaliana* peroxidases involved in lignin biosynthesis. *Plant Physiol. Biochem.* 67, 77–86. doi: 10.1016/j.plaphy.2013.02.019
- Iiyama, K., and Wallis, A. F. A. (1988). An improved acetyl bromide procedure for determining lignin in woods and wood pulps. *Wood Sci. Technol.* 22, 271–280. doi: 10.1007/BF00386022
- Junglee, S., Urban, L., Sallanon, H., and Lopez-Lauri, F. (2014). Optimized assay for hydrogen peroxide determination in plant tissue using potassium iodide. *Am. J. Analyt. Chem.* 5:48942. doi: 10.4236/ajac.2014.511081
- Kawaoka, A., Matsunaga, E., Endo, S., Kondo, S., Yoshida, K., Shinmyo, A., et al. (2003). Ectopic expression of a horseradish peroxidase enhances growth rate and increases oxidative stress resistance in hybrid aspen. *Plant Physiol.* 132, 1177–1185. doi: 10.1104/pp.102.019794
- Kim, D., Langmead, B., and Salzberg, S. L. (2015). HISAT: a fast spliced aligner with low memory requirements. *Nat. Methods* 12, 357–360. doi: 10.1038/nmeth.3317
- Kim, Y. H., Kim, C. Y., Song, W. K., Park, D. S., Kwon, S. Y., Lee, H. S., et al. (2008). Overexpression of sweetpotato *swpa4* peroxidase results in increased hydrogen peroxide production and enhances stress tolerance in tobacco. *Planta* 227, 867–881. doi: 10.1007/s00425-007-0663-3
- Koehler, L., Ewers, F. W., and Telewski, F. W. (2006). “Optimizing for multiple functions: mechanical and structural contributions of cellulose microfibrils and lignin in strengthening tissues,” in *Characterization of the Cellulosic Cell Wall*, eds D. D. Stokke, and L. H. Groom (Ames, IA: Blackwell Publishing), 20–29. doi: 10.1002/9780470999714.ch2
- Kooiman, P. (1960). A method for the determination of amyloid in plant seeds. *Recl. Trav. Chim. Pays Bas* 79, 675–678. doi: 10.1002/recl.19600790703
- Laemmli, U. K. (1970). Cleavage of structural proteins during the assembly of the head of bacteriophage T4. *Nature* 227, 680–685. doi: 10.1038/227680a0
- Li, F., Liu, S., Xu, H., and Xu, Q. (2018). A novel FC17/CESA4 mutation causes increased biomass saccharification and lodging resistance by remodeling cell wall in rice. *Biotechnol. Biofuels* 11:298. doi: 10.1186/s13068-018-1298-2
- Liszkay, A., Kenk, B., and Schopfer, P. (2003). Evidence for the involvement of cell wall peroxidase in the generation of hydroxyl radicals mediating extension growth. *Planta* 217, 658–667. doi: 10.1007/s00425-003-1028-1
- Liu, L., Shang-Guan, K., Zhang, B., Liu, X., Yan, M., Zhang, L., et al. (2013). Brittle Culm1, a COBRA-Like protein, functions in cellulose assembly through binding cellulose microfibrils. *PLoS Genet.* 9:e1003704. doi: 10.1371/journal.pgen.1003704
- Locato, V., Gadaleta, C., De Gara, L., and De Pinto, M. C. (2008). Production of reactive species and modulation of antioxidant network in response to heat shock: A critical balance for cell fate. *Plant Cell Environ.* 31, 1606–1619. doi: 10.1111/j.1365-3040.2008.01867.x
- López Núñez-Flores, M. J., Gutiérrez, J., Gómez-Ros, L. V., Novo Uzal, E., Sotomayor, M., and Ros Barceló, A. (2010). Downregulation of the basic peroxidase isoenzyme from *Zinnia elegans* by gibberellic acid. *J. Integr. Plant Biol.* 52, 244–251. doi: 10.1111/j.1744-7909.2010.00888.x
- López-Serrano, M., Fernández, M. D., Pomar, F., Pedreño, M. A., and Ros Barceló, A. (2004). *Zinnia elegans* uses the same peroxidase isoenzyme complement for cell wall lignification in both single-cell tracheary elements and xylem vessels. *J. Exp. Bot.* 55, 423–431. doi: 10.1093/jxb/erh036
- Marjamaa, K., Kukkola, E. M., and Fagerstedt, K. V. (2009). The role of xylem class III peroxidases in lignification. *J. Exp. Bot.* 60, 367–376. doi: 10.1093/jxb/ern278
- McFarlane, H. E., Döring, A., and Persson, S. (2014). The cell biology of cellulose synthesis. *Annu. Rev. Plant Biol.* 65, 69–94. doi: 10.1146/annurev-arplant-050213-040240
- Mélida, H., Largo-Gosens, A., Novo-Uzal, E., Santiago, R., Pomar, F., García, P., et al. (2015). Ectopic lignification in primary cellulose-deficient cell walls of maize cell suspension cultures. *J. Integr. Plant Biol.* 57, 357–372. doi: 10.1111/jipb.12346

- Mi, H., Muruganujan, A., Ebert, D., Huang, X., and Thomas, P. D. (2019). PANTHER version 14: more genomes, a new PANTHER-GO-slim and improvements in enrichment analysis tools. *Nucleic Acids Res.* 47, D419–D426. doi: 10.1093/nar/gky1038
- Noctor, G., Reichheld, J. P., and Foyer, C. H. (2018). ROS-related redox regulation and signaling in plants. *Semin Cell Dev. Biol.* 80, 3–12. doi: 10.1016/j.semcdb.2017.07.013
- Novo-Uzal, E., Gómez Ros, L. V., Pomar, F., Bernal, M. A., Paradelo, A., Albar, J. P., et al. (2009). The presence of sinapyl lignin in *Ginkgo biloba* cell cultures changes our views of the evolution of lignin biosynthesis. *Physiol. Plant.* 135, 196–213. doi: 10.1111/j.1399-3054.2008.01185.x
- Oliva, M., Theiler, G., Zámocký, M., Koua, D., Margis-Pinheiro, M., Passardi, F., et al. (2009). PeroxiBase: a powerful tool to collect and analyse peroxidase sequences from Viridiplantae. *J. Exp. Bot.* 60, 453–459. doi: 10.1093/jxb/ern317
- Persson, S., Wei, H., Milne, J., Page, G. P., and Somerville, C. R. (2005). Identification of genes required for cellulose synthesis by regression analysis of public microarray data sets. *Proc. Natl. Acad. Sci. U.S.A.* 102, 8633–8638. doi: 10.1073/pnas.0503392102
- Perte, M., Kim, D., Perte, G., Leek, J. T., and Salzberg, S. L. (2016). Transcript-level expression analysis of RNA-Seq experiments with HISAT, StringTie, and Ballgown. *Nat. Protoc.* 11, 1650–1667. doi: 10.1038/nprot.2016.095
- Perte, M., Perte, G. M., Antonescu, C. M., Chang, T. C., Mendell, J. T., and Salzberg, S. L. (2015). StringTie enables improved reconstruction of a transcriptome from RNA-Seq reads. *Nat. Biotechnol.* 33, 290–295. doi: 10.1038/nbt.3122
- Peters, L. P., Carvalho, G., Vilhena, M. B., Creste, S., Azevedo, R. A., and Monteiro-Vitorello, C. B. (2017). Functional analysis of oxidative burst in sugarcane smut-resistant and -susceptible genotypes. *Planta* 245, 749–764. doi: 10.1007/s00425-016-2642-z
- Pomar, F., Merino, F., and Ros Barceló, A. (2002). O-4-linked coniferyl and sinapyl aldehydes in lignifying cell walls are the main targets of the Wiesner (phloroglucinol-HCl) reaction. *Protoplasma* 220, 17–28. doi: 10.1007/s00709-002-0030-y
- Rebaque, D., Martínez-Rubio, R., Fornalé, S., García-Angulo, P., Alonso-Simón, A., Álvarez, J. M., et al. (2017). Characterization of structural cell wall polysaccharides in cattail (*Typha latifolia*): Evaluation as potential biofuel feedstock. *Carbohydr. Polym.* 175, 679–688. doi: 10.1016/j.carbpol.2017.08.021
- Richet, N., Afif, D., Huber, F., Pollet, B., Banvoy, J., El Zein, R., et al. (2011). Cellulose and lignin biosynthesis is altered by ozone in wood of hybrid poplar (*Populus tremulaxalba*). *J. Exp. Bot.* 62, 3575–3586. doi: 10.1093/jxb/err047
- Ros Barceló, A., Gómez Ros, L. V., and Esteban Carrasco, A. (2007). Looking for syringyl peroxidases. *Trends Plant Sci.* 12, 486–491. doi: 10.1016/j.tplants.2007.09.002
- Ros Barceló, A., Pomar, F., López-Serrano, M., Martínez, P., and Pedreño, M. A. (2002). Developmental regulation of the H<sub>2</sub>O<sub>2</sub>-producing system and of a basic peroxidase isoenzyme in the *Zinnia elegans* lignifying xylem. *Plant Physiol. Biochem.* 40, 325–332. doi: 10.1016/S0981-9428(02)01376-1
- Sasaki, S., Nishida, T., Tsutsumi, Y., and Kondo, R. (2004). Lignin dehydrogenative polymerization mechanism: a poplar cell wall peroxidase directly oxidizes polymer lignin and produces in vitro dehydrogenative polymer rich in β-O-4 linkage. *FEBS Lett.* 562, 197–201. doi: 10.1016/S0014-5793(04)00224-8
- Schmidt, G. W., and Delaney, S. K. (2010). Stable internal reference genes for normalization of real-time RT-PCR in tobacco (*Nicotiana tabacum*) during development and abiotic stress. *Mol. Genet. Genom.* 282, 233–241. doi: 10.1007/s00438-010-0511-1
- Shigeto, J., and Tsutsumi, Y. (2016). Diverse functions and reactions of class III peroxidase. *New Phytol.* 290, 1395–1402. doi: 10.1111/nph.13738
- Smith, R. A., Schuetz, M., Roach, M., Mansfield, S. D., Ellis, B., and Samuels, L. (2013). Neighboring parenchyma cells contribute to *Arabidopsis* xylem lignification, while lignification of interfascicular fibers is cell autonomous. *Plant Cell* 25, 3988–3999. doi: 10.1105/tpc.113.117176
- Strivastava, L. M. (1966). Histochemical studies on lignin. *Tappi* 49, 173–183.
- Sundaravelpandian, K., Chandrika, N. N., and Schmidt, W. (2013). PFT1, a transcriptional Mediator complex subunit, controls root hair differentiation through reactive oxygen species (ROS) distribution in *Arabidopsis*. *New Phytol.* 197, 151–161. doi: 10.1111/nph.12000
- Supek, F., Bošnjak, M., Škunca, N., and Šmuc, T. (2011). REVIGO summarizes and visualizes long lists of Gene Ontology terms. *PLoS One* 6:e21800. doi: 10.371/journal.pone.0021800
- Taylor-Teeples, M., Lin, L., de Lucas, M., Turco, G., Toal, T. W., Gaudinier, A., et al. (2015). An *Arabidopsis* gene regulatory network for secondary cell wall synthesis. *Nature* 517, 571–575. doi: 10.1038/nature14099
- Vanholme, R., Demedts, B., Morreel, K., Ralph, J., and Boerjan, W. (2010). Lignin biosynthesis and structure. *Plant Physiol.* 153, 895–905. doi: 10.1104/pp.110.155119
- Wang, H., Schoebel, S., Schmitz, F., Dong, H., and Hedfalk, K. (2020). Characterization of aquaporin driven hydrogen peroxide transport. *Biochim. Biophys. Acta Biomembr.* 1862:183065. doi: 10.1016/j.bbamem.2019.183065
- Wise, A. A., Liu, Z., and Binns, A. N. (2006). “Three methods for the introduction of foreign DNA into *Agrobacterium*,” in *Agrobacterium Protocols. Methods in Molecular Biology*, 343, ed. K. Wang (Totowa, NJ: Humana Press), 43–54. doi: 10.1385/1-59745-130-4:43
- Wrigley, C. W. (1971). Gel electrofocusing. *Methods Enzymol.* 22, 559–564. doi: 10.1016/0076-6879(71)22040-1
- Wu, F., Chi, Y., Jiang, Z., Xu, Y., Xie, L., Huang, F., et al. (2020). Hydrogen peroxide sensor HPCA1 is an LRR receptor kinase in *Arabidopsis*. *Nature* 578, 577–581. doi: 10.1038/s41586-020-2032-3
- Wu, J., Wang, L., and Baldwin, I. T. (2008). Methyl jasmonate-elicited herbivore resistance: does MeJa function as a signal without being hydrolyzed to JA? *Planta* 227, 1161–1168. doi: 10.1007/s00425-008-0690-8
- Wu, Y., Yang, Z., How, J., Xu, H., Chen, L., and Li, K. (2017). Overexpression of a peroxidase gene (*AtPrx64*) of *Arabidopsis thaliana* in tobacco improves plant's tolerance to aluminum stress. *Plant Mol. Biol.* 95, 157–168. doi: 10.1007/s11103-017-0644-2
- Yue, F., Lu, F., Sun, R. C., and Ralph, J. (2011). Syntheses of lignin-derived thiocidolysis monomers and their uses as quantitation standards. *J. Agric. Food Chem.* 60, 922–928. doi: 10.1021/jf204481x
- Zámocký, M., and Obinger, C. (2010). “Molecular phylogeny of heme peroxidases,” in *Biocatalysis Based on Heme Peroxidases. Peroxidases as Potential Industrial Biocatalysts*, eds E. Torres, and M. Ayala (Heidelberg: Springer-Verlag), 7–35. doi: 10.1007/978-3-642-12627-7
- Zhong, R., and Ye, Z. H. (2014). Complexity of the transcriptional network controlling secondary wall biosynthesis. *Plant Sci.* 229, 193–207. doi: 10.1016/j.plantsci.2014.09.009
- Zhong, R., and Ye, Z. H. (2015). Secondary cell walls: biosynthesis, patterned deposition and transcriptional regulation. *Plant Cell Physiol.* 56, 195–214. doi: 10.1093/pcp/pcu140

**Conflict of Interest:** The authors declare that the research was conducted in the absence of any commercial or financial relationships that could be construed as a potential conflict of interest.

Copyright © 2020 García-Ulloa, Sanjurjo, Cimini, Encina, Martínez-Rubio, Bouza, Barral, Estévez-Pérez, Novo-Uzal, De Gara and Pomar. This is an open-access article distributed under the terms of the Creative Commons Attribution License (CC BY). The use, distribution or reproduction in other forums is permitted, provided the original author(s) and the copyright owner(s) are credited and that the original publication in this journal is cited, in accordance with accepted academic practice. No use, distribution or reproduction is permitted which does not comply with these terms.



# Identification of Sulfenylated Cysteines in *Arabidopsis thaliana* Proteins Using a Disulfide-Linked Peptide Reporter

Bo Wei<sup>1,2,3,4,5†</sup>, Patrick Willems<sup>1,2†</sup>, Jingjing Huang<sup>1,2</sup>, Caiping Tian<sup>6</sup>, Jing Yang<sup>6</sup>, Joris Messens<sup>3,4,5\*</sup> and Frank Van Breusegem<sup>1,2\*</sup>

<sup>1</sup> Department of Plant Biotechnology and Bioinformatics, Ghent University, Ghent, Belgium, <sup>2</sup> VIB Center for Plant Systems Biology, Ghent, Belgium, <sup>3</sup> VIB-VUB Center for Structural Biology, Brussels, Belgium, <sup>4</sup> Brussels Center for Redox Biology, Brussels, Belgium, <sup>5</sup> Structural Biology Brussels, Vrije Universiteit Brussel, Brussels, Belgium, <sup>6</sup> State Key Laboratory of Proteomics, Beijing Proteome Research Center, National Center for Protein Sciences, Beijing Institute of Lifeomics, Beijing, China

## OPEN ACCESS

### Edited by:

Christian Lindemayr,  
Helmholtz Zentrum München,  
Germany

### Reviewed by:

Mirko Zaffagnini,  
University of Bologna, Italy  
Thomas Leustek,  
Rutgers, The State University  
of New Jersey, United States

### \*Correspondence:

Joris Messens  
Joris.messens@vub.be  
Frank Van Breusegem  
Frank.vanbreusegem@psb.vib-  
ugent.be;  
frbre@psb.vib-ugent.be

<sup>†</sup> These authors have contributed  
equally to this work

### Specialty section:

This article was submitted to  
Plant Abiotic Stress,  
a section of the journal  
Frontiers in Plant Science

**Received:** 17 March 2020

**Accepted:** 15 May 2020

**Published:** 02 July 2020

### Citation:

Wei B, Willems P, Huang J,  
Tian C, Yang J, Messens J and  
Van Breusegem F (2020) Identification  
of Sulfenylated Cysteines  
in *Arabidopsis thaliana* Proteins Using  
a Disulfide-Linked Peptide Reporter.  
Front. Plant Sci. 11:777.  
doi: 10.3389/fpls.2020.00777

In proteins, hydrogen peroxide (H<sub>2</sub>O<sub>2</sub>) reacts with redox-sensitive cysteines to form cysteine sulfenic acid, also known as S-sulfenylation. These cysteine oxidation events can steer diverse cellular processes by altering protein interactions, trafficking, conformation, and function. Previously, we had identified S-sulfenylated proteins by using a tagged proteinaceous probe based on the yeast AP-1-like (Yap1) transcription factor that specifically reacts with sulfenic acids and traps them through a mixed disulfide bond. However, the identity of the S-sulfenylated amino acid residues within a protein remained enigmatic. By using the same transgenic YAP1C probe, we present here a technological advancement to identify *in situ* sulfenylated cysteine sites in *Arabidopsis thaliana* cells under control condition and oxidative stress. Briefly, the total extract of transgenic YAP1C *A. thaliana* cells was initially purified on IgG-Sepharose beads, followed by a tryptic digest. Then, the mixed disulfide-linked peptides were further enriched at the peptide level on an anti-YAP1C-derived peptide (C<sub>598</sub>SEIHDR) antibody. Subsequent mass spectrometry analysis with pLink 2 identified 1,745 YAP1C cross-linked peptides, indicating sulfenylated cysteines in over 1,000 proteins. Approximately 55% of these YAP1C-linked cysteines had previously been reported as redox-sensitive cysteines (S-sulfenylation, S-nitrosylation, and reversibly oxidized cysteines). The presented methodology provides a noninvasive approach to identify sulfenylated cysteines in any species that can be genetically modified.

**Keywords:** S-sulfenylation (-SOH), YAP1C, hydrogen peroxide, cross-linked peptide identification, affinity purification, disulfide, *Arabidopsis thaliana*

## INTRODUCTION

Biotic and abiotic stresses increase the production of reactive oxygen species (ROS) in plants. Hydrogen peroxide (H<sub>2</sub>O<sub>2</sub>) is recognized as a secondary messenger and can cause posttranslational modifications on proteins by oxidizing sulfur-containing amino acids, such as methionine and cysteine (Jacques et al., 2015; Waszczak et al., 2015). Cysteine is one of the least abundant amino



acids, representing 1.86% of all amino acids in *Arabidopsis thaliana* (The UniProt Consortium, 2019), but its unique redox sensitivity properties make that it is often found at the active site of proteins (Backus, 2019). The redox sensitivity of Cys residues depends on its *pK<sub>a</sub>* and ionization state, both determined by the local structural environment in the protein. Sulfur-hydrogen bonds and neighboring positively charged residues (such as lysine, histidine, or arginine) can lower the *pK<sub>a</sub>* value of the thiol group, thereby stabilizing the thiolate form (Roos et al., 2013; Zaffagnini et al., 2019). In addition, also solvent accessibility and redox potential of cysteine will affect its reactivity (McConnell et al., 2019; Poole et al., 2020). Reaction of H<sub>2</sub>O<sub>2</sub> with proteinaceous redox-sensitive cysteine thiols leads to the formation of cysteine sulfinic acid (-SOH), which is generally unstable and frequently an intermediary modification *en route* to more stable oxidation forms (Roos and Messens, 2011; Gupta and Carroll, 2014). For instance, -SOH can form intra- or intermolecular disulfides or mixed disulfides with another free thiol or glutathione (GSH), making it enzymatically reversible by the action of thioredoxins (TRXs) or glutaredoxins (GRXs), respectively (Roos and Messens, 2011; Akter et al., 2015b). Recently, extracellular H<sub>2</sub>O<sub>2</sub> has been shown to be sensed through disulfide formation of extracellular cysteines in the plasma membrane receptor HYDROGEN PEROXIDE-INDUCED Ca<sup>2+</sup> INCREASES 1 (HPCA1), leading to Ca<sup>2+</sup> influx in guard cells (Wu et al., 2020). Conversely, besides disulfide formation, -SOH can further oxidize toward sulfinic (-SO<sub>2</sub>H) and sulfonic acid (-SO<sub>3</sub>H). Whereas -SO<sub>3</sub>H is generally considered as an irreversible modification associated with protein degradation (Huang et al., 2018), -SO<sub>2</sub>H can be reduced via sulfiredoxins (SRXs) (Biteau et al., 2003; Akter et al., 2018). Protein S-sulfenylation can directly regulate protein functions. For instance, in *Arabidopsis*, H<sub>2</sub>O<sub>2</sub>-dependent S-sulfenylation of BRASSINAZOLE-RESISTANT 1 (BZR1) promotes its interaction with transcriptional factors (TFs) and drives gene expression (Tian et al., 2018), whereas, S-sulfenylation of BRASSINOSTEROID INSENSITIVE 2 (BIN2) enhances the formation of phosphorylated BRI1-EMS-SUPPRESSOR 1 (BES1), which cannot transport and bind TFs in nuclei, thereby decreasing brassinosteroid (BR) signaling outputs (Song et al., 2019). Another example is the impact on the levels of the auxin biosynthetic precursor tryptophan by S-sulfenylation of a tryptophan synthetase  $\beta$  subunit 1 (Yuan et al., 2017). Alternatively, sulfenylation of catalytic cysteines can directly inhibit the enzymatic activity (Tanner et al., 2011; Gurrieri et al., 2019). As such, the identification of sulfenylated cysteine sites is a crucial step to advance our understanding of redox-regulated processes.

Over the past decade, indirect and direct approaches have been developed to capture and identify S-sulfenylated proteins (Takanishi et al., 2007; Yang et al., 2014, 2016; Gupta et al., 2017). Initially, carbon nucleophilic SOH-selective probes enabled the *in situ* detection of S-sulfenylation at the protein level in *Arabidopsis* and human cells (Leonard et al., 2009; Paulsen et al., 2012; Akter et al., 2015a). Further advancements in affinity-based enrichment strategies allowed the accurate identification of the sulfenylated cysteine residues within the proteins in both

human and plant cells (Yang et al., 2014; Yang J. et al., 2015; Akter et al., 2018; Huang et al., 2019). In addition to these chemoproteomics approaches, a genetic construct based on the yeast (*Saccharomyces cerevisiae*) AP-1-like (Yap1) transcription factor was utilized to detect S-sulfenylated proteins. Yap1 forms mixed disulfides via its redox-active Cys598, located in the C-terminal cysteine-rich domain (cCRD), with the sulfenylated Cys36 of the oxidant receptor protein 1 (Orp1) (Delaunay et al., 2002). A Yap1-cCRD construct, in which Cys620 and Cys629 were mutated to alanine (Ala) and threonine (Thr), respectively, and solely the redox-active Cys598 was retained, was used for the identification of S-sulfenylated proteins in *Escherichia coli* (Takanishi et al., 2007), yeast (Takanishi and Wood, 2011), and the legume model plant *Medicago truncatula* (Oger et al., 2012). In *Arabidopsis* cells, we generated a Yap1-cCRD construct fused to a tandem affinity purification (TAP) tag for improved capture and downstream identification of S-sulfenylated proteins (Waszczak et al., 2014). With this Yap1-cCRD construct, designated YAP1C hereafter, 97 and 132 S-sulfenylated proteins had previously been detected in the *Arabidopsis* cytosol and chloroplast, respectively (Waszczak et al., 2014; De Smet et al., 2019), but the sulfenylated cysteines remained unknown. Here, we describe how a tailored double affinity purification strategy enables the identification of *in situ* sulfenylated cysteines in a noninvasive manner.

## MATERIALS AND METHODS

### Plant Materials and Growth Conditions

Transgenic cells expressing the YAP1C construct were generated as previously reported (Waszczak et al., 2014). In summary, the Yap1 C-terminal cysteine-rich domain (cCRD) construct, entailing the *Saccharomyces cerevisiae* Yap1-coding region corresponding to Asn565 to Asn650, was codon-optimized for expression in *A. thaliana* (L.) Heynh. and synthesized with introduction of the mutations Cys620Ala and Cys629Thr. This genetic construct was fused with an N-terminal TAP tag, containing two IgG-binding domains of protein G and a streptavidin-binding peptide (SBP), separated by the Human Rhinovirus (HRV) 3C protease cleavage site. The YAP1C probe driven by a cauliflower mosaic virus 35S promoter was transformed in *Arabidopsis* cells. YAP1C expression levels were assessed by western blot analysis (Waszczak et al., 2014). The PSB-D *Arabidopsis* cell suspension cultures (NASC stock no. CCL84840) were maintained as described in the ABRC Cell Culture Handling Protocol<sup>1</sup>. For H<sub>2</sub>O<sub>2</sub> treatments, 500 mL of mid-log phase (3 days after culture refreshing, OD<sub>600</sub> = 0.9) cells in 1-L glass flasks were treated with 20 mM H<sub>2</sub>O<sub>2</sub> for 30 min before the cells were harvested through a vacuum filtration system (Pall Corporation, Port Washington, NY, United States) and snap-frozen in liquid nitrogen before storage at -70°C.

<sup>1</sup><https://abrc.osu.edu/researchers/cell>

## Protein Extraction

Frozen cell pellets harvested from approximately 1 L of suspension cultures were crushed with fine quartz granules (Merck, Darmstadt, Germany) with a precooled mortar and pestle in ice-cold lysis buffer (25 mM Tris, 15 mM MgCl<sub>2</sub>, 150 mM NaCl, 15 mM pNO<sub>2</sub> PhenylPO<sub>4</sub>, 60 mM β-glycerophosphate, 0.1% NP-40, 0.1 mM Na<sub>3</sub>VO<sub>4</sub>, 1 mM NaF, 1 mM phenylmethylsulfonyl fluoride, 1 μM *trans*-epoxysuccinyl-L-leucylamido(4-guanidino)butane [E64], 1/50 mL ethylenediaminetetraacetic acid [EDTA]-free Ultra Complete tablet, 5% [v/v] ethylene glycol, 0.1 mg/mL 4-(2-aminoethyl) benzenesulfonyl fluoride hydrochloride [AEBSF], 0.1% benzonase, and 1 μg/mL leupeptin, pH 7.6), supplemented with 10 mM iodoacetamide (IAM) to prevent artificial oxidation of cysteine residues during the extraction procedure. After two rounds of centrifugation (20,000 × *g* for 20 min; 4°C), the supernatant was collected and protein concentrations were determined with the Bradford Protein Assay (He, 2011).

## Anti-C<sub>598</sub>SEIWDR Antibody Production and Its Coupling on Magnetic Beads

The C<sub>598</sub>SEIWDR peptide was synthesized (purity >85%) and conjugated to Keyhole Limpet Hemocyanin (KLH) as a carrier (GenScript, Nanjing, China) and 0.2 mg of the C<sub>598</sub>SEIWDR-KLH conjugate, together with Freund's incomplete adjuvant, were injected subcutaneously into four New Zealand rabbits at 14, 28, and 42 days. Seven days after the second and third immunization, approximately 20 and 40 mL (60 mL) of serum, respectively, were obtained from each animal. Three sera were retained for further purification, based on their high specificity against the "C<sub>598</sub>SEIWDR" peptide (high ELISA titer, >1: 512,000), with a "C<sub>598</sub>SEIWDR" peptide-coupled affinity iodoacetyl resin. Subsequently, the anti-C<sub>598</sub>SEIWDR antibodies were coupled on BcMag<sup>TM</sup> Epoxy-Activated Magnetic Beads (Biolone Inc., San Diego, CA, United States) (Hamperl et al., 2014). Five mg of antibody was diluted to 3 mg/mL with coupling buffer (0.1 M sodium phosphate, pH 7.4) and incubated with 15 mg equilibrated Epoxy-Activated beads for 18 h at 30°C with gentle rotation (1000 rpm). After the beads had been washed twice with 100 mM glycine-HCl (pH 2.5) and then once with 10 mM Tris-HCl (pH 8.8), they were inactivated by 0.1 M trimethylamine and washed four times with phosphate-buffered saline (PBS) buffer (pH 7.4) and then twice with the PBS buffer (pH 7.4) containing 0.5% (w/v) Triton X-100. Finally, the antibody-coupled beads were suspended in 1 mL PBS buffer (pH 7.4), containing 0.02% (w/v) sodium azide and stored at 4°C until use.

## Affinity Purification

The initial purification at the protein level on IgG-Sepharose 6 Fast Flow beads (GE Healthcare, Chicago, IL, United States) was performed as described with some modifications (Van Leene et al., 2007). Briefly, 150 mg of protein extract was first incubated with 300 μL of IgG-Sepharose beads, preequilibrated with 3 × 1 mL washing buffer (10 mM Tris-HCl, pH 7.6, 150 mM NaCl, 1 μM E64, 0.5 mM EDTA-free Ultra Complete tablet,

0.1 mg/mL AEBSF, and 1 μg/mL leupeptin) for 2 h at 4°C with gentle rotation. IgG-Sepharose beads were transferred to a 1-mL Mobicol column (MoBiTec GmbH, Göttingen, Germany) and washed with 5 × 1 mL washing buffer and 2 × 1 mL digestion buffer (50 mM Tris-HCl, pH 8.0). Then, the IgG-enriched proteins were digested on the beads with mass spectrometry-grade Trypsin/Lys-C Mix (Promega, Madison, WI, United States) at a 1:50 (enzyme/substrate) ratio for 18 h at 37°C. Additional trypsin at a 1:100 (enzyme/substrate) ratio was added for an extra 4 h at 37°C. The peptides were collected by gentle rotation (1000 rpm for 1 min at 4°C), and the beads were eluted twice with digestion buffer. All three fractions were pooled. One-sixth of the tryptic digestion was used for protein-level identification with liquid chromatography-tandem mass spectrometry (LC-MS/MS) analysis. The remainder of the tryptic digestion was incubated with 200 μL magnetic beads coupled to anti-C<sub>598</sub>SEIWDR antibodies for 2 h at 4°C with gentle rotation (1000 rpm). The tube was placed in the magnetic separator until the beads were captured on the magnet side, where after, the clear supernatant was removed. Collected beads were washed three times with cold washing buffer (10 mM Tris, 150 mM NaCl, pH 7.6). The enriched peptides were eluted by incubation with 400 μL of 0.2 M glycine buffer (pH 2.5) for 10 min with rotation (1000 rpm). The supernatant was collected on the separator and supplemented with 100 μL 1 M Tris-HCl buffer (pH 9.0) for neutralization. After desalting with OMIX C18 pipette tips (Agilent, Santa Clara, CA, United States), the peptide samples were eluted with 100 μL 75% (v/v) acetonitrile containing 0.1% (v/v) formic acid and dried by vacuum centrifugation. The dried peptide samples were subjected to LC-MS/MS.

## LC-MS/MS

For the LC-MS/MS analyses, a Q Exactive Plus instrument was used (Thermo Fisher Scientific, Waltham, MA, United States) operated with an Easy-nLC1000 system (Thermo Fisher Scientific). Samples were reconstituted in 0.1% (v/v) formic acid, followed by centrifugation (16,000 × *g* for 10 min). The supernatants were pressure-loaded onto a 2-cm microcapillary precolumn packed with C18 (3 μm, 120 Å; SunChrom, Friedrichsdorf, Germany). The precolumn was connected to a 12-cm 150-μm-inner diameter microcapillary analytical column packed with C18 (1.9 μm, 120 Å; Dr. Maisch GmbH, Ammerbuch-Entringen, Germany) and equipped with a home-made electrospray emitter tip. The spray voltage was set to 2.0 kV and the heated capillary temperature to 320°C. The LC gradient A consisted of 0 min, 8% B; 14 min, 13% B; 51 min, 25% B; 68 min, 38% B; 69–75 min, 95% B [A, water; B, 80% (v/v) acetonitrile] at a flow rate of 600 nL/min. Higher-energy collisional dissociation (HCD) MS/MS spectra were recorded in the data-dependent mode with a Top20 method. The first MS spectra were measured with a resolution of 70,000, an AGC target of 3e<sup>6</sup>, a maximum injection time of 20 ms, and a mass range from *m/z* 300 to 1,400. The HCD MS/MS spectra were acquired with a resolution of 17,500, an AGC target of 1e<sup>6</sup>, a maximum injection time of 60 ms, a *m/z* 1.6 isolation window, and normalized collision energy of 30. The *m/z* of the

peptide precursors that triggered MS/MS scans were dynamically excluded from further MS/MS scans for 18 s.

## MS/MS Data Processing

RAW files were examined with pLink 2 algorithm version 2.3.5 (Chen et al., 2019) and converted to MGF files by the MSFileReader (Thermo Fisher Scientific). Spectra were searched against representative Araport11 proteins (27,655 entries, v1.10.4, release on 06/2016), supplemented with the YAP1C protein sequence. Notably, the last seven amino acids “RDWLESC” of AT1G74260, of which the reverse sequence is an isobaric “CSELWDR” peptide, were omitted, because they resulted in high-scoring decoy matches, reflecting the enriched YAP1C-derived “C<sub>598</sub>SEIWDR.” A precursor tolerance of 20 ppm and a fragment mass tolerance of 20 ppm (HCD spectra) were specified. A specific tryptic search was used with a maximum of two allowed missed cleavages. Variable modifications included methionine oxidation, cysteine carbamidomethylation, and protein N-terminal acetylation. No fixed modifications were set. Results were filtered at a false discovery rate (FDR) threshold of 1% at the spectrum, peptide, and protein levels.

## Bioinformatics

### Cross-Linked Peptide-to-Protein Assignment

Cross-linked peptides were extracted from pLink 2 cross-linked (CL) peptide reports ( $\leq 1\%$  FDR). Due to trypsin miscleavages, redundant CL peptides were identified for approximately 10% of the YAP1C-CL protein sites. To remove this redundancy, CL peptides matching an identical protein site were grouped and the peptide matching the least proteins was chosen as representative, resulting in 1,748 YAP1C-CL protein sites (Supplementary Dataset S1).

### Enrichment Analyses

The 570 proteins that uniquely matched CL peptides were analyzed for gene set enrichment in the Gene Ontology (GO) and the Kyoto Encyclopedia of Genes and Genomes (KEGG) pathways by means of the DAVID tool (Huang et al., 2009). In addition, the overrepresentation of Cys-SOHs was determined in protein domains (PROSITE profiles) (Sigrist et al., 2013) as described previously (Huang et al., 2019).

### C<sub>598</sub>SEIWDR Cross-Link Peptide Fingerprint Scanning

Peak list (MGF) files generated by pLink 2 (Chen et al., 2019) were parsed by an in-house script to detect the occurrence of the 10 characteristic fragment ions. Per MS/MS spectrum, the numbers of peaks with a matching  $m/z$  value ( $\leq 0.01$  Da) were counted, irrespective of their intensity. MS/MS spectra containing the full fingerprint or a high number of characteristic fragment ions hint at the fragmentation of C<sub>598</sub>SEIWDR CL peptides, although a CL search algorithm remains necessary to uncover their identity.

## Data Availability

Thermo RAW files and pLink 2 result tables are available on the PRIDE repository with the identifier PXD016723. The 1,747

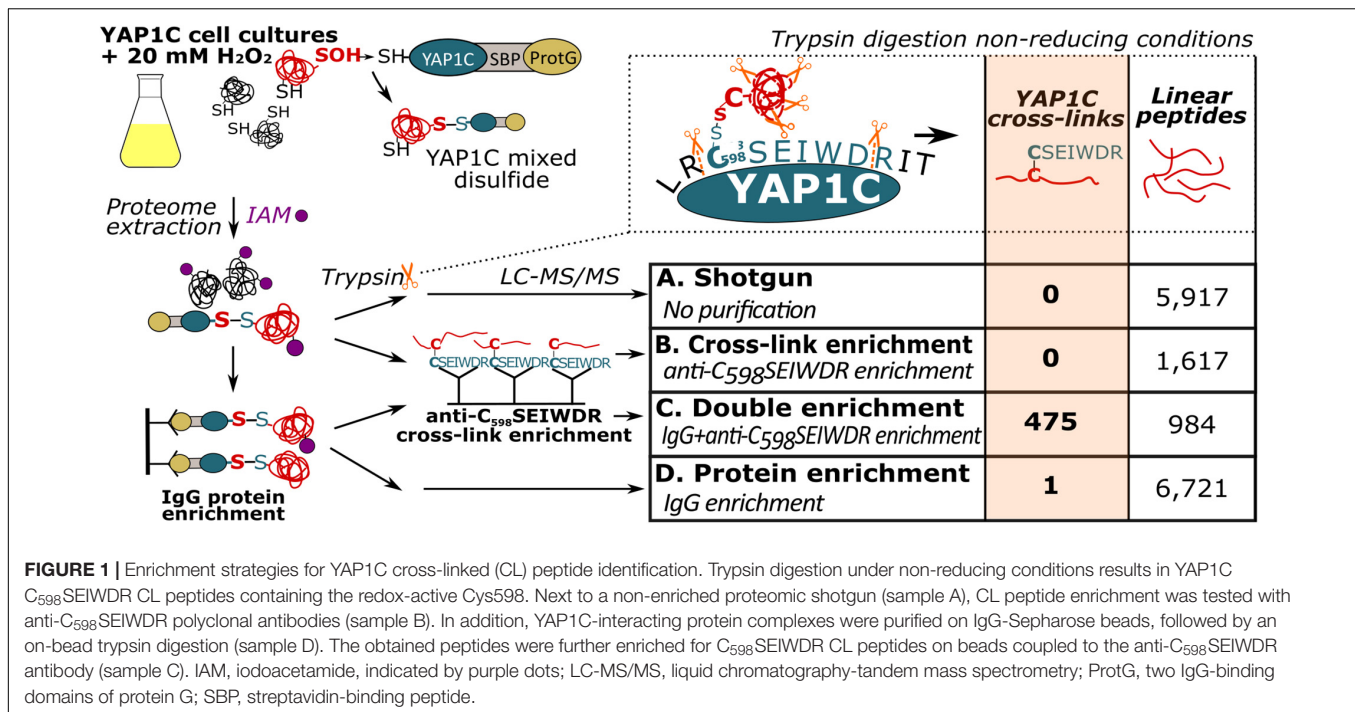
sulfenylated cysteine residues identified were submitted to the Plant PTM Viewer (Willems et al., 2019).

## RESULTS AND DISCUSSION

### Identification of YAP1C-Resolved S-Sulfenylated Sites Through a Protein- and Peptide-Level Purification Strategy

Previously, we had identified S-sulfenylated *Arabidopsis* proteins *in vivo* by means of a transgenically expressed YAP1C probe fused to an affinity purification tag (Waszczak et al., 2014; De Smet et al., 2019). Crucial steps in this strategy were the nucleophilic attack and the subsequent formation of a mixed disulfide bond by Cys598 of YAP1C and the sulfenylated Cys (Cys-SOH) residue in oxidized target proteins (Delaunay et al., 2002; Takanishi et al., 2007). In these approaches, the mixed disulfide YAP1C complexes were purified in a sequential affinity purification strategy, firstly by IgG-Sepharose beads trapping the IgG-binding domain of protein G (ProtG) and, subsequently, after cleavage with protease, by Streptavidin-Sepharose beads targeting the streptavidin-binding peptides (SBP). As such, approximately 230 *in vivo* S-sulfenylated protein targets had been detected by MS (Waszczak et al., 2014; De Smet et al., 2019). However, information on the identity of the S-sulfenylated sites remained unknown in the proteins harboring more than one cysteine. An average of 7.85 Cys residues per *Arabidopsis* protein (309,122 Cys residues in 39,364 proteins, The UniProt Consortium, 2019) implied that for most S-sulfenylation proteins downstream validation experiments are required, including mutational approaches and/or *in vitro* protein studies. We reasoned that, at least under non-reducing conditions, trypsin cleavage would result in disulfide-bound peptides between the nucleophilic YAP1C Cys598 and the sulfenylated cysteine in the target proteins. Hence, these mixed peptides entail the necessary information on the sulfenylated cysteines. Theoretically, trypsin cleavage around the disulfide bond generates a mixed peptide involving the 7-amino-acid peptide from the YAP1C probe “C<sub>598</sub>SEIWDR” that contains the redox-active Cys598, and the sulfenylated cysteine-containing peptide from the YAP1C-bound protein (Figure 1). Typically, CL peptides represent solely a minor fraction in complex peptide mixtures that are dominated by tryptic linear peptides. Therefore, enrichment procedures are performed in chemical cross-link proteomics (Barysz and Malmström, 2018). Similarly, we devised an enrichment strategy for the C<sub>598</sub>SEIWDR CL peptides by generating polyclonal antibodies directed toward the C<sub>598</sub>SEIWDR peptide (see Materials and Methods). Afterward, we tested four workflows for the detection of C<sub>598</sub>SEIWDR CL peptides by pLink 2 (Chen et al., 2019; Figure 1). Proteins were extracted from YAP1C cells treated with 20 mM H<sub>2</sub>O<sub>2</sub> for 30 min. Note that for all tested workflows, equal fractions of proteins were used for LC-MS/MS (0.5 mg). Firstly, a trypsin-digested proteome was submitted for MS (shotgun proteomics), resulting in the identification of 5,917 linear (regular) peptides that provided a general proteome reference (Figure 1, sample A). However, no





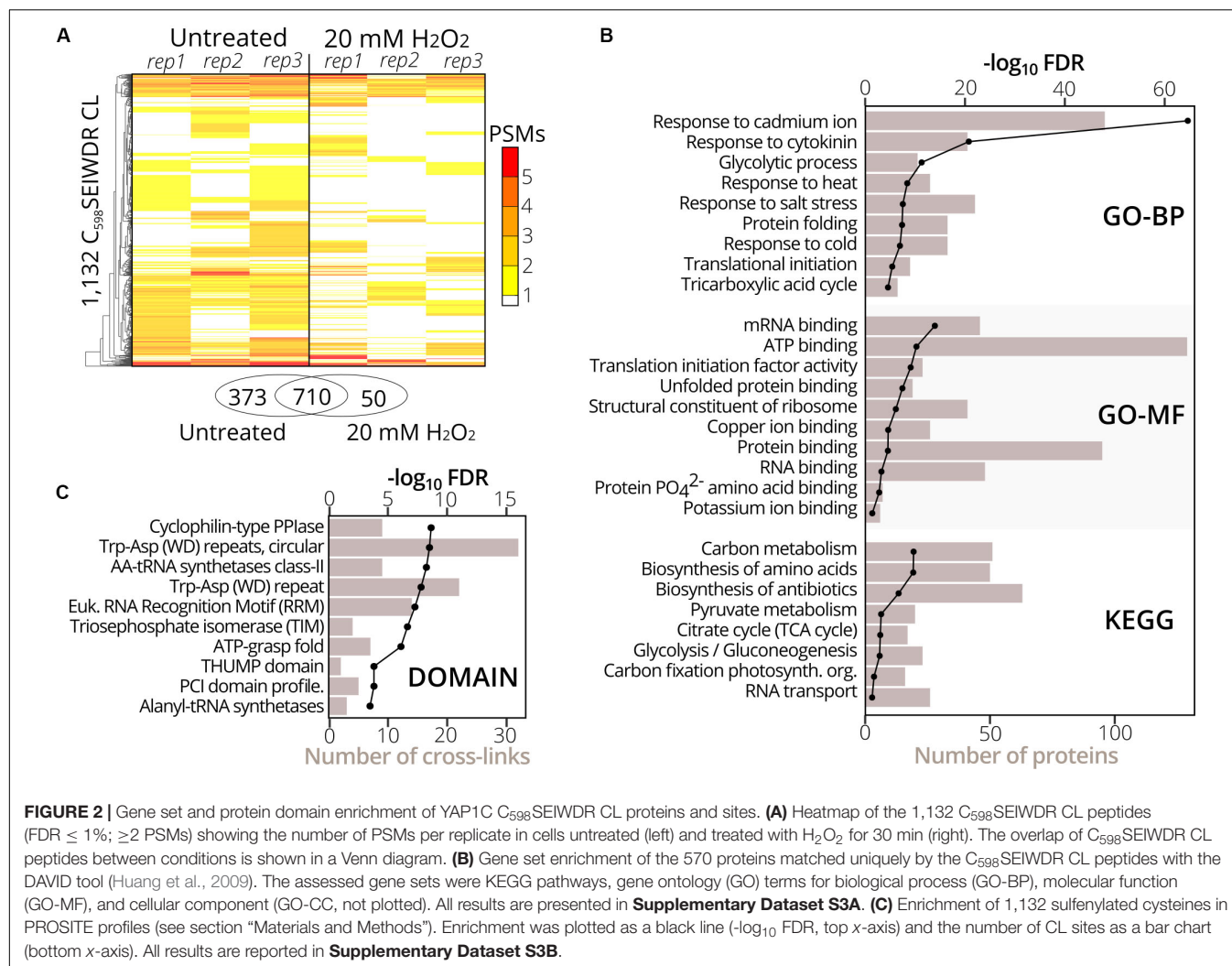
C<sub>598</sub>SEIWDR CL peptides were found, highlighting the need for YAP1C enrichment strategies. Hence, we subjected the digested proteome to an anti-C<sub>598</sub>SEIWDR enrichment (**Figure 1**, sample B). However, such direct peptide-level enrichment didn't result in C<sub>598</sub>SEIWDR CL peptide identifications. To reduce the peptide complexity prior to the anti-C<sub>598</sub>SEIWDR enrichment, the proteome was first enriched on the IgG-Sepharose beads and, second, after an on-beads trypsin digestion, the eluted sample was subjected to an anti-C<sub>598</sub>SEIWDR affinity purification and analyzed by MS (**Figure 1**, sample C). This double enrichment strategy proved highly successful, because 475 C<sub>598</sub>SEIWDR CL peptides were identified ( $\leq 1\%$  FDR; **Supplementary Dataset S1**). Lastly, we tested the CL peptide identifications of the eluted sample only after IgG-Sepharose enrichment (**Figure 1**, sample D). After protein-level enrichment, solely one single CL peptide, "C#SEIWDR-VIEYC#K" (with C#, indicating a CL cysteine), was identified that matched the S PHASE KINASE-ASSOCIATED PROTEIN (SPK)-like proteins. Hence, a dedicated cross-link enrichment step is required after the IgG-Sepharose enrichment for large-scale identification of YAP1C CL peptides. Moreover, the 6,721 identified linear peptides provide complementary information on the YAP1C protein interactors. Taken together, analysis of YAP1C protein interactors, after IgG-Sepharose enrichment, followed by the identification of YAP1C CL sites, after an additional anti-C<sub>598</sub>SEIWDR enrichment step, enables the proteome-wide detection of sulfenylated cysteines.

### Identification With YAP1C of Sulfenylated Cysteines Under H<sub>2</sub>O<sub>2</sub> Stress

To identify sulfenylated cysteines in untreated and treated (20 mM H<sub>2</sub>O<sub>2</sub> for 30 min) YAP1C cells (three replicates

per condition), we analyzed YAP1C protein complexes after IgG-Sepharose enrichment and their YAP1C CL sites after an additional anti-C<sub>598</sub>SEIWDR enrichment step. In total, 1,930 C<sub>598</sub>SEIWDR CL peptides were detected (7,040 peptide-to-spectrum matches (PSMs); **Supplementary Dataset S2**). Due to trypsin missed cleavages, some CL peptides specified the same sulfenylated cysteine. For instance, “C#ATITPDEGR-C#SEIWDR” and “C#ATITPDEGRVTEFGLK-C#SEIWDR,” both indicate S-sulfenylation of Cys75 in CYTOSOLIC NADP<sup>+</sup>-DEPENDENT ISOCITRATE DEHYDROGENASE. Removal of this redundancy (see Materials and Methods) resulted in a total of 1,747 non-redundant C<sub>598</sub>SEIWDR CL peptides (**Supplementary Dataset S2**). Of these 7,040 PSMs, 25 (0.36%) are indicative of inter-YAP1C cross-links between the redox-active Cys598, suggesting that a minor artifactual self-trapping of YAP1C is possible. In favor of high-confident identifications, we retained 1,132 out of the 1,747 C<sub>598</sub>SEIWDR CL peptides with at least two PSMs across the six samples (**Supplementary Dataset S2**). We identified more C<sub>598</sub>SEIWDR CL peptides in untreated samples (1,082 CL peptides) than in the H<sub>2</sub>O<sub>2</sub>-treated cells (759 CL peptides). The YAP1C probe is continuously overexpressed and trapping of S-sulfenylated cysteines starts before the addition of 20 mM H<sub>2</sub>O<sub>2</sub>. This oxidative stress treatment might result in the overoxidation of certain cysteines, leading to the formation of sulfinic and sulfonic acids, which cannot be trapped by YAP1C. Nevertheless, the majority of the C<sub>598</sub>SEIWDR CL peptides [709 out of 1,132 (63%)] were identified under both conditions and 50 CL peptides were exclusively identified after H<sub>2</sub>O<sub>2</sub> stress (**Figure 2A**). From the 1,132 C<sub>598</sub>SEIWDR CL peptides, 307 could not be determined unambiguously to a unique *Arabidopsis* protein, meaning that the YAP1C CL *Arabidopsis* peptides are present in at least two different proteins. The remaining 825 CL





peptides matched uniquely to 570 different proteins, implying that some *Arabidopsis* proteins contain multiple S-sulfenylated sites. For 94% of the 570 YAP1C CL proteins, at least one peptide was identified after IgG-Sepharose enrichment, thus complementarily confirmed as a YAP1C-interacting protein. From the 307 CL peptides that match multiple *Arabidopsis* proteins, protein-level evidence was exclusively available for solely one of the possible matching proteins, for instance, the CL peptide “KLKEC#EK-C#SEIWDR” represents a C<sub>598</sub>SEIWDR CL to either Cys124 in PROTEIN PHOSPHATASE5 (PP5, AT2G42810) or Cys487 in PROTON PUMP INTERACTOR2 (PPI2, AT3G15340) (**Supplementary Dataset S2**). Prior to the anti-C<sub>598</sub>SEIWDR purification step, 23 linear peptides (194 PSMs) were identified for PP5, whereas none for PPI2. As such, besides the complementary evidence of the YAP1C-interacting proteins, the MS analysis of the IgG-Sepharose-enriched samples are helpful for protein identification in case of ambiguous peptide-to-protein matching.

To functionally categorize the identified S-sulfenylated proteins, we carried out a gene set enrichment analysis on

the 570 proteins for which 825 sulfenylated cysteines had unambiguously been identified by C<sub>598</sub>SEIWDR CL peptides. In accordance with the cytosolic localization of the YAP1C probe, the strongest overrepresented GO term was the cellular component “cytosol” (FDR  $2.3 \times 10^{-202}$ ; **Supplementary Dataset S3A**). In addition, proteins of several stress-related adaptive processes (Cd<sup>2+</sup>, salt, heat, and cold), metabolism, and RNA processes were strongly enriched (**Figure 2B**), corresponding with our previous reports that demonstrated that enzymes involved in core carbon metabolic pathways, such as glycolysis, amino acid metabolism, and carbon fixation, were prone to S-sulfenylation (Huang et al., 2018, 2019). Also, the GO-MF term “mRNA-binding” and the KEGG pathway “RNA transport” were overrepresented (FDR  $3.6 \times 10^{-16}$  and 0.04, respectively) (**Figure 2B**). Sulfenylated cysteines were overrepresented in various protein domains (**Figure 2C**). For instance, in the *Arabidopsis* proteome, the amino acyl-transfer RNA (AA-tRNA) synthetase domain is present in seven proteins and contains 96 cysteines in total, of which nine found within the AA-tRNA synthetase domain were detected as sulfenylated and were

overrepresented (FDR  $5.9 \times 10^{-9}$ ; **Supplementary Dataset S3B**). In addition, the RNA-binding RNA-recognition motif (RRM) was overrepresented (FDR  $5.5 \times 10^{-8}$ ) that had previously been reported as a S-sulfenylation hotspot (Huang et al., 2019). Taken together, functional enrichment of S-sulfenylated proteins and cysteines identified by C<sub>598</sub>SEIWDR CL peptides match previous observations by other tools.

## YAP1C Cross-Linked Peptides Are Associated With Characteristic Disulfide Ions

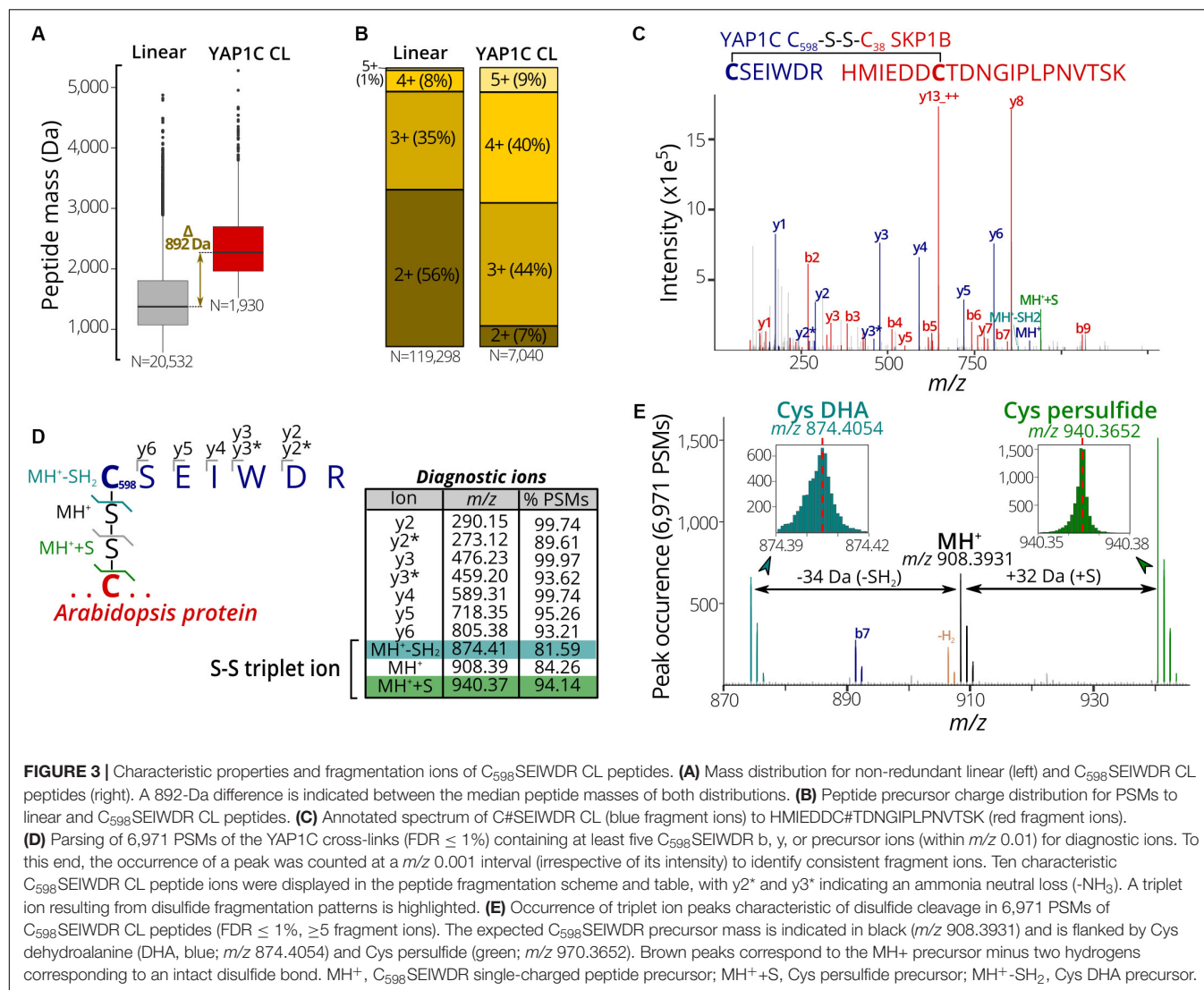
In a next phase, we used the 7,000 PSMs of C<sub>598</sub>SEIWDR CL peptides to characterize in detail their general properties and MS/MS fragmentation patterns. Firstly, we compared the properties of C<sub>598</sub>SEIWDR CL peptides to the linear peptides identified prior to the anti-C<sub>598</sub>SEIWDR purification. As CL peptides are the combination of two peptides with charged N-termini and tryptic C-termini ending on Arg/Lys, CL peptides typically have both a higher mass and precursor charge than the linear peptides. In accordance, the peptide mass of C<sub>598</sub>SEIWDR (907 Da) approximates the median peptide mass difference of identified C<sub>598</sub>SEIWDR CL peptides with linear peptides (**Figure 3A**, 892 Da). In addition, precursors of the C<sub>598</sub>SEIWDR CL peptides are more positively charged than the linear peptides, with approximately 93% of the PSMs charged  $\geq 3+$  (**Figure 3B**). As such, both peptide mass and charge are in line with typical CL peptide properties. Importantly, the CL peptide identification is more challenging than that of linear peptides, because the fragmentation of CL peptides results in intermixed fragment ions derived from both peptides. Noteworthy, the CL peptide search with pLink 2 was not biased toward C<sub>598</sub>SEIWDR CL and 27 intra-protein and 20 inter-protein (non-YAP1C) CL peptides were identified (102 PSMs, FDR  $\leq 1\%$ ) (**Supplementary Dataset S4**). Hence, despite the search for CL peptides between or within 26,000 Arabidopsis proteins, the YAP1C C<sub>598</sub>SEIWDR CL peptides are by far preponderant (7,040 C<sub>598</sub>SEIWDR CL PSMs versus 102 non-YAP1C PSMs), and emphasize the effectiveness and necessity of the anti-C<sub>598</sub>SEIWDR purification. Moreover, Cys598 of YAP1C was also CL to Arabidopsis peptides via the trypsin-missed cleaved peptides “EGSLRC#SEIWDR” and “C#SEIWDRITTHPK.” For instance, the peptide “HMIEDDC#TDNGIPLPNVTSK” of the E3 ubiquitin ligase SKP-like protein 1B (SKP1B; AT5G42190) was CL to both “C#SEIWDR” (**Figure 3C**) and “C#SEIWDRITTHPK” (**Supplementary Dataset S2**). This cytosolic protein had been identified previously to be S-sulfenylated by the original protein-level YAP1C-TAP strategy (Waszczak et al., 2014).

Next, we aimed to identify characteristic fragment ions of C<sub>598</sub>SEIWDR CL peptides. Such characteristic ions could help in the assessment of the PSM quality or future identification of C<sub>598</sub>SEIWDR CL peptides. To detect consistent fragment ions associated with C<sub>598</sub>SEIWDR CL peptide fragmentation, we counted the occurrence of MS/MS  $m/z$  peaks in 6,971 PSMs (98.8% of 7,040 total C<sub>598</sub>SEIWDR CL PSMs), containing at least five b, y, or precursor ions

of C<sub>598</sub>SEIWDR. The C<sub>598</sub>SEIWDR fragment y ions are well represented, occurring in 93% to 99% of the cases (**Figure 3D**), as well as y<sub>2</sub> and y<sub>3</sub> ions with neutral loss of NH<sub>3</sub> (**Figure 3D**, y<sub>2</sub><sup>\*</sup> and y<sub>3</sub><sup>\*</sup>, respectively). Interestingly, besides the C<sub>598</sub>SEIWDR precursor ion (MH<sup>+</sup>,  $m/z$  908.39), neighboring masses corresponding to the precursor ion with cysteine persulfide formation (blue; +S,  $m/z$  940.37) and a cysteine-to-dehydroalanine conversion (green; -SH<sub>2</sub>,  $m/z$  874.41) are consistently present in C<sub>598</sub>SEIWDR CL PSMs (**Figures 3D,E**). This distinctive pattern of triplet ions is characteristic for inter-protein disulfides (Janecki and Nemeth, 2011) and used, for instance, by dedicated disulfide CL identification algorithms, such as DBond (Na et al., 2015) and MS2DB+ (Murad et al., 2011). Together with the C<sub>598</sub>SEIWDR y fragment ions, these precursor triplet ions form a distinctive C<sub>598</sub>SEIWDR fragment ion fingerprint. For example, 4,220 PSMs (59.9%) of the identified C<sub>598</sub>SEIWDR CL PSMs contain all 10 of these characteristic ions, whereas 6,503 (92.4%) and 5,847 PSMs (83.1%) had eight and nine out of 10 ions, respectively. As such, these characteristic ions can help in PSM quality assessment of C<sub>598</sub>SEIWDR CL peptides, with, for instance, all characteristic ions present in the “HMIEDDC#TDNGIPLPNVTSK-C#SEIWDR” PSM (**Figure 3C**). In addition, we used the characteristic fragment ions (**Figure 3D**) as a fingerprint to scan potential C<sub>598</sub>SEIWDR CL peptides in the raw proteomics data obtained after IgG-Sepharose and/or anti-C<sub>598</sub>SEIWDR enrichment strategies (**Figure 1**). After IgG-Sepharose enrichment, 33 MS/MS spectra contained the full C<sub>598</sub>SEIWDR CL fingerprint (**Supplementary Dataset S5**), indicating that more than a single C<sub>598</sub>SEIWDR CL might be fragmented, but not identified in the pLink 2 search (FDR  $\leq 1\%$ ; **Supplementary Dataset S1**). Missing identifications can arise due to numerous reasons, such as the *Arabidopsis* peptide CL to C<sub>598</sub>SEIWDR being shorter than six amino acids (default pLink 2 search settings), noisy spectra with low-abundant fragment ions, or too stringent FDR scoring. In line with the high number of C<sub>598</sub>SEIWDR CL peptides identified by pLink 2 (475 peptides; **Supplementary Dataset S1**), 1,502 MS/MS spectra contained the full C<sub>598</sub>SEIWDR CL fingerprint after the additional anti-C<sub>598</sub>SEIWDR enrichment step (**Supplementary Dataset S5**). In contrast, no spectra with a full C<sub>598</sub>SEIWDR CL fingerprint were found in the proteome shotgun analysis or after direct anti-C<sub>598</sub>SEIWDR enrichment (**Figure 1**, samples A and B, respectively), indicating a high specificity for the fingerprint toward C<sub>598</sub>SEIWDR CL peptides. As such, the proposed 10 characteristic ions provide a useful and distinctive fingerprint for C<sub>598</sub>SEIWDR CL peptides for quality assessment of individual spectral matches or raw proteomics data.

## YAP1C Cross-Linked Cysteines Report Protein Redox-Sensitive Cysteine Sites

We assessed whether the identified C<sub>598</sub>SEIWDR CL peptides (**Supplementary Dataset S2**) are in agreement with related redox studies. First, in 67 out of the 97 S-sulfenylated



proteins (69%) identified previously as YAP1C interactors (Waszczak et al., 2014), 102 S-sulfenylated sites were found, including, for instance, Cys20 of DEHYDROASCORBATE REDUCTASE 2 (DHAR2) (Figure 4A) that had been shown to be S-glutathionylated via an S-sulfenylation intermediary by 5,5-dimethyl-1,3-cyclohexadione (dimedone) labeling and MS identification of recombinantly produced DHAR2 (Waszczak et al., 2014; Bodra et al., 2017). This laborious approach to identify the trapped S-sulfenylation sites can be avoided thanks to the identification of C<sub>598</sub>SEIWDR CL peptides, as shown here for DHAR2. In AtDHAR2, the sulfenylation of the active site cysteine is part of the ping-pong mechanistic cycle, which we described previously (Bodra et al., 2017). During the reduction of dehydroascorbate (DHA) to ascorbate (AsA), the active site thiol gets sulfenylated and becomes more electrophilic for the next step of the catalytic mechanism, being the formation of a mixed-disulfide with glutathione. Also, here, the micro-environment of this specific cysteine determines its reactivity with both DHA

and GSH. Besides Cys20 of DHAR2, Cys6 located at the protein N-terminus was identified as YAP1C CL site as well (Supplementary Dataset S2 and Figure 4B; Bodra et al., 2017). Furthermore, we highlighted the residues (96 out of 213, 45%) covered by 8 linear peptides (52 PSMs, Supplementary Dataset S2) identified after YAP1C protein-level enrichment and giving strong complementary evidence. Taken together, this procedure will help hypothetically formulate the mode-of-action of potential redox switches and fast-forward downstream experiments.

Then, the S-sulfenylated cysteines determined by C<sub>598</sub>SEIWDR CL peptides were compared to redox-sensitive *Arabidopsis* cysteines reported previously. Recently, we have identified more than 1,500 sulfenylated Cys residues in *Arabidopsis* cells by means of a chemoselective benzothiazindioxide (BTD)-based carbon nucleophile (Huang et al., 2019). Comparison of the 1,132 YAP1C CL peptides (Supplementary Dataset S2; ≥ 2 PSMs) revealed 406 sites (36%) that overlapped with BTD-targeted Cys (Figure 4C).



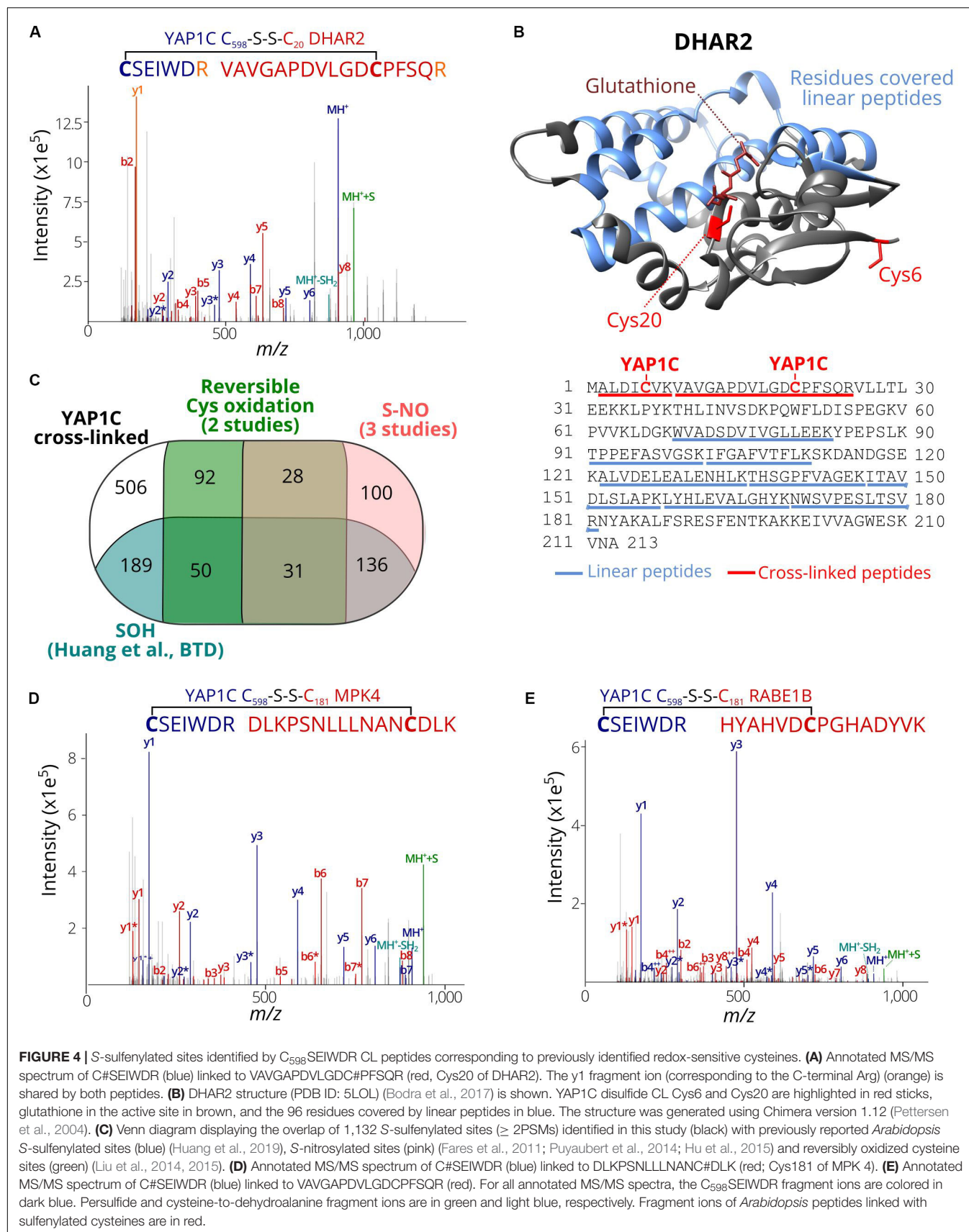


**FIGURE 4 |** S-sulfenylated sites identified by C<sub>598</sub>SEIWDR CL peptides corresponding to previously identified redox-sensitive cysteines. **(A)** Annotated MS/MS spectrum of C#SEIWDR (blue) linked to VAVGAPDVLGDCPFSSQR (red, Cys20 of DHAR2). The y1 fragment ion (corresponding to the C-terminal Arg) (orange) is shared by both peptides. **(B)** DHAR2 structure (PDB ID: 5L0L) (Bodra et al., 2017) is shown. YAP1C disulfide CL Cys6 and Cys20 are highlighted in red sticks, glutathione in the active site in brown, and the 96 residues covered by linear peptides in blue. The structure was generated using Chimera version 1.12 (Pettersen et al., 2004). **(C)** Venn diagram displaying the overlap of 1,132 S-sulfenylated sites (≥ 2PSMs) identified in this study (black) with previously reported *Arabidopsis* S-sulfenylated sites (blue) (Huang et al., 2019), S-nitrosylated sites (pink) (Fares et al., 2011; Puyaubert et al., 2014; Hu et al., 2015) and reversibly oxidized cysteine sites (green) (Liu et al., 2014, 2015). **(D)** Annotated MS/MS spectrum of C#SEIWDR (blue) linked to DLKPSNLLLNNANCDLK (red, Cys181 of MPK 4). **(E)** Annotated MS/MS spectrum of C#SEIWDR (blue) linked to VAVGAPDVLGDCPFSSQR (red). For all annotated MS/MS spectra, the C<sub>598</sub>SEIWDR fragment ions are colored in dark blue. Persulfide and cysteine-to-dehydroalanine fragment ions are in green and light blue, respectively. Fragment ions of *Arabidopsis* peptides linked with sulfenylated cysteines are in red.



For instance, the C<sub>598</sub>SEIWDR CL peptides “C#SEIWDR-DLKPSNLLNANC#DLK” (**Figure 4D**) matched the Cys181 of MITOGEN-ACTIVATED PROTEIN KINASE 4 (MPK4) that had been experimentally verified (Huang et al., 2019). Also, other site-specific reversibly oxidized cysteine studies (Liu et al., 2014, 2015) and S-nitrosylation studies (Fares et al., 2011; Puyaubert et al., 2014; Hu et al., 2015) were compared (Willems et al., 2019). In total, 295 S-nitrosylation and 201 reversible previously reported cysteine oxidation sites overlapped with the YAP1C CL sites (**Figure 4C**). Taken together, 626 out of the 1,132 sulfenylated cysteines identified here by C<sub>598</sub>SEIWDR CL peptides (55.3%) had already been reported as redox sensitive in independent studies, of which some had been confirmed biochemically. For instance, “C#SEIWDR-LRGLIAEKNC#APIMVR” matched Cys32 of ascorbate peroxidase 1 (APX1), an important ROS-scavenging enzyme, that has been identified previously as S-sulfenylated (Huang et al., 2019) and S-nitrosylated (Fares et al., 2011; Liu et al., 2014). Nitrosylation of Cys32 had been confirmed to increase its H<sub>2</sub>O<sub>2</sub>-scavenging enzymatic activity (Yang H. et al., 2015). Moreover, another C<sub>598</sub>SEIWDR CL Cys49 of APX1 was also found as S-nitrosylated (Hu et al., 2015) and S-sulfenylated (Huang et al., 2019). In addition, “C#SEIWDR-HYAHVDC#PGHADYVK” matched Cys149 of the chloroplastic elongation factor Tu (EF-Tu) RAB GTPASE HOMOLOG E1B (RABE1B) (**Figure 4E**), a site identified previously as S-sulfenylated (Huang et al., 2019) and S-nitrosylated (Hu et al., 2015). Interestingly, sulfenylation of the corresponding cysteine site (Cys82; **Supplementary Figure S1**) in the EF-Tu ortholog of *Cyanobacterium synechocystis*, a popular model organism for studies of photosynthesis as chloroplast ancestor, inactivates EF-Tu in a reversible manner (Puyaubert et al., 2014; Yutthanasirikul et al., 2016). Taken together with the approximately 3.0-fold increased S-sulfenylation under H<sub>2</sub>O<sub>2</sub> treatment (Huang et al., 2019), the plastidial EF-Tu protein probably exhibits a conserved redox sensitivity in *Arabidopsis*. All in all, the high agreement of the S-sulfenylated sites identified by C<sub>598</sub>SEIWDR CL peptides with other studies of redox-sensitive cysteines demonstrates that the YAP1C-resolved cysteines are in general highly susceptible to oxidative redox modifications. Identification of these redox-sensitive sites will greatly facilitate the possible formulation and our understanding of the redox signaling processes.

## CONCLUSION

Here, we report an innovative approach for *in situ* identification of S-sulfenylation sites by means of the transgenic probe YAP1C. By IgG purification at the protein level, followed by anti-C<sub>598</sub>SEIWDR purification at the peptide level, large-scale capture and identification of YAP1C CL peptides are possible, thereby uncovering *in vivo* S-sulfenylated protein sites. Importantly, this method can detect sulfenylated cysteines in a noninvasive manner and might easily be adapted to detect sulfenylated cysteines in specific organelles (De Smet et al., 2019). The

proposed genetically based methodology holds great promise for *in planta* mining of S-sulfenylated sites, in which rigid plant tissues limit the penetration and use of chemoselective probes. All in all, thanks to this noninvasive approach based on the YAP1C probe, the site-specific identification of protein S-sulfenylation was successfully shown for *Arabidopsis* cells under H<sub>2</sub>O<sub>2</sub> stress. Importantly, this method can be implemented for any species that can be genetically modified.

## DATA AVAILABILITY STATEMENT

The datasets generated for this study can be found in the PRIDE repository with the identifier-PXD016723, <https://www.ebi.ac.uk/pride/profile/reviewer06458>, Username: reviewer06458@ebi.ac.uk, Password: sFGF4SrQ, For data in Plant PTM Viewer, the linking is <https://www.psb.ugent.be/webtools/ptm-viewer/experiment.php?id=280&key=731ECC4C>.

## AUTHOR CONTRIBUTIONS

BW, PW, JH, JM, and FV conceived the research and wrote the manuscript. BW, CT, and JY conducted the experiments. BW and PW analyzed the data. All authors contributed to the article and approved the submitted version.

## FUNDING

This work was supported by the Research Foundation-Flanders, Fonds de la Recherche Scientifique (Excellence of Science project no. 30829584 to Claire Remacle, Kate Carroll, Didier Vertommen, JM and FV), the Research Foundation-Flanders (grants G0D7914N to JM and FV, 1508316N to JM, G003809N to Kris Gevaert and FV, G055416N and G06916N to FV), the China Scholarship Council (CSC no. 201606690036 to BW), the National Natural Science Foundation of China (no. 21922702 to JY), and the Ghent University Special Research Fund (BOF Grant 01J11311 to FV). JH is indebted to the Research Foundation-Flanders for a postdoctoral fellowship (no. 1227020N).

## ACKNOWLEDGMENTS

The authors thank Dr. Didier Vertommen and Dr. Barbara De Smet for helpful discussions, Dr. Lieven Sterck for submitting data to the Plant PTM Viewer, and Dr. Martine De Cock for excellent help in preparing the manuscript.

## SUPPLEMENTARY MATERIAL

The Supplementary Material for this article can be found online at: <https://www.frontiersin.org/articles/10.3389/fpls.2020.00777/full#supplementary-material>

## REFERENCES

- Akter, S., Fu, L., Jung, Y., Lo Conte, M., Lawson, J. R., Lowther, W. T., et al. (2018). Chemical proteomics reveals new targets of cysteine sulfinic acid reductase. *Nat. Chem. Biol.* 14, 995–1004. doi: 10.1038/s41589-018-0116-2
- Akter, S., Huang, J., Bodra, N., De Smet, B., Wahni, K., Rombaut, D., et al. (2015a). DYn-2 based identification of *Arabidopsis* sulfenomes. *Mol. Cell. Proteomics* 14, 1183–1200. doi: 10.1074/mcp.M114.046896
- Akter, S., Huang, J., Waszczak, C., Jacques, S., Gevaert, K., Van Breusegem, F., et al. (2015b). Cysteines under ROS attack in plants: a proteomics view. *J. Exp. Bot.* 66, 2935–2944. doi: 10.1093/jxb/erv044
- Backus, K. M. (2019). Applications of reactive cysteine profiling. *Curr. Top. Microbiol. Immunol.* 420, 375–417. doi: 10.1007/82.2018.120
- Barysz, H. M., and Malmström, J. (2018). Development of large-scale cross-linking mass spectrometry. *Mol. Cell. Proteomics* 17, 1055–1066. doi: 10.1074/mcp.R116.061663
- Biteau, B., Labarre, J., and Toledano, M. B. (2003). ATP-dependent reduction of cysteine-sulphinic acid by *S. cerevisiae* sulphiredoxin. *Nature* 425, 980–984. doi: 10.1038/nature02075
- Bodra, N., Young, D., Astolfi Rosado, L., Pallo, A., Wahni, K., De Proft, F., et al. (2017). *Arabidopsis thaliana* dehydroascorbate reductase 2: conformational flexibility during catalysis. *Sci. Rep.* 7:42494. doi: 10.1038/srep42494
- Chen, Z.-L., Meng, J.-M., Cao, Y., Yin, J.-L., Fang, R.-Q., Fan, S.-B., et al. (2019). A high-speed search engine pLink 2 with systematic evaluation for proteome-scale identification of cross-linked peptides. *Nat. Commun.* 10:3404. doi: 10.1038/s41467-019-11337-z
- De Smet, B., Willems, P., Fernandez-Fernandez, A. D., Alseekh, S., Fernie, A. R., Messens, J., et al. (2019). *In vivo* detection of protein cysteine sulfonylation in plastids. *Plant J.* 97, 765–778. doi: 10.1111/tpj.14146
- Delaunay, A., Pflieger, D., Barrault, M.-B., Vinh, J., and Toledano, M. B. (2002). A thiol peroxidase is an H<sub>2</sub>O<sub>2</sub> receptor and redox-transducer in gene activation. *Cell* 111, 471–481. doi: 10.1016/s0092-8674(02)01048-6
- Fares, A., Rossignol, M., and Peltier, J.-B. (2011). Proteomics investigation of endogenous S-nitrosylation in *Arabidopsis*. *Biochem. Biophys. Res. Commun.* 416, 331–336. doi: 10.1016/j.bbrc.2011.11.036
- Gupta, V., and Carroll, K. S. (2014). Sulfenic acid chemistry, detection and cellular lifetime. *Biochim. Biophys. Acta* 1840, 847–875. doi: 10.1016/j.bbagen.2013.05.040
- Gupta, V., Yang, J., Liebler, D. C., and Carroll, K. S. (2017). Diverse redoxome reactivity profiles of carbon nucleophiles. *J. Am. Chem. Soc.* 139, 5588–5595. doi: 10.1021/jacs.7b01791
- Gurrieri, L., Distefano, L., Pirone, C., Horrer, D., Seung, D., Zaffagnini, M., et al. (2019). The thioredoxin-regulated  $\alpha$ -amylase 3 of *Arabidopsis thaliana* is a target of glutathionylation. *Front. Plant Sci.* 10:993. doi: 10.3389/fpls.2019.00993
- Hamperl, S., Brown, C. R., Perez-Fernandez, J., Huber, K., Wittner, M., Babl, V., et al. (2014). “Purification of specific chromatin domains from single-copy gene loci in *Saccharomyces cerevisiae*,” in *Functional Analysis of DNA and Chromatin (Methods in Molecular Biology, 1094)*, eds J. C. Stockert, J. Espada, and A. Blázquez-Castro (Totowa, NJ: Humana Press), 329–341. doi: 10.1007/978-1-62703-706-8\_26
- He, F. (2011). Bradford protein assay. *Bio Protoc.* 1:e45. doi: 10.21769/BioProtoc.45
- Hu, J., Huang, X., Chen, L., Sun, X., Lu, C., Zhang, L., et al. (2015). Site-specific nitrosoproteomic identification of endogenously S-nitrosylated proteins in *Arabidopsis*. *Plant Physiol.* 167, 1731–1746. doi: 10.1104/pp.15.00026
- Huang, D. W., Sherman, B. T., and Lempicki, R. A. (2009). Systematic and integrative analysis of large gene lists using DAVID bioinformatics resources. *Nat. Protoc.* 4, 44–57. doi: 10.1038/nprot.2008.211
- Huang, J., Willems, P., Van Breusegem, F., and Messens, J. (2018). Pathways crossing mammalian and plant sulfenomic landscapes. *Free Radic. Biol. Med.* 122, 193–201. doi: 10.1016/j.freeradbiomed.2018.02.012
- Huang, J., Willems, P., Wei, B., Tian, C., Ferreira, R. B., Bodra, N., et al. (2019). Mining for protein S-sulfonylation in *Arabidopsis* uncovers redox-sensitive sites. *Proc. Natl. Acad. Sci. U.S.A.* 116, 21256–21261. doi: 10.1073/pnas.1906768116
- Jacques, S., Ghesquière, B., De Bock, P.-J., Demol, H., Wahni, K., Willems, P., et al. (2015). Protein methionine sulfoxide dynamics in *Arabidopsis thaliana* under oxidative stress. *Mol. Cell. Proteomics* 14, 1217–1229. doi: 10.1074/mcp.M114.043729
- Janecki, D. J., and Nemeth, J. F. (2011). Application of MALDI TOF/TOF mass spectrometry and collision-induced dissociation for the identification of disulfide-bonded peptides. *J. Mass Spectrom.* 46, 677–688. doi: 10.1002/jms.1938
- Leonard, S. E., Reddie, K. G., and Carroll, K. S. (2009). Mining the thiol proteome for sulfenic acid modifications reveals new targets for oxidation in cells. *ACS Chem. Biol.* 4, 783–799. doi: 10.1021/cb900105q
- Liu, P., Zhang, H., Wang, H., and Xia, Y. (2014). Identification of redox-sensitive cysteines in the *Arabidopsis* proteome using OxiTRAQ, a quantitative redox proteomics method. *Proteomics* 14, 750–762. doi: 10.1002/pmic.201300307
- Liu, P., Zhang, H., Yu, B., Xiong, L., and Xia, Y. (2015). Proteomic identification of early salicylate- and flg22-responsive redox-sensitive proteins in *Arabidopsis*. *Sci. Rep.* 5:8625. doi: 10.1038/srep08625
- McConnell, E. W., Berg, P., Westlake, T. J., Wilson, K. M., Popescu, G. V., Hicks, L. M., et al. (2019). Proteome-wide analysis of cysteine reactivity during effector-triggered immunity. *Plant Physiol.* 179, 1248–1264. doi: 10.1104/pp.18.01194
- Murad, W., Singh, R., and Yen, T.-Y. (2011). An efficient algorithmic approach for mass spectrometry-based disulfide connectivity determination using multi-ion analysis. *BMC Bioinformatics* 12(Suppl. 1):S12. doi: 10.1186/1471-2105-12-S1-S12
- Na, S., Paek, E., Choi, J.-S., Kim, D., Lee, S. J., and Kwon, J. (2015). Characterization of disulfide bonds by planned digestion and tandem mass spectrometry. *Mol. Biosyst.* 11, 1156–1164. doi: 10.1039/c4mb00688g
- Oger, E., Marino, D., Guignonis, J.-M., Pauly, N., and Puppo, A. (2012). Sulfenylated proteins in the *Medicago truncatula*-*Sinorhizobium meliloti* symbiosis. *J. Proteomics* 75, 4102–4113. doi: 10.1016/j.jpro.2012.05.024
- Paulsen, C. E., Truong, T. H., Garcia, F. J., Homann, A., Gupta, V., Leonard, S. E., et al. (2012). Peroxide-dependent sulfonylation of the EGFR catalytic site enhances kinase activity. *Nat. Chem. Biol.* 8, 57–64. doi: 10.1038/nchembio.736
- Pettersen, E. F., Goddard, T. D., Huang, C. C., Couch, G. S., Greenblatt, D. M., Meng, E. C., et al. (2004). UCSF chimera—a visualization system for exploratory research and analysis. *J. Comput. Chem.* 25, 1605–1612. doi: 10.1002/jcc.20084
- Poole, L. B., Furdui, C. M., and King, S. B. (2020). Introduction to approaches and tools for the evaluation of protein cysteine oxidation. *Essays Biochem.* 64, 1–17. doi: 10.1042/ebc20190050
- Puyaubert, J., Fares, A., Rézé, N., Peltier, J.-B., and Baudouin, E. (2014). Identification of endogenously S-nitrosylated proteins in *Arabidopsis* plantlets: effect of cold stress on cysteine nitrosylation level. *Plant Sci.* 21, 150–156. doi: 10.1016/j.plantsci.2013.10.014
- Roos, G., Foloppe, N., and Messens, J. (2013). Understanding the pKa of redox cysteines: the key role of hydrogen bonding. *Antioxid. Redox Signal.* 18, 94–127. doi: 10.1089/ars.2012.4521
- Roos, G., and Messens, J. (2011). Protein sulfenic acid formation: from cellular damage to redox regulation. *Free Radic. Biol. Med.* 51, 314–326. doi: 10.1016/j.freeradbiomed.2011.04.031
- Sigrist, C. J. A., de Castro, E., Cerutti, L., Cuche, B. A., Hulo, N., Bridge, A., et al. (2013). New and continuing developments at PROSITE. *Nucleic Acids Res.* 41, D344–D347. doi: 10.1093/nar/gks1067
- Song, S., Wang, H., Sun, M., Tang, J., Zheng, B., Wang, X., et al. (2019). Reactive oxygen species-mediated BIN2 activity revealed by single-molecule analysis. *New Phytol.* 223, 692–704. doi: 10.1111/nph.15669
- Takanishi, C. L., Ma, L.-H., and Wood, M. J. (2007). A genetically encoded probe for cysteine sulfenic acid protein modification in vivo. *Biochemistry* 46, 14725–14732. doi: 10.1021/bi701625s
- Takanishi, C. L., and Wood, M. J. (2011). A genetically encoded probe for the identification of proteins that form sulfenic acid in response to H<sub>2</sub>O<sub>2</sub> in *Saccharomyces cerevisiae*. *J. Proteome Res.* 10, 2715–2724. doi: 10.1021/pr1009542
- Tanner, J. J., Parsons, Z. D., Cummings, A. H., Zhou, H., and Gates, K. S. (2011). Redox regulation of protein tyrosine phosphatases: structural and chemical aspects. *Antioxid. Redox Signal.* 15, 77–97. doi: 10.1089/ars.2010.3611
- The UniProt Consortium (2019). UniProt: a worldwide hub of protein knowledge. *Nucleic Acids Res.* 47, D506–D515. doi: 10.1093/nar/gky1049
- Tian, Y., Fan, M., Qin, Z., Lv, H., Wang, M., Zhang, Z., et al. (2018). Hydrogen peroxide positively regulates brassinosteroid signaling through oxidation of

- the BRASSINAZOLE-RESISTANT1 transcription factor. *Nat. Commun.* 9:1063. doi: 10.1038/s41467-018-03463-x
- Van Leene, J., Stals, H., Eeckhout, D., Persiau, G., Van De Slijke, E., Van Isterdael, G., et al. (2007). A tandem affinity purification-based technology platform to study the cell cycle interactome in *Arabidopsis thaliana*. *Mol. Cell. Proteomics* 6, 1226–1238. doi: 10.1074/mcp.M700078-MCP200
- Waszczak, C., Akter, S., Eeckhout, D., Persiau, G., Wahni, K., Bodra, N., et al. (2014). Sulfenome mining in *Arabidopsis thaliana*. *Proc. Natl. Acad. Sci. U.S.A.* 111, 11545–11550. doi: 10.1073/pnas.1411607111
- Waszczak, C., Akter, S., Jacques, S., Huang, J., Messens, J., and Van Breusegem, F. (2015). Oxidative post-translational modifications of cysteine residues in plant signal transduction. *J. Exp. Bot.* 66, 2923–2934. doi: 10.1093/jxb/erv084
- Willems, P., Horne, A., Van Parys, T., Goormachtig, S., De Smet, I., Botzki, A., et al. (2019). The plant PTM Viewer, a central resource for exploring plant protein modifications. *Plant J.* 99, 752–762. doi: 10.1111/tpj.14345
- Wu, F., Chi, Y., Jiang, Z., Xu, Y., Xie, L., Huang, F., et al. (2020). Hydrogen peroxide sensor HPCA1 is an LRR receptor kinase in *Arabidopsis*. *Nature* 578, 577–581. doi: 10.1038/s41586-020-2032-3
- Yang, H., Mu, J., Chen, L., Feng, J., Hu, J., Li, L., et al. (2015). S-nitrosylation positively regulates ascorbate peroxidase activity during plant stress responses. *Plant Physiol.* 167, 1604–1615. doi: 10.1104/pp.114.255216
- Yang, J., Carroll, K. S., and Liebler, D. C. (2016). The expanding landscape of the thiol redox proteome. *Mol. Cell. Proteomics* 15, 1–11. doi: 10.1074/mcp.O115.056051
- Yang, J., Gupta, V., Carroll, K. S., and Liebler, D. C. (2014). Site-specific mapping and quantification of protein S-sulphenylation in cells. *Nat. Commun.* 5, 4776. doi: 10.1038/ncomms5776
- Yang, J., Gupta, V., Tallman, K. A., Porter, N. A., Carroll, K. S., and Liebler, D. C. (2015). Global, *in situ*, site-specific analysis of protein S-sulphenylation. *Nat. Protoc.* 10, 1022–1037. doi: 10.1038/nprot.2015.062
- Yuan, H. M., Liu, W. C., and Lu, Y. T. (2017). Catalase2 coordinates SA-mediated repression of both auxin accumulation and JA biosynthesis in plant defenses. *Cell Host Microbe* 21, 143–155. doi: 10.1016/j.chom.2017.01.007
- Yutthanasirikul, R., Nagano, T., Jimbo, H., Hihara, Y., Kanamori, T., Ueda, T., et al. (2016). Oxidation of a cysteine residue in elongation factor EF-Tu reversibly inhibits translation in the cyanobacterium *Synechocystis* sp. PCC 6803. *J. Biol. Chem.* 291, 5860–5870. doi: 10.1074/jbc.M115.706424
- Zaffagnini, M., Fermani, S., Marchand, C. H., Costa, A., Sparla, F., Rouhier, N., et al. (2019). Redox homeostasis in photosynthetic organisms: novel and established thiol-based molecular mechanisms. *Antioxid. Redox Signal.* 31, 155–210. doi: 10.1089/ars.2018.7617

**Conflict of Interest:** The authors declare that the research was conducted in the absence of any commercial or financial relationships that could be construed as a potential conflict of interest.

Copyright © 2020 Wei, Willems, Huang, Tian, Yang, Messens and Van Breusegem. This is an open-access article distributed under the terms of the Creative Commons Attribution License (CC BY). The use, distribution or reproduction in other forums is permitted, provided the original author(s) and the copyright owner(s) are credited and that the original publication in this journal is cited, in accordance with accepted academic practice. No use, distribution or reproduction is permitted which does not comply with these terms.



# The Contribution of Plant Dioxygenases to Hypoxia Signaling

Sergio Iacopino<sup>1,2,3</sup> and Francesco Licausi<sup>1,2,3\*</sup>

<sup>1</sup> Department of Biology, University of Pisa, Pisa, Italy, <sup>2</sup> Department of Plant Sciences, University of Oxford, Oxford, United Kingdom, <sup>3</sup> Institute of Life Sciences, Sant'Anna School of Advanced Studies, Pisa, Italy

## OPEN ACCESS

### Edited by:

Jörg-Peter Schnitzler,  
Helmholtz Zentrum München,  
Germany

### Reviewed by:

Daniel James Gibbs,  
University of Birmingham,  
United Kingdom  
Nobuhiro Suzuki,  
Sophia University, Japan

### \*Correspondence:

Francesco Licausi  
francesco.licausi@plants.ox.ac.uk

### Specialty section:

This article was submitted to  
Plant Physiology,  
a section of the journal  
Frontiers in Plant Science

**Received:** 20 March 2020

**Accepted:** 19 June 2020

**Published:** 08 July 2020

### Citation:

Iacopino S and Licausi F (2020) The  
Contribution of Plant Dioxygenases to  
Hypoxia Signaling.  
Front. Plant Sci. 11:1008.  
doi: 10.3389/fpls.2020.01008

Dioxygenases catalyze the incorporation of one or two oxygen atoms into target organic substrates. Besides their metabolic role, these enzymes are involved in plant signaling pathways as this reaction is in several instances required for hormone metabolism, to control proteostasis and regulate chromatin accessibility. For these reasons, alteration of dioxygenase expression or activity can affect plant growth, development, and adaptation to abiotic and biotic stresses. Moreover, the requirement of co-substrates and co-factors, such as oxygen, 2-oxoglutarate, and iron (Fe<sup>2+</sup>), invests dioxygenases with a potential role as cellular sensors for these molecules. For example, inhibition of cysteine deoxygenation under hypoxia elicits adaptive responses to cope with oxygen shortage. However, biochemical and molecular evidence regarding the role of other dioxygenases under low oxygen stresses is still limited, and thus further investigation is needed to identify additional sensing roles for oxygen or other co-substrates and co-factors. Here, we summarize the main signaling roles of dioxygenases in plants and discuss how they control plant growth, development and metabolism, with a focus on the adaptive responses to low oxygen conditions.

**Keywords:** dioxygenase, hypoxia, phytohormone, cell signaling, proteolysis

## INTRODUCTION

Dioxygenases comprise a large family of specialized enzymes that catalyze the incorporation of two oxygen atoms into an organic substrate or a primary organic substrate plus a co-substrate. In this redox reaction, four electrons are provided by the substrate or two by the substrate and two by an external donor (Bugg and Ramaswamy, 2008). The activity of dioxygenases results in a variety of modifications including dioxygenation, epoxidation, hydroxylation, and oxidative cleavage of C-C bonds, which affect plant metabolisms, physiology, and development.

Thanks to the vast set of reactions catalyzed by dioxygenases, the control of their activity constitutes a powerful tool for future biotechnological applications in plants. To date, dioxygenases have been effectively exploited in phytoremediation processes (Hernández-Vega et al., 2017) and development of biosensor (Iacopino et al., 2019). Moreover, from a synthetic biology perspective, their dependency on common cellular substrates and cofactors allows the transfer of dioxygenases between unrelated organisms (Iacopino et al., 2019; Masson et al., 2019; Puerta et al., 2019), opening possibilities towards the development of novel regulatory networks conferring new agronomical traits and improving fitness under challenging abiotic conditions.



The requirement of molecular oxygen as a co-substrate inevitably link dioxygenases activity to plant response to chronic and acute hypoxia, which is caused by ambient oxygen limitation, such as in the case of submergence or waterlogging, or as part of developmental programs (Weits et al., 2019). However, the affinity of each dioxygenase enzyme for oxygen and the protein expression levels can compensate for co-substrate shortage. Here, we summarize the different subfamilies of plant dioxygenases and their role of in plant metabolism and development, discussing their involvement and potential application under low oxygen stress.

## SUBFAMILIES OF PLANT DIOXYGENASES

Since dioxygen is a stable diradical triplet, it requires to be activated before reacting with organic substrates. To attain oxygen activation, most dioxygenases use a non-heme iron cofactor located into the catalytic site of the enzyme. The type of iron cofactor and its coordination, together with the requirement of additional co-substrates, allows the classification of dioxygenases into six subfamilies (Mitchell and Weng, 2019).

1. Catechol dioxygenases, comprising both non-heme iron-dependent intradiol and extradiol dioxygenases, mediate the conversion of catechol substrates in ring-opened products with the incorporation of oxygen into aldehydes and carbonylated functional groups (Bugg and Ramaswamy, 2008). Intradiol dioxygenases utilize a ferric cofactor coordinated by two His and two Tyr residues (Ohlendorf et al., 1988) while extradiol dioxygenases bind a ferrous cofactor through two His and one Asp/Glu residues (Hegg and Que, 1997). Both types of dioxygenases do not require additional co-substrates as electron sources (Wang et al., 2017).
2. Lipoygenases (LOX) are a group of non-heme iron dependent dioxygenases that catalyze the conversion of polyunsaturated fatty acids to hydroperoxides. In these proteins, the iron is coordinated by three His residues and the carboxyl terminal group of the protein (Andreou and Feussner, 2009).
3. The Rieske dioxygenases compose the smallest family of plant dioxygenases and catalyze the dihydroxylation of arene substrates (Mitchell and Weng, 2019). Together with oxygen, a NADH molecule is required as cofactor for the reaction. In this subfamily of enzymes, a 2Fe-2S cluster acts as a bridge to transfer electrons from the NADH to the catalytic site, where the iron atom is coordinated by two His and one acidic residue (Gibson et al., 1970).
4. Carotenoid cleavage dioxygenases (CCDs) mediate the cleavage of alkene chain in various tetraterpenoids. Differently from the other non-heme iron-dependent dioxygenases, the Fe atom in these enzymes is coordinated by four His residues whereas no carboxylate residue is involved (Harrison and Bugg, 2014).
5. Thiol dioxygenases catalyze the oxidation of the sulfur atom present in amino acid derivatives to their corresponding sulfinates. Green plants possess two types of thiol dioxygenases: cysteine dioxygenase (CDO), typical of green algae, which catalyze free cysteine catabolism and N-terminal plant cysteine oxidase (PCO), present also in land plants (Weits et al., 2014; Hildebrandt et al., 2015). While no information is available for PCO enzymes yet, in CDO proteins the Fe atom is coordinated by three His residues, a feature unique to this subfamily of dioxygenases (Joseph and Maroney, 2007).
6. Finally, 2-oxoglutarate (2OG)-dependent dioxygenases (2-ODDs) represent the largest family of plant dioxygenases with over 130 genes in Arabidopsis (Kawai et al., 2014) involved in a wide range of catalytic functions. The enzymes belonging to this subfamily utilize the ferrous cofactor, coordinated by the canonical two His and one acidic residue, and one acidic residue and 2-OG molecule to incorporate an atom of oxygen into the substrate. The second oxygen atom is instead transferred to the 2-OG molecule with the consequent production of succinate (Martinez and Hausinger, 2015).

These dioxygenases can participate to hypoxic signaling at two levels: they can generate cellular signals in an oxygen dependent manner, but they can also be the targets of hypoxia sensing, being regulated at the transcriptional or post-transcriptional level, as summarized in **Supplemental Table S1**.

## DIOXYGENASES PARTICIPATE TO HORMONE METABOLISM

Hormones are essential signaling molecules that regulate different aspects of plant development and physiology, and thus affect crop yield and response to biotic and abiotic stresses. Plants control hormone balance through the conversion from inactive precursor to active signaling molecules and vice versa. The widespread participation of dioxygenases to hormone homeostasis connects their signaling pathways to the availability of oxygen.

Dioxygenases are involved in the biosynthesis of gibberellins, abscisic acid (ABA), and ethylene (**Figures 1A–C**). The synthesis of gibberellic acids (GAs), phytohormones that regulate plant height, sex determination, and flowering time, requires the action of two 2-ODDs: GA20- and GA3- oxidases, which mediate the conversion of precursors into active GA molecules (Pimenta Lange and Lange, 2006) (**Figure 1A**). A key regulatory step in ABA biosynthesis, the oxidative cleavage of 9-cis-epoxycarotenoids is catalyzed by the CCD 9-cis-epoxycarotenoid dioxygenases (NCED) (Tan et al., 2003) (**Figure 1B**). Finally, the 2-ODD 1-aminocyclopropane-1-carboxylic acid (ACC) oxidase (ACO) catalyzes the final step of ethylene production (**Figure 1C**). Differently from most 2-ODD enzymes, ACO does not use 2-OG as co-substrate, and rather exploits reduced ascorbate as an electron donor (Gómez-Lim et al., 1993).

Interestingly, GAs, ethylene and ABA signaling pathways interact in plant adaptation to flooding. For instance, in wild rice species (*Oryza* spp) these hormones regulate internode elongation and the formation of aerenchymatic tissues. These

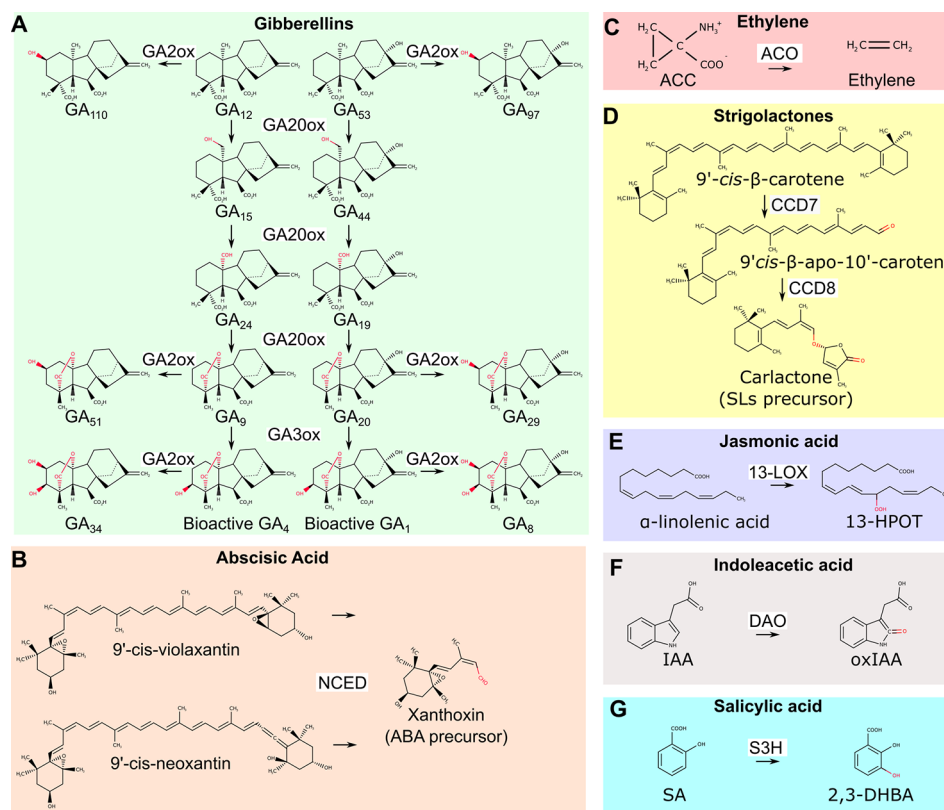


**FIGURE 1 |** Overview of biosynthetic and catabolic reactions of different hormones operated by dioxygenases. **(A)** GA20ox and GA3ox dioxygenases lead to the production of bioactive GA<sub>4</sub> and GA<sub>1</sub> molecules. GA20ox mediates their inactivation as well as the inactivation of other biosynthetic precursors. **(B)** The NCED enzyme is required for the production of the biosynthetic ABA precursor xanthoxin. **(C)** The ACO enzyme mediates the final step of ethylene biosynthetic pathway. **(D)** All SLs originates from carlactone, the product of CCD7 and CCD8 dioxygenases. **(E)** Dioxygenation of α-linolenic acid is the first step of jasmonic acid biosynthetic pathway. **(F)** The conversion of bioactive IAA into inactive oxidized IAA is mediated by DAO dioxygenase. **(G)** SA conversion to 2,3-DHBA by S3H dioxygenase. GA20ox, GA20-oxydases; GA3ox, GA 3-oxydases; GA2ox, GA 2-oxydases; NCED, 9-cis-epoxycarotenoid dioxygenases; ABA, abscisic acid; ACC, 1-aminocyclopropane-1-carboxylic acid; ACO, 1-aminocyclopropane-1-carboxylic acid oxidase; CCD7, carotenoid cleavage dioxygenases 7; CCD8, carotenoid cleavage dioxygenase 8; SLs, strigolactones; 13-LOX, 13-lipoxygenase; 13-HPOT, (13S)-hydroperoxyoctadecatrienoic acid; DAO, dioxygenase for auxin oxidation; IAA, indoleacetic acid; IAAox, oxidized indoleacetic acid; S3H, salicylic acid 3-hydroxylase; SA, salicylic acid; 2,3-DHBA, 2,3-dihydrobenzoic acid.

consist of large air cavities in the root cortex to facilitate gas diffusion. In case of submergence, ethylene concentration raises inside plant tissues to repress ABA biosynthesis and promotes GAs accumulation (Hoffmann-Benning and Kende, 1992; Hattori et al., 2009). Downstream targets of these hormones include genes involved in programmed cell death in the cortex and cell wall remodeling that enable cell expansion (Sasidharan and Voesenek, 2015). In concert, these events stimulate the formation of aerenchyma and promote in parallel rapid shoot elongation (Chen et al., 2010; Parlanti et al., 2011). Therefore, the shoot of submerged plants rapidly elongates, thus escaping from the water level and restoring gas exchange with the atmosphere. The increased synthesis of ethylene and active GAs in different plant species under submergence suggests that the biosynthetic dioxygenases involved in the synthesis of these hormones have a higher affinity for oxygen than its availability in these tissues (Atwell et al., 1988; Hattori et al., 2009). Moreover, low oxygen

stresses induces the upregulation of ACC synthase (ACS) and ACO in several plant (Wang and Arteca, 1992; Vriezen et al., 1999; Zhou et al., 2001). Finally, ethylene entrapment due to reduced gas diffusion rate in water, contributes to its local accumulation (Voesenek et al., 1993).

Strigolactones (SLs) are a group of molecules involved in the control of shoot branching, adventitious root development, establishment of symbiotic mycorrhiza and, recently, have been associated to root adaptation to abiotic stress conditions including waterlogging (Bashar, 2018). SLs biosynthetic pathways require the action of two CCD enzymes: CCD7 and CCD8 (Booker et al., 2004; Auldrige et al., 2006). They sequentially regulate the production of the precursor of all SLs, carlactone (Abe et al., 2014) (**Figure 1D**). Genetic inactivation of CCD7 and CCD8 is sufficient to block SLs biosynthesis, which results in a branched shoot phenotype (Gomez-Roldan et al., 2008). Since SLs repress the production of adventitious roots in waterlogged tomato plants,

manipulation of CCDs enzymes represents a promising strategy to improve nutrient and oxygen uptake and thus promote plant fitness (Vidoz et al., 2010; Kohlen et al., 2012).

Finally, dioxygenases also participate to the synthesis of jasmonic acid (JA), which is involved in seed germination, pollen development, plant aging and biotic stresses defense. The first step of JA biosynthesis, the dioxygenation of carbon 13 in  $\alpha$ -linolenic acid, requires the action of 13-LOX (**Figure 1E**). In Arabidopsis, 13-LOXs genes are upregulated after desubmergence, a condition where JA plays a fundamental role in the adaptation to the restoration of photosynthesis and aerobic metabolisms that cause a burst of reactive oxygen species (ROS) (Yuan et al., 2017; Yeung et al., 2019).

Dioxygenases also play key roles in the catabolism of plant hormones: auxin (IAA), salicylic acid (SA), and GAs catabolism relies on the action of 2-ODDs. IAA is oxidized to the inactive oxindole-3-acetic acid by DAO (**Figure 1F**), S3H, mediates the hydroxylation of SA to the inactive 2,3-dihydrobenzoic acid (2,3-DHBA) and GA2 oxidase is required for GA catabolism (Yamaguchi, 2008; Zhang et al., 2013; Stepanova and Alonso, 2016) (**Figure 1G**).

Overall, the involvement of dioxygenases in hormone homeostasis provides the opportunity for their exploitation as a tool to regulate plant development, anatomy, defense against pathogens, and survival under negative conditions. Specific dioxygenase activity can be manipulated by affecting the expression level of the relative coding gene, genetically altering the catalytic properties of the enzyme, modulating the abundance of cofactors, agonists and antagonists, or a combination of the interventions listed above. For example, pharmacological attempts to modulate the activity of these enzymes has led to the development of chemical inhibitors of GA biosynthesis and catabolism (King et al., 1997; Mander et al., 1998; Rademacher, 2000). In summary, dioxygenases control key aspects of hormone biosynthesis and catabolism, which in turn regulate plant growth and adaptation under challenging conditions. The requirement of oxygen as co-substrate makes dioxygenases a valuable tool for regulating hormone levels under low oxygen conditions such as submergence and waterlogging. The identification of enzyme variants with variable oxygen affinity, obtained by mutagenesis or isolated from alternative plant accessions, may support future breeding of crop varieties with optimized sensitivity to the ranges of oxygen concentrations encountered by the plant during submergence.

## DIOXYGENASES THAT OPERATE POST-TRANSLATIONAL MODIFICATIONS

Different classes of dioxygenases operate on protein substrates, to oxidize specific amino acid residues and thus alter the conformation or confer new properties to the polypeptide chain. About two-third of proteinogenic amino acids can be hydroxylated, with proline being the most commonly modified residue. In plants, part of the protein substrates serves a structural purpose, such as cell wall proteins, whose proline hydroxylation is a required for O-

glycosylation. Additionally, a large number of proteins involved in signaling events are co or post-translationally subjected to dioxygenase activity. These include, but are not limited to, signaling peptides, enzymes and transcription factors. The specific modification imposed by dioxygenases alters protein features, such as increased or decreased affinity for protein partners, reduced or enhanced stability and ability to bind DNA. Cysteine oxidation, proline hydroxylation and demethylation of histone proteins are the most common posttranslational modifications performed by dioxygenases (**Figure 2**), and thus the targets of most research endeavors.

### Proline Hydroxylation

Prolyl-residues can be hydroxylated at their  $\gamma$ -C atom by 2-ODDs enzymes defined as pro- and asn-4-hydroxylases (P4H) generating hydroxyproline (Hyp). In land plants, proline hydroxylation is frequently found in cell-wall proteins, such as arabinogalactan proteins (AGPs) and extensins (Fragkostefanakis et al., 2012; Fragkostefanakis et al., 2014), and in secreted peptide hormones including CLAVATA3 CLV3, root meristem growth factors (RGFs), and plant peptides containing sulfated tyrosine (PSYs) (Kondo et al., 2006; Amano et al., 2007; Matsuzaki et al., 2010). These small peptides act as short- and long-range signaling molecules regulating stem cell maintenance, proliferation and differentiation (Stuhrwohltdt and Schaller, 2019). They originate from longer peptides that are trimmed and subjected to a series of post translational modifications including proline hydroxylation (Matsubayashi, 2011). These modifications are often sequentially linked and appear to be required for full activity of the small peptides (**Figure 2A**). Although some sequence motifs are shared among the small peptides, a clear consensus sequence required for proline hydroxylation could not be identified so far. In mammals, P4Hs control the stability of the hypoxia inducible factor  $\alpha$  (HIF $\alpha$ ), a transcription factor regulating cellular responses to hypoxia stresses. (Epstein et al., 2001). The Arabidopsis genome contains 13 genes encoding for putative P4Hs. Those that have been tested, show different substrate specificity and subcellular localization, with the majority in the Endoplasmic Reticulum and Golgi Apparatus (Stuhrwohltdt and Schaller, 2019). The Arabidopsis At-P4H-1 could effectively hydroxylate a HIF $\alpha$  peptide *in vitro* and some P4Hs genes are differentially regulated in Arabidopsis in response to hypoxia (Hieta and Myllyharju, 2002; Vlad et al., 2007). However, endogenous PHDs were unable to hydroxylate a HIF fragment endogenously produced in Arabidopsis (Iacopino et al., 2019).

### Cysteine Oxidation

Cysteine oxidation proceeds through three states where oxygen atoms are progressively bound to the sulfur in the side-chain of the amino acid: sulfenic (-SOH), sulfinic (-SOOH), and sulfonic (-SOOOH), the latter being an irreversible reaction. N-terminal cysteine sulfinylation of specific proteins has been proposed to act as a molecular sensor of NO, O<sub>2</sub>, and heme in animal cells

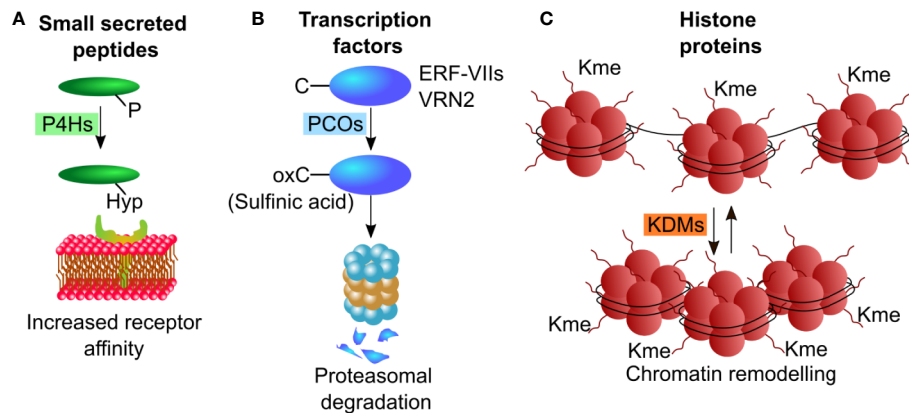


**FIGURE 2 |** Schematic representations of post-translational modifications operated by plant dioxygenases. **(A)** P4Hs hydroxylate proline residues on small secreted peptides thereby enhancing their receptor affinity. **(B)** PCO enzymes oxidize N-terminally located cysteine residue on ERF-VII and VRN2 transcription factors leading to their degradation through the N-degron pathway. **(C)** KDMs remove methyl groups from lysine residues on the N-terminal tails of histone proteins, thus altering chromatin compactness. P4H, proline hydroxylases; PCO, plant cysteine oxidases; KDM, Jumonji C (JmjC)-domain containing lysine demethylases.

since this post-translational modification labels proteins as substrates for proteasomal degradation by the Arg-branch of the N-degron pathway (Tasaki et al., 2009). Moreover, it was recently shown that animals possess N-terminal cysteine oxidase (NCOs) enzymes able to specifically catalyze the dioxygenation of N-terminally cysteine residues (Masson et al., 2019). Sulfenylated proteins are targets of arginyltransferases (ATE) that conjugate an arginine residue (White et al., 2017). This modification is finally recognized by N-recognition (Ubr1 in animals and PRT6 in plants) that mediate ubiquitination and subsequent targeting of the protein to the proteasome (Garzón et al., 2007) (**Figure 2B**). PCOs and animal aminoethanol dioxygenase (ADO) share moderate similarity between their amino acid sequences. The number of plant NCO substrates demonstrated experimentally is relatively low: enzymatic *in vitro* cysteine oxidation has been reported exclusively for the group VII of ethylene responsive factors (ERF-VIIs) and the polycomb group protein vernalization 2 (VRN2) (Gibbs et al., 2018) while it remains to be demonstrated for the Arg-degron substrate Little Zipper 2 (ZPR2) (Weits et al., 2019). These transcriptional regulators mediate plant responses to chronic and acute hypoxia, thereby conferring NCOs a role as oxygen sensors in plants and animals (Gibbs et al., 2011; Licausi et al., 2011).

Compatibly with this function, *in vitro* kinetics assays revealed that PCO and ADO have oxygen affinities that allow prompt inactivation under the hypoxic levels known to trigger a response in plants and animals respectively (White et al., 2018; Masson et al., 2019).

Besides hypoxia, conditions that reduce NCO activity such as nitric oxide and low temperature elicit a similar response (Gibbs et al., 2014; Gibbs et al., 2018; Hartman et al., 2019). For instance, stabilization of ERF-VII transcription factors and induction of anaerobic genes in conditions of iron deficiency and zinc excess has been proposed to result from the PCO inactivation that is observed in both conditions (Dalle Carbonare et al., 2019). These

observations support the proposed role of plant dioxygenases as metal sensors (Vigani et al., 2013).

## Histone Demethylation

Jumonji C (JmjC)-domain containing lysine demethylases (KDM) constitute a class of 2-ODD enzymes that act on mono-di- and trimethylated lysine residues in the N-terminal tail of histone proteins and thus play a critical role in defining the accession of the transcriptional complex to promoters (Strahl and Allis, 2000; Lan et al., 2008) (**Figure 2C**). For instance, the increase of the methylation state on K4 on histone H3 (H3K4me3) is associated to gene expression (Yu et al., 2009). Instead, increased methylation state on K9 and K27 of histone H3 is expected to negatively affect gene expression (Yu et al., 2009). The Arabidopsis genome codes for 21 JMJ enzymes, mainly characterized for their involvement in the regulation of flowering time and ABA responses (Gan et al., 2014; Wu et al., 2019).

KDM proteins have been proposed as oxygen sensors in animal cells. Indeed recent assessment of their low affinity for oxygen and consequent inactivation under hypoxia, associated with the widespread increase in histone methylation observed *in vivo* in such condition, confirmed this role (Chakraborty et al., 2002; Shmakova et al., 2014; Hancock et al., 2017; Batie et al., 2019; Chakraborty et al., 2019). A similar role for plant KDM has to be confirmed yet. In rice plants subjected to submergence, the trimethylation state of hypoxic genes was observed to increase significantly (Tsuji et al., 2006). Still, direct evidence of changes in histone methylation associated to a reduced activity of KDMs under hypoxia is missing. Interestingly, four Arabidopsis KDM mRNAs were observed to increase their association with polysomes in hypoxia, suggesting that these are preferentially translated (Branco-Price et al., 2008). Future research efforts will be directed at characterizing the affinity of plant KDMs for oxygen and their susceptibility to chronic and acute hypoxia, as well as the effect of hypoxia on specific histone methylation.



## FUTURE DIRECTIONS FOR RESEARCH ON PLANT DIOXYGENASE

Plant dioxygenases absolve different functions in biological systems, ranging from hormone biosynthesis to epigenetic chromatin rearrangements. Moreover, dioxygenases with low oxygen affinity have been developed by both animals and plants to perceive oxygen levels. The adaptation to environmental conditions that restrict oxygen availability, such as submergence, require changes in hormone profiles, chromatin rearrangements, and modulation of transcription factor activity. All these processes involve the participation of dioxygenases at different levels, thereby directly linking the intensity of the response to the oxygen content. Further structural and biochemical characterization of dioxygenases and the sensitivity of their targets to oxygen limitation will pave the way to deeper understating of molecular processes that enhance survival

under such adverse conditions and thus possibly support the generation of crops with increased submergence tolerance.

## AUTHOR CONTRIBUTIONS

SI and FL wrote the manuscript and conceptualized the figures. SI prepared the figures.

## SUPPLEMENTARY MATERIAL

The Supplementary Material for this article can be found online at: <https://www.frontiersin.org/articles/10.3389/fpls.2020.01008/full#supplementary-material>

## REFERENCES

- Abe, S., Sado, A., Tanaka, K., Kisugi, T., Asami, K., Ota, S., et al. (2014). Carlactone is converted to carlactonic acid by MAX1 in *Arabidopsis* and its methyl ester can directly interact with AtD14 in vitro. *Proc. Natl. Acad. Sci.* 111, 18084–18089. doi: 10.1073/pnas.1410801111
- Amano, Y., Tsubouchi, H., Shinohara, H., Ogawa, M., and Matsubayashi, Y. (2007). Tyrosine-sulfated glycopeptide involved in cellular proliferation and expansion in *Arabidopsis*. *Proc. Natl. Acad. Sci. U. S. A.* 104, 18333–18338. doi: 10.1073/pnas.0706403104
- Andreou, A., and Feussner, I. (2009). Lipoxygenases - Structure and reaction mechanism. *Phytochemistry* 70, 1504–1510. doi: 10.1016/j.phytochem.2009.05.008
- Atwell, B. J., Drew, M. C., and Jackson, M. B. (1998). The influence of oxygen deficiency on ethylene synthesis, 1-aminocyclopropane-1-carboxylic acid levels and aerenchyma formation in roots of *Zea mays*. *Physiol. Plant.* 75, 15–22. doi: 10.1111/j.1399-3054.1988.tb06616.x
- Auldrige, M. E., Block, A., Vogel, J. T., Dabney-Smith, C., Mila, I., Bouzayen, M., et al. (2006). Characterization of three members of the *Arabidopsis* carotenoid cleavage dioxygenase family demonstrates the divergent roles of this multifunctional enzyme family. *Plant J.* 45, 982–993. doi: 10.1111/j.1365-313X.2006.02666.x
- Bashar, K. K. (2018). Hormone dependent survival mechanisms of plants during post-waterlogging stress. *Plant Signal. Behav.* 13, 1–5. doi: 10.1080/15592324.2018.1529522
- Batie, M., Frost, J., Frost, M., Wilson, J. W., Schofield, P., and Rocha, S. (2019). Hypoxia induces rapid changes to histone methylation and reprograms chromatin. *Science* 363, 1222–1226. doi: 10.1126/science.aau5870
- Booker, J., Auldrige, M., Wills, S., McCarty, D., Klee, H., and Leyser, O. (2004). MAX3/CCD7 Is a Carotenoid Cleavage Dioxygenase Required for the Synthesis of a Novel Plant Signaling Molecule. *Curr. Biol.* 14, 1232–1238. doi: 10.1016/j.cub.2004.06.061
- Branco-Price, C., Kaiser, K. A., Jang, C. J. H., Larive, C. K., and Bailey-Serres, J. (2008). Selective mRNA translation coordinates energetic and metabolic adjustments to cellular oxygen deprivation and reoxygenation in *Arabidopsis thaliana*. *Plant J.* 56, 743–755. doi: 10.1111/j.1365-313X.2008.03642.x
- Bugg, T. D., and Ramaswamy, S. (2008). Non-heme iron-dependent dioxygenases: unravelling catalytic mechanisms for complex enzymatic oxidations. *Curr. Opin. Chem. Biol.* 12, 134–140. doi: 10.1016/j.cbpa.2007.12.007
- Chakraborty, U., Dutta, S., and Chakraborty, B. N. (2002). Response of tea plants to water stress. *Biol. Plant* 45, 557–562. doi: 10.1023/A:1022377126056
- Chakraborty, A. A., Laukka, T., Myllykoski, M., Ringel, A. E., Booker, M. A., Tolstorukov, M. Y., et al. (2019). Histone demethylase KDM6A directly senses oxygen to control chromatin and cell fate. *Science* 363, 1217–1222. doi: 10.1126/science.aaw1026
- Chen, X., Pierik, R., Peeters, A. J. M., Poorter, H., Visser, E. J. W., Huber, H., et al. (2010). Endogenous Abscissic Acid as a Key Switch for Natural Variation in Flooding-Induced Shoot Elongation. *Plant Physiol.* 154, 969–977. doi: 10.1104/pp.110.162792
- Dalle Carbonare, L., White, M., Shukla, V., Francini, A., Perata, P., Flashman, E., et al. (2019). Zinc excess induces a hypoxia-like response by inhibiting cysteine oxidases in poplar roots. *Plant Physiol.* 180, 1614–1628. doi: 10.1104/pp.18.01458
- Epstein, A. C. R., Gleadle, J. M., McNeill, L. A., Hewitson, K. S., O'Rourke, J., Mole, D. R., et al. (2001). *C. elegans* EGL-9 and mammalian homologs define a family of dioxygenases that regulate HIF by prolyl hydroxylation. *Cell* 107, 43–54. doi: 10.1016/S0092-8674(01)00507-4
- Fragkostefanakis, S., Dandachi, F., and Kalaitzis, P. (2012). Expression of arabinogalactan proteins during tomato fruit ripening and in response to mechanical wounding, hypoxia and anoxia. *Plant Physiol. Biochem. PPB* 52, 112–118. doi: 10.1016/j.plaphy.2011.12.001
- Fragkostefanakis, S., Sedeek, K. E. M., Raad, M., Zaki, M. S., and Kalaitzis, P. (2014). Virus induced gene silencing of three putative prolyl 4-hydroxylases enhances plant growth in tomato (*Solanum lycopersicum*). *Plant Mol. Biol.* 85, 459–471. doi: 10.1007/s11103-014-0197-6
- Gómez-Lim, M. A., Valdés-López, V., Cruz-Hernandez, A., and Saucedo-Arias, L. J. (1993). Isolation and characterization of a gene involved in ethylene biosynthesis from *Arabidopsis thaliana*. *Gene* 134, 217–221. doi: 10.1016/0378-1119(93)90096-L
- Gan, E.-S., Xu, Y., Wong, J.-Y., Geraldine Goh, J., Sun, B., Wee, W.-Y., et al. (2014). Jumonji demethylases moderate precocious flowering at elevated temperature via regulation of FLC in *Arabidopsis*. *Nat. Commun.* 5, 5098. doi: 10.1038/ncomms6098
- Garzón, M., Eifler, K., Faust, A., Scheel, H., Hofmann, K., Koncz, C., et al. (2007). PRT6/At5g02310 encodes an *Arabidopsis* ubiquitin ligase of the N-end rule pathway with arginine specificity and is not the CER3 locus. *FEBS Lett.* 581, 3189–3196. doi: 10.1016/j.febslet.2007.06.005
- Gibbs, D. J., Lee, S. C., Md Isa, N., Gramuglia, S., Fukao, T., Bassel, G. W., et al. (2011). Homeostatic response to hypoxia is regulated by the N-end rule pathway in plants. *Nature* 479, 415–418. doi: 10.1038/nature10534
- Gibbs, D. J., Md Isa, N., Movahedi, M., Lozano-Juste, J., Mendiondo, G. M., Berckhan, S., et al. (2014). Nitric Oxide Sensing in Plants Is Mediated by Proteolytic Control of Group VII ERF Transcription Factors. *Mol. Cell* 53, 369–379. doi: 10.1016/j.molcel.2013.12.020
- Gibbs, D. J., Tedds, H. M., Labandera, A.-M., Bailey, M., White, M. D., Hartman, S., et al. (2018). Oxygen-dependent proteolysis regulates the stability of angiosperm polycomb repressive complex 2 subunit VERNALIZATION 2. *Nat. Commun.* 9, 5438. doi: 10.1038/s41467-018-07875-7
- Gibson, D. T., Cardini, G. E., Maseles, F. C., and Kallio, R. E. (1970). Incorporation of oxygen-18 into benzene by *Pseudomonas putida*. *Biochemistry* 9, 1631–1635. doi: 10.1021/bi00809a024
- Gomez-Roldan, V., Feras, S., Brewer, P. B., Puech-Pagès, V., Dun, E. A., Pillot, J. P., et al. (2008). Strigolactone inhibition of shoot branching. *Nature* 455, 189–194. doi: 10.1038/nature07271
- Hancock, R. L., Masson, N., Dunne, K., Flashman, E., and Kawamura, A. (2017). The Activity of JmjC Histone Lysine Demethylase KDM4A Is Highly Sensitive

- to Oxygen Concentrations. *ACS Chem. Biol.* 12, 1011–1019. doi: 10.1021/acschembio.6b00958
- Harrison, P. J., and Bugg, T. D. H. (2014). Enzymology of the carotenoid cleavage dioxygenases: Reaction mechanisms, inhibition and biochemical roles. *Arch. Biochem. Biophys.* 544, 105–111. doi: 10.1016/j.abb.2013.10.005
- Hartman, S., Liu, Z., van Veen, H., Vicente, J., Reinen, E., Martopawiro, S., et al. (2019). Ethylene-mediated nitric oxide depletion pre-adapts plants to hypoxia stress. *Nat. Commun.* 10, 1–9. doi: 10.1038/s41467-019-12045-4
- Hattori, Y., Nagai, K., Furukawa, S., Song, X.-J., Kawano, R., Sakakibara, H., et al. (2009). The ethylene response factors SNORKEL1 and SNORKEL2 allow rice to adapt to deep water. *Nature* 460, 1026–1030. doi: 10.1038/nature08258
- Hegg, E. L., and Que, L. J. (1997). The 2-His-1-carboxylate facial triad—an emerging structural motif in mononuclear non-heme iron(II) enzymes. *Eur. J. Biochem.* 250, 625–629. doi: 10.1111/j.1432-1033.1997.t01-1-00625.x
- Hernández-Vega, J. C., Cady, B., Kayanja, G., Mauriello, A., Cervantes, N., Gillespie, A., et al. (2017). Detoxification of polycyclic aromatic hydrocarbons (PAHs) in *Arabidopsis thaliana* involves a putative flavonol synthase. *J. Hazard. Mater.* 321, 268–280. doi: 10.1016/j.jhazmat.2016.08.058
- Hieta, R., and Myllyharju, J. (2002). Cloning and characterization of a low molecular weight prolyl 4-hydroxylase from *Arabidopsis thaliana*. Effective hydroxylation of proline-rich, collagen-like, and hypoxia-inducible transcription factor alpha-like peptides. *J. Biol. Chem.* 277, 23965–23971. doi: 10.1074/jbc.M201865200
- Hildebrandt, T. M., Nunes Nesi, A., Araújo, W. L., and Braun, H. P. (2015). Amino Acid Catabolism in Plants. *Mol. Plant* 8, 1563–1579. doi: 10.1016/j.molp.2015.09.005
- Hoffmann-Benning, S., and Kende, H. (1992). On the role of abscisic Acid and gibberellin in the regulation of growth in rice. *Plant Physiol.* 99, 1156–1161. doi: 10.1104/pp.99.3.1156
- Iacopino, S., Jurinovich, S., Cupellini, L., Piccinini, L., Cardarelli, F., Perata, P., et al. (2019). A Synthetic Oxygen Sensor for Plants Based on Animal Hypoxia Signaling. *Plant Physiol.* 179, 986–1000. doi: 10.1104/pp.18.01003
- Joseph, C. A., and Maroney, M. J. (2007). Cysteine dioxygenase: structure and mechanism. *Chem. Commun.* 180 (32), 3338–3349. doi: 10.1039/B702158E
- Kawai, Y., Ono, E., and Mizutani, M. (2014). Evolution and diversity of the 2-oxoglutarate-dependent dioxygenase superfamily in plants. *Plant J.* 78, 328–343. doi: 10.1111/tjp.12479
- King, R. W., Blundell, C., Evans, L. T., Mander, L. N., and Wood, J. T. (1997). Modified Gibberellins Retard Growth of Cool-Season Turfgrasses†. *Crop Sci.* 37, 1878–1883. doi: 10.2135/cropsci1997.0011183X003700060036x
- Kohlen, W., Charnikhova, T., Lammers, M., Pollina, T., Tóth, P., Haider, I., et al. (2012). The tomato CAROTENOID CLEAVAGE DIOXYGENASE8 (SICCD8) regulates rhizosphere signaling, plant architecture and affects reproductive development through strigolactone biosynthesis. *New Phytol.* 196, 535–547. doi: 10.1111/j.1469-8137.2012.04265.x
- Kondo, T., Sawa, S., Kinoshita, A., Mizuno, S., Kakimoto, T., Fukuda, H., et al. (2006). A plant peptide encoded by CLV3 identified by in situ MALDI-TOF MS analysis. *Science* 313, 845–848. doi: 10.1126/science.1128439
- Lan, F., Nottke, A. C., and Shi, Y. (2008). Mechanisms involved in the regulation of histone lysine demethylases. *Curr. Opin. Cell Biol.* 20, 316–325. doi: 10.1016/j.ceb.2008.03.004
- Licausi, F., Kosmacz, M., Weits, D. A., Giuntoli, B., Giorgi, F. M., Voesenek, L. A. C. J., et al. (2011). Oxygen sensing in plants is mediated by an N-end rule pathway for protein destabilization. *Nature* 479, 419–422. doi: 10.1038/nature10536
- Mander, L. N., Sherburn, M., Camp, D., King, R. W., Evans, L. T., and Pharis, R. P. (1998). Effects of d-ring modified gibberellins on flowering and growth in *Lolium temulentum*. *Phytochemistry* 49, 2195–2206. doi: 10.1016/S0031-9422(98)00310-0
- Martinez, S., and Hausinger, R. P. (2015). Catalytic Mechanisms of Fe(II)- and 2-Oxoglutarate-dependent Oxygenases. *J. Biol. Chem.* 290, 20702–20711. doi: 10.1074/jbc.R115.648691
- Masson, N., Keeley, T. P., Giuntoli, B., White, M. D., Puerta, M. L., Perata, P., et al. (2019). Conserved N-terminal cysteine dioxygenases transduce responses to hypoxia in animals and plants. *Sci. (80-. )* 365, 65–9. doi: 10.1126/science.aaw0112
- Matsubayashi, Y. (2011). Post-translational modifications in secreted peptide hormones in plants. *Plant Cell Physiol.* 52, 5–13. doi: 10.1093/pcp/pcq169
- Matsuzaki, Y., Ogawa-Ohnishi, M., Mori, A., and Matsubayashi, Y. (2010). Secreted peptide signals required for maintenance of root stem cell niche in *Arabidopsis*. *Science* 329, 1065–1067. doi: 10.1126/science.1191132
- Mitchell, A. J., and Weng, J.-K. (2019). Unleashing the Synthetic Power of Plant Oxygenases: From Mechanism to Application. *Plant Physiol.* 179, 813–829. doi: 10.1104/pp.18.01223
- Ohlendorf, D. H., Lipscomb, J. D., and Weber, P. C. (1988). Structure and assembly of protocatechuate 3,4-dioxygenase. *Nature* 336, 403–405. doi: 10.1038/336403a0
- Parlanti, S., Kudahettige, N. P., Lombardi, L., Mensuali-Sodi, A., Alpi, A., Perata, P., et al. (2011). Distinct mechanisms for aerenchyma formation in leaf sheaths of rice genotypes displaying a quiescence or escape strategy for flooding tolerance. *Ann. Bot.* 107, 1335–1343. doi: 10.1093/aob/mcr086
- Pimenta Lange, M. J., and Lange, T. (2006). Gibberellin biosynthesis and the regulation of plant development. *Plant Biol.* 8, 281–290. doi: 10.1055/s-2006-923882
- Puerta, M. L., Shukla, V., Dalle Carbonare, L., Weits, D. A., Perata, P., Licausi, F., et al. (2019). A Ratiometric Sensor Based on Plant N-Terminal Degrons Able to Report Oxygen Dynamics in *Saccharomyces cerevisiae*. *J. Mol. Biol.* 431, 2810–2820. doi: 10.1016/j.jmb.2019.05.023
- Rademacher, W. (2000). GROWTH RETARDANTS : Effects on Gibberellin. *Annu. Rev. Plant Physiol. Plant Mol. Biol.* 51, 501–531. doi: 10.1146/annurev.arplant.51.1.501
- Sasidharan, R., and Voesenek, L. A. C. J. (2015). Ethylene-Mediated Acclimations to Flooding Stres. *Plant Physiol.* 169, 3–12. doi: 10.1104/pp.15.00387
- Shmakova, A., Batie, M., Druker, J., and Rocha, S. (2014). Chromatin and oxygen sensing in the context of JmjC histone demethylases. *Biochem. J.* 462, 385–395. doi: 10.1042/BJ20140754
- Stepanova, A. N., and Alonso, J. M. (2016). Auxin catabolism unplugged: Role of IAA oxidation in auxin homeostasis. *Proc. Natl. Acad. Sci. U. S. A.* 113, 10742–10744. doi: 10.1073/pnas.1613506113
- Strahl, B. D., and Allis, C. D. (2000). The language of covalent histone modifications. *Nature* 403, 41–45. doi: 10.1038/47412
- Stuhrwoldt, N., and Schaller, A. (2019). Regulation of plant peptide hormones and growth factors by post-translational modification. *Plant Biol. (Stuttg.)* 21 Suppl 1, 49–63. doi: 10.1111/plb.12881
- Tan, B.-C., Joseph, L. M., Deng, W.-T., Liu, L., Li, Q.-B., Cline, K., et al. (2003). Molecular characterization of the *Arabidopsis* 9-cis epoxycarotenoid dioxygenase gene family. *Plant J.* 35, 44–56. doi: 10.1046/j.1365-3113X.2003.01786.x
- Tasaki, T., Zakrzewska, A., Dudgeon, D. D., Jiang, Y., Lazo, J. S., and Kwon, Y. T. (2009). The substrate recognition domains of the N-end rule pathway. *J. Biol. Chem.* 284, 1884–1895. doi: 10.1074/jbc.M803641200
- Tsuji, H., Saika, H., Tsutsumi, N., Hirai, A., and Nakazono, M. (2006). Dynamic and reversible changes in histone H3-Lys4 methylation and H3 acetylation occurring at submergence-inducible genes in rice. *Plant Cell Physiol.* 47, 995–1003. doi: 10.1093/pcp/pcj072
- Vidoz, M. L., Loreti, E., Mensuali, A., Alpi, A., and Perata, P. (2010). Hormonal interplay during adventitious root formation in flooded tomato plants. *Plant J.* 63, 551–562. doi: 10.1111/j.1365-3113X.2010.04262.x
- Vigani, G., Morandini, P., and Murgia, I. (2013). Searching iron sensors in plants by exploring the link among 2'-OG-dependent dioxygenases, the iron deficiency response and metabolic adjustments occurring under iron deficiency. *Front. Plant Sci.* 4, 169. doi: 10.3389/fpls.2013.00169
- Vlad, F., Spano, T., Vlad, D., Daher, F. B., Ouelhadj, A., Fragkostefanakis, S., et al. (2007). Involvement of *Arabidopsis* prolyl 4 hydroxylases in hypoxia, anoxia and mechanical wounding. *Plant Signal. Behav.* 2, 368–369. doi: 10.4161/psb.2.5.4462
- Voesenek, L. A. C. J., Banga, M., Thier, R. H. C., Mudde, M., Harren, F. J. M., Barendse, G. W. M., et al. (1993). Submergence-Induced Ethylene Synthesis, Entrapment, and Growth in Two Plant Species With Contrasting Flooding Resistances. *Plant Physiol.* 103, 783–791. doi: 10.1104/pp.103.3.783
- Vriezen, W. H., Huzink, R., Mariani, C., and Voesenek, L. A. C. J. (1999). 1-Aminocyclopropane-1-carboxylate oxidase activity limits ethylene biosynthesis in *Rumex palustris* during submergence. *Plant Physiol.* 121, 189–195. doi: 10.1104/pp.121.1.189
- Wang, T. W., and Arteca, R. N. (1992). Effects of low O<sub>2</sub> root stress on ethylene biosynthesis in tomato plants (*Lycopersicon esculentum* mill cv heinz 1350). *Plant Physiol.* 98, 97–100. doi: 10.1104/pp.98.1.97

- Wang, Y., Li, J., and Liu, A. (2017). Oxygen activation by mononuclear nonheme iron dioxygenases involved in the degradation of aromatics. *J. Biol. Inorg. Chem.* 22, 395–405. doi: 10.1007/s00775-017-1436-5
- Weits, D. A., Giuntoli, B., Kosmacz, M., Parlanti, S., Hubberten, H. M., Riegler, H., et al. (2014). Plant cysteine oxidases control the oxygen-dependent branch of the N-end-rule pathway. *Nat. Commun.* 5, 1–10. doi: 10.1038/ncomms4425
- Weits, D. A., Kunkowska, A. B., Kamps, N. C. W., Portz, K. M. S., Packbier, N. K., Nemec Venza, Z., et al. (2019). An apical hypoxic niche sets the pace of shoot meristem activity. *Nature* 569, 714–717. doi: 10.1038/s41586-019-1203-6
- White, M. D., Klecker, M., Hopkinson, R. J., Weits, D. A., Mueller, C., Naumann, C., et al. (2017). Plant cysteine oxidases are dioxygenases that directly enable arginyl transferase-catalysed arginylation of N-end rule targets. *Nat. Commun.* 8. doi: 10.1038/ncomms14690
- White, M. D., Kamps, J. J. A. G., East, S., Taylor Kearney, L. J., and Flashman, E. (2018). The plant cysteine oxidases from *Arabidopsis thaliana* are kinetically tailored to act as oxygen sensors. *J. Biol. Chem.* 293, 11786–11795. doi: 10.1074/jbc.RA118.003496
- Wu, J., Ichihashi, Y., Suzuki, T., Shibata, A., Shirasu, K., Yamaguchi, N., et al. (2019). Abscisic acid-dependent histone demethylation during postgermination growth arrest in *Arabidopsis*. *Plant Cell Environ.* 42, 2198–2214. doi: 10.1111/pce.13547
- Yamaguchi, S. (2008). Gibberellin Metabolism and its Regulation. *Annu. Rev. Plant Biol.* 59, 225–251. doi: 10.1146/annurev.arplant.59.032607.092804
- Yeung, E., Bailey-Serres, J., and Sasidharan, R. (2019). After The Deluge: Plant Revival Post-Flooding. *Trends Plant Sci.* 24, 443–454. doi: 10.1016/j.tplants.2019.02.007
- Yu, Y., Bu, Z., Shen, W. H., and Dong, A. (2009). An update on histone lysine methylation in plants. *Prog. Nat. Sci.* 19, 407–413. doi: 10.1016/j.pnsc.2008.07.015
- Yuan, L.-B., Dai, Y.-S., Xie, L.-J., Yu, L.-J., Zhou, Y., Lai, Y.-X., et al. (2017). Jasmonate Regulates Plant Responses to Postsubmergence Reoxygenation through Transcriptional Activation of Antioxidant Synthesis. *Plant Physiol.* 173, 1864–1880. doi: 10.1104/pp.16.01803
- Zhang, K., Halitschke, R., Yin, C., Liu, C. J., and Gan, S. S. (2013). Salicylic acid 3-hydroxylase regulates *Arabidopsis* leaf longevity by mediating salicylic acid catabolism. *Proc. Natl. Acad. Sci. U. S. A.* 110, 14807–14812. doi: 10.1073/pnas.1302702110
- Zhou, Z., Vriezen, W., Van Caeneghem, W., Van Montagu, M., and Van Der Straeten, D. (2001). Rapid induction of a novel ACC synthase gene in deepwater rice seedlings upon complete submergence. *Euphytica* 121, 137–143. doi: 10.1023/A:1012059425624

**Conflict of Interest:** The authors declare that the research was conducted in the absence of any commercial or financial relationships that could be construed as a potential conflict of interest.

Copyright © 2020 Iacopino and Licausi. This is an open-access article distributed under the terms of the Creative Commons Attribution License (CC BY). The use, distribution or reproduction in other forums is permitted, provided the original author(s) and the copyright owner(s) are credited and that the original publication in this journal is cited, in accordance with accepted academic practice. No use, distribution or reproduction is permitted which does not comply with these terms.



# Novel Role of JAC1 in Influencing Photosynthesis, Stomatal Conductance, and Photooxidative Stress Signalling Pathway in *Arabidopsis thaliana*

Weronika Czarnocka<sup>1,2\*</sup>, Anna Rusaczzonek<sup>1,2</sup>, Patrick Willems<sup>3,4</sup>, Marzena Sujkowska-Rybikowska<sup>1</sup>, Frank Van Breusegem<sup>3,4</sup> and Stanisław Karpiński<sup>2</sup>

<sup>1</sup> Department of Botany, Institute of Biology, Warsaw University of Life Sciences, Warsaw, Poland, <sup>2</sup> Department of Plant Genetics, Breeding and Biotechnology, Institute of Biology, Warsaw University of Life Sciences, Warsaw, Poland, <sup>3</sup> Department of Plant Biotechnology and Bioinformatics, Ghent University, Ghent, Belgium, <sup>4</sup> Center of Plant Systems Biology, VIB, Ghent, Belgium

## OPEN ACCESS

### Edited by:

Joerg Durner,  
Helmholtz Zentrum München,  
Germany

### Reviewed by:

Peter J. Gollan,  
University of Turku, Finland  
Vivek Dogra,  
Institute of Himalayan Bioresource  
Technology (CSIR), India

### \*Correspondence:

Weronika Czarnocka  
weronika\_czarnocka@sggw.edu.pl

### Specialty section:

This article was submitted to  
Plant Abiotic Stress,  
a section of the journal  
Frontiers in Plant Science

**Received:** 22 March 2020

**Accepted:** 08 July 2020

**Published:** 29 July 2020

### Citation:

Czarnocka W, Rusaczzonek A,  
Willems P, Sujkowska-Rybikowska M,  
Van Breusegem F and Karpiński S  
(2020) Novel Role of JAC1 in  
Influencing Photosynthesis, Stomatal  
Conductance, and Photooxidative  
Stress Signalling Pathway in  
*Arabidopsis thaliana*.  
Front. Plant Sci. 11:1124.  
doi: 10.3389/fpls.2020.01124

Regulation of light absorption under variable light conditions is essential to optimize photosynthetic and acclimatory processes in plants. Light energy absorbed in excess has a damaging effect on chloroplasts and can lead to cell death. Therefore, plants have evolved protective mechanisms against excess excitation energy that include chloroplast accumulation and avoidance responses. One of the proteins involved in facilitating chloroplast movements in *Arabidopsis thaliana* is the J domain-containing protein required for chloroplast accumulation response 1 (JAC1). The function of JAC1 relates to the chloroplast actin filaments appearance and disappearance. So far, the role of JAC1 was studied mainly in terms of chloroplasts photorelocation. Here, we demonstrate that the function of JAC1 is more complex, since it influences the composition of photosynthetic pigments, the efficiency of photosynthesis, and the CO<sub>2</sub> uptake rate. JAC1 has positive effect on water use efficiency (WUE) by reducing stomatal aperture and water vapor conductance. Importantly, we show that the stomatal aperture regulation is genetically coupled with JAC1 activity. In addition, our data demonstrate that JAC1 is involved in the fine-tuning of H<sub>2</sub>O<sub>2</sub> foliar levels, antioxidant enzymes activities and cell death after UV-C photooxidative stress. This work uncovers a novel function for JAC1 in affecting photosynthesis, CO<sub>2</sub> uptake, and photooxidative stress responses.

**Keywords:** chloroplast movement, stomata, photosynthesis, oxidative stress, transcriptome

## INTRODUCTION

Plants regulate the light absorption under naturally variable conditions, which is essential for photosynthesis optimization and acclimation. Light energy absorbed in excess (excess excitation energy, EEE) leads to photoinhibition and chloroplast retrograde-signalling and may cause chloroplast damage and ultimately cell death (Mühlenbock et al., 2008; Wituszyńska and



Karpiński, 2013; Wituszyńska et al., 2015; Czarnecka and Karpiński, 2018; Górecka et al., 2020). Therefore, plants have evolved EEE avoidance and dissipation mechanisms to ensure the proper functionality of the photosynthetic apparatus and photosynthesis. One of these mechanisms is chloroplast movement (Demarsy et al., 2018).

Chloroplast photorelocation is an essential mechanism to adapt to the fluctuating light conditions (Gabrys, 2004; Suetsugu et al., 2010a). In the dark, chloroplasts are located along the anticlinal walls and at the cells' bottom. Upon transferring plants to weak or moderate light, chloroplasts reposition themselves along the periclinal walls in order to efficiently capture light energy, which is termed the accumulation response. However, after exposure to strong light intensities, chloroplasts demonstrate avoidance response, which manifests itself by positioning at anticlinal cell walls and is aimed at lowering the risk of photoinhibition and photodamage (Wada and Kong, 2018). So far, only a couple of proteins have been identified to facilitate light intensity perception and light-mediated chloroplast movements. Well-characterized are blue and UV-A/B photoreceptors, phototropins. *Arabidopsis thaliana* (*Arabidopsis*) possesses two such receptors, phototropin 1 (*phot1*) and phototropin 2 (*phot2*), that redundantly mediate the chloroplast accumulation response (Sakai et al., 2001). However, the avoidance response is regulated only by *phot2* and not by *phot1* (Kagawa et al., 2001). In *Arabidopsis*, the movement of chloroplasts and their anchoring to the plasma membrane is dependent on short actin filaments located along the chloroplast periphery (cp-actin filaments). Under light induction cp-actin filaments relocate to the leading edge of chloroplasts and cause chloroplast movement that is regulated by both *phot1* and *phot2* (Kadota et al., 2009), and additionally by a J-domain protein required for chloroplast accumulation response 1 (*JAC1*) (Ichikawa et al., 2011).

*JAC1* was originally identified in an *Arabidopsis* mutant screen deficient in chloroplast accumulation responses (Suetsugu et al., 2005). In *jac1* mutant, chloroplasts remain localized to the side walls of palisade cells (Suetsugu et al., 2005; Gotoh et al., 2018). Apart from the important role in chloroplast accumulation at the cell surface in weak light, *JAC1* is also required for the chloroplast relocation to the cell's bottom in the darkness (Suetsugu et al., 2005). In palisade cells, the chloroplast dark positioning in the *jac1* mutant is different from wild-type plants, because chloroplasts gather at the anticlinal cell walls (Hermanowicz et al., 2019). In addition, it was proven that under excess light, *JAC1*, to some extent, is also needed in the regulation of the avoidance response as cp-actin filament reorganization is impaired in *jac1* (Kodama et al., 2010; Ichikawa et al., 2011). A similar perturbed cp-actin reorganization was observed in two other mutants, *weak chloroplast movement under blue light 1* (*web1*) and *plastid movement impaired 2* (*pmi2*) (Kodama et al., 2010), which show weak chloroplast movement during accumulation and avoidance responses. Even though the physical interaction between *phot1* and *phot2* (Sztatelman et al., 2016), as well as between *WEB1* and *PMI2* has been documented (Kodama et al., 2010), *JAC1* does not physically interact with any of them (Suetsugu et al., 2005; Kodama et al., 2010). Therefore, a yet

unidentified signal from plasma membrane-localized phototropins is received by *JAC1* and passed along to chloroplasts to regulate the direction of their movement (Suetsugu et al., 2005). Moreover, it was shown that *JAC1* is dispensable for *phot2*-mediated chloroplast avoidance response induced by high-light irradiation (Suetsugu et al., 2005).

The *Arabidopsis JAC1* protein is 651 amino acids long and contains a 70 amino acid long auxilin-like J-domain at the C-terminus, which is essential for *JAC1*-mediated chloroplast photorelocation (Takano et al., 2010). A sequence-based classification assigned *JAC1* to the group of type III J-proteins, including cochaperones of the heat shock protein 70 (*Hsp70*) chaperones (Takano et al., 2010). The *JAC1* J-domain is similar to the J-domain of auxilins, enzymes that uncoat clathrin from the mature vesicles to promote the recycling of clathrin during endocytosis (Suetsugu et al., 2005). The highly conserved His-Pro-Asp (HPD) tripeptide within J-domain has been shown to facilitate the interactions with *Hsp70* chaperones (Jiang et al., 2003). Structural analysis of the *JAC1* J-domain indicates that HPD motif is indispensable for *JAC1*-dependent chloroplast light-induced movement and suggests that *JAC1* cooperation with heat shock protein cognate 70 (*Hsc70*) chaperone is needed in this process (Suetsugu et al., 2010b). Auxilin J-domain targets and activates the *Hsc70* that mediates clathrin uncoating (Eisenberg and Greene, 2007). *JAC1* overexpression was shown to inhibit endocytosis process in root hair cells, which indirectly supports its role in clathrin uncoating (Ezaki et al., 2007). However, so far there is no evidence on the involvement of *Hsc70* and clathrin-mediated endocytosis in chloroplast movement (Adamowski et al., 2018). The localization of *JAC1* is most probably cytoplasmic, but its presence in the nucleus (Suetsugu et al., 2005) or within cellular membranes, cannot be excluded (Suetsugu et al., 2015). Furthermore, neither the expression level of *JAC1* gene nor the protein level are regulated by light or by the phototropins (Suetsugu et al., 2005).

Even though the role of *JAC1* has been broadly studied in terms of chloroplast movements, so far little is known about the other molecular and physiological processes that involve *JAC1*. This study demonstrates that *JAC1* influences photosynthetic reactions, stomatal aperture and thus water vapor conductance and CO<sub>2</sub> uptake. This regulation, at least partially, involves *JAC1*-dependent gene expression changes. In addition, we prove that *JAC1* takes part in the fine-tuning of photooxidative-stress induced accumulation of hydrogen peroxide (H<sub>2</sub>O<sub>2</sub>), regulation of antioxidant enzymes activities and cell death. Our results shed a new light on the role of *JAC1* in *Arabidopsis*.

## MATERIALS AND METHODS

### Plant Material and Growth Conditions

*Arabidopsis thaliana jac1-1* mutant in Columbia-0 gl1 (*Col-0* gl1) background together with wild-type *Col-0* gl1 plants were used in this study. The seeds were a kind gift from Prof. Masamitsu Wada (Tokyo Metropolitan University, Tokyo, Japan). Seeds were sown on Jiffy pots, stratified for two days in

4°C and moved for germination to standard laboratory conditions (8 h photoperiod, PPFD: 80  $\mu\text{mol photons m}^{-2} \text{ s}^{-1}$ ), 50% relative air humidity and temperature day/night: 22/18°C).

## Measurements of Morphological and Physiological Traits

All morphological and physiological parameters were measured for four-week-old plants. Rosette size was analyzed with a FluorCam (Photon System Instruments PSI, Brno, Czech Republic) for 15 plants *per* genotype in two independent experiments (n=15). Rosette dry weight was measured for 12 plants for each genotype (n=12) after desiccation in 105°C for three days. The determination of water use efficiency (WUE) was performed for 12 plants *per* genotype in two independent experiments (n=12) according to the previously published protocol (Wituszyńska et al., 2013b; Wituszyńska and Karpiński, 2014).

## Microscopy and Image Analysis

The calculation of stomata number *per* mm<sup>2</sup> of leaf area was performed using the transparent glue imprints of the abaxial leaf side and with the use of Olympus AX70 Provis microscope (Olympus, Tokio, Japan). Three leaves, 6<sup>th</sup>, 7<sup>th</sup> and 8<sup>th</sup> were analyzed for 9 individual plants for each genotypes in two independent experiments (n=27). The number of stomata *per* mm<sup>2</sup> of leaf area was calculated from three frames of each microscopic sample. Stomatal aperture was measured with Image J program (Version 1.52e, National Institutes of Health, Bethesda, MD, USA) for 6<sup>th</sup>, 7<sup>th</sup>, and 8<sup>th</sup> leaf, for 77 and 74 individual stomata in the wild type and *jac1* mutant, respectively (n=74–77). Arabidopsis mesophyll cells were assayed for intracellular chloroplast location with Leica TCS Sp5 confocal microscope (Leica Camera AG, Wetzlar, Germany), using chlorophyll autofluorescence upon argon laser (488 nm) excitation. 6<sup>th</sup>, 7<sup>th</sup> or 8<sup>th</sup> leaf was analyzed for 5 plants *per* each genotype *per* treatment in two independent experiments (n=5).

## Chlorophyll a Fluorescence and Gas Exchange Parameters Measurements

Chlorophyll *a* fluorescence parameters and OJIP test were measured with a FluorCam system (Photon System Instruments PSI, Brno, Czech Republic), including four super bright LED panels 130 x 130 mm, providing actinic light (300  $\mu\text{mol photons m}^{-2} \text{ s}^{-1}$ ) and saturation pulses (4,000  $\mu\text{mol photons m}^{-2} \text{ s}^{-1}$ ). Measurements were performed with standard “Quenching” protocol implemented in the FluorCam7 software for 11–21 plants *per* genotypes *per* treatment in two separate experiments (n=11–21). Prior the measurements, plants were dark-adapted for 30 min in order to determine  $F_0$  and  $F_m$  parameters. Chlorophyll fluorescence terminology has been previously described (Baker, 2008; Wituszyńska et al., 2013a). CO<sub>2</sub> uptake and water vapor conductance (GH<sub>2</sub>O) in variable conditions of photosynthetic active radiation (PAR) ranging between 0 and 1,900  $\mu\text{mol m}^{-2} \text{ s}^{-1}$  were determined using Portable Gas Exchange System GFS-3000 (Heinz Walz GmbH, Effeltrich, Germany) for 8–10 plants *per* genotype in two independent experiments (n=8–10). In order to obtain the slope of the regression line for each tested genotype, all

the values for CO<sub>2</sub> uptake (or GH<sub>2</sub>O) for each tested PAR intensity were used. To compare the regression line slopes the procedure from Wonnacott and Wonnacott (1990) was used. The statistical analysis was performed in the “R” version 2.12.1 using stats packages.

## Photosynthetic Pigments Measurements

The determination of photosynthetic pigment compositions was performed according to the procedure described previously (Rusaczek et al., 2015; Wituszyńska et al., 2015) for 12 plants *per* genotypes in two independent experiments (n=12).

## Hydrogen Peroxide Levels Determination

The hydrogen peroxide (H<sub>2</sub>O<sub>2</sub>) content was determined for nine plants *per* genotype *per* treatment from two independent experiments (n=9), as previously described (Rusaczek et al., 2015; Wituszyńska et al., 2015).

## Antioxidant Enzyme Activity Measurements

The activities of superoxide dismutase (SOD), catalase (CAT), and ascorbate peroxidase (APX) were determined for nine plants *per* genotype *per* treatment from two independent experiments (n=9), as previously described (Rusaczek et al., 2015; Wituszyńska et al., 2015).

## UV-C Treatment and Cell Death Analysis

UV-C radiation (100 mJ cm<sup>-2</sup>) was used as oxidative-stress inducing factor. UV-C radiation was applied with 500 Crosslinker (Hoefer Pharmacia Biotech, San Francisco, CA, USA), equipped with lamps emitting light in the wavelength ranging from 250 to 258 nm (type G8T5, 8W; Sankyo Denki, Hiratsuka, Japan). Cell death analysis was performed by the measurement of ion leakage for 9–12 plants *per* genotype *per* treatment in two independent experiments (n=9–12), as previously described (Rusaczek et al., 2015; Wituszyńska et al., 2015). Cell death visualization was performed by staining five leaves *per* genotype *per* treatment with 1% (m/v) Evans blue and vacuum infiltration for 30 min (Mergemann and Sauter, 2000). After staining, the leaves were washed three times with deionized water and chlorophyll was removed by the incubation in chloral hydrate (2.5 mg/mL) for two days. The pictures of representative leaves are presented.

## RNA Extraction and cDNA Synthesis

The RNA was extracted from whole rosettes in three biological replicates, each consisting of at least four rosettes. Total RNA extraction was performed with a use of GeneMATRIX Universal RNA Purification Kit (EURX, Gdańsk, Poland). Additional step of on-column DNaseI digestion was performed. RNA concentration and purity were analyzed spectrophotometrically with Eppendorf BioSpectrometer (Eppendorf, Hamburg, Germany). The RNA integrity was tested by electrophoretic separation in 1% agarose gel and the same amount of RNA for each sample was used for reverse transcription. cDNA synthesis was performed with a High Capacity cDNA Reverse Transcription Kit (Thermo Fisher Scientific, Waltham, MA, USA).

## Relative Gene Expression Measurement by Real-Time qPCR

Real-time qPCR was performed for four-week-old non-treated and UV-C treated plants (3, 6, 12, and 24 h after UV-C exposure), using the 7500 Fast Real-Time PCR System and Power SYBR Green Master Mix (Thermo Fisher Scientific, Waltham, MA, USA). Each of three biological repeats *per* treatment was tested in three technical repeats. The following cycling programme was used in qPCR: 95°C for 10 min, followed by 40 cycles of denaturation in 95°C for 15 s and annealing/extension in 60°C for 60 s. Primers for *JAC1* (AT1G75100) were designed with Primer3 software (Primer3Plus, Free Software Foundation, Inc., Boston, MA, USA) and their sequence was as follows, forward 5'-gatggttctaataccaaggaa-3' and reverse 5'-tgaaggttctgatcccgatt-3'. *YELLOW-LEAF-SPECIFIC GENE 8* (YLS8, AT5G08290) was used as a reference, according to the RefGenes tool incorporated in Genevestigator (Hruz et al., 2008) and amplified with the following primers: forward 5'-ttactgttctggttctccattt-3' and reverse 5'-cactgaatcatgttcgaagcaagt-3'. The specificity of each primer pair was analyzed by melting curve. The efficiency of real-time qPCR was calculated using LinRegPCR tool (Ramakers et al., 2003). Calculation of relative gene expression levels and the significance of difference between tested samples was performed using REST2009 (Pfaffl et al., 2002).

## RNA Sequencing and RNA-Seq Analysis

The RNA was extracted as described above from four-week-old non-treated and UV-C treated plants 30 min after exposure to 100 mJ cm<sup>-2</sup> of UV-C radiation. RNA was isolated from three biological replicates, each consisting of at least four rosettes. RNA concentration and purity were determined spectrophotometrically using the Nanodrop ND-1000 (Nanodrop Technologies) and RNA integrity was assessed using a BioAnalyzer 2100 (Agilent). An amount of 1,000 ng of total RNA *per* sample was used as input. Poly-A containing mRNA was purified from the total RNA, using poly-T oligo-attached magnetic beads and the Illumina TruSeq® Stranded mRNA Sample Prep Kit (protocol version: Document # 1000000040498 v00 - October 2017). RNA was transcribed to cDNA in a reverse transcription reaction using random primers, and subsequently converted into double-stranded cDNA using DNA Polymerase I and RNase H. The cDNA fragments were extended with a single 'A' base at the 3' ends of the blunt-ended cDNA fragments, after which multiple indexing adapters were ligated introducing different barcodes for each sample. Finally, PCR was performed to enrich DNA fragments that possess adapter molecules on both ends. Sequence-libraries of each sample were equimolarly pooled and sequenced on Illumina HiSeq 4000 (Paired-end kit, 76 cycles, Dual Index, 4 lanes) at the VIB Nucleomics Core (www.nucleomics.be). Reads were aligned to the Arabidopsis genome by STAR (v2.5.2b) (Dobin et al., 2013), using the Araport11 annotation (Cheng et al., 2017). The number of reads *per* gene was quantified with the featureCounts function as implemented in the Subread package v1.6.2 (Liao et al., 2014). Only protein-coding genes quantified by at least 5 reads in at least three samples (20,013 genes) were retained for downstream differential gene expression analysis using the

software package edgeR (Robinson et al., 2010) in R (v3.4.1). TMM normalization (Robinson and Oshlack, 2010) was applied using the calcNormFactors function. Variability in the data set was assessed with a MDS plot, showing clear separation according to genotype and UV-C treatment. In order to test user-defined hypotheses, a no-intercept single-factor model was defined combining genotype and treatment factors, e.g. such as *jac1*\_UV. Dispersions were estimated with the estimateGLMRobustDisp function. A negative binomial regression model was used to model the overdispersed counts for each gene separately with fixed values for the dispersion parameter as outlined (McCarthy et al., 2012) and as implemented in the function glmFit using the above described model. Hypothesis testing was based on likelihood ratio tests. Contrasts of interest were the response between different genotypes under control conditions, the effect of UV stress in each genotype, and the interaction effect of UV stress and genotype. False discovery rate adjustments of the P values were performed with the method described by Benjamini and Hochberg (1995). The gene expression data were deposited in Gene Expression Omnibus (GEO; <http://www.ncbi.nlm.nih.gov/geo/>) under accession number GSE143762. Gene ontology enrichment analysis was performed using ThaleMine tool (v4.1.2-20200127) within the Araport portal (Krishnakumar et al., 2015). Functional analysis of differentially expressed genes was performed using the MapMan tool (Thimm et al., 2004).

## RESULTS

### JAC1 Influences Photosynthetic Efficiency and the Level of Photosynthetic Pigments

Since JAC1 is involved in the regulation of chloroplast movements (**Supplementary Figure 1**), our first aim was to assess if it has an influence on photosynthetic efficiency. Chlorophyll *a* fluorescence measurements proved that the *jac1* mutant has higher maximum quantum efficiency of photosystem II (PSII) ( $F_v/F_m$ ) (**Figure 1A**), but lower non-photochemical (NPQ) (**Figure 1B**) and photochemical quenching ( $qP$ ) (**Figure 1C**), as compared to the wild-type plants.

In order to obtain better insight into the specific photosynthetic reactions that are JAC1-dependent, we analyzed the fluorescence transient using the O–J–I–P test (Strasser et al., 2004). This demonstrated functional changes within light harvesting complexes (LHCs) and photosystems in *jac1* mutant (**Supplementary Figure 2**). More specifically, a decreased ABS/RC ratio was apparent. This ratio represents the total number of photons absorbed by chlorophylls of all the reaction centres (RCs) divided by the total number of active RCs and thus suggests that *jac1* mutant had more active RCs than wild-type plants. Besides measuring active RCs, the TRo/RC ratio is an estimate of maximal rate by which excitation is trapped by the RC resulting in the reduction of quinone A ( $Q_A$ ). The decreased TRo/RC ratio in *jac1* suggests that not the whole  $Q_A$  pool was reduced in this mutant, unlike in the wild-type. Furthermore, the



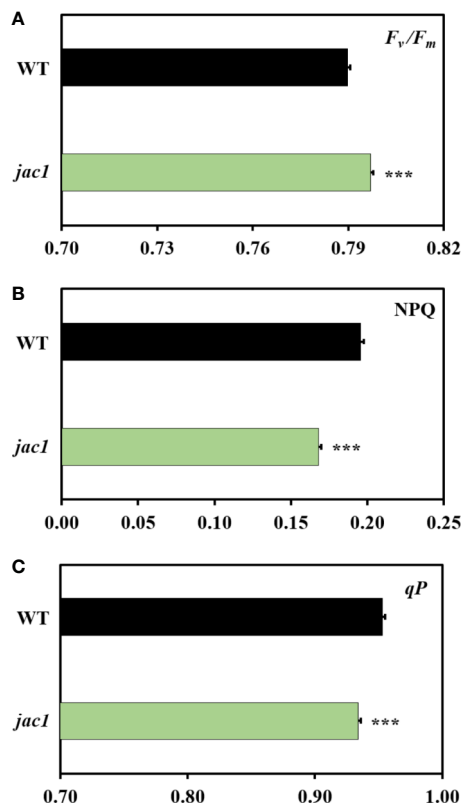


**FIGURE 1** | Chlorophyll a fluorescence parameters of 4-week-old *Arabidopsis thaliana* wild-type (WT) and *jac1* mutant. **(A)**  $F_v/F_m$ , maximum quantum efficiency of PSII; **(B)** NPQ, non-photochemical quenching; **(C)**  $qP$ , photochemical quenching. Values are means ( $\pm$  SD) of 11–21 plants per genotype from two independent experiments ( $n=11$ – $21$ ). Asterisks indicate significant difference in comparison with the wild-type plants at the level  $P < 0.001$  (\*\*\*) according to the Tukey's HSD multiple comparison test.

*jac1* mutant showed a significantly decreased reoxidation of reduced  $Q_A$  via electron transport in active RCs (ETo/RC). Because ETo/RC is represented only by the active centres, the lower ratio in the *jac1* mutant implies again that there were more active centres than in the wild type. Finally, the effective dissipation of untrapped excitation energy from all RCs with respect to the number of active RCs (DIO/RC ratio) was also lower in *jac1* mutant, indicating a better connectivity between the structurally heterogeneous units of PSII (Force et al., 2003; Wituszyńska et al., 2013a).

To study whether the observed JAC1-dependent changes in photosynthetic efficiency are caused by altered photosynthetic pigments levels, we analyzed their composition (Figure 2). The total chlorophyll level, concentration of chlorophyll *b* (but not chlorophyll *a*) were significantly elevated in *jac1*. We also observed that Chl *a/b* ratio was significantly decreased in *jac1* mutant in relation to the wild type. Moreover, while  $\beta$ -carotene level was elevated in *jac1* mutant, the content of violaxanthin, antheraxanthin and zeaxanthin were decreased in *jac1* mutant, in comparison to the control plants.

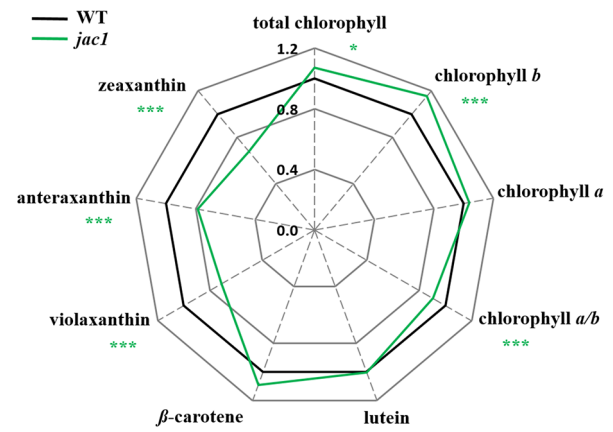


**FIGURE 2** | Photosynthetic pigment contents in 4-week-old *Arabidopsis thaliana* wild type and mutant plants. Total chlorophyll, chlorophyll *a*, chlorophyll *b*, chlorophyll *a/b* ratio; lutein;  $\beta$ -carotene; violaxanthin; antheraxanthin; zeaxanthin. Values are means ( $\pm$  SD) of 12 plants per genotype from two independent experiments ( $n=12$ ) expressed as the peak area (mg of dry weight<sup>-1</sup>). Asterisks indicate significant differences from the wild type according to the Tukey HSD test at the level of  $P < 0.05$  (\*), or  $P < 0.001$  (\*\*\*)

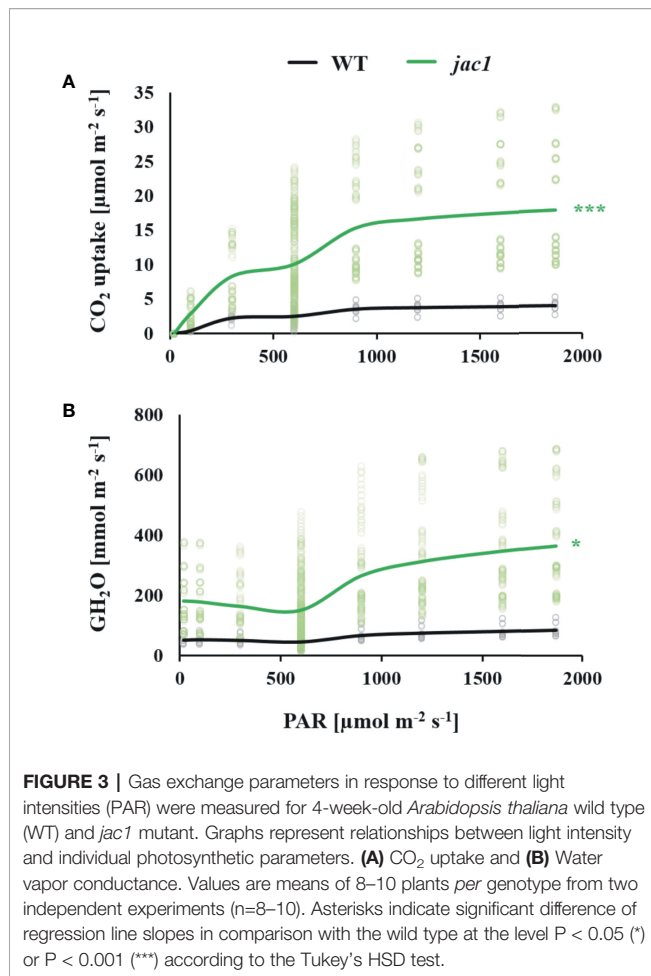
## CO<sub>2</sub> Uptake Rate and Water Vapor Conductance Are Negatively Affected by JAC1

Due to altered light-phase photosynthetic reactions in *jac1* mutant, our next step was to assess whether JAC1 influences the carbon dioxide (CO<sub>2</sub>) uptake. In a range of photosynthetic active radiation (PAR) intensities that were tested, the CO<sub>2</sub> uptake was consistently higher in *jac1*, reaching more than three times higher uptake in high light intensities (Figure 3A). The simultaneously measured water vapor conductance (GH<sub>2</sub>O) was elevated up to three times in low PAR intensities and, similarly to the CO<sub>2</sub> uptake rate, a greater relative increase in *jac1*, compared to wild-type was apparent under high PAR (Figure 3B). Interestingly, the variation of CO<sub>2</sub> uptake and GH<sub>2</sub>O parameters in a single measuring point was much greater in *jac1* background, compared to the wild type.

## JAC1 Has an Impact on Water Use Efficiency Through the Reduction of Stomatal Conductance

Such high water vapor conductance and CO<sub>2</sub> uptake rate in *jac1* prompted us to analyze the impact of JAC1 activity on stomatal density and aperture. While the stomatal density was reduced in *jac1* mutant, stomatal aperture was significantly elevated (Figures 4A–C). Moreover, water use efficiency (WUE), measured as dry weight per water used, proved to be significantly decreased in *jac1* compared to wild-type plants (Figure 4D). Hence, *jac1* consumed relatively more water for the production of dry weight, which is in agreement with the previously observed elevated water vapor conductance (Figure 3B), a measure of leaf transpiration efficiency. Importantly, our results showed that the rosette size and





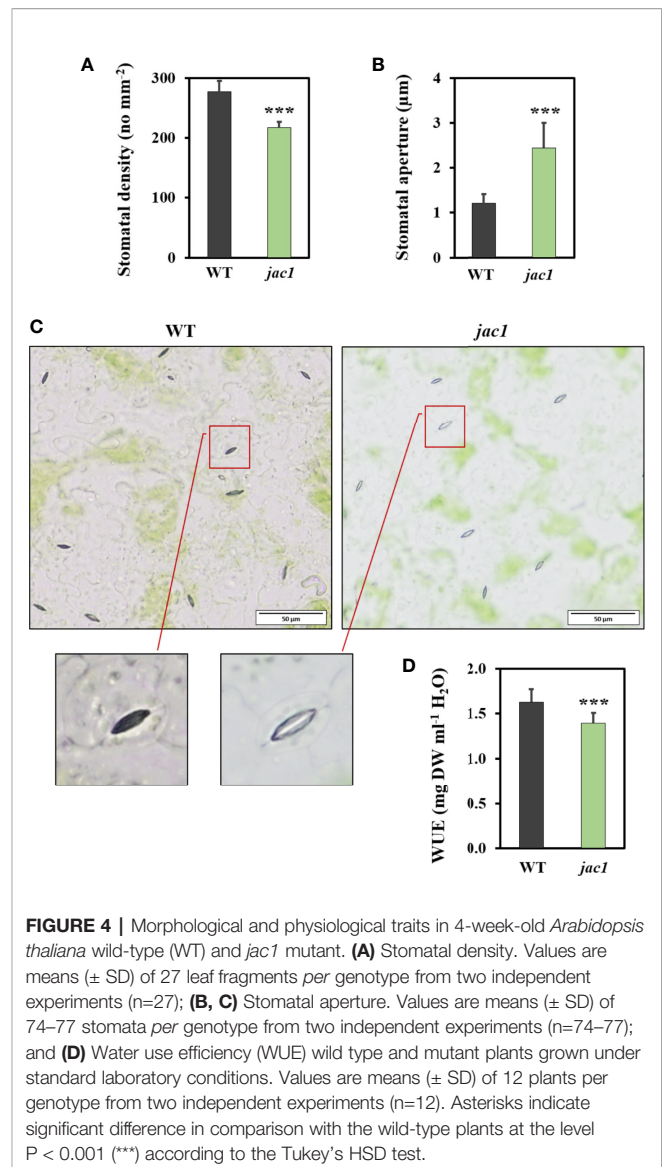
dry weight were not different between *jac1* mutant and the wild type (Supplementary Figure 3, Supplementary Figures 4A, B).

## Photooxidative Stress Causes Changes in JAC1 Expression Level and Shows the Influence of JAC1 on Photosynthetic Activity, Redox Homeostasis, and Cell Death Regulation

UV-C radiation has been shown to induce oxidative stress and photoinhibition. It was demonstrated that changes within chloroplasts are the first observed symptoms of UV-C induced cell death (Wituszyńska et al., 2015). Therefore, we used UV-C treatment to explore the influence of JAC1 in the photooxidative stress response and cell death.

Firstly, we examined how the *JAC1* expression changes after UV-C exposure (Figure 5). In the early hours (3 and 6 h) after UV-C treatment, *JAC1* transcript abundance was slightly induced. However, between 6 and 12 h post UV-C stress, *JAC1* expression dropped severely to reach 10% of the initial expression level after 12 h and 30% after 24 h.

In the next step, we explored the role of JAC1 during photosynthetic acclimation to oxidative stress. Our results demonstrated that both 48 and 96 h post UV-C exposure, *jac1*



had higher values of maximum and operational quantum efficiency of PSII ( $F_v/F_m$  and  $\Phi_{PSII}$ , respectively), as compared to the wild-type plants (Figures 6A, B). However, 96 h after UV-C incident, *jac1* plants, compared to wild-type, exhibited decreased levels of the photochemical quenching ( $qP$ ) parameter, signifying a lower proportion of PSII reaction centres to be open in *jac1* (Figure 6C). In addition, the level of EEE dissipation through the NPQ reactions was decreased in *jac1*, compared to the wild type (Figure 6D). The overall leaf photosynthetic capacity, indicated by  $R_{fd}$  parameter, was elevated in *jac1* mutant in relation to the control plants (Figure 6E). Taken together, this ensemble of parameters shows JAC1 to negatively influence the photosynthetic activity under photooxidative stress.

Next, to examine the role of JAC1 in UV-C-triggered photooxidative stress response, we analyzed the concentration of H<sub>2</sub>O<sub>2</sub> and activities of antioxidant enzymes in *jac1* mutant and

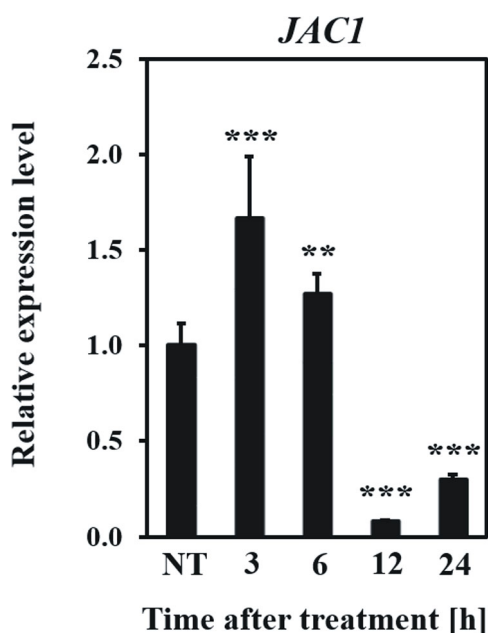


**FIGURE 5 |** Relative expression level of *JAC1* in the *Arabidopsis thaliana* wild-type plants in non-stress conditions (NT) and 3, 6, 12, 24 h after UV-C exposure. Values are means ( $\pm$  SD) from three biological replicates, for which three individual qPCR reactions were performed ( $n=9$ ). Asterisks indicate statistically significant differences from non-treated plants, at the level  $P < 0.01$  (\*\*) or  $P < 0.001$  (\*\*\*).

wild-type plants. Before the UV-C exposure, the  $H_2O_2$  content, as well as superoxide dismutase (SOD) and catalase (CAT) activities were similar in *jac1* and wild-type plants (Figures 7A–C). In contrast, non-stressed *jac1* plants showed significantly higher activity of ascorbate peroxidase (APX) (Figure 7D).

Twelve hours after UV-C exposure, *jac1* mutant demonstrated higher levels of  $H_2O_2$  (Figure 7A), which corresponded with elevated CAT activity (Figure 7C). In contrast, samples analyzed in all time points after 24 h post UV-C stress showed lower content of  $H_2O_2$  (Figure 7A). The pattern of SOD and APX activities in *jac1* mutant was similar to the wild-type, except 96 h after UV-C exposure, when activities of those antioxidant enzymes were significantly decreased in relation to the controls (Figures 7B, D).

In order to assess the influence of JAC1 activity on UV-C-triggered cell death, we performed the analysis of cellular leakage and Evans blue staining of dead cells. Our results proved that 48 h after UV-C treatment, *jac1* mutant demonstrated significantly higher ion leakage (Figure 8A). Higher cell death level was also confirmed by Evans blue staining (Figure 8B), which was visibly more intense at all time points starting from 12 h after UV-C stress.

## UV-C Stress Reshapes the Arabidopsis Transcriptome

In a next phase, we profiled gene expression changes under UV-C stress using high-throughput mRNA sequencing (RNA-seq). In the wild type, UV-C treatment resulted in 2,094 differentially

expressed genes (DEGs) ( $FDR < 0.01$ , absolute  $\log_2$  fold change (FC)  $> 1$ ) (Supplementary Data Sheet 2). In total, 1,579 of these DEGs (75.4%) showed higher expression level after UV-C treatment. Gene set enrichment demonstrated that many DEGs encode membrane, cell wall and chloroplast proteins, especially those integral to thylakoids (Supplementary Data Sheet 3). Interestingly, 73 genes encoded by chloroplast genome were highly upregulated after UV-C treatment (Supplementary Table 1). In addition, amongst the DEGs, there were many genes encoding stress-responsive proteins, including transcription factors and proteins possessing oxidoreductase activity (Supplementary Data Sheet 3). There was also an enrichment of genes encoding tetrapyrrole (including chlorophyll)-binding proteins, light-harvesting complex proteins and photosystems subunits (Supplementary Figure 5), as well as biotic- and abiotic-stress responsive proteins (Supplementary Figure 6), mitochondrial electron transport chain proteins (Supplementary Figure 7), cell wall modification proteins, proteins involved in hormone and redox homeostasis, and protein modifying/degrading enzymes (Supplementary Figure 8). These results indicate that UV-C treatment in wild-type plants has pronounced effects on gene expression level.

## Changes in *jac1* Transcriptome in Non-Stress and After Oxidative Stress Conditions

Under control conditions, 558 DEGs were apparent in *jac1* in comparison to the wild type ( $FDR < 0.01$ ,  $|\log_2 FC| > 1$ ) (Supplementary Data Sheet 2). Enrichment analysis showed that relatively high proportion of DEGs encoded extracellular (16%) and cell wall (6%) proteins (Supplementary Data Sheet 4). In terms of biological processes, *jac1* mutant, in relation to the wild type, demonstrated changes in expression level of genes encoding proteins involved in abiotic stresses (mainly light-induced stress), circadian rhythm and transcriptional regulation (Supplementary Data Sheet 4). Given the observed redox- and photosynthetic-related changes in non-stressed *jac1*, we inspected the gene expression of several photosynthetic components and redox homeostasis enzymes. We observed induced expression of both LHCI (LHCA1, LHCA4) and LHCII (LHCB1.1, LHCB1.2, LHCB1.4, LHCB2.1, LHCB2.2, LHCB2.3, LHCB3) components in *jac1*, in comparison to the wild type (Supplementary Data Sheet 4). Furthermore, in non-stress conditions we found five DEGs involved in redox regulation, encoding thioredoxins, glutaredoxins, and enzymes involved in ascorbate and glutathione metabolism. For instance, monodehydroascorbate reductase (ATMDAR, AT3G09940) was highly induced in *jac1* background. This enzyme takes part in ascorbate recovery, which provides reducing power to APX. In addition, we observed a relatively high number of DEGs encoding cell wall modifying enzymes in non-treated *jac1*, compared to the wild type. Also, genes encoding proteins involved in proteolysis and signalling, especially light- and calcium-induced signal transduction demonstrated changed expression in *jac1*, in relation to wild-type plants. Interestingly, seven genes involved in calcium signalling expressed in stomata

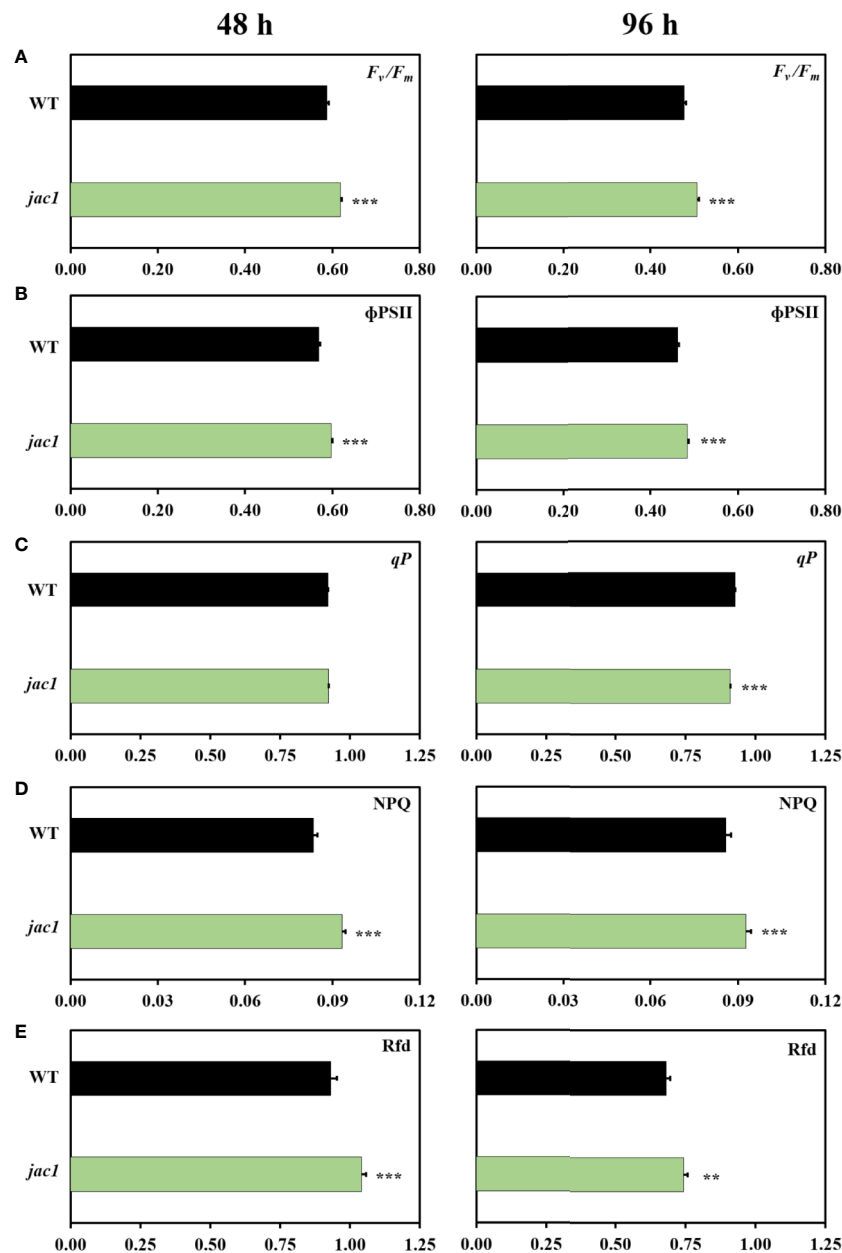


**FIGURE 6 |** Chlorophyll a fluorescence parameters measured in 4-week-old *Arabidopsis thaliana* wild type and *jac1* mutant 48 and 96 h after UV-C exposure (100 mJ cm<sup>-2</sup>). (A)  $F_v/F_m$ , maximum quantum efficiency of PSII; (B)  $\Phi_{PSII}$ , quantum yield of PSII; (C)  $qP$ , photochemical quenching; (D) NPQ, non-photochemical quenching; (E) Rfd, plant vitality parameter. Values are means ( $\pm$  SD) of 11–21 plants per genotype and time point from two independent experiments ( $n=11-21$ ). Asterisks indicate significant difference in comparison with the wild-type plants at the level  $P < 0.005$  (\*\*), or  $P < 0.001$  (\*\*\*) according to the Tukey's HSD multiple comparison test.

guard cells were significantly induced in *jac1* when compared to the wild type (**Supplementary Data Sheet 4**): *MULTICOPY SUPPRESSORS OF SNF4 DEFICIENCY IN YEAST 3* (AT2G43290), calmodulin binding *SAR DEFICIENT 1* (AT1G73805), *CALMODULIN LIKE 23* (AT1G66400), *CALMODULIN 9* (AT3G51920), *TOUCH 2* (AT5G37770), *TOUCH 3* (AT2G41100) and a calcium-binding endonuclease/exonuclease/phosphatase family gene (AT5G54130)

(Obulareddy et al., 2013). Moreover, a gene encoding calcium-binding EF hand family protein (AT4G27280), engaged in stomata movements (Cominelli et al., 2005) was up-regulated in *jac1*, compared to the wild type. CHLORIDE CHANNEL B (AT3G27170), and two water channels, PLASMA MEMBRANE INTRINSIC PROTEIN 2 (AT3G53420) and RESPONSIVE TO DESICCATION 28 (AT2G37180), all expressed in guard cells (Obulareddy et al., 2013; Wang et al., 2016), also demonstrated

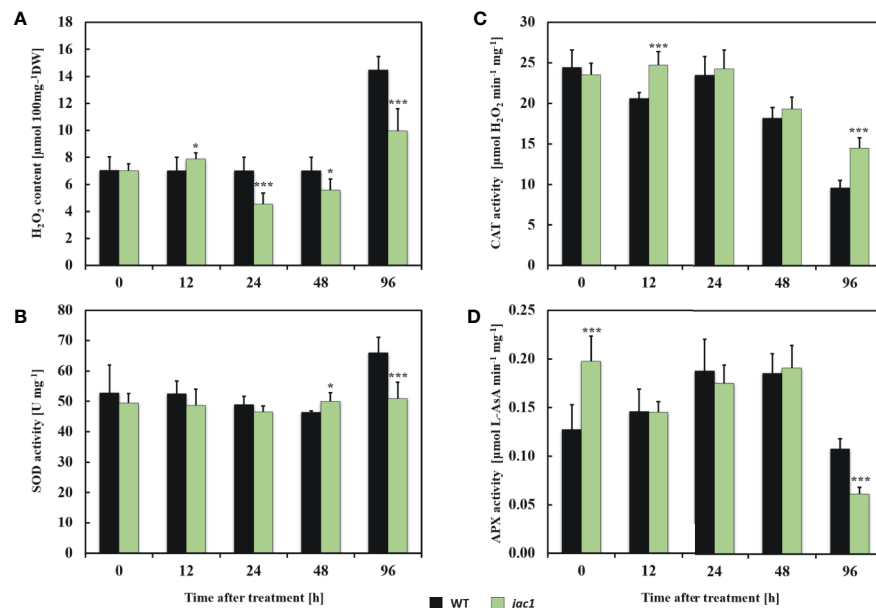


**FIGURE 7 |** Hydrogen peroxide content and activities of selected antioxidant enzymes in 4-week-old *Arabidopsis thaliana* wild type and *jac1* mutant plants measured for untreated plants and 12, 24, 48, and 96 h after UV-C exposure (100 mJ cm<sup>-2</sup>). **(A)** H<sub>2</sub>O<sub>2</sub>, hydrogen peroxide content; **(B)** SOD, superoxide dismutase activity; **(C)** CAT, catalase activity; **(D)** APX, ascorbate peroxidase activity. Values are means (± SD) of 9 plants *per* genotype *per* time point from two independent experiments (n=9). Asterisks indicate significant difference in comparison with the wild-type plants at the level P<0.05 (\*) or P<0.001 (\*\*\*) according to the Tukey's HSD test.

significantly higher expression level in *jac1* mutant, compared to wild-type counterparts.

After UV-C stress, *jac1* displayed 1,017 DEGs in comparison to wild-type plants (**Supplementary Data Sheet 2**). Within the “cellular component” category we observed enrichment in genes encoding components of cell wall, plasma membrane and photosystems (**Supplementary Data Sheet 5**). DEGs in UV-treated *jac1* versus UV-treated wild type were over-represented by genes encoding proteins engaged in response to stimulus (especially abiotic stress), and response to hormones. Among stress-related genes, we identified genes encoding proteins involved in oxidative stress signalling and response, such as catalase 3 (CAT3, AT1G20620), galactinol synthase 2 (GolS2, AT1G56600), and GolS3 (AT1G09350) to be up-regulated, in comparison to the wild type (Sun et al., 2013; Song et al., 2016; Selvaraj et al., 2017). Moreover, significantly changed expression level in UV-C treated *jac1* background, in relation to the wild type, included genes encoding transcription factors (10% of all the DEGs), enzymes with oxidoreductase activity (8% of all the DEGs), tetrapyrrole-binding proteins (3% of all the DEGs). Furthermore, MapMan categorization proved that after UV-C stress in *jac1* mutant, compared to wild-type plants, there were a lot of genes (both up- and down-regulated) encoding proteins involved in signal transduction (i.e. receptor kinases, proteins involved in light-, calcium-dependent signalling), intra- and inter-cellular transport, protein degradation and development (i.e. senescence-associated genes) (**Supplementary Data Sheet 5**). After UV-C treatment, similarly to non-treated samples, *jac1* demonstrated higher expression level of LHCI (LHCA1,

LHCA3, LHCA4) and LHCII (LHCB1.1, LHCB1.2, LHCB1.4, LHCB2.2, LHCB2.4, LHCB3, LHCB4.2) components.

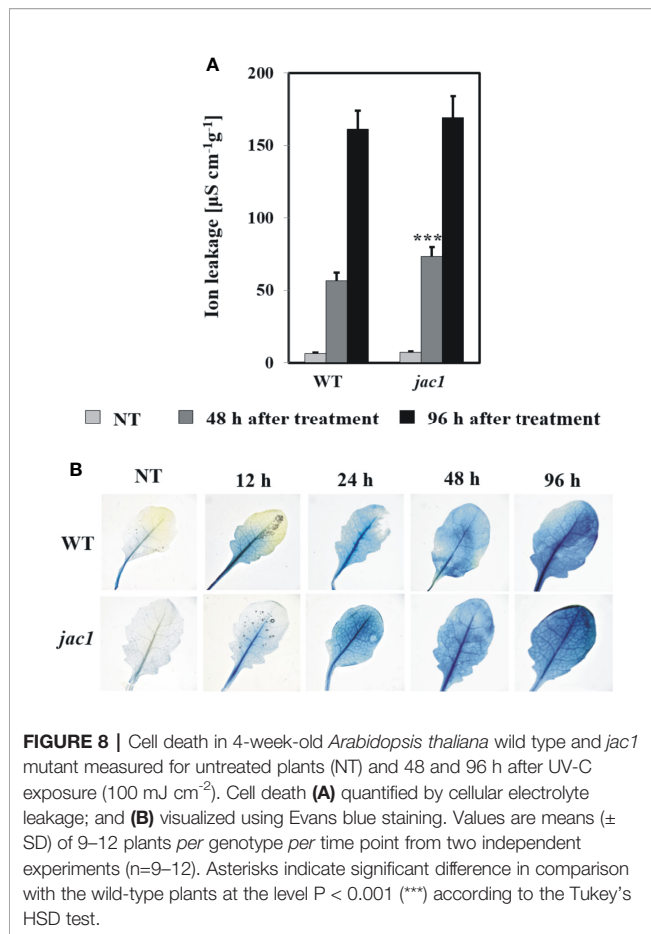
## DISCUSSION

Under variable natural conditions plants need to optimize the absorption of light in order to efficiently perform photosynthetic reactions. EEE, which is the energy absorbed in excess, may lead to photoinhibition, photosystem damage, chloroplasts disruption, and finally to cell death. Thus, plants are equipped in various avoidance and dissipation mechanisms that enable them to protect photosynthetic apparatus from EEE and perform optimal, condition-dependent photosynthesis.

Among the EEE protective mechanisms we can distinguish chloroplast movements, NPQ, and state-transitions (Karpiński et al., 2013; Gawroński et al., 2014; Gilroy et al., 2016; Czarnocka and Karpiński, 2018; Górecka et al., 2020). Chloroplast accumulation and avoidance response are dependent on blue light and UV-A/B radiation receptors, phototropins, and a non-receptor protein, JAC1 (Suetsugu et al., 2005; Kodama et al., 2010; Ichikawa et al., 2011). Even though the JAC1 function was well described in terms of chloroplast movements, so far little was known about its involvement in photosynthetic reactions, response to EEE and cell death.

The analysis of chlorophyll *a* fluorescence performed in this study proved that *jac1* mutant has elevated value of maximum quantum efficiency of PSII ( $F_v/F_m$ ), more active centres, better connectivity between the structurally heterogeneous PSII units





and lower  $Q_A$  pool reduction, compared to the wild type. The results indicate that even though the mutation in JAC1 positively influences PSII maximum quantum efficiency ( $F_v/F_m$ ), it has negative impact on the conversion of the absorbed photon energy into photochemistry ( $qP$ ). Higher  $F_v/F_m$  in *jac1*, compared to the wild type, may be connected with the lack of chloroplast accumulation ability and thus the need of induced potential photosynthetic efficiency and suggests that the *jac1* mutant has elevated capacity of acclimation to variable light conditions, in relation to the wild type. Moreover, higher  $F_v/F_m$  in *jac1* *versus* wild type was in agreement with elevated level of total chlorophyll and up-regulation of genes encoding LHC subunits.

We also observed decreased values of NPQ in *jac1* mutant, compared to the wild type, which well corresponded with decreased xanthophyll pigments level. Xanthophyll pigments are involved in light energy dissipation during violaxanthin-antheraxanthin-zeaxanthin (VAZ) cycle (Demmig-Adams and Adams, 1992) and thus protect plants against photodamage (Havaux and Niyogi, 1999). Lower NPQ value and reduced content of xanthophyll pigments in *jac1*, in relation to the wild type, may be caused by the defects in *jac1* chloroplasts photorelocation. Because the *jac1* chloroplasts are constantly located close to the anticlinal cell walls, low light-acclimated mutant has less necessity in energy quenching. These results

indicate that JAC1-dependent chloroplast movement positively influences non-photochemical reaction rates and light energy dissipation.

Most importantly, we proved that apart from positively affecting photosynthetic electron transport, JAC1 negatively influences plant  $\text{CO}_2$  uptake. The *jac1* mutant demonstrated significantly elevated  $\text{CO}_2$  uptake rate, compared to the wild type, especially in higher light intensities. This observation was most probably caused by the chloroplasts inhibited mobility. It was shown that chloroplast surface area exposed to intercellular airspaces positively correlates with the  $\text{CO}_2$  conductance, and thus it was suggested that chloroplast movement control the  $\text{CO}_2$  uptake by modulating the  $\text{CO}_2$  diffusion path length from intercellular airspaces to the chloroplast stroma (Terashima et al., 2006). It was also proven that the chloroplast avoidance response decreases the internal conductance to  $\text{CO}_2$  diffusion in *Arabidopsis* leaves (Tholen et al., 2008). Taking into consideration that *jac1* mutant is to some extent disturbed in avoidance response (Kodama et al., 2010; Ichikawa et al., 2011), relatively higher chloroplast surface area should be adjacent to intercellular airspaces, in comparison to wild-type plants, especially in high light intensities. Therefore, the diffusion path length of  $\text{CO}_2$  to the chloroplast stroma may be lower in *jac1*, in relation to control plants, which can be one of the factors increasing the  $\text{CO}_2$  uptake rate in *jac1* mutant. Furthermore, higher variation of  $\text{CO}_2$  uptake and  $\text{GH}_2\text{O}$  parameters in a single measuring point in *jac1* mutant, compared to the wild type, suggests that the lack of functional JAC1 affects the ability of whole-leaf stomatal aperture stabilization, most likely due to changes in the guard cells functioning.

Increased  $\text{CO}_2$  uptake rate, correlated with JAC1 absence, was connected with almost three-times elevated water vapor conductance and two-times higher stomatal aperture. Performed transcriptomic profiling showed that many genes, expressed in stomata guard cells and involved in stomata movements, were all up-regulated in *jac1*, compared to wild-type counterparts. These were genes encoding proteins involved in calcium binding (Cominelli et al., 2005; Obulareddy et al., 2013) as well as chloride and water channel proteins (Obulareddy et al., 2013; Wang et al., 2016). Therefore, it indicates that JAC1 activity is genetically coupled with the negative regulation of stomatal conductance, and thus, affects water vapor conductance and  $\text{CO}_2$  uptake rate. We cannot exclude that JAC1 regulates the gene expression directly, because of its possible presence in the nucleus (Suetsugu et al., 2005). Higher stomatal aperture and water vapor conductance in *jac1* mutant were most probably the reason for higher transpiration and water loss. Therefore, JAC1 activity positively influenced water use efficiency (WUE). Despite these changes, we did not observe any statistically important changes in *jac1* mutant size or dry weight, as compared to the wild-type plants. Interestingly, elevated  $\text{CO}_2$  uptake in *jac1* mutant did not correlate with increased biomass production. Our observations are contrary to the study by Gotoh and co-workers (2018), where reduced photosynthesis,  $\text{CO}_2$  uptake, smaller rosette size and lesser biomass production were observed for *jac1* mutant.

However, this research was performed in moderate light conditions ( $120 \mu\text{mol photons m}^{-2} \text{ s}^{-1}$ ), while the experiments described in the current work were all performed for relatively low light conditions ( $80 \mu\text{mol photons m}^{-2} \text{ s}^{-1}$ ). This may indicate that, similarly to our previous studies on the regulators of EEE responses, such as LSD1 (Wituszyńska et al., 2013b; Wituszyńska et al., 2015), the role of JAC1 may be condition-dependent. Therefore, we postulate that JAC1 may participate in the condition-dependent optimization of the photon energy use in photosynthetic light phase reaction and the  $\text{CO}_2$  uptake.

We have shown before that UV-C treatment induces chloroplast retrograde signalling, causes photoinhibition, photooxidative stress and finally cell death (Rusaczonok et al., 2015; Wituszyńska et al., 2015). Since chloroplast movement is an important mechanism of EEE avoidance, we wanted to define the role of JAC1 protein in the activation of UV-C triggered cellular response. In a very recent study, it was shown that UV-B treatment did not trigger chloroplast rearrangements in the upper parts of palisade cells in the *jac1* mutant, which means that upon UV-B, the *jac1* chloroplasts were stuck and did not demonstrate avoidance response (Hermanowicz et al., 2019). Despite the greater exposure of chloroplasts to UV-C, we demonstrated that the *jac1* mutant had higher values of maximum and operational quantum efficiency of PSII, and the overall leaf photosynthetic capacity (Rfd), when compared to the wild-type counterparts, thus indicating that JAC1 activity negatively affects the PSII protection under UV-C stress. These results suggest that JAC1 influences acclimatory processes, leading to LHCs and PS photo-protection.

When assessing differences in  $\text{H}_2\text{O}_2$  levels and antioxidant enzyme activities in *jac1* mutant and wild type plants after UV-C exposure, *jac1* mutant showed higher level of  $\text{H}_2\text{O}_2$  12 h after treatment. In contrast, in later time points,  $\text{H}_2\text{O}_2$  levels were decreased, when compared to the wild type. The  $\text{H}_2\text{O}_2$  content 12 h after UV-C exposure corresponded well with the CAT activity, which was higher in *jac1*, when compared to the wild type, and thus processed  $\text{H}_2\text{O}_2$  more efficiently. In fact, transcriptomic profiling proved that the expression of CAT3 (AT1G20620), located in peroxisomes (Li et al., 2015), was up-regulated in *jac1* background after UV-C treatment. Additionally, in non-treated *jac1* we observed higher APX activity, which corresponded with higher expression of monodehydroascorbate reductase (ATMDAR), engaged in ascorbate recovery.

Moreover, UV-induced cell death was more pronounced in *jac1* mutant after 48 h, but not after 96 h post UV-C exposure, which suggests that JAC1 negatively influences the fine-tuning of cell death signalling and progression. The only work so far studying the impact of JAC1 on stress response showed that Arabidopsis line with significantly higher expression of JAC1 demonstrated lower level of aluminium-induced oxidative stress and higher resistance towards Al stress, than the wild-type plants (Ezaki et al., 2007). This study is convergent with our conclusion on the role of JAC1 in the increasing of resistance towards cell death. Interestingly, the expression level of JAC1 demonstrated dynamic pattern, as it was up-regulated 3 and 6 h after UV-C exposure and strongly down-regulated afterwards. It seems that

Arabidopsis wild-type plants tend to diminish JAC1 expression to reduce its negative impact on photosynthetic activity and lower the spread of cell death under oxidative stress. All these results indicate that JAC1 is most important at the early stages of photooxidative stress as it is engaged in the fine-tuning of the cellular redox homeostasis and cell death.

In the present work, we also identified genes that are transcriptionally affected by the absence of JAC1 activity. Interestingly, in *jac1* mutant, when compared to the wild type, we found deregulation of many genes encoding proteins engaged in calcium signalling, such as calmodulins (CaMs), CaM-like and CaM-binding proteins. It was previously shown that JAC1 binds calmodulin 1 (CaM1) and CaM-like CML10 (Popescu et al., 2007). Here, we prove that the regulation of CaMs is not only at the protein-protein interaction level, but also at the transcriptional stage. Importantly, two times more genes showed significant change in the expression level in UV-C treated *jac1*, compared to the UV-C treated wild type. It may be caused by altered chloroplast positioning in *jac1*, that due to impaired avoidance response capture more UV-C and hence provoke more plastid signals affecting nuclear gene expression. Although we have identified many genes that are influenced by the lack of JAC1 activity, the identification of JAC1-interacting proteins may further clarify the role of JAC1 in chloroplast movement, photosynthetic reactions, stomatal conductance, and stress responses.

In conclusion, we have identified a new role of JAC1 in the photosynthetic apparatus efficiency and plant stomatal conductance and thus  $\text{CO}_2$  uptake. Our results prove that the movements of stomata are genetically coupled with JAC1 activity. From a broader perspective, we demonstrate that chloroplast altered positioning, dependent on JAC1, influences plant photosynthetic performance,  $\text{H}_2\text{O}_2$  foliar levels, antioxidant enzymes activities, and cell death after UV-C photooxidative stress.

## DATA AVAILABILITY STATEMENT

The datasets presented in this study can be found in online repositories. The names of the repository/repositories and accession number(s) can be found in the article/Supplementary Material.

## AUTHOR CONTRIBUTIONS

WC, AR, and SK planned the experiments and postulated the hypotheses tested in this paper. WC measured hydrogen peroxide content and activities of antioxidant enzymes, prepared the RNA for NGS sequencing, performed the qPCRs, and analyzed functionally the RNAseq results. AR performed morphological analyses (measured plant size, dry weight, stomatal density), analyzed water use efficiency, chlorophyll *a* fluorescence, and ion leakage. PW did the annotation and statistical analysis of the RNAseq data. MS-R performed analysis of stomatal aperture and Evans Blue staining. WC wrote the manuscript and together with AR prepared the figures. SK and FB reviewed and approved its final version.

## ACKNOWLEDGMENTS

This work was supported by the Maestro 6 project (2014/14/A/NZ1/00218) granted to SK by the National Science Centre. PW is supported by the FWO grant 3G006916.

## REFERENCES

- Adamowski, M., Narasimhan, M., Kania, U., Glanc, M., De Jaeger, G., and Friml, J. (2018). A Functional Study of AUXILIN-LIKE1 and 2, Two Putative Clathrin Uncoating Factors in Arabidopsis. *Plant Cell* 30, 700–716. doi: 10.1105/tpc.17.00785
- Baker, N. R. (2008). Chlorophyll fluorescence: a probe of photosynthesis in vivo. *Annu. Rev. Plant Biol.* 59, 89–113. doi: 10.1146/annurev.arplant.59.032607.092759
- Benjamini, Y., and Hochberg, Y. (1995). Controlling the False Discovery Rate: A Practical and Powerful Approach to Multiple Testing. *J. R. Stat. Soc. Ser. B Methodol.* 57, 289–300. doi: 10.1111/j.2517-6161.1995.tb02031.x
- Cheng, C.-Y., Krishnakumar, V., Chan, A. P., Thibaud-Nissen, F., Schobel, S., and Town, C. D. (2017). Araport11: a complete reannotation of the Arabidopsis thaliana reference genome. *Plant J. Cell Mol. Biol.* 89, 789–804. doi: 10.1111/tjp.13415
- Cominelli, E., Galbiati, M., Vavasseur, A., Conti, L., Sala, T., Vuylsteke, M., et al. (2005). A Guard-Cell-Specific MYB Transcription Factor Regulates Stomatal Movements and Plant Drought Tolerance. *Curr. Biol.* 15, 1196–1200. doi: 10.1016/j.cub.2005.05.048
- Czarnocka, W., and Karpiński, S. (2018). Friend or foe? Reactive oxygen species production, scavenging and signaling in plant response to environmental stresses. *Free Radic. Biol. Med.* 122, 4–20. doi: 10.1016/j.freeradbiomed.2018.01.011
- Demarsy, E., Goldschmidt-Clermont, M., and Ulm, R. (2018). Coping with “Dark Sides of the Sun” through Photoreceptor Signaling. *Trends Plant Sci.* 23, 260–271. doi: 10.1016/j.tplants.2017.11.007
- Demmig-Adams, B., and Adams, W. W. (1992). Photoprotection and Other Responses of Plants to High Light Stress. *Annu. Rev. Plant Physiol. Plant Mol. Biol.* 43, 599–626. doi: 10.1146/annurev.pp.43.060192.003123
- Dobin, A., Davis, C. A., Schlesinger, F., Drenkow, J., Zaleski, C., Jha, S., et al. (2013). STAR: ultrafast universal RNA-seq aligner. *Bioinform. Oxf. Engl.* 29, 15–21. doi: 10.1093/bioinformatics/bts635
- Eisenberg, E., and Greene, L. E. (2007). Multiple roles of auxilin and hsc70 in clathrin-mediated endocytosis. *Traffic Cph. Den.* 8, 640–646. doi: 10.1111/j.1600-0854.2007.00568.x
- Ezaki, B., Kiyohara, H., Matsumoto, H., and Nakashima, S. (2007). Overexpression of an auxilin-like gene (F9E10.5) can suppress Al uptake in roots of Arabidopsis. *J. Exp. Bot.* 58, 497–506. doi: 10.1093/jxb/erl221
- Force, L., Critchley, C., and van Rensen, J. J. S. (2003). New fluorescence parameters for monitoring photosynthesis in plants. *Photosynth. Res.* 78, 17. doi: 10.1023/A:1026012116709
- Gabryś, H. (2004). Blue light-induced orientation movements of chloroplasts in higher plants: Recent progress in the study of their mechanisms. *Acta Physiol. Plant* 26, 473–479. doi: 10.1007/s11738-004-0038-3
- Gawroński, P., Witoń, D., Vashutina, K., Bederska, M., Betliński, B., Rusaczek, A., et al. (2014). Mitogen-activated protein kinase 4 is a salicylic acid-independent regulator of growth but not of photosynthesis in Arabidopsis. *Mol. Plant* 7, 1151–1166. doi: 10.1093/mp/ssu060
- Gilroy, S., Bialasek, M., Suzuki, N., Górecka, M., Devireddy, A. R., Karpiński, S., et al. (2016). ROS, Calcium, and Electric Signals: Key Mediators of Rapid Systemic Signaling in Plants1[OPEN]. *Plant Physiol.* 171, 1606–1615. doi: 10.1104/pp.16.00434
- Górecka, M., Lewandowska, M., Dąbrowska-Bronk, J., Bialasek, M., Barczak-Brzyżek, A., Kulasek, M., et al. (2020). Photosystem II 22kDa protein level - a prerequisite for excess light-inducible memory, cross-tolerance to UV-C and regulation of electrical signalling. *Plant Cell Environ.* 43, 649–661. doi: 10.1111/pce.13686
- Gotoh, E., Suetsugu, N., Yamori, W., Ishishita, K., Kiyabu, R., Fukuda, M., et al. (2018). Chloroplast Accumulation Response Enhances Leaf Photosynthesis and Plant Biomass Production. *Plant Physiol.* 178, 1358–1369. doi: 10.1104/pp.18.00484
- Havaux, M., and Niyogi, K. K. (1999). The violaxanthin cycle protects plants from photooxidative damage by more than one mechanism. *Proc. Natl. Acad. Sci.* 96, 8762–8767. doi: 10.1073/pnas.96.15.8762
- Hermanowicz, P., Banaś, A. K., Sztatelman, O., Gabryś, H., and Łabuz, J. (2019). UV-B Induces Chloroplast Movements in a Phototropin-Dependent Manner. *Front. Plant Sci.* 10:1279. doi: 10.3389/fpls.2019.01279
- Hruz, T., Laule, O., Szabo, G., Wessendorp, F., Bleuler, S., Oertle, L., et al. (2008). Genevestigator v3: a reference expression database for the meta-analysis of transcriptomes. *Adv. Bioinforma.* 2008:420747. doi: 10.1155/2008/420747
- Ichikawa, S., Yamada, N., Suetsugu, N., Wada, M., and Kadota, A. (2011). Red light, Phot1 and JAC1 modulate Phot2-dependent reorganization of chloroplast actin filaments and chloroplast avoidance movement. *Plant Cell Physiol.* 52, 1422–1432. doi: 10.1093/pcp/pcr087
- Jiang, J., Taylor, A. B., Prasad, K., Ishikawa-Brush, Y., Hart, P. J., Lafer, E. M., et al. (2003). Structure-function analysis of the auxilin J-domain reveals an extended Hsc70 interaction interface. *Biochemistry* 42, 5748–5753. doi: 10.1021/bi034270g
- Kadota, A., Yamada, N., Suetsugu, N., Hirose, M., Saito, C., Shoda, K., et al. (2009). Short actin-based mechanism for light-directed chloroplast movement in Arabidopsis. *Proc. Natl. Acad. Sci. U. S. A.* 106, 13106–13111. doi: 10.1073/pnas.0906250106
- Kagawa, T., Sakai, T., Suetsugu, N., Oikawa, K., Ishiguro, S., Kato, T., et al. (2001). Arabidopsis NPL1: a phototropin homolog controlling the chloroplast high-light avoidance response. *Science* 291, 2138–2141. doi: 10.1126/science.291.5511.2138
- Karpiński, S., Szechyńska-Hebda, M., Wituszyńska, W., and Burdiak, P. (2013). Light acclimation, retrograde signalling, cell death and immune defences in plants. *Plant Cell Environ.* 36, 736–744. doi: 10.1111/pce.12018
- Kodama, Y., Suetsugu, N., Kong, S.-G., and Wada, M. (2010). Two interacting coiled-coil proteins, WEB1 and PM12, maintain the chloroplast photorelocation movement velocity in Arabidopsis. *Proc. Natl. Acad. Sci. U. S. A.* 107, 19591–19596. doi: 10.1073/pnas.1007836107
- Krishnakumar, V., Hanlon, M. R., Contrino, S., Ferlanti, E. S., Karamycheva, S., Kim, M., et al. (2015). Araport: the Arabidopsis Information Portal. *Nucleic Acids Res.* 43, D1003–D1009. doi: 10.1093/nar/gku1200
- Li, J., Liu, J., Wang, G., Cha, J.-Y., Li, G., Chen, S., et al. (2015). A chaperone function of NO CATALASE ACTIVITY1 is required to maintain catalase activity and for multiple stress responses in Arabidopsis. *Plant Cell* 27, 908–925. doi: 10.1105/tpc.114.135095
- Liao, Y., Smyth, G. K., and Shi, W. (2014). featureCounts: an efficient general purpose program for assigning sequence reads to genomic features. *Bioinform. Oxf. Engl.* 30, 923–930. doi: 10.1093/bioinformatics/btt656
- McCarthy, D. J., Chen, Y., and Smyth, G. K. (2012). Differential expression analysis of multifactor RNA-Seq experiments with respect to biological variation. *Nucleic Acids Res.* 40, 4288–4297. doi: 10.1093/nar/gks042
- Mergemann, H., and Sauter, M. (2000). Ethylene induces epidermal cell death at the site of adventitious root emergence in rice. *Plant Physiol.* 124, 609–614. doi: 10.1104/pp.124.2.609
- Mühlenbock, P., Szechyńska-Hebda, M., Plaszczyca, M., Baudo, M., Mateo, A., Mullineaux, P. M., et al. (2008). Chloroplast signaling and LESION SIMULATING DISEASE1 regulate crosstalk between light acclimation and immunity in Arabidopsis. *Plant Cell* 20, 2339–2356. doi: 10.1105/tpc.108.059618
- Obularedy, N., Panchal, S., and Melotto, M. (2013). Guard Cell Purification and RNA Isolation Suitable for High-Throughput Transcriptional Analysis of Cell-Type Responses to Biotic Stresses. *Mol. Plant-Microbe Interact.* 26, 844–849. doi: 10.1094/MPMI-03-13-0081-TA
- Pfaffl, M. W., Horgan, G. W., and Dempfle, L. (2002). Relative expression software tool (REST) for group-wise comparison and statistical analysis of relative expression results in real-time PCR. *Nucleic Acids Res.* 30, e36. doi: 10.1093/nar/30.9.e36

## SUPPLEMENTARY MATERIAL

The Supplementary Material for this article can be found online at: <https://www.frontiersin.org/articles/10.3389/fpls.2020.01124/full#supplementary-material>



- Popescu, S. C., Popescu, G. V., Bachan, S., Zhang, Z., Seay, M., Gerstein, M., et al. (2007). Differential binding of calmodulin-related proteins to their targets revealed through high-density Arabidopsis protein microarrays. *Proc. Natl. Acad. Sci.* 104, 4730–4735. doi: 10.1073/pnas.0611615104
- Ramakers, C., Ruijter, J. M., Deprez, R. H. L., and Moorman, A. F. M. (2003). Assumption-free analysis of quantitative real-time polymerase chain reaction (PCR) data. *Neurosci. Lett.* 339, 62–66. doi: 10.1016/s0304-3940(02)01423-4
- Robinson, M. D., and Oshlack, A. (2010). A scaling normalization method for differential expression analysis of RNA-seq data. *Genome Biol.* 11, R25. doi: 10.1186/gb-2010-11-3-r25
- Robinson, M. D., McCarthy, D. J., and Smyth, G. K. (2010). edgeR: a Bioconductor package for differential expression analysis of digital gene expression data. *Bioinform. Oxf. Engl.* 26, 139–140. doi: 10.1093/bioinformatics/btp616
- Rusaczonok, A., Czarnocka, W., Kacprzak, S., Witoń, D., Ślesak, I., Szechyńska-Hebda, M., et al. (2015). Role of phytochromes A and B in the regulation of cell death and acclimatory responses to UV stress in Arabidopsis thaliana. *J. Exp. Bot.* 66, 6679–6695. doi: 10.1093/jxb/erv375
- Sakai, T., Kagawa, T., Kasahara, M., Swartz, T. E., Christie, J. M., Briggs, W. R., et al. (2001). Arabidopsis nph1 and npl1: blue light receptors that mediate both phototropism and chloroplast relocation. *Proc. Natl. Acad. Sci. U. S. A.* 98, 6969–6974. doi: 10.1073/pnas.101137598
- Selvaraj, M. G., Ishizaki, T., Valencia, M., Ogawa, S., Dedicova, B., Ogata, T., et al. (2017). Overexpression of an Arabidopsis thaliana galactinol synthase gene improves drought tolerance in transgenic rice and increased grain yield in the field. *Plant Biotechnol. J.* 15, 1465–1477. doi: 10.1111/pbi.12731
- Song, C., Chung, W. S., and Lim, C. O. (2016). Overexpression of Heat Shock Factor Gene HsfA3 Increases Galactinol Levels and Oxidative Stress Tolerance in Arabidopsis. *Mol. Cells* 39, 477–483. doi: 10.14348/molcells.2016.0027
- Strasser, R. J., Tsimilli-Michael, M., and Srivastava, A. (2004). “Analysis of the Chlorophyll a Fluorescence Transient,” in *Chlorophyll a Fluorescence: A Signature of Photosynthesis Advances in Photosynthesis and Respiration*. Eds. G. C. Papageorgiou and Govindjee, (Dordrecht: Springer Netherlands), 321–362. doi: 10.1007/978-1-4020-3218-9\_12
- Suetsugu, N., Kagawa, T., and Wada, M. (2005). An auxilin-like J-domain protein, JAC1, regulates phototropin-mediated chloroplast movement in Arabidopsis. *Plant Physiol.* 139, 151–162. doi: 10.1104/pp.105.067371
- Suetsugu, N., Dolja, V. V., and Wada, M. (2010a). Why have chloroplasts developed a unique motility system? *Plant Signal. Behav.* 5, 1190–1196. doi: 10.4161/psb.5.10.12802
- Suetsugu, N., Takano, A., Kohda, D., and Wada, M. (2010b). Structure and activity of JAC1 J-domain implicate the involvement of the cochaperone activity with HSC70 in chloroplast photorelocation movement. *Plant Signal. Behav.* 5, 1602–1606. doi: 10.4161/psb.5.12.13915
- Suetsugu, N., Higa, T., Kong, S.-G., and Wada, M. (2015). Plastid Movement Impaired1 and Plastid Movement Impaired1-Related1 Mediate Photorelocation Movements of Both Chloroplasts and Nuclei. *Plant Physiol.* 169, 1155–1167. doi: 10.1104/pp.15.00214
- Sun, Z., Qi, X., Wang, Z., Li, P., Wu, C., Zhang, H., et al. (2013). Overexpression of TsGOLS2, a galactinol synthase, in Arabidopsis thaliana enhances tolerance to high salinity and osmotic stresses. *Plant Physiol. Biochem.* 69, 82–89. doi: 10.1016/j.plaphy.2013.04.009
- Sztatelman, O., Łabuz, J., Hermanowicz, P., Banaś, A. K., Bażant, A., Zgłobicki, P., et al. (2016). Fine tuning chloroplast movements through physical interactions between phototropins. *J. Exp. Bot.* 67, 4963–4978. doi: 10.1093/jxb/erw265
- Takano, A., Suetsugu, N., Wada, M., and Kohda, D. (2010). Crystallographic and functional analyses of J-domain of JAC1 essential for chloroplast photorelocation movement in Arabidopsis thaliana. *Plant Cell Physiol.* 51, 1372–1376. doi: 10.1093/pcp/pcq089
- Terashima, I., Hanba, Y. T., Tazoe, Y., Vyas, P., and Yano, S. (2006). Irradiance and phenotype: comparative eco-development of sun and shade leaves in relation to photosynthetic CO<sub>2</sub> diffusion. *J. Exp. Bot.* 57, 343–354. doi: 10.1093/jxb/erj014
- Thimm, O., Bläsing, O., Gibon, Y., Nagel, A., Meyer, S., Krüger, P., et al. (2004). MAPMAN: a user-driven tool to display genomics data sets onto diagrams of metabolic pathways and other biological processes. *Plant J. Cell Mol. Biol.* 37, 914–939. doi: 10.1111/j.1365-3113.2004.02016.x
- Tholen, D., Boom, C., Noguchi, K., Ueda, S., Katase, T., and Terashima, I. (2008). The chloroplast avoidance response decreases internal conductance to CO<sub>2</sub> diffusion in Arabidopsis thaliana leaves. *Plant Cell Environ.* 31, 1688–1700. doi: 10.1111/j.1365-3040.2008.01875.x
- Wada, M., and Kong, S.-G. (2018). Actin-mediated movement of chloroplasts. *J. Cell Sci.* 131, 1–8. doi: 10.1242/jcs.210310
- Wang, C., Hu, H., Qin, X., Zeise, B., Xu, D., Rappel, W.-J., et al. (2016). Reconstitution of CO<sub>2</sub> Regulation of SLAC1 Anion Channel and Function of CO<sub>2</sub>-Permeable PIP2<sub>1</sub> Aquaporin as CARBONIC ANHYDRASE4 Interactor. *Plant Cell* 28, 568–582. doi: 10.1105/tpc.15.00637
- Wituszyńska, W., and Karpiński, S. (2013). Programmed Cell Death as a Response to High Light, UV and Drought Stress in Plants. *Abiotic Stress - Plant Responses Appl. Agric.* 207–246. doi: 10.5772/53127
- Wituszyńska, W., and Karpiński, S. (2014). Determination of Water Use Efficiency for Arabidopsis thaliana. *BIO-Protoc.* 4 (3), e1041. doi: 10.21769/BioProtoc.1041
- Wituszyńska, W., Gałązka, K., Rusaczonok, A., Vanderauwera, S., Van Breusegem, F., and Karpiński, S. (2013a). Multivariable environmental conditions promote photosynthetic adaptation potential in Arabidopsis thaliana. *J. Plant Physiol.* 170, 548–559. doi: 10.1016/j.jplph.2012.11.016
- Wituszyńska, W., Ślesak, I., Vanderauwera, S., Szechyńska-Hebda, M., Kornaś, A., Kelen, K. V. D., et al. (2013b). Lesion Simulating Disease1, Enhanced Disease Susceptibility1, And Phytoalexin Deficient4 Conditionally Regulate Cellular Signaling Homeostasis, Photosynthesis, Water Use Efficiency, and Seed Yield in Arabidopsis. *Plant Physiol.* 161, 1795–1805. doi: 10.1104/pp.112.208116
- Wituszyńska, W., Szechyńska-Hebda, M., Sobczak, M., Rusaczonok, A., Kozłowska-Makulska, A., Witoń, D., et al. (2015). Lesion simulating disease 1 and enhanced disease susceptibility 1 differentially regulate UV-C-induced photooxidative stress signalling and programmed cell death in Arabidopsis thaliana. *Plant Cell Environ.* 38, 315–330. doi: 10.1111/pce.12288
- Wonnacott, T. H., and Wonnacott, R. J. (1990). *Introductory statistics for business and economics* (United States: Wiley), 1990.

**Conflict of Interest:** The authors declare that the research was conducted in the absence of any commercial or financial relationships that could be construed as a potential conflict of interest.

Copyright © 2020 Czarnocka, Rusaczonok, Willems, Sujkowska-Rybkowska, Van Breusegem and Karpiński. This is an open-access article distributed under the terms of the Creative Commons Attribution License (CC BY). The use, distribution or reproduction in other forums is permitted, provided the original author(s) and the copyright owner(s) are credited and that the original publication in this journal is cited, in accordance with accepted academic practice. No use, distribution or reproduction is permitted which does not comply with these terms.





# Improving Air Quality by Nitric Oxide Consumption of Climate-Resilient Trees Suitable for Urban Greening

Jiangli Zhang<sup>1,2</sup>, Andrea Ghirardo<sup>3</sup>, Antonella Gori<sup>4,5</sup>, Andreas Albert<sup>3</sup>, Franz Buegger<sup>1</sup>, Rocco Pace<sup>6,7</sup>, Elisabeth Georgii<sup>1</sup>, Rüdiger Grote<sup>6</sup>, Jörg-Peter Schnitzler<sup>3</sup>, Jörg Durner<sup>1,8</sup> and Christian Lindermayr<sup>1\*</sup>

<sup>1</sup> Institute of Biochemical Plant Pathology, Helmholtz Zentrum München, Neuherberg/Munich, Germany, <sup>2</sup> College of Life Sciences, Henan Normal University, Xinxiang, China, <sup>3</sup> Research Unit Environmental Simulation, Institute of Biochemical Plant Pathology, Helmholtz Zentrum München, Neuherberg/Munich, Germany, <sup>4</sup> Department of Agriculture, Food, Environment, and Forestry (DAGRI), University of Florence, Florence, Italy, <sup>5</sup> Department of Biology, Agriculture and Food Sciences, Institute for Sustainable Plant Protection, The National Research Council of Italy (CNR), Florence, Italy, <sup>6</sup> Institute of Meteorology and Climate Research — Institute of Atmospheric Environmental Research, Karlsruhe Institute of Technology, Garmisch-Partenkirchen, Germany, <sup>7</sup> Institute of Research on Terrestrial Ecosystems (IRET), National Research Council (CNR), Porano, Italy, <sup>8</sup> Chair of Biochemical Plant Pathology, Technische Universität München, Freising, Germany

## OPEN ACCESS

### Edited by:

Christiane Werner,  
University of Freiburg, Germany

### Reviewed by:

Lina Fusaro,  
Italian National Research Council, Italy  
Astrid Moser-Reischl,  
Technical University of Munich,  
Germany

### \*Correspondence:

Christian Lindermayr  
lindermayr@helmholtz-muenchen.de

### Specialty section:

This article was submitted to  
Plant Physiology,  
a section of the journal  
Frontiers in Plant Science

**Received:** 07 April 2020

**Accepted:** 10 September 2020

**Published:** 29 September 2020

### Citation:

Zhang J, Ghirardo A, Gori A, Albert A, Buegger F, Pace R, Georgii E, Grote R, Schnitzler J-P, Durner J and Lindermayr C (2020) Improving Air Quality by Nitric Oxide Consumption of Climate-Resilient Trees Suitable for Urban Greening. *Front. Plant Sci.* 11:549913. doi: 10.3389/fpls.2020.549913

Nitrogen oxides (NO<sub>x</sub>), mainly a mixture of nitric oxide (NO) and nitrogen dioxide (NO<sub>2</sub>), are formed by the reaction of nitrogen and oxygen compounds in the air as a result of combustion processes and traffic. Both deposit into leaves via stomata, which on the one hand benefits air quality and on the other hand provides an additional source of nitrogen for plants. In this study, we first determined the NO and NO<sub>2</sub> specific deposition velocities based on projected leaf area (sV<sub>d</sub>) using a branch enclosure system. We studied four tree species that are regarded as suitable to be planted under predicted future urban climate conditions: *Carpinus betulus*, *Fraxinus ornus*, *Fraxinus pennsylvanica* and *Ostrya carpinifolia*. The NO and NO<sub>2</sub> sV<sub>d</sub> were found similar in all tree species. Second, in order to confirm NO metabolization, we fumigated plants with <sup>15</sup>NO and quantified the incorporation of <sup>15</sup>N in leaf materials of these trees and four additional urban tree species (*Celtis australis*, *Alnus spaethii*, *Alnus glutinosa*, and *Tilia henryana*) under controlled environmental conditions. Based on these <sup>15</sup>N-labeling experiments, *A. glutinosa* showed the most effective incorporation of <sup>15</sup>NO. Third, we tried to elucidate the mechanism of metabolization. Therefore, we generated transgenic poplars overexpressing *Arabidopsis thaliana* phytoalbumin 1 or 2. Phytoalbumins are known to metabolize NO to nitrate in the presence of oxygen. The <sup>15</sup>N uptake in phytoalbumin-overexpressing poplars was significantly increased compared to wild-type trees, demonstrating that the NO uptake is enzymatically controlled besides stomatal dependence. In order to upscale the results and to investigate if a trade-off exists between air pollution removal and survival probability under future climate conditions, we have additionally carried out a modeling exercise of NO and NO<sub>2</sub> deposition for the area of central Berlin. If the actually dominant deciduous tree species (*Acer platanoides*, *Tilia cordata*, *Fagus sylvatica*, *Quercus robur*) would be replaced by the species suggested for future conditions, the total annual NO and NO<sub>2</sub>

deposition in the modeled urban area would hardly change, indicating that the service of air pollution removal would not be degraded. These results may help selecting urban tree species in future greening programs.

**Keywords:** nitric oxide, nitrogen dioxide,  $^{15}\text{N}$ , phytohemoglobin, air pollution mitigation, urban trees

## INTRODUCTION

Urban air is posing a risk to health in most parts of the world, with emissions from industrial processes, residential heating, and heavy traffic based on fossil fuels being the principal causes. This results in high levels of particles, nitrogen oxides ( $\text{NO}_x$ ), and other dangerous compounds.

Particularly  $\text{NO}_x$ , which is formed by the reaction of nitrogen and oxygen compounds as a result of combustion processes, is a pollutant of great concern since it is directly related to cardiovascular diseases and respiratory malfunctions (Mannucci et al., 2015) as well as being a precursor for ozone formation (Sillman, 1999). Additionally, they have also been found to increase the allergenicity of pollen (Zhao et al., 2016). In areas with heavy vehicle traffic, such as in large cities and conurbations, the amount of  $\text{NO}_x$  emitted as an air pollutant into the lower troposphere is significant, and the resulting concentrations often exceed national regulation. For instance, in 2017, around 10% of all the air quality monitoring stations in Europe recorded average annual concentrations above the annual limit value of  $40 \mu\text{g m}^{-3}$  (EEA, 2019). Plants can play an important role in mitigating the  $\text{NO}_x$  related damages on health and environment because their large surface represents efficient “sinks” for air pollutants (Hill, 1971). In cities, the air phytoremediation abilities combined with other ecosystem services of trees (e.g., mitigate air temperature extremes) give urban greening the potential to improve human health while mitigating the effects of climate change (Salmond et al., 2016; Kabisch and van den Bosch, 2017). Plants remove gaseous air pollutants such as  $\text{NO}_x$  and ozone mainly by uptake through the stomata of leaves, although some gaseous compounds may also be deposited on the plant surface (Elkiey et al., 1982; Jud et al., 2016). The ability to absorb  $\text{NO}_2$  has been reported for a variety of plant species, including many tree species, such as loblolly pine (*Pinus taeda*), white oak (*Quercus alba*), silver birch (*Betula pendula*), European beech (*Fagus sylvatica*), pedunculate oak (*Quercus robur*), holm oak (*Quercus ilex*), California oak (*Quercus agrifolia*), Scots pine (*Pinus sylvestris*), and Norway spruce (*Picea abies*) (Rogers et al., 1979; Geßler et al., 2002; Eller and Sparks, 2006; Chaparro-Suarez et al., 2011; Breuning et al., 2013; Delaria et al., 2018).  $\text{NO}_2$  deposition is influenced by stomata aperture, nitrogen status, leaf development and -age, photosynthetic rate, and the position of leaves within the plant canopy (Morikawa et al., 1998; Sparks et al., 2001; Takahashi et al., 2005; Hu and Sun, 2010). Thus, a clear difference between tree species and dependence on vitality can be expected. In contrast to  $\text{NO}_2$  deposition, studies on NO uptake by plants are scarce in the literature. Nevertheless, measurements of atmospheric NO levels in the presence of horticultural crops, including lettuce, strawberry, apple, and

banana, showed a significant decrease in atmospheric NO concentrations, indicating the ability of these plants to absorb NO (Hanson and Lindberg, 1991; Soegiarto et al., 2003).

If  $\text{NO}_x$  is taken up through the stomata, it needs to be further processed or deposited into the plant structure. In fact, evidence exists that various enzymes have the ability to metabolize  $\text{NO}_x$ . For example, phytohemoglobins (PGBs) are proteins regarded as important for the nitrogen metabolisms and are ubiquitously distributed in plants (Becana et al., 2020). These proteins play a major role in regulating many biological processes, such as normal growth and development, hypoxic stress, symbiotic nodulation and nitrogen fixation, and are activated in response to low mineral nutrient status and abiotic stress (Hebelstrup et al., 2006; Mira et al., 2016; Mira et al., 2017; Shankar et al., 2018; Becana et al., 2020; Berger et al., 2020). Particularly, PGBs can oxidize NO to nitrate during hypoxic stress, which is called the PGB/NO cycle (Igamberdiev and Hill, 2004; Igamberdiev et al., 2006; Becana et al., 2020). In previous publications on *Arabidopsis* and barley, we reported on the ability of PGBs (Kuruthukulangarakoola et al., 2017; Zhang et al., 2019) to fix atmospheric NO and incorporate N into the nitrogen metabolism of the plants. Atmospheric nitrogen supply has been formerly regarded as gaseous nitrogen fixation or ammonia uptake only in connection with microbial or fungal associations (Granhall and Lindberg, 1980; Papen et al., 2002). This new NO fixation process seems to be a new pathway in this cycle, which can potentially play an important role within the whole nitrogen cycle, which is essential for building up proteins, nucleic acids, chlorophyll and many other organic compounds. Although the ability for  $\text{NO}_x$  uptake may be ubiquitous in plants, the actual uptake capacity of different species is likely to vary (Takahashi et al., 2005).

In the near future, tree species composition in urban areas is likely to change towards climate-change resilient species, which can cope with increases in intensity, frequency, and severity of abiotic stresses (Burley et al., 2019). In particular, drought and heat resistance are primary selection criteria for urban greening programs (e.g., Roloff et al., 2009). Therefore, stress-tolerant species such as *C. betulus*, *F. ornus*, *F. pennsylvanica*, *O. carpinifolia*, *C. australis*, *Ahnus x spaethii*, *A. glutinosa*, and *T. henryana* are currently being proposed (e.g., Böll, 2017; Dickhaut and Eschenbach, 2019). However, it is known that different tree species have different pollution removal capacities that are related to various leaf traits that influence deposition velocity and to their stomatal behavior in response to drought (Grote et al., 2016). The ability to process  $\text{NO}_x$  may thus be a further trait that influences the uptake of gaseous nitrogen compounds. Particularly trees that are considered suitable under future environmental conditions and which, therefore, might have a reduced stomatal conductance adapted to high temperatures and low water supply, could be

assumed to have less NO<sub>x</sub> removal capacity. Therefore, tree species that are selected to withstand increasing heat and drought stress in urban areas need to be checked for their ability to provide the same degree of ecosystem services, i.e. air pollution removal.

To provide a quantitative estimate of pollution removal of current and potential future tree species, we determined the deposition rates of NO and NO<sub>2</sub> in tree species that are regarded as suitable candidates for urban trees under future climatic conditions in Central Europe (Böll, 2017; Böll, 2018a; Böll, 2018b). Moreover, we used gas exchange measurements and followed the capacity of NO uptake and metabolization in eight different tree species fumigated with <sup>15</sup>NO under controlled environmental conditions. Additionally, we demonstrated that the NO uptake could be enhanced in trees by introducing the *Arabidopsis* phytohemoglobin 1 and 2 (*AtPGB1*, *AtPGB2*) genes into poplars. Finally, using the newly determined deposition rates, we compared the potential NO<sub>x</sub> removal for a scenario that assumes a high abundance of tree species proposed for adaptation to climate change conditions with the removal capacities of the current urban tree distribution. This should indicate potential changes in NO<sub>x</sub> removal due to the selection of these species in future urban planning under “real world conditions”. For this exercise, we use state-of-the-art calculation processes, parameters from literature for the current tree species, and the boundary conditions for a Metropolitan area, Central Berlin.

## MATERIALS AND METHODS

### Plants Material

All plant species with altered PGB expression used in this study are listed in **Table 1**. *Arabidopsis thaliana* (Columbia-0) with

overexpressing class 1 PGB (*AtPgb1+*) or class 2 PGB (*AtPgb2+*), as well as plants with reduced (*AtPgb1-*) or knocked out (*AtPgb2-*) Pgb expression were obtained in Aarhus University as described in Hebelstrup et al. (2006). Transgenic hybrid poplars [*Populus x canescens*, syn. *P. tremula* x *P. alba*, number 7171-B4, Institute de la Recherche Agronomique (INRA), Nancy, France] were generated following the protocol of Bi et al. (2015). PcPgb1+ and PcPgb2+ lines are grey poplars with overexpressing *Arabidopsis* class 1 PGB gene (*AtPgb1*) and *Arabidopsis* class 2 PGB gene (*AtPgb2*). The different tree species *Carpinus betulus* ‘Frans Fontaine’, *Fraxinus ornus* ‘Loisa Lady’, *Fraxinus pennsylvanica* ‘Summit’, *Ostrya carpinifolia*, *Celtis australis* L., *Alnus x spaethii* (syn. *A. japonica* x *A. subcordata*), *Alnus glutinosa* ‘Imperialis’, and *Tilia henryana* were obtained from Wilhelm Ley Baumschule (Meckenheim, Germany) and plants were 2–4 years old. These climate-resilient tree species are tested for their suitability for future urban greening in Germany ([http://www.lwg.bayern.de/landespflege/urbanes\\_gruen/085113/index.php](http://www.lwg.bayern.de/landespflege/urbanes_gruen/085113/index.php); Böll, 2018a; Böll, 2018b).

### Experimental Setup and Determination of NO/NO<sub>2</sub> Specific Leaf Deposition Velocities

All experiments were performed in the phytotron chambers of Helmholtz Center in Munich, under highly controlled conditions (for a detailed description of the chambers, see Ghirardo et al., 2020). In brief, the phytotron is composed of unique climate chambers for exposure experiments of reactive gasses (Kozovits et al., 2005), and analyses of gas-exchange of CO<sub>2</sub>, H<sub>2</sub>O (Vanzo et al., 2015) under a realistic simulation of the solar radiation spectra of UV-Vis-NIR (Seckmeyer and Payer, 1993; Döhring et al., 1996; Thiel et al., 1996).

**TABLE 1** | Tree species and plants with altered PGB expression used for the different experiments in the study.

Abbreviation	Plant species	Characteristics	Number of used individual/samples
<b>At</b>	<i>A. thaliana</i> (Col-0)	Wild-type	4 ( <sup>15</sup> NO uptake)
<b>AtPgb1+</b>	<i>A. thaliana</i> (Col-0)	Overexpressing <i>Arabidopsis</i> <i>PGB1</i>	4 ( <sup>15</sup> NO uptake)
<b>AtPgb2+</b>	<i>A. thaliana</i> (Col-0)	Overexpressing <i>Arabidopsis</i> <i>PGB2</i>	4 ( <sup>15</sup> NO uptake)
<b>AtPgb1-</b>	<i>A. thaliana</i> (Col-0)	Knock-down of <i>PGB1</i> (RNAi)	4 ( <sup>15</sup> NO uptake)
<b>AtPgb2-</b>	<i>A. thaliana</i> (Col-0)	Knock-out of <i>PGB2</i>	4 ( <sup>15</sup> NO uptake)
<b>Pc</b>	<i>Populus x canescens</i>	Wild-type	4 old, 3 young ( <sup>15</sup> NO uptake)
<b>PcPgbOx1</b>	<i>Populus x canescens</i>	Overexpressing <i>Arabidopsis</i> <i>PGB1</i>	4 old, 3 young ( <sup>15</sup> NO uptake)
<b>PcPgbOx2</b>	<i>Populus x canescens</i>	Overexpressing <i>Arabidopsis</i> <i>PGB2</i>	4 old, 3 young ( <sup>15</sup> NO uptake)
<b>T1</b>	<i>Carpinus betulus</i> ‘Frans Fontane’		3 (C and N content, <sup>15</sup> NO uptake)
<b>T2</b>	<i>Fraxinus ornus</i> ‘Loisa Lady’		4 NO and NO <sub>2</sub> deposition) 3 (C and N content, <sup>15</sup> NO uptake)
<b>T3</b>	<i>Fraxinus pennsylvanica</i> ‘Summit’		4 NO and NO <sub>2</sub> deposition) 3 (C and N content, <sup>15</sup> NO uptake)
<b>T4</b>	<i>Ostrya carpinifolia</i>		4 NO and NO <sub>2</sub> deposition) 3 (C and N content, <sup>15</sup> NO uptake)
<b>T5</b>	<i>Alnus glutinosa</i> ‘Imperialis’		4 NO and NO <sub>2</sub> deposition) 4 (C and N content, <sup>15</sup> NO uptake)
<b>T6</b>	<i>Tilia henryana</i>		4 (C and N content, <sup>15</sup> NO uptake)
<b>T7</b>	<i>Alnus x spaethii</i>		4 (C and N content, <sup>15</sup> NO uptake)
<b>T8</b>	<i>Celtis australis</i> L.		4 (C and N content, <sup>15</sup> NO uptake)

To determinate the ability of plants to emit or remove NO/NO<sub>2</sub> from the atmosphere, we performed NO and NO<sub>2</sub> fumigation experiments on four different tree species (*C. betulus*, *F. ornus*, *F. pennsylvanica*, and *O. carpinifolia*) under steady-state conditions by using a dynamic branch enclosure system. Experiments were repeated using different trees to obtain four replicates ( $n = 4$ ). Plants were moved inside the climate chambers two days before starting the fumigation experiment, and one tree branch containing 5–8 mature leaves was enclosed the day before the NO/NO<sub>2</sub> experiment. The cuvette system consisted of eight odorless polyethylene terephthalate (PET) bags (size: 60x31cm) without plasticizer (Toppits Cofresco, Minden, Germany). All the line tubes (1/4"), fittings, and T-pieces were made of the inert material polytetrafluoroethylene (PTFE). The inlet air tube was placed on the side of the stem and tightened together. Each of the eight cuvettes was continuously flushed with 1,000 ml min<sup>-1</sup> of humidified (60% RH) NO<sub>x</sub>-free air (Ghirardo et al., 2020) containing ambient CO<sub>2</sub> concentrations (~ 400 ppm).

The environmental conditions of the enclosed branches were: leaf temperatures of 25/12°C and relative humidity (RH) of 60/80% (light/dark); light intensities of maximum incident photosynthetically active quantum flux density (PPFD) levels of 300 μmol m<sup>-2</sup> s<sup>-1</sup> and a photoperiod of 14 h. Experiments started four hours after switching on the light to ensure steady-state photosynthetic conditions (Ghirardo et al., 2010; Ghirardo et al., 2014). Overall, measurements followed the experimental procedures described elsewhere (Wildt et al., 1997; Chaparro-Suarez et al., 2011), although specific leaf deposition velocities of NO/NO<sub>2</sub> were determinate on tree branches. Branches of healthy trees were exposed to six different mixing ratios of NO and NO<sub>2</sub> of 0, 2.5, 12.5, 25, 45, 90 ppb. Clean air enriched in NO/NO<sub>2</sub> was produced by dilution steps using mass flow controllers (MKS, Andover, USA), starting from a gas cylinder containing 2% NO in N<sub>2</sub> (Air Liquide, Düsseldorf, Germany), and converting 50% NO to NO<sub>2</sub> using pure O<sub>2</sub> and reaction chambers as previously described (Mayer et al., 2018).

NO and NO<sub>2</sub> concentrations at the inlet and outlet of the cuvettes were measured online throughout all experiments by chemiluminescence technique and using an ultra-high precision and sensitive NO/NO<sub>2</sub> analyzer (limit of detection <0.025 ppb; model nCLD 899Y SupremeLine, Eco Physics AG, Duernten, Switzerland). Calibration of the instrument was achieved by using N<sub>2</sub> (purity 5.0) for the zero measurements and certified NO standards at 850 ppb (Air Liquide) for the span calibration.

The cuvettes were run in parallel, and NO/NO<sub>2</sub> were measured sequentially by switching automatically every 9 min using an automatic multiport valve in a similar manner as described before (Ghirardo et al., 2010; Ghirardo et al., 2020). The first 8 min of measurements were used as flushing time, and the corresponding acquisition data were disregarded from the data analysis to remove any interference from the previous cuvette measurement. The last 1 min containing six measurement points (10 s integration time) were averaged and used for calculation of gas-exchange based on projected leaf area (m<sup>2</sup>) as previously described (Ghirardo et al., 2011). As the

reference of the fumigation levels, the inlet air was measured every four cuvettes. Therefore, the entire measurement cycle through all eight cuvettes and two references took 1 h and 30 min, before switching to the next concentration and waiting another 30 min for reaching the equilibrium of NO/NO<sub>2</sub> concentrations.

Fluxes ( $F$ ) of NO (FNO) and NO<sub>2</sub> (FNO<sub>2</sub>) (nmol m<sup>-2</sup> s<sup>-1</sup>) were calculated following Chaparro-Suarez et al. (2011) as:

$$F = ([C_{out}] - [C_{in}]) \times Q/A \quad \text{eq. (1)}$$

based on the concentration differences between the outlet ports of the branch cuvette and the inlet air reference ( $[C_{out}]$  and  $[C_{in}]$ , respectively, in nmol mol<sup>-1</sup>), the enclosed project leaf area ( $A$ , in m<sup>2</sup>), and the airflow rate through the cuvettes ( $Q$ , in mol s<sup>-1</sup>). The linear relationship was calculated between FNO/FNO<sub>2</sub> and the fumigated NO/NO<sub>2</sub> concentration:

$$y = kx + b \quad \text{eq. (2)}$$

(where  $x$  represents the fumigated NO/NO<sub>2</sub> concentration;  $y$ , the net exchange rates of NO (FNO) or NO<sub>2</sub> (FNO<sub>2</sub>),  $b$ , the leaf emission rate of NO/NO<sub>2</sub> (in nmol m<sup>-2</sup> s<sup>-1</sup>). The deposition potential (in nmol m<sup>-2</sup> s<sup>-1</sup> ppb<sup>-1</sup>) is the slope ( $k$ ) value of eq. 2, and the compensation point is determined as the  $x$  value when  $y$  equals zero (i.e., the NO/NO<sub>2</sub> air concentrations when leaf emission equals uptake and therefore net exchange rate is zero). Deposition potentials were converted to absolute values of specific deposition velocities ( $sV_d$ , in m s<sup>-1</sup>) using the ideal gas equation for conditions of 1 atm and 20°C. Background measurements were conducted using empty cuvettes and all the data have been corrected, accordingly. All calculations were performed using data of stable leaf gas-exchange of NO/NO<sub>2</sub> collected under steady-state conditions of photosynthesis. The total projected leaf area was determined from drawings of leaves on paper prior cuvette enclosure to allow an immediate harvest after the fumigation experiment.

## Determination of <sup>15</sup>N Content in Leaves

30 day-old Arabidopsis, 15 day-old grey poplar (the height was around 15 cm), 40 day-old grey poplar (the height was around 50 cm), and 8 different urban tree species were used in this fumigation experiment. All plants were transferred to the climate chamber two days before fumigation. <sup>15</sup>NO (99 % atom isotopic abundance) was obtained from Linde (Pullach, Germany) and diluted to 2% (v/v) with nitrogen by Westfalen AG (Münster, Germany). Fumigation with 50 ppb of <sup>15</sup>NO and 50 ppb of unlabeled NO (control) was performed for 4 days. After the experiment, plant leaf material was dried at 60°C for 48 h and ground to a homogenous powder using a ball mill (Tissue Lyser II, Qiagen, Venlo, Netherlands). Aliquots of about 2 mg leaf powder was transferred into tin capsules (IVA Analysentechnik, Meerbusch, Germany). <sup>15</sup>N abundance as well as N and C contents were determined with an Isotope Ratio Mass Spectrometer (IRMS, delta V Advantage, Thermo Fisher, Dreieich, Germany) coupled to an Elemental Analyzer (Euro EA, Eurovector, Milano, Italy). IRMS measurements were



always be performed in comparison with one or more standards with known isotope composition in the same range of the analyzed samples. For that purpose, a laboratory standard (acetanilide), being part of every sequence in intervals, was used. A series of working standards of different weights were measured to determine the isotope linearity of the system. All lab standard measurements were also the base for the calibration of N and C content calculation. The lab standard itself was calibrated against several suitable international isotope standards (International Atomic Energy Agency, Vienna, Austria). International and suitable laboratory isotope standards were also part of every sequence to create a final correction of  $^{15}\text{N}$  covering all  $^{15}\text{N}$  results of this sequence. The accuracy of the  $^{15}\text{N}$  measurements can be described by a coefficient of variation of less than 0.5%. That of the element analyses is less than 2%.

## Modeling the $\text{NO}_2$ and NO Deposition for Central Berlin

The deposition potentials measured for the four species (*C. betulus*, *F. ornus*, *F. pennsylvanica* and *O. carpinifolia*) were used to investigate the effect that planting these species may have on dry  $\text{NO}_x$  deposition under realistic conditions. For this purpose, we have calculated total atmospheric NO and  $\text{NO}_2$  deposition fluxes into the street tree foliage ( $F$ , in  $\text{g m}^{-2} \text{s}^{-1}$ ) within the central district of Berlin (Mitte), simplified as the product of the deposition velocity ( $vd$ ,  $\text{m s}^{-1}$ ) and the NO/ $\text{NO}_2$  concentration ( $C$ , in  $\text{g m}^{-3}$ ):

$$F = vd \times C \quad \text{eq. (3)}$$

For this exercise, 78,000 trees within one district area of Berlin (Mitte, 39.47  $\text{km}^2$ ) were considered, available from the city-tree inventory presented by Tigges et al. (2017). Species and dimension of each tree is known, indicating that the four most prominent genera in this area are *Acer* (26.2%, mostly *A. platanoides*), *Tilia* (25.7%, mostly *T. cordata*), *Fagus sylvatica* (17%), and *Quercus* (10.9%, mostly *Q. robur*) which together have a share of about 80%. The leaf area (LA) has been calculated using a formula based on the Beer-Lambert Law according to Nowak (1996), considering the crown dimension, which is available from the inventory.

In order to demonstrate the potential impact of the new parameters, we determined the deposition first by considering the prescribed species selection using a daytime  $vd$  value of  $0.001 \text{ m s}^{-1}$  for  $\text{NO}_2$  and  $0.0001 \text{ m s}^{-1}$  for NO for all trees (standard run). The  $\text{NO}_2$  value is the average of published measurements from tree species that are relevant for Central European urban areas, i.e., maple, oaks, and birches (Elkley et al., 1982; Chaparro-Suarez et al., 2011). It is at the lower end of the range suggested by Lovett (1994) considering a wide range of plant species. For NO deposition velocity, we assumed a 10-fold smaller value as recommended by Hanson and Lindberg (1991), which is consistent with findings from Neubert et al. (1993). The simulation was carried out for the entire year 2014 using measured precipitation (data obtained from the German Weather Service) and air pollution data (from station “Mitte”,

available from the BLUME network Berlin on request, <https://www.berlin.de/senuvk/umwelt/umweltratgeber/de/spiu/luft.shtml>). In a second simulation (scenario run), all trees of the aforementioned most abundant genera were replaced by the four species which had been investigated in the laboratory, using the experimentally measured  $sV_d$  based on projected leaf area measurements that were converted into deposition velocity ( $\text{m s}^{-1}$ ) to leaf canopy according to:

$$vd = sV_d \times LAI \quad \text{eq. (4)}$$

Where  $LAI$  is the leaf area index, assumed a value of 3, commonly found for urban trees (Öztürk et al., 2015; Massetti et al., 2019). To have the largest effect, we replaced species in the order of descending  $vd$  for  $\text{NO}_2$ , which is *C. betulus* ( $0.933 \text{ mm s}^{-1}$ ) replacing *Acer*, *O. carpinifolia* ( $0.666 \text{ mm s}^{-1}$ ) replacing *Tilia*, *F. pennsylvanica* ( $0.600 \text{ mm s}^{-1}$ ) replacing *Fagus* and *F. ornus* ( $0.453 \text{ mm s}^{-1}$ ) replacing *Quercus* trees. All other boundary conditions were the same as in the standard run. The respective  $vd$ s for NO are  $0.568 \text{ mm s}^{-1}$  for *C. betulus*,  $0.1152 \text{ mm s}^{-1}$  for *O. carpinifolia*,  $0.184 \text{ mm s}^{-1}$  for *F. pennsylvanica*, and  $0.169 \text{ mm s}^{-1}$  for *F. ornus*. In addition, we considered a decrease in  $vd$  to one-fifth of the daytime value during night as suggested by Lovett (1994), assuming the stomata to be mostly closed.

## Statistics

All experiments were performed using three or four different plants as independent replicates ( $n = 3\text{--}4$ , Table 1). Principal component analysis and group comparisons were done in R version 3.6.0 (R Core Team, 2019). Normality and homogeneity of variances were checked via the Shapiro-Wilk test (R Core Team, 2019) and Levene's test with group medians (Fox and Weisberg, 2019), respectively. If both assumptions were not rejected ( $p > 0.05$ ), ANOVA was applied, otherwise the non-parametric Kruskal-Wallis test. Raw p-values were Bonferroni-corrected across all variables of a data set. For posthoc analysis of significant ANOVA results, we applied Tukey's test (Hothorn et al., 2008) to identify group differences. Letter assignment to groups was performed with multcompView (Graves et al., 2015).

## RESULTS

### $\text{NO}_x$ Deposition Velocities and $^{15}\text{NO}$ Labeling Studies in Different Tree Species

To determine the NO and  $\text{NO}_2$  specific deposition velocities to the leaf surface of *Carpinus betulus*, *Fraxinus ornus*, *Fraxinus pennsylvanica*, and *Ostrya carpinifolia*, we performed fumigation experiments and dynamic branch enclosure measurements. The experiment was performed under highly controlled environmental conditions of a phytotron. For each of the four plant species, one branch containing 5–8 mature leaves was enclosed in parallel into a respective odorless bag inside the climate chambers (Figure 1A). Increasing concentrations of NO and  $\text{NO}_2$  up to 90 ppb were applied via the inlet air, and the concentration-dependent capacity of the different tree species to remove atmospheric NO/ $\text{NO}_2$  was observed (Figures 1B, C). Then, deposition and compensation

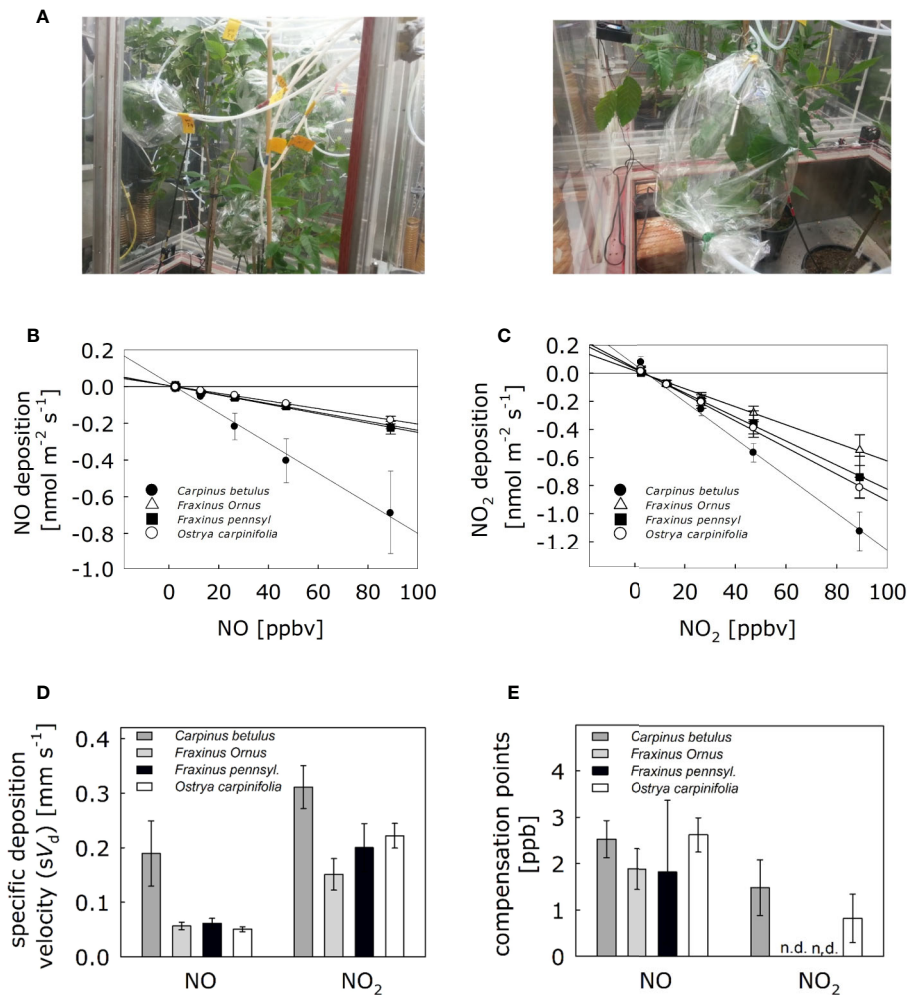


**FIGURE 1** | Exchange of NO and  $\text{NO}_2$  fluxes of four tree species resilient to heat and drought stresses suitable for urban greening. **(A)** Trees (*C. betulus*, *F. ornus*, *F. pennsylvanica* and *O. carpinifolia*) were placed into the climate chambers two days before fumigation to adapt to the environmental conditions. Fumigation experiments were performed with a dynamic branch enclosure system under steady-state conditions using NO and  $\text{NO}_2$ . One branch was enclosed in odorless polyethylene terephthalate bags serving as cuvette system during fumigations and online measurements of NO/ $\text{NO}_2$ . The inlet air tube was placed on the side of the stem and tightened together. Each cuvette was continuously flushed with  $1,000 \text{ ml min}^{-1}$  of humidified (60% RH)  $\text{NO}_x$ -free air containing ambient  $\text{CO}_2$  concentrations ( $\sim 400 \text{ ppm}$ ).  $\text{NO}_x$  was measured sequentially by switching automatically every 9 min using an automatic multipoint valve. **(B)** Linear regressions of NO deposition fluxes and **(C)**  $\text{NO}_2$  deposition fluxes are shown. **(D)** Specific deposition velocities based on projected leaf area for each tree species was calculated from the corresponding linear regressions. **(E)** Compensation points, the NO/ $\text{NO}_2$  air concentrations (in ppb) when leaf emission equals uptake (i.e., net exchange rate is zero). nd, not detectable. Bars in **(C)** represents means  $\pm$  SD. Experiments were replicated with four different trees. None of the NO and  $\text{NO}_2$  parameters in **(D)** and **(E)** showed significant differences [Kruskal-Wallis test for NO in **(D)**:  $p > 0.05$ ; ANOVA for  $\text{NO}_2$  in **(D)** and for NO and  $\text{NO}_2$  in **(E)**:  $p > 0.05$ ; Shapiro-Wilk test:  $p < 0.05$  for NO in **(D)**,  $p > 0.05$  otherwise; Levene's test:  $p < 0.001$  for NO in **(D)**,  $p > 0.05$  otherwise].

parameters were determined for NO and  $\text{NO}_2$ . Experiments were repeated using four different trees ( $n = 4$ ) per plant species. Although the different tree species did not fall into clearly distinct groups (**Supplementary Figure S1**), the foliage of *C. betulus* showed the highest NO deposition velocity, although not statistically different from that of the others (**Figure 1D**). Similarly, the  $\text{NO}_2$  deposition velocity in *C. betulus* leaves tend to be higher compared to the other tree species (**Figure 1D**). Detected compensation points for NO were in the range of 1.8–2.6 ppb and for  $\text{NO}_2$  in the range of 0.8–1.5 ppb (**Figure 1E**).

To study the NO uptake capacity of tree foliage, a  $^{15}\text{NO}$  labeling experiment was performed with three trees of each species listed above. Moreover, four additional tree species (*Celtis australis*, *Alnus spaethii*, *Alnus glutinosa*, and *Tilia henryana*; four trees of each species) were included in the analysis. The trees were exposed to 50 ppb of  $^{15}\text{NO}$  for 5 days, while fumigation with 50 ppb of unlabeled NO was used as control. Then total N and C content, C/N ratio and  $^{15}\text{N}$  content were determined. Overall, the different tree species formed characteristic gradients, with *Fraxinus ornus*, *Celtis australis*,

and *Alnus glutinosa* representing the extremes (Supplementary Figure S2). The trees differed in their total dry matter N content ranging from 0.016 g per g dry matter (*F. ornus*) to 0.036 g per g dry matter (*C. australis*) (Figure 2A). The total C content was in the range of 0.42 to 0.51 g per g of dry matter, with significantly larger values in both *Alnus* species than in *C. australis*, *F. ornus* and *C. betulus* (Figure 2B). Consequently, we observed a C/N ratio between 13 (*C. australis*) and 26 (*F. ornus*) (Figure 2C). The highest daily  $^{15}\text{N}$  uptake was found in *A. glutinosa* (3.6 mg per kg dry matter), followed by *C. betulus* and *C. australis*, respectively. The lowest daily uptake of  $^{15}\text{N}$  was detected in *F. ornus* (0.8 mg per kg dry matter) (Figure 2D).

## Modelling $\text{NO}_2$ and NO Dry Deposition for Central Berlin.

The  $\text{NO}_x$  specific deposition velocities are not plant-species dependent (Figure 1D), concluding that all the tree species investigated are suitable for urban greening. Based on our determined  $\text{NO}_x$  deposition rates, we defined a tree population for the effective reduction of  $\text{NO}_x$  in Central Berlin. Therefore, the four dominant tree genera in this area as depicted in Figure 3A, which represent the standard simulation, were replaced by *C. betulus*, *F. ornus*, *F. pennsylvanica*, and *O. carpinifolia*. For discussion, we also present the distribution of each tree species within the Berlin district Mitte in Figure 3B. The simulations indicate that the overall pollution removal of the newly

investigated species was in the same range as that of the four currently dominant genera. According to our rough estimates that assume no changes in tree dimensions or tree positions and an equal share of the abundance of the new species, the total annual NO deposition would more than double, but the  $\text{NO}_2$  deposition would slightly decrease by ~23% (Figure 3C).

## Improved NO Uptake in Phytooglobin Transgenic Arabidopsis and Poplar

As previously reported for *Arabidopsis* and barley, PGBs are able to fix atmospheric NO into nitrogen metabolites (Kuruthukulangarakoola et al., 2017; Zhang et al., 2019). The reaction mechanism of the NO-fixation by PGB is illustrated in Figure 4A. To investigate if an enhanced expression of PGBs can enhanced NO uptake in trees, we generated transgenic grey poplar overexpressing the Arabidopsis class 1 and class 2 PGB gene.

The enzymatically dependent NO uptake capacity of these transgenic lines was studied in four 40-day-old trees and three 15-day-old poplars. We exposed the trees to 50 ppbv of labeled  $^{15}\text{NO}$  for 5 consecutive days under controlled environmental conditions, and we studied the  $^{15}\text{N}$  label in the harvested leaf materials. Wild type poplar of the corresponding age, as well as transgenic Arabidopsis plants with enhanced and reduced expression of PGB genes, were used as controls (Figures 4B, C).  $^{15}\text{N}$  levels in *AtPGB* overexpressing plants were higher than in

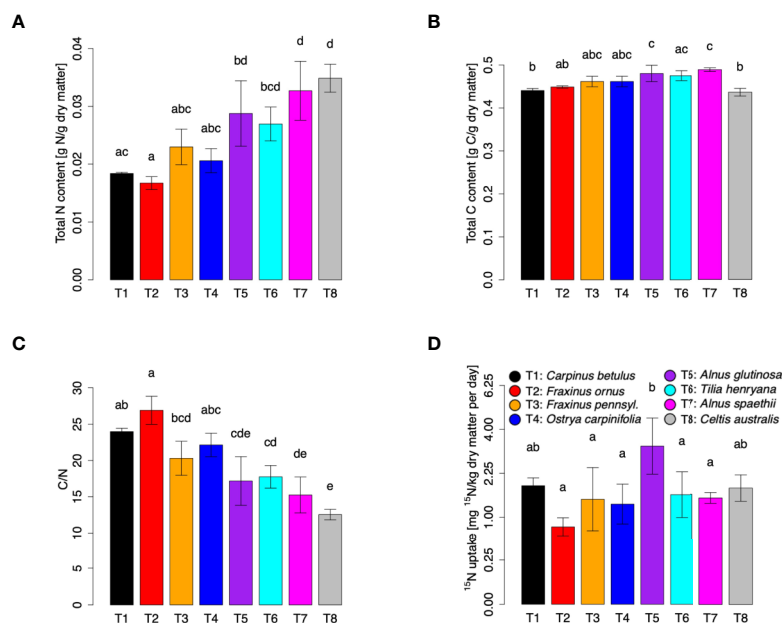


**FIGURE 2** | N, C, C/N ratio and  $^{15}\text{N}$  content in different tree species after fumigation with 50 ppbv of  $^{15}\text{NO}$  for 5 days. Trees were exposed to 50 ppbv of  $^{15}\text{NO}$  in climate chambers, and leaf samples were taken for  $^{15}\text{N}$  measurements after 4 days of treatment. Total N (A) and C (B) contents as well as  $^{15}\text{N}$  (D) content were determined with an Isotope Ratio Mass Spectrometer (IRMS) coupled to an Elemental Analyzer (EA). Calculated C/N ratio for each tree is shown in (C).  $^{15}\text{N}$  uptake values are shown after square root transformation. Each plot represents means  $\pm$  SD. Three individuals of *Carpinus betulus*, *Fraxinus ornus*, *Fraxinus pennsylvanica*, and *Ostrya carpinifolia* were measured ( $n = 3$ ). Four individuals of *Celtis australis*, *Alnus spaethii*, *Alnus glutinosa*, and *Tilia henryana* were measured ( $n = 4$ ). Significant species differences were observed for N, C, C/N and  $^{15}\text{N}$  (ANOVA:  $p < 0.01$ ; Shapiro-Wilk test:  $p > 0.05$ ; Levene's test:  $p > 0.05$ ). Different letters indicate significant differences according to Tukey's posthoc test ( $p < 0.05$ ).

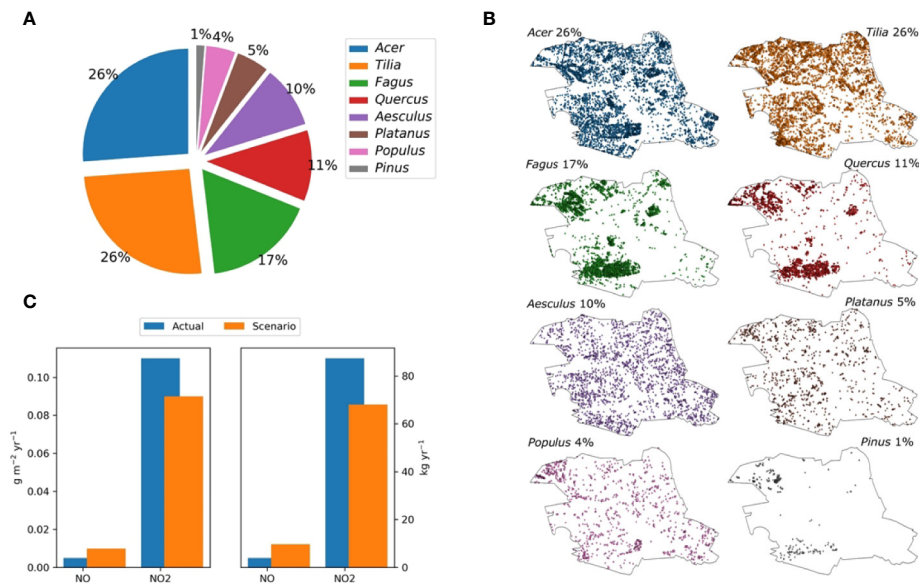


**FIGURE 3** | Tree population in Central Berlin and modeling of NO<sub>x</sub> deposition. The calculations are done with NO<sub>2</sub> and NO concentrations of the year 2014 for the central district of Berlin (Mitte). This area hosts about 78,000 trees with the species composition indicated in **(A)** and the spatial distribution depicted in **(B)**. The overall annual deposition of NO<sub>2</sub> and NO per m<sup>2</sup> regarding this species composition (standard) and alternative species composition (scenario) is shown in **(C)**. For the scenario, the four urban climate-resilient tree-species (*Carpinus betulus*, *Fraxinus ornus*, *Fraxinus pennsylvanica*, *Ostrya carpinifolia*) replaced the four actual dominant tree genera as indicated by the senate of Berlin. For parameterization, we assume that the genera can be characterized by the most abundant species in each genera group (*Acer platanoides*, *Tilia cordata*, *Fagus sylvatica*, *Quercus robur*, *Aesculus hypocastanum*, *Platanus hispanica*, *Populus nigra/alba*, and *Pinus sylvestris*).

the corresponding WT and PGB knockdown/knockout mutants (**Figure 4B**), confirming that enhanced production of the protein PGB can significantly increase the enzymatic process towards higher foliage NO uptake capacity in trees. Interestingly, we observed a higher level of <sup>15</sup>N incorporation in young poplars (15 day-old poplars) in comparison to older (40 day-old poplars) plants (**Figure 4B**).

## DISCUSSION

Our results showed that under well-watered conditions, *A. glutinosa* has the most effective NO uptake. Overall, specific deposition velocities measured in this study are in the same order of magnitude as observed in other tree species relevant for Central European urban areas such as *A. platanoides*, *A. pseudoplatanus*, *Q. robur*, *Q. petraea*, and *Betula pendula* (Elkies et al., 1982; Chaparro-Suarez et al., 2011). However, some species seem to deviate from this average, as demonstrated in our study for *C. betulus* which at least tended to have higher *s*V<sub>d</sub> for NO and NO<sub>2</sub> deposition rates. Assuming a standard transformation procedure, the resulting uptake/deposition velocities were between 0.15 and 0.56 mm s<sup>-1</sup> for NO and 0.45 and 0.95 mm s<sup>-1</sup> for NO<sub>2</sub>. This strongly agrees with previous studies (Hanson and Lindberg, 1991; Hereid and Monson, 2001; Teklemariam and Sparks, 2006; Breuninger et al., 2013; Delaria et al., 2018). The reasons for the considerable difference between NO and NO<sub>2</sub> are manifold: The assimilation of NO<sub>x</sub> is controlled

by several factors, including the resistance to the entry of NO<sub>x</sub> gas molecules through the stomata and mesophyll conductance, cuticle layer, and intercellular cavity to reach the surface of mesophyll cells (Morikawa et al., 1998). Overall, NO is low soluble in water, whereas NO<sub>2</sub> quickly reacts in water to form nitrate and nitrite in the apoplast (Lee and Schwartz, 1981a; Lee and Schwartz, 1981b). Because air pollutants need to go through the extracellular aqueous covering plant cell when they enter the mesophyll cells, it is logical to expect much lower deposition velocities for NO than for NO<sub>2</sub>. Also, the permeability of nitrate and nitrite ions through cell walls and plasma membranes (Lee and Schwartz, 1981a; Lee and Schwartz, 1981b; Ramge et al., 1993; Ammann et al., 1995), as well as the activity in the primary nitrate assimilation pathway through which NO<sub>2</sub>-nitrogen is reported to be metabolized do play a role in NO<sub>x</sub> uptake (Rogers et al., 1979; Yoneyama and Sasakawa, 1979; Wellburn, 1990). The NO<sub>2</sub> uptake by leaves of the same plant species is furthermore affected by stomatal dynamics, rate of photosynthesis, and position within the canopy (Sparks et al., 2001; Chaparro-Suarez et al., 2011). Altogether, these features can largely explain the different uptake/deposition rates for NO.

In addition to the physicochemical controls on NO/NO<sub>2</sub> deposition velocities, we demonstrate that the fixation of NO is also under the control of an enzymatic process. The amount of PGB proteins and the activity of the NO-fixing machinery are important factors for an effective NO uptake and might differ between tree species. According to the biochemical activities of PGBs as NO dioxygenase [EC 1.14.12.17] (Perazzolli et al., 2004),



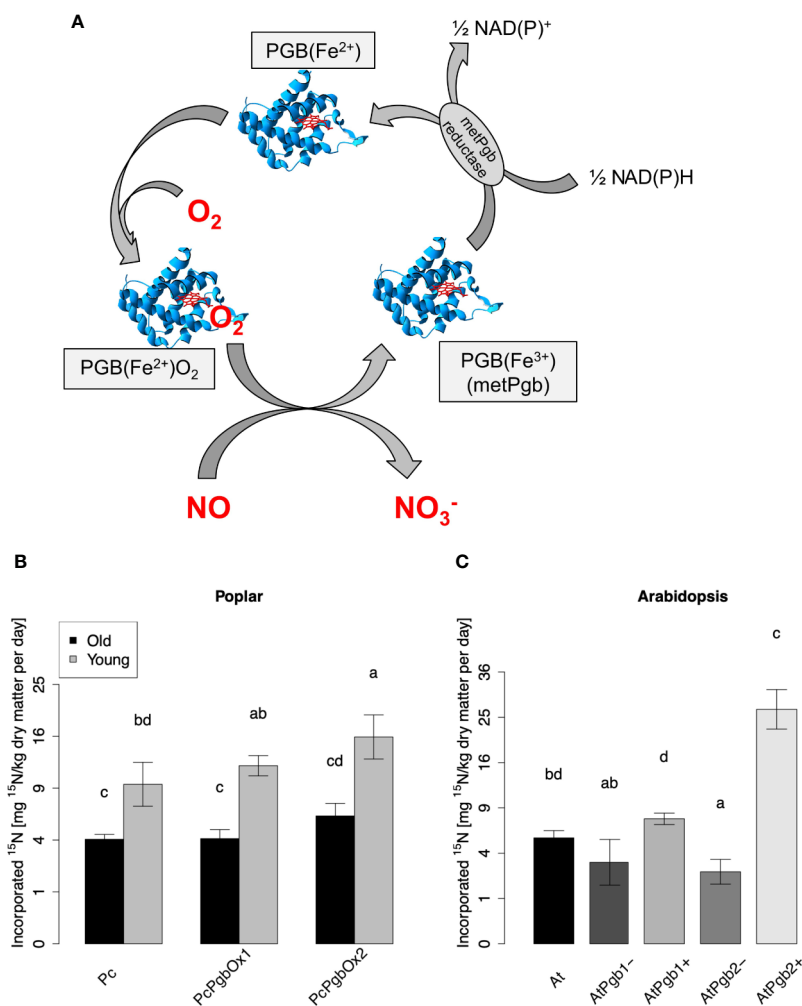


**FIGURE 4 |** NO-fixation by plant phytohemoglobin. **(A)** Illustration of the biochemical NO-fixing reaction mechanism. NO is converted to nitrate ( $\text{NO}_3^-$ ) by the oxygenated ferrous phytohemoglobin [ $\text{PGB(Fe}^{2+})$ ], which turns to the metPgb form [ $\text{PGB(Fe}^{3+})$ ]. The latter is reduced by a NAD(P)H-dependent reductase (metPgb) and then oxygenated again. **(B)**  $^{15}\text{N}$  content in transgenic poplar and **(C)** *Arabidopsis* determined 5 days after fumigation with 50 ppbv of  $^{15}\text{NO}$ . In **(B)** leaves of old (40 day-old) and young (15 day-old) poplar tree have been analyzed. Each plot depicts means  $\pm$  SD. Four samples of *Arabidopsis* and old poplar trees were measured ( $n = 4$ ) and three samples of the young poplar trees were measured ( $n = 3$ ).  $^{15}\text{N}$  content values are shown after square root transformation. Different letters indicate significant differences according to Tukey's posthoc test ( $p < 0.05$ ) after significant ANOVA ( $p < 0.001$ ; Shapiro-Wilk test:  $p > 0.05$ ; Levene's test:  $p > 0.05$ ).

nitrite reductase [EC 1.7.2.1] (Sturms et al., 2011a; Tiso et al., 2012; Kumar et al., 2016), and hydroxylamine reductase [EC 1.7.1.10] (Sturms et al., 2011b), they seem to be of general importance for the nitrogen metabolism. Since different PGB isoforms differ in their kinetic properties regarding oxygen and NO binding as well as NO deoxygenase activity (Smagghe et al., 2008; Calvo-Begueria et al., 2017; Eriksson et al., 2019), inducing the biosynthesis of PGBs and improving the biochemical features for NO-fixation might increase the uptake of atmospheric NO. We demonstrated that overexpression of *Arabidopsis* PGB 1 and 2 in grey poplar could indeed significantly enhance the NO uptake capacity. Therefore, producing and planting highly efficient  $\text{NO}_x$  removing trees, transgenic ones or after derived from “natural” selection from phenotype screening, could be a

potential means to reduce the atmospheric  $\text{NO}_x$  level and improve air quality in urban areas.

Our modeling exercise resulted in only moderate to minor changes in overall  $\text{NO}_x$  removal during a full year in a Metropolitan area. Nevertheless, differences between compounds exist, indicating that the total  $\text{NO}_2$  deposition would only slightly decrease while NO deposition would increase by a factor of more than two, if the four dominant tree genera grown in Central Berlin would be replaced by the four tree species considered for climate change adaptation. This is partly due to the differences between the investigated species but also due to the relatively rough estimate that the standard run was based upon. Indeed, this run is parametrized with very few deposition velocity data available for the tree species populating urban areas. Besides, the scaling of

specific deposition velocities based on leaf area that is also estimated with a relatively crude method includes considerable uncertainties. As a criterion for deposition removal capacity, we used stomatal conductance that is easily scalable with LAI to obtain a canopy- or regional level result (Teklemariam and Sparks, 2006; Chaparro-Suarez et al., 2011; Breuninger et al., 2013; Delaria et al., 2018). Respective functions consider crown size and competition that are estimated based on site conditions (e.g., Pace et al., 2018). Since we did this estimation based on species-specific parameterization, the differences in LAI due to the new tree species are already considered in the calculations. Nevertheless, LAI estimates may still considerably deviate from reality because the estimation method provides high uncertainty and pruning intensity as well as frequency. Thus, crown size strongly depends on the management practice of the city, which may differ with species. In addition, the stomatal dependency of gas uptake implies that growing under dry conditions substantially decrease removal capacity. Different water-use strategies thus result in differences in gaseous uptake. For example, an isohydric species such as *A. platanoides* that establishes drought resistance by closing stomata early would perform less well under medium water supply compared to an anisohydric species such as *Alnus* or *Carpinus* (Li et al., 2016). Considering this behavior, we can assume that the removal capacity of the tree species resilient to drought episodes would be higher under realistic environmental conditions and even higher under projected future climate conditions, provided the drought episodes are moderate. The picture, however, might change under more severe drought that might deplete water reservoirs completely and may induce mortality.

It is, overall, desirable to choose city tree species that have a relatively high NO and NO<sub>2</sub> uptake/deposition capacity since they could provide a viable means to reduce atmospheric NO<sub>x</sub> level and help meet clean air standards. The selection of appropriate tree species able to cope with increased heat and drought stress while keeping a high capacity to “clean” air may thus support urban planning strategies. Also, the NO-fixing capability of PGBs could be a valuable trait that might be increasingly applied to characterize tree species in the context of urban air quality.

## REFERENCES

- Ammann, M., von Ballmoos, P., Stalder, M., Suter, M., and Brunold, C. (1995). Uptake and assimilation of atmospheric NO<sub>2</sub> - N by spruce needles (*Picea abies*): A field study. *Water Air Soil Pollut.* 85, 1497–1502. doi: 10.1007/BF00477193
- Becana, M., Yruea, I., Sarath, G., Catal, P., and Hargrove, M. S. (2020). Plant hemoglobins: a journey from unicellular green algae to vascular plants. *New Phytol.* 227, 1618–1635. doi: 10.1111/nph.16444
- Berger, A., Guinand, S., Boscari, A., Puppo, A., and Brouquisse, R. (2020). *Medicago truncatula* Phytoglobin 1.1 controls symbiotic nodulation and nitrogen fixation via the regulation of nitric oxide concentration. *New Phytol.* 227, 84–98. doi: 10.1111/nph.16462
- Bi, Z., Merl-Pham, J., Uehlein, N., Zimmer, I., Mühlhans, S., Aichler, M., et al. (2015). RNAi-mediated downregulation of poplar plasma membrane intrinsic proteins (PIPs) changes plasma membrane proteome composition and affects leaf physiology. *J. Proteomics* 128, 321–332. doi: 10.1016/j.jprot.2015.07.029

## DATA AVAILABILITY STATEMENT

Datasets from this study are shown as graphs in the article/**Supplementary Material**. Original data are available upon request.

## AUTHOR CONTRIBUTIONS

JZ, AGh, AGo, RP, FB, and CL contributed conception and design of the study and performed the experiments/analysis. JZ AGh, and EG performed the statistical analysis. JZ and CL wrote the first draft of the manuscript. AGh, RG, EG, and J-PS wrote sections of the manuscript. All authors contributed to the article and approved the submitted version.

## FUNDING

JZ gratefully acknowledges the financial support from China Scholarship Council (CSC, File No. 201406300083).

## ACKNOWLEDGMENTS

We thank Felix Anritter, Elke Mattes, Lucia Gößl, and Rosina Ludwig for excellent technical assistance. Moreover, we thank Susanne Böll for selecting the tree species that are regarded suitable candidates for urban trees under future climatic conditions. This work was supported by the Bundesministerium für Bildung und Forschung (BMBF) and by the Graduate School for Climate and Environment (GRACE).

## SUPPLEMENTARY MATERIAL

The Supplementary Material for this article can be found online at: <https://www.frontiersin.org/articles/10.3389/fpls.2020.549913/full#supplementary-material>

- Böll, S. (2017). *7 Jahre “Stadtgrün 2021” - Einfluss des regionalen Klimas auf das Baumwachstum an drei bayerischen Standorten* (Verlag HAYMARKET, Braunschweig: Jahrbuch der Baumpflege), S. 91–S.114.
- Böll, S. (2018a). *Stadtbäume der Zukunft – Wichtige Erkenntnisse aus dem Forschungsprojekt (Stadtgrün 2021: Bayerische Landesanstalt für Weinbau und Gartenbau, Veitshöchheim)*. Available at: [http://www.lwg.bayern.de/landespflege/urbanes\\_gruen/085113/index.php](http://www.lwg.bayern.de/landespflege/urbanes_gruen/085113/index.php).
- Böll, S. (2018b). “Projekt Stadtgrün 2021” Selektion, Anzucht und Verwendung von Gehölzen unter sich ändernden klimatischen Bedingungen (Abschlussbericht zum Forschungsvorhaben Nr: KL/17/03).
- Breuninger, C., Meixner, F. X., and Kesselmeier, J. (2013). Field investigations of nitrogen dioxide (NO<sub>2</sub>) exchange between plants and the atmosphere. *Atmospheric Chem. Phys.* 13, 773–790. doi: 10.5194/acp-13-773-2013
- Burley, H., Beaumont, L. J., Ossola, A., Baumgartner, J. B., Gallagher, R., Laffan, S., et al. (2019). Substantial declines in urban tree habitat predicted under climate change. *Sci. Total Environ.* 685, 451–462. doi: 10.1016/j.scitotenv.2019.05.287

- Calvo-Begueria, L., Cuypers, B., Van Doorslaer, S., Abbruzzetti, S., Bruno, S., Berghmans, H., et al. (2017). Characterization of the heme pocket structure and ligand binding kinetics of non-symbiotic hemoglobins from the model legume *Lotus japonicus*. *Front. Plant Sci.* 8, 407. doi: 10.3389/fpls.2017.00407. eCollection 2017.
- Chaparro-Suarez, I. G., Meixner, F. X., and Kesselmeier, J. (2011). Nitrogen dioxide (NO<sub>2</sub>) uptake by vegetation controlled by atmospheric concentrations and plant stomatal aperture. *Atmospheric Environ.* 45, 5742–5750. doi: 10.1016/j.atmosenv.2011.07.021
- Delaria, E. R., Vieira, M., Cremieux, J., and Cohen, R. C. (2018). Measurements of NO and NO<sub>2</sub> exchange between the atmosphere and *Quercus agrifolia*. *Atmospheric Chem. Phys.* 18, 14161–14173. doi: 10.5194/acp-18-14161-2018
- Dickhaut, W., and Eschenbach, A. (2019). *Entwicklungskonzept Stadtbäume - Anpassungsstrategien an sich verändernde urbane und klimatische Rahmenbedingungen* (Hamburg: HafenCity Universität Hamburg).
- Döhning, T., Köfferlein, M., Thiel, S., and Seidlitz, H. K. (1996). Spectral shaping of artificial UV-B irradiation for vegetation stress research. *J. Plant Physiol.* 148, 115–119. doi: 10.1016/S0176-1617(96)80302-6
- EEA (2019). *Air quality in Europe 2019*, European Environmental Agency, EEA report No 10/2018. Luxembourg: European Environmental Agency, Publications Office of the European Union.
- Elkay, T., Ormrod, D. P., and Marie, B. (1982). Foliar sorption of sulfur dioxide, nitrogen dioxide and ozone by ornamental woody plants. *HortScience* 17, 358–359.
- Eller, A. S. D., and Sparks, J. P. (2006). Predicting leaf-level fluxes of O<sub>3</sub> and NO<sub>2</sub>: The relative roles of diffusion and biochemical processes. *Plant Cell Environ.* 29, 1742–1750. doi: 10.1111/j.1365-3040.2006.01546.x
- Eriksson, N. L., Reeder, B. J., Wilson, M. T., and Bülow, L. (2019). Sugar beet hemoglobins: reactions with nitric oxide and nitrite reveal differential roles for nitrogen metabolism. *Biochem. J.* 476, 2111–2125. doi: 10.1042/BCJ20190154
- Fox, J., and Weisberg, S. (2019). *An R Companion to Applied Regression*. 3rd ed. (Thousand Oaks CA: Sage). Available at: <https://socialsciences.mcmaster.ca/jfox/Books/Companion/>.
- Geffler, A., Rienks, M., and Rennenberg, H. (2002). Stomatal uptake and cuticular adsorption contribute to dry deposition of NH<sub>3</sub> and NO<sub>2</sub> to needles of adult spruce (*Picea abies*) trees. *New Phytol.* 156, 179–194. doi: 10.1046/j.1469-8137.2002.00509.x
- Ghirardo, A., Koch, K., Taipale, R., Zimmer, I., Schnitzler, J.-P., and Rinne, J. (2010). Determination of de novo and pool emissions of terpenes from four common boreal/alpine trees by <sup>13</sup>CO<sub>2</sub> labelling and PTR-MS analysis. *Plant Cell Environ.* 33, 781–792. doi: 10.1111/j.1365-3040.2009.02104.x
- Ghirardo, A., Gutknecht, J., Zimmer, I., Brüggemann, N., and Schnitzler, J.-P. (2011). Biogenic volatile organic compound and respiratory CO<sub>2</sub> emissions after <sup>13</sup>C-labeling: online tracing of C translocation dynamics in poplar plants. *PLoS One* 6, e17393. doi: 10.1371/journal.pone.0017393
- Ghirardo, A., Wright, L. P., Bi, Z., Rosenkranz, M., Pulido, P., Rodríguez-Concepción, M., et al. (2014). Metabolic flux analysis of plastidic isoprenoid biosynthesis in poplar leaves emitting and nonemitting isoprene. *Plant Physiol.* 165, 37–51. doi: 10.1104/pp.114.236018
- Ghirardo, A., Lindstein, F., Koch, K., Buegger, F., Schlöter, M., Albert, A., et al. (2020). Origin of VOC emissions from subarctic ecosystems under global warming. *Global Change Biol.* 26, 1908–1925. doi: 10.1111/gcb.14935
- Granhall, U., and Lindberg, T. (1980). "Nitrogen input through biological nitrogen fixation," in *Structure and function of northern Coniferous forests - An ecosystem Study*. Ed. T. Persson (Stockholm: Ecol. Bull.).
- Graves, S., Piepho, H.-P., Selzer, L., and Dorai-Raj, S. (2015). *multcompView: Visualizations of Paired Comparisons*. R package version 0.1-7. Available at: <https://CRAN.R-project.org/package=multcompView>.
- Grote, R., Samson, R., Alonso, R., Amorim, J. H., Cariñanos, P., Churkina, G., et al. (2016). Functional traits of urban trees in relation to their air pollution mitigation potential: A holistic discussion. *Front. Ecol. Environ.* 14, 543–550. doi: 10.1002/fee.1426
- Hanson, P. J., and Lindberg, S. E. (1991). Dry deposition of reactive nitrogen compounds: A review of leaf, canopy and non-foliar measurements. *Atmos. Environ.* 25, 1615–1634. doi: 10.1016/0960-1686(91)90020-8
- Hebelstrup, K. H., Hunt, P., Dennis, E., Jensen, S. B., and Jensen, E. Ø. (2006). Hemoglobin is essential for normal growth of Arabidopsis organs. *Physiol. Plant.* 127, 157–166. doi: 10.1111/j.1399-3054.2006.00653.x
- Hereid, D. P., and Monson, R. K. (2001). Nitrogen oxide fluxes between corn (*Zea mays* L.) leaves and the atmosphere. *Atmospheric Environ.* 35, 975–983. doi: 10.1016/S1352-2310(00)00342-3
- Hill, A. C. (1971). Vegetation: A sink for atmospheric pollutants. *J. Air Pollut. Control Assoc.* 21, 341–346. doi: 10.1080/00022470.1971.10469535
- Hothorn, T., Bretz, F., and Westfall, P. (2008). Simultaneous Inference in General Parametric Models. *Biometrical J.* 50, 346–363. doi: 10.1002/bimj.200810425
- Hu, Y., and Sun, G. (2010). Leaf nitrogen dioxide uptake coupling apoplastic chemistry, carbon/sulfur assimilation, and plant nitrogen status. *Plant Cell Rep.* 29, 1069–1077. doi: 10.1007/s00299-010-0898-5
- Igamberdiev, A. U., and Hill, R. D. (2004). Nitrate, NO and haemoglobin in plant adaptation to hypoxia: An alternative to classic fermentation pathways. *J. Exp. Bot.* 55, 2473–2482. doi: 10.1093/jxb/erh272
- Igamberdiev, A. U., Bykova, N. V., and Hill, R. D. (2006). Nitric oxide scavenging by barley hemoglobin is facilitated by a monodehydroascorbate reductase-mediated ascorbate reduction of methemoglobin. *Planta* 223, 1033–1040. doi: 10.1007/s00425-005-0146-3
- Jud, W., Fischer, L., Canaval, E., Wohlfahrt, G., Tissier, A., and Hansel, A. (2016). Plant surface reactions: an ozone defence mechanism impacting atmospheric chemistry. *Atmospheric Chem. Phys.* 16, 277–292. doi: 10.5194/acp-16-277-2016
- Kabisch, N., and van den Bosch, M. A. (2017). "Urban green spaces and the potential for health improvement and environmental justice in a changing climate," in *Nature-Based Solutions to Climate Change Adaptation in Urban Areas. Theory and Practice of Urban Sustainability Transitions*. Eds. N. Kabisch, H. Korn, J. Stadler and A. Bonn (Cham: Springer).
- Kozovits, A. R., Matyssek, R., Blaschke, H., Göttele, A., and Grams, T. E. E. (2005). Competition increasingly dominates the responsiveness of juvenile beech and spruce to elevated CO<sub>2</sub>/O<sub>3</sub> concentrations throughout two subsequent growing seasons. *Global Change Biol.* 11, 1387–1401. doi: 10.1111/j.1365-2486.2005.00993.x
- Kumar, N., Astegno, A., Chen, J., Giorgetti, A., and Dominici, P. (2016). Residues in the distal heme pocket of *Arabidopsis* non-symbiotic hemoglobins: Implication for Nitrite Reductase Activity. *Int. J. Mol. Sci.* 17, 640–656. doi: 10.3390/ijms17050640
- Kuruthukulangarakoola, G. T., Zhang, J., Albert, A., Winkler, J. B., Lang, H., Buegger, F., et al. (2017). Nitric oxide-fixation by non-symbiotic haemoglobin proteins in *Arabidopsis thaliana* under N-limited conditions. *Plant Cell Environ.* 40, 36–50. doi: 10.1111/pce.12773
- Lee, Y. N., and Schwartz, S. E. (1981a). Evaluation of the rate of uptake of nitrogen dioxide by atmospheric and surface liquid water. *J. Geophys. Res.* 86, 11971–11983. doi: 10.1029/JC086iC12p11971
- Lee, Y. N., and Schwartz, S. E. (1981b). Reaction kinetics of nitrogen dioxide with liquid water at low partial pressure. *J. Phys. Chem.* 85, 840–848. doi: 10.1021/j150607a022
- Li, S., Feifel, M., Karimi, Z., Schuldt, B., Choat, B., and Jansen, S. (2016). Leaf exchange performance and the lethal water potential of five European species during drought. *Tree Physiol.* 36, 179–192. doi: 10.1093/treephys/tpv117
- Lovett, G. M. (1994). Atmospheric deposition of nutrients and pollutants in North America: an ecological perspective. *Ecol. Appl.* 4, 629–650. doi: 10.2307/1941997
- Mannucci, P. M., Harari, S., Martinelli, I., and Franchini, M. (2015). Effects on health of air pollution: a narrative review. *Internal Emergency Med.* 10, 657–662. doi: 10.1007/s11739-015-1276-7
- Massetti, L., Petralli, M., Napoli, M., Brandani, G., Orlandini, S., and Pearlmutter, D. (2019). Effects of deciduous shade trees on surface temperature and pedestrian thermal stress during summer and autumn. *Int. J. Biometeorol.* 63, 467–479. doi: 10.1007/s00484-019-01678-1
- Mayer, D., Kanawati, B., Schmitt-Kopplin, P., Schnitzler, J.-P., Ghirardo, A., Georgii, E., et al. (2018). Short-term exposure to nitrogen dioxide provides basal pathogen resistance. *Plant Physiol.* 178, 468–487. doi: 10.1104/pp.18.00704
- Mira, M. M., Hill, R. D., and Stasolla, C. (2016). Pgbs improve hypoxic root growth by alleviating apical meristem cell death. *Plant Physiol.* 172, 2044–2056. doi: 10.1104/pp.16.01150
- Mira, M. M., Huang, S., Kapoor, K., Hammond, C., Hill, R. D., and Stasolla, C. (2017). Expression of Arabidopsis class 1 Pgb (AtPgb1) delays death and degradation of the root apical meristem during severe PEG-induced water deficit. *J. Exp. Bot.* 68, 5653–5668. doi: 10.1093/jxb/erx371
- Morikawa, H., Higaki, A., Nohno, M., Takahashi, M., Kamada, M., Nakata, M., et al. (1998). More than a 600-fold variation in nitrogen dioxide assimilation

- among 217 plant taxa. *Plant Cell Environ.* 21, 180–190. doi: 10.1046/j.1365-3040.1998.00255.x
- Neubert, A., Kley, D., Wildt, J., Segsneider, H., and Förstel, H. (1993). Uptake of NO, NO<sub>2</sub> and O<sub>3</sub> by sunflower (*Helianthus annuus*) and tobacco plants (*Nicotiana tabacum*): Dependence on stomatal conductivity. *Atmospheric Environ.* 27A, 2137–2145. doi: 10.1016/0960-1686(93)90043-X
- Nowak, D. J. (1996). Estimating leaf area and leaf biomass of open-grown deciduous urban trees. *For. Sci.* 42, 504–507. doi: 10.1093/forestscience/42.4.504
- Öztürk, M., Bolat, İ., and Ergün, A. (2015). Influence of air–soil temperature on leaf expansion and LAI of *Carpinus betulus* trees in a temperate urban forest patch. *Agric. For. Meteorol.* 200, 185–191. doi: 10.1016/j.agrformet.2014.09.014
- Pace, R., Biber, P., Pretzsch, H., and Grote, R. (2018). Modelling ecosystem services for park trees: Sensitivity of i-Tree Eco simulations to light exposure and tree species classification. *Forests*. 9, 89–106. doi: 10.3390/f9020089
- Papen, H., Geßler, A., Zumbusch, E., and Rennenberg, H. (2002). Chemolithoautotrophic nitrifiers in the phyllosphere of a spruce ecosystem receiving high atmospheric nitrogen input. *Curr. Microbiol.* 44, 56–60. doi: 10.1007/s00284-001-0074-9
- Perazzolli, M., Dominici, P., Romero-Puertas, M. C., Zago, E., Zeier, J., Sonoda, M., et al. (2004). Arabidopsis nonsymbiotic hemoglobin AHb1 modulates nitric oxide bioactivity. *Plant Cell* 16, 2785–2794. doi: 10.1105/tpc.104.025379
- R Core Team (2019). *R: A language and environment for statistical computing* (Vienna, Austria: R Foundation for Statistical Computing). Available at: <https://www.R-project.org/>.
- Ramge, P., Badeck, F.-W., Plöchl, M., and Kohlmaier, G. H. (1993). Apoplastic antioxidants as decisive elimination factors within the uptake process of nitrogen dioxide into leaf tissues. *New Phytol.* 125, 771–785. doi: 10.1111/j.1469-8137.1993.tb03927.x
- Rogers, H. H., Campbell, J. C., and Volk, R. J. (1979). Nitrogen-15 dioxide uptake and incorporation by *Phaseolus vulgaris* (L.). *Science* 206, 333–335. doi: 10.1126/science.206.4416.333
- Roloff, A., Korn, S., and Gillner, S. (2009). The Climate-Species-Matrix to select tree species for urban habitats considering climate change. *Urban For. Urban Greening* 8, 295–308. doi: 10.1016/j.ufug.2009.08.002
- Salmond, J. A., Tadaki, M., Vardoulakis, S., Arbutnot, K., Coutts, A., Demuzere, M., et al. (2016). Health and climate related ecosystem services provided by street trees in the urban environment. *Environ. Health* 15, S36. doi: 10.1186/s12940-016-0103-6
- Seckmeyer, G., and Payer, H. D. (1993). A new sunlight simulator for ecological research on plants. *J. Photochem. Photobiol. B: Biol.* 21, 175–181. doi: 10.1016/1011-1344(93)80180-H
- Shankar, A., Fernandes, J. L., Kaur, K., Sharma, M., Kundu, S., and Pandey, G. K. (2018). Rice Pgbs regulate responses under low mineral nutrients and abiotic stresses in *Arabidopsis thaliana*. *Plant Cell Environ.* 41, 215–230. doi: 10.1111/pce.13081
- Sillman, S. (1999). The relation between ozone, NO<sub>x</sub> and hydrocarbons in urban and polluted rural environments. *Atmospheric Environ.* 33, 1821–1845. doi: 10.1016/S1352-2310(98)00345-8
- Smaghe, B. J., Trent, J. T. III, and Hargrove, M. S. (2008). NO dioxygenase activity in hemoglobins is ubiquitous in vitro, but limited by reduction in vivo. *PLoS One* 3, e2039. doi: 10.1371/journal.pone.0002039
- Soegiarto, L., Wills, R. B. H., Seberry, J. A., and Leshem, Y. Y. (2003). Nitric oxide degradation in oxygen atmospheres and rate of uptake by horticultural produce. *Postharvest Biol. Technol.* 28, 327–331. doi: 10.1016/S0925-5214(02)00199-0
- Sparks, J. P., Monson, R. K., Sparks, K. L., and Lerdau, M. (2001). Leaf uptake of nitrogen dioxide (NO<sub>2</sub>) in a tropical wet forest: Implications for tropospheric chemistry. *Oecologia* 127, 214–221. doi: 10.1007/s004420000594
- Sturms, R., DiSpirito, A. A., and Hargrove, M. S. (2011a). Plant and cyanobacterial hemoglobins reduce nitrite to nitric oxide under anoxic conditions. *Biochemistry* 50, 3873–3878. doi: 10.1021/bi2004312
- Sturms, R., DiSpirito, A. A., Fulton, D. B., and Hargrove, M. S. (2011b). Hydroxylamine reduction to ammonium by plant and cyanobacterial hemoglobins. *Biochemistry* 50, 10829–10835. doi: 10.1021/bi201425f
- Takahashi, M., Higaki, A., Nohno, M., Kamada, M., Okamura, Y., Matsui, K., et al. (2005). Differential assimilation of nitrogen dioxide by 70 taxa of roadside trees at an urban pollution level. *Chemosphere* 61, 633–639. doi: 10.1016/j.chemosphere.2005.03.033
- Teklemariam, T. A., and Sparks, J. P. (2006). Leaf fluxes of NO and NO<sub>2</sub> in four herbaceous plant species: The role of ascorbic acid. *Atmospheric Environ.* 40, 2235–2244. doi: 10.1016/j.atmosenv.2005.12.010
- Thiel, S., Döhring, T., Köfferlein, M., Kosak, A., Martin, P., and Seidlitz, H. K. (1996). A phytotron for plants stress research: How far can artificial lighting compare to natural sunlight? *J. Plant Physiol.* 148, 456–463. doi: 10.1016/S0176-1617(96)80279-3
- Tigges, J., Churkina, G., and Lakes, T. (2017). Modeling above-ground carbon storage: a remote sensing approach to derive individual tree species information in urban settings. *Urban Ecosyst.* 20, 97–111. doi: 10.1007/s11252-016-0585-6
- Tiso, M., Tejero, J., Kenney, C., Frizzell, S., and Gladwin, M. T. (2012). Nitrite reductase activity of nonsymbiotic hemoglobins from *Arabidopsis thaliana*. *Biochemistry* 51, 5285–5292. doi: 10.1021/bi300570v
- Vanzo, E., Jud, W., Li, Z., Albert, A., Domagalska, M. A., Ghirardo, A., et al. (2015). Facing the future: Effects of short-term climate extremes on isoprene-emitting and non-emitting poplar. *Plant Physiol.* 169, 560–575. doi: 10.1104/pp.15.00871
- Wellburn, A. R. (1990). Why are atmospheric oxides of nitrogen usually phytotoxic and not alternative fertilizers? *New Phytol.* 115, 395–429. doi: 10.1111/j.1469-8137.1990.tb00467.x
- Wildt, J., Kley, D., Rockel, A., Rockel, P., and Segsneider, H. J. (1997). Emission of NO from several higher plant species. *J. Geophys. Res.* 102, 5919–5927. doi: 10.1029/96JD02968
- Yoneyama, T., and Sasakawa, H. (1979). Transformation of atmospheric NO<sub>2</sub> absorbed in spinach leaves. *Plant Cell Physiol.* 20, 263–266. doi: 10.1093/oxfordjournals.pcp.a075801
- Zhang, J., Buegger, F., Albert, A., Ghirardo, A., Winkler, J. B., Schnitzler, J.-P., et al. (2019). Phytoglobin overexpression promotes barley growth in the presence of enhanced level of atmospheric nitric oxide. *J. Exp. Bot.* 70, 4521–4537. doi: 10.1093/jxb/erz249
- Zhao, F., El Kelish, A., Durner, J., Lindermayr, C., Winkler, J. B., Ruëff, F., et al. (2016). Common ragweed (*Ambrosia artemisiifolia* L.): allergenicity and molecular characterization of pollen after plant exposure to elevated NO<sub>2</sub>. *Plant Cell Environ.* 39, 147–164. doi: 10.1111/pce.12601

**Conflict of Interest:** The authors declare that the research was conducted in the absence of any commercial or financial relationships that could be construed as a potential conflict of interest.

Copyright © 2020 Zhang, Ghirardo, Gori, Albert, Buegger, Pace, Georgii, Grote, Schnitzler, Durner and Lindermayr. This is an open-access article distributed under the terms of the Creative Commons Attribution License (CC BY). The use, distribution or reproduction in other forums is permitted, provided the original author(s) and the copyright owner(s) are credited and that the original publication in this journal is cited, in accordance with accepted academic practice. No use, distribution or reproduction is permitted which does not comply with these terms.



# Advantages of publishing in Frontiers



## OPEN ACCESS

Articles are free to read  
for greatest visibility  
and readership



## FAST PUBLICATION

Around 90 days  
from submission  
to decision



## HIGH QUALITY PEER-REVIEW

Rigorous, collaborative,  
and constructive  
peer-review



## TRANSPARENT PEER-REVIEW

Editors and reviewers  
acknowledged by name  
on published articles

## Frontiers

Avenue du Tribunal-Fédéral 34  
1005 Lausanne | Switzerland

Visit us: [www.frontiersin.org](http://www.frontiersin.org)

Contact us: [frontiersin.org/about/contact](http://frontiersin.org/about/contact)



## REPRODUCIBILITY OF RESEARCH

Support open data  
and methods to enhance  
research reproducibility



## DIGITAL PUBLISHING

Articles designed  
for optimal readership  
across devices



## FOLLOW US

@frontiersin



## IMPACT METRICS

Advanced article metrics  
track visibility across  
digital media



## EXTENSIVE PROMOTION

Marketing  
and promotion  
of impactful research



## LOOP RESEARCH NETWORK

Our network  
increases your  
article's readership